

2.5 Geology, Seismology, and Geotechnical Engineering

The geological, seismological, and geotechnical engineering properties of the VEGP site are presented in this section. **Subsection 2.5.1** describes basic geological and seismologic data. **Subsection 2.5.2** describes the vibratory ground motion at the site, including an updated seismicity catalog, description of seismic sources, and development of the Safe Shutdown Earthquake (SSE) ground motion. **Subsection 2.5.3** describes the potential for surface faulting in the site area, and **Subsections 2.5.1, 2.5.5, and 2.5.6** describe the stability of subsurface materials and foundations at the site.

NRC Regulatory Guide 1.165, *Identification and Characterization of Seismic Sources and Determination of Safe Shutdown Earthquake Ground Motion* (RG 1.165) (1997), Appendix D, *Geological, Seismological and Geophysical Investigations to Characterize Seismic Sources*, provides guidance for the level of investigation recommended at different distances from a proposed site for a nuclear facility.

The following four terms for site map areas are designated by RG 1.165:

- Site region - area within 200 mi (320 km) of the site location.
- Site vicinity - area within 25 mi (40 km) of the site location.
- Site area - area within 5 mi (8 km) of the site location.
- Site - area within 0.6 mi (1 km) of the proposed VEGP Unit 3 and 4 locations.

These terms are used in **Subsections 2.5.1** through **2.5.3** to describe these specific areas of investigation. These terms are not applicable to other sections of this ESP application.

SNC conducted field investigations and performed extensive research of relevant geologic literature to reach the conclusion that no geologic or seismic hazards have the potential to affect the VEGP site except the Charleston seismic zone and a small magnitude local earthquake occurring in the site region. These topics are discussed in greater technical detail in **Subsection 2.5.2**. There is only limited potential for non-tectonic surface deformation in shallow deposits within the 5-mi site area radius, and this potential can be mitigated by means of excavation.

RG 1.165 states that the vibratory design ground motion for a new nuclear power plant may be developed using either the Electric Power Research Institute (EPRI) or Lawrence Livermore National Laboratory (LLNL) probabilistic seismic hazard methodology. As described in **Subsection 2.5.2**, the EPRI methodology has been used to develop the SSE ground motion for the VEGP site. RG 1.165 further requires that the geological, seismological, and geophysical database be updated and any new data be evaluated to determine whether revisions to the 1986 EPRI seismic source model are required (presented in **Subsection 2.5.2**). This section, therefore, provides an update of the geological, seismological, and geophysical database for the VEGP site, focusing on whether any data published since the 1980s indicates a significant change to the 1986 EPRI seismic source model. In addition, the geotechnical properties of the VEGP site location are described to evaluate the ground motion site response characteristics of the site (i.e., non-tectonic geologic and man-made hazards at the site presented in **Subsection 2.5.2**).

2.5.1 Basic Geologic and Seismic Information

This section presents information on the geological and seismological characteristics of the VEGP site region and site area. The information is divided into two parts. **Subsection 2.5.1.1** describes the geologic and tectonic setting of the site region (200 mi), and **Subsection 2.5.1.2** describes the geology and structural geology of the site area (5 mi). The geological and seismological information was developed in accordance with the guidance presented in NRC Regulatory Guide 1.70, *Standard Format and Content of Safety Analysis Reports for Nuclear Power Plants, LWR Edition* (RG 1.70) (1978), **Subsection 2.5.1**, *Basic Geologic and Seismic Information*, and RG 1.165 and is intended to satisfy the requirements of 10 CFR 100.23(c). The geological and seismological information presented in this section is used as a basis for evaluating the detailed geologic, seismic, and man-made hazards at the site.

The geological and seismological information presented in this section was developed from a review of previous reports prepared for the existing VEGP Units 1 and 2, published geologic literature, new boreholes drilled at the VEGP Units 3 and 4 site and a seismic refraction and reflection survey. A review of published geologic literature was used to supplement and update the existing geological and seismological information. A list of the references used to compile the geological and seismological information presented in the following sections is provided at the end of each major subsection within **Section 2.5**.

2.5.1.1 Regional Geology (200 mi radius)

This section discusses the regional geology within a 200-mi radius of the VEGP site. The physiography and geomorphology, geologic setting and stratigraphy, and tectonic setting are discussed below. The information provided is a brief summary of this broad area, with an extensive and current bibliography. The information also provides the basis for evaluating the geologic and seismologic hazards discussed in the succeeding sections.

2.5.1.1.1 Regional Physiography and Geomorphology

From northwest to southeast the site region includes parts of the Valley and Ridge, Blue Ridge, Piedmont, and Coastal Plain provinces. The VEGP site is located on the upper Coastal Plain, about 30 mi (48 km) southeast of the Fall Line that separates the Piedmont and Coastal Plain provinces (**Figure 2.5-204**).

The Valley and Ridge Physiographic Province

The Valley and Ridge physiographic province extends from the 25-mi wide Hudson Valley in New York State to a wider 75-mi zone in Pennsylvania, Maryland, and Virginia and is about 50 mi wide from southern Virginia southward to Alabama. This physiographic province is underlain by a folded and faulted sequence of Paleozoic sedimentary rocks. The linear valleys and ridges typical of this province are the result of differential weathering and erosion in a humid environment of lithologies that are more or less resistant to these geomorphic processes.

The Blue Ridge Physiographic Province

The Blue Ridge physiographic province is located west of and adjacent to the Piedmont province. The Blue Ridge province extends from Pennsylvania to northern Georgia. It varies from about 10 to 75 mi (16 to 120 km) wide, north to south. Elevations are highest in North Carolina and Tennessee, with several peaks in North Carolina exceeding 5,900 ft (1,800 m) msl, including Mount Mitchell, North Carolina, the highest point (6,684 ft [2,037 m] msl) in the Appalachian Mountains. The Blue Ridge front, with a maximum elevation of about 3,950 ft (1,200 m) msl in North Carolina, is an east-facing escarpment between the Blue Ridge and Piedmont provinces in the southern Appalachians.

The Blue Ridge province is comprised primarily of relatively more resistant granites and granitic gneisses that form a broad mountainous upland area in Georgia.

The Piedmont Physiographic Province

The Piedmont physiographic province extends southwest from New York to Alabama and lies west of and adjacent to the Atlantic Coastal Plain. It is the eastern-most physiographic and structural province of the Appalachian Mountains. The Piedmont is a seaward-sloping plateau whose width varies from about 10 mi (16 km) in southeastern New York to almost 125 mi (200 km) in North Carolina; it is the least rugged of the Appalachian provinces. Elevation of the inland boundary ranges from about 200 ft (60 m) msl in New Jersey to over 1,800 ft (550 m) msl in Georgia.

The Piedmont province is divided into the Piedmont Upland section to the west and the Piedmont Lowland section to the east. The Piedmont Upland section is underlain by metamorphosed sedimentary and crystalline rocks of Precambrian to Paleozoic age. These lithologies are relatively resistant, and their erosion has resulted in a moderately irregular surface. Topographically higher terrain is underlain by Cambrian quartzites and Precambrian crystalline rocks. The Piedmont Lowland section is a less rugged terrain containing fault-bounded basins filled with sedimentary and igneous rocks of Triassic and Early Jurassic age (referred to as the Triassic Basin Rocks).

The Coastal Plain Physiographic Province

The Atlantic Coastal Plain extends southward from Cape Cod, Massachusetts, to south-central Georgia where it merges with the Gulf Coastal Plain. The surface of the Coastal Plain slopes gently seaward. The province is underlain by a seaward-dipping wedge of unconsolidated and semiconsolidated sediments that extend from the contact with the crystalline Piedmont province at the Fall Line to the edge of the continental shelf. In Georgia, the province is known as the Coastal Plain province. Sediment thickness increases from zero at the Fall Line to about 4,000 ft (1,200 m) at the Georgia - South Carolina coastline.

The VEGP site is located within a portion of the Coastal Plain in which depositional landforms have been obliterated by fluvial erosion based on studies in South Carolina (Reference 241). The lower coastal plain south of the site is dominated by primary depositional topography that has been modified slightly by fluvial erosion. In addition, the Coastal Plain contains numerous, minor geomorphic features, called Carolina bays. Since the origin of these minor geomorphic features has been controversial they are discussed in more detail in the following paragraphs. However, it is believed that these features formed as a result of erosion by predominantly southwesterly winds (Reference 448).

Carolina bays are shallow, elliptical depressions with associated sand rims that are found on the surface of the Coastal Plain sediments. These features, common throughout the Atlantic Coastal Plain, are most numerous in North and South Carolina, with major axes of the depressions up to 1.1 mi (1.8 km) long (Reference 437). The depressions are found from southern New Jersey to northern Florida, with the greatest occurrence in the Carolinas (Reference 448). One hundred ninety-four confirmed or suspected Carolina bays have been identified at the Savannah River Site (SRS), a US Department of Energy (DOE) reservation located directly east of the VEGP site area on the South Carolina side of the Savannah River. The long axes of the bays are oriented S50°E (Reference 338), and the sand rims generally are observed on the east and southeast flanks. Various authors have provided a range of hypotheses for the timing and mode of origin of these bays [e.g., (Reference 290; Reference 410; Reference 248; Reference 385; Reference 344)]. Theories regarding the origin of bays include meteorite impact, sinks, wind, and water currents [e.g., (Reference 385; Reference 410; Reference 248; Reference 464; Reference 290; Reference 344)]. The origin of these features remains indeterminate.

Prouty (1952), Savage (1982), and Kaczorowski (1976) provide the most likely explanation of formation: the bays formed by action of strong unidirectional wind on water ponded in surface depressions (Reference 448). The resulting waves caused the formation of the sand rims as shoreline features, and the sand rims formed perpendicular to the wind direction. The wind bays observed today formed in response to a southwesterly wind (Reference 448).

The Carolina bays are surficial features that have no effect on the subsurface sediments. Based on subsurface core data, a clay layer mapped beneath the bays and outside their rims has no greater relief beneath the bays than beyond them (Reference 290). Bryant and McCracken (1964), Preston and Brown (1964), and Thom (1970) provide additional evidence of the surficial character of Carolina bays. In these studies, certain identified strata were mapped and were found to be continuous and undeformed beneath bay and interbay areas. In Horry and Marion counties, South Carolina, there was no evidence of solution-related subsidence of the Carolina bays in spite of the presence of carbonate-rich strata in the subsurface and some localized sink holes of irregular shape with depths on the order of 20 ft. Early studies suggest that the bay-like depressions in the vicinity of the VEGP site (at SRS) probably resulted from dissolution of carbonate from the underlying geological formations (Reference 437). However, this has not been substantiated.

The age of the Carolina bays is based on Soller (1988) and Thom (1970). A minimum age has been set at middle to late Wisconsinan based on radiocarbon date (Reference 464). The maximum age can be constrained by examination of the formations on which the bays rest (Reference 448). This places bay formation between 100,000 and 200,000 years ago (ka) (Reference 448). If there is more than one generation, then the bays could be as old as the formations on which they rest.

2.5.1.1.2 Geologic History

The VEGP site is located in the Coastal Plain Physiographic province. Portions of all the major lithotectonic divisions of the Appalachian orogen (mountain belt) are found within a 200-mile (320-km) radius of the VEGP site. The structures and stratigraphic sequences within these divisions represent a complex geologic evolution that ends in the modern day passive margin of the Atlantic continental margin. Subsections 2.5.1.1.3 and 2.5.1.1.4 provide additional detail.

Within the Appalachian orogen, several lithotectonic terranes that have been extensively documented include the foreland fold belt (Valley and Ridge) and western Blue Ridge Precambrian–Paleozoic continental margin; the eastern Blue Ridge–Chauga Belt–Inner Piedmont Terrane; the volcanic-plutonic Carolina-Avalon Terrane; and the geophysically defined basement terrane beneath the Atlantic Coastal Plain [for an expanded bibliography see (Reference 315, Reference 316, Reference 318, Reference 319)]. These geological divisions contain the regional geologic record for the complete cycles of Precambrian and Paleozoic orogens and subsequent opening and closing of ocean basins (Proterozoic Iapetus Ocean and the opening of the Atlantic Ocean) (Reference 316).

The late Proterozoic rifting is recorded in rift-related sediments at the edge of the frontal Blue Ridge province and the Ocoee and Tallulah Falls basins in the western and eastern Blue Ridge, respectively. Passive margin conditions began in the middle Cambrian and persisted through early Ordovician. The Cambro–Ordovician sedimentary section in the Valley and Ridge reflects this condition. The collision-accretionary phase of the Appalachians began in the middle Ordovician and persisted with pulses through the early Permian (Penobscot/Taconic, Acadian, Alleghanian orogenies). Subsection 2.5.1.1.4 provides additional discussion.

The modern continental margin includes the Triassic basins that record the beginning of extension and continental rifting during the early to middle Mesozoic leading to the formation of the current Atlantic Ocean. One locus of major extension during early stages was in the South Georgia rift, which extends from Georgia into South Carolina. The Dunbarton Basin, underlying the VEGP site and SRS, is likely structurally related to the South Georgia rift basin (Reference 453) (Figure 2.5-205).

Subsection 2.5.1.1.3.4 provides additional discussion. During the later stage of rifting (early Jurassic), the focus of extension shifted eastward to the major marginal basins that would become the site of the Atlantic Ocean basin. The extension in the onshore, western-most basins, such as the Dunbarton, waned. Eventually, rifting of continental crust ceased as sea floor spreading began in the Atlantic spreading center sometime around 175 million years ago (Ma) ([Reference 356](#)). The oldest ocean crust in contact with the eastern continental margin is late middle Jurassic ([Reference 355](#)). The significance of the transition from rifting to sea floor spreading is that the tectonic regime of rifting is no longer acting on the continental crust along the Eastern Atlantic margin.

After the continental extension and rifting ended, a prograding shelf-slope began to form over the passive continental margin. The offshore Jurassic–Cretaceous clastic-carbonate bank sequence covered by younger Cretaceous and Tertiary marine sediments, and onshore Cenozoic sediments, represent a prograding shelf-slope [Reference 316](#) and the final evolution to a passive margin. Cretaceous and Cenozoic sediments thicken from near zero at the Fall Line to about 1,000 ft (335 m) in the center of the VEGP area, to approximately 4,000 ft (1,219 m) at the Georgia and South Carolina coast. The fluvial-to-marine sedimentary wedge consists of alternating sand and clay with tidal and shelf carbonates common in the downdip Tertiary section. Other offshore Continental margin elements include the Florida–Hatteras shelf and slope and the unusual Blake Plateau basin and Escarpment ([Reference 264](#); [Reference 356](#); [Reference 406](#)).

2.5.1.1.3 Regional Stratigraphy and Geologic Setting

The regional stratigraphy within each of the physiographic provinces is presented below. The generalized geology and stratigraphy within a 200-mi radius of the VEGP site is shown on [Figures 2.5-206](#) and [2.5-207](#). The stratigraphy shown on [Figures 2.5-206](#) and [2.5-207](#) is from a portion of The Geologic Map of the United States ([Reference 352](#)). The regional stratigraphy of the rock units shown on [Figure 2.5-206](#) is illustrated by the legend ([Figure 2.5-207](#)). The rock units are classified based on age and type.

2.5.1.1.3.1 Valley and Ridge Province

The Valley and Ridge lithotectonic terrane contains Paleozoic sedimentary rock consisting of conglomerate, sandstone, shale, and limestone ([Figures 2.5-204](#), [2.5-206](#) and [2.5-217](#)). This continental shelf sequence was extensively folded and thrust faulted during the Alleghanian collisional event. The physiography is expressed as a series of parallel ridges and valleys. To the east is the boundary with the Blue Ridge province, at the Blue Ridge–Piedmont fault system. This boundary is fairly distinct in most places along the strike of the Appalachians and marks the change from folded rocks that are not penetratively deformed to rocks that are penetratively deformed.

2.5.1.1.3.2 Blue Ridge Province

The Blue Ridge lithotectonic province is bounded on the southeast by the Brevard fault zone and on the northwest by a predominantly thrust fault system ([Reference 310](#); [Reference 308](#); [Reference 349](#)) ([Figure 2.5-217](#)). The province is a metamorphosed basement/cover sequence that has been complexly folded, faulted, penetratively deformed, and intruded. These rocks record multiple late Proterozoic to late Paleozoic deformation (extension and compression) associated with the formation of the Iapetus Ocean and the Appalachian orogen ([Reference 310](#); [Reference 324](#); [Reference 312](#); [Reference 390](#); [Reference 306](#)). The province consists of a series of westward-vergent thrust sheets, each with different tectonic histories and different lithologies, including gneisses, plutons, and metavolcanic and metasedimentary rift sequences, as well as continental and platform deposits [see ([Reference 310](#) and [Reference 316](#))] for an expanded bibliography). The Blue Ridge–Piedmont fault system thrust the entire Blue Ridge province northwest over Paleozoic sedimentary rock of the Valley and Ridge province during the Alleghanian orogeny ([Reference 304](#),

[Reference 305](#); [Reference 245](#); [Reference 249](#)). The Blue Ridge geologic province reaches its greatest width in the southern Appalachians.

The Blue Ridge is divided into a western and an eastern belt separated by the Hayesville-Gossan Lead fault. Thrust sheets in the western Blue Ridge consist of a rift-facies sequence of clastic sedimentary rocks deposited on continental basement, whereas thrust sheets in the eastern Blue Ridge consist of slope and rise sequences deposited in part on continental basement and on oceanic crust ([Reference 310](#); [Reference 306](#)). Western Blue Ridge stratigraphy consists of basement gneisses and metasedimentary, metaplutonic, and metavolcanic rocks, whereas Eastern Blue Ridge stratigraphy consists of fewer lithologies, more abundant mafic rocks, and minor amounts of continental basement.

Western Blue Ridge

The western Blue Ridge consists of an assemblage of Middle Proterozoic crystalline continental (Grenville) basement rock nonconformably overlain by Late Proterozoic to Early Paleozoic rift and drift facies sedimentary rock ([Reference 316](#)). The basement consists of various types of gneisses, amphibolite, gabbroic and volcanic rock, and metasedimentary rock. All basement rock is metamorphosed to granulite or uppermost amphibolite facies ([Reference 316](#)). The calculated ages of these rocks generally range from 1,000 to 1,200 million years old (Ma) [e.g., [Reference 289](#); [Reference 286](#); [Reference 288](#)].

The rifting event during the Late Proterozoic through Early Paleozoic that formed the Iapetus Ocean is recorded in the rift-drift sequence of the Ocoee Supergroup and Chilhowie Group [e.g., [Reference 478](#); [Reference 418](#); [Reference 354](#); [Reference 392](#); [Reference 350](#)]. These rocks, basement, and sedimentary cover were later affected by Taconic and possibly Acadian deformation and metamorphism. The entire composite thrust sheet was transported west as an intact package during the Alleghanian collision event on the Blue Ridge–Piedmont thrust.

Eastern Blue Ridge

The eastern Blue Ridge is located southeast of the western Blue Ridge and is separated from that province by the Hayesville-Gossan Lead fault. The Brevard fault zone forms the southeastern boundary with the Inner Piedmont. The eastern Blue Ridge is composed of metasedimentary rocks originally deposited on a continental slope and rise and ocean floor metasedimentary rocks in association with oceanic or transitional to oceanic crust [for expanded bibliography see ([Reference 316](#); [Reference 324](#))]. This is in contrast to the previously discussed western Blue Ridge that contains metasedimentary rocks suggesting continental rift-drift facies of a paleomargin setting. The eastern Blue Ridge is structurally complex, with several major thrust faults, multiple fold generations, and two high-grade metamorphic episodes ([Reference 316](#)). Metamorphism took place during the Taconic and possibly Acadian orogenies.

The stratigraphy within the eastern Blue Ridge includes rare Grenville (Precambrian) gneisses, metasedimentary rocks of the Tallulah Falls Formation and the Coweeta Group, metamorphosed Paleozoic granitoids, and mafic and ultramafic complexes and rocks of the Dahlonge Gold Belt. The Paleozoic granitoids are a part of a suite of similar granites found in the western Inner Piedmont, suggesting a common intrusive history. Metasedimentary rock sequences in the eastern Blue Ridge are correlated along strike as well as across some thrust fault boundaries, also suggesting a commonality in the original depositional history. Based on geochemical data, the mafic and ultramafic complexes found in particular thrust sheets in the eastern Blue Ridge have oceanic as well as continental affinities. However, their exact tectonic origin is not clear because the contacts with the host metasedimentary rock are obscure.

2.5.1.1.3.3 Piedmont Province

The Piedmont province in northwestern Georgia and South Carolina consists of variably deformed and metamorphosed igneous and sedimentary rocks ranging in age from Middle Proterozoic to Permian (1,100 to 265 Ma). The province consists of the Western (Inner) Piedmont and the Carolina-Avalon Terrane ([Figure 2.5-217](#)). This designation is made because of different tectonic origins for the western and eastern parts of the province. The province can also be subdivided into seven distinctive tectonostratigraphic belts separated by major faults, contrasts in metamorphic grade, or both. The Charlotte and Carolina Slate belts are combined and discussed as the Carolina-Avalon Terrane. The rocks of the Piedmont have been deformed into isoclinal recumbent and upright folds, which have been refolded and are contained in several thrust sheets or nappes. These metamorphic rocks extend beneath the Coastal Plain sediments in Georgia and South Carolina. The southeastern extent of the Piedmont province underneath the Coastal Plain is unknown.

Western Piedmont

The Western Piedmont encompasses the Inner Piedmont block, the Smith River Allochthon in Virginia and North Carolina, and the Sauratown Mountains Anticlinorium in north central North Carolina ([Reference 327](#)) ([Figure 2.5-208](#)). The Western (Inner) Piedmont is separated from the Blue Ridge province on the northwest by the Brevard Fault zone. It is separated from the Carolina–Avalon Terrane on the southeast by the Towaliga fault, a complex series of fault zones approximately coincident with the Central Piedmont suture ([Reference 307](#)). These faults include: Lowndesville, Kings Mountain, Eufola, Shacktown, and Chatham Fault zones ([Reference 327](#)). The province is a composite stack of thrust sheets containing a variety of gneisses, schists, amphibolite, sparse ultramafic bodies, and intrusive granitoids ([Reference 391](#); [Reference 295](#); [Reference 308](#)). The protoliths are immature quartzo-feldspathic sandstone, pelitic sediments, and mafic lavas.

The Sauratown Mountains anticlinorium is a complex structural window of four stacked thrust sheets that have been exposed in eroded structural domes. Each sheet contains Precambrian basement with an overlying sequence of younger Precambrian-to-Cambrian metasedimentary and metaigneous rocks ([Reference 327](#)). The Smith River Allochthon contains two predominantly metasedimentary units and a suite of plutonic rocks. It is a completely fault-bounded terrane, as is the Sauratown Mountains anticlinorium. The Inner Piedmont block is a fault-bounded, composite thrust sheet with metamorphic complexes of different tectonic affinities ([Reference 327](#)). There is some continental basement within the block ([Reference 295](#)) and scattered mafic and ultramafic bodies and complexes ([Reference 386](#)), suggesting the presence of oceanic crustal material ([Reference 327](#)). The rest of the block contains a coherent, though poorly understood, stratigraphy of metasedimentary rock, metavolcanic gneisses, and schists ([Reference 327](#)). The eastern Blue Ridge and Inner Piedmont contain some stratigraphically equivalent rocks ([Reference 313](#)).

The stratigraphy and structural geologic data in the western Piedmont reflects the effects of a complex tectonic history from the Precambrian Grenville through Late Paleozoic Alleghanian orogenies. Metamorphism affected the basement rocks of the Sauratown Mountains anticlinorium at least twice: during the Precambrian Grenville and later during the Paleozoic. The metasedimentary cover sequence as well as the Smith River allochthon and the Inner Piedmont block were affected by one metamorphic event (prograde and retrograde) in the Paleozoic ([Reference 327](#)). The Alleghanian continental collision is reflected in the thrust and dextral strike slip fault systems such as the Brevard and Bowens Creek fault zones. A few late Paleozoic granites were emplaced in the Inner Piedmont block; however, most lie further east in the Carolina Terrane. Early Mesozoic extension resulted in the formation of rift basins (Dan River and Davie County basins).

Carolina-Avalon Terrane

The Carolina Terrane is part of a late Precambrian–Cambrian composite arc terrane exotic to North America ([Reference 430](#); [Reference 425](#)) and accreted sometime during the Ordovician to Devonian

(Reference 473; Reference 393). It consists of felsic to mafic volcanic rock and associated volcanoclastic rock. Middle Cambrian fossil fauna indicate a European or African affinity (Reference 430).

The northwestern boundary of the Carolina–Avalon Terrane is formed by a complex of faults that constitute the Central Piedmont suture (Figures 2.5-208 and 2.5-209) and separate the terrane from rocks of North American affinity [see (Reference 314; Reference 323; Reference 450; Reference 297; Reference 260; Reference 421; Reference 326; Reference 322; Reference 383)]. This structure was reactivated during the later Alleghanian collisional events as a dextral shear fault system (Reference 218). Subsequent investigators have further enhanced the geological knowledge of the complicated structure (Reference 431, Reference 432; Reference 309; Reference 323). Dennis (1991) suggested that the Central Piedmont suture is a low-angle normal fault. The Carolina–Avalon Terrane (also known as the Carolina Terrane) is bounded on the southeast by the Modoc fault zone and the Kiokee belt (Figure 2.5-209).

The Carolina–Avalon Terrane is the combination of the earlier Charlotte and Carolina slate belts. The belts were initially distinguished by metamorphic grade (Reference 349) and were later recognized as the same protolith and thus were combined (Reference 316). Metamorphic grade increases to the northwest from lower greenschist facies to upper amphibolite facies. Pre-Alleghanian structure is dominated by large northeast trending folds with steeply dipping axial surfaces. All country rock of the Carolina–Avalon Terrane has been penetratively deformed, thereby producing axial plane cleavage and foliation (Reference 316).

The Charlotte belt contains numerous intrusions and moderate- to high-grade metamorphic rock. Much of the belt was metamorphosed to amphibolite grade during the Taconic orogeny (Reference 230), but retrograde metamorphism is also widespread. The oldest rocks are amphibolite, biotite gneiss, hornblende gneiss, and schist, and probably were derived from volcanic, volcanoclastic, or sedimentary protoliths.

The Carolina Slate belt (Figure 2.5-209) is characterized by thick sequences of metasedimentary rocks derived from volcanic source areas and felsic to mafic metavolcanic rocks. The oldest rocks within the Carolina Slate belt consist of intermediate to felsic ashflow tuff and associated volcanoclastic rocks. These rocks are overlain by a sequence of mudstone, siltstone, sandstone, greywacke, and greenstone, with some interbedded volcanic tuff and flows. The belt was subjected to low- to medium-grade regional metamorphism and folding from 500 to 300 Ma and was intruded subsequently by granitic and gabbroic plutons about 300 Ma.

Kiokee Belt

The Kiokee belt is located between the Carolina–Avalon Terrane and the Belair belt in Georgia and South Carolina (Figure 2.5-209). It is referred to as the Savannah River Terrane in some of the recent literature (Reference 368). The Kiokee belt is bounded on the northwest by the Modoc fault zone and on the southeast by the Augusta fault (the Modoc fault zone and the Augusta fault are discussed in Subsection 2.5.1.1.4.3). The Kiokee belt is a medium- to high-grade metamorphic belt with associated plutonism (Reference 258). Snoke et al. (1980) concluded that the Kiokee belt was part of the Alleghanian metamorphic core. That core was deformed and metamorphosed prior to the development of the plastic shear zones bounding it (Reference 431). The bounding faults are mylonite zones that overprint the amphibolite facies infrastructure of the core of the belt (Reference 316).

The Kiokee belt is an antiformal structure that strikes northeast. The interior is a migmatitic complex of biotite amphibole paragneiss, leucocratic paragneiss, sillimanite schist, amphibolite, ultramafic schist, serpentinite, feldspathic metaquartzite, and granitic intrusions of Late Paleozoic age (Reference 429). Some of the lithologic units found in the Carolina slate belt may occur at higher metamorphic grade in the Kiokee belt (Reference 316).

From extensive field studies and geochronological dating, a complex Alleghanian history can be derived from the studies of the Kiokee belt ([Reference 225](#); [Reference 366](#); [Reference 444](#); [Reference 257](#); [Reference 287](#); [Reference 445](#); [Reference 303](#); [Reference 424](#)). The pre-Alleghanian structure and stratigraphy are only partially known. The nature of the crustal rock that played a part in the metamorphism, deformation, and intrusion is still unknown. The possible role of a Precambrian basement in the Kiokee belt is a key question proposed by Hatcher et al. (1994). No rock in the Kiokee belt has been identified at this time as Precambrian basement. However, Long and Chapman (1977), suggested, based on gravity data, that a large rifted block of continental crust underlies the Kiokee belt.

Belair Belt

The Belair belt, also known as the Augusta Terrane ([Reference 366](#), [Reference 367](#)), is locally exposed in the Savannah River valley, near Augusta, Georgia ([Figure 2.5-209](#)). It is largely concealed beneath the Atlantic Coastal Plain, but is exposed in several small erosional windows through the Coastal Plain sediments in eastern Georgia ([Reference 226](#)). The Belair belt consists of intermediate to felsic volcanic tuffs and related volcanoclastic sediments penetratively deformed and metamorphosed to greenschist facies ([Reference 226](#); [Reference 365](#), [Reference 366](#), [Reference 367](#), [Reference 311](#); [Reference 414](#); [Reference 411](#); [Reference 395](#)). The Belair belt displays similar characteristics as the Carolina-Avalon Terrane ([Reference 370](#)). Geophysical and well data indicate that the Belair belt extends beneath the Atlantic Coastal Plain ([Reference 258](#)). Near Augusta, the Augusta fault and the southeast edge of the Kiokee belt appear to be offset by the north-northeast trending Cenozoic Belair fault ([Figure 2.5-209](#)) (discussed in [Subsection 2.5.1.1.4.3](#)).

2.5.1.1.3.4 Mesozoic Rift Basins

While primarily exposed in the Piedmont Province, Mesozoic-age rift basins are found along the entire eastern continental margin of North America from the Gulf Coast through Nova Scotia ([Figure 2.5-210](#)). The basins formed in response to the continental rifting episode that broke up the supercontinent, Pangea, and led to the formation of the Atlantic Ocean basin. Rift basins are exposed in the Piedmont province as well as buried beneath Cretaceous and younger Coastal Plain sediments. Many underlie offshore regions. Structurally, the basins are grabens or half grabens elongated in a northeast direction and bounded by normal faults on one or both sides ([Reference 371](#)). Several basins were localized along reactivated Paleozoic ductile or brittle fault zones ([Reference 404](#); [Reference 336](#); [Reference 419](#); [Reference 359](#); [Reference 293](#)).

The basins are located in extended or rifted continental crust, identified as the Eastern Seaboard domain (subdomain of North American stable continental crust) ([Reference 345](#)). Rifted crust is crust that has been stretched, faulted, and thinned slightly by rifting but is still recognizable as continental crust. The faulting is extensional or normal, and down-dropped blocks form rift basins. The western boundary of this zone of extended crust is defined by the western-most edge of Triassic–Jurassic onshore rift basins or the boundaries of the structural blocks in which they occur ([Reference 356](#); [Reference 346](#); [Reference 345](#)). The eastern boundary is the continental shelf ([Reference 298](#)).

Two belts of basins occur in the Eastern Seaboard domain, from the Carolinas to Pennsylvania ([Olsen et al. 1991](#)): an eastern belt of basins buried by Atlantic Coastal Plain Sediments and a western belt exposed in the Piedmont Physiographic Province. In North and South Carolina, the Deep River, Elberbe, and Crowburg basins are in the eastern belt, and the Dan River and Davie County basins are in the western belt ([Reference 402](#)). In addition, the Dunbarton, Florence, Riddleville, and South Georgia basins are buried beneath Coastal Plain sediments in the eastern belt ([Figure 2.5-210](#)).

The basins are generally filled with lacustrine sedimentary and igneous rock. Sedimentary strata consist mainly of non-marine sandstone, conglomerate, siltstone, and shale. Carbonate rocks and coal are found locally in several basins. Igneous rocks of basaltic composition occur as flows, sills,

and stocks within the basins and as extensive dike swarms within and outside the basins (Reference 351). These basin fill strata have been described and named the Newark Supergroup (Reference 400; Reference 285; Reference 402). In general, the stratigraphy can be divided into three sections. The lower section is characteristically fluvial (Reference 440; Reference 296) and contains reddish-brown, arkosic, coarse-grained sandstone and conglomerate. The middle section mainly includes sediments of lacustrine origin (Reference 440). These sediments include gray-black fossiliferous siltstone, carbonaceous shale, and thin coal beds (Reference 402). The upper section is a complex of deltaic, fluvial, and lacustrine environments (Reference 401; Reference 428). These sediments include red-brown siltstone, arkosic sandstone, pebble sandstone, red and gray mudstone, and conglomerate (Reference 402).

In Georgia and South Carolina, the Dunbarton Triassic rift basin, a sub-basin within the South Georgia Basin, is located beneath Coastal Plain sediments below the SRS and the VEGP sites (Figure 2.5-210). The Dunbarton Basin was first identified based on aeromagnetic and well data (Reference 437). Subsequent seismic reflection surveys, potential field surveys, and additional well data have led to the current understanding of the basin (Reference 372, Reference 373; Reference 374; Reference 232; Reference 208; Reference 451; Reference 362; Reference 266). The structure is interpreted as an asymmetric graben approximately 31 mi long and 6 to 9 mi wide. The axis of the basin strikes northeast, parallel to the regional strike of crystalline basement (Reference 374). The basin extends 5 mi southwest of the Savannah River and 25 mi to the northeast of the SRS, where it terminates against a granite body interpreted from magnetic data (Reference 437; Reference 372, Reference 373; Reference 208). The primary fault controlling basin formation, the Pen Branch fault, bounds the northwest side of the basin. The fault appears to have been an earlier Paleozoic reverse fault that was reactivated as an extensional normal fault during Mesozoic continental rifting. The fault was subsequently reactivated in the Cenozoic as a reverse fault or right-oblique slip fault (Reference 409; Reference 442; Reference 453). The Pen Branch fault dips to the southeast. The master fault to the Riddleville Basin in Georgia also dips to the southeast (Reference 404). Subsections 2.5.1.1.4.3 and 2.5.1.2.4.1 provide further discussion of the Mesozoic basins and the Pen Branch fault, respectively. The southeast boundary of the Dunbarton basin is poorly constrained but is interpreted as fault bounded (Reference 280; Reference 443).

Fourteen wells drilled at the SRS penetrated sedimentary rocks of the Dunbarton Basin. Recovered core is Mesozoic clastic rock (Reference 403; Reference 374). Conglomerate, fanglomerate, sandstone, siltstone, and mudstone are the dominant lithologies. These rocks are similar to the clastic facies in other Newark Supergroup basins. Conglomerate and red clayey siltstone are the dominant lithologies in those cores. Parsons Brinckerhoff (1973) concluded that the lithology and stratigraphy identified in the core indicate that the proximal side of the basin is to the northwest. A larger component of coarse-grained rock types occurs to the northwest than on the southeast side of the basin. This suggests an asymmetric basin with greater cumulative separation on the northwest than to the southeast. This asymmetry led to greater local relief along the northern boundary, where high energy fluvial processes dominated, and the resulting sediments are coarser grained than farther out in the basin.

Gravity and magnetic modeling suggests that the Triassic section in the Dunbarton Basin is at least 1.2 mi (2 km) thick. Boreholes have encountered up to 899 m of Triassic fill, but the base of the Dunbarton was not encountered (Reference 374). Seismic reflection data do not unequivocally constrain the base of the basin; the transition between the Triassic rock and the crystalline terrane is unclear. However, interpreted Triassic reflectors are at least as deep as 1 to 2.3 mi (1.6 to 3.7 km) (Reference 266).

The South Georgia Basin, further east and south in Georgia and South Carolina, is a much larger, deeper, and more complex basin than the Dunbarton Basin. The basin is as wide as 62 mi and as deep as 4 mi (Reference 380). It is not a single basin, but a complex of isolated synrift grabens with

limited major crustal extension. The major border fault dips northward ([Reference 380](#)), as opposed to southeastward, for the controlling faults bounding the Dunbarton Basin.

Further to the northeast, in North Carolina, two major basins are exposed: the Dan River and Deep River basins. Both basins exhibit half-graben geometry, bounded on one side by a major normal fault zone. However, the border faults on the two basins are on opposite flanks of the basin: Dan River's Chatham fault zone dips to the southeast and Deep River's Jonesboro fault zone dips northwest ([Reference 402](#)).

2.5.1.1.3.5 Coastal Plain

In the Coastal Plain, rocks of Paleozoic and Triassic age have been beveled by erosion and are unconformably overlain by unconsolidated to poorly consolidated Coastal Plain sediments ([Reference 247](#); [Reference 437](#); [Reference 241](#)). The sediments of the Coastal Plain in Georgia and South Carolina are stratified sand, clay, limestone, and gravel that dip gently seaward and range in age from Late Cretaceous to Recent. The sedimentary sequence thickens from essentially zero at the Fall Line to more than 4,000 ft (1,219 m) at the coast ([Colquhoun et al. 1983](#)). Regional dip is to the southeast, although beds dip and thicken locally in other directions because of locally variable depositional regimes and differential subsidence of basement features.

Many investigations have provided insight into the evolution of the southeastern United States Coastal Plain, including: Cooke (1936), Siple (1967), Huddlestun and Hetrick (1978), Colquhoun and Steele (1985), Prowell et al. (1985a, 1985b), Dennehy et al. (1988), Fallaw et al. (1990a, 1990b, 1992, 1995), Nystrom et al. (1990), Aadland and Bledsoe (1990), Huddlestun and Summerour (1996) and, most recently, Falls and Prowell (2001). The Coastal Plain section is divided into several rock-stratigraphic groups based principally on age and lithology ([Figure 2.5-211](#)).

The VEGP Units 3 and 4 site is located on the Coastal Plain. Numerous geologic studies have been conducted in the surrounding area since initial studies were conducted for the existing VEGP units. Most of these studies were conducted in the vicinity of the SRS and focused on correlating both geologic and hydrogeologic formations present in Georgia and South Carolina resulting in an updated stratigraphic nomenclature. A correlation chart showing the Vogtle FSAR, current USGS, Georgia Geological Survey, South Carolina and SRS nomenclature is provided in [Figure 2.5-211](#). The following sections describe each geologic unit (from oldest to youngest), largely taken from the recent work of the USGS ([Reference 278](#)) and the Georgia Geological Survey ([Reference 334](#)).

Cretaceous Sediments

Five deep test holes were drilled in the Georgia Coastal Plain sediments of Burke and Screven counties by the USGS and the Georgia Geologic Survey to determine the stratigraphy of the Upper Cretaceous and Tertiary sediments in eastern Georgia near the Savannah River ([Figure 2.5-212](#)) ([Reference 278](#)). The Cretaceous sections in the cores are divided into the Cape Fear Formation, the Pio Nono/Middendorf Formation, the Gaillard/Black Creek Formation (regionally, the Black Creek Group), and the Steel Creek Formation ([Figure 2.5-211](#)). These units consist of siliciclastic sediments. Evidence for possible unconformities led the investigators to recognize two subunits in the Middendorf and three subunits in the Black Creek Group. Each contact between units is a regional unconformity and denotes considerable hiatus in sedimentation. The depositional environment for all four units is interpreted as a set of large deltaic systems that prograded across the continental shelf in east-central Georgia and western South Carolina.

Cape Fear Formation

The Cape Fear Formation consists of partially lithified to unlithified, poorly to very poorly-sorted clayey sand and sandy clay with a few beds of silty clay. The sand is fine to very coarse with granules and pebbles and is predominantly angular to subangular quartz with some feldspar. Cristobalite in

the clay matrix results in lithologies that are harder and denser than sediments in the other Cretaceous units. The cristobalitic clay matrix imparts a yellowish-green to greenish-gray color to most of the lithologies and occludes most of the intergranular porosity in the sand beds. In three out of the five test holes evaluated by the USGS, the bottom of the Cape Fear Formation was drilled through and the formation ranges in total thickness from 96 to 212 ft, thickening in the downdip direction.

The Cape Fear Formation contains multiple fining-upward cycles that range in thickness from 3 to 15 ft. Each cycle grades upward from a basal pebbly coarse sand to a clayey sand or clay. The clays are oxidized and are generally stained with reddish-brown and yellowish-brown patches of iron oxide. A root-trace pattern is present at the top of a few of the fining-upward cycles. The upper contact sediments are typically stained with iron oxides.

Most of the strata in this unit are without fossils; however, a silty clay sample from one of the cores contains low-abundance and low-diversity pollen assemblages. Palynologic analysis indicates a Coniacian microflora ([Reference 284](#)). This is consistent with the microflora of the Cape Fear Formation of South Carolina and North Carolina ([Reference 237](#); [Reference 236](#); [Reference 446](#)). Prowell et al. (1985a) and Fallaw and Price (1995) suggested a Santonian age for unit UK1 and the Cape Fear Formation at the SRS. Huddleston and Summerour (1996) suggested that the Cape Fear Formation is equivalent to the Cenomanian-Turonian Tuscaloosa Formation of western Georgia.

The presence of a terrestrial microflora and the absence of dinoflagellates (marine fossils) in the Cape Fear Formation suggest deposition in a nonmarine environment. The multiple fining-upward cycles, the coarse texture of the sand layers, the iron-oxide staining, and the root-trace patterns in the clay layers suggest that most of this unit was deposited in channel and overbank environment during aggradation of a fluvially dominated, subaerially exposed part of a delta-plain environment.

Pio Nono/Middendorf Formation

The Pio Nono/Middendorf Formation unconformably overlies the Cape Fear Formation with a distinct contact. The formation is marked by an abrupt change from the moderately indurated clay and clayey sand of the underlying Cape Fear to the slightly indurated sand and lesser clayey sand of the Pio Nono/Middendorf. The Pio Nono/Middendorf sand units are moderately to poorly-sorted and are very porous and permeable in comparison to the sand units in the underlying Cape Fear. The Pio Nono/Middendorf consists predominantly of unlithified sand, which is locally fine to very coarse or fine to medium quartz. The mineral assemblage includes smoky-quartz granules and pebbles, mica, lignite, and generally very little clay matrix. The basal zone is often pebbly. The formation has a maximum known thickness of about 520 ft (158 m) in Georgia ([Reference 238](#)). Total thickness of the unit in the USGS test holes ranges from 157 to 207 ft.

The Pio Nono/Middendorf Formation contains two distinct subunits (informal, ascending Subunits 1 and 2) in the Millhaven, Girard, and Millers Pond cores ([Figure 2.5-212](#)). Each includes a basal lag deposit of poorly-sorted sand that grades upward to interbedded and interlaminated clay and sand. Micaceous and lignitic sand laminae are common in the Middendorf sections, particularly near the top of each subunit. Clay beds in some of the cores display more abundant iron-oxide staining near the top of the subunits. A root-trace pattern is observed in the clay bed at the top of Subunit 2 in the Girard core.

A Santonian age is suggested by current research ([Reference 278](#)). Lithologic and geophysical log patterns indicate the upper contact of the Pio Nono/Middendorf Formation in Georgia correlates to the UK2/UK4 boundary of Prowell et al. (1985a) and to the upper contact of the Pio Nono/Middendorf in South Carolina ([Reference 273](#)).

Dinoflagellates and other marine indicators are sparse and suggest a marginal-marine environment in the downdip cores and a nonmarine environment for this unit in the other cores.

Near Bamberg, South Carolina, the Pio Nono/Middendorf Formation consists of poorly-sorted, gray, medium to very coarse grained, angular to subangular quartz sand with quartz pebbles and sparse feldspar grains ([Reference 360](#)). Silt and fine sand are present. The angularity and large overall grain size of the quartz and the presence of feldspar indicate that deposition occurred relatively close to the source area, most likely in an upper delta plain environment. In southeastern Georgia, the Middendorf includes some shallow shelf sediments. Farther downdip, sediments of the Middendorf become finer grained. In Allendale County, South Carolina, in the vicinity of Millet, the unit consists of light gray to colorless, fine to coarse grained quartzose sand, clayey sand, and silty clay. The sand is unconsolidated and poorly to moderately-sorted. Trace amounts of heavy minerals and lignite are present. Deposition most probably occurred on a lower delta plain ([Reference 360](#)).

Gaillard /Black Creek Formation (regionally the Black Creek Group)

The Gaillard/Black Creek Formation (Black Creek Group) is distinguished from the overlying and underlying Cretaceous units by its better-sorted sand, fine grained texture, and relatively high clay content. It is generally darker, more lignitic, and more micaceous, especially in the updip part of the section, than the other Cretaceous units. The total thickness of the unit in the study area ranges from 270 to 333 ft. Falls and Prowell (2001) found that, in Georgia, the Gaillard Formation typically consists of three subunits:

- Subunit 1 - Basal, lignitic sand
- Subunit 2 - Laminated black clay and sand
- Subunit 3 - Coarsening upward sand sequence

The lag deposits observed at the bases of these subunits suggest unconformities. However, the Gaillard Formation/Black Creek Group in the Millers Pond core (updip location) is coarser and more sandy, with no recognizable subunits.

Subunit 1 is similar to the underlying Pio Nono/Middendorf Formation. The sediments consist of moderate to poorly-sorted, fine to coarse grained quartz sand. The sequence grades upward into fine and very fine sand with thin beds of clay. Sand layers contain fine lignite and mica with little clay matrix.

Subunit 2 has two sharp contacts within the subunit, observed in the downdip cores. Each contact is overlain by a basal lag of very poorly-sorted sand. Most of Subunit 2 is calcareous and contains laminae and lenses of very fine sand and sand-filled burrows. There are thick sections of silty laminated black clay. The sand layers typically contain mica, lignite, and minor glauconite.

Bioturbation features in Subunit 2 include clay-lined burrows, mottled textures, and discontinuous laminae of clay in the sands. Subunit 2 has the most abundant and diverse marine macrofaunas, microfaunas, and microfloras in the Cretaceous section in the study area, including shark teeth, pelecypods, ostracodes, benthic and planktonic foraminifers, spicules, dinoflagellates, pollen, and calcareous nannofossils.

Subunit 3 typically consists of a coarsening upward sequence with very poorly-sorted lag deposit at the base. Moderate to well-sorted, very fine to medium sand occurs above the basal lag deposit. Fine to coarse sand is found higher in the section. There are laminae and thin beds of dark gray clay, large and small lignite pieces, mica and cross-bedding.

Paleontological data from the Gaillard Formation/Black Creek Group indicate a Campanian age for the unit ([Reference 284](#); [Reference 229](#); [Reference 294](#)). Units UK4 and UK5 ([Reference 416](#)) and the Black Creek Group at the SRS ([Reference 273](#)) are assigned an age of Campanian to Maastrichtian. The diversity and abundance of dinoflagellates, the abundance of marine faunas, and

the presence of glauconite at Millhaven and Girard coreholes suggest a strong marine influence during the deposition of Subunit 2, probably in the distal part of a deltaic complex. Dinoflagellates in Subunit 3 suggest a marginal-marine depositional environment. The composition of the microflora and the absence of other marine indicators suggest that Subunit 1 at Millhaven and Girard, and the entire section of the Gaillard Formation/Black Creek Group at Millers Pond reflect sedimentation in a nonmarine part of the delta ([Reference 284](#)).

Steel Creek Formation

The contact between the Steel Creek Formation and the underlying Gaillard Formation/Black Creek Group is subtle in most of the test cores in the region ([Reference 348](#); [Reference 334](#)). The contact may be conformable, paraconformable, or gradational at various locations in the region. The USGS study ([Reference 278](#)) identified the contact as unconformable and placed the boundary based on projection of the contact from a downdip test hole. The Steel Creek Formation in the study area ranges from 38 to 197 ft thick.

The Steel Creek Formation in Georgia typically consists of poorly to very poorly-sorted, fine to very coarse sand with granules and pebbles of smoky quartz. Clay matrix ranges from 5 to 15 percent. Basal lags are characteristically overlain by thick sections of oxidized clay. There are multiple fining-upward sequences in the formation. Cross-bedding is common. Lignite and mica are common accessories.

The formation is mostly barren of fossils. Some core samples yielded Cretaceous and Paleocene palynomorphs ([Reference 284](#)). Paleontology data from the Black Creek Group below and the Tertiary Black Mingo/Ellenton Formation above restrict the age to Maastrichtian.

Coarse grained sediments, fining-upward sequences, iron oxide staining, and indications of root-bearing zones indicate channel and overbank deposits in a delta-plain environment.

Tertiary Sediments

Tertiary sediments in the site area range in age from Early Paleocene to Miocene and were deposited in open marine shelf environments (downdip) to marginal-marine environments (updip) ([Reference 334](#), [Reference 278](#)). The Tertiary sequence is divided into five units: Black Mingo/Ellenton Formation, Snapp Formation, Congaree Formation [regionally, the Fourmile Branch/Congaree/Warley Hill (FM/C/W) unit], Lisbon Formation (regionally, the Santee Limestone), and Barnwell Group/unit ([Figure 2.5-211](#)). The section is generally more calcareous in the downdip area than in the updip area, with greater diversity and abundance of marine microflora and fauna. The thickness of the entire Tertiary section in the study area ranges from 284 to 642 ft.

Black Mingo Formation

The Black Mingo Formation varies from a predominantly clay-rich section in the downdip area into a more sandy, clayey, and calcareous area further updip and finally to a predominantly sandy section in the most updip locations. The formation varies in total thickness from 33 to 72 ft. In the downdip core, the section contains well-sorted, fine to medium sand with large portions of well laminated clay and silty clay. The top of the section in the downdip area is calcareous and non-calcareous clay. Further updip in the Girard core, the section contains sandy carbonate, limestone, calcareous sand, and abundant glauconite, along with well laminated, non-calcareous silty clay. The sand layers are typically fine to medium grained. Several lag deposits examined have 10 to 20 percent glauconite, rounded phosphatic clasts, and shark teeth. In the updip core, the section is generally fine to very coarse sand interbedded with sandy clay. Midway in this section are interlaminated black lignitic clay and very fine to medium sand. The top of the section is clayey, fine to medium sand.

Paleontologic studies identify a diverse microflora of dinoflagellates, pollen, and calcareous nannofossils and a faunal component of ostracodes, planktonic foraminifers, pelecypods, and

gastropods in the downdip sections ([Reference 270](#)). The updip section at Millers Pond contains a low-diversity microflora of dinoflagellates and pollen ([Reference 239](#)). The marine fossils, glauconite, and carbonate in downdip sediments indicate an open-marine environment, possibly distal prodelta. The low diversity and the low abundance of dinoflagellates and the absence of other marine indicators at Millers Pond suggest a change to a more restricted marginal-marine environment.

Snapp Formation

The Snapp Formation in all test holes in the study area consists of moderate to poorly-sorted, fine to very coarse sand. The sand typically contains granules and pebbles and less than 10 percent clay matrix. The formation in the study area is from 50 to 67 ft thick. The sand section is overlain by a very light gray colored kaolin zone that is oxidized and stained red and yellow by iron oxides. Pedogenic structures are found in the clay and include root traces and desiccation cracks. Pyrite is disseminated in the clay and also concentrates along desiccation cracks. In general, there is a strong fining-upward sequence from bottom to top within the formation.

The Snapp Formation pinches out in the vicinity of the VEGP site. Snapp was not found in the Thompson Oak core. This is consistent with the described updip limit of Snapp in South Carolina, near the Upper Three Runs creek in Aiken County ([Reference 273](#)).

Paleontology samples from the downdip core hole (Millhaven) provided sparse dinoflagellates ([Reference 270](#)).

The stratigraphic position of the Snapp Formation between the Black Mingo Formation and the overlying early Eocene part of the Congaree Formation suggests that the age of the strata is either late Paleocene ([Reference 416](#); [Reference 273](#)) or early Eocene ([Reference 302](#)).

Sedimentary characteristics suggest a fluvially dominated depositional environment in either an upper delta plain or an incised alluvial valley. The presence of dinoflagellates in the Millhaven core suggests a marginal-marine environment in the downdip part of the study area.

Congaree Formation

The Congaree Formation unit consists of mixed siliciclastic/carbonate sections in the downdip test cores and grades to siliciclastic sediments in updip holes. The total section varies from 9 to 103 ft thick.

The Congaree Formation in the downdip area of the VEGP site vicinity contains interbedded quartz sand, marl, and limestone. The sand is moderately well-sorted, very fine to fine at the bottom, grading to fine to medium grained higher in the same section. Carbonate layers, some of which are lithified, include glauconite, and have a clay matrix and fossils. Extensive burrowing is described in the sandy carbonate material.

Further updip in the Girard core, the sand layers range from fine to medium grained at the bottom of the section and grade up into medium to coarse sand interbedded with sandy carbonate, and limestone. Unlithified sandy carbonate and partially lithified calcareous sand are typical in the top portion of the section. In the most updip test hole, the unit is a 9-ft section of well-sorted, very fine to fine sand with less than 5 percent clay matrix ([Reference 278](#)). However, there are clay-lined burrows.

Dinoflagellates, pollen, and calcareous nannofossils were recovered from the core samples of the Congaree Formation unit at Millhaven and Girard. Dinoflagellates and pollen were recovered from the Thompson Oak and Millers Pond cores. Paleontologic examination of these core samples indicate that this unit is early Eocene to early middle Eocene in age and that it includes more than one biostratigraphic unit ([Reference 231](#); [Reference 283](#); [Reference 269](#)). Other fossils observed in the Millhaven core included bryozoans, pelecypods, and foraminifers below a depth of 462 ft, and

pelecypods and foraminifers above a depth of 462 ft. In the Girard core, pelecypods, bryozoans, and shark teeth were observed above a depth of 342 ft. Biomoldic pores indicate that gastropods also were present ([Reference 278](#)).

Sedimentary characteristics of the Still Branch Formation sections in the Girard and Thompson Oak cores suggest a nearshore-marine environment. Sedimentary characteristics of the overlying Congaree beds suggest an open-marine shelf environment for deposits in the downdip core and a fluvially dominated to marginal-marine environment for deposits in the updip cores in the vicinity of Millers Pond. However, the Warley Hill Formation at Millhaven also was deposited in an open-marine shelf environment ([Reference 278](#)).

Lisbon Formation

The Lisbon Formation is predominantly calcareous clay with limestone with a few beds of calcareous sand and clay. As discussed, the Lisbon Formation in eastern Georgia ([Reference 334](#)) includes lithologies assigned to other units ([Reference 449](#); [Reference 382](#); [Reference 272](#); [Reference 273](#), and [Reference 278](#)); the Blue Bluff Marl of the Lisbon Formation ([Reference 333](#)); the Santee Limestone ([Reference 438](#)); and the McBean Limestone Formation (currently considered a Member of the Lisbon Formation) ([Reference 472](#); [Reference 334](#)). The unit ranges between 52 and 173 ft in thickness in the VEGP site vicinity.

In the downdip Millhaven core, the Lisbon Formation can be divided into lower, middle, and upper sections. The lower section is a medium to coarse grained calcareous sand that grades into a fine to medium sandy carbonate with large oyster shells. The contact between the lower and middle sections is distinguished by a layer that is phosphatized and pyritized. The middle portion of the section is predominantly carbonate sediments that vary from marl to carbonate, with little sand in either lithology. The carbonate is well lithified with biomoldic porosity. The marl is burrow mottled to wavy laminated with minor amounts of lignite and pyrite. Fossils include foraminifers, spicules, shark teeth, pelecypods, gastropods, bryozoans, echinoids, and brachiopods. The upper section contains fine to medium sand with glauconite and marine fossils, including pelecypods, gastropods, and bryozoans.

The Lisbon Formation in the Girard test hole further updip contains a very sandy limestone with glauconite base layer. This lithology has biomoldic porosity. A marl overlies the limestone. The contact between them is pyrite rich. The marl is a fine sandy carbonate with up to 30 percent clay matrix. The sand content continues to increase to 25 percent and is very fine to fine grained. There are few macrofossils in this portion of the Lisbon.

The Lisbon Formation in the updip Millers Pond core consists of a lower sandy limestone and calcareous sand. A thin basal lag of very poorly-sorted sand separates the calcareous material from a more sandy section above. The quartz sand is fine to very coarse in calcareous sand beds and fine to medium in sandy limestone beds. The limestone below a depth of 121 ft is finely crystalline and contains glauconite and marine fossils, including pelecypods, spicules, foraminifers, and shark teeth. Marine fossils in the limestone above a depth of 100 ft include oysters and other pelecypods, foraminifers, and echinoid fragments. Biomoldic porosity also is present above a depth of 100 ft and reflects dissolution of aragonitic pelecypods and gastropods.

Calcareous nannofossils, planktonic foraminifers, dinoflagellates, and pollen from the core localities indicate a late middle Eocene (late Claibornian) age for the Lisbon sections ([Reference 270](#)). Marine fossils and carbonate suggest that this unit was deposited in an open-marine, shallow-shelf environment. The distribution of siliciclastic sediments and the diversity of marine fossils in the carbonate facies suggest that the updip Millers Pond core is more proximal to a source of siliciclastic sediments than the downdip Millhaven core.

Barnwell Unit

The Barnwell unit, as described in Falls and Prowell (2001), includes the Barnwell Groups plus post-Eocene strata in the study area. The Barnwell Group includes the Utley Limestone Member, Clinchfield and Dry Branch Formations, and the Tobacco Road Sand. The unit is 82 to 250 ft thick in the site vicinity.

In the downdip Millhaven core, the section begins with calcareous clay overlain by moderately well to well-sorted, fine to medium grained, calcareous quartz sand followed by partially lithified sandy limestone. Glauconite is a typical accessory mineral in the sand. Higher in the section, thin beds of silica-replaced limestone are common. Other lithologies in the upper section include unlithified carbonate, partially lithified limestone, and irregularly shaped phosphatized limestone clasts. The top of this unit consists of a coarsening-upward sequence of clayey sand and sandy clay.

Fossils observed in the core include pelecypods, bryozoans, echinoids, and foraminifers. Biomoldic pores are present and reflect dissolution of aragonitic pelecypods and gastropods.

The Barnwell unit in the Girard core consists of a lower portion of clay, sand, and carbonate layers. A basal calcareous clay is overlain by partially silicified, phosphatized, and glauconitic limestone; a calcareous quartz sand; a sandy limestone; a marl; and a sandy limestone that grades into an overlying quartz sand. Sand is fine to coarse near the base and grades into very fine to fine for the rest of the section. The clay matrix ranges from 20 to 40 percent. The top part of the Barnwell unit section is noncalcareous and contains clayey sand and clay. The sand ranges from fine to coarse grained.

Fossils include pelecypods and bryozoans. Biomoldic porosity ranges from 5 to 20 percent in the limestone and reflects dissolution of aragonitic pelecypods.

At the updip Millers Pond test hole, the unit contains siliciclastic sediments with essentially no limestone or carbonate. It includes thin beds of fine to medium sand and fine to very coarse sand and thin beds of well-laminated clay. The sand contains fine lignite, clay clasts, and 10 to 20 percent clay matrix. The top of the section is a coarsening-upward sequence of sand that ranges from fine to medium sand up to fine to very coarse sand with a clay matrix from 5 to 25 percent. Sedimentary structures include clay laminae and clay wisps. The Barnwell unit is mapped as the uppermost stratigraphic unit at the Millers Pond site ([Reference 278](#)), where it includes the Tobacco Road Sand and Irwinton Sand members of the Dry Branch Formation.

Paleontologic data for the Millhaven and Girard cores suggest a late Eocene to questionably early Oligocene age for the Barnwell sections ([Reference 270](#)). The Barnwell Group contains equivalent units to E6, E7, E8, and MI ([Reference 416](#)) in addition to the Clinchfield Formation, Dry Branch Formation, and Tobacco Road Sand of the Barnwell Group at the SRS ([Reference 273](#)). Throughout the study area, the abundance of carbonate, the presence of glauconite and phosphate, and the abundance of marine macrofossils and microfossils in the calcareous part of the section indicate that the Barnwell strata were deposited in open-marine environments. The calcareous sand probably was deposited in a shallow-shelf environment, and the fossil bed at the base is a lag deposit produced by a late Eocene marine transgression. The noncalcareous sand and clay, the ovoid flattened pebbles, and the clay wisps in the upper part of the Barnwell unit suggest that these strata were deposited in nearshore-marine environments.

Quaternary Surfaces and Deposits

The Quaternary record in the VEGP area is preserved primarily in the fluvial terraces along the Savannah River and its major tributaries and in deposits of colluvium, alluvium, and eolian sediments on upland interfluvial areas.

The drainage systems within the site consist entirely of streams tributary to the Savannah River. A series of nested fluvial terraces are preserved along the east side of the Savannah River (Figure 2.5-232). Fluvial terraces are the primary geomorphic surface that can be used to evaluate Quaternary deformation within the Savannah River area. However, limited data are available for the estimation of ages of river terraces in both the Atlantic and Gulf coastal plains (Reference 376; Reference 240; Reference 387; Reference 375; Reference 447).

Along the east side of the Savannah River in the vicinity of the VEGP site, there are two prominent terraces above the modern flood plain (Qal): the Bush Field (Qtb) and the Ellenton (Qte) terraces (Figure 2.5-232) (Reference 292; Reference 301). These designations are based on morphology and relative height above local base level, which is the present elevation of the Savannah River channel. In addition, there are other minor terraces, one lower than the Bush Field and several higher older terrace remnants. Other investigators have delineated essentially the same terraces (Reference 452; Reference 227); however, there are significant differences in the estimated ages of these terraces.

The Bush Field (Qtb) and Ellenton (Qte) terraces are laterally extensive and are mapped over 15 mi both upstream and downstream from the VEGP site (Reference 292). The development of a sequence of laterally extensive fluvial terraces along the Savannah River is characteristic of other major Piedmont-draining river systems. Similar sequences of laterally extensive fluvial terraces are found along other rivers, such as the Pee Dee River in South Carolina and the Cape Fear River in North Carolina (Reference 292).

The modern flood plain is a broad alluvial surface that is 6 to 9 ft (2 to 3 m) above the channel. Local relief is about 3 ft (1 m). More extensive details are provided by Stevenson (1982). The next terrace at a structurally higher position is the Qty terrace, but that terrace is minor and not laterally continuous (Reference 292) (Figure 2.5-232).

The Bush Field terrace (Qtb), like the modern floodplain, includes a number of terrace surfaces of slightly differing heights above the modern base level (Reference 292). These surfaces range from 26 to 43 ft (8 to 13 m) above the Savannah River at SRS. This terrace is preserved primarily on the northeast side of the river. Limited subsurface data indicate the terrace is 29 to 49 ft (9 to 15 m) thick. The Ellenton terrace (Qte) is the higher of the two major terraces and includes surfaces that range from 56 to 82 ft (17 to 25 m) above the river channel. Subsurface data indicate the terrace is a minimum of 26 to 33 ft (8 to 10 m) thick (Reference 292).

Estimated ages of the terraces are based on several techniques, including radiometric Carbon-14 dates, soil chronosequences, relative position above base level, and correlation to other dated river or marine terraces (Reference 292). Alluvium within the modern floodplain ranges in age from latest Holocene to possibly latest Pleistocene (Reference 292). The Qty terrace is estimated to be 29 to 120 ka. The Qtb terrace appears to be about 90 ka based on correlation, relative position, and terrace morphology and as much as 200 ka based on soil chronosequences. Geomatrix (1993) assigned a best estimate age of the Qtb terrace of 100 to 250 ka. The Qte terrace is about 200 ka to more than 760 ka, based on regional correlation and morphology and at least 400 ka to perhaps 1 Ma based on soil chronosequences. Considering the various methods for estimating the age of the Qte terrace, Geomatrix (1993) assigned an age estimate of 350 ka to 1 Ma for the Qte terrace.

2.5.1.1.4 Regional Tectonic Setting

The regional tectonic setting of the VEGP site is presented below. This section includes discussions of regional plate tectonic evolution, regional tectonic stresses, and principal regional tectonic structures.

2.5.1.1.4.1 Plate Tectonic Evolution of the Appalachian Orogenic Belt at the Latitude of the Site Region

The VEGP site lies within the southern part of the northeast-southwest-trending Appalachian orogenic belt, which extends nearly the entire length of the eastern United States from Alabama to southern New York State. The Appalachian orogenic belt formed during the Paleozoic Era and records the opening and closing of the proto-Atlantic along the eastern margin of ancestral North America. The geologic history of the region surrounding the VEGP site is discussed in [Subsection 2.5.1.1.2](#).

Depending on the focus of a given study, the Appalachian orogenic belt has been subdivided in a variety of ways by various researchers. These subdivisions include provinces, belts, and terranes. Provinces, which are generally more regional in extent, are defined based on both physiography (landforms) and geology. Five physiographic provinces have been defined across the Appalachian belt. From west to east, these include the Appalachian Plateaus (the “Cumberland Plateau” at the latitude of the site region) and the Valley and Ridge, Blue Ridge, Piedmont, and the Coastal Plain physiographic provinces ([Figure 2.5-204](#)). The Blue Ridge and Piedmont physiographic provinces are further divided into different lithotectonic belts of similar rock type and/or tectonic origin ([Figure 2.5-217](#)). Some geologists further divide the lithotectonic belts into individual fault-bounded terranes [e.g., ([Reference 328](#), [Reference 329](#); [Reference 316](#))]. The terms “belt” and “terrane” are used interchangeably in this section to describe fault-bounded crustal blocks that share a common tectonic history.

Since the publication of EPRI (1986), geologists such as Hatcher (1987) and Horton et al. (1989, 1991) have proposed models for the development of the Appalachian orogen and its component provinces in the context of collisional tectonic events that added new fragments of crust to the eastern margin of North America and finally closed an ancestral ocean basin between ancestral North America (“Laurentia”) and ancestral Africa (“Gondwana”). The most recent synthesis of the Appalachian orogen at the latitude of the ESP study region is by Hatcher et al. (1994) and incorporates analysis of gravity, magnetic, and seismic reflection data in the interpretation. From northwest to southeast, Hatcher et al. (1994) recognized the following principal tectonic elements of the Appalachian orogen:

- The Valley and Ridge Province. This province encompasses a sequence of sedimentary rocks originally deposited on North American crust and subsequently deformed by folds and thrust faults during the Alleghanian orogeny, which resulted from the collision of Gondwana with Laurentia at the end of the Paleozoic Era.
- The Blue Ridge Province: The western part of the Blue Ridge province is a thrust-bounded sheet of crystalline rocks with overlying sedimentary strata that originally lay along the Paleozoic eastern margin of Laurentia. The eastern part of the Blue Ridge province is underlain by high-grade metamorphic rocks, some or all of which may be exotic to ancestral North America. At the latitude of the VEGP site region, the eastern and western parts of the Blue Ridge province are separated by the Hayesville fault. The eastern tectonic boundary between the Blue Ridge and Piedmont provinces is the Brevard fault.
- The Piedmont Province: The Piedmont province is subdivided into the Inner Piedmont belt on the west, and the Carolina–Avalon Terrane ([Reference 316](#)) on the east. The boundary between these two units is the Towaliga fault. Rocks of the Carolina–Avalon Terrane extend east of the Piedmont province beneath the overlying sedimentary cover of the Coastal Plain province.

- The Coastal Plain Province: This province is defined by a sequence of predominantly Cretaceous and Tertiary marine sediments overlying Paleozoic crystalline rocks and Mesozoic sedimentary rocks. The Coastal Plain strata record development of a passive continental margin along the eastern United States following Mesozoic rifting and opening of the Atlantic Ocean basin.

Modern plate tectonic reconstructions of the southern Appalachian orogenic belt published since EPRI (1986) interpret that at least some of the major regional Paleozoic deformation events (i.e., Penobscottian, Taconic, Acadian, and Alleghanian) are associated with collisions of exotic or suspect terranes with ancestral North America [e.g., (Horton et al. 1989; Hatcher et al. 1994)] (Figure 2.5-213). Most geologists generally agree that folded strata in the Valley and Ridge province and the crystalline rocks in the western Blue Ridge province are native to North America [e.g., (Horton et al. 1991; Hatcher et al. 1994)] and that these units have been transported westward from their original position along Paleozoic east-dipping, west-verging thrust faults. Key differences between plate tectonic models arise from varying interpretations of which belts and terranes represent exotic or suspect terranes and the location of primary tectonic boundaries or sutures that juxtapose such exotic terranes against North American crust and to one another. At the latitude of the VEGP site, there is general agreement among geologists regarding which belts and terranes are native to North America and which are exotic. The primary differences among models concern the precise location and downdip geometry of the major faults and sutures [e.g., alternative interpretations in (Hatcher et al. 1994)] that separate these terranes.

Development of the Appalachian orogen began in the late Precambrian with rifting of the Precambrian basement of ancestral North America, opening of an ocean basin, and formation of a passive margin (Figure 2.5-213). Sediments accumulated in local fault-bounded basins in the early phases of rifting, followed by deposition of a characteristic off-lapping, passive-margin sequence of marine carbonate and siliciclastic sediments.

The Grenville Front is the leading edge of a northeast-southwest-trending Precambrian collisional orogen that involved rocks of the pre-Appalachian basement of Laurentia (i.e., ancestral North America) (Figures 2.5-213 and 2.5-215). The following discussion is summarized from White et al. (2000). Like the younger Appalachian orogen, the Grenville orogen may have formed in part from exotic terranes that were assembled prior to 1,160 Ma, then deformed and thrust westward over the pre-Grenville Laurentian margin between 1,120 and 980 Ma. The Grenville orogen and Grenville front primarily are exposed in southeastern Canada, and can be traced in outcrop southwest to the latitude of Lake Ontario. Grenville-age rocks and structures continue on trend to the southeast into the United States, but are depositionally and structurally overlain by younger rocks, including terranes of the Appalachian orogen (Reference 217; Reference 320). Seismic reflection profiles indicate that the Grenville front and other prominent reflectors generally dip toward the east and extend to lower crustal depths (Reference 485).

The Penobscottian event is the earliest major orogeny recognized in the Appalachian belt and primarily is expressed in the northern Appalachians. Horton et al. (1989) stated that evidence for the Penobscottian orogeny has not been observed south of Virginia. The earliest Paleozoic deformation along or adjacent to the ancestral North American margin at the latitude of the VEGP site region occurred in the Middle Ordovician and is known as the Taconian event or orogeny (Figure 2.5-213). The onset of the Taconian event is marked regionally throughout much of the Appalachian belt by an unconformity in the passive-margin sequence and deposition of clastic sediments derived from an uplifted source area or areas to the east. The Taconic event at the latitude of the VEGP site region is interpreted by Horton et al. (1989) and Hatcher et al. (1994) to have resulted from the collision of one or more terranes with North America. Rocks of the eastern Blue Ridge and Inner Piedmont are interpreted to have originated east of the Laurentian passive margin in Middle Ordovician time and, thus, are candidates for Taconic collision(s).

Horton et al. (1989) included the eastern Blue Ridge at the latitude of the ESP study region in the Jefferson Terrane, a large body of sandstones, shales, basalt, and ultramafic rocks interpreted to be a metamorphosed accretionary wedge that accumulated above a subduction zone. Hatcher et al. (1994) suggested that the Hayesville thrust, which forms the western structural boundary of the eastern Blue Ridge and dips eastward beneath it, may be the “up-dip leading edge of an early Paleozoic subduction zone.” If this interpretation is correct, then the Hayesville thrust fault may be a Taconic suture. The Carolina-Avalon Terrane also is interpreted by Horton et al. (1989) and Hatcher et al. (1994) to have been accreted during the Taconic orogeny. If this is correct, then the Towaliga fault between the Inner Piedmont and Carolina-Avalon Terranes also may be a Taconic structure.

According to Horton et al. (1989), evidence for the middle Paleozoic Acadian orogeny is “neither pervasive nor widespread” south of New England. The Acadian event primarily is expressed at the latitude of the ESP study region by unconformities in foreland stratigraphic succession, plutonism, and activity of several major faults (Reference 316), and possibly ductile folding elsewhere in the southern Appalachians (Reference 328). To date, geologists have not observed compelling evidence for a major accretion event at the latitude of the VEGP site region during the Acadian orogeny (Reference 328; Reference 316).

The final and most significant collisional event in the formation of the Appalachian belt was the late Paleozoic Alleghanian orogeny, during which Gondwana collided with Laurentia, closing the intervening Paleozoic ocean basin (Figure 2.5-213). At the latitude of the VEGP site region, the Alleghanian collision telescoped the previously accreted Taconic terranes and drove them westward up and across the Laurentian basement, folding the passive margin sequence before them and creating the Valley and Ridge fold-and-thrust belt. The collisional process also thrust a fragment from the underlying Laurentian basement eastward over the passive margin sequence, forming the western Blue Ridge. Significant strike-slip faulting and lateral transport of terranes also are interpreted to have occurred during the Alleghanian orogeny (Reference 316).

At the latitude of the VEGP site region, the Alleghanian suture between rocks of ancestral Africa and terranes accreted to North America is buried beneath the Coastal Plain sediments and not exposed. Hatcher et al. (1994) offered alternative interpretations that the Alleghanian suture (1) coincides with the western edge of the Mesozoic Dunbarton Basin, which implies that the suture was reactivated as a normal fault during Mesozoic rifting and opening of the modern Atlantic basin or (2) is located somewhere east of the Dunbarton Basin, and its location and geometry are not known precisely. Based on detailed petrologic and geochemical analyses of basement samples from deep boreholes at the SRS, Dennis et al. (2004) concluded that the basement rocks there correlate with meta-igneous rocks of the Carolina–Avalon Terrane, which implies that the Alleghanian suture must lie east of the VEGP site.

Despite uncertainties regarding the precise origin, emplacement, and boundaries of belts and terranes, there is good agreement among tectonic models regarding first-order structural features of the southern Appalachian orogenic belt. At the latitude of the VEGP site region, the ancestral North American basement of the Paleozoic passive margin underlies the Valley and Ridge, Blue Ridge, and Inner Piedmont provinces at depths of less than 6 to 9 mi (10 to 15 km), and possibly as shallow as 3.1 mi (5 km) or less beneath the Valley and Ridge (Figure 2.5-214). A basal decollement along the top of the North American basement is the root zone for Paleozoic thrust faults in the Valley and Ridge, Blue Ridge, and Inner Piedmont provinces. Although potential seismogenic sources may be present within the North American basement below the decollement (Reference 480), the locations, dimensions, and geometries of these deeper potential sources are not necessarily expressed in the exposed fold-thrust structures above the detachment.

Wheeler (1995) suggests that many earthquakes in the eastern part of the Piedmont province and beneath the Coastal Plain province may be associated spatially with buried normal faults related to rifting that occurred during the Mesozoic Era (Figure 2.5-213). Normal faults in this region that bound

Triassic basins may be listric into the Paleozoic detachment faults [e.g., (Reference 263)] or may penetrate through the crust as high-angle faults. However, no definitive correlation of seismicity with Mesozoic normal faults has been conclusively demonstrated.

2.5.1.1.4.2 Tectonic Stress in the Mid-Continent Region

Earth science teams (ESTs) that participated in the EPRI (1986) evaluation of intra-plate stress found that tectonic stress in the Central and Eastern United States (CEUS) region primarily is characterized by northeast-southwest-directed horizontal compression. In general, the ESTs concluded that the most likely source of tectonic stress in the mid-continent region was ridge-push force associated with the Mid-Atlantic ridge, transmitted to the interior of the North American plate by the elastic strength of the lithosphere. Other potential forces acting on the North American plate were judged to be less significant in contributing to the magnitude and orientation of the maximum compressive principal stress. Some of the ESTs noted that the regional northeast-southwest trend of principal stress may vary in places along the east coast of North America and in the New Madrid region. They assessed the quality of stress indicator data and discussed various hypotheses to account for what were interpreted as variations in the regional stress trajectories.

During the 1980s, an international effort to collate and evaluate stress indicator data culminated in the publication of a new World Stress Map (Reference 491). Data for this map are ranked in terms of quality. Plate-scale trends in the orientations of principal stresses are assessed qualitatively based on analysis of high-quality data (Reference 490). Subsequent statistical analyses of stress indicators confirmed that the trajectory of the maximum compressive principal stress is uniform across broad continental regions at a high level of statistical confidence. In particular, the northeast-southwest orientation of principal stress in the CEUS inferred by the EPRI ESTs is statistically robust and is consistent with the theoretical trend of compressive forces acting on the North American plate from the mid-Atlantic ridge (Reference 490).

The more recent assessments of lithospheric stress do not support inferences by some EPRI ESTs that the orientation of the principal stress may be locally perturbed in the New England area, along the east coast of the United States, or in the New Madrid region. Zoback and Zoback (1989) summarized a variety of data, including well-bore breakouts, results of hydraulic fracturing studies, and newly calculated focal mechanisms, which indicate that the New England and eastern seaboard regions of the US are characterized by uniform horizontal northeast-southwest to east-west compression. Similar trends are present in the expanded set of stress indicators for the New Madrid region. Zoback and Zoback (1989) grouped all of these regions, along with a large area of eastern Canada, with the CEUS in an expanded "Mid-Plate" stress province characterized by northeast-southwest-directed horizontal compression.

A detailed study by Moos and Zoback (2001) evaluated the orientations and magnitudes of the principal stresses at the Savannah River Site, north of the VEGP site, to a depth of about 4,000 ft (1,220 m) using data and observations from the New Production Reactor (NPR) borehole. They inferred that the maximum horizontal compressive stress is oriented N50°E to N70°E in the upper 2,100 ft (640 m) depth range, similar to regional trends in the eastern United States reported by Zoback (1992). Moos and Zoback (2001) estimated that the magnitude of the differential stress in the upper 2,100 ft (640 m) is close to the limit of the frictional strength on NW-striking reverse faults. In the depth range of about 3,000 ft to 3,700 ft (915 to 1130 m), Moos and Zoback (2001) found that the maximum horizontal compressive stress was directed about N33°E, more toward the north and counterclockwise of regional trends, and that the magnitude of the differential stress would likely favor strike-slip displacement rather than reverse faulting. In the 4,000 ft (1,220 m) depth range near the bottom of the hole, breakouts and other stress indicators suggest that the maximum horizontal compressive stress is directed toward N55°E, subparallel to regional trends.

The observations from the NPR borehole at the Savannah River Site thus appear to document a counterclockwise rotation of the maximum horizontal compressive stress restricted to a narrow depth range in the upper 4,000 ft (1,220 m) of the crust. Stress indicators from depth intervals above and below this excursion suggest that the NE-SW orientation of the maximum horizontal compressive stress is consistent with regional trends documented in the eastern United States ([Reference 490](#)).

The significance of these results for tectonic stress and fault activity in the vicinity of the VEGP site are equivocal. The clockwise excursion in the orientation of the maximum horizontal compressive stress in the NPR borehole is limited to a narrow depth range, and may be similarly limited in horizontal extent. The specific cause of the stress rotation in the NPR borehole is not known. Moos and Zoback (2001) discuss several physical reasons why it is “not reasonable” to linearly extrapolate estimates of stress magnitudes at shallow depths to mid-crustal depths where moderate to large magnitudes typically nucleate. Thus, the data from the NPR borehole only provide information on the state of stress in the shallow crust directly adjacent to the borehole. The data suggest that while there may be local perturbations in the stress field near the borehole, the average state of crustal stress is probably characterized by horizontal NE-SW compression, similar to regional trends.

In addition to better documenting the orientation of stress, research conducted since 1986 has addressed quantitatively the relative contributions of various forces that may be acting on the North American plate to the total stress within the plate. Richardson and Reding (1991) performed numerical modeling of stress in the continental US interior and considered the contribution to total tectonic stress to be from three classes of forces:

- Horizontal stresses that arise from gravitational body forces acting on lateral variations in lithospheric density. These forces commonly are called buoyancy forces. Richardson and Reding (1991) emphasized that what is commonly called ridge-push force is an example of this class of force. Rather than a line-force that acts outwardly from the axis of a spreading ridge, ridge-push arises from the pressure exerted by positively buoyant, young oceanic lithosphere near the ridge against older, cooler, denser, less buoyant lithosphere in the deeper ocean basins ([Reference 465](#)). The force is an integrated effect over oceanic lithosphere ranging in age from about 0 to about 100 Ma ([Reference 256](#)). The ridge-push force is transmitted as stress to the interior of continents by the elastic strength of the lithosphere.
- Shear and compressive stresses transmitted across major plate boundaries (strike-slip faults and subduction zones).
- Shear tractions acting on the base of the lithosphere from relative flow of the underlying asthenospheric mantle.

Richardson and Reding (1991) concluded that the observed northeast-southwest trend of principal stress in the CEUS dominantly reflects ridge-push body forces. They estimated the magnitude of these forces to be about 2 to 3×10^{12} N/m (i.e., the total vertically integrated force acting on a column of lithosphere 3.28 ft [1 m] wide), which corresponds to average equivalent stresses of about 40 to 60 MPa distributed across a 30-mi-thick elastic plate. Richardson and Reding (1991) found that the fit of the model stress trajectories to data was improved by adding compressive stress (about 5 to 10 MPa) acting on the San Andreas fault and Caribbean plate boundary structures. The fit of the model stresses to data further indicates that shear stresses acting on these plate boundary structures must also be in the range of 5 to 10 MPa. Humphreys and Coblenz (in review) also found that the fit of numerical stress models for the North American plate was improved by imposing large compressive stresses on the San Andreas fault and Caribbean plate boundary structures.

Richardson and Reding (1991) noted that the general northeast-southwest orientation of principal stress in the CEUS also could be reproduced in numerical models that assume horizontal shear

tractions acting on the base of the North American plate. Richardson and Reding (1991) did not favor this as a significant contributor to total stress in the mid-continent region, however, because their model would require an order-of-magnitude increase in the horizontal compressive stress from the eastern seaboard to the Great Plains. Using numerical models, Humphreys and Coblenz (in review) also evaluated the contribution of shear tractions on the base of the North American lithosphere to intra-continental stress, and concluded that (1) there is a viscous drag or resisting force acting on the cratonic root of North America as it moves relative to the asthenospheric mantle and that this drag supports part of the ridge-push force acting from the east and creates a stress shadow for the western US and (2) shear tractions on the base of North America from flow of the underlying asthenospheric mantle are a minor contribution, if any, to stress in the mid-continental lithosphere. Humphreys and Coblenz (in review) concluded that the dominant control on the northeast-southwest orientation of the maximum compressive principal stress in the CEUS is ridge-push force from the Atlantic basin.

To summarize, analyses of regional tectonic stress in the CEUS since EPRI (1986) have not significantly altered the characterization of the northeast-southwest orientation of the maximum compressive principal stress. The orientation of a planar tectonic structure relative to the principal stress direction determines the magnitude of shear stress resolved onto the structure. Given that the current interpretation of the orientation of principal stress is similar to that adopted in EPRI (1986), a new evaluation of the seismic potential of tectonic features based on a favorable or unfavorable orientation to the stress field would yield similar results. Thus, there is no significant change in the understanding of the static stress in the CEUS since the publication of the EPRI source models in 1986, and there are no significant implications for existing characterizations of potential activity of tectonic structures.

2.5.1.1.4.3 Principal Regional Tectonic Structures

Principal tectonic structures and features in the southeastern United States and within the 200-mi VEGP site region can be divided into four categories based on their age of formation or reactivation, and are shown in **Figures 2.5-215 and 2.5-216**. These categories include structures that were most active during Paleozoic, Mesozoic, Tertiary, or Quaternary time. Most of the Paleozoic and Mesozoic structures are regional in scale and geologically and geophysically recognizable. The Mesozoic rift basins and bounding faults show a high degree of parallelism with the structural grain of the Paleozoic Appalachian orogenic belt, which generally reflects reactivation of pre-existing Paleozoic structures. Tertiary and Quaternary structures are generally more localized and may be related to reactivation of portions of older bedrock structures.

Regional Paleozoic Tectonic Structures

The VEGP site region encompasses portions of the Coastal Plain, Piedmont, Blue Ridge, and Valley and Ridge physiographic provinces (**Figure 2.5-204**). Rocks and structures within these provinces are associated with thrust sheets that formed during convergent Appalachian orogenic events of the Paleozoic Era. Tectonic structures of this affinity also exist beneath the sedimentary cover of the Coastal Plain province. These types of structures include the following: (1) sutures juxtaposing allochthonous (tectonically transported) rocks with North American crust, (2) regionally extensive Appalachian thrust faults and oblique-slip shear zones, and (3) a multitude of smaller structures that accommodated Paleozoic deformation within individual belts or terranes (**Figure 2.5-14**). The majority of these structures dip eastward and shallow into a low-angle, basal Appalachian decollement. The Appalachian orogenic crust is relatively thin across the Valley and Ridge province, Blue Ridge province, and western part of the Piedmont province and thickens eastward beneath the eastern part of the Piedmont province and the Coastal Plain province (**Figure 2.5-11**). Below the decollement are rocks that form the North American basement complex. The basement rocks contain northeast-striking, Late Precambrian to Cambrian normal faults that formed during the rifting that preceded the deposition of Paleozoic sediments (See **Subsection 2.5.1.1.4.1**).

Researchers have observed that much of the sparse seismicity in eastern North America occurs within the North American basement below the basal decollement. Therefore, seismicity within the Appalachians may be unrelated to the abundant, shallow thrust sheets mapped at the surface (Reference 480). For example, seismicity in the Giles County seismic zone (Figure 2.5-218), located in the Valley and Ridge province, is occurring at depths ranging from 3 to 16 mi (5 to 25 km) (Reference 233) which is generally below the Appalachian thrust sheets and basal decollement (Reference 222).

Paleozoic faults within 200 mi of the site are shown on Figure 2.5-216, and are described as follows:

- **Augusta Fault:** The Augusta fault zone is located near Augusta, Georgia, about 30 mi north of the VEGP site and separates amphibolite facies gneisses and schists of the Kiokee belt to the northwest from greenschist facies volcanic and volcanoclastic rocks of the Belair belt to the southeast (Reference 431; Reference 367; Reference 429) (Figures 2.5-209 and 2.5-219). The Augusta fault trends east-northeast and dips moderately to the southeast. The Augusta fault zone is characterized as a zone of quartzofeldspathic mylonites, ultramylonites, and blastomylonites with minor amphibolites, schists, and a variety of light-colored granitic veins (Reference 367). The fault contains two distinct deformation fabrics: a mylonite about 800 ft thick is overprinted by a brittle fabric. Until Maher (1987) performed a detailed structural analysis of the fault zone rocks, the Augusta fault had been characterized variably as a thrust fault, a dextral strike-slip fault, a strain gradient with little displacement, and a possible listric normal fault within the early Mesozoic (Reference 445; Reference 246; Reference 218). The sense of movement of the fault zone is now constrained by regional context, mesoscopic structures, and microscopic textures. Maher (1987) notes five observations that indicate a hanging-wall-down, oblique sense of slip: (1) geometry and orientation of folded discordant granitic veins, (2) a sporadically developed lineation, (3) composite planar fabric (S and C surfaces), (4) “mica fish”, and (5) regional geologic relations. The significant normal component of slip during the Alleghanian collisional orogeny is seemingly contradictory, but extension on the Augusta fault (and others within the region) is consistent with a model involving gravitational collapse of a thickened crust, similar to examples from the Himalaya (Reference 370). Geologic relations and the $40\text{Ar}/39\text{Ar}$ cooling ages of Maher et al. (1994) suggest that extensional movement on the Augusta fault zone initiated about 274 Ma. Maher et al. (1994) constrains Augusta fault extension as occurring late in the Alleghanian phase and well after initiation of Alleghanian crustal shortening in the Valley and Ridge and Blue Ridge. Some discontinuous silicified breccias occur along the Augusta fault zone, and minor brittle faults utilizing the mylonitic fabric have striae subparallel to the mylonitic lineation (Reference 367). The brittle striae and faults record the same sense and direction of shear as the mylonitic fabric, indicating Alleghanian movement on the Augusta fault occurred during transition from ductile to brittle conditions (Reference 367; Reference 370). Alleghanian extensional events have been interpreted for not only the Augusta fault, but also other faults within the Eastern Piedmont fault system, suggesting that extension played a significant role in the development of the Appalachians. Maher et al. (1994) suggest that the new geochronology indicates Piedmont normal faulting is not solely Mesozoic, but includes late Alleghanian episodes. No seismicity is attributed to the Augusta fault.
- **Modoc Fault Zone:** The Modoc zone, located in South Carolina and Georgia about 40 mi north of the VEGP site, is a region of high ductile strain separating the Carolina Terrane (Carolina Slate and Charlotte belts) from the amphibolite facies migmatitic and gneissic rocks of the Kiokee belt (Reference 226; Reference 429) (Figures 2.5-209 and 2.5-219). The northeast-trending Modoc zone dips steeply to the northwest and can be traced from central Georgia to central South Carolina based on geological and geophysical data. Mylonitic rocks are common within the zone, although the intensity of mylonitization varies widely (Reference 226). Regional relationships and structures within the zone reflect predominantly dextral motion with a northwest-side-down normal component, related to early Alleghanian

extension ([Reference 423](#)). Geochronologic data from Dallmeyer et al. (1986) indicate movement occurred between 315 and 290 Ma, during the Alleghanian Lake Murray deformation, D2. Recent exposures created for the construction of Saluda Dam on Lake Murray exposed a portion of the Modoc fault zone where four Paleozoic ductile deformational events are recognized. The D4 deformation is recognized as an east-northeast-striking zone at least 20 km wide, and it shows a transition from ductile to brittle behavior, which correlates with retrograde mineral assemblages in D4 faults in the Modoc zone ([Reference 331](#)). Brittle features observed in the Saluda Dam foundation are interpreted to be the result of a readjustment from differential loading and unloading, as well as tectonic movement associated with latest Alleghanian deformation and initial Triassic rifting ([Reference 381](#)). No seismicity is attributed to the Modoc fault zone.

- Eastern Piedmont Fault System: Hatcher et al. (1977) suggested that the Modoc shear zone, the Irmo shear zone, and the Augusta fault are part of the proposed Eastern Piedmont Fault System, an extensive series of faults and splays extending from Alabama to Virginia ([Figure 2.5-216](#)). Aeromagnetic, gravity, and seismic reflection data indicate that the Augusta fault zone continues in the crystalline basement beneath the Coastal Plain province sediments.
- Other Paleozoic Faults: Other Paleozoic faults within the site region include the Brevard fault, the Hayesville fault, the Towliga fault, the Central Piedmont suture, and the Eastern Piedmont fault system ([Figures 2.5-216 and 2.5-217](#)). No seismicity is attributed to these Paleozoic faults, and published literature does not indicate that any of these faults offset late Cenozoic deposits or exhibit geomorphic expression indicative of Quaternary deformation. In addition, Crone and Wheeler (2000) and Wheeler (2005) do not show any of these faults to be potentially active Quaternary faults. Therefore, these Paleozoic structures in the site region are not considered to be capable tectonic sources, as defined in Appendix A of RG 1.165.

No new information has been published since 1986 on any Paleozoic fault in the site region that would cause a significant change in the EPRI seismic source model.

Regional Mesozoic Tectonic Structures

Wheeler (1995) suggested that many earthquakes in the eastern part of the Piedmont province and beneath the Coastal Plain province may be associated spatially with buried normal faults related to rifting that occurred during the Mesozoic Era. However, no definitive correlation of seismicity with Mesozoic normal faults has been conclusively demonstrated. Normal faults in this region that bound Triassic basins may be listric into the Paleozoic detachment faults [e.g., or may penetrate through the crust as high-angle faults (e.g., [Reference 427](#)). Within regions of stable continental cratons, areas of extended crust potentially contain the largest earthquakes ([Reference 343](#)). Mesozoic basins have long been considered potential sources for earthquakes along the eastern seaboard ([Reference 479](#)) and were considered by most EPRI teams in their definition of seismic sources ([Reference 271](#)). Mesozoic basins and faults in the site region include:

- Mesozoic Rift Basins - A broad zone of fault-bounded, elongate depositional basins associated with crustal extension and rifting formed during the opening of the Atlantic Ocean in early Mesozoic time. These rift basins are common features along the eastern coast of North America from Florida to Newfoundland ([Figures 2.5-210 and 2.5-216](#)). The VEGP site is located within the Dunbarton Basin. This basin is discussed in detail below ([Figure 2.5-216](#)).
- Dunbarton Basin - The Dunbarton Basin is a roughly east-northeast-trending Mesozoic rift basin located beneath the VEGP site and the SRS ([Figure 2.5-219](#)). The basin is approximately 31 mi long and 6 to 9 mi wide. Siple (1967) and Marine and Siple (1974) originally identified the general extent and shape of the Dunbarton Basin on the basis of Coastal Plain sediment cores and a limited amount of seismic data from the SRS, as well as

aeromagnetic data from Petty et al. (1965). The Dunbarton Basin coincides with both gravity and magnetic lows and is bounded on the north by the Pen Branch fault ([Reference 374](#); [Reference 232](#); [Reference 451](#); [Reference 253](#), [Reference 254](#), [Reference 255](#); [Reference 265](#)). The Pen Branch fault has had a long and varied history. The Pen Branch fault likely formed in the Paleozoic Era, and was reactivated as a normal fault during the Triassic Period. The Pen Branch fault was most recently reactivated as an oblique-reverse fault in the Cenozoic Era ([Reference 253](#), [Reference 254](#), [Reference 255](#)) and is discussed in greater detail in [Subsection 2.5.1.2.4](#). It has been suggested that the Martin fault (discussed in [Subsection 2.5.1.1.4.5](#)) is the southeastern bounding fault of the Dunbarton Basin ([Reference 442](#)), although Domoracki et al. (1999b) suggested that the Dunbarton Basin is instead a half-graben bounded only by the Pen Branch fault to the north.

Regional Tertiary Tectonic Structures

Within 200 mi of the VEGP site, only a few tectonic features, including arches, domes, and embayments, were active during the Tertiary Period. A series of topographic highs and lows in the crust (arches and embayments, respectively) oriented perpendicular to the hinge zone have exerted control over Coastal Plain sedimentation from late Cretaceous through Pleistocene time and are indicative of episodic, differential tectonic movement. The arches are broad anticlinal upwarps, whereas the embayments are broad, sediment-filled basement flexures.

The most prominent arches in the VEGP site region include the Cape Fear Arch on the South Carolina–North Carolina border and the Yamacraw Arch on the Georgia–South Carolina border. The Cape Fear Arch is bordered by the Salisbury embayment to the northeast and the Georgia embayment to the southeast. There is no evidence that these structures are active, and Crone and Wheeler (2000) classified the Cape Fear Arch as a Class C feature, based on lack of evidence for Quaternary faulting ([Figure 2.5-220](#)).

Regional Quaternary Tectonic Structures

In an effort to provide a comprehensive database of Quaternary tectonic features, Crone and Wheeler (2000) and Wheeler (2005) compiled geological information on Quaternary faults, liquefaction features, and possible tectonic features in the CEUS. They evaluated and classified these features into one of four categories (Classes A, B, C, and D; see [Table 2.5-201](#) for definitions) based on strength of evidence for Quaternary activity.

Within a 200-mi radius of the VEGP site, Crone and Wheeler (2000) and Wheeler (2005) identified 11 potential Quaternary features ([Table 2.5-201](#) and [Figure 2.5-220](#)). These include: the Charleston, Georgetown, and Bluffton paleoliquefaction features (Class A), the East Coast fault system (Class C), the Cooke fault (Class C), the Helena Banks fault zone (Class C), the Pen Branch fault (Class C), the Belair fault (Class C), the fall lines of Weems (1998) (Class C), the Cape Fear Arch (Class C), and the Eastern Tennessee seismic zone (Class C).

The Charleston features (including the East Coast fault system; the Cooke fault, the Helena Banks fault zone; and the Charleston, Georgetown, and Bluffton paleoliquefaction features) are discussed in detail in [Subsection 2.5.1.1.4.4](#). The Pen Branch fault is discussed in detail [Subsection 2.5.1.2.4.1](#), and the Eastern Tennessee Seismic Zone is discussed in detail in [Subsection 2.5.1.1.4.6](#). The Belair fault zone and the fall lines of Weems (1998) are discussed in detail below:

- **Belair Fault Zone** - The Belair fault zone has been mapped for at least 15 mi (24 km) as a series of northeast-trending, southeast-dipping, oblique-reverse slip faults near Augusta, Georgia, that generally parallel the structural grain of the Piedmont ([Figures 2.5-219](#) and [2.5-220](#)). The Belair fault juxtaposes Paleozoic phyllite over Late Cretaceous sands of the Coastal Plain province ([Reference 414](#)). No geomorphic expression of the fault has been reported ([Reference 251](#)). Shallow trenches excavated across the Belair fault near Fort

Gordon in Augusta, Georgia, were initially interpreted as revealing evidence for Holocene movement (Reference 415), but the apparent youthfulness of movement was probably the result of contaminated radiocarbon samples (Reference 413). (Reference 414) demonstrated that the Belair fault cuts beds of Late Cretaceous and Eocene age. Overlying, undeformed strata provide a minimum constraint on the last episode of faulting, which is constrained to sometime between post-late Eocene and pre-26,000 years ago (Reference 413). There is no evidence of historic or recent seismicity associated with the Belair fault. Crone and Wheeler (2000) classified the Belair fault zone as a Class C feature, since the most recent faulting is not demonstrably of Quaternary age. Quaternary slip on the Belair fault zone is allowed, but not demonstrated, by the available data.

Mapping and structural analysis by Bramlett et al. (1982) indicate that the Belair fault likely formed as a lateral ramp or tear associated with the Augusta fault when displacement on these faults initiated during the Paleozoic Alleghanian orogeny. The timing and sense-of-slip for the most-recent movements on the Belair and Augusta faults, however, demonstrate that these two structures have not reactivated as a single tectonic element in Cenozoic or younger time. Powell et al. (1975) and Powell and O'Connor (1978) document Cenozoic, brittle, reverse slip on the Belair fault. In contrast, the latest movement on the Augusta fault, as demonstrated by brittle overprinting of ductile fabrics, exhibits a normal sense-of-slip and is constrained to have occurred in late Alleghanian time during the transition from ductile to brittle conditions (Reference 367; Reference 370). The brittle overprinting on the Augusta fault is consistent with the ductile normal sense of slip. In contrast, the Belair fault exhibits a reverse sense-of-slip during its Cenozoic reactivation. Therefore, different slip histories and opposite senses of dip-slip for the Belair and Augusta faults demonstrate that these two faults have not been reactivated as a single structure during the Cenozoic.

- Fall Lines of Weems (1998) - In his examination of longitudinal profiles of large streams flowing across the Piedmont and Blue Ridge provinces of North Carolina, Virginia and Tennessee, Weems (1998) identified numerous anomalously steep stream segments (Figure 2.5-220). These “fall zones” are aligned from stream to stream along curvilinear paths, and these paths are generally subparallel to the regional structural grain. Weems (1998) presented three hypotheses to explain these phenomena, including climatic factors, rock hardness, and neotectonics. Although some fall zones are spatially coincident with changes in rock hardness, Weems (1998) favored a neotectonic origin for the fall lines. Wheeler (2005) classified the fall lines as a Class C feature, since the fall zones are not demonstrably reproducible and tectonic faulting is not demonstrated by available data.
- The Cape Fear Arch - The Cape Fear Arch is previously discussed in this section (under Regional Tertiary Tectonic Structures). Crone and Wheeler (2000) classified the Cape Fear Arch as a Class C feature based on lack of evidence for Quaternary faulting.

Regional Geophysical Anomalies and Major Tectonic Features

In addition to the tectonic structures described above, a number of regional geophysical anomalies, lineaments, and major tectonic features are located within about 300 mi of the VEGP site (Figure 2.5-215). From southeast to northwest, these include the East Coast Magnetic Anomaly, Appalachian gravity gradient, the southeast boundary of Iapetan normal faulting, Clingman lineament, Ocoee lineament, New York-Alabama lineament, the Appalachian gravity gradient, the northwest boundary of Iapetan normal faulting, Appalachian thrust front, and the Grenville front. These features are described below with more detail provided for those features within the 200-mi site region.

- East Coast Magnetic Anomaly - The East Coast Magnetic Anomaly (ECMA) is a broad, 200 to 300 nT magnetic high that is located approximately 30 to 120 mi (50 to 200 km) off the coast of North America, and which is continuously expressed for about 1,200 mi (1,900 km)

from the latitude of Georgia to Nova Scotia (Reference 356; Reference 487) (Figure 2.5-215). The ECMA is subparallel to the Atlantic coastline, and is spatially associated with the eastern limit of North American continental crust (Reference 356). The ECMA has been variously interpreted to be a discrete, relatively magnetic body such as a dike or ridge, or an “edge effect” due to the juxtaposition of continental crust on the west with higher susceptibility oceanic crust on the east (see summary and additional references in Austin et al. 1990). In the vicinity of the ECMA, deep seismic reflection profiling in the Atlantic basin has imaged packages of east-dipping reflectors that underlie the sequence of Mesozoic-Tertiary passive-margin marine strata (Reference 435). The rocks associated with the east-dipping reflectors are interpreted to be an eastward-thickening wedge of volcanic and volcanoclastic rocks that were deposited during the transition between rifting of the continental crust and opening of the Atlantic basin during the Mesozoic (Reference 487). Models of the magnetic data show that the presence of this volcanic “wedge” can account for the wavelength and amplitude of the ECMA (Reference 356).

To summarize, the ECMA is a relict of the Mesozoic opening of the Atlantic basin, and probably arises from the presence of a west-tapering wedge of relatively magnetic volcanic rocks deposited along the eastern margin of the continental crust as the Atlantic basin was opening, rather than juxtaposition of rocks with differing magnetic susceptibilities across a fault. The ECMA is not directly associated with a fault or tectonic feature, and thus is not a potential seismic source.

- Appalachian Gravity Gradient – This regional gravity gradient extends the length of the Appalachian orogen and exhibits a southeastward rise in Bouguer gravity values as much as 50 to 80 mGal (Reference 222; Reference 481). The Appalachian gravity gradient represents the southeastern thinning of relatively intact Precambrian continental crust, and the early opening of the Iapetus Ocean (e.g., Reference 222).
- Southeast and northwest boundaries of Iapetus normal faults - The southeast and northwest boundaries of Iapetus normal faults shown in Figure 2.5-215 define the extent of the Iapetus margin of the craton containing normal faults that accommodated extension during the late Proterozoic to early Paleozoic rifting that formed the Iapetus Ocean basin. Wheeler (1996) defined the southeast boundary as the southeastern limit of the intact Iapetus margin, which is nearly coincident with the Appalachian gravity gradient in the southeastern United States. The Iapetus normal faults are concealed beneath Appalachian thrust sheets that overrode the margin of the craton during the Paleozoic. A few of these Iapetus faults are thought to be reactivated and responsible for producing earthquakes in areas such as eastern Tennessee; Giles County, Virginia; and Charlevoix, Quebec (Reference 222; Reference 481).

The southeast margin of the Iapetus normal faults shown on Figure 2.5-215 does not represent a potential seismic source since it does not represent a discrete crustal discontinuity or tectonic structure. The linear feature shown in the figure represents the southeastern extent of the intact Iapetus margin (with a location uncertainty of 30 to 35 km), and therefore, the southeastern limit of potentially seismogenic Iapetus faults (Reference 481).

- The New York-Alabama, Clingman, and Ocoee Lineaments - King and Zietz (1978) identified a 1,000-mi- (1,600-km-) long lineament in aeromagnetic maps of the eastern United States that they referred to as the “New York-Alabama lineament” (NYAL) (Figure 2.5-215). The NYAL primarily is defined by a series of northeast-southwest-trending linear magnetic gradients in the Valley and Ridge province of the Appalachian fold belt that systematically intersect and truncate other magnetic anomalies. The NYAL also is present as complementary but less-well-defined lineament on regional gravity maps (Reference 353).

The Clingman lineament is an approximately 750-mi- (1,200-km-) long, northeast-trending aeromagnetic lineament that passes through parts of the Blue Ridge and eastern Valley and Ridge provinces from Alabama to Pennsylvania ([Reference 389](#)). The Ocoee lineament is described as a splay that branches southwest from the Clingman lineament at about latitude 36°N (see summary in Johnston et al. 1985). The Clingman-Ocoee lineaments are sub-parallel to and located about 30 to 60 mi (50 to 100 km) east of the NYAL.

King and Zeitz (1978) interpreted the NYAL to be a major strike-slip fault in the Precambrian basement beneath the thin-skinned fold-and-thrust structures of the Valley and Ridge, and suggested that it may separate rocks on the northwest that acted as a mechanical buttress from the intensely deformed Appalachian fold belt to the southeast. Shumaker (2000) interpreted the NYAL to be a right-lateral wrench fault that formed during an initial phase of late Proterozoic continental rifting that eventually led to the opening of the Iapetus Ocean. The Clingman lineament also is interpreted to arise from a source or sources in the Precambrian basement beneath the accreted and transported Appalachian terranes ([Reference 389](#)).

Johnston et al. (1985) observed that the “preponderance of southern Appalachian seismicity” occurs within the “Ocoee block”, a Precambrian basement block bounded by the NYAL and Clingman-Ocoee lineaments [the Ocoee block was previously defined by ([Reference 340](#))]. The proximity of these lineaments to current seismicity in the Eastern Tennessee seismic zone therefore suggests the possibility that they are potential seismic sources. Based on the orientations of nodal planes from focal mechanisms of small earthquakes, Johnston et al. (1985) noted that most events within the Ocoee block occurred by strike-slip displacement on north-south and east-west striking faults, and thus these geologists did not favor the interpretation of seismicity occurring on a single, through-going NE-SW-trending structure parallel to the Ocoee block boundaries.

The Ocoee block lies within a zone defined by Wheeler (1995, 1996) as the cratonward limit of normal faulting along the ancestral rifted margin of North America that occurred during the opening of the Iapetus Ocean in late Precambrian to Cambrian time. Synthesizing geologic and geophysical data, Wheeler (1995, 1996) mapped the northwest extent of the Iapetus faults in the subsurface below the Appalachian detachment, and proposed that earthquakes within the region defined by Johnston and Reinhold (1985) as the Ocoee block may be the result of reactivation of Iapetus normal faults as reverse or strike-slip faults in the modern tectonic setting.

- **Appalachian Thrust Front** – The northwestern limit of allochthonous crystalline Appalachian crust was termed the Appalachian thrust front by Seeber and Armbruster (1988). This front, which lies beyond the 200-mi site region, is a sharply defined boundary interpreted as a major splay of the master Appalachian detachment.
- **Grenville Front** – The Grenville front, which is located beyond the 200-mi site region, is defined by geophysical, seismic reflection, and scattered drill hole data in the southeastern United States. This feature lies within the continental basement and is interpreted to separate the relatively undeformed granite-rhyolite province on the northwest from the more highly deformed rocks of the Grenville province on the southeast ([Reference 471](#)).

2.5.1.1.4.4 Charleston Tectonic Features

The August 31, 1886, Charleston, South Carolina, earthquake is one of the largest historical earthquakes in the eastern United States. The event produced Modified Mercalli Intensity (MMI) X shaking in the epicentral area and was felt strongly as far away as Chicago (MMI V) ([Reference 339](#)). As a result of this earthquake, considerable effort has gone into identifying the source of the earthquake and recurrence history of large magnitude events in the region. In spite of this effort, the

source of the 1886 earthquake has not been definitively attributed to any particular fault shown in [Figures 2.5-221](#) and [2.5-222](#).

The 1886 Charleston earthquake produced no identifiable primary tectonic surface deformation; therefore, the source of the earthquake has been inferred based on the geology, geomorphology, and instrumental seismicity of the region ([Figures 2.5-221](#) and [2.5-222](#)). Talwani (1982) infers that the 1886 event was produced by the north-northeast-striking Woodstock fault (inferred from seismicity) near its intersection with the northwest-striking Ashley River fault (also inferred from seismicity). Marple and Talwani (2000) have more recently suggested that a northeast-trending zone of river anomalies, referred to as the East Coast fault system, represents the causative fault for the 1886 Charleston event. The southern segment of the East Coast fault system coincides with a linear zone of micro-seismicity that defines the northeast-trending Woodstock fault of Talwani (1982) and the isoseismal zone from the 1886 earthquake.

Johnston (1996) estimated a moment magnitude of (**M**) 7.3 ± 0.26 for the 1886 Charleston event. More recently, Bakun and Hopper (2004) estimated a smaller magnitude of **M** 6.9 with a 95 percent confidence level corresponding to a range of **M** 6.4 to 7.1. Both of these more recent estimates of maximum magnitude (**M**_{max}) are similar to the upper-bound maximum range of **M**_{max} values used in EPRI (1986) (body wave magnitude [**m**_b] 6.8 to 7.5). However, significant new information regarding the source geometry and earthquake recurrence of the Charleston seismic source warrants an update of the EPRI (1986) source models in the PSHA. The updated Charleston seismic source parameters are presented in [Subsection 2.5.2.2.2.4](#).

Potential Charleston Source Faults

Since the EPRI (1986) source models were developed, a number of faults have been identified or described in the literature as possible sources related to the 1886 Charleston earthquake. These include numerous faults localized in the Charleston meizoseismal area approximately 85 mi from the site ([Figure 2.5-221](#)).

There is evidence, in the form of paleoliquefaction features in the South Carolina Coastal Plain, that the source of the 1886 Charleston earthquake has repeatedly generated vibratory ground motion. Paleoliquefaction evidence is lacking for prehistoric earthquakes elsewhere along much of the eastern seaboard [e.g., ([Reference 205](#); [Reference 207](#), [Reference 206](#))]. At a minimum, the Charleston seismic source is defined as a seismogenic source according to RG 1.165. Whereas the 1886 Charleston earthquake almost certainly was produced by a capable tectonic source, that specific tectonic structure has yet to be identified. Various studies have proposed potential causative faults for the 1886 event; however, a positive linkage between a discrete structure and the Charleston earthquake has yet to be determined.

These potential causative faults are shown in [Figures 2.5-221](#) and [2.5-222](#) and described below:

- **East Coast Fault System** - The inferred East Coast fault system (ECFS, the southern section of which is also known as the “zone of river anomalies” or ZRA based on the alignment of river bends) is a northeast-trending, approximately 373-mi-long (600-km-long) fault system extending from west of Charleston, South Carolina, to southeastern Virginia ([Reference 378](#)). The ECFS comprises three, approximately 124-mi-long (200-km-long), right-stepping sections (southern, central, and northern; [Figure 2.5-221](#)). Evidence for the southern section is strongest, with evidence becoming successively weaker northward ([Reference 482](#)). Marple and Talwani (1993) identified a series of geomorphic anomalies (i.e., ZRA) located along and northeast of the Woodstock fault and attributed these to a buried fault much longer than the Woodstock fault. Marple and Talwani (1993, 2000) suggested that this structure, the ECFS, may have been the source of the 1886 Charleston earthquake. Marple and Talwani (2000) provided additional evidence for the existence of the southern section of the ECFS, including seismic reflection data, linear aeromagnetic anomalies, exposed Plio-Pleistocene

faults, local breccias, and upwarped strata. Since most of the geomorphic anomalies associated with the southern section of the ECFS are in late Pleistocene sediments, Marple and Talwani (2000) speculated that the fault has been active in the past 130–10 ka, and perhaps remains active. Wildermuth and Talwani (2001) used gravity and topographic data to postulate the existence of a pull-apart basin between the southern and central sections of the ECFS, which would imply a component of right-lateral slip on the fault. Wheeler (2005) classified the ECFS as a Class C feature based on the lack of demonstrable evidence that the ECFS has or can generate strong ground motion and the lack of any demonstrable evidence for any sudden uplift anywhere along the proposed fault.

- Adams Run Fault - Weems and Lewis (2002) postulated the existence of the Adams Run fault (Figure 2.5-222) on the basis of microseismicity and borehole data. Their interpretation of borehole data suggests the presence of areas of uplift and subsidence separated by the inferred fault. However, review of these data shows that the pattern of uplift and subsidence does not appear to persist through time (i.e., successive stratigraphic layers) in the same locations and that the intervening structural lows between the proposed uplifts are highly suggestive of erosion along ancient river channels. In addition, there is no geomorphic evidence for the existence of the Adams Run fault, and analysis of microseismicity in the vicinity of the proposed Adams Run fault does not clearly define a discrete structure (Figure 2.5-223).
- Ashley River Fault - The Ashley River fault was identified by Talwani (1982) on the basis of a northwest-oriented, linear zone of seismicity located about 6 mi west of Woodstock, South Carolina, in the meizoseismal area of the 1886 Charleston earthquake (Figure 2.5-222). The postulated Ashley River fault, a southwest-side-up reverse fault, is thought to offset the north-northeast-striking Woodstock fault about 3 to 4 miles to the northwest near Summerville (Reference 457; Reference 459; Reference 476).
- Charleston Fault - Lennon (1986) proposed the Charleston fault on the basis of geologic map relations and subsurface borehole data (Figure 2.5-222). Weems and Lewis (2002) suggested that the Charleston fault is a major, high-angle reverse fault that has been active at least intermittently in Holocene to modern times. The Charleston has no clear geomorphic expression, nor is it clearly defined by microseismicity (Figure 2.5-223).
- Cooke Fault - Behrendt et al. (1981) and Hamilton et al. (1983) identified the Cooke fault based on seismic reflection profiles in the meizoseismal area of the 1886 Charleston earthquake (Figure 2.5-222). This east-northeast-striking, steeply northwest-dipping fault has a total length of about 6.2 mi (10 km) (Reference 214; Reference 300). Marple and Talwani (1993, 2000) reinterpreted these data to suggest that the Cooke fault may be part of a longer, more northerly striking fault (i.e., the ZRA of Marple and Talwani [1993] and the ECFS of Marple and Talwani [2000]). Crone and Wheeler (2000) classified the Cooke fault as a Class C feature based on lack of evidence for faulting younger than Eocene.
- Drayton Fault – The Drayton fault is imaged on onshore seismic reflection lines and was known to the six EPRI ESTs at the time of EPRI (1986). The Drayton fault is mapped as a 5.5-mi-long, apparently northeast-trending, high-angle, reverse fault in the meizoseismal area of the 1886 Charleston earthquake (Reference 300) (Figures 2.5-222 and 2.5-223). The Drayton fault terminates upward at approximately 2,500 ft below the ground surface within a Jurassic-age basalt layer (Reference 300), precluding significant Cenozoic slip on this fault.
- Gants Fault – The Gants fault is imaged on onshore seismic reflection lines and was known to the six EPRI ESTs at the time of EPRI (1986) as a possible Cenozoic-active fault. The Gants fault is mapped as a 5.5-mi-long, apparently northeast-trending, high-angle, reverse fault in the meizoseismal area of the 1886 Charleston earthquake (Reference 214;

Reference 300) (Figures 2.5-222 and 2.5-223). The Gants fault displaces vertically a Jurassic-age basalt layer by about 150 ft at approximately 2,500 ft below the ground surface (Reference 300). Overlying Cretaceous and Cenozoic beds show apparent decreasing displacement with decreasing depth (Reference 300), indicating likely Cenozoic activity, but with decreasing displacement on the Gants fault during the Cenozoic.

- Helena Banks Fault Zone - The Helena Banks fault zone is clearly imaged on seismic reflection lines offshore of South Carolina (Reference 215; Reference 213) and was known to the six EPRI ESTs at the time of EPRI (1986) as a possible Cenozoic-active fault zone (Figure 2.5-222). Some ESTs recognized the offshore fault zone as a candidate tectonic feature for producing the 1886 event and included it in their Charleston seismic source zones. However, since 1986, three additional sources of information have become available:
 - In 2002, two magnitude m_b 3.5 earthquakes (m_b 3.5 and 4.4) occurred offshore of South Carolina in the vicinity of the Helena Banks fault zone in an area previously devoid of seismicity (Figure 2.5-222).
 - Bakun and Hopper (2004) reinterpreted intensity data from the 1886 Charleston earthquake and show that the calculated intensity center is located about 100 mi offshore from Charleston (although they ultimately concluded that the epicentral location most likely lies onshore near the Middleton Place-Summerville seismic zone; Figure 2.5-222).
 - Crone and Wheeler (2000) described the Helena Banks fault zone as a potential Quaternary tectonic feature (although it was classified as a Class C feature that lacks sufficient evidence to demonstrate Quaternary activity). The occurrence of the 2002 earthquakes and the location of the Bakun and Hopper (2004) intensity center offshore suggest, at a low probability, that the fault zone could be considered a potentially active fault. If the Helena Banks fault zone is an active source, its length and orientation could possibly explain the distribution of paleoliquefaction features along the South Carolina coast.
- Sawmill Branch Fault - Talwani and Katuna (2004) postulated the existence of the Sawmill Branch fault on the basis of microseismicity and further speculated that this feature experienced surface rupture in the 1886 earthquake. According to Talwani and Katuna (2004), this approximately 3-mi-long (5-km-long), northwest-trending fault, which is a segment of the larger Ashley River fault, offsets the Woodstock fault in a left-lateral sense (Figure 2.5-222). Earthquake damage at three localities was used to infer that surface rupture occurred in 1886. These localities were reviewed in the field as part of this ESP project. Features along the banks of the Ashley River (small, discontinuous cracks in a tomb that dates to 1671 AD and displacements [less than 10 cm] in the walls of colonial Fort Dorchester) are almost certainly the product of shaking effects as opposed to fault rupture. Moreover, assessment of microseismicity in the vicinity of the proposed Sawmill Branch fault does not clearly define a discrete structure distinct or separate from the larger Ashley River fault, which was defined based on seismicity (Figure 2.5-223).
- Summerville Fault - Weems et al. (1997) postulated the existence of the Summerville fault near Summerville, South Carolina, on the basis of previously located microseismicity (Figure 2.5-222). However, there is no geomorphic or borehole evidence for the existence of the Summerville fault, and analysis of microseismicity in the vicinity of the proposed Summerville fault does not clearly define a discrete structure (Figure 2.5-223).
- Woodstock Fault - The Woodstock fault, a postulated north-northeast-trending, dextral strike-slip fault, was identified by Talwani (1982) on the basis of a linear zone of seismicity located approximately 6 mi west of Woodstock, South Carolina, in the meizoseismal area of the 1886

Charleston earthquake (Figure 2.5-222). Madabhushi and Talwani (1990, 1993) used a revised velocity model to relocate Middleton Place–Summerville seismic zone earthquakes, and the results of this analysis were used to further refine the location of the postulated Woodstock fault. Talwani (1999, 2000) subdivided the Woodstock fault into two segments that are offset in a left-lateral sense across the northwest-trending Ashley River fault. Marple and Talwani include the Woodstock fault as part of their larger ZRA (1993) and ECFS (2000).

Charleston Area Seismic Zones

Three zones of microseismic activity have been identified in the greater Charleston area. These include the Middleton Place–Summerville, Bowman, and Adams Run seismic zones. Each of these features is described in detail below, and the specifics of the seismicity catalog are discussed in Subsection 2.5.2.1.

- **Middleton Place–Summerville Seismic Zone.** The Middleton Place–Summerville seismic zone is an area of elevated microseismic activity located about 12 mi northwest of Charleston (Reference 462; Reference 223; Reference 364; Reference 460) (Figure 2.5-222). Between 1980 and 1991, 58 events with mb 0.8 to 3.3 were recorded in an 11-by-14-km area, with hypocentral depths ranging from about 1 to 7 mi (2 to 11 km) (Reference 364). The elevated seismic activity of the Middleton Place–Summerville seismic zone has been attributed to stress concentrations associated with the intersection of the Ashley River and Woodstock faults (Reference 457; Reference 364; Reference 460; Reference 291). Persistent foreshock activity was reported in the Middleton Place–Summerville seismic zone area (Reference 268), and it has been speculated that the 1886 Charleston earthquake occurred within this zone [e.g., (Reference 457; Reference 462; Reference 210)].
- **Bowman Seismic Zone.** The Bowman seismic zone is located about 50 mi northwest of Charleston, South Carolina, outside of the meizoseismal area of the 1886 Charleston earthquake and about 60 mi east-northeast of the VEGP site (Figures 2.5-221 and 2.5-222). The Bowman seismic zone was identified on the basis of a series of $3 < M_L < 4$ earthquakes that occurred between 1971 and 1974 (Reference 463; Reference 223).
- **Adams Run Seismic Zone.** The Adams Run seismic zone, located within the meizoseismal area of the 1886 Charleston earthquake, was identified on the basis of four $M < 2.5$ earthquakes, three of which occurred in a 2-day period in December 1977 (Reference 462). The Adams Run seismic zone is located about 75 mi east-southeast of the VEGP site. Bollinger et al. (1991) downplayed the significance of the Adams Run seismic zone, noting that, in spite of increased instrumentation, no additional events were detected after October 1979.

Charleston Area Seismically Induced Liquefaction Features

The presence of liquefaction features in the geologic record may be indicative of past earthquake activity in a region (e.g., Reference 397). Liquefaction features have been recognized throughout coastal South Carolina and have been attributed to both the 1886 Charleston and earlier moderate to large earthquakes in the region.

- **1886 Charleston Earthquake Liquefaction Features -** Liquefaction features produced by the 1886 Charleston earthquake are most heavily concentrated in the meizoseismal area (Reference 268; Reference 434; Reference 205), but have been reported as far away as Columbia, Allendale, Georgetown (Reference 434) and Bluffton, South Carolina (Reference 461) (Figure 2.5-221).

- Paleoliquefaction Features in Coastal South Carolina - Liquefaction features predating the 1886 Charleston earthquake are found throughout coastal South Carolina (Figures 2.5-221 and 2.5-222). The spatial distribution and ages of paleoliquefaction features in coastal South Carolina constrain possible locations and recurrence rates for large earthquakes [e.g., (Reference 398, Reference 399; Reference 205; Reference 207, Reference 206)]. Talwani and Schaeffer (2001) combined previously published data with their own studies of liquefaction features in the South Carolina coastal region to derive possible earthquake recurrence histories for the region. Talwani and Schaeffer's (2001) Scenario 1 allows for the possibility that some events in the paleoliquefaction record are smaller in magnitude (approximately M 6+), and that these more moderate events occurred to the northeast (Georgetown) and southwest (Bluffton) of Charleston. In Talwani and Schaeffer's (2001) Scenario 2, all earthquakes in the record are large events (approximately M 7+) located near Charleston. Talwani and Schaeffer (2001) estimated recurrence intervals of about 550 years and approximately 900 to 1,000 years from their two scenarios. Subsection 2.5.2.2.4.3 provides discussion of the interpretation of the paleoliquefaction record used to define earthquake recurrence for the Charleston earthquake source.

Because there is no surface expression of faults within the Charleston seismic zone, earthquake recurrence estimates are based largely on dates of paleoliquefaction events. The most recent summary of paleoliquefaction data (Reference 461) suggests a mean recurrence time of 550 years for Charleston, which was used in the 2002 USGS model (Reference 282). This recurrence interval is less than the 650-year recurrence interval used in the USGS hazard model (Reference 281) and is roughly an order of magnitude less than the seismicity-based recurrence estimates used in EPRI (1986). Refinements of the estimate of Charleston area earthquake recurrence are presented in detail in Subsection 2.5.2.2.4.

2.5.1.1.4.5 Savannah River Site Tectonic Features

A number of faults have been identified on the Savannah River Site (SRS), located in South Carolina directly across the Savannah River from the VEGP site (Figures 2.5-224, 2.5-225, and 2.5-226). Fault locations are based on a combination of seismic reflection and refraction studies, borehole studies, and groundwater investigations [e.g., (Reference 442; Reference 265; Reference 453; Reference 254, Reference 255)]. There are a greater number of faults recognized east of the Savannah River because the Savannah River Site has been the focus of several decades of subsurface exploration and research over a much larger area than the VEGP site. However, the availability of high quality, high resolution seismic reflection data collected as part of the Vogtle ESP project make the existence of any unrecognized faults at the VEGP site unlikely.

The interpreted locations of the SRS faults have changed through time among different researchers and with the availability of additional data. Because most SRS faults are defined in the subsurface primarily from interpretation of seismic reflection profiles, there is considerable uncertainty regarding the strike, extent, and continuity of some features. Mapping of these subsurface structures between limited data points on seismic profiles has evolved to where some faults defined by name in earlier studies are no longer identified in more recent compilations. For example, the Ellenton fault was initially mapped by Domoracki (1994) as northerly striking fault between the Pen Branch and Crackerneck faults (Figure 2.5-224). The Ellenton fault, however, does not appear in the most recent SRS fault maps (Reference 254, Reference 255) (Figure 2.5-226).

The most significant perturbations in subsurface basement topography are associated with the Pen Branch, Steel Creek, ATTA, Crackerneck, Martin, and Tinker Creek faults (these are the so-called "first order SRS faults" of Cumest et al. [2000]; Figure 2.5-226). Other faults that have been identified or postulated to exist on the SRS include the Ellenton, Lost Lake, Millett, and Upper Three Runs faults (Figures 2.5-224 and 2.5-225). Four of the Savannah River faults are located within the

VEGP site area (i.e., the Pen Branch, Steel Creek, Ellenton, and Upper Three Runs faults). Each SRS fault is discussed below, beginning with the four faults that lie within the VEGP site area:

- Pen Branch Fault - Because it extends under the VEGP site, the Pen Branch fault is discussed in detail in [Subsections 2.5.1.2.4](#) and [2.5.3](#).
- Steel Creek Fault - The Steel Creek fault is located in the southwest portion of the SRS, about 2.5 mi (4 km) from the VEGP site ([Reference 453](#); [Reference 255](#)) ([Figure 2.5-224](#)). The Steel Creek fault is an approximately 10-mi-long, steeply northwest-dipping, southeast-side-down reverse fault that terminates to the northeast on the Savannah River Site ([Reference 265](#)). The Steel Creek fault is subparallel to, and southeast of, the Pen Branch fault. Together the Pen Branch and Steel Creek faults form the boundaries of an uplifted block of Triassic basement, indicating that the Steel Creek fault is genetically associated with, and probably an antithetic feature to, the Pen Branch fault. The Steel Creek fault extends upward into Cretaceous units, but the uppermost extent of faulting remains unresolved ([Reference 453](#)). The orientation of the Steel Creek fault is similar to that of the southeast-dipping Pen Branch fault relative to the maximum horizontal compressive stress field ([Reference 388](#)), thereby making both the Steel Creek and Pen Branch faults unfavorably oriented to be reactivated in a reverse or strike-slip sense. Geomatrix (1993) addressed the potential capability of the Steel Creek fault in conjunction with the Pen Branch fault and concluded that there is no discernible warping or faulting of Quaternary fluvial terraces across both faults within a resolution of 7 to 10 ft.
- Ellenton Fault - The Ellenton fault is located in the southeastern portion of the SRS, about 5 mi from the VEGP site ([Figure 2.5-224](#)). The Ellenton fault strikes north-northwest and is near vertical to steeply east-dipping ([Reference 453](#); [Reference 254](#)). The Ellenton fault appears to have an east-side-down sense of slip, but data quality are poor ([Reference 453](#)), and the latest mapping does not show this fault ([Reference 254](#), [Reference 255](#)).
- Upper Three Runs Fault - The Upper Three Runs fault is located in the northwest portion of the SRS, about 5 mi from the VEGP site ([Reference 255](#)) ([Figure 2.5-224](#)). The northeast-trending Upper Three Runs fault is restricted to crystalline basement; seismic reflection profiling revealed no evidence for this fault offsetting Coastal Plain sediments ([Reference 232](#); [Reference 453](#)). The Upper Three Runs fault has been interpreted as an older (initially Paleozoic) fault that soles into the Augusta fault at depth, possibly reactivated as a Mesozoic normal fault ([Reference 252](#); [Reference 265](#); [Reference 453](#)).
- ATTA Fault - The ATTA fault is located in the northeast portion of the SRS, about 16 mi from the VEGP site ([Figure 2.5-226](#)). The near-vertical ATTA fault strikes approximately N36°E. Based on geometrical analysis of seismic reflection data, the maximum east-side-up vertical separation of basement rocks by the ATTA fault is about 82 ft (25 m) ([Reference 255](#)). Upward penetration of the ATTA fault is uncertain because of the lack of good reflectors overlying the fault in the shallow section ([Reference 453](#)).
- Crackerneck Fault - The Crackerneck fault is located in the northwestern portion of the SRS, about 10 mi from the VEGP site ([Figure 2.5-226](#)). The Crackerneck fault strikes N22°E and dips steeply to the east ([Reference 254](#)). Based on geometrical analysis of seismic reflection data, the maximum vertical separation of basement rocks by the Crackerneck fault is about 98 ft (30 m) ([Reference 255](#)). Offset decreases upward within the Coastal Plain section to 23 ft (7 m) at the top of the Upper Eocene Dry Branch formation (approximately 38.8 Ma) ([Reference 255](#)).

- Martin Fault - The Martin fault is located just south of the SRS, about 9 mi from the VEGP site (Reference 255) (Figures 2.5-225 and 2.5-226). There is little subsurface control constraining the location and extent of the Martin fault, but aeromagnetic data anomalies associated with this fault trend N55°E for a distance of about 25 mi (Reference 255). The dip direction of the Martin fault is unknown (Reference 255). Based on data from two boreholes, Snipes et al. (1993a) estimated about 60 to 100 ft of vertical separation of the basement surface associated with the Martin fault. It has been suggested that the Martin fault is the southeastern bounding fault of the Dunbarton Basin (Reference 442), although Domoracki et al. (1999b) suggested that the Dunbarton Basin is instead a half-graben bounded only by the Pen Branch fault to the north.
- Tinker Creek Fault - The Tinker Creek fault is located in the northern portion of the SRS, about 12 mi from the VEGP site (Reference 255) (Figure 2.5-226). The Tinker Creek fault strikes approximately N36°E and dips steeply to the southeast. Based on geometrical analysis of seismic reflection data, the vertical separation of basement rocks by the Tinker Creek fault increases to the northeast to a maximum of about 79 ft (24 m) (Reference 255). Cumest et al. (1998) suggested that the Tinker Creek fault may be of regional importance, but the southeastern extent of the fault remains unresolved.
- Lost Lake Fault -. The Lost Lake fault is located in the northwestern portion of the SRS, about 12 mi from the VEGP site (Reference 252) (Figure 2.5-225). The Lost Lake fault has been mapped based on its apparent control on contaminant flow paths. Seismic reflection and borehole data constraining the location, geometry, sense of slip, and recency of movement on the Lost Lake fault are lacking (Reference 254).
- Millett Fault - A USGS Open File Report by Faye and Prowell (1982) postulated the existence of the Millett and Statesboro faults. Based on the interpretation of (1) lithic fragments in cuttings from two water wells, (2) groundwater data, and (3) changes in Savannah River sinuosity, Faye and Prowell (1982) proposed a 40-mi-long, northeast-striking Millett fault that vertically separates the buried Triassic/Cretaceous contact by 600 ft in a southeast-side-up sense.

A detailed multidisciplinary study was undertaken by Georgia Power Company (GPC) to investigate the postulated Millett and Statesboro faults (Reference 211). This study included:

- Geologic mapping
- Analysis of aerial and Landsat imagery
- Core drilling along two transects
- Petrographic, X-ray, and heavy minerals analysis of core samples
- Downhole geophysical surveys
- Seismic reflection profiling
- Water level monitoring
- Groundwater modeling
- Analysis of surface water flow

The Bechtel (1982) study concludes that there is no evidence for a capable fault or any fault as young as the undeformed Blue Bluff Marl of mid-Eocene age (40 Ma). This study also demonstrated that the original interpretation of a 600-ft (183-m) vertical separation of the base of the Coastal Plain sediments was incorrect. Core VSC-4, located 200 ft (61 m) from the original well (AL66) where Triassic rock was interpreted in the cuttings, demonstrated the presence of Cretaceous Coastal Plain sediments 400 ft (122 m) below where Triassic rock had originally been interpreted by Faye and Prowell (1982).

Upon review of the Bechtel (1982) study, the NRC staff concluded that the Millett fault is not a capable fault as defined in Appendix A to 10 CFR Part 100 in the vicinity of the VEGP site. (Reference 357).

2.5.1.1.4.6 Seismic Sources Defined by Regional Seismicity

Within 200 mi of the VEGP site, there are four areas of concentrated seismicity. Three of these (the Middleton Place-Summerville, Bowman, and Adams Run seismic zones) are located in the Charleston, South Carolina area and are discussed in Subsection 2.5.1.1.4.4. The fourth area of concentrated seismicity in the site region is the Eastern Tennessee seismic zone, a northeast-trending concentration of small-to-moderate earthquakes (Figure 2.5-218).

Eastern Tennessee Seismic Zone

The Eastern Tennessee seismic zone (ETSZ) is a pronounced seismic source in the central and southeastern United States (Figure 2.5-218). Most of the seismicity associated with the Eastern Tennessee seismic zone is located more than 200 mi from the VEGP site, but diffuse seismicity associated with the southeastern margin of the Eastern Tennessee seismic zone is located just within 200 mi of the VEGP site. The zone, located in the Valley and Ridge province of eastern Tennessee, is about 185 mi (300 km) long and 30 mi (50 km) wide and has not produced a damaging earthquake in historical time (Reference 407). However, this zone is the second most active seismic area in the United States east of the Rocky Mountains, after the New Madrid seismic zone (Reference 223), and produced the second highest release of seismic strain energy in the CEUS during the 1980s, when normalized by crustal area (Reference 407).

Earthquakes in the Eastern Tennessee seismic zone are occurring at depths from 3 to 16 mi (5 to 26 km) within Precambrian crystalline basement rocks buried beneath the exposed thrust sheets of Paleozoic rocks. None of the Eastern Tennessee seismic zone earthquakes has exceeded a moment magnitude (*M*) of 4.6 (Reference 234). The mean focal depth within the seismic zone is 9 mi (15 km), which is well below the Appalachian basal decollement's maximum depth of 3 mi (5 km) (Reference 407). The lack of seismicity in the shallow Appalachian thrust sheets implies that the seismogenic structures in the Eastern Tennessee zone are unrelated to the surface geology of the Appalachian orogen (Reference 342). The majority of earthquake focal mechanisms show right-lateral slip on northerly-trending planes or left-lateral slip on easterly-trending planes (Reference 234). A smaller number of focal plane solutions show right-lateral motion on northeasterly trending planes that parallel the overall trend of seismicity (Reference 235). Statistical analyses of focal mechanisms and epicenter locations suggest that seismicity is occurring on a series of northeast-trending en-echelon basement faults intersected by several east-west-trending faults (Reference 234). Potential structures most likely responsible for the seismicity in Eastern Tennessee are reactivated Cambrian or Precambrian normal faults formed during rifting that led to the Iapetus Ocean and presently located beneath the Appalachian thrust sheets (Reference 222; Reference 480).

Earthquakes within the Eastern Tennessee seismic zone cannot be attributed to known faults (Reference 407), and no capable tectonic sources have been identified within the seismic zone. However, the seismicity is spatially associated with major geophysical lineaments. The western margin of the Eastern Tennessee seismic zone is sharply defined and is coincident with the

prominent gradient in the magnetic field defined by the New York-Alabama magnetic lineament (Reference 235). Most seismicity lies between the New York–Alabama lineament on the west and the Clingman and Ocoee lineaments on the east (Reference 342).

In spite of the observations of small to moderate earthquakes in the Eastern Tennessee seismic zone, no geological evidence has demonstrated the occurrence of prehistoric earthquakes larger than any historical shocks within the seismic zone (Reference 235; Reference 482). Some researchers have suggested secondary evidence for possible large, prehistoric earthquakes in the region [e.g., (Reference 317)], but none of this work is conclusive. As a result, Wheeler (2005) classifies the Eastern Tennessee seismic zone as a Class C feature for lack of geological evidence of large earthquakes.

The EPRI source model (Reference 271) includes various source geometries and parameters to represent the seismicity of the Eastern Tennessee seismic zone. Subsequent hazard studies have used M_{\max} values within the range of maximum magnitudes used by the six EPRI models. Collectively, upper-bound maximum values of M_{\max} used by the EPRI teams ranged from m_b 6.6 to 7.4. Using three different methods specific to the Eastern Tennessee seismic source, Bollinger (1992) estimated a M_{\max} of m_b 6.45. Chapman and Krimgold (1994) used a M_{\max} of m_b 7.25 for the Eastern Tennessee zone and most other sources in their seismic hazard analysis of Virginia. Both of these more recent estimates of M_{\max} are similar to the range of M_{\max} values used in EPRI (1986). (Equivalencies between m_b and M as used in this SSAR are discussed in Subsection 2.5.2.2.1 and listed in Table 2.5-209). Therefore, it is concluded that no new information has been developed since 1986 that would require a significant revision to the EPRI seismic source model. Additional discussion of the significance of the ETSZ on the Vogtle ESP seismic hazard is provided in Subsection 2.5.2.2.5

Selected Seismogenic and Capable Tectonic Sources Beyond the Site Region

Because of the potential for distant, large earthquakes in the CEUS contributing to the long period ground motion hazard at the VEGP site, a discussion of three additional seismic sources located beyond 200 mi from the site is warranted. These sources are the Central Virginia, New Madrid, and Giles County seismic zones.

Central Virginia Seismic Zone

The Central Virginia seismic zone is an area of persistent, low-level seismicity in the Piedmont province, located more than 350 mi from the VEGP site (Figure 2.5-218). The zone extends about 75 mi in a north-south direction and about 90 mi in an east-west direction from Richmond to Lynchburg (Reference 221). The largest historical earthquake to occur in the Central Virginia seismic zone was the body-wave magnitude (m_b) 5.0 Goochland County event on December 23, 1875 (Reference 221). The maximum intensity estimated for this event was MMI VII in the epicentral region.

Seismicity in the Central Virginia seismic zone ranges in depth from about 2 to 8 mi (4 to 13 km) (Reference 484). Coruh et al. (1988) suggested that seismicity in the central and western parts of the zone may be associated with west-dipping reflectors that form the roof of a detached antiform, while seismicity in the eastern part of the zone near Richmond may be related to a near-vertical diabase dike swarm of Mesozoic age. However, given the depth distribution of 2 to 8 mi (4 to 13 km) (Reference 484) and broad spatial distribution, it is difficult to uniquely attribute the seismicity to any known geologic structure, and it appears that the seismicity extends both above and below the Appalachian detachment.

No capable tectonic sources have been identified within the Central Virginia seismic zone, but two paleoliquefaction sites have been identified within the seismic zone (Reference 251; Reference 396).

The paleoliquefaction sites reflect prehistoric occurrences of seismicity within the Central Virginia seismic zone and do not indicate the presence of a capable tectonic source.

The 1986 EPRI source model includes various source geometries and parameters to capture the seismicity of the Central Virginia seismic zone (Reference 271). Subsequent hazard studies have used Mmax values that are within the range of maximum magnitudes used by the six EPRI models. Collectively, upper-bound maximum values of Mmax used by the EPRI ESTs range from m_b 6.6 to 7.2 (discussed in Subsection 2.5.2.2). More recently, Bollinger (1992) has estimated a Mmax of m_b 6.4 for the Central Virginia seismic source. Chapman and Krimgold (1994) have used a Mmax of m_b 7.25 for the Central Virginia seismic source and most other sources in their seismic hazard analysis of Virginia. This more recent estimate of Mmax is similar to the Mmax values used in EPRI (1986). Similarly, the distribution and rate of seismicity in the Central Virginia seismic source have not changed since the 1986 EPRI study (discussed in Section 2.5.2.8). Thus, there is no change to the source geometry or rate of seismicity. Therefore, the conclusion is that no new information has been developed since 1986 that would require a significant revision to the EPRI seismic source model.

New Madrid Seismic Zone

The New Madrid seismic zone extends from southeastern Missouri to southwestern Tennessee and is located more than 400 mi west of the VEGP site (Figure 2.5-218). The New Madrid seismic zone lies within the Reelfoot rift and is defined by post-Eocene to Quaternary faulting and historical seismicity. Given the significant distance between the site and the seismic zone, the New Madrid seismic zone did not contribute to 99 percent of the hazard at the VEGP site in EPRI (1986). However, it is described in this section because several recent studies provide significant new information regarding magnitude and recurrence interval for the seismic zone.

The New Madrid seismic zone is approximately 125 mi (220 km) long and 25 mi (40 km) wide. Research conducted since 1986 has identified three distinct fault segments embedded within the seismic zone. These three fault segments include a southern northeast-trending dextral slip fault, a middle northwest-trending reverse fault, and a northern northeast-trending dextral strike-slip fault (Reference 483). In the current east-northeast to west-southwest directed regional stress field, Precambrian and Late Cretaceous age extensional structures of the Reelfoot rift appear to have been reactivated as right-lateral strike-slip and reverse faults.

The New Madrid seismic zone produced three historical, large magnitude earthquakes between December 1811 and February 1812 (Reference 330). The December 16, 1811, earthquake is associated with strike-slip fault displacement along the southern portion of the New Madrid seismic zone. Johnston (1996) estimated a magnitude of M 8.1±0.31 for the December 16, 1811, event. However, Hough et al. (2000) re-evaluated the isoseismal data for the region and concluded that the December 16 event had a magnitude of M 7.2 to 7.3. Bakun and Hopper (2004) similarly concluded this event had a magnitude of M 7.2.

The February 7, 1812, New Madrid earthquake is associated with reverse fault displacement along the middle part of the New Madrid seismic zone (Reference 341). This earthquake most likely occurred along the northwest-trending Reelfoot fault that extends approximately 43 mi from northwestern Tennessee to southeastern Missouri. The Reelfoot fault is a northwest-trending, southwest-vergent reverse fault. The Reelfoot fault forms a topographic scarp developed as a result of fault-propagation folding (Reference 470; Reference 347; Reference 469). Johnston (1996) estimated a magnitude of M 8.0±0.33 for the February 7, 1812, event. However, Hough et al. (2000) re-evaluated the isoseismal data for the region and concluded that the February 7 event had a magnitude of M 7.4 to 7.5. More recently, Bakun and Hopper (2004) estimated a similar magnitude of M 7.4.

The January 23, 1812, earthquake is associated with strike-slip fault displacement on the East Prairie fault along the northern portion of the New Madrid seismic zone. Johnston (1996) estimated a

magnitude of $M 7.8 \pm 0.33$ for the January 23, 1812, event. Hough et al. (2000), however, re-evaluated the isoseismal data for the region and concluded that the January 23 event had a magnitude of $M 7.1$. More recently, Bakun and Hopper (2004) estimated a similar magnitude of $M 7.1$.

Because there is very little surface expression of faults within the New Madrid seismic zone, earthquake recurrence estimates are based largely on dates of paleoliquefaction and offset geological features. The most recent summaries of paleoseismologic data (Reference 466, Reference 467; Reference 299) suggest a mean recurrence time of 500 years, which was used in the 2002 USGS model (Reference 282). This recurrence interval is half of the 1,000-year recurrence interval used in the 1996 USGS hazard model (Reference 281), and an order of magnitude less than the seismicity-based recurrence estimates used in EPRI (1986).

The upper-bound maximum values of M_{max} used in EPRI (1986) range from $m_b 7.2$ to 7.9 . Since the EPRI study, estimates of M_{max} have generally been within the range of maximum magnitudes used by the six EPRI models. The most significant update of source parameters in the New Madrid seismic zone since the 1986 EPRI study is the reduction of the recurrence interval to 500 years.

Giles County Seismic Zone

The Giles County seismic zone is located in Giles County, southwestern Virginia, near the border with West Virginia and more than 250 mi from the VEGP site (Figure 2.5-218). The largest known earthquake to occur in Virginia and the second largest earthquake in the entire southeastern United States is the 1897 $M 5.9$ (Reference 343) Giles County event, which likely produced an MMI VIII in the epicentral area.

Earthquakes in the Giles County seismic zone occur within Precambrian crystalline basement rocks beneath the Appalachian thrust sheets at depths from 3 to 16 mi (5 to 25 km) (Reference 222). Earthquake foci define a 25-mi-long (40-km-long), northeasterly striking, tabular zone that dips steeply to the southeast beneath the Valley and Ridge thrust sheets (Reference 222; Reference 233). The lack of seismicity in the shallow Appalachian thrust sheets, estimated to be about 2 to 3.5 mi (4 to 6 km) thick, implies that the seismogenic structures in the Giles County seismic zone, similar to those inferred for the Eastern Tennessee seismic zone, are unrelated to the surface geology of the Appalachian orogen (Reference 222). The spatial distribution of earthquake hypocenters, together with considerations of the regional tectonic evolution of eastern North America, suggests that the earthquake activity is related to contractional reactivation of late Precambrian or Cambrian normal faults that initially formed during rifting associated with opening of the Iapetus Ocean (Reference 222; Reference 223).

No capable tectonic sources have been identified within the Giles County seismic zone, nor does the seismic zone have recognizable geomorphic expression (Reference 482). Thus, in spite of the occurrence of small to moderate earthquakes, no geological evidence has demonstrated the occurrence of prehistoric earthquakes larger than any historical shocks within the zone (Reference 482). As a result, Wheeler (2005) classifies the Giles County seismic zone as a Class C feature for lack of geological evidence of large earthquakes.

A zone of small Late Pliocene to Early Quaternary age faults has been identified within the Giles County seismic zone, near Pembroke, Virginia (Reference 251). The Pembroke zone is a set of extensional faults exposed in terrace deposits overlying limestone bedrock along the New River. Crone and Wheeler (2000) rated these faults as Class B features because it has not yet been determined whether these faults are tectonic or the result of solution collapse in underlying limestone units. The shallow Pembroke faults do not appear to be related to the seismicity within the Giles County seismic zone, which is occurring beneath the Appalachian basal decollement in the North American basement.

The EPRI source model includes various source geometries and parameters to represent the seismicity of the Giles County seismic zone (Reference 271). Subsequent hazard studies have used Mmax values that were within the range of maximum magnitudes used by the six EPRI models. Collectively, upper-bound maximum values of Mmax used by the EPRI teams ranged from m_b 6.6 to 7.2 (discussed in Subsection 2.5.2.2). More recently, Bollinger (1992) estimated a Mmax of m_b 6.3 for the Giles County seismic source using three different methods. Chapman and Krimgold (1994) used a Mmax of m_b 7.25 for the Giles County zone and most other sources in their seismic hazard analysis of Virginia. Both of these more recent estimates of Mmax are similar to the range of Mmax values used in EPRI (1986). Therefore, no new information has been developed since 1986 that would require a significant revision to the EPRI seismic source model.

2.5.1.1.5 Regional Gravity and Magnetic Data

Regional maps of the gravity and magnetic fields in North America were published by the Geological Society of America in 1987 as part of the Society's Decade of North American Geology (DNAG) project. The maps present the potential field data at 1:5,000,000-scale and thus are useful for identifying and assessing regional gravity and magnetic anomalies with wavelengths on the order of about 6 mi (10 km) or greater. Gravity and magnetic data also have been incorporated in the E-5 DNAG crustal transect, which traverses the Appalachian orogen from eastern Tennessee to the offshore Atlantic basin (Reference 316), and encompasses the VEGP site region. At a local scale, Cumbest et al. (1992) developed models of gravity and magnetic data to evaluate the geometry and structure of the Mesozoic Dunbarton basin beneath the SRS northeast of the VEGP site. These models in particular provide important insights for the interpretation of potential field data in the VEGP site region.

2.5.1.1.5.1 Regional Gravity Data

The 1987 DNAG gravity map and the gravity profile along the E-5 DNAG crustal transect document low gravity values beneath the Valley and Ridge and Blue Ridge provinces relative to the Cumberland Plateau province to the west (Figure 2.5-214). The approximately 40 to 60 mGal eastward decrease in gravity along the western margin of the Valley and Ridge province is likely due to eastward thickening of the relatively less dense carbonate and siliciclastic rocks above the Grenville metamorphic basement in the Valley and Ridge province relative to the Cumberland Plateau.

Bouguer gravity values increase by about 80 mGal across an approximately 62 mi (100 km) distance from the eastern Blue Ridge to the Inner Piedmont Terrane (Reference 244; Reference 316). As documented by the DNAG gravity map, this gradient is present across the Piedmont physiographic province along much of the length of the Appalachian belt. At the latitude of Virginia, north of the VEGP site region, this gradient has been interpreted to reflect the eastward thinning of the North American continental crust and associated positive relief on the Moho with proximity to the Atlantic margin. Inspection of the crustal structure interpreted by Hatcher et al. (1994) along the E-5 transect (Figure 2.5-214) indicates that the eastward increase in gravity across the Inner Piedmont at the latitude of the ESP study region also is associated with obducted metavolcanic rocks of the Carolina–Avalon Terrane that have been overthrust onto the Grenvillian basement. A gravity model by Iverson and Smithson (1983) along the southern Appalachian COCORP seismic reflection profile suggests that the gradient probably arises from both eastward thinning of continental crust and the obduction of the Inner Piedmont and Carolina Terranes, which have higher average densities than the underlying Grenvillian crust.

The gravity profile along the DNAG E-5 crustal transect indicates that the gravity field east of the Inner Piedmont is relatively uniform (Figure 2.5-214), and the 1987 DNAG gravity map shows that the Coastal Plain is characterized by relatively low amplitude anomalies with wavelengths on the order of about 12 to 25 mi (20 to 40 km) superimposed on this uniform field. Detailed modeling of the

gravity field in this region by Cumbest et al. (1992) indicates that the most prominent anomalies are associated with monzogranite plutons, which are relatively less dense than the intruded country rock and thus give rise to local gravity lows, and mafic intrusions, which are relatively more dense and give rise to local gravity highs. From modeling of gravity data, Cumbest et al. (1992) found that the predicted anomaly associated with the Mesozoic Dunbarton Basin is a subordinate feature of the gravity field compared to the anomalies associated with the plutons and mafic intrusions.

The relationship between gravity anomalies in the VEGP site vicinity and bedrock geology inferred by Dennis et al. (2004) to underlie the Coastal Plain sediments from borehole and other subsurface data is illustrated in [Figure 2.5-227](#). The extremes in the local gravity field are highs associated with Triassic-Jurassic mafic intrusive complexes southeast of the VEGP site and lows associated with granitic plutons mapped to the north-northeast and east-northeast of the site. The lateral extent of the gravity lows associated with the Graniteville and Springfield plutons suggest that these bodies may be larger than inferred by Dennis et al. (2004). The Dunbarton Basin is spatially associated with an approximately 5-mi-wide (8-km-wide), northeast-southwest-trending gravity low northwest of the mafic intrusive complexes and associated gravity high southeast of the VEGP site. A northwest-southeast profile of the gravity data through the VEGP site ([Figure 2.5-228](#)) illustrates in detail that the gravity low associated with the Dunbarton Basin is a very modest second-order feature superimposed on the 25-mi-long (40-km-long) west-to-east increase in gravity between the granitic plutons and mafic intrusive complexes, consistent with the findings of Cumbest et al. (1992).

The gravity profile also shows that the Belair fault, which separates the Kiokee belt on the northwest from the Belair belt to the southeast, is adjacent to an approximately 35 mGal gravity difference ([Figure 2.5-228](#)). This eastward decrease in gravity shows that the high-grade metamorphic rocks of the Kiokee belt are generally denser than the relatively lower-grade rocks of the Belair belt. However, the magnitude of the gradient also could be affected by the presence of the relatively lower density granitic plutons to the east and southeast of the Belair fault.

To summarize, gravity data published since the mid-1980s document that long-wavelength anomalies along the E-5 DNAG crustal transect through the VEGP site region are characteristic of large parts of the Appalachian belt and reflect first-order features of the various provinces and accreted Paleozoic terranes and west-to-east thinning of the ancestral North American (Grenvillian) continental crust during the Mesozoic. The dominant short-wavelength characteristics of the gravity field in the vicinity of the VEGP site are gravity highs and lows associated with Mesozoic mafic and Paleozoic granitic intrusions, respectively. Detailed gravity modeling by Cumbest et al. (1992) shows that the gravity low associated with the Triassic Dunbarton Basin is a subordinate feature in the regional field. The gravity data acquisition and modeling studies performed to date do not show any evidence for Cenozoic tectonic activity or specific Cenozoic structures. There are no large, unexplained anomalies in the gravity data.

2.5.1.1.5.2 Regional Magnetic Data

Data compiled for the DNAG magnetic map reveal numerous northeast-southwest-trending magnetic anomalies that are generally parallel to the structural grain of the Paleozoic Appalachian orogenic belt ([Reference 244](#)). For example, a magnetic profile along the DNAG E-5 crustal transect ([Reference 316](#)) reveals an approximately 800 nT southeastward decrease in magnetic intensity between the Cumberland Plateau and western Valley and Ridge provinces, and the western Blue Ridge province ([Figure 2.5-214](#)). The DNAG magnetic map indicates that this difference is present to the southwest and northeast along the western Appalachian belt in adjacent parts of Alabama and Kentucky and is spatially associated with the contact between Precambrian metamorphic basement and overlying Paleozoic accreted terranes. In general, the western Valley and Ridge province and eastern Blue Ridge along the E-5 crustal transect are characterized by relatively low magnetic intensities, and the western Blue Ridge and Inner Piedmont are relative magnetic highs, probably

indicating a greater abundance of mafic rocks in the accreted Taconic units east of the Hayesville thrust.

The accreted Carolina–Avalon Terrane is characterized by short-wavelength, high-amplitude anomalies (approximately 200 nT over distances of about 6.2 mi [10 km]). Detailed modeling of magnetic data from the SRS northeast of the VEGP site indicates that these anomalies may be associated with mafic intrusions that are vertically elongated and have east-dipping boundaries (Reference 253). Felsic plutons in this region, which are inferred to exist from borehole data and gravity modeling, have modest susceptibility contrasts with the country rock they intrude and thus do not generate high-amplitude magnetic anomalies (Reference 253). Similarly, Mesozoic basin sediments are inferred to have relatively low susceptibility contrasts with the pre-intrusive basement rock, and modeling by Cumbest et al. (1992) suggests that the anomaly associated with the sediments and margins of the Dunbarton Basin is a second-order feature of the magnetic field relative to the amplitudes of the anomalies produced by the intrusive mafic rocks. The Towaliga fault along the western margin of the Carolina–Avalon Terrane is associated with alternating low and high short wavelength magnetic anomalies (Reference 316) characteristic of those produced by a susceptibility contrast across a dipping structural contact.

Comparison of aeromagnetic data from the VEGP site region (Reference 259) with bedrock geology inferred by Dennis et al. (2004) to underlie the Coastal Plain sediments from borehole and other subsurface data illustrates the relationships described by Cumbest et al. (1992). The Dunbarton Basin is associated with a northeast-southwest-trending magnetic low and is bounded on the south by pronounced magnetic highs associated with Triassic–Jurassic mafic intrusive complexes (Figure 2.5-229). A northwest-southeast-trending profile of the magnetic intensities that passes through the VEGP site shows that the magnetic low associated with the Dunbarton Basin is similar to a magnetic low approximately 12 mi to the southeast that is not associated with a known Triassic basin (Figure 2.5-230); also, the figure shows that the high magnetic anomalies associated with the mafic intrusive complexes extend northward into the basin (Figure 2.5-229). These relations are consistent with the conclusion of Cumbest et al. (1992) that the magnetic signature of the Dunbarton Basin is very modest relative to that of the mafic intrusive complexes.

The magnetic map and profile (Reference 259) also include the Kiokee and Belair belts of the Carolina arc terrane northwest of the VEGP site. Both of these belts are characterized by closely spaced, short-wavelength anomalies with amplitudes of about 100 to 200 gammas (Figure 2.5-230). In general, the magnetic intensities in the Belair belt are slightly higher than those of the Kiokee belt. Daniels (1974) noted that the bulk composition of the Kiokee belt is probably more felsic than that of the Belair belt and thus has a lower magnetic susceptibility.

To summarize, magnetic data published since the mid-1980s provide additional characterization of the magnetic field in the VEGP site region. Detailed modeling of magnetic data from the SRS provides insights into the origins of magnetic anomalies that extend southwest into the vicinity of the VEGP site. The first-order magnetic anomalies in the VEGP site region are associated primarily with northeast-southwest-trending Paleozoic and Mesozoic intrusive rock bodies. The magnetic data do not show evidence for any Cenozoic structures in the site region and do not have sufficient resolution to identify or map discrete faults, such as border faults along the Dunbarton Basin. No large, unexplained anomalies are found in the magnetic data.

2.5.1.2 Site Area Geology

This section describes the geology and structural geology of the site area (within a 5-mi radius of the VEGP site).

2.5.1.2.1 Site Area Physiography and Geomorphology

The site area lies in the Upper Coastal Plain of the Coastal Plain Physiographic Province and is bordered by the Savannah River to the east (Figures 2.5-204 and 2.5-231). The surrounding topography consists of gently rolling hills with a principally dendritic drainage pattern. Surficial soils are typically well drained. All major streams are tributary to the Savannah River.

The site area lies at the northern extent of a broad westward migrating meander in the Savannah River where the sinuosity decreases from about 1.8 to 1.3 (Reference 292). Incision of the river has formed steep bluffs and topographic relief of nearly 150 ft from the river surface to the plant site. The river level adjacent to the plant site is at an elevation of approximately 80 ft msl, with a gradient of less than 1 ft/mi (Reference 292). The flood plain is a broad alluvial surface that is 4 to 10 ft above the channel. The youngest alluvium lies along the western side of the river, while older terraces are preserved on the east side of the flood plain (Figures 2.5-232 and 2.5-234). Stream valleys are predominantly symmetrical, with slopes ranging from 0.2 to 0.6 percent. The surface topography ranges from an elevation of about 90 to nearly 300 ft msl across the VEGP site (Figures 2.5-233 and 2.5-235).

Several surface depressions were noted during the initial site investigation and were extensively studied. The topography and surface drainage within the site has been modified during and after construction of the existing VEGP units, making evaluation of these features impractical. In the Coastal Plain, surface depressions can be categorized as eolian features known as Carolina bays, whereas others may result from solution of underlying calcareous sediment (Reference 437; Reference 468; Reference 439).

Carolina bays, which are shallow, elliptical depressions with associated sand rims, are common throughout the Atlantic Coastal Plain and are most numerous in North and South Carolina. They are surficial features that have no effect on the subsurface sediments. Distinguishing features of Carolina bays are the elliptical shape, preferential orientation of the long axis at S50°E, and sand rims along the east and southeast flanks (Reference 338). A discussion of various hypotheses for the timing and mode of origin of these bays is provided in Subsection 2.5.1.1.1.

Surface depressions that do not meet the criteria of Carolina bays are typically irregularly shaped, localized features resulting most likely from the dissolution of calcareous stratum at depth. Initial site studies conducted for the existing VEGP Units 1 and 2 concluded that these features resulted principally from dissolution of a limestone unit and that lower-lying carbonate-bearing units were not involved. Subsection 2.5.3.8.2.1 contains a discussion of the significance of these features.

2.5.1.2.2 Site Area Geologic History

The Upper Coastal Plain is essentially a flat-lying section of unconsolidated fluvial and marine sediments overlying a basement complex of Paleozoic crystalline metamorphic and igneous rock as well as Triassic–Jurassic basin sediments. Evolution of the basement complex and the effect on the Coastal Plain section is regional in nature and is discussed in Subsections 2.5.1.1.2 and 2.5.1.1.4.

The Paleozoic rocks and the Triassic sediments were beveled by erosion, forming the base for Coastal Plain sediment deposition. The erosional surface dips southeast approximately 50 ft/mi (Reference 273). The Coastal Plain section consists of stratified sand, clay, limestone, and gravel that dip gently seaward. The oldest Coastal Plain sediments beneath the site area are Late Cretaceous and consist of predominantly siliciclastics deposited in an upper deltaic, fluvial setting that continued throughout the Late Cretaceous. Paleocene sedimentation continued, with a strong fluvial influence changing to more marginal marine to shallow shelf deposition well into the Middle Eocene, marked by deposition of mixed clastic-carbonate sediments. Upper Eocene sedimentation occurred in more marginal and inner-tidal settings. Miocene (or younger) high energy fluvial deposits

are present at higher topographic locations and in some areas incised deeply into the underlying Eocene section. A thin veneer of late Miocene to early Pliocene eolian sands overlies some of the higher topographic areas. The youngest sediments consist of Quaternary alluvium present within the stream and river valleys.

2.5.1.2.3 Site Area Stratigraphy

The site area stratigraphy is based on site-specific data obtained during the ESP and COL site investigations as well as regional geologic studies and includes the following sources of information:

- Regional geologic maps and studies
- Site area studies performed for VEGP Units 1 and 2 and for the ESP investigation
- Borehole data, including core and geophysical logs acquired during the ESP and COL investigations ([Figures 2.5-236 and 2.5-249](#))
- Surface geophysical surveys performed as part of the ESP investigation, including seismic reflection and refraction ([Figures 2.5-237, 2.5-238, 2.5-239, and 2.5-240](#)).

Numerous geologic studies have been conducted in the surrounding area since initial studies were conducted for VEGP Units 1 and 2. Most of these studies were focused in the vicinity of the SRS. Many of these studies focused on correlating both geologic and hydrogeologic formations present in South Carolina and Georgia, resulting in an updated stratigraphic nomenclature. The most current stratigraphic nomenclature from Huddlestun and Summerour (1996) and Falls and Prowell (2001) is used below. A correlation chart showing current USGS, Georgia Geological Survey, South Carolina, and SRS and VEGP Units 1 and 2 FSAR nomenclature is provided as [Figure 2.5-211](#). A site stratigraphic column based mainly on data from borehole B-1003, supplemented by data from other ESP and COL investigation borings, is shown on [Figure 2.5-241](#).

2.5.1.2.3.1 Basement Rock

The regional basement surface has been leveled by erosion and dips to the southeast approximately 50 ft/mi ([Reference 273](#)). Basement rock lithology within the site area consists of Paleozoic crystalline rock as well as Triassic–Jurassic sedimentary rock of the Dunbarton Basin. Basement rock lithology has been determined directly from core data from boring B-1003 and inferred from seismic reflection and refraction surveys performed as part of the ESP investigation. These data are corroborated regionally with other core data and geophysical surveys, as discussed in [Subsection 2.5.1.1.3.5](#).

Boring B-1003 was drilled within the VEGP site to acquire detailed stratigraphic, lithologic, geophysical (including natural gamma, electrical resistivity, compressional velocity, and shear wave velocity) and depth-to-basement data. Data from B-1003 identifies Triassic–Jurassic basement rock at a depth of 1,049 ft (-826 ft msl). Data from four seismic reflection and refraction lines described in [Subsection 2.5.1.2.4.2](#), as well as borehole and seismic reflection data from other regional studies including the SRS ([Reference 253](#); [Reference 442](#)), determine the northern boundary of the Dunbarton Basin to strike northeast-southwest across the site area, defining the approximate boundary between the Triassic–Jurassic sedimentary rock underlying the southeastern portion and Paleozoic crystalline rock underlying the northwestern portion of the site area ([Figure 2.5-242](#)).

Although no borehole data confirm the lithology of the Paleozoic crystalline rock within the site area, data from regional studies, as well as regional gravity and magnetic surveys, suggest a complex of metavolcanics ([Reference 253](#); [Reference 442](#)). The Triassic–Jurassic sedimentary rocks of the

Dunbarton Basin consist of mudstones, sandstones, and conglomerates of varying degrees of lithification, as determined from borehole B-1003.

2.5.1.2.3.2 Site Area Coastal Plain Stratigraphy

The Paleozoic and Triassic basement complex is unconformably overlain by poorly consolidated to unconsolidated Coastal Plain sediments that dip and thicken to the southeast. These sediments range in age from Upper Cretaceous to Miocene except where the Miocene Hawthorne Formation has been removed by excavation and are approximately 1,049 ft thick in the site area, based on boring B-1003 that was drilled as part of the ESP investigation.

The stratigraphy defined for the site area adopts the nomenclature of Huddlestun and Summerour (1996), as shown on [Figures 2.5-211](#), and [2.5-241](#), and was based primarily on lithology except where carbonate fossils provided more definitive stratigraphic correlation. Cretaceous sediments that had been assigned to the Tuscaloosa Formation were assigned to the Cape Fear, Pio Nono, Gaillard/Black Creek and Steel Creek formations. Tertiary sediments were further subdivided based on both lithology and carbonate fossils where present. The youngest sediments of Quaternary age consisted of alluvial deposits within stream and river valleys.

More recent investigations in the VEGP site vicinity have included detailed lithological and paleontological studies to correlate stratigraphic units between Georgia and South Carolina ([Reference 278](#)). Over the last two decades, detailed work that focused on the SRS ([Figure 2.5-211](#)), has resulted in a more detailed lithostratigraphic column. Cross-well correlation using lithologic data from both the core and downhole geophysical logs provides a means to correlate many of the same geologic units present at the site area with those mapped in the VEGP site vicinity.

The following sub-sections describe each geologic unit, from oldest to youngest, and are based primarily on lithologic descriptions of the core log from boring B-1003 drilled and logged as part of the ESP site investigation ([Appendix 2.5A](#)) ([Figure 2.5-241](#)). The most recent stratigraphic column published by the USGS ([Reference 278](#)) is cited where those studies provide confirmatory information that is directly applicable to the site area. In addition, geologic studies and correlation with SRS stratigraphic units are cited where they provide confirmatory information directly applicable to the site area.

Cretaceous Stratigraphy

Upper Cretaceous age sediments unconformably overlie both crystalline and Triassic–Jurassic basement rock in the site area. The initial site stratigraphy for the VEGP Units 1 and 2 assigned all Cretaceous sediments to the Tuscaloosa Formation. More recent investigations have identified four geologic formations within the Cretaceous section. The following discussions rely primarily on core log data from boring B-1003 ([Appendix 2.5A](#)). Contacts, as interpreted from geophysical well logs might vary from the depths identified on the boring logs. The following sections describe these units from oldest to youngest.

Cape Fear Formation

In boring B-1003, the base of the Cape Fear Formation was determined to be at a 1,049 ft depth (-826 ft msl) and the top at a depth of 858 ft (-635 msl). This results in a thickness of 191 ft. The base of the Cape Fear Formation in Boring B-1003 consists of sandy silt overlain by well-sorted quartz gravel with subrounded to angular grains. This is overlain by generally well-sorted gray sandy silt with layers of subrounded gravels, pebbles and silty sand. The silty sand is overlain by sandy silt that in turn is overlain by a clayey sand grading up into a sandy elastic clay. The top portion of the Cape Fear formation is logged as a gray to dark gray, well-sorted, subrounded to subangular fine to coarse clayey sand with a weak cementation zone near the top and arkosic layers.

In boreholes in the site vicinity, the Cape Fear Formation consists of poorly-sorted, silty to clayey quartz, occasionally arkosic, sands with interbedded clays. Grains tend to be subangular to angular. The sands are medium to coarse, with occasional pebble zones. Lithification ranges from moderate to high due to the presence of cristobalite in the clay matrix, which can also yield a greenish blue hue to the sediments. Numerous stacked fining-upward sequences, lack of marine fossils, and the presence of terrestrial microflora and root clasts suggest deposition within a fluvial dominated delta plain ([Reference 278](#)).

Pio Nono Formation

In boring B-1003 the base of the Pio Nono Formation is logged at a depth of 858 ft (-635 msl) and the top is logged at a depth of 798 ft (-575 msl). The base consists of a light gray, well-sorted clayey sand. This is overlain primarily by well-sorted sand with silt that grades upward from a gray-tan fine to medium grained unit into a white-gray fine to coarse unit with some gravel. This formation consists primarily of moderately to well-sorted quartz sands with little silt and clayey sands. Traces of manganese staining and mica are present. Grains tend to be rounded to subangular, medium to coarse, with some gravel lags. The sands are typically non-lithified, with a few slightly cemented zones. The top of the formation is logged as a tan-white poorly-sorted fine to medium sand with silt. A fining-up sequence was logged between depths of 808 and 803 ft.

Both fining and coarsening upward sequences are noted in nearby boreholes. The top of the formation may be marked by a thick bed of oxidized clay. In borehole B-1003, this clay was logged as marking the base of the overlying Gaillard/Black Creek formations. The lack of marine fossils, presence of oxidized zones, and gravel lags suggest a deltaic environment.

Upper Gaillard Formation/Black Creek Formation

The Upper Gaillard/Black Creek Formation consists of thick alternating sequences of moderately to well-sorted silty, clayey sands and silty clay beds. The sands tend to be medium to coarse grained, rounded to subrounded, and contain trace amounts of mica and glauconite. Fining-upward sequences are present, as well as gravel lag deposits. The more clayey beds tend to be dark and oxidized, with trace amounts of lignite and root clasts. The presence of marine fauna and glauconite suggests a marine influence, while oxidation in the clay beds and the presence of root clasts suggest a more lagoonal setting, which together indicate a prograding delta sequence.

The base of the Upper Gaillard/Black Creek Formation in boring B-1003 was noted at a 798-ft depth (-575 ft msl) and the top at a 587-ft depth (-364 ft msl), resulting in an overall thickness of 211 ft. As noted above, the base is logged as a 12-ft layer of black to dark gray clay. The clay is overlain by poorly graded silty sands to sandy silts. A 24-ft layer of gray sandy silt with clayey sand layers occurs between depths of 603 ft to 627 ft. The top of the Gaillard/Black Creek Formation consists of well-sorted gray fine to coarse sand with silt.

Steel Creek Formation

The basal contact of the Steel Creek Formation with the underlying upper Gaillard/Black Creek Formation is at a depth of 587 ft (-364 ft msl). The top of the Steel Creek Formation is noted at a depth of 477 ft (-254 ft msl), resulting in a total thickness of 110 ft.

Sediments of the Steel Creek Formation are predominantly sands and silty sands. These sands are well to poorly-sorted, with trace amounts of mica, kaolin, and lignite. Sand grains are subrounded to subangular. Multiple fining-upward sequences, the presence of lignite, and the oxidation of clays indicate a more fluvial, delta plain depositional setting. The top of the Steel Creek Formation in boring B-1003 is marked by a transition from gray poorly-sorted fine to coarse sand with a kaolinitic clay matrix to a clayey sand of the overlying Black Mingo Formation.

Tertiary Stratigraphy

Tertiary sediments ranging from Paleocene to Miocene age unconformably overlie the Cretaceous section in the site area. The site stratigraphy defined for the VEGP UFSAR divided the Tertiary section into the Ellenton Formation, Huber Formation, Lisbon Formation, Barnwell Group, Suwanee Limestone (not recognized at the ESP project site), and Hawthorne Formation. Further subdivisions were made for the Lisbon and Barnwell Group because these units are more easily mapped due to exposure within incised valleys as well as to more available borehole data units due to the relative shallow depth of these units. The Tertiary section also contains considerably more calcareous sediments, thus providing more biostratigraphic constraint.

More recent investigations, including detailed palynologic and paleontologic studies, have refined the Tertiary stratigraphy in the vicinity of the site area ([Reference 273](#); [Reference 278](#)). Huddlestun and Summerour (1996) divide the Tertiary units, from oldest to youngest, into the Black Mingo, Snapp and Congaree formations, the Bennock Millpond/Still Branch Sand, the Lisbon Formation and the Barnwell Group. As with the Cretaceous section, core log data from boring B-1003 are used to describe the site stratigraphy. The following sections describe these units from oldest to youngest.

Black Mingo Formation

In boring B-1003, the base of the Black Mingo Formation was noted at a depth of 477 ft (-254 ft msl) and the top at a depth of 438 ft (-215 ft msl), giving an overall thickness of 39 ft. The base of the unit is marked by the occurrence of a gray, poorly-sorted fine to coarse sand and is overlain by a 15-ft thick layer of gray sandy clay with some coarse subangular quartz sand and lignite fragments. This, in turn is overlain by light gray well-sorted fine to medium clayey sand and sand with silt. The top of the Black Mingo Formation is logged as a 7-ft thick layer of dark gray sandy clay.

Snapp Formation

The base of the Snapp Formation in boring B-1003 is logged at a depth of 438 ft (-215 ft msl) and the top at a depth of 331 ft (-108 ft msl), resulting in an overall thickness of 107 ft. The base is marked by well-sorted sand with quartz gravel that appears to be a channel lag deposit. This grades upward into a tan-gray well-sorted silty fine to medium sand that is overlain by 18 ft of gray-red silty clay containing some 4- to 6-inch layers of white and gray fine to coarse silty quartz sand. The clay is overlain by well-sorted clayey sand that is overlain by a sandy to silty gray to red-brown clay. This 12-ft clay layer is overlain by a silty to clayey sand sequence overlain by about 5 ft of gray-reddish brown clay. The top of the Snapp Formation is a light grayish white poorly-sorted medium to coarse grained clayey sand.

Congaree Formation

The base of the Congaree Formation is logged at a depth of 331 ft (-108 ft msl) and the top at a depth of 216 ft (7 ft msl), resulting in a thickness of 115 ft. Although the core was not recovered in one 5-ft run, the base of the Congaree Formation appears to be marked by a 14-ft thick dark grayish black clay. This clay is overlain by black, well-sorted silty sand overlain by a 1-ft thick black clay layer. This clay layer is overlain by gray, well-sorted clayey sand that grades upward into a light gray, well-sorted silty sand overlain by a sandy silt. The top of the Congaree Formation consists of gray, well-sorted silty sands.

Still Branch Sand

Based on ESP and COL borings, the base of the Still Branch Sand is noted at a depth of 216 ft (7 ft msl) and the top at a depth of 173 ft (50 ft msl), resulting in a thickness of 43 ft. The base of the Still Branch is marked by the occurrence of dark greenish gray sandy silt containing 1- to 3-inch thick sand layers. This silt is overlain by light gray well-sorted medium to coarse sand that is overlain by dark gray, well-sorted clayey sand. This is overlain by dark, greenish gray calcareous silty sand

overlain by calcareous clayey sand. An overlying silty to clayey sand sequence is overlain by a gray well-sorted fine to medium sand at the top of the unit.

Lisbon Formation

The middle Eocene Lisbon Formation includes members that have been extensively mapped in the upper Coastal Plain of Georgia and South Carolina. These include the Blue Bluff Marl, McBean Limestone, and, in South Carolina, the Tinker Formation. These units commonly interfinger. In general, the Lisbon Formation is more fossiliferous and ranges from calcareous sands to coquina, while the Tinker Formation in South Carolina is the clastic equivalent consisting predominantly of well-sorted quartz sands. The Blue Bluff Marl Member tends to be more micritic, with shell fragments suspended in a micrite matrix with occasional shell-rich zones. Lithologies, fossil assemblage, and the interfingering nature suggest shallow shelf to neritic environment. In the VEGP site area, the Blue Bluff Marl is noted as the dominant facies and is exposed in the western bluffs along the site boundary with the Savannah River. In Burke County, the Blue Bluff Member disconformably overlies the Still Branch Sand. In general, the Blue Bluff Member disconformably underlies the Utley Limestone Member of the Clinchfield Formation, but locally, where the Utley Limestone is absent, the Blue Bluff Member is overlain disconformably by the Dry Branch Formation of the Barnwell Group (Reference 334). The Blue Bluff Member was extensively studied and mapped as the foundation bearing unit for VEGP Units 1 and 2 and as part of the subsurface investigation for VEGP Units 3 and 4. The regional occurrence of the Blue Bluff Marl is discussed in Subsection 2.5.1.2.6. The Lisbon Formation also contains a carbonate unit called the McBean Limestone Member (Figures 2.5-231 and 2.5-241) that occurs in an area limited to the north and northwest of the VEGP site vicinity (Reference 334). The McBean Member has not been recognized in borings at the VEGP site. At the Georgia Geological Survey reference locality, near McBean, Georgia, the McBean Member is disconformably overlain by the Utley Limestone and rests paraconformably on the Still Branch Sand (Reference 334).

A total of 186 borings were drilled as part of the ESP and COL subsurface investigations for VEGP Units 3 and 4. The boring locations are shown on Figure 2.5-249. The boring logs drilled during the VEGP Units 1 and 2 and the recent Units 3 and 4 subsurface investigations describe the Blue Bluff Member (referred to as the Blue Bluff Marl on boring logs and geotechnical data report tables [Appendices 2.5A, and 2.5C]) as a fine-grained, calcareous silty clay that directly underlies the Utley Limestone. The Blue Bluff Marl is defined as very stiff to hard carbonate-rich clayey silt to silty clay with trace amounts of very fine to fine grained sand (Appendix 2.5C). Distinguishing features in the field are the marl's greenish gray color, the presence of shell and phosphatic fragments in localized horizons, and the abundance of partially cemented, well-indurated layers consisting of very fine grained to fine grained quartz sand with carbonate mud cement. Breakage of the well-indurated (limestone) zones by the split spoon sampler often resulted in forming gravel-sized particles (Appendix 2.5C).

A total of 182 borings have penetrated the top of the Blue Bluff Marl within the VEGP site and indicate that the Utley Limestone/Blue Bluff Marl contact ranges in elevation between 96.1 ft msl and 151.6 ft msl. A structure contour map of the top of the Blue Bluff Marl, incorporating these data, is shown on Figure 2.5-250. The top of the Blue Bluff Marl is at elevations ranging from 126.2 ft msl to 136.8 ft msl in the vicinity of Unit 3 and from 121.9 to 138.2 ft msl in the vicinity of Unit 4 (Figure 2.5-250). In general, the top of the Blue Bluff Marl is located at elevations above 130 ft msl east of a monoclinical fold that downwarps the Blue Bluff Marl toward the northwest to elevations lower than 100 ft msl. This feature is shown on the structure contour map (Figure 2.5-250) and on the geologic cross sections A-A' and B-B' (Figures 2.5-249, 2.5-251, and 2.5-252) and was formed by reverse faulting along the Pen Branch fault (Subsection 2.5.1.2.4.1). The cross sections illustrate the geology beneath the nuclear islands and the monocline appears as a subtle downwarp at the top of the Blue Bluff Marl. Cross section C-C' trends to the northeast from Unit 3 (Figure 2.5-253); east of and generally parallel to the monocline.

Where fully penetrated by 85 borings, the marl thickness ranges from a minimum of 5 feet where it has been scoured by the Savannah River and overlain with alluvium (Boring B-1159) to a maximum of approximately 95 ft (Boring B-1004). The mean thickness of the marl is approximately 63 ft. An isopach map of the Blue Bluff Marl indicates that it is more than 60 ft thick at the locations of Units 3 and 4 (Figure 2.5-254).

In boring B-1003, the base of the Lisbon Formation is noted at a depth of 149 ft (74 ft msl) and the top at a depth of 86 ft (137 ft msl), with an overall thickness of 63 ft (Figure 2.5-241). The base of the Lisbon Formation is marked by the occurrence of a 12 ft-thick greenish gray, sandy non-plastic silt with fossil fragments and 1- to 3-in thick layers of fossiliferous limestone. This is overlain by a 23-ft thick layer of greenish gray highly plastic sandy silt with fossil fragments and 1- to 3-inch layers of hard fossiliferous limestone. This in turn is overlain by greenish gray well-sorted, strongly cemented sand with 1- to 2-inch layers of hard fossiliferous limestone. This is overlain by a light greenish gray fossiliferous limestone. The top of the Lisbon Formation is marked by the occurrence of dark green-gray non-plastic calcareous sandy silt (Blue Bluff Marl). The marl contains 2- to 4-in-thick layers of hard fossiliferous limestone.

Barnwell Group

The Barnwell Group overlying the Blue Bluff Marl member includes three subdivisions, from oldest to youngest, the Clinchfield Formation (including the Utley Limestone member), Dry Branch Formation, and the Tobacco Road Sand. Due to the location and surface elevation of boring B-1003, the portion of the Barnwell Group penetrated by boring B-1003 includes only the Clinchfield Formation and lower portion of the Dry Branch Formation. However, most of these units are exposed along the bluffs of the Savannah River or within stream valleys, or lie on topographically higher areas within the site and site vicinity (Figures 2.5-231 and 2.5-234). The Formations described below are logged as undifferentiated sands, clays, and silts of the Barnwell Group in the ESP and COL borings (Appendices 2.5A and 2.5C). The thickness of this group is variable and ranges from approximately 26 to 162 ft in borings where the undifferentiated sediments of the Barnwell Group are fully penetrated.

Clinchfield Formation

In Boring B-1003 the base of the Clinchfield Formation (Utley Limestone member) occurs at a depth of 88 ft (130 ft msl) and the top at a depth of 74 ft (144 ft msl), with an overall thickness of 14 ft (Figure 2.5-241). The thickness of this unit was noted as variable within the VEGP Units 1 and 2 excavation, which is consistent with dissolution of carbonate material. Based on observations during the COL subsurface investigation, identification of the Utley Limestone member in ESP drill holes was re-evaluated on the basis of descriptions in Huddlestun and Summerour (1996), additional samples obtained during the COL investigation and on field observations of outcrops along the Savannah River. Where observed in the excavations for VEGP Units 1 and 2, the Utley Limestone Member of the Clinchfield Formation is recognized as fossiliferous limestone that grades into coquina. The Utley Limestone contains minor amounts of silt and clay. Larger fossils visible in outcrop include oyster shells, unidentified shell fragments and phosphatic mineral fragments. Well-cemented zones consist of quartz sand and/or shell fragments with a carbonate cement matrix. Based on the ESP and COL data set, where well-indurated, as indicated by high blow counts during split-barrel sampling and generally low recovery, the indurated Utley breaks down into gravel-size particles with varying amounts of silt and clay. This unit contains softer zones and areas in which drilling fluid circulation was lost (Appendices 2.5A and 2.5C).

As discussed in Subsection 2.4.12.1.2, the Utley Limestone is discontinuous across the site. It is absent in 54 of the 152 borings drilled through the stratigraphic interval where this unit was expected to occur (Table 2.4-253). This variation in thickness is shown on the geologic cross sections (Figures 2.5-251, 2.5-252, and 2.5-253) and on the structure contour and isopach maps (Figures 2.5-255 and 2.5-256). As discussed in Subsection 2.5.1, all geologic units overlying the Blue

Bluff Marl will be excavated from the nuclear island foundation. The isopach map indicates that the Utley Limestone is irregularly present in the area of Units 3 and 4 (Figure 2.5-256) where it ranges in thickness from 0 to 25 ft (Boring B-3039) at Unit 3 and 0 to 15 ft (Boring 4020) at Unit 4. Based on the borings that fully penetrated the Utley Limestone, its mean thickness is 10.5 ft. The Utley Limestone also tends to be present to the north of the nuclear islands and south towards the Units 3 and 4 cooling towers. The structure contour map indicates that the limestone is a linear feature in its areal extent with the axis of maximum thickness extending approximately north-northeast from the Units 3 and 4 cooling towers to approximately 1200 feet east of Mallard Pond (Subsection 2.4.12).

The average elevation of the top of the Utley Limestone is 142.4 ft msl at Units 3 and 4 (Figure 2.5-255). This is the approximate elevation of the base of the overlying undifferentiated Barnwell Group. The Clinchfield Formation consists predominantly of calcareous sands and biomoldic limestones. Some silty and clayey sands are also present, with varying amounts of carbonate material and silicified zones.

Exposures of the Clinchfield Formation along the Savannah River and within excavations for VEGP Units 1 and 2 noted varying degrees of weathering and evidence of solution cavities, indicating that the process of carbonate removal is ongoing. This process could be a primary contributing factor to the development of surface depressions noted in the site area.

Dry Branch Formation

In boring B-1003, the Dry Branch Formation overlying the Clinchfield Formation contains more clayey, laminated sands and silty sands. The base was logged at a depth of 74 ft (144 ft msl) and this unit occurs at the ground surface. The Dry Branch Formation consists primarily of silty, clayey quartz sands. Varying amounts of carbonate material are sometimes present, often in the form of bioherms. The sands are generally moderately to well-sorted and subrounded to subangular. Lignite and manganese staining is often present, with a notable lack of glauconite. Portions of the Dry Branch Formation become significantly more clayey, with finely laminated beds reaching thicknesses of several to tens of feet. The lithology, absence of glauconite, and inclusion of bioherms indicate a back barrier depositional setting.

Tobacco Road Sand

The Tobacco Road Sand consists of moderately to poorly-sorted sands and clayey sands with varying amounts of kaolin. Sands tend to be subrounded to rounded, with coarse rounded pebbly zones present as a basal lag in some areas. Where this unit is exposed, the sediments are oxidized and, in many cases, Ophiomorpha burrows are present, as well as cross-beds and convoluted bedding indicative of an open bay, tidal flat setting.

Boring B-1003 did not penetrate this unit due to the surface elevation surrounding the boring location; however, the unit is exposed in stream valleys and road cuts within the site area and vicinity. The thickness of the Tobacco Road Sand varies due to incision by the overlying Hawthorne Formation but can be in excess of 50 ft. Where present at the VEGP site, the top of the Tobacco Road Sand generally occurs at the ground surface.

Hawthorne Formation

The Hawthorne Formation consists of poorly-sorted sands and clayey sands. Sands range from fine to coarse and are well rounded. Clay is present in the form of laminae to cobble-size clasts. This unit was not identified in any of the borings drilled as part of the ESP subsurface investigation program. It was likely removed during excavation for the existing units and, therefore, is no longer present in the developed portions of the VEGP site. However, it is present in higher elevations of the site area. Obvious incision and cross-cutting channels are noted in exposures, with channel sequences often indicated by coarse channel lags indicative of a high energy fluvial setting. The age of the Hawthorne

Formation is problematic due to the lack of fossils. However, Falls and Prowell (2001) indicate a Miocene age for this formation.

Pinehurst Formation

The Pinehurst Formation was not mapped by the USGS, nor is it considered to be a significant stratigraphic unit regionally. The Pinehurst Formation is encountered sporadically within the site area and at the VEGP site. Where preserved, the Pinehurst Formation is less than a few meters thick, and therefore does not appear on geologic maps of the VEGP site. The unit is typically clean, well-sorted fine sand. Although bedding is often absent, cross-bedding and remnant dune morphology have been noted in a few exposures, indicative of an eolian deposit ([Reference 412](#)).

Although the age of these sediments is not definitive, the unconformable position above the Hawthorne and lack of these sediments overlying Late Pliocene marine sediments down-dip of the site area place the relative age as lower Pliocene ([Reference 412](#)).

Quaternary Stratigraphy

Alluvium exists within the surrounding stream and river valleys and forms terraces that can be locally delineated and mapped. As noted on [Figures 2.5-232](#) and [2.5-234](#), in the vicinity of the site area, a modern alluvial flood plain and several alluvial terraces are present on the east side of the Savannah River. The higher terraces show distinctive oxidation and weathering, and the relative position above the Holocene flood plain indicates a Pleistocene age ([Reference 412](#)). Quaternary deposits are discussed in [Subsections 2.5.1.1.3.5](#) and [2.5.1.2.4.3](#).

2.5.1.2.4 Site Area Structural Geology

In the site vicinity, the basement rock beneath the Coastal Plain consists of Paleozoic crystalline rock as well as Triassic–Jurassic sedimentary rock of the Dunbarton Basin. The VEGP site lies near the buried northwest margin of the approximately 9-mi-wide (15-km-wide) Dunbarton Basin, which formed during Mesozoic rifting and opening of the Atlantic Ocean. Deep boreholes within and adjacent to the SRS that penetrate basement indicate that the Paleozoic crystalline rock northwest of the Dunbarton basement has been overprinted with a foliation that dips about 40 to 60 degrees. Based on regional correlations, the foliation strikes northeast and dips to the southeast ([Reference 263](#)).

The upper surface of the basement has been leveled by erosion and dips to the southeast between 48 ft/mi ([Reference 442](#)) and 37 ft/mi ([Reference 488](#)). In the site area, the regional basement surface is unconformably overlain by loosely consolidated, fluvial, deltaic, and shallow marine Coastal Plain sediments. The depth to the Triassic–Jurassic basement rock beneath the site is 1,049 ft (-826 ft msl), based on borehole B-1003.

Within the 5-mi site area radius, a total of four basement-involved faults have been identified, namely the Pen Branch, Ellenton, Steel Creek, and Upper Three Runs faults ([Figure 2.5-224](#)). The Ellenton fault does not appear in the most recent SRS fault maps ([Reference 254](#), [Reference 255](#)) and, if it exists, is not considered a capable structure. The Upper Three Runs fault is restricted to basement rocks, with no evidence that it offsets Coastal Plain sediments ([Reference 232](#); [Reference 453](#)). Similarly, the Steel Creek fault is not considered a capable tectonic source. The Pen Branch fault is thought to have been the northern bounding (normal) fault of the Mesozoic Dunbarton extensional basin, subsequently reactivated as a reverse or reverse-dextral slip fault, as documented by post-extension, reverse offsets of Late Cretaceous and younger horizons ([Reference 442](#); [Reference 254](#), [Reference 255](#)). The Pen Branch fault is discussed in detail below.

Only one fold potentially of tectonic origin has been identified in the site area. Bechtel site drawings AX6DD377 (“Top of the bearing horizon”) and AX6DD378 (“Bottom of the bearing horizon”) show an

apparent monoclinial flexure of the Blue Bluff Marl, with a hingeline that trends approximately northeast-southwest (Figure 2.5-242). Because of its spatial association with the Pen Branch fault, it is likely that this feature is the result of reverse or reverse-oblique slip on the Pen Branch fault. In previous studies [e.g., (Reference 212)], this monocline has been referred to as a 3° dip reversal and interpreted to be of sedimentary origin.

2.5.1.2.4.1 Pen Branch Fault

The Pen Branch fault is neither exposed nor expressed at the surface at the SRS, but its location at the SRS is constrained by dense subsurface well control, as well as seismic-reflection geophysical data [e.g., (Reference 442; Reference 453; Reference 321; Reference 254, Reference 255)]. The Pen Branch exceeds 25 mi in length and is interpreted to comprise several subparallel segments that strike N46-66°E and dip 60-75°SE (Reference 255) and is projected southwestward from SRS to beneath the VEGP site. Crone and Wheeler (2000) assigned the Pen Branch fault to Class C because of the lack of evidence for post-Eocene slip. Due to its proximity to the VEGP site, however, the Pen Branch fault is examined in detail in this SSAR.

The Pen Branch fault was first discovered in the subsurface of the SRS in 1989 from the interpretation of earlier seismic reflection surveys and other geologic studies (Reference 374; Reference 232; Reference 442; Reference 454). A brief history of the Pen Branch fault and issues concerning the VEGP site and the NRC are as follows:

- January 8, 1989: Draft report on newly discovered Pen Branch fault issued by David Snipes (Clemson University), Wallace Fallaw (Furman University), and Van Price, Jr. (SRS). This report (Reference 441) was provided to the NRC, which received it on January 12, 1989. The authors presented evidence of late Eocene movement, but emphasized “compelling evidence for absence of recent movement” and that the fault should not be assumed to be capable. The nearest seismic line data were located about 7 mi east of the VEGP site. This draft report also projected the fault toward the VEGP site based on an interpreted offset of Utley Limestone outcrop located near the existing VEGP intake structure and the dip reversal in the Blue Bluff Marl (Figure 2.5-237).
- January 18, 1989: The NRC formally requested the Georgia Power Company to assess capability and impact of the proposed Pen Branch fault on the VEGP site. Southern Company assembled a field review team to review field conditions within and nearby the VEGP site.
- January 29, 1989: Bechtel submitted a response to the NRC.
- February 1989: The NRC issued Supplement No. 8 to the VEGP Units 1 and 2 SER. The NRC concluded that the Pen Branch fault is not capable and that there was no evidence that suggested Tertiary offset on the Pen Branch fault within 6 mi northeast of the VEGP site.
- September 1989: Bechtel issued the Pen Branch fault report (Reference 212) that summarized work performed for the January 29, 1989, response to the NRC.
- 1991: A high-resolution shallow seismic reflection survey focused on the uppermost 300 ft of Coastal Plain strata at the SRS conducted by Berkman (1991) was designed to investigate the capability of the Pen Branch fault (Figure 2.5-237). Deformation associated with the Pen Branch fault was observed in the Cretaceous Cape Fear Formation but no higher in the stratigraphic section, confirming the non-capable status of the Pen Branch fault.
- October 1993: Snipes et al. (1993a) concluded that the Pen Branch fault must lie more than 2 mi upstream from the VEGP site, based on SRS borehole PBF-6 (which encountered sheared Triassic basin sediments) (Figure 2.5-237).

- 1993: Savannah River fluvial terrace study ([Reference 292](#)) concluded that the Pen Branch fault has no geomorphic expression, no tectonic deformation is observed within a resolution of approximately 7 to 10 ft, and the Pen Branch fault is not capable.
- 1994: The Confirmatory Drilling Project was designed to investigate the capability of the Pen Branch fault at the SRS ([Reference 454](#)). This report combined previous data with 18 borings to conclude that deformation associated with the Pen Branch fault likely pre-dates the Williamsburg Unconformity (about 50 Ma) and that the Pen Branch fault is therefore not capable.
- 1995: As part of a groundwater contamination study in Burke County, Georgia, Henry (1995) collected and interpreted a total of 70 mi of high-resolution seismic reflection data from the Savannah River between the Richmond/Burke county line and the Burke/Screven county line. In addition, a medium-resolution seismic survey was conducted in the Savannah River between Hancock Landing and the VEGP boat ramp ([Figure 2.5-237](#)). Henry (1995) concluded that the Pen Branch fault appears as a high-angle, southeast-side-up reverse fault located about 1,000 ft downstream from Hancock Landing. Henry (1995) interpreted the Pen Branch fault as extending upward through the Paleocene Ellenton Formation and into strata dated as possible Eocene that lie below the unconformity at the base of Savannah River alluvium.
- 1998: As part of an investigation of tritium in the Gordon Aquifer and other aquifers in Burke County, Georgia, Summerour et al. (1998) reported seismic reflection data collected and interpreted by Waddell et al. (1995). This land-based seismic reflection survey was located on an unimproved road about 0.5 mi west of River Road ([Figure 2.5-237](#)). Numerous, minor faults were interpreted to cut reflectors within the Coastal Plain section. The basement reflector, however, is not clearly faulted and, therefore, the interpretation that the Pen Branch fault is imaged in this profile ([Reference 455](#)) is questionable. Based in part on the Waddell et al. (1995) seismic reflection data, Summerour et al. (1998) reported that the Gordon Aquifer is not affected by Pen Branch fault.
- 1998: Cumbest et al. (1998) integrated more than 60 basement borings and 100 mi of seismic reflection profiling to refine the location of the Pen Branch fault at the SRS. Based on their review of existing data, Cumbest et al. (1998) concluded that no faults on the SRS, including the Pen Branch fault, are capable.
- 2000: Based on geometrical analysis of seismic reflection data, the maximum vertical separation of the contact between basement rocks and overlying Coastal Plain sediments by the Pen Branch fault (segment 4) is estimated to be about 92 ft ([Reference 255](#)). The offset decreases upward within the Coastal Plain section to 30 ft at the top of the Upper Cretaceous/Lower Paleocene Pee Dee/Ellenton formation (approximately 66.4 Ma) ([Reference 255](#)).

2.5.1.2.4.2 Site Subsurface Investigation of the Pen Branch Fault

The Pen Branch fault, which juxtaposes Paleozoic crystalline rock against Triassic (Dunbarton) Basin sedimentary rock at the SRS, has been interpreted to project southwestward into Georgia near the VEGP site. Past interpretations have projected the fault and basin boundary at VEGP site ([Reference 441](#)), north of the VEGP site ([Reference 442](#)), and south of VEGP ([Reference 254](#); [Reference 255](#)). These and all other available data on the location of the fault were compiled and assessed for this ESP investigation. The study concluded that the Pen Branch fault is located in proximity to the VEGP site.

The seismic acquisition program was designed to image the subsurface structure and characterize the basement lithology and velocities beneath the VEGP site as input to the development of the Safe Shutdown Earthquake (SSE). An additional, specific goal of this study was to image the northeast-striking, non-capable Pen Branch fault, which has been imaged and mapped on the SRS northeast of the VEGP site [e.g., (Reference 255)], and determine its precise location, strike, and dip beneath the VEGP site.

Seismic reflection and refraction data were collected within the VEGP site area in January and February 2006. The seismic data were acquired by Bay Geophysical under contract to Southern Nuclear Operating Company (SNC); details of the acquisition and preliminary processing of the data are fully documented in the final technical report (Appendix 2.5B). The survey included four seismic reflection and three seismic refraction lines (Figures 2.5-238 and 2.5-239, respectively). The seismic array was designed to: (1) image the Pen Branch fault, with the assumption that it continues on strike to the southwest from the SRS into the VEGP site area and (2) assess the depth and character of the basement rocks beneath the Atlantic Coastal Plain deposits.

As noted in the report by Bay Geophysical (Appendix 2.5B), vibrations from the existing VEGP generated coherent noise that significantly compromised the quality of the seismic data for lines 1, 2, and 3. The noise masked the first arrivals along most or substantial parts of these three lines, which made it impossible to apply refraction static corrections to the reflection data. Consequently, these lines have anomalies in the reflector geometries that arise from the lack of a proper static solution rather than real earth structure, making detailed geologic interpretation of these lines problematic. Similarly, masking of refractor first breaks by noise from the existing VEGP on lines 1 and 3 made it impossible to confidently and accurately pick the first arrivals for use in 2-D P-wave velocity inversions (Appendix 2.5B). Based on a field assessment of the quality of the refraction data for lines 1 and 3 by Dr. Cumbest, SNC decided not to collect refraction data along line 2, as initially planned.

Reflection and refraction data from line 4 were not affected by noise problems from the existing VEGP. Consequently, line 4 has greater detail than the other three lines in the seismic survey (Figure 2.5-240).

Strike of the Pen Branch Fault

The seismic reflection data acquired for this ESP study clearly document that the Pen Branch fault strikes northeast and dips southeast beneath the VEGP site. When the intersections of the Pen Branch fault with the top of basement interpreted from reflection data are plotted on a map, it is apparent that the strike of the fault through the VEGP site is not uniform. The fault-basement intersections on lines 1, 2, and 3 fall along a common trend of about N34°E. In contrast, the fault-basement intersections on lines 4 and 1 define a more westerly trend of about N45°E (Figures 2.5-242 and 2.5-245). Although it is possible that uncertainty in picking the fault-basement intersection on the eastern three lines (especially lines 1 and 2) may account for some of the difference in strike across the plant site, the different strike east and west of line 2 is likely real for the following reasons:

- The fault and basement offset are best imaged and most confidently interpreted on lines 1 and 4. Thus, the N45°E strike of the fault determined between these two lines is likely accurate.
- The trends of the structure contours on the monoclinally folded Blue Bluff Marl beneath the VEGP site range from about N25°E to N40°E and are similar to the N34°E strike of the fault measured between lines 1, 2, and 3 (Figure 2.5-242). Most kinematic models of fault-related folding assume that the axes of fault-propagation folds and monoclines are parallel to the strike of an underlying thrust or reverse fault [e.g., (Reference 456; Reference 384)]. If these assumptions are correct, then the strike of the fault beneath the monocline is closer to N32°E, as inferred from seismic lines 1, 2, and 3, than to N45°E.

- Cumbest et al. (2000) have documented that the strike of the Pen Branch fault is not constant beneath the SRS northeast of the VEGP site. They found that the fault consists of several discrete reaches or segments variously separated by small offsets and changes in strike. The range in strike of the fault northeast of Savannah River is about N46°E to N66°E (Reference 255).

The change in strike of the Pen Branch fault across the VEGP site may be part of a regional trend. On the SRS northeast of VEGP, the Pen Branch fault includes a distinct reach that strikes about N58°E between seismic lines SRL-7 and PBF-2A and another distinct reach that strike about N53°E between seismic line PBF-2A and point in the Savannah River channel where the fault was imaged by Henry (1995), representing a counterclockwise rotation in strike from northeast to southwest. Southwest of the Savannah River, the fault strike rotates counterclockwise again to about N34°E beneath the VEGP site. The strike of the fault rotates clockwise to about N45°E between seismic lines 1 and 4. The overall trend is a bend or left jog in the strike of the fault. It is possible that the changes in strike between individual reaches of the fault also include small offsets of the fault plane, as inferred for the fault on the SRS to the north (Reference 255).

Dip of the Pen Branch Fault

The dip of the Pen Branch fault is estimated primarily from its expression in the version of seismic line 4 displayed at a constant velocity of 12,000 ft/s (Figure 2.5-240). Based on measurements of P-wave velocities for Triassic basin rocks in boreholes throughout the region (Reference 232), 12,000 ft/s probably best characterizes the average velocity of the Triassic rocks in the hanging wall of the Pen Branch fault along line 4. The dip of the Pen Branch fault reflector in the version of line 4 displayed at a velocity of 12,000 ft/s is about 40° (Figure 2.5-240).

The geometry of the fault in line 4 reflects an apparent dip because the seismic line is not perpendicular to the fault. The general trend of the section of line 4 corresponding to the well-imaged fault plane (i.e., between shotpoints 225 and 310) intersects the N45°E strike of the fault at an angle of about 55°. Using the apparent dip relation [(Reference 379), equation 3-7] to account for the obliquity of the seismic line relative to fault strike, a true dip of about 45° to the southeast is derived for the fault plane imaged on line 4 in Figure 2.5-243.

Fault-Fold Relationships

The plan projection of the intersection of the Pen Branch fault with the top of basement on lines in the seismic reflection array is located beneath or slightly to the southeast of the antiformal hinge at the top of the monocline in the Blue Bluff Marl (Figure 2.5-242). This relationship is shown more directly by two geologic cross sections that pass through borehole B-1003 (Figures 2.5-243 and 2.5-244).

The northwest-southeast cross section (Figure 2.5-243) is oriented perpendicular to the local strike of the Pen Branch fault and displays the fault and its relationship to the monoclinical fold in the Blue Bluff Marl with a minimum of geometric distortion. The plan projection of the offset of the basement surface is located about 100 ft northwest of the upper axial hinge of the monocline (Figure 2.5-242). The projection of the fault beyond its termination in the Cretaceous Coastal Plain deposits approximately intersects the synformal hinge at the base of the monocline in the marl (Figure 2.5-243). The east-west cross section (Figure 2.5-244) is oriented to pass through the locations of boreholes B-1002, B-1003, and B-1004; because the section is oblique rather than perpendicular to the fault and monocline, the geometry of the structures is slightly distorted. In particular, the apparent dip of the fault in the east-west section (35°; Figure 2.5-244) is lower than the true dip (about 45°) in the northwest-southeast section (Figure 2.5-243). Although the base of the monocline in the marl is poorly constrained by available borehole data at the west end of the east-west cross section, the Pen Branch fault appears to project toward the base of the fold (Figure 2.5-243).

2.5.1.2.4.3 Evaluation of Quaternary River Terrace Overlying Pen Branch Fault

The seismic reflection profiles and deep borehole (B-1003) performed at the VEGP site as part of the ESP study helped refine the location of the Pen Branch fault in Georgia and in the westernmost portion of the SRS in South Carolina. These new data combined with reflection profiles in the Savannah River (Reference 321) and earlier SRS studies were integrated to develop a more accurate representation of the fault's location and geometry beneath the VEGP site and Quaternary terraces flanking the Savannah River on the SRS (Figure 2.5-237). Previous geomorphic study of the fluvial terraces by Geomatrix (1993) concluded that the Pen Branch fault is not a capable tectonic source and that there is no observable deformation within a resolution of 7 to 10 ft, in the overlying Ellenton Terrace (Qte) surface estimated to be 350 ka to 1 Ma. The 10-ft contour interval of the USGS 7.5-minute topographic maps limited the resolution of this previous study.

Given the higher degree of confidence in the location of the Pen Branch fault beneath the Savannah River fluvial terraces, which represent the only significant Quaternary deposits and surfaces that straddle the Pen Branch fault, a focused study was undertaken to survey and interpret remnants of the Ellenton Terrace (Qte) surface located approximately 4 miles east-northeast of the VEGP site (Figure 2.5-212 and Figure 2.5-246). The purpose of this effort was to improve the resolution of the terrace surface elevation and independently assess the presence or absence of Quaternary tectonic deformation on the Pen Branch fault, which has been classified by Crone and Wheeler (2000) as a potential Quaternary fault having insufficient geologic evidence to demonstrate Quaternary slip or deformation (Class C in Table 2.5-201).

The scope of this investigation included a review of previous studies, as well as geomorphic mapping, analysis of aerial photographs, surveying the portion of the Qte terrace surface at the SRS that overlies the Pen Branch fault, and the construction and analysis of longitudinal terrace profiles.

Geomorphic mapping and field reconnaissance

Prior to surveying the study area to acquire elevation data, a geomorphic map of the Qte terrace surface at the SRS in the vicinity of the Pen Branch fault was prepared in order to establish geologic context, to ground-truth and refine the mapping of Geomatrix (1993), and to investigate the degree of erosion and/or anthropogenic disturbance of the terrace surface. The primary focus of the geomorphic mapping was to define the portions of the Qte surface that appear best preserved (minimal deflation and modification) (Figure 2.5-247). Preparation of this map included inspection of aerial photographs dating from 1943 to 2004, field reconnaissance, and hand-auger soil borings. A review of multiple sets of aerial photography reveals the presence of several closed depressions (of variable size), marshy areas, and tributary drainages in the study area (Figure 2.5-247). The aerial photographs also show that the study area was farmland at least as early as 1943. Today the study area is crossed by an SRS power line right-of-way and several dirt roads, and timber has been sporadically logged from portions of the study area over the past few decades.

Survey data acquisition

A total of approximately 2,600 elevation data points were collected by a Georgia Power Company survey team using a combination of differential Global Positioning System (DGPS) and total station survey techniques. Survey data were collected in UTM zone 17N coordinates, using NAD 27 geographic datum and NAVD 88 elevation datum.

The preponderance of survey data was collected from, and adjacent to, dirt roads and the power line right-of-way (Figures 2.5-246 and 2.5-247). The Qte terrace surface in the vicinity of the Pen Branch fault on the SRS is largely covered by trees and dense undergrowth. This dense vegetative cover hinders the acquisition of survey data. Fortunately, a power line right-of-way oriented approximately normal to the local strike of the Pen Branch fault and approximately parallel to the long-axis of the Qte terrace deposits extends through the study area. As much as possible, survey data were

collected away from obviously disturbed, eroded, and/or modified areas as identified by geologic reconnaissance and aerial photograph interpretation.

Terrace surface longitudinal profiles

A longitudinal profile of the Qte terrace surface was constructed by projecting elevation data onto a profile line oriented approximately N35°W (approximately normal to the local strike of the Pen Branch fault and approximately parallel to the long-axis of the Qte terrace and paleo-Savannah River valley in the study area) (Figures 2.5-246 and 2.5-247). Data points interpreted as representing the best-preserved remnants of the Qte terrace surface (as determined from field reconnaissance and aerial photograph inspection) are shown on the longitudinal profile in red (Figure 2.5-248). Data points interpreted as representing more modified or eroded portions of Qte terrace surface and those points collected away from the Qte terrace surface are shown on the longitudinal profile in gray.

Sources of error/uncertainty

There are three main sources of uncertainty and error that contribute to the overall uncertainty in the original elevation and variability of the Qte terrace surface. Each of these is discussed below:

Geologic context – The largest contributor to the overall uncertainty in characterizing the Qte terrace surface elevation is due to ambiguities regarding geologic and geomorphic context. The Qte terrace surface was initially deposited as a planar feature with some inherent variability. Since the river abandoned this surface 350 ka to 1 Ma, however, the Qte surface has been modified by geologic and anthropogenic processes. Geologic processes of deposition, erosion, and settlement resulting from dissolution of the underlying carbonate sands have all contributed to the modification the original surface. Significant deflation of the surface has occurred as a result of dissolution collapse as evidenced from the abundant closed depressions across the Qte and younger Qtb terrace surfaces (Figures 2.5-232 and 2.5-248). Incision of tributary drainages into the terrace have locally removed the deposits and surface as well as the deflated adjacent portions of the surface. Deposition of alluvial and colluvial material onto the eastern margin of the Qte terrace near the mouth of Fourmile Branch and along the base of the southwest-facing slopes has locally increased the ground surface elevation. Anthropogenic processes that have modified the original terrace surface, to a much lesser extent, include agricultural land use practices (logging and farming) and other human activities related to development of the SRS. A primary focus of this study was to define those portions of the Qte terrace surface that best preserved remnants of the original terrace (least modified) and to resolve the magnitude of the scatter in elevation data. Any remaining perturbations, if any, in the overall Qte terrace surface that cannot be explained by erosion, settlement, deposition, and/or anthropogenic modification can be considered to be of possible tectonic origin.

Survey error – The uncertainty due to both systematic and random errors associated with the collection and processing of survey data is estimated to be about 3 cm (about 1.2 inches) in the horizontal dimension and about 5 cm (about 2 inches) in the vertical dimension. The contribution of survey error to overall uncertainty is considered to be negligible.

Profile construction error – The projection of elevation data onto profile line A-A' (Figure 2.5-248) introduces a minimal amount of error into the analysis. The magnitude of the positional error resulting from profile construction is minimized by minimizing the distance over which points are projected, and by constructing the profile approximately parallel to the long-axis of the Qte terrace surface in the study area and approximately normal to the local strike of the Pen Branch fault. The amount of error introduced into this analysis from the construction of the longitudinal profile is minimal.

Results

The geomorphic map presented in Figure 2.5-247 shows the best-preserved remnants of the Qte terrace surface in the study area (red shaded areas). The influence of dissolution collapse-related depressions on the terrace surface is most clearly seen in the vicinity of depressions D1 and D2, as

short-wavelength variations in the topographic surface. In addition, portions of the Qte terrace surface have been sites for the local deposition of alluvium and colluvium. These two areas are located at the northwestern-most extent of the survey and southeast of depression D2 (Figure 2.5-248).

Taken together, the overall uncertainty in the elevation of the best-preserved remnants of the Qte terrace surface is estimated to be about 3 ft. As shown in Figure 2.5-248, the elevation data for the terrace remnant range between elevations of 153 and 156 ft.

Longitudinal profile A-A' (Figure 2.5-248) indicates about 25 ft of variability in the present topography of the Qte terrace deposit in the study area. Most of this variability is the result of erosion and deflation of the terrace surface.

A longitudinal profile of the Qte fluvial terrace surface in the study area provides evidence demonstrating the absence of discernible tectonic deformation due to the underlying Pen Branch fault within the limit of resolution of the terrace elevation data (Figure 2.5-248). The results of this study demonstrate a lack of tectonic deformation in the 350 ka to 1 Ma year old fluvial terrace surface within a resolution of about 3 ft. This observation is consistent with previous studies at both the VEGP site and the SRS that have concluded the Pen Branch fault is not a capable tectonic source.

2.5.1.2.5 Site Area Geologic Hazard Evaluation

No geologic hazards have been identified within the VEGP site area. Surface depressions associated with dissolution of carbonate bearing stratum of the Utley member of the Clinchfield Formation are discussed in Subsections 2.5.1.2.3.2 and 2.5.3.8.2.1 and do not affect the foundation-bearing layer (Blue Bluff Marl). However, structures founded above the Blue Bluff Marl will require subsurface exploration to identify low-bearing-strength layers associated with dissolution processes noted in the site area.

2.5.1.2.6 Site Engineering Geology Evaluation

2.5.1.2.6.1 Engineering Soil Properties and Behavior of Foundation Materials

Engineering soil properties, including index properties, static and dynamic strength, and compressibility are discussed in Subsection 2.5.1. Variability and distribution of properties for the foundation bearing layer will be evaluated and mapped as the excavation is completed.

Heave monitor installation will be required prior to excavation, and settlement monitoring will be required during and post construction. Heave measurements will be used to quantify recompression during reloading to measure actual net settlements.

2.5.1.2.6.2 Zones of Alteration, Weathering, and Structural Weakness

The Blue Bluff Marl will form the foundation-bearing layer and consists of unweathered, slightly lithified, micritic limestone. Some desiccation is expected; however, visual examination of the exposure will be required, and long-term exposure may require a thin application of shotcrete for protection. Any noted desiccation, weathered zones, joints, or fractures will be mapped and evaluated.

2.5.1.2.6.3 Deformational Zones

No deformational zones within the Blue Bluff Marl were reported from the detailed excavation mapping for VEGP. However, proximity of the Pen Branch fault to the VEGP site (Figures 2.5-237 and 2.5-245) may have produced deformational features during development of the anticlinal

structure described in [Subsection 2.5.1.2.4.1](#). However, these features, if present, are not expected to compromise the foundation-bearing capacity. Excavation mapping will be required during construction, and any noted deformational zones will be evaluated.

2.5.1.2.6.4 Prior Earthquake Effects

Extensive studies of outcrops and alluvial terrace and flood plain deposits have not indicated any evidence for post-Miocene earthquake activity, as discussed in [Subsection 2.5.1.2.4](#).

2.5.1.2.6.5 Effects of Human Activities

No mining operations (other than borrow of surficial soils), excessive extraction or injection of groundwater, or impoundment of water has occurred within the site area that can affect geologic conditions.

2.5.1.2.7 Site Groundwater Conditions

A detailed discussion of groundwater conditions is provided in [Subsection 2.4.12](#).

2.5.2 Vibratory Ground Motion

The AP1000 is designed for an earthquake defined by a peak ground acceleration (PGA) of 0.30g and the design response spectra specified in [Subsection 3.7.1.1](#), and [Figures 3.7.1-1](#) and [3.7.1-2](#). The AP1000 design earthquake is referred to as the AP1000 Certified Seismic Design Response Spectra (CSDRS). The AP1000 CSDRS was developed using the Regulatory Guide 1.60 response spectra as the base and modified to include additional high frequency amplification at a control point at 25 Hz. The peak ground accelerations in the two horizontal and the vertical directions are equal. The CSDRS also represents the AP1000 Foundation Input Response Spectra (FIRS) at a hard rock site.

The AP1000 is evaluated for high frequency input using the response spectra specified in [Appendix 3I](#), [Figures 3I.1-1](#) and [3I.1-2](#). The seismic response spectra given in [Figures 3I.1-1](#) and [3I.1-2](#) are envelope response spectra with high frequency content.

2D Analyses

Where features of the site are not within the parameters specified for the AP1000, site-specific soil structure interaction analyses may be performed using the 2D SASSI models described in [Appendix 3G](#) for variations in site conditions that can be represented in these models. Results should be compared to the results of the 2D SASSI analyses described in [Appendix 3G](#). Such analyses may be used to demonstrate that local features, such as soil degradation properties or backfill, are well within the bounds established by the design cases. If the results are not clearly enveloped at the significant frequencies of response at the six key locations compared with the floor response spectra of the certified design at 5-percent damping, then a 3D SASSI analysis may be required.

3D Analyses

If required, a 3D evaluation will consist of a site-specific dynamic analysis and generation of in-structure response spectra at six key locations to be compared with the floor response spectra of the certified design at 5-percent damping. The certified seismic site design response spectra at the foundation level in the free-field given in [Figures 3.7.1-1](#) and [3.7.1-2](#) were used to develop the floor response spectra. They were applied at foundation level for the hard rock site and at finished grade level for the soil sites. The site is acceptable if the floor response spectra from the site-specific evaluation do not exceed the AP1000 spectra for each of the locations identified below or the exceedances are justified:

Containment internal structures at elevation of reactor vessel support	Figure 3G.4-5X to 3G.4-5Z
Containment operating floor	Figure 3G.4-6X to 3G.4-6Z
Auxiliary building NE corner at elevation 116'-6"	Figure 3G.4-7X to 3G.4-7Z
Shield building at fuel building roof	Figure 3G.4-8X to 3G.4-8Z
Shield building roof	Figure 3G.4-9X to 3G.4-9Z
Steel containment vessel at polar crane support	Figure 3G.4-10X to 3G.4-10Z

Site-specific soil structure interaction analyses are performed using the 3D SASSI models described in [Appendix 3G](#). The site-specific soil structure interaction analyses use the site-specific soil conditions (including variation in soil properties in accordance with Standard Review Plan 3.7.2 and site-specific soil degradation models). The three components of the site-specific ground motion time history must satisfy the regulatory requirements for statistical independence and enveloping of the site design spectra at 5% damping. Floor response spectra determined from the site-specific analyses should be compared against the design basis of the AP1000 described above.

If the site-specific spectra at foundation level at a rock site exceed the response spectra in [Figures 3I.1-1 and 3I.1-2](#) at any frequency, a site-specific evaluation can be performed similar to that described in [Appendix 3I](#).

This section provides a detailed description of the vibratory ground motion assessment that was carried out for the VEGP ESP site resulting in the development of the VEGP ESP site Ground Motion Response Spectrum (GMRS). This assessment was performed to address seismic hazard update guidance in Regulatory Guide 1.165, Identification and Characterization of Seismic Sources and Determination of Safe Shutdown Earthquake Ground Motion, Rev. 0, March 1997 (RG 1.165), and meet the SSE requirements in paragraph (d) of 10CFR 100.23. The starting point for this site assessment is the EPRI-SOG probabilistic seismic hazard analysis (PSHA) evaluation ([Reference 514](#)).

[Subsection 2.5.1.2](#) through [Subsection 2.5.2.4](#) document the review and update of the available EPRI seismicity, seismic source, and ground motion models. [Subsection 2.5.2.5](#) summarizes information about the seismic wave transmission characteristics of the ESP site with reference to more detailed discussion of all engineering aspects of the subsurface in [Subsection 2.5.1](#).

[Subsection 2.5.2.6](#) describes the development of the horizontal GMRS for the VEGP ESP site. The selected ground motion is based on the risk-consistent/performance-based approach from NUREG/CR-6728 ([Reference 525](#)) and ASCE 43-05 ([Reference 494](#)). Site-specific horizontal ground motion amplification factors are developed using site-specific estimates of near-surface rock, soil, and engineered backfill properties. These amplification factors are then used to scale the hard rock spectra to develop Uniform Hazard Spectra (UHS) accounting for site-specific conditions using Approach 2A of NUREG/CR-6769. Horizontal GMRS spectra are developed from these ground surface Uniform Hazard Spectra (UHS) using the performance-based approach of ASCE 43-05. Companion outcrop motions are defined in [Subsection 2.5.2.6](#) for the highest competent in situ layer and at the depth of the bottom of the Nuclear Island basemat. The highest competent in situ layer is at the top of the Blue Bluff Marl, at a depth of 86 ft. The bottom of the Nuclear Island basemat is at a depth of 40 ft. See [Subsections 2.5.1](#) and [2.5.2.5](#) for further discussion of the subsurface conditions.

Ratios of vertical to horizontal motions appropriate to the site area are developed in [Subsection 2.5.2.7](#) and applied to the horizontal spectra to derive recommended vertical spectra.

The GMRS described in this section are considered performance goal-based (risk-informed) site-specific response spectra. The spectra at the top of the Blue Bluff Marl reflect the seismic hazard in terms of a PSHA and *in situ* geologic characteristics of the site. The spectra at the bottom of the Nuclear Island basemat are used to define the Foundation Input Response Spectra (FIRS) used to help confirm the adequacy of the Certified Seismic Design Response Spectra (CSDRS) design basis of the Nuclear Island.

The site-specific SSE motion of Section 3.7.1 of the COLA is consistent with the description of the free-field ground motion at the site provided in this [Subsection 2.5.2](#). The OBE is discussed in [Subsection 2.5.2.8](#).

Finally, two complementary sensitivity studies, incorporating information from supplemental site-specific subsurface investigations, are discussed in [Subsection 2.5.2.9](#).

2.5.2.1 Seismicity

The seismic hazard analysis conducted by EPRI (NP-6395-D 1989) relied on an analysis of historical seismicity in the Central and Eastern United States (CEUS) to estimate seismicity parameters (rates of activity and Richter b-values) for individual seismic sources. The historical earthquake catalog

used in the EPRI analysis was complete through 1984. The earthquake data for the site region occurring since 1984 was reviewed and used to update the EPRI catalog.

2.5.2.1.1 Regional Seismicity Catalog Used for 1989 EPRI Seismic Hazard Analysis Study

Many seismic networks record earthquakes in the CEUS. A large effort was made during the EPRI seismic hazard analysis study to combine available data on historical earthquakes and to develop a homogeneous earthquake catalog that contained all recorded earthquakes for the region.

“Homogeneous” means that estimates of body-wave magnitude, m_b , for all earthquakes are consistent, that duplicate earthquakes have been eliminated, that non-earthquakes (e.g., mine blasts and sonic booms) have been eliminated, and that significant events in the historical record have not been missed. Thus, the EPRI catalog (Reference 512) forms a strong basis on which to estimate seismicity parameters.

2.5.2.1.2 Updated Seismicity Data

NRC Regulatory Guide 1.165, Identification and Characterization of Seismic Sources and Determination of Safe Shutdown Earthquake Ground Motion, Revision 0, March 1997 (RG 1.165) specifies that earthquakes of Modified Mercalli Intensity (MMI) greater than or equal to IV or magnitude greater than or equal to 3.0 should be listed for seismic sources “any part of which is within a radius of 200 mile (320 km) of the site (the site region).” In updating the EPRI catalog a latitude-longitude window of 30° to 37° N, 78° to 86° W was used. This window incorporates the 200 mi (320 km) radius “site region” and all seismic sources contributing significantly to VEGP ESP site earthquake hazard. Figure 2.5-204 shows the VEGP ESP site and its associated site region. Figures 2.5-257 through 2.5-262 show this site region and the defined latitude-longitude window.

The updated catalog was compiled from the following sub-catalogs:

EPRI Catalog. The various data fields of the EPRI catalog are described in EPRI NP-4726-A 1988.

SEUSSN Catalog. The SEUSSN catalog is available from the Virginia Tech Seismological Observatory FTP site (Reference 535). On the June 3, 2005 date of the catalog update, the SEUSSN catalog had 2,483 records dating from March 1698 to December 2003 within the site region latitude-longitude window. Of these, 1,355 records occurred in 1985 or later.

ANSS Catalog. The ANSS catalog (Reference 493) was searched on June 3, 2005, for all records within the site region latitude-longitude window, resulting in 1,710 records from 1928 to April 14, 2005. Of these, 1,375 records occurred in 1985 or later.

The Southeastern US Seismic Network (SEUSSN) and Advanced National Seismic System (ANSS) catalogs were used for the temporal update (1985 to present) of the EPRI seismicity catalog. The SEUSSN has coverage over the entire site region (defined above) and is the primary catalog used to compile the national ANSS seismicity catalog. While the SEUSSN catalog is taken as the preferred catalog, some additional events listed only in the ANSS catalog are also included in the update.

The magnitudes given in both catalogs were converted to best or expected estimate of m_b magnitude ($E[m_b]$, also called Emb), using the conversion factors given as equation 4-1 and Table 4-1 in EPRI NP-4726-A 1988:

$$Emb = 0.253 + 0.907 \cdot Md \quad (\text{Equation 2.5.2-1})$$

$$Emb = 0.655 + 0.812 \cdot ML \quad (\text{Equation 2.5.2-2})$$

where Md is duration or coda magnitude and ML is “local” magnitude.

Equation 4-2 of EPRI (NP-4726-A 1988) indicates that the equation from which m_b^* or Rmb is estimated from the best estimate of magnitude $E[m_b]$ or Emb and the variance of m_b , σ_{mb}^2 , or Smb^2 is :

$$m_b^* = E[m_b] + (1/2) \cdot \ln(10) \cdot b \cdot \sigma_{mb}^2 \quad (\text{Equation 2.5.2-3})$$

where $b = 1.0$.

Values for σ_{mb}^2 or Smb were estimated for the two catalogs, and m_b [Rmb] was assigned to each event added to the updated catalog.

The result of the above process was a catalog of 61 earthquakes shown in [Table 2.5-202](#) as the update of the EPRI NP-4726-A seismicity catalog recommended for the site region. For the purpose of recurrence analysis, these should be considered independent events.

The 61 events in the 30° to 37° N, 78° to 86° W latitude-longitude window, incorporating the 200 mi (320 km) radius site region, from 1985 to April 2005 with Emb magnitude 3.0 or greater have been incorporated into a number of figures, including tectonic features discussed in [Subsection 2.5.1](#) and EPRI Earth Science Team source maps in this section.

2.5.2.2 Geologic Structures and EPRI Seismic Source Model for the Site Region

As described in [Subsection 2.5.1](#), a comprehensive review of available geological, seismological, and geophysical data has been performed for the VEGP ESP site region and adjoining areas. The following sections summarize seismic source interpretations from the 1989 EPRI probabilistic seismic hazard analysis (PSHA) study (EPRI NP-6395-D 1989) and from relevant post-EPRI seismic source characterization studies and the updated interpretations of new and existing sources based on more recent data.

Since publication of the EPRI seismic source model, significant new information has been developed for assessing the earthquake source that produced the 1886 Charleston earthquake. This new information shows that the Charleston seismic source should be updated according to RG 1.165. Paleoliquefaction features and other new information published since the 1986 EPRI project ([Reference 511](#)) have significant implications regarding the geometry, M_{max} , and recurrence of M_{max} in the Charleston seismic source. Results from the 1989 EPRI study also show that the Charleston seismic source is the most significant contributor to seismic hazard at the VEGP ESP site ([Reference 514](#)). Thus, an update of the Charleston seismic source has been developed as part of the work performed for this ESP application. Details of the Updated Charleston Seismic Source (UCSS) model are presented in [Subsection 2.5.2.2.4](#) and in a separate Engineering Study Report ([Reference 498](#)).

Sensitivity studies were performed to evaluate the potential significance of the UCSS model to seismic hazard at the VEGP ESP site, as described in detail in [Subsection 2.5.2.4](#). Based on this analysis, it is found that the UCSS interpretations for the Charleston area show that the Charleston seismic source still dominates the seismic hazard at the VEGP ESP site. These new interpretations of the possible locations, sizes, and recurrence intervals of large earthquakes in the Charleston area form a strong basis with which to calculate the seismic ground motion hazard for the site.

2.5.2.2.1 Summary of EPRI Seismic Sources

This section summarizes the seismic sources and parameters used in the 1986 EPRI project ([Reference 511](#)). The description of seismic sources is limited to those sources within 200 mi of the VEGP ESP site (i.e., the site region) and those at distances greater than 200 mi that may affect the hazard at the VEGP ESP site.

In the 1986 EPRI project, six independent Earth Science Teams (ESTs) evaluated geological, geophysical, and seismological data to develop a model of seismic sources in the CEUS. These sources were used to model the occurrence of future earthquakes and evaluate earthquake hazards at nuclear power plant sites across the CEUS.

The six ESTs involved in the 1986 EPRI project were Bechtel Group, Dames & Moore, Law Engineering, Rondout Associates, Weston Geophysical Corporation, and Woodward-Clyde Consultants. Each team produced a report (volumes 5 through 10 of EPRI NP-4726) providing detailed descriptions of how they identified and defined seismic sources. The results were implemented into a PSHA study (Reference 514). For the computation of hazard in the 1989 study, a few seismic source parameters were modified or simplified from the original parameters determined by the six ESTs. EPRI NP-6452-D (1989) summarized the parameters used in the final PSHA calculations, and this reference is the primary source for the seismicity parameters used in this current ESP application. Each EST provides more detailed descriptions of the rationale and methodology used in evaluating tectonic features and establishing the seismic sources (refer to volumes 5 through 10 of EPRI NP-4726).

The most significant seismic sources (Reference 514) developed by each EST are shown in Figures 2.5-257 through 2.5-262. For the 1989 EPRI seismic hazard calculations, a screening criterion was implemented to identify those sources whose combined hazard exceeded 99 percent of the total hazard from all sources, for two ground motions measures (Reference 514). These sources are identified in the descriptions below as “primary” seismic sources. Other sources, which together contributed less than one percent of the total hazard from all sources for the two ground motion measures, are identified in the descriptions below as “additional” seismic sources. Earthquakes with body-wave magnitude m_b 3.0 are also shown in Figures 2.5-257 through 2.5-262 to show the spatial relationships between seismicity and seismic sources. Earthquake epicenters include both events from the EPRI earthquake catalog and for the period between 1985 and April 2005 as described in Subsection 2.5.2.1.2.

The maximum magnitude, interdependencies, and probability of activity for each EPRI EST’s seismic sources are presented in Tables 2.5-203 through 2.5-208. These tables present the parameters assigned to each source within 200 mi of the VEGP ESP site and include primary and additional seismic sources as defined above. The tables also indicate whether new information has been identified that would lead to a revision of the source’s geometry, maximum magnitude, or recurrence parameters. The seismicity recurrence parameters (a- and b-values) used in the seismic hazard studies were computed for each 1° latitude and longitude cell that intersects any portion of a seismic source.

The nomenclature used by each EST to describe the various seismic sources in the CEUS varies from team to team. In other words, a number of different names may have been used by the EPRI teams to describe the same or similar tectonic features or sources, or one team may describe seismic sources that another team does not. For example, the Charleston seismic source was modeled by each team but was called the Charleston Area and Charleston Faults by the Bechtel Group team; the Charleston Seismic Zone by the Dames & Moore, Law, and Weston teams; and Charleston by the Rondout and Woodward-Clyde teams. Each team’s source names, data, and rationale are included in its team-specific documentation (volumes 5 through 10 of EPRI NP-4726).

The EPRI PSHA study expressed maximum magnitude (M_{max}) values in terms of body-wave magnitude (m_b), whereas most modern seismic hazard analyses describe M_{max} in terms of moment magnitude (M). To provide a consistent comparison between magnitude scales, this study relates body-wave magnitude to moment magnitude using the arithmetic average of three equations, or their inversions, presented in Atkinson and Boore (1995), Frankel et al (1996), and EPRI TR-102293 (1993). The conversion relations are very consistent for magnitudes 4.5 and greater and begin to show divergence at lower magnitudes. (Table 2.5-209 lists m_b and M equivalences developed from

these relations over the range of interest for this study.) Throughout this section, the largest assigned values of M_{\max} distributions assigned by the ESTs to seismic sources are presented for both magnitude scales (m_b and M) to give perspective on the maximum earthquakes that were considered possible in each seismic source. For example, EPRI m_b values of M_{\max} are followed by the equivalent M value.

The following sections describe the most significant EPRI sources (both primary and additional seismic sources) for each EST with respect to the VEGP ESP site. Assessment of these and other EPRI sources within the site region shows that the EPRI source parameters (M_{\max} , geometry, and recurrence) are sufficient to capture the current understanding of the seismic hazard in the site region.

Except for the Charleston seismic source, no new geological, geophysical, or seismological information in the literature published since the EPRI NP-6395-D source model suggests that these sources should be modified. Each EST's characterization of the Charleston seismic source was replaced by four alternative source geometries. For each geometry, large earthquake occurrences (M 6.7 to 7.5) were modeled with a range of mean recurrence rates, and smaller earthquakes (m_b 5 to 6.7) were modeled with an exponential magnitude distribution, with rates and b-values determined from historical seismicity. Also, all surrounding sources for each team were redrawn so that the new Charleston source geometries were accurately represented as a "hole" in the surrounding source, and seismic activity rates and b-values were recalculated for the modified surrounding sources, based on historical seismicity. Further details and the results of sensitivity analyses performed on the modified seismic sources are presented in [Subsection 2.5.2.4](#).

2.5.2.2.1.1 Sources Used for EPRI PSHA – Bechtel Group

Bechtel Group identified and characterized six primary seismic sources. All six of these primary seismic sources are located within the site region (200 mi); they are:

- Charleston Area (H)
- Charleston Faults (N3)
- Atlantic Coastal Region (BZ4)
- S Appalachians (BZ5)
- SE Appalachians (F)
- NW South Carolina (G)

Bechtel Group also characterized four additional seismic sources. These additional seismic sources are:

- Eastern Mesozoic Basins (13)
- Bristol Trends (24)
- Rosman Fault (15)
- Belair Fault (16)

Primary and additional seismic sources characterized by the Bechtel Group team within the site region are listed in [Table 2.5-203](#). A map showing the locations and geometries of the Bechtel

primary seismic sources is provided in [Figure 2.5-257](#). Following is a brief discussion of each of the primary seismic sources characterized by the Bechtel Group team.

Charleston Area (H). The Charleston Area source (H) is located about 60 mi from the VEGP ESP site. This oblong combination source area is defined based on the historic earthquake pattern (including the Middleton Place-Summerville and Bowman seismic zones), is elongated northwest-southeast, and encompasses all of source zone N3 (described below). Sources H and N3 are interdependent; if N3 is active, it is unlikely that H is active, and vice versa. The largest M_{\max} assigned by Bechtel Group to this zone is m_b 7.4 (**M** 7.9), reflecting its assumption that Charleston-type earthquakes are produced within this zone.

Charleston Faults (N3). The Charleston Faults (N3) source zone is a small area set within the Charleston Area (H) source zone and encompassing a number of identified and postulated faults in the Charleston, South Carolina, area, including the Ashley River, Charleston, and Woodstock faults. Source N3 is located approximately 85 mi from the VEGP ESP site. Sources H and N3 are interdependent; if N3 is active, it is unlikely that H is active, and vice versa. According to EPRI NP-4726, this combination was created for computational simplicity. The largest M_{\max} assigned by the Bechtel Group team to this zone is m_b 7.4 (**M** 7.9), reflecting its assumption that Charleston-type earthquakes are produced within this zone.

Atlantic Coastal Region (BZ4). The VEGP ESP site is located within the Atlantic Coastal Region background source (BZ4). Source BZ4 is a large background zone that extends from offshore New England to Alabama and encompasses portions of the Coastal Plain from Georgia to southern Virginia. The largest M_{\max} assigned by the Bechtel Group team to this zone is m_b 7.4 (**M** 7.9), reflecting its assumption that there is a small probability that a Charleston-type earthquake could occur within this region.

S Appalachians (BZ5). The Southern Appalachians background source (BZ5) is located about 10 mi from the VEGP ESP site. This source is a large background region that extends from New York to Alabama, including portions of the Southern Appalachians, Piedmont, and Coastal Plain. The largest M_{\max} assigned by the Bechtel Group team to this zone is m_b 6.6 (**M** 6.5).

SE Appalachians (F). The VEGP ESP site is located about 10 mi from the Southeastern Appalachians source (F), a combination source zone that includes parts of Georgia and the Carolinas and flanks the southwest and northeast borders of Zone G (described below). Source Zone F is mutually exclusive with Zone G; if F is active, G is inactive, and vice versa. The largest M_{\max} assigned by the Bechtel Group team to this zone is m_b 6.6 (**M** 6.5).

NW South Carolina (G). The VEGP ESP site is located about 10 mi from the Northwestern South Carolina combination source (G). Source Zone G is mutually exclusive with Zone F; if G is active, F is inactive, and vice versa. The largest M_{\max} assigned by the Bechtel Group team to this zone is m_b 6.6 (**M** 6.5).

2.5.2.2.1.2 Sources Used for EPRI PSHA – Dames & Moore

Dames & Moore identified and characterized five primary seismic sources. All five of these seismic sources are located within the site region; they are:

- Charleston Seismic Zone (54)
- Charleston Mesozoic Rift (52)
- S Appalachian Mobile Belt (Default Zone) (53)

- S Cratonic Margin (Default Zone) (41)
- S Coastal Margin (20)

Dames & Moore also identified seven additional seismic sources within the site region. These sources are:

- Appalachian Fold Belts (4)
- Kink in Fold Belt (4A)
- Jonesboro Basin (49)
- Buried Triassic Basins (50)
- Florence Basin (51)
- Dunbarton Triassic Basin (65)
- Combination Zone 4A-4B-4C-4D (C01)

Primary and additional seismic sources characterized by the Dames & Moore team within the site region are listed in [Table 2.5-204](#). A map showing the locations and geometries of the Dames & Moore primary seismic sources is provided in [Figure 2.5-258](#). Following is a brief discussion of these primary seismic sources.

Charleston Seismic Zone (54). The Charleston Seismic Zone (54) is a northwest-southeast oriented polygon located about 45 mi from the VEGP ESP site. This source includes the Ashley River, Woodstock, Helena Banks, and Cooke faults, as well as the Bowman and Middleton Place-Summerville seismic zones and was designed to capture the occurrence of Charleston-type earthquakes. The largest M_{\max} assigned by the Dames & Moore team to this zone is m_b 7.2 (**M** 7.5).

Charleston Mesozoic Rift (52). The Charleston Mesozoic Rift source (52) is a large polygon located less than 5 mi from the VEGP ESP site. This source extends from offshore South Carolina to Gulf Shore Florida, including portions of the South Carolina and Georgia Coastal Plain. The largest M_{\max} assigned by the Dames & Moore team to this zone is m_b 7.2 (**M** 7.5).

S Appalachian Mobile Belt (Default Zone) (53). The VEGP ESP site is located within the Southern Appalachian Mobile Belt (Default Zone) source (53). This default zone comprises crustal rocks that have undergone several periods of divergence and convergence. The source is bounded on the east by the East Coast magnetic anomaly and on the west by the westernmost boundary of the Appalachian gravity gradient. The largest M_{\max} assigned by the Dames & Moore team to this zone is m_b 7.2 (**M** 7.5).

S Cratonic Margin (Default Zone) (41). The Southern Cratonic Margin (Default Zone) source is located about 65 mi from the VEGP ESP site. This large default zone is located between the Appalachian Fold Belt (4) and the Southern Appalachian Mobile Belt (53) and includes the region of continental margin deformed during Mesozoic rifting. Located within this default zone are many Triassic basins and border faults. The largest M_{\max} assigned by the Dames & Moore team to this zone is m_b 7.2 (**M** 7.5).

S Coastal Margin (20). The Southern Coastal Margin regional source (20) is located approximately 90 mi from the VEGP ESP site. This zone is roughly parallel to the rifted continental margin from Texas to Alabama and incorporates a region of diffuse seismicity. Located within this source is a

down-warped wedge of miogeosynclinal sediments of Cretaceous age and younger. The largest M_{\max} assigned by the Dames & Moore team to this zone is m_b 7.2 (**M** 7.5).

2.5.2.2.1.3 Sources Used for EPRI PSHA – Law Engineering

Law Engineering identified and characterized 15 primary seismic sources all within the site region; They are:

- Charleston Seismic Zone (35)
- Eastern Basement (17)
- Reactivated E Seaboard Normal (22)
- Brunswick, NC Background (108)
- Mesozoic Basins (8 – Bridged) (C09)
- 8 – 35 (C10)
- 22 – 35 (C11)
- Eight mafic pluton sources (M33 and M36 through M42)

Law Engineering also characterized five additional seismic sources within the site region that do not contribute to 99 percent of the hazard at the VEGP ESP site. These are:

- Eastern Basement Background (217)
- Eastern Piedmont (107)
- 22 – 24 – 35 (GC13)
- 22 – 24 (GC12)
- Mesozoic Basins (8)

Primary and additional seismic sources characterized by the Law Engineering team within the site region are listed in **Table 2.5-205**. A map showing the locations and geometries of the Law Engineering primary seismic sources is provided in **Figure 2.5-259**. Following is a brief discussion of Law's primary seismic sources

Charleston Seismic Zone (35). The Charleston Seismic Zone source (35) is a northeast-southwest elongated polygon that includes the Charleston, Ashley River, and Woodstock faults, as well as parts of the offshore Helena Banks fault and most of the more recently discovered liquefaction features identified by Amick (1990). This source was designed to capture the occurrence of Charleston-type earthquakes. This source is located about 75 mi from the VEGP ESP site and overlaps with the Reactivated E Seaboard Normal (22; described below) and Buried Mesozoic Basins (8; not a 99 percent contributor) sources. The largest M_{\max} assigned by the Law Engineering team to this zone is m_b 6.8 (**M** 6.8).

Eastern Basement (17). The VEGP ESP site is located 90 mi from the Eastern Basement (17) source. This source was defined as an area containing pre-Cambrian and Cambrian normal faults, developed during the opening of the proto-Atlantic Ocean, in the basement rocks beneath the

Appalachian decollement. The Giles County and eastern Tennessee zones of seismicity are included in this source. The largest M_{\max} assigned by the Law Engineering team to this zone is m_b 6.8 (**M** 6.8).

Reactivated E Seaboard Normal (22). The VEGP ESP site is located within the Reactivated Eastern Seaboard Normal (22) source. This source was characterized as a region along the eastern seaboard in which Mesozoic normal faults are reactivated as high-angle reverse faults. The Law Engineering team assigned a single M_{\max} of m_b 6.8 (**M** 6.8) to this zone.

Brunswick, NC Background (108). The VEGP ESP site is located within the Brunswick NC Background source zone (108). The source 108 site represents a zone defined by a low-amplitude, long-wavelength magnetic anomaly pattern. The Law Engineering team interpreted this pattern as possibly indicating a zone of Mesozoic extended crust. The largest M_{\max} assigned by the Law Engineering team to this zone is m_b 6.8 (**M** 6.8).

Mesozoic Basins (8 – Bridged) (C09). The VEGP ESP site is located within the Mesozoic Basins (C09) source, which comprises eight bridged basins. This source was defined based on northeast-trending sediment-filled troughs in basement rock bounded by normal faults. The largest M_{\max} assigned by the Law Engineering team to this zone is m_b 6.8 (**M** 6.8).

8 – 35 (C10). The VEGP ESP site is located within the 8 – 35 combination source (C10). The largest M_{\max} assigned by the Law Engineering team to this zone is m_b 6.8 (**M** 6.8).

22 – 35 (C11). The VEGP ESP site is located within the 22 – 35 combination source (C11). The largest M_{\max} assigned by the Law Engineering team to this zone is m_b 6.8 (**M** 6.8).

Eight Mafic Pluton Sources (M33 and M36 through M42). The Law Engineering team identified a number of mafic pluton sources, eight of which are located within about 130 mi of the VEGP ESP site. The Law Engineering team considered pre- and post-metamorphic plutons in the Appalachians to be stress concentrators and, thus, earthquake sources. Law Engineering assigned a single M_{\max} of m_b 6.8 (**M** 6.8) to all mafic pluton sources.

2.5.2.2.1.4 Sources Used for EPRI PSHA – Rondout Associates

Rondout Associates characterized two primary seismic sources both within the site region; they are:

- Charleston (24)
- South Carolina (26)

Rondout Associates also identified eight additional seismic sources within the site region. These are:

- Appalachian (49)
- Background 49 (C01)
- 49 + 32 (C09)
- Grenville (50)
- Background 50 (C02)
- 50 (02) + 12 (C07)
- Southern Appalachians (25)

- Tennessee-VA Border Zone (27)

Primary and additional seismic sources characterized by the Rondout Associates team within the site region are listed in **Table 2.5-206**. A map showing the locations and geometries of the Rondout Associates primary seismic sources is provided in **Figure 2.5-260**. Following is a brief discussion of both of these primary seismic sources.

Charleston (24). The Charleston source is a northwest-southeast-oriented area set within the larger South Carolina (26) source and located about 35 mi from the VEGP ESP site. Source 24 includes the Helena Banks, Charleston, Ashley River, and Woodstock faults, as well as the Bowman and Middleton Place-Summerville seismic zones, and was designed to capture the occurrence of Charleston-type earthquakes. The largest M_{\max} assigned by the Rondout Associates team to this zone is m_b 7.0 (**M 7.2**).

South Carolina (26). The VEGP ESP site is located within the South Carolina source (26). The South Carolina source (26) is a northwest-southeast elongated area that surrounds, but does not include, Source 24 (described above). Source 26 includes most of South Carolina except the Charleston area. The largest M_{\max} assigned by the Rondout Associates team to this zone is m_b 6.8 (**M 6.8**).

2.5.2.2.1.5 Sources Used for EPRI PSHA – Weston Geophysical

Weston Geophysical identified and characterized 12 primary seismic sources, all within the site region; they are:

- Charleston Seismic Zone (25)
- South Carolina (26)
- Southern Coastal Plain (104)
- 103 – 23 – 24 (C19)
- 104 – 22 (C20)
- 104 – 25 (C21)
- 104 – 22 – 26 (C23)
- 104 – 22 – 25 (C24)
- 104 – 28BCDE – 22 (C26)
- 104 – 28BCDE – 22 – 25 (C27)
- 26 – 25 (C33)
- 104 – 28BE – 25 (C35)

Weston Geophysical also characterized 13 additional seismic sources within the site region. These sources are:

- 104 – 26 (C22)

- 104 – 28BE – 26 (C34)
- 104 – 28BCDE (C25)
- 104 – 28BCDE – 22 – 26 (C28)
- Zone of Mesozoic Basin (28B)
- 28A through E (C01)
- Southern Appalachians (103)
- 103 – 23 (C17)
- 103 – 24 (C18)
- Zone of Mesozoic Basin (28D)
- Zone of Mesozoic Basin (28E)
- Appalachian Plateau (102)
- New York-Alabama-Clingman (24)

Primary and additional seismic sources characterized by the Weston Geophysical team are listed in [Table 2.5-207](#). A map showing the locations and geometries of the Weston Geophysical primary seismic sources is provided in [Figure 2.5-262](#). Following is a brief discussion of each of the Weston Geophysical team's primary seismic sources.

Charleston Seismic Zone (25). The Charleston Seismic Zone source is an irregularly shaped hexagon centered just northeast of Charleston, South Carolina, and located about 60 mi from the VEGP ESP site. This source includes the Helena Banks, Charleston, Ashley River, and Woodstock faults, but does not include the Bowman seismic zone. This source was designed to capture the occurrence of Charleston-type earthquakes. The largest M_{\max} assigned by the Weston Geophysical team to this zone is m_b 7.2 (**M 7.5**).

South Carolina (26). The South Carolina source (26) is a large area covering most of South Carolina and the VEGP ESP site. The largest M_{\max} assigned by the Weston Geophysical team to this zone is m_b 7.2 (**M 7.5**).

Southern Coastal Plain (104). The Southern Coastal Plain source (104) extends from New York to Alabama and from the Towaliga-Lowdenville-Kings Mountain fault trends on the west to the offshore East Coast magnetic anomaly on the east. Source 104 was designed to include the Central Virginia seismic zone, the Charleston seismic zone, and a number of Mesozoic basins. The largest M_{\max} assigned by the Weston Geophysical team to this zone is m_b 6.6 (**M 6.5**).

Nine Combination Zones: (103 – 23 – 24 (C19); 104 – 22 (C20); 104 – 25 (C21); 104 – 22 – 26 (C23); 104 – 22 – 25 (C24); 104 – 28BCDE – 22 (C26); 104 – 28BCDE – 22 – 25 (C27); 26 – 25 (C33); and 104 – 28BE – 25 (C35)). Weston Geophysical specified a number of combination seismic source zones, nine of which are primary sources for the VEGP ESP site. The largest M_{\max} assigned by the Weston Geophysical team to these combination zones is m_b 6.6 (**M 6.5**).

2.5.2.2.1.6 Sources Used for EPRI PSHA – Woodward-Clyde Consultants

Woodward-Clyde Consultants identified and characterized five primary seismic sources, all five located within the site region; they are:

- Charleston (includes “none of the above,” NOTA) (30)
- S Carolina Gravity Saddle (Extended) (29)
- SC Gravity Saddle No. 2 (Combo C3) (29A)
- SC Gravity Saddle No. 3 (NW Portion) (29B)
- Vogtle Background

Woodward-Clyde Consultants also identified two additional seismic sources within the site region. These sources are:

- Blue Ridge Combo (31)
- Blue Ridge Combination – Alternate Configuration (31A)

Primary and additional seismic sources characterized by the Woodward-Clyde team within the site region are listed in [Table 2.5-208](#). A map showing the locations and geometries of the Woodward-Clyde primary seismic sources is provided in [Figure 2.5-261](#). Following is a brief discussion of each of the primary seismic sources identified by the Woodward-Clyde team.

Charleston (includes NOTA) (30). The Charleston seismic source (30) is a northeast-southwest-oriented rectangle that includes most of the Charleston earthquake MMI IX and X area and the Charleston Ashley River and Woodstock faults. Source 30 is located about 70 mi from the VEGP ESP site and was designed to capture the occurrence of Charleston-type earthquakes. The Charleston source (30) is mutually exclusive with Sources 29, 29A, and 29B; if 30 is active, the other three are inactive, and vice versa. The largest M_{\max} assigned by the Woodward-Clyde Consultants team to this zone is m_b 7.5 (**M 8.0**).

S Carolina Gravity Saddle (Extended) (29). The South Carolina Gravity Saddle (Extended) source (29) covers most of South Carolina and parts of Georgia, including the VEGP ESP site. The South Carolina Gravity Saddle source (29) is mutually exclusive with Sources 29A, 29B, and 30; if 29 is active, the other three are inactive, and vice versa. The largest M_{\max} assigned by the Woodward-Clyde Consultants team to this zone is m_b 7.4 (**M 7.9**), reflecting its assumption that Charleston-type earthquakes can occur in this zone.

SC Gravity Saddle No. 2 (Combo C3) (29A). The South Carolina Gravity Saddle No. 2 source (29A) is an irregularly shaped polygon set within the larger area of Source 29. The SC Gravity Saddle No. 2 source (29A) is mutually exclusive with Sources 29, 29B, and 30; if 29A is active, the other three are inactive, and vice versa. The largest M_{\max} assigned by the Woodward-Clyde Consultants team to this zone is m_b 7.4 (**M 7.9**), reflecting its assumption that Charleston-type earthquakes can occur in this zone.

SC Gravity Saddle No. 3 (NW Portion) (29B). The South Carolina Gravity Saddle No. 3 source (29B) is an irregularly shaped polygon set within the larger area of Source 29 and includes the VEGP ESP site. The SC Gravity Saddle No. 3 source (29B) is mutually exclusive with Sources 29, 29A, and 30; if 29B is active, the other three are inactive, and vice versa. The largest M_{\max} assigned by the Woodward-Clyde Consultants team to this zone is m_b 7.0 (**M 7.2**).

Vogtle Background. The VEGP ESP Background source is a large box containing the VEGP ESP site and covering most of South Carolina and Georgia as well as parts of adjoining states and extending offshore. This source is a background zone defined as a rectangular area surrounding the VEGP ESP site and is not based on any geological, geophysical, or seismological features. The largest M_{\max} assigned by the Woodward-Clyde Consultants team to this zone is m_b 6.6 (**M** 6.5).

2.5.2.2.2 Post-EPRI Seismic Source Characterization Studies

Since the EPRI (NP-4726 1986, NP-6395-D 1989) seismic hazard project, three recent studies have been performed to characterize seismic sources within the VEGP ESP site region for PSHAs. These studies include the US Geological Survey's (USGS) National Seismic Hazard Mapping Project ([Reference 281](#), [Reference 282](#)), the South Carolina Department of Transportation's seismic hazard mapping project ([Reference 504](#)), and the Nuclear Regulatory Commission's Trial Implementation Project (TIP) study ([Reference 533](#)). These three studies are described below (i.e., [Subsections 2.5.2.2.2.1](#) through [2.5.2.2.2.3](#)). Based on review of recent studies it was determined that an update of the Charleston seismic source for the EPRI (NP-4726 1986, NP-6395-D 1989) seismic hazard project was required. This update is presented in [Subsection 2.5.2.2.2.4](#). In addition, at the perimeter of the VEGP ESP site region is what is now identified as the Eastern Tennessee Seismic Zone (ETSZ). The significance of the ETSZ on the VEGP ESP seismic hazard is discussed in [Subsection 2.5.2.2.2.5](#).

2.5.2.2.2.1 US Geological Survey Model (Frankel et al. 2002)

In 2002, the USGS produced updated seismic hazard maps for the conterminous United States based on new seismological, geophysical, and geological information ([Reference 282](#)). The 2002 maps reflect changes to the source model used to construct the previous version of the national seismic hazard maps ([Reference 281](#)). The most significant modifications to the CEUS portion of the source model include changes in the recurrence, M_{\max} , and geometry of the Charleston and New Madrid sources.

Unlike the EPRI models that incorporate many local sources, the USGS source model in the CEUS includes only five sources: the Extended Margin background, Stable Craton background, Charleston, Eastern Tennessee, and New Madrid ([Table 2.5-209](#)). Except for the Charleston and New Madrid zones, where earthquake recurrence is modeled by paleoliquefaction data, the hazard for the large background or "maximum magnitude" zones is largely based on historical seismicity and the variation of that seismicity. The USGS source model defines the M_{\max} distribution for the Extended Margin background source zone as a single magnitude of **M** 7.5 with a weight of 1.0. The EPRI model, however, includes multiple source zones for each of the six ESTs for this region containing the eastern seaboard and the Appalachians. The EPRI M_{\max} distributions for these sources capture a wide range of magnitudes and weights, reflecting considerable uncertainty in the assessment of M_{\max} for the CEUS. An **M** 7.5 M_{\max} is captured in most of the EPRI source zones, although at a lower weight than assigned by the USGS model.

As part of the 2002 update of the National Seismic Hazard Maps, the USGS developed a model of the Charleston source that incorporates available data regarding recurrence, M_{\max} , and geometry of the source zone. The USGS model uses two equally weighted source geometries, one an areal source enveloping most of the tectonic features and liquefaction data in the greater Charleston area and the second a north-northeast-trending elongated areal source enveloping the southern half of the southern segment of the East Coast fault system (ECFS) ([Table 2.5-209](#) and [Figure 2.5-263](#)). The Frankel et al. (2002) report does not specify why the entire southern segment of the ECFS is not contained in the source geometry. For M_{\max} , the study defines a distribution of magnitudes and weights of **M** 6.8 [.20], 7.1 [.20], 7.3 [.45], 7.5 [.15]. For recurrence, Frankel et al. (2002) adopt a mean paleoliquefaction-based recurrence interval of 550 years and represent the uncertainty with a continuous lognormal distribution.

2.5.2.2.2.2 South Carolina Department of Transportation Model (Chapman and Talwani 2002)

Chapman and Talwani (2002) created probabilistic seismic hazard maps for the South Carolina Department of Transportation (SCDOT). In the SCDOT model, treatment of the 1886 Charleston, South Carolina, earthquake and similar events dominates estimates of hazard statewide.

The SCDOT model employs a combination of line and area sources to characterize Charleston-type earthquakes in three separate geometries and uses a slightly different M_{\max} range (M 7.1 to 7.5) than the USGS 2002 model (Table 2.5-210 and Figure 2.5-264). Three equally-weighted source zones defined for this study include (1) a source capturing the intersection of the Woodstock and Ashley River faults, (2) a larger Coastal South Carolina zone that includes most of the paleoliquefaction sites, and (3) a southern ECFS source zone. The respective magnitude distributions and weights used for M_{\max} are M 7.1 [.20], 7.3 [.60], 7.5 [.20]. The mean recurrence interval used in the SCDOT study is 550 years, based on the paleoliquefaction record.

2.5.2.2.2.3 The Trial Implementation Project Study (Savy et al. 2002)

The purpose of the Lawrence Livermore National Laboratory Trial Implementation Project (TIP) study is to “test and implement the guidelines developed by the Senior Seismic Hazard Analysis Committee (SSHAC) developed under FIN L2503 (NRC 1997)” (Reference 533, p. 1). To test the SSHAC PSHA methodology, the TIP study focuses on seismic zonation and earthquake recurrence models for the Watts Bar site in Tennessee and the VEGP site. The TIP study uses an expert elicitation process to characterize the Charleston seismic source, considering published data through 1996. The TIP study identifies multiple alternative zones for the Charleston source and for the South Carolina–Georgia seismic zone, as well as alternative background seismicity zones for the Charleston region. However, the TIP study focuses primarily on implementing the Senior Seismic Hazard Advisory Committee (SSHAC) PSHA methodology (Reference 538) and was designed to be as much of a test of the methodology as a real estimate of seismic hazard. As a result, its findings are not included explicitly in this report.

2.5.2.2.2.4 Updated Charleston Seismic Source (UCSS) Model (Bechtel 2006d)

It has been nearly 20 years since the six EPRI ESTs evaluated hypotheses for earthquake causes and tectonic features and assessed seismic sources in the CEUS (Reference 511). The EPRI Charleston source zones developed by each EST are shown in Figure 2.5-266 and summarized in Table 2.5-211. Several studies that post-date the 1986 EPRI EST assessments have demonstrated that the source parameters for geometry, M_{\max} , and recurrence of M_{\max} in the Charleston seismic source need to be updated to capture a more current understanding for both the 1886 Charleston earthquake and the seismic source that produced this earthquake. In addition, recent PSHA studies of the South Carolina region (Reference 533; Reference 504) and the southeastern United States (Reference 282) have developed models of the Charleston seismic source that differ significantly from the earlier EPRI characterizations. Therefore, the Charleston seismic source was updated as part of this ESP application.

The UCSS model is summarized below and presented in detail in Bechtel (2006d). Methods used to update the Charleston seismic source follow guidelines provided in RG 1.165. An SSHAC Level 2 study was performed to incorporate current literature and data and the understanding of experts into an update of the Charleston seismic source model. This level of effort is outlined in the SSHAC (1997) report, which provides guidance on incorporating uncertainty and the use of experts in PSHA studies.

The UCSS model incorporates new information to re-characterize geometry, M_{\max} , and recurrence for the Charleston seismic source. These components are discussed in the following sections.

Paleoliquefaction data imply that the Charleston earthquake process is defined by repeated, relatively frequent, large earthquakes located in the vicinity of Charleston, indicating that the Charleston source is different from the rest of the eastern seaboard.

2.5.2.2.2.4.1 UCSS Geometry

The UCSS model includes four mutually exclusive source zone geometries (A, B, B', and C; [Figure 2.5-265](#)). The latitude and longitude coordinates that define these four source zones are presented in [Table 2.5-212](#). Details for each source geometry are given below. The four geometries of the UCSS are defined based on current understanding of geologic and tectonic features in the 1886 Charleston earthquake epicentral region; the 1886 Charleston earthquake shaking intensity; distribution of seismicity; and geographic distribution, age, and density of liquefaction features associated with both the 1886 and prehistoric earthquakes. These features, shown in [Figures 2.5-221](#) and [2.5-222](#), strongly suggest that the majority of evidence for the Charleston source is concentrated in the Charleston area and is not widely distributed throughout South Carolina. [Table 2.5-211](#) provides a subset of the Charleston tectonic features differentiated by pre- and post-EPRI ([Reference 511](#)) information. In addition, pre- and post-1986 instrumental seismicity, $m_b \geq 3$, are shown on [Figures 2.5-221](#) and [2.5-222](#). Seismicity continues to be concentrated in the Charleston region in the Middleton Place–Summerville seismic zone (MPSSZ), which has been used to define the intersection of the Woodstock and Ashley River faults ([Reference 463](#); [Reference 364](#)). Notably, two earthquakes in 2002 (m_b 3.5 and 4.4) are located offshore of South Carolina along the Helena Banks fault zone in an area previously devoid of seismicity of $m_b > 3$. A compilation of the EPRI EST Charleston source zones is provided in [Figure 2.5-266](#) as a comparison to the UCSS geometries shown in [Figure 2.5-265](#).

Geometry A - Charleston

Geometry A is an approximately 100 x 50 km, northeast-oriented area centered on the 1886 Charleston meizoseismal area ([Figure 2.5-265](#)). Geometry A is intended to represent a localized source area that generally confines the Charleston source to the 1886 meizoseismal area (i.e., a stationary source in time and space). Geometry A completely incorporates the 1886 earthquake MMI X isoseismal ([Reference 219](#)), the majority of identified Charleston-area tectonic features and inferred fault intersections, and the majority of reported 1886 liquefaction features. Geometry A excludes the northern extension of the southern segment of the East Coast fault system because this system extends well north of the meizoseismal zone and is included in its own source geometry (Geometry C). Geometry A also excludes outlying liquefaction features, because liquefaction occurs as a result of strong ground shaking that may extend well beyond the areal extent of the tectonic source. Geometry A also envelopes instrumentally located earthquakes spatially associated with the MPSSZ ([Reference 463](#); [Reference 462](#); [Reference 364](#)).

The preponderance of evidence strongly supports the conclusion that the seismic source for the 1886 Charleston earthquake is located in a relatively restricted area defined by Geometry A. Geometry A envelopes (1) the meizoseismal area of the 1886 earthquake, (2) the area containing the majority of local tectonic features (although many have large uncertainties associated with their existence and activity, as described earlier), (3) the area of ongoing concentrated seismicity, and (4) the area of greatest density of 1886 liquefaction and prehistoric liquefaction. These observations show that future earthquakes having magnitudes comparable to the Charleston earthquake of 1886 most likely will occur within the area defined by Geometry A. A weight of 0.70 is assigned to Geometry A ([Figure 2.5-267](#)). To confine the rupture dimension to within the source area and to maintain a preferred northeast fault orientation, Geometry A is represented in the model by a series of closely spaced, northeast-trending faults parallel to the long axis of the zone.

Geometries B, B', and C

While the preponderance of evidence supports the assessment that the 1886 Charleston meizoseismal area and Geometry A define the area where future events will most likely be centered, it is possible that the tectonic feature responsible for the 1886 earthquake either extends beyond or lies outside Geometry A. Therefore, the remaining three geometries (B, B', and C) are assessed to capture the uncertainty that future events may not be restricted to Geometry A. The distribution of liquefaction features along the entire coast of South Carolina and observations from the paleoliquefaction record that a few events were localized (moderate earthquakes to the northeast and southwest of Charleston), suggest that the Charleston source could extend well beyond Charleston proper. Geometries B and B' are assessed to represent a larger source zone, while Geometry C represents the southern segment of the East Coast fault system as a possible source zone. The combined geometries of B and B' are assigned a weight of 0.20, and Geometry C is assigned a weight of 0.10. Geometry B' a subset of B, formally defines the onshore coastal area as a source (similar to the SCDOT coastal source zone) that would restrict earthquakes to the onshore region. Geometry B, which includes the onshore and offshore regions, and Geometry B' are mutually exclusive and given equal weight in the UCSS model. Therefore, the resulting weights are 0.10 for Geometries B and B'.

Geometry B - Coastal and Offshore Zone

Geometry B is a coast-parallel, approximately 260 x 100 km source area that (1) incorporates all of Geometry A, (2) is elongated to the northeast and southwest to capture other, more distant liquefaction features in coastal South Carolina ([Reference 205](#); [Reference 207](#); [Reference 206](#); [Reference 461](#)), and (3) extends to the southeast to include the offshore Helena Banks fault zone ([Reference 213](#); [Figure 2.5-265](#)). The elongation and orientation of Geometry B is roughly parallel to the regional structural grain as well as roughly parallel to the elongation of 1886 isoseismals. The northeastern and southwestern extents of Geometry B are controlled by the mapped extent of paleoliquefaction features [e.g., ([Reference 205](#); [Reference 207](#); [Reference 206](#); [Reference 461](#))].

The location and timing of paleoliquefaction features in the Georgetown and Bluffton areas to the northeast and southwest of Charleston have suggested to some researchers that the earthquake source may not be restricted to the Charleston area ([Reference 530](#); [Reference 207](#); [Reference 461](#)). A primary reason for defining Geometry B is to account for the possibility that there may be an elongated source or multiple sources along the South Carolina coast. Paleoliquefaction features in the Georgetown and Bluffton areas may be explained by an earthquake source both northeast and southwest of Charleston, as well as possibly offshore.

Geometry B extends southeast to include an offshore area and the Helena Banks fault zone. The Helena Banks fault zone is clearly shown by multiple seismic reflection profiles and has demonstrable late Miocene offset ([Reference 213](#)). Offshore earthquakes in 2002 (m_b 3.5 and 4.4) suggest a possible spatial association of seismicity with the mapped trace of the Helena Banks fault system ([Figures 2.5-265](#) and [2.5-222](#)). Whereas these two events in the vicinity of the Helena Banks fault system do not provide a positive correlation with seismicity or demonstrate recent fault activity, these small earthquakes are considered new data since the EPRI studies. The EPRI earthquake catalog ([Reference 512](#)) was devoid of any events ($m_b \geq 3.0$) offshore from Charleston. The recent offshore seismicity also post-dates the development of the USGS and SCDOT source models that exclude any offshore Charleston source geometries.

A low weight of 0.10 is assigned to Geometry B ([Figure 2.5-267](#)), because the preponderance of evidence indicates that the seismic source that produced the 1886 earthquake lies onshore in the Charleston meizoseismal area and not in the offshore region. To confine the rupture dimension to within the source area and to maintain a preferred northeast fault orientation, Geometry B is represented in the model by a series of closely spaced, northeast-trending faults parallel to the long axis of the zone.

Geometry B' - Coastal Zone

Geometry B' is a coast-parallel, approximately 260 x 50 km source area that incorporates all of Geometry A, as well as the majority of reported paleoliquefaction features (Reference 205; Amick et al. 1990a, Reference 206; Reference 461). Unlike Geometry B, however, Geometry B' does not include the offshore Helena Banks fault zone (Figure 2.5-265).

The Helena Banks fault system is excluded from Geometry B' to recognize that the preponderance of the data and evaluations support the assessment that the fault system is not active and because most evidence strongly suggests that the 1886 Charleston earthquake occurred onshore in the 1886 meizoseismal area and not on an offshore fault. Whereas there is little uncertainty regarding the existence of the Helena Banks fault, there is a lack of evidence that this feature is still active. Iseoseismal maps documenting shaking intensity in 1886 indicate an onshore meizoseismal area (the closed bull's eye centered onshore north of downtown Charleston, Figure 2.5-222). An onshore source for the 1886 earthquake as well as the prehistoric events is supported by the instrumentally recorded seismicity in the MPSSZ and the corresponding high density cluster of 1886 and prehistoric liquefaction features.

Similar to Geometry B above, a weight of 0.10 is assigned to Geometry B' and reflects the assessment that Geometry B' has a much lower probability of being the source zone for Charleston-type earthquakes than Geometry A (Figure 2.5-267). To confine the rupture dimension to within the source area and to maintain a preferred northeast fault orientation, Geometry B' is represented in the model by a series of closely spaced, northeast-trending faults parallel to the long axis of the zone.

Geometry C - East Coast Fault System - South (ECFS-s)

Geometry C is an approximately 200 x 30 km, north-northeast-oriented source area enveloping the southern segment of the proposed East Coast fault system (ECFS-s) shown in Figure 3 of Marple and Talwani (2000) (Figures 2.5-265 and 2.5-268). The USGS hazard model (Reference 282) (Figure 2.5-263) incorporates the ECFS-s as a distinct source geometry (also known as the zone of river anomalies [ZRA]); however, as described earlier, the USGS model truncates the northeastern extent of the proposed fault segment. The South Carolina Department of Transportation hazard model (Reference 504) also incorporates the ECFS-s as a distinct source geometry; however, this model extends the southern segment of the proposed East Coast fault system farther to the south than originally postulated by Marple and Talwani (2000) to include, in part, the distribution of liquefaction in southeastern South Carolina (Reference 503) (Figure 2.5-265).

In this ESP evaluation the area of Geometry C is restricted to envelope the original depiction of the ECFS-s by Marple and Talwani (2000). Truncation of the zone to the northeast as shown by the 2002 USGS model is not supported by available data, and the presence of liquefaction in southeastern South Carolina is best captured in Geometries B and B', rather than extending the ECFS-s farther to the south than defined by the data of Marple and Talwani (2000).

A low weight of 0.10 is assigned to Geometry C to reflect the assessment that Geometries B, B', and C all have equal, but relatively low, likelihood of producing Charleston-type earthquakes (Figure 2.5-267). As with the other UCSS geometries, Geometry C is represented as a series of parallel, vertical faults oriented northeast-southwest and parallel to the long axis of the narrow rectangular zone. The faults and extent of earthquake ruptures are confined within the rectangle depicting Geometry C.

UCSS Model Parameters

Based on studies by Bollinger et al. (1985, 1991) and Bollinger (1992), a 20-km-thick seismogenic crust is assumed for the UCSS. To model the occurrence of earthquakes in the characteristic part of the Charleston distribution ($M > 6.7$), the model uses a series of closely-spaced, vertical faults parallel to the long axis of each of the four source zones (A, B, B', and C). Faults and earthquake

ruptures are limited to within each respective source zone and are not allowed to extend beyond the zone boundaries, and ruptures are constrained to occur within the depth range of 0 to 20 km. Modeled fault rupture areas are assumed to have a width-to-length aspect ratio of 0.5, conditional on the assumed maximum fault width of 20 km. To obtain M_{\max} earthquake rupture lengths from magnitude, the Wells and Coppersmith (1994) empirical relationship between surface rupture length and M for earthquakes of all slip types is used.

To maintain as much similarity as possible with the original EPRI model, the UCSS model treats earthquakes in the exponential part of the distribution ($M < 6.7$) as point sources uniformly distributed within the source area (full smoothing), with a constant depth fixed at 10 km.

2.5.2.2.4.2 UCSS Maximum Magnitude

The six EPRI ESTs developed a distribution of weighted M_{\max} values and weights to characterize the largest earthquakes that could occur on Charleston seismic sources. On the low end, the Law Engineering team assessed a single M_{\max} of m_b 6.8 to seismic sources it considered capable of producing earthquakes comparable in magnitude to the 1886 Charleston earthquake. On the high end, four teams defined M_{\max} upper bounds ranging between m_b 7.2 and 7.5. For this ESP application, the m_b magnitude values have been converted to moment magnitude (M) as described previously. The m_b value and converted moment magnitude value for each team are shown below. The range in M for the six ESTs is 6.5 to 8.0.

<u>Team</u>	<u>Charleston M_{\max} range</u>
Bechtel Group	m_b 6.8 to 7.4 (M 6.8 to 7.9)
Dames & Moore	m_b 6.6 to 7.2 (M 6.5 to 7.5)
Law Engineering	m_b 6.8 (M 6.8)
Rondout	m_b 6.6 to 7.0 (M 6.5 to 7.2)
Weston Geophysical	m_b 6.6 to 7.2 (M 6.5 to 7.5)
Woodward-Clyde Consultants	m_b 6.7 to 7.5 (M 6.7 to 8.0)

The M equivalents of EPRI m_b estimates for Charleston M_{\max} earthquakes show that the upper bound values are similar to, and in two cases exceed, the largest modern estimate of M 7.3 ± 0.26 (Reference 339) for the 1886 earthquake. The upper bound values for five of the six ESTs also exceed the preferred estimate of M 6.9 by Bakun and Hopper (2004) for the Charleston event. The EPRI M_{\max} estimates are more heavily weighted toward the lower magnitudes, with the upper bound magnitudes given relatively low weights by several ESTs (Tables 2.5-203 through 2.5-208). Therefore, updating the M_{\max} range and weights to reflect the current range of technical interpretations is warranted for the UCSS.

Based on assessment of the currently available data and interpretations regarding the range of modern M_{\max} estimates (Table 2.5-213), the UCSS model modifies the USGS magnitude distribution (Reference 282) to include a total of five discrete magnitude values, each separated by 0.2 M units (Figure 2.5-267). The UCSS M_{\max} distribution includes a discrete value of M 6.9 to represent the Bakun and Hopper (2004) best estimate of the 1886 Charleston earthquake magnitude, as well as a lower value of M 6.7 to capture a low probability that the 1886 earthquake was smaller than the Bakun and Hopper (2004) mean estimate of M 6.9. Bakun and Hopper (2004) do not explicitly report a 1-sigma range in magnitude estimate of the 1886 earthquake, but do provide a 2-sigma range of M 6.4 to M 7.2.

The UCSS magnitudes and weights are as follows:

M	Weight	
6.7	0.10	
6.9	0.25	Bakun and Hopper (2004) mean
7.1	0.30	
7.3	0.25	Johnston (1996) mean
7.5	0.10	

This results in a weighted M_{\max} mean magnitude of **M** 7.1 for the UCSS, which is slightly lower than the mean magnitude of **M** 7.2 in the USGS model (Reference 282).

2.5.2.2.2.4.3 UCSS Recurrence Model

In the 1989 EPRI study (Reference 514), the six EPRI ESTs used an exponential magnitude distribution to represent earthquake sizes for their Charleston sources. Parameters of the exponential magnitude distribution were estimated from historical seismicity in the respective source areas. This resulted in recurrence intervals for M_{\max} earthquakes (at the upper end of the exponential distribution) of several thousand years.

The current model for earthquake recurrence is a composite model consisting of two distributions. The first is an exponential magnitude distribution used to estimate recurrence between the lower-bound magnitude used for hazard calculations and m_b 6.7. The parameters of this distribution are estimated from the earthquake catalog, as they were for the 1989 EPRI study. This is the standard procedure for smaller magnitudes and is the model used, for example, by the USGS 2002 national hazard maps (Reference 282). In the second distribution, M_{\max} earthquakes (**M** \geq 6.7) are treated according to a characteristic model, with discrete magnitudes and mean recurrence intervals estimated through analysis of geologic data, including paleoliquefaction studies. In this document, M_{\max} is used to describe the range of largest earthquakes in both the characteristic portion of the UCSS recurrence model and the EPRI exponential recurrence model.

This composite model achieves consistency between the occurrence of earthquakes with **M** < 6.7 and the earthquake catalog and between the occurrence of large earthquakes (**M** \geq 6.7) with paleoliquefaction evidence. It is a type of “characteristic earthquake” model, in which the recurrence rate of large events is higher than what would be estimated from an exponential distribution inferred from the historical seismic record.

M_{\max} Recurrence

This section describes how the UCSS model determines mean recurrence intervals for M_{\max} earthquakes. The UCSS model incorporates geologic data to characterize the recurrence intervals for M_{\max} earthquakes. As described earlier, identifying and dating paleoliquefaction features provides a basis for estimating the recurrence of large Charleston area earthquakes. Most of the available geologic data pertaining to the recurrence of large earthquakes in the Charleston area were published after 1990 and therefore were not available to the six EPRI ESTs. In the absence of geologic data, the six EPRI EST estimates of recurrence for large, Charleston-type earthquakes were based on a truncated exponential model using historical seismicity (Reference 511; Reference 514). The truncated exponential model also provided the relative frequency of all earthquakes greater than m_b 5.0 up to M_{\max} in the EPRI PSHA. The recurrence of M_{\max} earthquakes in the EPRI models was on the order of several thousand years, which is significantly greater than more recently published estimates of about 500 to 600 years, based on paleoliquefaction data (Reference 461).

Paleoliquefaction Data

Strong ground shaking during the 1886 Charleston earthquake produced extensive liquefaction, and liquefaction features from the 1886 event are preserved in geologic deposits at numerous locations in the region. Documentation of older liquefaction-related features in geologic deposits provides evidence for prior strong ground motions during prehistoric large earthquakes. Estimates of the recurrence of large earthquakes in the UCSS are based on dating paleoliquefaction features. Many potential sources of ambiguity and/or error are associated with dating and interpreting paleoliquefaction features. This assessment does not reevaluate field interpretations and data; rather, it reevaluates criteria used to define individual paleoearthquakes in the published literature. In particular, the UCSS reevaluates the paleoearthquake record interpreted by Talwani and Schaeffer (2001) based on that study's compilation of sites with paleoliquefaction features.

Talwani and Schaeffer (2001) compiled radiocarbon ages from paleoliquefaction features along the coast of South Carolina. These data include ages that provide contemporary, minimum, and maximum limiting ages for liquefaction events. Radiocarbon ages were corrected for past variability in atmospheric ^{14}C using well established calibration curves and converted to “calibrated” (approximately calendric) ages. From their compilation of calibrated radiocarbon ages from various geographic locations, Talwani and Schaeffer (2001) correlated individual earthquake episodes. They identified an individual earthquake episode based on samples with a “contemporary” age constraint that had overlapping calibrated radiocarbon ages at approximately 1-sigma confidence interval. The estimated age of each earthquake was “calculated from the weighted averages of overlapping contemporary ages” (Reference 461) (p. 6,632). They defined as many as eight events (named 1886, A, B, C, D, E, F, and G in order of increasing age) from the paleoliquefaction record, and offered two scenarios to explain the distribution and timing of paleoliquefaction features (Table 2.5-214).

The two scenario paleoearthquake records proposed by Talwani and Schaeffer (2001) have different interpretations for the size and location of prehistoric events (Table 2.5-214). In their Scenario 1, the four prehistoric events that produced widespread liquefaction features similar to the large 1886 Charleston earthquake (A, B, E, and G) are interpreted to be large, Charleston-type events. Three events, C, D, and F, are defined by paleoliquefaction features that are more limited in geographic extent than other events and are interpreted to be smaller, moderate-magnitude events (approximately M 6). Events C and F are defined by features found north of Charleston in the Georgetown region, and Event D is defined by sites south of Charleston in the Bluffton area. In their Scenario 2, all events are interpreted as large, Charleston-type events. Furthermore, Events C and D are combined into a large Event C'. Talwani and Schaeffer (2001) justify the grouping of the two events based on the observation that the calibrated radiocarbon ages that constrain the timing of Events C and D are indistinguishable at the 95 percent (2-sigma) confidence interval.

The length and completeness of the paleoearthquake record based on paleoliquefaction features is a source of epistemic uncertainty in the UCSS. The paleoliquefaction record along the South Carolina coast extends from 1886 to the mid-Holocene (Reference 461). The consensus of the scientists who have evaluated these data (Reference 461; Reference 540; Reference 529) is that the paleoliquefaction record of earthquakes is complete only for the most recent about 2,000 years and that it is possible that liquefaction events are missing from the older portions of the record. The suggested incompleteness of the paleoseismic record is based on the argument that past fluctuations in sea level have produced time intervals of low water table conditions (and thus low liquefaction susceptibility), during which large earthquake events may not have been recorded in the paleoliquefaction record (Reference 461). While this assertion may be true, it cannot be ruled out that the paleoliquefaction record may be complete back to the mid-Holocene.

2-Sigma Analysis of Event Ages

Analysis of the coastal South Carolina paleoliquefaction record performed for the VEGP ESP application is based on the Talwani and Schaeffer (2001) data compilation. As described above, Talwani and Schaeffer (2001) use calibrated radiocarbon ages with 1-sigma error bands to define the timing of past liquefaction episodes in coastal South Carolina. The standard in paleoseismology, however, is to use calibrated ages with 2-sigma (95.4 percent confidence interval) error bands [e.g., (Reference 536; Reference 518)]. Likewise, in paleoliquefaction studies, to more accurately reflect the uncertainties in radiocarbon dating, the use of calibrated radiocarbon dates with 2-sigma error bands (as opposed to narrower 1-sigma error bands) is advisable (Reference 544). The Talwani and Schaeffer (2001) use of 1-sigma error bands may lead to over-interpretation of the paleoliquefaction record such that more episodes are interpreted than actually occurred. In recognition of this possibility, the conventional radiocarbon ages presented in Talwani and Schaeffer (2001) have been recalibrated and reported with 2-sigma error bands. The recalibration of individual radiocarbon samples and estimation of age ranges for paleoliquefaction events show broader age ranges with 2-sigma error bands which are used to obtain broader age ranges for paleoliquefaction events in the Charleston area.

Event ages based on overlapping 2-sigma ages of paleoliquefaction features are presented in Table 2.5-214. Paleoearthquakes have been distinguished based on grouping paleoliquefaction features that have contemporary radiocarbon samples with overlapping calibrated ages. Event ages have then been defined by selecting the age range common to each of the samples. For example, an event defined by overlapping 2-sigma sample ages of 100 to 200 cal yr BP and 50 to 150 cal yr BP would have an event age of 100 to 150 cal yr BP. The UCSS study considers the “trimmed” ages to represent the approximately 95 percent confidence interval, with a “best estimate” event age as the midpoint of the approximately 95 percent age range.

The 2-sigma analysis identified six distinct paleoearthquakes in the data presented by Talwani and Schaeffer (2001). As noted by that study, Events C and D are indistinguishable at the 95 percent confidence interval, and in the UCSS, those samples define Event C' (Table 2.5-214). Additionally, the UCSS 2-sigma analysis suggests that Talwani and Schaeffer (2001) Events F and G may have been a single, large event, defined in the UCSS as F'. One important difference between the UCSS result and that of Talwani and Schaeffer (2001) is that the three Events C, D, and F in their Scenario 1, which are inferred to be smaller, moderate-magnitude events, are grouped into more regionally extensive Events C' and F' (Table 2.5-214). Therefore, in the UCSS, all earthquakes in the 2-sigma analysis have been interpreted to represent large, Charleston-type events. The incorporation of large Events C' and F' into the UCSS model is, in effect, a conservative approach. In the effort to estimate the recurrence of M_{\max} events (M 6.7 to 7.5), moderate-magnitude (about M 6) earthquakes C and D would be eliminated from the record of large (M_{\max}) earthquakes in the UCSS model, thereby increasing the calculated M_{\max} recurrence interval and lowering the hazard without sufficient justification. For these reasons the UCSS model uses a single, large Event C' (instead of separate, smaller Events C and D) and a single, large Event F' (instead of separate, smaller Events F and G). Analysis suggests that there have been four large earthquakes in the most-recent, about 2,000-year portion of the record (1886 and Events A, B, C', E, F'; Table 2.5-214). Figure 2.5-269 shows the geographic distribution of liquefaction features associated with each event in the UCSS model. The distributions of paleoliquefaction sites for Events A, B, C', E, and F' are all very similar to the coastal extent of the liquefaction features from the 1886 earthquake.

Recurrence intervals developed from the earthquakes recorded by paleoliquefaction features assume that these features were produced by large M_{\max} events and that both the about 2,000-year and about 5,000-year records are complete. However, the UCSS mentions at least two concerns regarding the use of the paleoliquefaction record to characterize the recurrence of past M_{\max} events. First, it is possible that the paleoliquefaction features associated with one or more of these pre-1886 events were produced by multiple moderate-sized events closely spaced in time. If this were the

case, then the calculated recurrence interval would yield artificially short recurrence for M_{\max} , since it was calculated using repeat times of both large (M_{\max}) events and smaller earthquakes. Limitations of radiocarbon dating and limitations in the stratigraphic record often preclude identifying individual events in the paleoseismologic record that are closely spaced in time (i.e., separated by only a few years to a few decades). Several seismic sources have demonstrated tightly clustered earthquake activity in space and time that are indistinguishable in the radiocarbon and paleoseismic record:

- New Madrid (1811, 1811, 1812)
- North Anatolian Fault (1999 and 1999)
- San Andreas Fault (1812 and 1857)

Therefore the UCSS acknowledges the distinct possibility that M_{\max} occurs less frequently than what is calculated from the paleoliquefaction record.

A second concern is that the recurrence behavior of the M_{\max} event may be highly variable through time. For example, the UCSS considers it unlikely that M 6.7 to M 7.5 events have occurred on a Charleston source at an average repeat time of about 500 to 600 years (Reference 461) throughout the Holocene Epoch. Such a moment release rate would likely produce tectonic landforms with clear geomorphic expression, such as are present in regions of the world with comparably high rates of moderate to large earthquakes (for example, faults in the Eastern California shear zone with sub-millimeter per year slip rates and recurrence intervals on the order of about 5,000 years have clear geomorphic expression (Reference 531). Perhaps it is more likely that the Charleston source has a recurrence behavior that is highly variable through time, such that a sequence of events spaced about 500 years apart is followed by quiescent intervals of thousands of years or longer. This sort of variability in inter-event time may be represented by the entire mid-Holocene record, in which both short inter-event times (e.g., about 400 years between Events A and B) are included in a record with long inter-event times (e.g., about 1,900 years between Events C' and E).

Recurrence Rates

The UCSS model calculates two average recurrence intervals covering two different time intervals, which are used as two recurrence branches on the logic tree (Figure 2.5-267). The first average recurrence interval is based on the four events that occurred within the past about 2,000 years. This time period is considered to represent a complete portion of the paleoseismic record based on published literature [e.g., (Reference 461)] and feedback from those researchers questioned (Reference 540; Reference 529). These events include 1886, A, B, and C' (Table 2.5-214). The average recurrence interval calculated for the most recent portion of the paleoliquefaction record (four events over the past about 2,000 years) is given 0.80 weight on the logic tree (Figure 2.5-267).

The second average recurrence interval is based on events that occurred within the past about 5,000 years. This time period represents the entire paleoseismic record based on paleoliquefaction data (Reference 461). These events include 1886, A, B, C', E, and F' as listed in Table 2.5-214. As mentioned previously, published papers and researchers questioned suggest that the older part of the record (older than about 2,000 years ago) may be incomplete. Whereas this assertion may be true, it is also possible that the older record, which exhibits longer inter-event times, is complete. The average recurrence interval calculated for the 5,000-year record (six events) is given 0.20 weight on the logic tree (Figure 2.5-267). The 0.80 and 0.20 weighting of the 2,000-year and 5,000-year paleoliquefaction records, respectively, reflect incomplete knowledge of both the current short-term recurrence behavior and the long-term recurrence behavior of the Charleston source.

The mean recurrence intervals for the most-recent 2,000-year and past 5,000-year records represent the average time interval between earthquakes attributed to the Charleston seismic source. The mean recurrence intervals and their parametric uncertainties were calculated according to the

methods outlined by Savage (1991) and Cramer (2001). The methods provide a description of mean recurrence interval, with a best estimate mean T_{ave} and an uncertainty described as a lognormal distribution with median $T_{0.5}$ and parametric lognormal shape factor $\sigma_{0.5}$.

The lognormal distribution is one of several distributions, including the Weibull, Double Exponential, and Gaussian, among others, used to characterize earthquake recurrence (Reference 510). Ellsworth et al. (1999a) and Matthews et al. (2002) propose a Brownian-passage time model to represent earthquake recurrence, arguing that it more closely simulates the physical process of strain build-up and release. This Brownian-passage time model is currently used to calculate earthquake probabilities in the greater San Francisco Bay region (Reference 547). Analyses show that the lognormal distribution is very similar to the Brownian-passage time model of earthquake recurrence for cases where the time elapsed since the most recent earthquake is less than the mean recurrence interval (Reference 508; Reference 510). This is the case for Charleston, where 120 years have elapsed since the 1886 earthquake and the mean recurrence interval determined over the past 2,000 years is about 548 years. The UCSS study has chosen to calculate average recurrence interval using a lognormal distribution because its statistics are well known (Reference 527) and it has been used in numerous studies [e.g., (Reference 532; Reference 546; Reference 509)].

The average interval between earthquakes is expressed as two continuous lognormal distributions. The average recurrence interval for the 2,000-year record, based on the three most recent inter-event times (1886-A, A-B, B-C'), has a best estimate mean value of 548 years and an uncertainty distribution described by a median value of 531 years and a lognormal shape factor of 0.25. The average recurrence interval for the 5,000-year record, based on five inter-event times (1886-A, A-B, B-C', C'-E, E-F'), has a best estimate mean value of 958 years and an uncertainty distribution described by a median value of 841 years and a lognormal shape factor of 0.51. At one standard deviation, the average recurrence interval for the 2,000-year record is between 409 and 690 years; for the 5,000-year record, it is between 452 and 1,564 years. Combining these mean values of 548 and 958 years with their respective logic tree weights of 0.8 and 0.2 results in a weighted mean of 630 years for Charleston M_{max} recurrence.

The mean recurrence interval values used in the UCSS model are similar to those determined by earlier studies. Talwani and Schaeffer (2001) consider two possible scenarios to explain the distribution in time and space of paleoliquefaction features. In their Scenario 1, large earthquakes have occurred with an average recurrence of 454 ± 21 years over about the past 2,000 years; in their Scenario 2, large earthquakes have occurred with an average recurrence of 523 ± 100 years over the past 2,000 years. Talwani and Schaeffer (2001) state that, "In anticipation of additional data we suggest a recurrence rate between 500 and 600 years for **M** 7+ earthquakes at Charleston". For the 2,000-year record, the 1-standard-deviation range of 409 to 690 years completely encompasses the range of average recurrence interval reported by Talwani and Schaeffer (2001). The best-estimate mean recurrence interval value of 548 years is comparable to the midpoint of the Talwani and Schaeffer (2001) best-estimate range of 500 to 600 years. The best estimate mean recurrence interval value from the 5,000-year paleoseismic record of 958 years is outside the age ranges reported by Talwani and Schaeffer (2001), although they did not determine an average recurrence interval based on the longer record.

In the updated seismic hazard maps for the conterminous United States, Frankel et al. (2002) use a mean recurrence value of 550 years for characteristic earthquakes in the Charleston region. This value is based on the above-quoted 500 to 600 year estimate from Talwani and Schaeffer (2001). Frankel et al. (2002) do not incorporate uncertainty in mean recurrence interval in their calculations.

For computation of seismic hazard, discrete values of activity rate (inverse of recurrence interval) are required as input to the PSHA code (Cornell 1968). To evaluate PSHA based on mean hazard, the mean recurrence interval and its uncertainty distribution should be converted to mean activity rate with associated uncertainty. The final discretized activity rates used to model the UCSS in the PSHA

reflect a mean recurrence of 548 years and 958 years for the 2,000-year and 5,000-year branches of the logic tree, respectively. Lognormal uncertainty distributions in activity rate are obtained by the following steps: (1) invert the mean recurrence intervals to get mean activity rates; (2) calculate median activity rates using the mean rates and lognormal shape factors of 0.25 and 0.51 established for the 2,000-year and 5,000-year records, respectively; and (3) determine the lognormal distributions based on the calculated median rate and shape factors. The lognormal distributions of activity rate can then be discretized to obtain individual activity rates with corresponding weights.

2.5.2.2.2.5 Eastern Tennessee Seismic Zone

The Eastern Tennessee Seismic Zone (ETSZ) is one of the most active seismic zones in Eastern North America. This region of seismicity in the southern Appalachians is described in [Subsection 2.5.1.1.4.6](#). Despite its high rate of activity, the largest known earthquake was magnitude 4.6 ([Reference 505](#)). No evidence for larger prehistoric earthquakes, such as paleoliquefaction features, has been discovered ([Reference 505](#); [Reference 482](#)). While the lack of large earthquakes in the relatively short historical record cannot preclude the future occurrence of large events, there is a much higher degree of uncertainty associated with the assignment of M_{\max} for the ETSZ than other CEUS seismic source zones, such as New Madrid and Charleston, where large historical earthquakes are known to have occurred.

The EPRI source model ([Reference 511](#)) includes various source geometries and parameters to represent the seismicity of the ETSZ. All but one of the EPRI Earth Science Teams (ESTs) modeled local source zones to capture this area of seismicity and some ESTs included more than one zone. The Law team did not include a specific, local source for the ETSZ, however the ETSZ and Giles County seismic zones were included in a larger seismic source zone called the Eastern Basement (17). A wide range of M_{\max} values and associated probabilities were assigned to these sources to reflect the uncertainty of multiple experts from each EST. The moment magnitude (M) equivalents of body-wave magnitude (m_b) M_{\max} values assigned by the ESTs range from M 4.8 to 7.5. The Dames & Moore sources for the ETSZ included the largest upper-bound M_{\max} value of M 7.5. Sources from the Woodward-Clyde and Rondout teams were also assigned large upper-bound M_{\max} values of M 7.2.

Subsequent hazard studies have used M_{\max} values within the range of maximum magnitudes used by the six EPRI models. Collectively, upper-bound maximum values of M_{\max} used by the EPRI teams ranged from M 6.3 to 7.5. Using three different methods specific to the Eastern Tennessee seismic source, Bollinger (1992) estimated an M_{\max} of M 6.3. The Bollinger (1992) model also included the possibility that the ETSZ was capable of generating a larger magnitude event and included an M 7.8 (m_b 7.37) with a low probability of 5% in the M_{\max} distribution. The 5% weighted M 7.8 by Bollinger (1992) slightly exceeds the EPRI range, but the M 6.3 value was given nearly the entire weight (95%) in his characterization of the ETSZ. This smaller magnitude is much closer to the mean magnitude (about M 6.2) of the EPRI study. The Trial Implementation Project (TIP) ([Reference 533](#)) also provided a broad M_{\max} distribution for the ETSZ. This study developed magnitude distributions for all ETSZ source zone representations that ranged from as low as M 4.5 to as high as M 7.5, with a mode of about M 6.5 for almost each distribution ([Reference 533](#), pages F-12 to F-19 of Appendix F). The broad distribution of the TIP study magnitude distribution for the ETSZ source zones is very similar to the EPRI distribution of M 4.8 to M 7.5. The USGS source model assigns a single M_{\max} value of M 7.5 for the ETSZ ([Reference 282](#)). The most recent characterizations of the ETSZ M_{\max} by the USGS and TIP study consider M 7.5 as the largest magnitude in the distribution, and this magnitude is captured by the range of M_{\max} values used in EPRI (NP-4726 1986). Therefore, it is concluded that no new information has been developed since 1986 that would require a significant revision to the EPRI seismic source model.

For the VEGP ESP site, the contribution to hazard from the ETSZ sources in the EPRI study was minimal. With the exception of the Law source 17 (Eastern Basement), none of the ETSZ sources

contributed more than one percent of the site hazard, and thus were excluded from the final hazard calculations ([Reference 513](#)). The ground motion hazard at the VEGP ESP site is dominated by the Charleston seismic source, and the inclusion of new recurrence values for Charleston based on paleoliquefaction serves to increase the relative contribution of Charleston with respect to any distant source, such as the ETSZ. No modifications to the EPRI parameters for ETSZ source zones were made as part of this ESP study.

2.5.2.3 Correlation of Seismicity with Geologic Structures and EPRI Sources

The final part of the review and update of the 1989 EPRI seismic source model was a correlation of updated seismicity with the 1989 model source. The EPRI seismicity catalog covers earthquakes in the CEUS through 1984, as described in [Subsection 2.5.2.1](#). [Figures 2.5-257 through 2.5-262](#) shows the distribution of earthquake epicenters from both the EPRI (pre-1985) and updated (post-1984 through April 2005) earthquake catalogs in comparison to the seismic sources identified by each of the EPRI ESTs.

Comparison of the additional events of the updated earthquake catalog to the EPRI earthquake catalog shows:

- There are no new earthquakes within the site region that can be associated with a known geologic structure.
- There are no unique clusters of seismicity that would suggest a new seismic source not captured by the EPRI seismic source model.
- The updated catalog does not show a pattern of seismicity that would require significant revision to the geometry of any of the EPRI seismic sources.
- The updated catalog neither shows nor suggests any increase in M_{\max} for any of the EPRI seismic sources.
- The updated catalog does not imply a significant change in seismicity parameters (rate of activity, b-value) for any of the EPRI seismic sources (see also [Subsection 2.5.2.4.2](#)).

2.5.2.4 Probabilistic Seismic Hazard Analysis and Controlling Earthquakes

PSHA is an accepted method for determining seismic design levels (RG 1.165). The PSHA developed here relies on seismic source inputs from the EPRI-SOG study ([Reference 514](#)) which is accepted by the NRC (RG 1.165), on updates to those sources as described in [Subsection 2.5.2.2](#), and on ground motion models ([Reference 516](#)) that have been accepted under other ESP applications.

The final GMRS ground motion for the VEGP ESP site is developed using a performance-based approach, which has as its foundation a well-justified PSHA for the VEGP ESP site. Ground motion levels corresponding to mean annual frequencies of exceedance (MAFEs) of 10^{-4} to 10^{-6} are developed, because this range encompasses the range of motions necessary to establish the GMRS ground motion under several criteria.

The seismic hazard at the VEGP ESP was first calculated using the assumptions of the EPRI (NP-6395-D 1989) study. This was to confirm that the 1989 results could be replicated. Then the seismic sources were updated with the UCSS models, including sources surrounding the Charleston source for each team, as described in [Subsection 2.5.2.2.2](#). Also, the EPRI (1009684 2004) ground motion model was adopted for calculations of seismic hazard at seven structural frequencies. Sensitivity studies were conducted to determine the effects of these changes.

The seismic hazard was calculated for hard rock conditions for a range of ground motions corresponding to a range of annual frequencies of exceedance. This hard rock hazard formed the basis with which to integrate the effects of surficial materials on ground motion, to calculate the seismic hazard at a horizon appropriate for seismic design. The ASCE 43-05 2005 procedure was used to recommend an appropriate GMRS seismic spectrum. This procedure requires ground motion amplitudes and slopes of seismic hazard curves in the range of 10^{-4} to 10^{-5} mean annual frequency of exceedance. To obtain a full design spectrum from structural frequencies of 0.1 to 100 Hz, a smooth site-specific spectral shape was fit to the seven structural frequencies for which specific seismic hazard calculations were made.

2.5.2.4.1 Replication of 1989 EPRI Probabilistic Seismic Hazard Results

PSHA calculations were initially made using the original 1989 EPRI-SOG seismic sources and ground motion assumptions (Reference 514). The purpose of these calculations was to validate Risk Engineering Inc.'s (REI) proprietary FRISK88 seismic hazard code, the EPRI-SOG seismic sources, the EPRI-SOG source combinations, and the EPRI-SOG attenuation equations, as modeled by the FRISK88 code. The results used in this replication were the peak ground acceleration (PGA) results available for VEGP site (see Appendix E, Table 3-103 of Reference 514).

Seismic sources used to represent the seismic hazard for each of the six teams in the EPRI-SOG study are shown in Table 2.5-215. These are the primary sources used for the VEGP site in the original EPRI-SOG study, as documented in the EQHAZARD input files transmitted by EPRI.

The ground motion attenuation relations and their relative weights used in this analysis are those specified in the EPRI-SOG study (see Table 4-1 of Reference 514). Following Table 4-1 of EPRI NP-6395-D, a standard deviation of (log) amplitude of 0.5 was assumed for each ground motion equation. These equations were used to calculate hard rock hazard.

The VEGP site is classified in EPRI NP-6395-D 1989 as a "Soil V" site (see Table 2-2 of Reference 514). The site amplification factor versus PGA for this site class is shown in Figure 2-6 of EPRI NP-6395-D. To avoid having to apply site amplification factors to the rock curves, the results calculated here were compared to original EPRI-SOG hard rock results received from EPRI.

Results of this seismic hazard calculation are compared to the EPRI-SOG results in Table 2.5-216.

Agreement is excellent, generally within 5.1 percent in hazard for amplitudes up to 1g. For the 85 percent, replication is slightly less accurate, with a difference of -11.5 percent and -11.7 percent at 0.05g and 0.1g, respectively. This slight difference is of less concern, because the mean hazard curve is used to develop the GMRS ground motions. Comparison plots of the mean, median, and 85 percent PGA hazard curves are shown in Figures 2.5-270 through 2.5-272.

This comparison validates the FRISK88 code, the EPRI-SOG seismic sources, the EPRI-SOG source combinations, and the EPRI-SOG attenuation equations.

2.5.2.4.2 Effects of New Regional Earthquake Catalog

The effects of the new regional earthquake catalog were examined by comparing seismicity rates in two regions critical to seismic hazard at the VEGP ESP site: the Charleston, South Carolina, region and the local region in South Carolina and into Georgia around the VEGP ESP site. The importance of these regions to seismic hazard is addressed in Subsection 2.5.2.4.6. The effects of two seismicity catalogs were compared: (1) the EPRI-SOG (Reference 512) earthquake catalog (through 1984) and (2) the EPRI-SOG catalog updated to include more recent seismicity (Subsection 2.5.2.1). The fundamental question to be addressed is whether or not the seismicity recorded since 1984 indicates

that the seismic activity rates used in the EPRI-SOG study (Reference 514) are inadequate or insufficiently conservative for assessment of the seismic hazard at the VEGP ESP site.

Seismicity rates were assessed for two sources in the site region, as follows: (1) a small rectangular source around the Charleston seismicity and (2) a triangular-shaped source representing seismicity in South Carolina and a strip of Georgia incorporating the VEGP ESP site. Figure 2.5-273 shows a map of these two sources, along with the earthquakes from the EPRI-SOG catalog and from the updated catalog.

The seismicity in these two sources was investigated by running program EQPARAM (from the EPRI EQHAZARD package), first for the original EPRI catalog and then using the updated EPRI catalog (through April 2005). Full smoothing of a- and b-values was selected for the comparison because this was a common choice of many of the ESTs in the EPRI-SOG study. Further, if comparisons were made on an individual degree-cell basis, the rates in some cells might increase and in others might decrease; furthermore, for a source such as the triangular South Carolina source, a composite rate would have to be used to compare seismic rates using the earthquake catalog through 1984 to those using the earthquake catalog through April 2005. The choice of full smoothing achieves this composite rate directly and automatically, since it is a composite rate for the entire source.

From the a- and b-values calculated with EQPARAM, recurrence rates were calculated for different magnitudes. Figures 2.5-274 and 2.5-275 compare the annual recurrence rates for the Charleston source and for the triangular South Carolina source, respectively. For the rectangular Charleston source, the updated catalog indicates that seismicity rates are about the same. For the triangular South Carolina source, the updated catalog indicates that seismicity rates have decreased when the seismicity from 1985 to April 2005 is added.

The conclusion is that the seismicity recorded since 1984 does not indicate that seismic activity rates have increased in those sources contributing most to the hazard at the VEGP ESP site under the assumptions of the EPRI-SOG study. Therefore, for original sources of the EPRI-SOG teams and the original seismicity rates from the EPRI-SOG (Reference 512) earthquake catalog (through 1984) were used here for calculations of seismic hazard. These rates give an accurate estimate of seismicity for Charleston sources, and are slightly conservative for local sources, when compared to rates from the updated (through April 2005) catalog. Where the geometries of EPRI-SOG sources were modified to account for new information on the Charleston earthquake source (see Subsection 2.5.2.4.4 below), new seismicity rates were calculated using the updated earthquake catalog (through April 2005) in order to use the most recent information available.

2.5.2.4.3 New Maximum Magnitude Information

Geological and seismological data published since the 1986 EPRI seismic source model are presented in Subsection 2.5.1. Based on a review of these data, there are no significant changes in the EPRI M_{\max} parameters, with the exception of the Charleston seismic source. A summary of M_{\max} values for each EPRI EST is provided in Tables 2.5-203 through 2.5-208.

Changes to M_{\max} for the Charleston seismic source are discussed in Subsection 2.5.2.2.2 and in a separate Engineering Study Report (Reference 498).

2.5.2.4.4 New Seismic Source Characterizations

The effect of new geoscience information is to modify the interpretations for the Charleston seismic source. The EPRI-SOG teams used an exponential model to represent earthquakes for sources in the Charleston area, and some teams adopted interpretations that included (with a low weight) the possibility that a specific Charleston source did not exist (i.e., that large earthquakes could occur in a large region in the eastern US). The new interpretation of the Charleston source (see

Subsection 2.5.2.2.2) indicates that a unique source of large earthquakes exists with weight 1.0 and that large magnitudes occur with a rate of occurrence unrelated to the rate of smaller magnitudes. Typical recurrence intervals for large Charleston earthquakes for the EPRI-SOG teams were on the order of 2,000 years, whereas the new information indicates recurrence intervals of 500 to 1,000 years.

In addition, the geometry of the Charleston sources has changed. Some EPRI-SOG teams drew relatively broad zones within which a Charleston-size earthquake could occur or specified (under some interpretations) that Charleston-size earthquakes were not restricted to southeast South Carolina but could occur over broad areas. The new geologic and tectonic information presented in **Subsection 2.5.2.2.2** describes a relatively restricted zone within which Charleston-size earthquakes are modeled.

These changes in rate of occurrence and location of Charleston sources generally have the effect of increasing seismic hazard at the VEGP ESP site, compared to the EPRI-SOG study. It is not possible to determine the specific effect of one change, because (for example) changing the geometry of the Charleston source affects the geometries and seismicity rates of local sources and background sources for each EPRI-SOG team. The total effect of the new geoscience information is taken into account in the revised PSHA results presented in **Subsection 2.5.2.4.6**.

Figure 2.5-276 (reproducing **Figure 2.5-265** content relevant to this discussion) shows the geometry of the four sources used to characterize the Charleston seismic source (**Subsection 2.5.2.2.2**).

To update the EPRI-SOG model, these four geometries of the Charleston source were overlaid onto each of the six EPRI-SOG team sources, and new geometries were created for all EPRI-SOG team sources surrounding the Charleston source. **Figure 2.5-277** shows an example of the original geometry, and **Figures 2.5-278** through **2.5-281** show the new geometries created for the Rondout team, source 26. The purpose in creating the new geometries was to ensure that, in incorporating the new Charleston sources, no area was left without seismicity. Seismicity parameters for the new EPRI-SOG team source geometries were calculated using the same methodology and same smoothing assumptions as in the EPRI-SOG project and using the updated seismicity catalog (through April 2005). This procedure ensured that the principles underlying the seismicity representations for each EPRI-SOG team source surrounding Charleston were maintained.

The four geometries used to represent the Charleston source were modeled, for seismic hazard calculations, with parallel faults striking northeast-southwest and spaced at 10 km intervals. This spacing was narrow enough not to affect the calculated hazard (i.e., a spacing of 5 km would not have produced significantly different results). Activity rates for the faults were equally divided among the faults, and they were represented as vertical faults from the surface to a depth of 20 km. A rupture length equation (given magnitude) was used to represent a finite rupture length, and an aspect ratio (width-to-length) of 0.5 was assumed. The specific equation selected was for surface rupture length for all rupture types from Wells and Coppersmith (1994).

A characteristic earthquake was modeled for the new Charleston source geometries, with the following magnitudes and weights (**Figure 2.5-267**):

<u>M</u>	<u>Weight</u>
6.7	0.1
6.9	0.25
7.1	0.3
7.3	0.25
7.5	0.1

The magnitudes and weights were discussed in [Subsection 2.5.2.2.4.2](#). The rate of occurrence of the characteristic earthquake was modeled with two 5-point discrete distributions representing (respectively) the 2,000-year and 5,000-year paleoliquefaction intervals described in [Subsection 2.5.2.2.4.3](#). These distributions are as follows:

<u>2,000-Year Interval</u>		<u>5,000-Year Interval</u>	
<u>Activity Rate</u>	<u>Weight</u>	<u>Activity Rate</u>	<u>Weight</u>
1.22×10^{-3}	0.101	3.65×10^{-4}	0.101
1.45×10^{-3}	0.244	6.12×10^{-4}	0.244
1.77×10^{-3}	0.310	9.20×10^{-4}	0.310
2.16×10^{-3}	0.244	1.38×10^{-3}	0.244
2.78×10^{-3}	0.101	2.32×10^{-3}	0.101

These distributions give mean activity rates of 1.823×10^{-3} and 1.044×10^{-3} , respectively, which correspond to recurrence intervals of 548 years and 958 years, and have logarithmic shape factors of 0.25 and 0.51, as described in [Subsection 2.5.2.2.4.3](#).

In addition to the characteristic earthquake, smaller earthquakes were modeled for each of the four source geometries for magnitudes between the lower-bound magnitude ($m_b = 5.0$) and M_{\max} value of $m_b = 6.7$, with an exponential magnitude distribution. The activity rate and b-value for this distribution were determined using the EPRI-SOG catalog, EQPARAM software, and full smoothing of seismicity parameters across the source. For this exponential model, the rectangular geometries of the Charleston sources were assumed (see [Figure 2.5-276](#)), with earthquakes uniformly distributed within the source.

The source combinations of the EPRI-SOG teams were reviewed and modified to accurately incorporate the four new Charleston seismic sources into each team's model. This generally resulted in four times as many source combinations, because a single Charleston source was being replaced by four alternative Charleston sources. As an example, the Rondout team originally had one source combination applicable to the VEGP ESP site:

<u>Source Combination</u>	<u>Weight</u>	<u>Sources</u>
1	1.0	26, 24

The revised model for the Rondout team had four source combinations applicable to the VEGP ESP site:

<u>Source Combination</u>	<u>Weight</u>	<u>Sources</u>
1	0.7	Charleston-A, 26-A
2	0.1	Charleston-B, 26-B
3	0.1	Charleston-B', 26-B'
4	0.1	Charleston-C, 26-C

where, for example, "26-A" indicates Rondout source 26 with new Charleston source geometry A removed. See [Figures 2.5-278 through 2.5-281](#) for maps of these source geometries.

Incorporating this new geoscience information into the PSHA for the VEGP ESP site ensures that the PSHA results reflect the most recent information and interpretations of seismicity in the southeastern US. This provides a strong basis for the GMRS ground motions.

2.5.2.4.5 New Ground Motion Models

The ground motion models developed by the 2004 EPRI-sponsored study ([Reference 516](#)) were used to examine the effects on seismic hazard of current estimates of seismic shaking as a function of earthquake magnitude and distance. For general area sources, nine estimates of median ground motion are combined with four estimates of aleatory uncertainty, giving 36 combinations. For fault sources in rifted regions, which applies to the ECFS fault segments, 12 estimates of median ground motion are combined with four estimates of aleatory uncertainty, giving 48 combinations. When both area sources and faults are active, a specific correlation of area source models and fault source models is used to represent ground motion models that might apply together. These families of models (36 for area sources, 48 for fault sources) represent the epistemic uncertainty in ground motion, and contribute to the epistemic uncertainty in seismic hazard.

Conclusions regarding a comparison of the EPRI NP-6395-D (1989) ground motion models with the EPRI 1009684 (2004) ground motion models depend on the specific magnitude, distance, and structural frequency being compared. Some comparison plots are shown in EPRI 1009684. In general, median ground motion amplitudes are similar at high frequencies. At low frequencies, the EPRI 1009684 models show lower median ground motions, because these models incorporate the possibility of a two-corner seismic source. Seismic hazard is affected by the median ground motion and also by the standard deviation. The EPRI 1009684 standard deviations are universally higher than those of EPRI NP-6395-D, which leads to higher seismic hazards.

2.5.2.4.6 Updated EPRI Probabilistic Seismic Hazard Analysis, Deaggregation, and 1 Hz, 2.5 Hz, 5 Hz, and 10 Hz Spectral Accelerations Incorporating Significant Increases Based on the Above Sensitivity Studies

Sensitivity studies were conducted to determine which magnitudes and distances contribute most to the seismic hazard at the VEGP ESP site. This was done following the guidelines of RG 1.165, modified for use in calculating GMRS spectra using a performance-based procedure. Specifically, the seismic hazard was deaggregated at mean annual frequencies of exceedance (MAFEs) of 10^{-4} , 10^{-5} , and 10^{-6} . Deaggregations were conducted for two sets of spectral frequencies: a “high-frequency” (HF) set consisting of 10 Hz and 5 Hz and a “low-frequency” (LF) set consisting of 2.5 Hz and 1 Hz. [Figure 2.5-282](#) shows a mean uniform hazard spectrum (UHS) for hard rock conditions at the VEGP ESP site for several MAFEs from 10^{-4} to 10^{-6} , and [Table 2.5-217](#) lists the values of the mean UHS for hard rock conditions for these MAFEs for frequencies of 100 Hz (PGA), 25 Hz, 10 Hz, 5 Hz, 2.5 Hz, 1 Hz, and 0.5 Hz.

[Figures 2.5-283](#) through [2.5-288](#) show the hard rock magnitude-distance deaggregations for three MAFEs and for the high- and low-frequency sets. For the low frequencies, earthquakes from the Charleston sources dominate the hazard at all MAFEs considered. For the high frequencies, local earthquakes contribute substantially to the hazard at 10^{-5} and dominate the contribution to hazard at the 10^{-6} MAFE level.

[Figures 2.5-289](#) and [2.5-290](#) show marginal magnitude distributions for hard rock PSHA from the deaggregations for high- and low-frequencies, respectively, for the three MAFEs. For the low frequencies, the large earthquakes from the Charleston dominate the hazard at all three MAFEs. For the high frequencies, large earthquakes dominate 10^{-4} but the smaller earthquakes dominate 10^{-6} .

[Figures 2.5-291](#) and [2.5-292](#) show marginal distance distributions for hard rock PSHA from the deaggregations for high- and low-frequencies, respectively, for the three MAFEs. These deaggregations are consistent with those for magnitude, in terms of the contribution of large earthquakes from the Charleston sources.

The contribution of the Charleston sources to hazard can be understood by plotting and comparing hazard curves from individual sources. [Figure 2.5-293](#) shows such a comparison, using as an example the sources from the Rondout team (which is the simplest interpretation). [Figure 2.5-293](#), for 10 Hz spectral acceleration, shows that the main Charleston source (geometry A, marked “C-A” in [Figure 2.5-293](#), with a weight of 0.7) dominates for MAFEs of 10^{-3} to 10^{-4} but that the local source “RND-26-A” dominates for lower MAFEs (below about 3×10^{-5}). At the 10^{-6} MAFE, most of the contribution to total hazard is from the local source. [Figure 2.5-294](#), showing hazard curves for the Rondout team for 1 Hz spectral acceleration, indicates that the Charleston sources dominate the total hazard at all MAFEs (at least above 10^{-7}). Note that in both [Figures 2.5-293](#) and [2.5-294](#), the mean hazard curve for each source includes the probability that source is active. Thus, the hazard curves for Charleston sources B, B’, and C (labeled C-B, C-B’, and C-C) are lower than the hazard curve for Charleston source A (labeled C-A), primarily because the former three have much lower probabilities of activity than does source A.

These results indicate that seismic sources representing earthquakes in the Charleston region have a large contribution to seismic hazard for hard rock conditions at the VEGP ESP site. The local seismic source representing seismicity in South Carolina also can have an important contribution to hazard for high frequency ground motion, particularly for MAFEs around 10^{-5} and lower.

2.5.2.5 Seismic Wave Transmission Characteristics of the Site

The uniform hazard spectra described in the preceding section are defined on hard rock (shear-wave velocity of 9,200 ft/sec), which is located more than 1,000 ft below the current ground surface at the VEGP ESP site. The subsurface materials at the VEGP ESP site are described in detail in [Subsection 2.5.1](#). The material characterization is summarized in the following groups:

- I. Upper Sand Stratum (Barnwell Group) – predominantly sands, silty sands, and clayey sands, with occasional clay seams. A Shelly Limestone (Utley Limestone) layer was encountered at the base of the Upper Sand Stratum or the top of the Blue Bluff Marl. The limestone contains solution channels, cracks, and discontinuities, and was the cause of severe fluid loss observed during drilling for the VEGP ESP site subsurface investigation.
- II. Marl Bearing Stratum (Blue Bluff Marl or Lisbon Formation) – slightly sandy, cemented, calcareous clay.
- III. Lower Sand Stratum (comprises several formations from the Still Branch just beneath the Blue Bluff Marl to the Cape Fear just above the Dunbarton Triassic Basin rock) – fine to coarse sand with interbedded silty clay and clayey silt.
- IV. Dunbarton Triassic Basin Rock – red sandstone, breccia, and mudstone, weathered along the upper 120 ft.
- V. Paleozoic Crystalline Rock – a competent rock with high shear-wave velocity that underlies the Triassic Basin rock. The non-capable Pen Branch fault forms the boundary between the Triassic Basin and Paleozoic basement rocks (see [Subsection 2.5.1.2.4](#) for a detailed discussion of the Pen Branch fault).

The Upper Sand Stratum (Barnwell Group) will be removed because it is not considered competent material. It is susceptible to liquefaction ([Subsection 2.5.4.8](#)) and dissolution-related ground deformation ([Subsection 2.5.3.8.2](#)); also the shear-wave velocity of the Upper Sand Stratum is generally below 1000 ft/sec, see [Table 2.5-218](#).

All safety-related structures will be founded on structural backfill that will be placed on top of the Blue Bluff Marl after complete removal of the Upper Sand Stratum. The structural fill will be a sandy or silty

sand material following the guidelines used during construction of VEGP Units 1 and 2. The properties of this structural backfill are described in [Subsection 2.5.4.2](#).

The GMRS is defined at the free ground surface of this site-specific rock, soil, fill column. The FIRS is defined as hypothetical outcrop motion at the 40-ft depth horizon within this column. The highest in situ competent material for the VEGP ESP site is the Blue Bluff marl at 86-ft depth.

To determine the GMRS, FIRS, and 86-ft depth horizon ground motions, it is necessary to adjust the uniform hazard hard rock spectra (presented in [Subsection 2.5.2.4](#)) for amplification or deamplification as vibratory ground motion is propagated through the subsurface materials above the 9,200 ft/s shear-wave velocity horizon. This section describes the analyses performed to develop site amplification functions associated with the different hard rock ground motions presented in [Subsection 2.5.2.4](#). These site amplification factors are used in [Subsection 2.5.2.6](#) (GMRS, FIRS, and top of Blue Bluff Marl) along with the hard rock ground motions to develop site-specific ground motions at these three horizons.

2.5.2.5.1 Development of Site Amplification Factors

2.5.2.5.1.1 Methodology

The method adopted here to account for the effects of surficial soils on seismic hazard follows the procedure in NUREG/CR-6728 and NUREG/CR-6769 ([Reference 525](#), [Reference 526](#)), described as “Approach 2A.” This procedure requires 6 steps:

1. The seismic hazard is calculated for hard rock conditions for the seven structural frequencies, over a range of ground motion amplitudes, resulting in a range of annual frequencies of exceedance.
2. For ground motion amplitudes corresponding to annual frequencies of 10^{-4} , 10^{-5} , and 10^{-6} , the seismic hazard is deaggregated for high frequencies (HF) and low frequencies (LF), as described in [Subsection 2.5.2.4.6](#), to determine the dominant magnitudes and distances for those amplitudes and frequencies.
3. HF hard rock spectra are developed to represent earthquakes dominating the 5-10 Hz ground motions, and LF hard rock spectra are developed to represent earthquakes dominating the 1-2.5 Hz ground motions. These hard rock spectra represent the mean magnitude and distance of earthquakes that dominate the seismic hazard for those structural frequencies.
4. The rock and soil column is modeled, and soil amplitudes are calculated for input hard rock motions corresponding to frequencies of exceedance of 10^{-4} , 10^{-5} , and 10^{-6} . These calculations are made separately for ground motions dominating the HF hard rock motion and the LF hard rock motion, and the input motions have a spectrum determined by the HF or LF hard rock spectral shape, as appropriate. Multiple hard rock motions are used, and multiple soil column properties are used, so that the mean soil amplitudes can be determined accurately.
5. The soil amplification factors (AFs) are developed at 300 frequencies using analyses described in this section based on the HF and LF hard rock spectral shapes. The AFs for a given horizon represent the mean spectral acceleration (SA) at that horizon, divided by input SA at hard rock, at each frequency. At each frequency, the envelope motion is determined. This is the motion (HF or LF) that gives the higher mean soil motion, for that structural

frequency and MAFE. At frequencies above 8 Hz, this is always the HF motion. At frequencies below 2 Hz, this is always the LF motion. At intermediate frequencies, the envelope motion depends on the frequency and the MAFE.

6. The uniform hazard response spectra at MAFEs of 10^{-4} and 10^{-5} at each horizon are calculated as follows. Starting from the 10^{-4} and 10^{-5} SA hard rock values (from the hazard calculations described in [Subsection 2.5.2.4](#)) at the seven structural frequencies, interpolation is performed between those SA values to obtain 10^{-4} and 10^{-5} SA values at the 300 structural frequencies using the HF and LF spectral shapes for hard rock. The choice of HF or LF is based on the envelope motion determined in the previous step. The UHS for 10^{-4} at each horizon is calculated by multiplying the hard rock 10^{-4} SA values at the 300 frequencies by the mean AFs for 10^{-4} from step 5, again using the HF or LF mean AF corresponding to the envelope motion. (At some intermediate frequencies between 2 and 8 Hz, the HF and LF AFs are weighted in order to achieve a smooth transition between HF and LF spectra.) The UHS for 10^{-5} is calculated in a similar way, using the 10^{-5} rock SA values and the 10^{-5} AFs.

This gives an accurate calculation of the soil hazard at each horizon. In step 3, it is sufficiently accurate to use the mean magnitude to generate spectral shapes for the HF and LF spectra (Approach 2A of NUREG/CR-6728 and NUREG/CR-6769 ([Reference 525](#), [Reference 526](#))). Using multiple magnitudes (Approach 2B of NUREG/CR-6728 and NUREG/CR-6769) does not materially affect the calculated soil spectra, as documented in NUREG/CR-6769 ([Reference 526](#))).

From the 10^{-4} and 10^{-5} SA values at each horizon, spectra are calculated using the procedure recommended by ASCE 43-05 2005. This procedure is used to establish the spectral amplitudes at the 300 structural frequencies. To obtain final horizontal spectra smoothing of the raw spectral shape is performed as described in [Subsection 2.5.2.6.3](#).

2.5.2.5.1.2 Base Case Soil/Rock/Fill Column and Uncertainties

Development of a base case rock/soil/fill column, is described in [Subsection 2.5.1](#). Summaries of the low strain shear wave velocity, material damping, and strain-dependency properties of the base case materials, as these parameters are used in the site response analyses, are provided below in [Subsection 2.5.2.5.1.2.1](#). [Subsection 2.5.2.5.1.2.2](#) describes the methodology and results of randomization to address the uncertainties in rock/soil/fill column parameters. Additional subsurface data in the power block has been collected for the COL site investigation. These data are presented in [Subsection 2.5.1](#). The COL information includes RCTS testing and measurements of dynamic properties of the proposed backfill. [Subsection 2.5.2.9.3](#) presents an evaluation of the effects of the combined COL and ESP geotechnical data on site response to determine its significance on site response.

2.5.2.5.1.2.1 Base Case Rock/Soil/Fill Column

2.5.2.5.1.2.1.1 Soil Column

The base case shear-wave velocity model for the soil column is provided in [Figure 2.5-378](#), and the corresponding values are listed in [Table 2.5-251](#). Additional shear-wave velocity data have been collected for the COL site investigation of the in-situ material. [Figure 2.5-379](#) shows the base case shear-wave velocity model for the combined COL and ESP data. The COL plus ESP data shear-wave velocity model is not used to develop the ESP site amplification factors. This is discussed further below. The base case assumes that the uppermost 86 feet of native material will be excavated and replaced with structural fill. Shear-wave velocity was not measured for the compacted backfill during the ESP subsurface investigation ([Appendix 2.5A](#)). Interpolated values based on measurements made on fill for existing Units 1 and 2 ([Bechtel 1984](#)) are used instead. The backfill

shear-wave velocity values are summarized in [Table 2.5-249](#) (these values are also included in [Table 2.5-251](#)).

The variation with strain of shear modulus and damping of the soil were developed for two sets of degradation relationships:

- Based on relationships developed for EPRI ([Reference 515](#)) and
- Based on relationships developed for SRS ([Reference 519](#)).

Site-specific soil degradation and damping ratio curves were developed as part of the COL site investigation. These curves are presented in [Figures 2.5-382](#) and [2.5-385](#), respectively.

The EPRI relationships are widely used and accepted in the industry and, while the SRS curves were developed for the adjacent SRS site, the Blue Bluff Marl soil unit at the ESP site has higher velocities than the corresponding soil unit at the SRS site. Analyses are performed for both sets of degradation curves and equally weighted in developing the final spectral amplification factors. Details of the derivation and extension of the degradation curves are presented in [Subsection 2.5.4.7.2](#).

The base case degradation curves for shear modulus and damping for the EPRI-based assumption are presented in [Figures 2.5-381](#) and [2.5-384](#), respectively. The base case degradation curves for shear modulus and damping for the SRS-based assumption are presented in [Figures 2.5-383](#) and [2.5-386](#), respectively. The corresponding tables of values are presented in [Tables 2.5-254](#) and [2.5-256](#), for the EPRI-based and SRS-based relationships, respectively.

Unit weights, derived from the ESP laboratory testing program ([Appendix 2.5A](#)) for the shallow soils and calculation ([Reference 548](#)) for the deep sands, are provided in [Table 2.5-241](#).

2.5.2.5.1.2.1.2 Rock Column

Due to the geometry of the Pen Branch fault, the shear-wave velocity character of the Triassic Basin and Paleozoic crystalline rocks below the Coastal Plain sediments, and the possible presence of a low velocity zone between the Triassic Basin and the Paleozoic crystalline rocks, a set of six (6) rock column models were used in combination with the base case soil column, described above, to adequately model uncertainty in the rock/soil column for site response analysis.

As discussed in [Subsection 2.5.4.2.5](#), a rock density of 2.75 gm/cc (172 pcf) is used for the crystalline rock, and 2.53 gm/cc (158 pcf) for the Triassic rock. Based on inspection of [Figures 2.5-384](#) and [2.5-386](#), the low strain damping of soils is on the order of 0.5 percent, which generally increases to 0.6 percent to 2 percent for strain compatible conditions. Rock, which would be expected to have lower damping than soil, was therefore assumed to behave as a linearly elastic material with one percent damping for all rock types.

The above-described shear-wave velocity profile, degradation relationships, and material densities were then used to develop randomized soil/rock profiles described in the following section.

2.5.2.5.1.2.2 Randomization of Site Profiles

To account for variations in shear-wave velocity across the site, sixty artificial profiles were generated using the stochastic model described in EPRI ([Reference 515](#)) and extended in Toro (1996), with some modifications to account for the conditions at the VEGP ESP site. These artificial profiles represent the soil/rock/fill column from the top of the Paleozoic crystalline rock (with a shear-wave velocity of 9,200 feet/s) to the ground surface. This model uses as inputs the following quantities: (1) the median shear-wave velocity profile, which is equal to the base-case soil and rock profiles defined

in **Subsections 2.5.2.5.1.2.1.1** and **2.5.2.5.1.2.1.2**; (2) the logarithmic standard deviation of shear-wave velocity as a function of depth, which is set to 10 percent for the structural backfill, is set to values obtained from soil-randomization studies performed at the SRS site (**Reference 542**; **Reference 543**) for the soil strata, and is set to values consistent with the six rock-column models described in **Subsection 2.5.2.5.1.2.1.2**; (3) the correlation coefficient between velocities in adjacent layers, which is taken from the second SRS soil-randomization study referenced above; (4) the probabilistic characterization of layer thickness as a function of depth, which is taken from the second SRS soil-randomization study referenced above, modified to allow for sharp changes in the base-case velocity profile; and (5) the depth to bedrock, which is randomized to account for the range of depths associated with the Pen Branch fault described in **Subsection 2.5.2.5.1.2.1.2**.

Figure 2.5-295 depicts the summary statistics for the 60 shear-wave velocity profiles. It is worth noting that the depth to the Blue Bluff Marl and to the Triassic Basin rock vary little between the profiles, and that the logarithmic standard deviation in shear-wave velocity is lower than typical values (e.g., **Reference 541**). These features are a consequence of the availability of shear-wave velocity data from the VEGP ESP site and from the nearby SRS, and of the uniformity exhibited by these data. As a consequence of this uniformity, the average amplification factors computed from site-response calculations using these profiles may not be as smooth as those obtained using artificial profiles with more variability.

Figure 2.5-296 shows the upper part of the soil column shear wave velocity profile. The ESP base case shear-wave model is shown in red, each of the 60 individual randomizations used in the site amplification factor analysis are shown in light gray lines, and the statistical characterization of the randomization is shown in black lines. In addition, the COL plus ESP shear-wave velocity base case model is shown in turquoise. The COL plus ESP shear-wave velocity model falls well within the range of randomized ESP base case velocity models. Pending additional COL data on site-specific soil degradation and damping ratio curves and measured dynamic properties for the proposed backfill, the differences in the ESP to ESP plus COL soil column shear wave velocity do not warrant at this time recalculation of site amplification factors and the GMRS.

The degradation curves for shear modulus and damping were also randomized to account for the epistemic and aleatory uncertainty in these properties. These randomizations used as input the following quantities: (1) the median degradation curves, which are equal to the base-case degradation curves in **Subsections 2.5.2.5.1.2.1.1** and **2.5.2.5.1.2.1.2**; (2) the uncertainties in the degradation properties of soil, which are taken from Costantino (1996), except for the engineered backfill, for which they are reduced by 1/3; and (3) the uncertainty in the damping ratio for the Triassic Basin rock, which is represented by a 5-95 percentile range of 0.7-1.5, which corresponds to a logarithmic standard deviation of 0.41. For each randomized velocity profile, one set of randomized degradation curves was generated for the EPRI curves and another set was generated for the SRS curves.

2.5.2.5.1.3 Development of Low-Frequency and High-Frequency Hard Rock Target Spectra

Hard rock target spectra were developed for the two different frequency ranges: HF (5-10 Hz) and LF (1-2.5 Hz), as defined in Reg. Guide 1.165, at each of three annual probability levels (10^{-4} , 10^{-5} , and 10^{-6}). The target spectra are based on the computed mean magnitude (Mbar) and distance (Dbar) values from the deaggregation of the hazard curves. For the HF cases (5-10 Hz), only those sources less than 105 km were used to compute the Mbar and Dbar values. For the LF cases (1-2.5 Hz), only those sources at distances greater than 105 km from the site were used to compute the Mbar and Dbar values. This distinction was made based on the noted dominance of the Charleston source for low frequencies and long return periods. The computed Mbar and Dbar results were based on the average of the 5 – 10 Hz values for the HF cases and the average of the 1 – 2.5 Hz for the LF cases. These computed values are given in **Table 2.5-218**. Based on the similar Mbar and Dbar values for

each of the three probability levels for the HF and LF cases, a single recommended Mbar and Dbar pair was selected to represent the computed values for each of the HF and LF cases. For the LF case, the recommended distance was set at 130 km to model the Charleston source. For the HF case, the recommended distance is approximately equal to the log-average of the three computed values rounded to the nearest km. The recommended magnitude value is approximately equal to the linear average of the three computed magnitude values. The recommended magnitude values for both the high- and low-frequency cases are equal to the linear average of the three magnitude values rounded to the nearest tenth of a magnitude unit.

Given the Mbar and Dbar values, the Central and Eastern United States spectral shape (log-average of the single and double corner source models) from NUREG/CR-6728 (Reference 525) were computed for both the HF and LF cases. These spectral shapes were scaled to the corresponding uniform hazard spectral (UHS) values (see Table 2.5-217) at 7.5 Hz and 1.75 Hz for the HF and LF cases, respectively. An additional requirement that the envelop spectrum of the scaled target spectra for a given annual probability level be no less than 90 percent of the UHS was applied. In any case for which this requirement was not met, either the scaled HF or LF target spectrum was increased to meet this requirement at the seven frequencies at which the hard rock UHS is computed. For the HF case, this requirement caused an increase of the 25 Hz spectral acceleration value at the 10^{-6} probability level. For the LF case at all three probability levels, the scaled LF spectra fall below the 90 percent UHS limit at 1 and 0.5 Hz. Thus, the scaled LF spectra were increased to 90 percent of the UHS value for the 1 and 0.5 Hz values, and for frequencies less than 0.5 Hz, the spectral shape of the LF spectrum scaled to the 90 percent of the 0.5 Hz UHS value was used.

The scaled hard rock target spectra were interpolated (log-log) to the recommended sampling rate of 100 equally log spaced values per frequency decade. The HF and LF target spectra for the three annual probability levels used to develop the spectrum-compatible time histories are shown in Figures 2.5-297 and 2.5-298.

2.5.2.5.1.4 Selection of Seed Time Histories

The selection of the seed input time histories used in the spectral matching procedure was guided by the deaggregation results described in the previous section. For the HF case, the recommended Mbar and Dbar values are 5.6 and 12 km. For the low frequency case, the recommended Mbar and Dbar values are 7.2 and 130 km. These values were considered appropriate for all three MAFEs. Based on these recommended magnitude and distance values, a total of 30 seed time histories were selected for both the HF and LF cases.

Because of the limited number of strong ground motion acceleration time histories from stations located in the Eastern North America, 58 of the 60 selected seed input time histories were recorded at stations located in other regions than the Eastern North America. The additional two seed time histories that are used for the HF case were recorded in Eastern Canada. Time histories were selected based on the database of recorded strong ground motion records, recommended magnitude and distance values, and shear-wave velocities in the top 30 meters at recording sites of greater than 600 m/sec (about 1,970 ft/sec). The selected seed time histories are listed in Table 2.5-219 and Table 2.5-220, for the HF and LF cases, respectively.

The spectral matching was performed based on a given horizontal target spectra with a spectral damping of 5 percent. The spectral matching procedure is a time domain spectral matching procedure and emphasis was placed on maintaining the phasing characteristics of the initial time history in the final modified spectrum-compatible time history. In addition, emphasis was placed on maintaining the characteristic of the normalized Arias intensities (the integral of the square of the acceleration-time history, a ground motion parameter that captures the potential destructiveness of an earthquake) of the initial and final modified spectrum-compatible time histories. The spectral matching criteria given in NUREG/CR-6728 (Reference 525) that are applicable with the use of

multiple time histories were used to check the average spectrum from the 30 time histories for a given frequency range (high- or low-frequency) and annual probability level. This is the recommended procedure in NUREG/CR-6728 (Reference 525) when multiple time histories are being generated and used.

The selected 60 seed time histories were first matched to their respective 10^{-6} high and low frequency target spectra. As an example, the acceleration, velocity, and displacement time histories for one of the thirty 10^{-6} HF target spectrum seed time histories are shown in Figure 2.5-319. The final modified spectrum-compatible acceleration, velocity, and displacement time histories (matched to the 10^{-6} HF target spectrum) are plotted in Figure 2.5-320. Figure 2.5-321 shows the 10^{-6} HF target spectrum (thick grey line), the response spectrum from the initial acceleration time history scaled to the target PGA value (thin blue line), and the response spectrum from the final modified spectrum-compatible time history (thin red line). The initial and final modified spectrum-compatible normalized Arias intensities for this example are plotted in Figure 2.5-322. These results are representative of the goodness of fit for all spectrum-compatible time histories. For the 10^{-5} probability level, the final modified spectrum-compatible time histories from the 10^{-6} probability level were used as the input time histories for the spectral matching. In a similar fashion, the final modified spectrum-compatible time histories for the 10^{-5} probability level were used as the input time histories for the spectral matching at the 10^{-4} probability level. The results of the spectral matching for the high and low frequency cases at each of the three annual probability levels are shown in Figures 2.5-299 through 2.5-304. These spectrum-compatible time histories were used in the site response analysis presented in the next section.

2.5.2.5.1.5 Site Response Analyses

The site response analyses were conducted using the randomized shear-wave velocity profiles and soil modulus and damping relationships discussed in Subsection 2.5.2.5.1.2.1.1 to account for variation in the dynamic soil properties across the VEGP ESP Site. Two separate sets of degradation relationships for shear modulus and damping were applied in the site response analyses: EPRI-based curves and SRS-based curves (see Subsection 2.5.2.5.1.2). The depth to hard rock ($V_s > 9200$ fps) was also randomized to reflect its uncertainty. All site response analyses assumed that the sedimentary rock below 1049 ft (depth to bottom of Coastal Plain sediments) remains linear during earthquake shaking with one percent damping for all rock types. This randomization process resulted in 60 randomized rock/soil/fill profiles (that included combinations of depths to hard rock and degradation relationships) for each family of degradation curves (i.e., EPRI or SRS). Additional details about the generation of profiles for the site response analyses are included in Subsection 2.5.2.5.1.2.

Each of the 60 randomized soil profiles was paired with 30 seed time histories (each time history was applied to two of the randomized soil profiles) for each of the hard rock input motions (i.e., 30 time histories for the HF spectra and 30 time histories for the low frequency spectra). Three different mean annual frequency of exceedance events (10^{-4} , 10^{-5} , and 10^{-6} , see Subsection 2.5.2.5.1.3) were analyzed for each profile—seed time history pairing in order to calculate the amplification factors, defined as the ratios of five percent damped spectral accelerations for rock input motion at the 9,200 ft/s shear-wave velocity horizon to the five percent damped spectral accelerations motions computed at a hypothetical outcrop at the top of the Blue Bluff Marl (86-ft depth) at a hypothetical outcrop at the 40-ft depth horizon, and at the ground surface.

The computer program SHAKE (Reference 497) was used to perform these analyses and amplification factors were extracted from each analysis resulting in 720 spectral amplifications (see Table 2.5-221) for each horizon.

The mean of the site amplification functions based on the suite of multiple input spectrum-compatible time histories for each group of 60 randomized soil profiles was used to develop site amplification factors for the VEGP ESP Site, as described in NUREG/ CR-6728 (Reference 525).

Figure 2.5-307 depicts the mean spectral amplification results of a typical analysis for HF content of a 10^{-4} MAFE seismic event using EPRI degradation curves for the ground surface. Similar plots of the computed amplification results for the 40-ft and 86-ft horizons are shown in Figures 2.5-306 and 2.5-305, respectively. The curves shown were determined by averaging the logarithms of amplification values for each frequency. As described in Subsection 2.5.2.5.1.2.1.1, analyses are performed for both sets of degradation curves and equally weighted in the subsequent development of the final spectral amplification factors.

In order to implement site response analysis Approach 2A, as discussed in Subsection 2.5.2.5.1.1, the amplification factors are prepared as a function of hard rock input motion. Tables 2.5-226 and 2.5-227 present the amplification factors at the ground surface for input hard rock motions corresponding to 10^{-4} , 10^{-5} , and 10^{-6} HF and LF MAFE target spectra, respectively (see Figures 2.5-297 and 2.5-298). Similar results for the 40-ft horizon outcrop motion and the top of the Blue Bluff Marl are given in Tables 2.5-224 and 2.5-225 and Tables 2.5-222 and 2.5-223, respectively. These results are presented for 30 structural frequencies, including the seven structural frequencies at which seismic hazards were calculated.

2.5.2.6 Horizontal Ground Motion

2.5.2.6.1 Criterion for GMRS

The criterion used to calculate the recommended design spectrum comes from ASCE 43-05 (Reference 494). This criterion is based on the mean seismic hazard curves for multiple structural frequencies at the ground surface, taking into account the effect of rock, soil, and fill above the hard rock horizon. The spectral amplitudes at this horizon corresponding to a mean annual frequency of exceedance (MAFE) of 10^{-4} are scaled so that structures and components designed to the scaled spectral amplitudes will achieve a target performance goal corresponding to a mean annual frequency of onset of significant inelastic deformation (FOSID) of 10^{-5} per year. The soil hazard values that form the basis for this calculation were developed following Approach 2A as described in Subsection 2.5.2.5.1.1.

2.5.2.6.2 Discrete Frequency Horizontal GMRS Amplitudes

Table 2.5-230 shows ground motion amplitudes corresponding to MAFEs of 10^{-4} , 10^{-5} , and (for information purposes only) 10^{-6} for hard rock conditions. Thirty structural frequencies are tabulated, including the seven frequencies developed in Subsection 2.5.2.4 and an additional twenty three frequencies from the 300 frequency values per step 6 of Subsection 2.5.2.5.1.1. Table 2.5-230 also shows ground motion amplitudes for the free ground surface of the site-specific rock/soil/fill column that were calculated from the hard rock motions and the amplification factors of Subsection 2.5.2.5.

The horizontal GMRS (the design response spectrum (DRS) in the nomenclature of the ASCE 43-05 Reference 494) is derived from the amplitudes for MAFEs of 10^{-4} and 10^{-5} in Table 2.5-230. That is, the Amplitude Ratio, AR, of 10^{-5} to 10^{-4} amplitudes is determined for spectral accelerations (SA) at each structural frequency:

$$A_R = SA(10^{-5})/SA(10^{-4}) \quad (\text{Equation 2.5.2-4})$$

and the horizontal GMRS is calculated as:

$$GMRS = SA(10^{-4}) \times \max(1.0, 0.6 A_R^{0.8}) \quad (\text{Equation 2.5.2-5})$$

Table 2.5-233 shows thirty of the GMRS values calculated from Equation 2.5.2-5, at the free ground surface. In Table 2.5-233, the last term in Equation 2.5.2-5, $0.6 A_R^{0.8}$, is indicated as “DF2” in the table.

2.5.2.6.3 Full GMRS Horizontal Spectrum

The horizontal GMRS values at the 300 structural frequencies, thirty of which are provided in Table 2.5-233, are used to define the raw horizontal GMRS. This spectrum is then smoothed by a running average filter for the 100-points-per-decade spectral amplitudes above 1 Hz, but is constrained to go through the seven structural frequencies at which hazard calculations were made. (An exception was made for 5 Hz, where the site amplification analysis indicated a trough, so the 5 Hz GMRS value was smoothed based on amplitudes at adjacent frequencies, which raised the 5 Hz GMRS value slightly and improved the shape of the spectrum.) This step smooths out the spectral peaks and troughs above 1 Hz, which are not statistically significant, but maintains the low-frequency peaks and troughs representing lower-mode soil column response for this site.

Figure 2.5-310 shows the raw spectrum and the smoothed VEGP ESP horizontal GMRS.

2.5.2.6.4 Foundation Input Response Spectrum (FIRS) and Top of In Situ Competent Material (top of Blue Bluff Marl) Ground Motions

2.5.2.6.4.1 Development of FIRS and Top of In Situ Competent Material Spectra

The criterion used to calculate the recommended outcrop FIRS and top of Blue Bluff Marl spectra (at the 40-ft and 86-ft depth horizons, respectively) are the same as was used to develop the ground surface GMRS motion. That is, as described above the methodology of ASCE 43-05 (Reference 494) was used. And, as for the GMRS, the soil hazard values that form the basis for this calculation were developed following Approach 2A and the characterization of subsurface materials as described in Subsection 2.5.2.5.1.1.

Table 2.5-229 shows ground motion amplitudes corresponding to MAFEs of 10^{-4} , 10^{-5} , and (for information purposes only) 10^{-6} for hard rock conditions (thirty structural frequencies are tabulated including, the seven frequencies developed in Subsection 2.5.2.4 and an additional twenty three frequencies from the 300 frequency values per step 6 of Subsection 2.5.2.5.1.1). Table 2.5-229 also shows ground motion amplitudes for an outcrop at the 40-ft depth horizon; these were calculated from the hard rock motions and the amplification factors of Subsection 2.5.2.5.

Table 2.5-228 shows similar values for the top of Blue Bluff Marl horizon.

The FIRS and top of Blue Bluff Marl horizons outcrop spectra are derived from the amplitudes for MAFEs of 10^{-4} and 10^{-5} in Tables 2.5-229 and 2.4.2-21, respectively. That is, the Amplitude Ratio, AR, of 10^{-5} to 10^{-4} amplitudes are determined for spectral accelerations (SA) at each structural frequency using the ASCE 43-05 formula given above in the development of the GMRS spectra.

Tables 2.5-232 and 2.5-231 shows thirty of the FIRS and top of Blue Bluff Marl values calculated at the hypothetical outcrops at the 40-ft and 86-ft horizons, respectively.

The FIRS and top of Blue Bluff Marl values at the 300 structural frequencies, thirty of which are provided in Tables 2.5-232 and 2.5-231, are used to define the raw ground motion response spectra. These spectra are then smoothed, as were the GMRS spectra, by a running average filter for the 100-points-per-decade spectral amplitudes above 1 Hz, but is constrained to go through the seven structural frequencies at which hazard calculations were made.

Figures 2.5-309 and Figure 2.5-308 show the raw and smoothed spectrum.

The vertical FIRS and top of Blue Bluff Marl spectra were computed by applying the V/H spectral ratio presented in [Subsection 2.5.2.7.1.3](#) to the smoothed FIRS and top of Blue Bluff Marl horizontal spectra plotted in [Figure 2.5-309](#) and [Figure 2.5-308](#). The resulting VEGP ESP vertical and horizontal FIRS and top of Blue Bluff Marl spectra are plotted in [Figures 2.5-317](#) and [2.5-316](#).

2.5.2.6.4.2 Selection of Time Histories and Spectral Matching to the FIRS

Time histories matching the FIRS are used in several sensitivity analyses summarized in [Subsection 2.5.2.9](#). Therefore, these time histories are developed here. Given the FIRS horizontal and vertical spectra presented in [Subsection 2.5.2.7.1](#) and plotted in [Figure 2.5-317](#), one set of three component time histories was developed to be spectrum compatible to the FIRS target spectra. The single three component set was selected based on the deaggregation of the low frequency (LF) results. For the low frequency case, the recommended Mbar and Dbar values are 7.2 and 130 km. These values were considered appropriate for all three MAFEs. For this analysis, the three component time histories from the 1999 Hector Mine earthquake ($M_w=7.13$) recorded at the Heart Bar State Park station ($R=61.21$ km) were selected. This was one of the 30 sets of time histories selected for the site response analysis (see [Table 2.5-220](#)).

The spectral matching procedure is a time domain procedure and emphasis was placed on maintaining the phase characteristics of the initial time history in the final modified spectrum-compatible time history. In addition, emphasis was placed on maintaining the characteristic of the normalized Arias intensities (the integral of the square of the acceleration-time history, a ground motion parameter that captures the potential destructiveness of an earthquake) of the initial and final modified spectrum-compatible time histories. The spectral matching criteria given in NUREG/CR-6728 ([Reference 525](#)) that are applicable were used to check the acceptability of the modified spectrum compatible time history. In most cases, an additional scale factor which is applied after the spectral matching process is used to assure that the final modified time history satisfies the spectral matching criteria given in NUREG/CR-6728. A common scale factor of 1% (i.e., 1.01) was used for each of the three components. The modified acceleration, velocity, and displacement time history prior to the application of this 1.01 scale factor is shown in [Figure 2.5-323](#) for the first horizontal component. [Figure 2.5-324](#) shows target FIRS horizontal spectrum, 1.3*FIRS target spectrum, 0.9*FIRS target spectrum and the modified time history response spectrum including the 1.01 scale factor. The normalized Arias intensities for this first horizontal component are shown in [Figure 2.5-325](#). The results for the second horizontal component are shown in [Figures 2.5-326](#) through [2.5-328](#). The vertical component results are presented in [Figures 2.5-329](#) through [2.5-331](#).

2.5.2.7 Vertical GMRS Spectrum

The method to develop the vertical GMRS is to develop a vertical-to-horizontal scaling factor [V/H], which is then applied to the horizontal GMRS at the 3 horizons (GMRS, FIRS, and top of Blue Bluff Marl), presented above.

2.5.2.7.1 Development of V/H

Reg. Guide 1.60 presents acceptable standard response spectral shapes as a function of frequency that may be considered for the seismic design of nuclear power plants. These shapes are given for both horizontal and vertical ground motions as a function of damping. The shapes are independent of peak ground acceleration (PGA), which is used as a scaling factor. The ratio of the vertical to horizontal spectral shapes results in a V/H scaling function that is a value of 2/3 for frequencies less than 0.25 Hz, 1.0 for frequencies higher than 3.5 Hz, and varies between 2/3 and 1 for frequencies between 0.25 and 3.5 Hz.

A significant increase in the number of strong ground motion observations and advances in earthquake ground motion modeling since the publication of Reg. Guide 1.60 suggest that the V/H

ratios implied in Reg. Guide 1.60 may not be appropriate for a given site (Reference 515; Reference 525). The horizontal and vertical ground motions and the V/H ratios are observed to depend on magnitude, distance, site conditions, and regional tectonic setting (e.g. western US [WUS] vs. central and eastern US [CEUS]), which presents distinctive characteristics of earthquake source, attenuation along regional path, and shallow crust).

NUREG/CR-6728 (Reference 525) presents V/H ratios for soft rock WUS sites and hard rock CEUS sites as a function of horizontal peak acceleration, as a proxy for the combined dependence on magnitude and distance. While the WUS rock V/H ratios are based on the significant empirical database of WUS strong ground motion, there are too few CEUS recordings to develop empirically-based CEUS V/H relations. NUREG/CR-6728 follows up on a technique presented in EPRI TR-102293 of using earthquake ground motion modeling to develop CEUS rock V/H. Due to assumptions and the estimation of various required parameters, the explicit results of the CEUS modeling are not considered robust, but can be used as guidelines for the difference between V/H ratios for WUS and CEUS rock sites. For the rock CEUS V/H ratios NUREG/CR-6728 uses the WUS ratios and modifies them based on the difference in trends obtained between WUS and CEUS rock sites from their modeling studies. For example, a peak in the V/H ratio is expected to occur at higher frequencies for CEUS than for WUS sites because site kappa values in the CEUS are typically lower than in the WUS.

The VEGP ESP site, however, is a deep soil site, not a hard rock site. V/H relations for soil sites are not given in NUREG/CR-6728 (Reference 525), and, again, an insufficient number of ground motion observations have been made to develop empirical CEUS relationships for soil sites. Appendix J of NUREG/CR-6728, however, does discuss the use of modeling by which V/H ratios can be developed for CEUS soil sites. The method mirrors that used in NUREG/CR-6728 in developing the CEUS rock V/H relations, and can be represented by the following formula:

$$V/H_{\text{CEUS,Soil}} = V/H_{\text{WUS,Soil,Empirical}} * [V/H_{\text{CEUS,Soil,Model}} / V/H_{\text{WUS,Soil,Model}}] \quad (\text{Equation 2.5.2-6})$$

The first term of Equation 2.5.2-6 can be a readily available WUS relationship, such as Abrahamson and Silva (1997), which presents both vertical and horizontal ground motion attenuation relations for deep soil sites. Magnitude and distance is specified, which allows hazard contribution-appropriate specification for a given location.

The second term is a WUS-to-CEUS “transfer function” to modify the WUS ratios from the first term to give the required $V/H_{\text{CEUS,Soil}}$. The development of this second term entails ground motion modeling of both CEUS [numerator] and WUS [denominator] ground motions appropriate for the given site (e.g., the major contributing or controlling earthquake by magnitude and distance) and considers the site-specific conditions. The model for developing $V/H_{\text{WUS,Soil,Model}}$ considers generic site soil conditions, as implicitly considered in the $V/H_{\text{WUS,Soil,Empirical}}$ term. The model for developing $V/H_{\text{CEUS,Soil,Model}}$ model can consider as site-specific soil conditions as possible.

Upon developing $V/H_{\text{CEUS,Soil}}$ from Eq. 2.5.2-6, the vertical GMRS response spectrum is then defined by

$$S_{\text{GMRD,Vertical}} = S_{\text{GMRS,Horizontal}} * V/H_{\text{CEUS,Soil}} \quad (\text{Equation 2.5.2-7})$$

As discussed above, the first term on the right-hand side of Equation 2.5.2-6 can be implemented using the ground motion attenuation relationship of Abrahamson and Silva (1997). The development of the WUS-to-CEUS transfer function (the second right-hand side term of Equation 2.5.2-6) needs significant analytical effort, contains potentially significant uncertainties, and requires a number of assumptions. Two studies guide the development of a best estimate of $V/H_{\text{CEUS,Soil}}$ and, through Equation 2.5.2-7, the definition of the vertical GMRS response spectrum.

2.5.2.7.1.1 Estimate of V/H from NUREG/CR-6728

Appendix J of NUREG/CR-6728 (Reference 525) discusses various characteristics of vertical strong motions and, building upon the work presented in EPRI TR-102293, presents the methodology to estimate V/H for CEUS rock and soil sites. This method is that represented by Equation 2.5.2-6, above. A generic CEUS soil column is considered in their presentation of the method. In the appendix, plots of the numerator and denominator of the WUS-to-CEUS transfer function are shown, Figures J-32 and J-31, respectively, for **M6.5** and a suite of distances [1, 5, 10, 20, and 40km]. An estimate of the WUS-to-CEUS transfer function can be made for **M6.5** at the given distances using these results shown in these figures.

As discussed above, the GMRS response spectrum is based on slopes of the 10⁻⁴ and 10⁻⁵ ground motion hazard curves and the scaling of the 10⁻⁴ ground motions. The resulting horizontal GMRS ground motions at the seven spectral control points are generally only slightly higher than the 10⁻⁴ ground motion levels. That is, the horizontal GMRS is dominated by the 10⁻⁴ ground motion.

In reviewing the high-frequency distance deaggregation at the 10⁻⁴ hazard level (Figure 2.5-291), about one-quarter of the hazard is coming from “near” events, or about distances less than 20 km, while about three-quarters of the hazard is coming from “far” events, or distances centered at about 130 km. In reviewing the corresponding distance deaggregation at the 10⁻⁵ hazard level in the same figure, the bimodal nature of the deaggregation is yet apparent, but the relative contribution of the near and far events is about the same.

In reviewing the low-frequency magnitude-distance deaggregations at both the 10⁻⁴ and 10⁻⁵ hazard levels (Figure 2.5-292), hazard contribution is clearly dominated by the distant event centered on about 130 km.

The magnitudes and distances that can be attributed to the near and far events are taken as those used in the development of the high-frequency and low-frequency target spectra for the site response analysis: **M5.6** at a distance of 12 km and **M7.2** at a distance of 130 km, respectively.

Figure 2.5-311 is a plot of the first term of Equation 2.5.2-6 for both near and far events using the attenuation relationship of Abrahamson and Silva (1997).

Figure 2.5-312 is a plot of estimates of the second term of Equation 2.5.2-6 (ratio of V/H ratios) developed as the quotient of the curves in NUREG/CR-6728 (Reference 525) Figure J-32 and J-31 for highest available distances of 10, 20, and 40 km. The Appendix J figures are given only for **M6.5**. Therefore, an estimate of an equivalent ground motion proxy magnitude and distance must be made to estimate the second term of Equation 2.5.2-6. The **M6.5**, 20 km curve may be considered a reasonable proxy for the “near” event of **M5.6** at 12 km. The greatest distance given in the two figures of Appendix J is 40 km, so this has to be used as the proxy, along with the associated **M6.5**, for the “far” event of **M7.2** at 130 km. Given the trend of the V/H values (decreasing with distance for a given magnitude), it is expected that the “far” event proxy may be conservative (high in value), as compared to the value expect if equivalent ratio of ratio curves had been explicitly available for **M7.2** at 130 km. Figure 2.5-312 shows the recommended “near” and “far” versions of the second term of Equation 2.5.2-6. Some smoothing has been applied that may be reflecting certain aspects (peaks, valleys) of the response reflecting the generic soil models used.

Figure 2.5-313 is a plot of $V/H_{\text{CEUS,Soil}}$ of Equation 2.5.2-6 considering both “near” and “far” events. Given the observations made earlier with regard to the relative contributions of the deaggregation “near” and “far” events to the 10⁻⁴ and 10⁻⁵ hazards, and the relative contribution of these two hazard levels to the horizontal GMRS design response spectrum, the “near” and “far” estimates of $V/H_{\text{CEUS,Soil}}$ are weighted approximately 1:3, resulting in the final $V/H_{\text{CEUS,Soil}}$ shown in Figure 2.5-313, as derived from the available results in NUREG/CR-6728.

2.5.2.7.1.2 Estimate of V/H from Lee (2001)

As a second estimate of the required V/H ratio, the results of the study for the MOX Fuel Fabrication Facility [MFFF] at the Savannah River Site are considered (Reference 520). The methodology used in that study followed the same approach as presented in NUREG/CR-6728 and EPRI TR-102293, and used in the section above, with the primary exception that the function $V/H_{CEUS,Soil,Model}$ of Equation 2.5.2-6 is developed using a site-specific model of the soil conditions. Lee (2001) notes that the following vertical and horizontal modeling assumptions are made based on validations:

Vertical motions are modeled as a combination of pure SV-waves and SV-P converted waves arriving at the base of the soil/alluvium materials at inclined angles of incidence computed using ray tracing methods;

Horizontal component spectra are computed assuming pure S-waves arriving at vertical incidence;

Linear elastic analysis is assumed for computing the vertical motions;

Low strain behavior (i.e., no wave induced dynamic strain degradation) compressional and shear-wave site velocity profiles are used in computing vertical spectra;

Damping for computing vertical spectra is the low strain level damping used to compute horizontal spectra;

For computing horizontal motions, wave induced dynamic strain degradation of the shear-wave velocity and increased damping of the profile is permitted (in an equivalent linear analysis).

The consequence of these assumptions is that the model-derived V/H ratios (particularly for the MFFF site) may be conservatively high over some range of spectral frequencies and at high loading levels.

Lee (2001) directly presents final V/H ratios (i.e., the resulting $V/H_{CEUS,Soil}$ of Equation 2.5.2-6) for several magnitudes and distances. V/H ratios for **M5.5** at 10 and 20 km and **M6.0** at 10 and 20 km were interpolated to estimate the “near” V/H ratio for **M5.6** at 12 km. V/H ratios for **M7.0** at 100 km and **M7.5** at 100 km were interpolated to estimate a “far” V/H ratio for **M7.2** at 100 km. The distance of 100 km was the greatest considered in Lee (2001), but is considered adequate, if not slightly conservative, for a proxy of the 130 km desired for the “far” event.

Figure 2.5-314 is a plot of $V/H_{CEUS,Soil}$ of Equation 2.5.2-6 considering both “near” and “far” events. As before, given the observations made earlier with regard to the relative contributions of the deaggregation “near” and “far” events to the 10^{-4} and 10^{-5} hazards, and the relative contribution of these two hazard levels to the horizontal GMRS response spectrum, the “near” and “far” estimates of $V/H_{CEUS,Soil}$ are weighted approximately 1:3, resulting in the final $V/H_{CEUS,Soil}$ shown in Figure 2.5-314, as derived from the available results in Lee (2001).

2.5.2.7.1.3 Recommended V/H

The results of two studies have been used to guide in the development of best estimates of $V/H_{CEUS,Soil}$, as discussed above and summarized in Figure 2.5-315. The $V/H_{CEUS,Soil}$ developed from Lee (2001) gives a higher value V/H ratio than that developed from the available NUREG/CR-6728 results for frequencies greater than about 0.7 Hz. Both results give minimum V/H values, particularly in the lower frequencies, which appear lower than engineering judgment may suggest acceptable in the current state-of-knowledge.

Given the site specific nature of the Lee (2001) estimate, which would argue against considering an average of the two results, an approximate envelope of the results is recommended, wherein some smoothing is considered and a minimum V/H value of 0.5 is considered. The recommended final V/H ratio is shown in [Figure 2.5-315](#). This V/H ratio is described as follows:

Frequencies	V/H ratio
≤ 1 Hz	0.5
1 to 15 Hz	log-log interpolate between 0.5 and 0.9
≥ 15 Hz	0.9

In [Figure 2.5-315](#) the V/H ratio from RG 1.60 is shown for comparison. The recommended V/H ratio is marginally less than the Reg. Guide ratio at all frequencies.

2.5.2.7.1.4 Recommended Vertical GMRS Spectrum

To develop the vertical spectra, the horizontal spectra is scaled by the recommended V/H ratios provided in [Subsection 2.5.2.7.1.3](#). [Figures 2.5-318](#), [2.5-317](#), and [2.5-316](#) show the resulting vertical and horizontal GMRS, FIRS, and top of Blue Bluff Marl spectra, respectively.

2.5.2.8 Operating Basis Earthquake Ground Motion

The Operating Basis Earthquake (OBE) ground motion spectra was not determined as part of the Vogtle ESP submittal. Requirements related to the OBE are provided in paragraph IV (a) (2) of Appendix S to 10 CFR Part 50, "Earthquake Engineering Criteria for Nuclear Power Plants." Under General Information in this appendix, the following statement is made: "This appendix applies to applications for the design certification or combined license pursuant to part 52 of this chapter or a construction permit..." Since OBE requirements are related to the design and performance of safety related systems, the OBE ground motion spectra have been determined during the COL stage as required under Appendix S.

2.5.2.9 Sensitivity Studies

2.5.2.9.1 Sensitivity for Backfill Vs

During the COL investigation and prior to conducting the Phase I test pad program, a study was conducted to evaluate the sensitivity of the AP1000 responses to the change in backfill shear wave velocity. The shear wave velocity used for the backfill sensitivity analysis (sensitivity study) is compared with the backfill velocity used for GMRS and FIRS computation (ESP profile) in [Figure 2.5-332](#). The analyses included randomization of the entire soil column with the new backfill properties and development of the new outcrop motion at the foundation level of the AP1000 Nuclear Island. The new time history and associated strain-compatible soil properties were used in the SSI analysis of the AP1000.

The study confirmed that, even with a large variation of the backfill property, the AP1000 design is applicable to the Vogtle site with a large margin. [Appendix 2.5E](#), Vogtle Site Specific Seismic Evaluation Report provides the results of this sensitivity analysis.

2.5.2.9.2 Study of the Effects of Backfill Geometry

Due to the large volume of excavation and the lateral extent of the backfill at the Vogtle site, the backfill layers were modeled as free-field soil layers in the modeling of the soil profile for both the soil amplification for development of the ground motion (GMRS and FIRS) and the site-specific seismic SSI analysis of the AP1000.

To verify the validity of this assumption, a two-dimensional site response analysis followed by a two-dimensional SSI analysis of the AP1000 model were used to evaluate the effect of the extent of backfill on the site response and on the SSI response of the NI. The plant layout is shown in [Figure 2.5-333](#). For the 2D analysis, the cross section shown in the East-West direction shown in [Figure 2.5-334](#) was used. The analysis consists of two parts.

In part I, 2D site response analysis was performed. The 2D SASSI model of the site is based on Section A shown in [Figure 2.5-334](#) that represent a "bathtub" model of the site with backfill modeled with plane strain elements. The 2D SASSI model for site response analysis is shown in [Figure 2.5-335](#). An axis of symmetry was used to consider the backfill geometry for both units. The in-situ upper sand layers are modeled using the site-specific dynamic properties measured at the site. The properties of the backfill, blue bluff marl, the lower sand layers and layers extending to the rock at the base were the same as those used in the site response analysis to develop GMRS and FIRS. However, since computation of GMRS and FIRS were based a wide range of soil columns and input motions (60 randomized profiles, 30 time histories for HF and 30 time histories for LF rock motion), only a subset of the properties and input motion were considered. The analysis in part I included the upper, mean and lower bound soil profiles and only 3 time histories for each of HF and LF rock input motion. The results of the site amplification for the 2D site response analysis was compared with the site amplification factors from the 1D SHAKE results for the same set of input motion and soil properties. The differences in site amplification factors are shown in [Figures 2.5-336](#), [2.5-338](#), and [2.5-340](#). The results from SHAKE are represented in terms "in-column" motions to be comparable with the 2D SASSI nodal response motions at the three locations at centerline of the backfill ([Figure 2.5-335](#)). As shown in these figures, the differences are very small confirming that geometry of the backfill has insignificant effect on GMRS and FIRS. Additionally in [Figure 2.5-336](#) the mean amplification used to develop the GMRS motion is plotted as a red dotted line; the close fit of the curves confirms the adequacy of the selection of limited number of soil columns and time histories for this study. In addition, transfer functions are obtained from the same set of calculations that provided the spectral amplifications. Transfer functions represent the harmonic amplification of the input motion used as input to soil column analysis to the "in-column" motion at the two horizons (0 ft and 40 ft depth). Transfer functions for the mean (Best Estimate) soil profile subjected to one HF input motion are compared for the 1D SHAKE and 2D SASSI analysis at two horizons, 0 ft and 40 ft depth, in [Figure 2.5-337](#) and [Figure 2.5-339](#), respectively. The comparison of transfer function also confirms that 1D SHAKE analysis is adequate for the development of the ground motion given the geometry of the backfill at the site.

In part II, a new Vogtle 2D SASSI model of the NI was created to include the backfill as part of the structural model as shown in [Figure 2.5-341](#). This model is similar to the "bathtub" model shown in [Figure 2.5-335](#) except the AP1000 NI model is included. For this model the strain-compatible soil properties for the in-situ upper sand layer were used as part of the free-field SASSI model. The analysis in Part II was limited to the mean soil profile and for one time history from the analysis performed in Part I. The input motions for the two SSI analyses are obtained from the respective 1D SHAKE analysis in part I consistent with the free-field model used in each SASSI model. The SSI responses for the Vogtle "bathtub" 2D SASSI NI model (Bathtub Model-d5) at key locations in the NI are compared with the SSI results of the Vogtle 2D SASSI NI model (2D-AP-d5) that assumes backfill extends to infinity in lateral directions. The results of the analysis are compared at the following key locations in the NI.

Nodes	Elevation (ft)	Description
4041	99.000	NI at Reactor Vessel Support Elevation
4061	116.5	Auxiliary Shield Building at Control Room Floor
4120	179.560	ASB Auxiliary Building Roof Area
4310	327.41	ASB Shield Building Roof Area
4412	224	Steel Containment Vessel near Polar Crane
4535	134.250	Containment Internal Structure at Operating Deck

These comparisons are shown in **Figures 2.5-342 through 2.5-347**. The response spectra are similar and the differences are considered negligible. For information the generic AP1000 standard design response spectra are plotted for comparison purposes which confirms significant margin between the AP1000 generic response and the Vogtle 2D results. A more detailed discussion of the Vogtle "bathtub" 2D SASSI NI model and a comparison of transfer functions are documented in Appendix A of **Appendix 2.5E**.

The comparison of the results confirms that the extent and geometry of the backfill has negligible effects on GMRS and FIRS and has small effects on the structural responses which are well within the range of the margin of the design.

2.5.2.9.3 Updated Site Response Analyses

As discussed in **Subsection 2.5.4.7**, additional geotechnical data was collected as part of COL investigation and the ESP data was supplemented with the new data. The completed data set is referred to as "COL" data. **Subsection 2.5.4.7.1** presents a discussion of the shear wave velocity profile of the ESP and COL data sets and **Subsection 2.5.4.7.2** presents a discussion of the strain-dependent soil properties of the two data sets. Site specific (COL) strain-dependant soil properties are presented in **Figures 2.5-382 and 2.5-385** and in **Table 2.5-255**. **Subsection 2.5.4.7.5** presents the comparison of the data in terms of the shear wave velocity profile (**Figure 2.5-379**) and strain-dependent soil properties (**Figures 2.5-392 through 2.5-397**). Soil amplification analysis and development of FIRS described in **Subsection 2.5.2.5.1** are based on the ESP data. In this section, the effect of COL data on the soil amplification at the depth of 40 ft (FIRS) is presented. The FIRS at 40 ft depth has been used as input for the site specific evaluation of the AP1000 design.

As described in **Subsection 2.5.2.5.1**, development of soil amplification using ESP data is based on 60 randomized velocity profiles and associated EPRI and SRS strain-dependent soil properties incorporating 30 time histories for the HF and LF motions at each MAFE of 10^{-4} , 10^{-5} , and 10^{-6} levels. However for the purpose of sensitivity analysis and evaluation of the effects of COL data, a limited number of soil column analysis have been performed as described below.

Using the best estimate COL velocity profile (**Figure 2.5-379**), the upper bound and lower bound profiles were developed using a variation of the data set. The three COL velocity profiles and the associated COL strain-dependent soil properties were analyzed using three HF and three LF time histories corresponding to MAFE of 10^{-4} . All analyses were performed twice to consider the low and high PI strain-dependent soil properties for BBM (**Figures 2.5-393 and 2.5-396**). Several iterations were performed in each run to converge on the soil properties. The strain-compatible velocity profiles and damping profiles obtained from the analysis are shown in **Figures 2.5-349 and 2.5-350** labeled as COL. From each run, the response motion in terms of 5% acceleration response spectrum at the depth of 40 ft as SHAKE "outcrop" motion was computed. The results of HF input motion were averaged over the three time histories and over the three soil profiles as well as the low and high PI cases of the BBM. The same averaging method was used for the LF input motions. The averaged results were divided by the corresponding HF and LF input response spectrum at MAFE of 10^{-4} to

compute the spectral amplification at the 40 ft horizon. The resultant two amplifications curves were enveloped. The enveloped amplification values are shown in [Figure 2.5-351](#) labeled as COL.

To provide a consistent soil amplification for comparison with the results using COL data, from the ESP set of runs described in [Subsection 2.5.2.5.1](#) the strain-compatible velocity and damping profiles were used to obtain the median and upper and lower bound profiles (using one standard deviation as the variation). The velocity and damping profiles are compared with the corresponding profiles from the analysis of the COL data in [Figures 2.5-349](#) and [2.5-350](#), respectively. Except for the damping profile at shallow depths, the two sets of data are consistent. The three profiles selected from the analysis of the ESP data were subsequently analyzed using the same three HF and LF time histories used in the analysis of the COL data. Since the soil properties are already compatible with shear strains, no further iteration on soil properties was performed. The results in terms of acceleration response spectrum at 5% damping at 40 ft depth as outcrop motion were obtained. The spectra for each HF and LF motions were averaged over the three time histories and over the three profiles. The averaged responses were divided by the respective HF and LF response spectra at MAFE of 10^{-4} and the resultant amplifications were enveloped. [Figure 2.5-351](#) shows the amplification labeled as ESP.

To confirm the adequacy of the limited number of profiles and time histories for the purpose of this evaluation, the amplification corresponding to the analyses of the fully randomized ESP soil profiles ([Subsection 2.5.2.](#)) is also shown in [Figure 2.5-351](#) labeled as “ESP-all”. The comparison of the two sets of results based on ESP data shows the selection of limited number of profiles and time histories are adequate for the purpose of the evaluation of the impact of the COL data. Furthermore, the comparison of the amplification between ESP and COL data is considered small and is expected to be reduced to be negligible if the fully randomized soil profiles were used in the COL set of analyses.

In addition, an assessment of the small differences in the amplification of the FIRS motion on the structural response of the AP1000 has been made. The AP1000 has significant margin when compared to Vogtle site specific seismic floor response spectra associated with the ESP and sensitivity soil profiles. Based on this evaluation, it has been determined that the AP1000 certified Design remains acceptable for the Vogtle site.

2.5.2.9.4 Study of Engineered Granular Backfill Placed Over the Slopes of the Excavation

Backfill within the defined excavation permits using an engineered granular backfill (EGB) material over the slopes of the excavation as shown in [Figure 2.5-389](#). This is an alternate backfill geometry to that considered in [Subsection 2.5.2.9.2](#). This section discusses the significance of backfill material, other than Category 1 and 2, placed over the slopes and demonstrates that the results and conclusions provided in [Subsection 2.5.2.9.2](#) remain valid.

As described in [Subsection 2.5.1](#) the removal of the Upper Sands is required since this in-situ material is variable, contains dissolution features, is susceptible to liquefaction, and is not a competent bearing stratum. Directly below the approximately 90 feet of Upper Sands is the first competent in-situ stratum called the Blue Bluff marl (BBM). [Figures 2.5-388](#) and [2.5-389](#) show the defined width and length of the exposed BBM surface for each excavation, which is approximately 347 ft by 812 ft, respectively, producing a bearing surface area of approximately 282,000 sq ft per unit. This width and length is based on a zone of influence forming from the bottom of the foundations of the power block structures extending down to the BBM at approximately 45 degrees. Directly above this bearing surface area of the BBM, Category 1 and 2 backfill is placed to provide:

- A uniform bearing subsurface for the foundations of the major power block structures.
- Adequate static and dynamic bearing capacities ([2.5.4.10.1](#)).

- Acceptable total settlement and minimum differential settlement (2.5.4.10.2).
- No potential for liquefaction due to earthquake ground motion (2.5.4.8).

Figures 2.5-388 and 2.5-389 show that the actual amount of excavation of the upper sands is significantly larger than required to simply expose the BBM surface to provide an adequate bearing surface for the power block structure foundations. This is due to the need for a safe excavation of the upper sands, which dictate 2-horizontal to 1-vertical slopes. The slopes of the excavation are for construction purposes only and not a foundation design requirement nor needed to assure the safety performance of the Nuclear Island (NI).

For analytical purposes it was assumed the lateral extent of backfill can be considered infinite for site response and seismic SSI analyses. To demonstrate the reasonableness of this assumption a sensitivity study of the backfill geometry is provided in Subsection 2.5.2.9.2. In this sensitivity analyses, 2D SASSI bathtub models are used to represent the ESP defined excavation cross section including the slopes. The Best Estimate ESP Category 1 and 2 backfill properties were used for this sensitivity study.

Since Category 1 and 2 backfill over the defined slopes is not a foundation design requirement, this section evaluates the importance of backfill placed directly over the slopes with regard to the study of backfill geometry provided in Subsection 2.5.2.9.2. This is accomplished by comparing the 2D SASSI bathtub model results of Subsection 2.5.2.9.2 to results of the same 2D SASSI bathtub models and inputs while varying the backfill properties, primarily stiffness, directly over the slopes of the excavation. Figure 2.5-335 and Figure 2.5-341 from Subsection 2.5.2.9.2 show the 2D SASSI bathtub models for site response (Part I) and the site seismic SSI analysis (Part II) respectively. These same models are used for this study herein except the backfill properties over the slopes are varied. A range of material properties for backfill over the slopes was considered while maintaining the Best Estimate ESP backfill properties directly above the BBM. A comparison that shows no significant differences between the 2D SASSI bathtub model results for different cases of backfill over the slopes with the 2D SASSI bathtub model results of Subsection 2.5.2.9.2 will demonstrate that the results and conclusions in Subsection 2.5.2.9.2 are still valid and therefore will support the use of backfill other than Category 1 and 2 backfill over the slopes.

For this evaluation three cases are considered for material other than Category 1 and 2 backfill placed over the excavation slopes:

Case 1 is a hypothetical case of no excavation slopes (a vertical cut) with the full depth of the Upper Sands brought up to the bottom toe of the exposed BBM. This is considered an extreme contrast to the Best Estimate Category 1 and 2 backfill modeled above the BBM and would represent the most limiting lateral extent of the backfill possible.

Case 2 is a hypothetical lower bound of well-compacted engineered granular backfill. It is considered an extreme lower bound for engineered backfill, with shear wave velocities less than 1000 fps at the NI foundation elevation.

Case 3 is a hypothetical upper bound of well-compacted engineered granular backfill. It is considered an extreme upper bound for engineered granular backfill, with shear wave velocities well over 1000 fps at the NI foundation elevation.

The well-compacted engineered granular backfill would have a similar parabolic shear wave velocity profile as the ESP Category 1 and 2 backfill, but with possibly a larger potential range of values.

The three cases provide a significant range of shear wave velocity over the slopes, which create various contrasting boundaries to the adjacent best estimate ESP backfill shear wave velocity

modeled directly above the BBM. Therefore, the comparison of the 2D SASSI bathtub model results for these different cases of material over the slopes to the 2D SASSI bathtub model results of [Subsection 2.5.2.9.2](#) is sufficient to demonstrate that engineered backfill other than Category 1 and 2 backfill placed over the slopes would not invalidate the results and conclusions provided in [Subsection 2.5.2.9.2](#).

[Figure 2.5-352](#) is a plot of the Lower Bound (LB), Best Estimate (BE), and Upper Bound (UB) low strain profiles for the ESP Category 1 and 2 backfill, Case 1, Case 2, and Case 3. This figure demonstrates the breadth of the variation of the shear wave velocity profiles considered for backfill material over the slopes of the excavation in order to assess the significance of material placed over the slopes on the results and conclusions provided in [Subsection 2.5.2.9.2](#). [Figure 2.5-353](#) is a comparison of the strain compatible BE shear wave velocity profiles for ESP Category 1 and 2 backfill used in the sensitivity analysis of [Subsection 2.5.2.9.2](#) (identified as Base Case in the figure) along with Cases 1, 2, and 3 used in the 2D SASSI SSI bathtub models.

Part I of [Subsection 2.5.2.9.2](#) provides the sensitivity study for seismic site response. The same 2D SASSI bathtub model shown in [Figure 2.5-335](#) was used, except the material over the slopes was changed. Three cases described above were considered, the results of Cases 1, 2, and 3 are compared to the 2D SASSI bathtub results of [Subsection 2.5.2.9.2](#) identified as “SASSI-BF-IS.” The results in the form of spectral amplification factors versus frequency are shown in [Figures 2.5-354](#), [2.5-355](#), and [2.5-356](#) at three horizons: at a depth of 0 ft (GMRS Horizon), at 40 ft depth (FIRS horizon), and at 86 ft depth (top of Blue Bluff Marl), respectively. As shown in these figures the differences are very small confirming that backfill with shear wave velocities lower and higher than Category 1 and 2 backfill can be placed over the slopes without invalidating the results and conclusions provided in [Subsection 2.5.2.9.2](#).

Part II of [Subsection 2.5.2.9.2](#) provides the sensitivity study for site seismic SSI analyses. The same 2D SASSI SSI bathtub model shown in [Figure 2.5-341](#) was used here except the material over the slopes was changed. Three cases described above were considered, the results of cases 1, 2, and 3 are compared to the 2D SASSI SSI bathtub results of [Subsection 2.5.2.9.2](#). These results are the horizontal in-structure response spectra at the six key locations in the NI and are shown on [Figures 2.5-357](#) through [2.5-362](#). The 2D SASSI SSI bathtub results of [Subsection 2.5.2.9.2](#) with the Best Estimate Category 1 and 2 backfill properties used throughout the excavation are identified as “Bathtub Model-d5.” The generic AP1000 standard 2D design response spectra are plotted for comparison purposes as was done in [Subsection 2.5.2.9.2](#). As shown in these figures the differences are very small confirming that backfill with shear wave velocities lower and higher than Category 1 and 2 backfill can be placed over the slopes without invalidating the results and conclusions provided in [Subsection 2.5.2.9.2](#).

In summary, the seismic models for VEGP 3 and 4 are based on an assumption of infinite lateral extent of backfill. The sensitivity study described in [Subsection 2.5.2.9.2](#) demonstrated that the ESP-defined lateral extent of the excavation is adequate to support the infinite backfill assumptions of the seismic models. The results from the sensitivity studies described above show that this conclusion remains valid when the Category 1 and 2 backfill over the slopes is replaced with backfill with conservatively low shear wave velocities, backfill with conservatively higher shear wave velocities, and no backfill at all (in situ material). Thus it can be concluded that an engineered fill other than Category 1 and 2 backfill can be used over the slopes of the excavation without invalidating the results and conclusions of [Subsection 2.5.2.9.2](#).

2.5.3 Surface Faulting

NRC Regulatory Guide 1.165, *Identification and Characterization of Seismic Sources and Determination of Safe Shutdown Earthquake Ground Motion* (RG 1.165), defines a capable tectonic source as a tectonic structure that can generate both vibratory ground motion and tectonic surface deformation, such as faulting or folding at or near the earth's surface in the present seismotectonic regime. This section evaluates the potential for tectonic surface deformation and non-tectonic surface deformation at the site. Information contained in **Subsection 2.5.3** was developed in accordance with RG 1.165 and is intended to satisfy 10 CFR 100.23, *Geologic and Seismic Siting Criteria*.

There are no capable tectonic sources within the 5-mi VEGP site area radius, and there is a negligible potential for tectonic fault rupture. There is only limited potential for non-tectonic surface deformation in shallow deposits within the 5-mi site area radius, and this potential can be mitigated by means of excavation. The following sections provide the data, observations, and references to support these conclusions.

2.5.3.1 Geological, Seismological, and Geophysical Investigations

The following investigations were performed to assess the potential for tectonic and non-tectonic deformation at and within a 5-mi radius of the VEGP site:

- Compilation and review of existing data and literature
- Interpretation of aerial photography
- Field reconnaissance
- Aerial reconnaissance
- Review of historical and recorded seismicity
- Collection and interpretation of seismic reflection data at the VEGP site
- Discussions with current researchers in the area
- Collection and interpretation of survey data collected from a Quaternary fluvial terrace located at the SRS overlying the surface projection of the Pen Branch fault.

An extensive body of information is available for the VEGP site. This information is contained in five main sources:

- Work performed for the existing VEGP Units 1 and 2.
- Published geologic mapping performed by the US Geological Survey (USGS), the South Carolina Department of Natural Resources, and other researchers.
- Numerous, detailed investigations of the nearby Savannah River Site (SRS), perhaps the most extensively studied portion of the US Atlantic Coastal Plain.
- Seismicity data compiled and analyzed in published journal articles, EPRI (1986a), and the updated EPRI catalog, performed as part of this study.

- Seismic reflection data collected near the site within the Savannah River channel (Reference 321).

This existing information was supplemented by aerial and field reconnaissance performed within and beyond the 25-mi site vicinity radius, and by interpretation of aerial photography within the 5-mi site area radius. Given the extensive geologic and geomorphic studies performed previously at the SRS, the interpretation of aerial photography performed for the ESP study focused on the area southeast of the SRS. These studies were performed to document, where possible, the presence or absence of geomorphic features indicative of potential Quaternary fault activity within the Coastal Plain sediments or underlying bedrock.

2.5.3.1.1 Previous VEGP Site Investigations

This section summarizes previous site investigations performed for existing VEGP Units 1 and 2. Previous investigations for VEGP Units 1 and 2 did not identify the existence of tectonic faulting (Reference 551, Reference 552, Reference 553, Reference 554, Reference 212). Detailed geologic mapping and inspection of excavations during VEGP construction revealed no evidence of geologically recent or active faulting. However, minor, non-tectonic dissolution-induced collapse features (including minor folds and small joints and faults confined to the near-surface) were recognized and logged in detail on site Reference 555.

Bechtel (1974a) identified, discussed in Subsection 2.5.1.2.3, a northwest-dipping monoclinial flexure beneath the site in the Blue Bluff Marl. This feature, referred to as a dip reversal because the strata locally dip gently northwest against the regional southeast dip of the Coastal Plain sediments, was interpreted as a syndepositional, sedimentary feature (Reference 552). Later investigations by Bechtel (1978, 1981) describe “stratigraphic irregularities” recognized in site excavations associated with the Blue Bluff Marl. Because these stratigraphic irregularities were observed to be underlain by flat-lying, laterally continuous strata, Bechtel (1978, 1981) concluded that these irregularities were produced by syn-depositional processes.

Alterman (1984) reported observing a number of “clastic dikes” at the VEGP site and in the site vicinity during an NRC visit. Alterman’s report does not, however, interpret the origin of these features. Bechtel (1984) identified the presence of a variety of small-scale deformation structures in the walls of a garbage trench on the VEGP site within Tertiary Coastal Plain sediments. These structural features, including warped bedding, fractures, joints, minor offsets, and injected sand dikes, were interpreted as local phenomena related to dissolution of the underlying Utley Limestone and resultant plastic and brittle collapse of overlying Tertiary sediments. These features and their potential for non-tectonic surface deformation at the site are further discussed in Subsection 2.5.3.8.2.1 below. Bechtel (1984) also noted the presence of “clastic dikes” in the garbage trench and interpreted these features to be the result of near-surface pedogenic processes.

As described in Subsection 2.5.1.2.4.1, the Pen Branch fault was first discovered at the SRS in 1989, which initiated investigations at the VEGP site and a series of studies at the SRS. Investigations at the VEGP site concluded that the fault was not onsite or in close proximity to Units 1 and 2 (Reference 212). Studies of the Pen Branch fault at the SRS continued through the 1990s, but had still not definitively located the southwestward projection of the fault to the Georgia side of the Savannah River. As shown in Figures 2.5-224, 2.5-225, 2.5-227 and 2.5-237, projections of the fault into Georgia included locations northwest of the VEGP site (Reference 442) and directly southeast of the VEGP site (Reference 255).

In light of the data gathered from studies of the Pen Branch fault at the SRS during the 1990s and recent investigations at the VEGP site, some conclusions of the previous studies regarding the location of the Pen Branch fault in site studies and the FSAR should be revised. Because the Pen Branch fault has been located adjacent to the VEGP site and beneath the monocline in the Blue Bluff

Marl, it is now clear that the Pen Branch fault is associated with the monocline (or dip reversal) and that there is a Tertiary fault within 5 mi of the VEGP site. However, the new information only alters the past location of the Pen Branch fault. After considerable study, no new information gathered on the Pen Branch fault has changed the original conclusions of Snipes et al. (1989) that the youngest strata deformed by the fault are late Eocene and that the fault is not a capable tectonic source. In fact, recent studies, for this ESP study, have provided additional lines of evidence to support the non-capable status of the Pen Branch fault, a conclusion that has been supported in multiple NRC and DOE reviews (NUREG-1137, NUREG-1137-8, NUREG-1821).

2.5.3.1.2 Published Geologic Mapping

Geologic mapping of the site vicinity (25-mi radius) and site area (5-mi radius) in the past two decades has been largely focused on the SRS and surrounding regions of South Carolina (Figure 2.5-231). The USGS has published 1:100,000 scale and 1:48,000 scale geologic maps of the SRS area (Reference 558, Reference 412). In addition, the South Carolina Department of Natural Resources has published numerous 1:24,000 scale geologic maps within the site vicinity. Significantly fewer and less detailed geologic maps have been published for the Georgia portion of the VEGP site vicinity (Figure 2.5-231).

Additional studies focused on mapping and assessing specific geologic and/or tectonic features in the site vicinity. These include mapping and interpreting small-scale deformation structures (Reference 556; Reference 550) and possible Quaternary tectonic features (Reference 251; Reference 482).

McDowell and Houser (1983) mapped the distribution of small-scale deformation structures in the Upper Coastal Plain in the greater Columbia, South Carolina, to Augusta, Georgia, area. They identified small-scale folds, brittle faults, and convoluted bedding features exposed in roadcuts, excavations, and stream cuts. McDowell and Houser noted that some of these features appear to be non-tectonic in origin, whereas others are less clear and may be related to strong ground shaking.

Bartholomew et al. (2002) described exposures of “clastic dikes” in the VEGP site vicinity. One of these exposures is located in the upper Eocene Tobacco Road sand near Hancock landing (north of existing VEGP Units 1 and 2 within the VEGP site area). They interpret these clastic dikes as evidence for “strong paleoearthquakes, probably associated with late Eocene to late Miocene oblique-slip”.

In addition, the USGS has published a compilation of all known Quaternary faults, liquefaction features, and possible tectonic features in the central and eastern United States (Reference 251), updated in (Reference 482) (Figure 2.5-220). The only feature within the 5-mi VEGP site area radius identified by this compilation is the Pen Branch fault (discussed in detail in Subsection 2.5.1.2.4.1). Crone and Wheeler (2000) classified the Pen Branch fault as a Class C feature (Table 2.5-201) because of its demonstrated early Cenozoic activity but absence of evidence for post-Eocene slip.

2.5.3.1.3 Previous Savannah River Site Investigations

SRS studies include numerous geological, geophysical, seismologic, and hydrologic investigations. These studies identified a number of basement faults that are mapped at the SRS based on interpretation of seismic reflection data, borehole data, gravity and magnetic data, and/or groundwater anomalies. Several of these faults are located within the 5-mi radius of the VEGP site (Figures 2.5-224, 2.5-225, and 2.5-226).

The SRS is one of the most extensively studied portions of the Coastal Plain in terms of geology. Accordingly, an exhaustive description of all SRS geologic studies is not given here. Instead, the key studies that locate and characterize tectonic features of the SRS are summarized in this section.

These studies include Chapman and DiStefano (1989), Snipes et al. (1993), Stieve et al. (1991), Stephenson and Stieve (1992), Geomatrix (1993), Domoracki (1994), Stieve and Stephenson (1995), and Cumbest et al. (1998, 2000). As described in [Subsection 2.5.1.1.4.5](#), the majority of evidence for the presence of faults at the SRS is based on the interpretation of seismic reflection surveys; therefore, the depiction of buried fault locations differs between researchers and has also evolved through time with the successive availability of additional data.

Chapman and DiStefano (1989) conducted a vibroseis seismic reflection survey to refine existing knowledge of the basement structure beneath the SRS. This survey identifies first-order features of the basement surface, including the northern boundary fault of the Mesozoic Dunbarton Basin, later named the Pen Branch fault.

Based on core logs and supplemented by seismic reflection data from Chapman and DiStefano (1989), Snipes et al. (1993) mapped the location of the Pen Branch fault across the SRS. Snipes et al. (1993) recognized up-to-the-southeast movement for the Pen Branch fault and suggested that the fault formed originally as a Mesozoic normal fault bordering the northwestern Dunbarton Basin that was later reactivated in the Tertiary as a reverse fault.

Stieve et al. (1991) presented the results of a drilling program designed to further characterize the displacement history of the Pen Branch fault on the SRS. This study concludes that the base of the late Miocene Upland Formation is not deformed across the projected trace of the fault and thus provides direct stratigraphic evidence for the absence of activity on the Pen Branch fault within the past 5 Ma (million years ago).

Stephenson and Stieve (1992) and Stieve and Stephenson (1995) combined seismic data, borehole data, and potential field data to construct a subsurface structure model for the SRS. Their subsurface fault map identifies six basement-involved faults, including the Pen Branch, Steel Creek, ATTA, Ellenton, Crackerneck, and Upper Three Runs faults ([Figure 2.5-224](#)). These faults are described in [Subsection 2.5.1.1.4.5](#) and [Subsection 2.5.3.2](#).

Geomatrix (1993) performed a Quaternary and neotectonic study to assess geologic and geomorphic evidence for active tectonic deformation at the SRS. No evidence for active tectonic deformation was observed. Longitudinal profiles on Savannah River fluvial terraces show no evidence for warping or faulting of terrace surfaces associated with the surface projections of the Pen Branch and Steel Creek faults within a resolution of 7 to 10 ft (2 to 3 m).

Domoracki (1994) used 170 mi of reprocessed seismic reflection lines to map the geometry of the Dunbarton Basin and to refine the subsurface locations of SRS basement-involved faults. The report identified the Dunbarton Basin as a half-graben bounded solely by the Pen Branch fault and suggested that the Pen Branch fault possiblysoles into the Augusta fault at depth (see [Subsection 2.5.1.1.4.3](#) for discussion of the Augusta fault).

Cumbest et al. (1998, 2000) integrated data from more than 60 boreholes and more than 100 mi of seismic reflection profiles to provide the most-recent mapping of subsurface structure and basement-involved faults at the SRS. Cumbest et al. (1998) found no evidence for capability on any faults at the SRS. These data were used in combination with geometrical fault models to constrain slip histories for the Pen Branch and Crackerneck faults ([Reference 255](#)).

Cumbest et al. (2000) also compared the SRS faults with other Atlantic Coastal Plain faults and concluded that both sets of faults exhibit the same general characteristics and are closely associated. These characteristics include:

- Maximum offset less than 80 m (260 ft) at the base of the Coastal Plain sediments

- Regional-scale features that strike approximately northeast-southwest
- Predominantly reverse sense of slip
- Movement beginning in the Cretaceous Period and decreasing with time

Based on the strength of this association, and based on the fact that many of the other Coastal Plain faults are known to be non-capable, Cumbest et al. (2000) concluded by association that the SRS faults are also non-capable.

In situ stress measurements in basement rocks have been made in deep boreholes at the SRS. As part of a study of seismic hazards, magnitudes and orientations of in situ stresses were determined in five boreholes in 1998 and a 4,000-ft-deep borehole in 1992 (Reference 388). Results from the 4,000-ft-deep well (NPR hole) and previous borehole measurements at the SRS are consistent with a northeast-southwest direction of maximum compressive stress in the Atlantic Coastal Plain province (Reference 388). While the orientation of maximum horizontal stress was observed to range from N75°E to N33°E in the NPR hole, the majority of other orientations are closer to approximately N60°E. Thus, the maximum horizontal stress is oriented roughly parallel to the Pen Branch fault (about N55°E), indicating that it is unlikely to accommodate reverse or strike-slip faulting earthquakes in the present stress regime (Reference 388).

2.5.3.1.4 Previous Seismicity Data

The EPRI catalog of historical seismicity has demonstrated that no known earthquake greater than body wave magnitude (m_b) 3 has occurred within the VEGP site vicinity (25-mi radius) prior to 1984 (Figure 2.5-219). Considering micro-seismicity ($m_b < 3$) recorded since 1976 by the SRS seismic recording network, there has been no recent earthquake activity within the site area (5-mi radius) (Figure 2.5-219). The nearest micro-earthquake to the VEGP site is about 7 mi (about 11 km) to the northeast and located on the SRS (Reference 561).

The local SRS seismic network recorded three small earthquakes in 1985 (magnitude 2.6), 1988 (magnitude 2.0), and 1997 (magnitude 2.5), and a small earthquake sequence in 2001–2002 within the boundaries of the SRS (Reference 561). These small SRS earthquakes, as well as a 1993 event located north of the SRS in Aiken, South Carolina, have been studied by researchers in an effort to evaluate possible correlations to tectonic features. As described in Subsection 2.5.3.3, this minor activity is not correlated with any known faults.

2.5.3.1.5 Previous Seismic Reflection Data

In addition to the numerous seismic reflection surveys conducted at the SRS, several other seismic reflection studies have been performed in the VEGP site area. These include two surveys conducted within the Savannah River (Reference 211; Reference 321) and one conducted in a land-based survey located about 1.5 mi west of VEGP Units 1 and 2 (Reference 455).

As part of its investigation of the postulated Millett fault, Bechtel (1982) collected seismic reflection data along the Savannah River. Nelson (1989) reprocessed and re-interpreted these data from Utey Point southeastward to about 1 mi northwest of Griffins Landing to evaluate whether the Pen Branch fault extends southwest across the Savannah River beneath the VEGP site (Figure 2.5-237). Nelson (1989) concluded that there is no evidence of faulting and concluded that if the Pen Branch fault does occur in the SRS area in South Carolina, its upward termination is below the limit of survey penetration at approximately 750 ft (beneath at least the upper part of the Late Cretaceous Tuscaloosa Formation).

As part of a groundwater contamination study in Burke County, Georgia, Henry (1995) collected and interpreted seismic reflection data from two lines located in the Savannah River between Hancock Landing and the VEGP boat ramp (Figure 2.5-237). Henry (1995) concluded that the Pen Branch fault appears as a high-angle, southeast-side-up reverse fault located approximately 1,000 ft downstream from Hancock Landing (Figure 2.5-237). Henry (1995) interpreted the Pen Branch fault as a growth fault extending upward through the Paleocene Black Mingo Formation and into Eocene strata that lie below the unconformity at the base of Savannah River alluvium.

A land-based seismic reflection survey was performed along an unimproved road about 0.5 mi west of River Road (about 1.5 mi west of VEGP Units 1 and 2) and included in a report by Summerour et al. (1998) (Figure 2.5-237). Similar to Henry (1995), this research was also part of a groundwater contamination study in Burke County, Georgia. The seismic line was roughly situated across the westward projection of the Pen Branch fault within the site area and southwest of the VEGP site. Numerous, minor faults belonging to the Pen Branch fault were interpreted to cut reflectors within the Coastal Plain section. The basement reflector, however, is not clearly faulted and, therefore, these data suggesting the location of the Pen Branch fault are questionable.

2.5.3.1.6 Current Seismic Reflection Studies

Seismic reflection and refraction data were collected on the VEGP site in January and February 2006 as part of this ESP study. The seismic array was designed to: (1) image the Pen Branch fault, with the assumption that it continues on strike to the southwest from the SRS into the VEGP site area, and (2) assess the depth and character of the basement rocks beneath the Coastal Plain deposits. The survey included four seismic reflection and three seismic refraction lines (Figures 2.5-238 and 2.5-239, respectively). The results of this seismic reflection profiling clearly document that the Pen Branch fault is imaged in the basement beneath the VEGP site (see discussion in Subsection 2.5.1.2.4.2, and Figures 2.5-237 and 2.5-240). These data indicate that the Pen Branch fault strikes between N34°E and N45°E across the VEGP site, and dips 45° to the southeast.

2.5.3.1.7 Current Aerial and Field Reconnaissance

Field and aerial reconnaissance inspections reveal no evidence for surface rupture, surface warping, or the offset of geomorphic features indicative of active faulting. Likewise, interpretation of aerial and satellite photography and topographic maps reveals no evidence of geomorphic features indicative of potential for tectonic surface deformation (faulting or warping).

As part of the field reconnaissance performed for the ESP study, many of the features previously mapped within the site vicinity (25-mi radius) as evidence for possible tectonic activity have been observed [including those mapped by (Reference 556) and (Reference 550)]. Based on field observations and similar characteristics to features studied in a large excavation at the VEGP site (Reference 555), these features are assessed to be of non-tectonic origin. Even if the Bartholomew et al. (2002) “clastic dikes” are of tectonic origin, they interpret these features to be evidence for earthquakes that occurred during or prior to the late Miocene. “Clastic dikes” are discussed in detail in Subsection 2.5.3.8.2.2.

2.5.3.2 Geological Evidence, or Absence of Evidence, for Surface Deformation

As shown in Figure 2.5-224, four bedrock faults are mapped within 5 mi of the VEGP site (Reference 254, Reference 255; Reference 453). These four faults are:

- Pen Branch fault
- Ellenton fault

- Steel Creek fault
- Upper Three Runs fault

These faults were first identified on the SRS based on the interpretation of seismic reflection, borehole, gravity and magnetic, and/or groundwater data (Reference 232; Reference 562; Reference 451; Reference 442; Reference 265; Reference 453; and Reference 253, Reference 254, Reference 255). Each of these faults appears to terminate upward beneath the near surface. The youngest deposits deformed are Eocene in age. No deformation or geomorphic features indicative of potential Quaternary activity have been reported in the literature for these faults. Aerial and field reconnaissance and air photo interpretation performed for the current ESP study show that no geomorphic features indicative of Quaternary activity exist along any of the mapped fault traces. These four faults are summarized in Table 2.5-235 and described below.

2.5.3.2.1 Pen Branch Fault

The more than 20-mi-long (more than 30-km-long) Pen Branch fault is the northwest bounding fault of the Mesozoic Dunbarton Basin, strikes northeast, traverses the central portion of the SRS, and trends southwestward into Georgia near the VEGP site (Reference 441, Reference 442). Seismic reflection profiling performed as part of this ESP study has imaged the southeast-dipping Pen Branch fault beneath the VEGP site (see discussion in Subsection 2.5.1.2.4.2, Figure 2.5-243). The Pen Branch fault was reactivated in the Tertiary as an up-to-the-southeast reverse fault (Reference 442), and possibly soles into the Augusta fault (described in Subsection 2.5.1.1.4.3) at depth (Reference 265; Reference 453).

The Pen Branch fault is not exposed or expressed at the surface (Reference 442; Reference 453; Reference 255). Borehole and seismic reflection data collected from the SRS show no evidence for post-Eocene slip on the Pen Branch fault (Reference 255). SRS studies have been specifically designed to assess the youngest deformed strata overlying the fault through shallow, high-resolution reflection profiles, drilling of boreholes, and geomorphic analyses and have consistently concluded that late Eocene is the youngest strata deformed as described in Subsection 2.5.1.2.4.1.

The Pen Branch fault is not expressed geomorphically, nor is microseismicity associated with this fault. Therefore, it is concluded that the Pen Branch fault is not a capable fault within the site area. Within a resolution of 7 to 10 ft (2 to 3 m), longitudinal profiles along Quaternary fluvial terraces overlying the surface projection of the Pen Branch fault show no evidence of warping or faulting of the 350 ka to 1 Ma Ellenton (Qte) fluvial terrace (Reference 292).

Additional work performed for the ESP study has more accurately located the Pen Branch fault beneath a remnant of this terrace (Figure 2.5-246). The geomorphic evaluation of the Quaternary Ellenton terrace (Qte) surface overlying the Pen Branch fault is described in Subsection 2.5.1.2.4.3. The results of this study demonstrate a lack of tectonic deformation in the 350 ka to 1 Ma fluvial terrace surface within a resolution of about 3 ft. This observation is consistent with previous studies at both the VEGP site and the SRS that have concluded the Pen Branch fault is not a capable tectonic source.

2.5.3.2.2 Ellenton Fault

The Ellenton fault had been located in the southeastern portion of the SRS, about 4.6 mi from the VEGP site (Figure 2.5-224), but the Ellenton fault does not appear on the most recent SRS fault maps (Reference 254, Reference 255). The approximately 4-mi-long Ellenton fault had been interpreted to strike north-northwest, with near vertical to steeply east dip and east-side-down sense of slip (Reference 265; Reference 453). No clear relationship exists between the previously located Ellenton fault and regional structural features.

Because the data originally used to identify this fault are of poor quality according to Stieve and Stephenson (1995), the fault is not expressed geomorphically, and microseismicity is not associated with this fault; the current assessment is that this fault likely does not exist. Therefore, it is concluded that the Ellenton fault is not a capable tectonic source within the site area. Neither the Crone and Wheeler (2000) compilation of Quaternary faults and tectonic features in the central and eastern United States, nor the Wheeler (2005) compilation update, identifies the Ellenton fault as a potential Quaternary feature.

2.5.3.2.3 Steel Creek Fault

The Steel Creek fault is located in the northwest portion of the SRS, about 3 mi from the VEGP site (Reference 453; Reference 255) (Figures 2.5-224 and 2.5-226). This greater than 11-mi-long, northeast-trending, northwest-dipping, up-to-the-northwest reverse fault is located within the Dunbarton Basin and, along with the Pen Branch fault, forms a horst structure within the basin (Reference 453). The Steel Creek fault extends upward into Cretaceous units, but the uppermost extent of faulting remains unresolved (Reference 453).

Within a resolution of 7 to 10 ft (2 to 3 m), longitudinal profiles along Quaternary fluvial terraces overlying the surface projection of the Steel Creek fault show no evidence of warping or faulting of the fluvial terraces (Reference 292). The Steel Creek fault is not expressed geomorphically, nor is microseismicity associated with this fault. Therefore, it is concluded that this fault is not a capable tectonic source within the site area. Neither the Crone and Wheeler (2000) compilation of Quaternary faults and tectonic features in the central and eastern United States, nor the Wheeler (2005) compilation update, identifies the Steel Creek fault as a potential Quaternary feature.

2.5.3.2.4 Upper Three Runs Fault

The Upper Three Runs fault is located in the northwest portion of the SRS, about 5 mi from the VEGP site (Reference 453) (Figure 2.5-224). The location of the Upper Three Runs fault is mapped based on potential field data and interpretation of seismic reflection profiles (Reference 453). The Upper Three Runs fault has been interpreted as an older (initially Paleozoic) fault that soles into the Augusta fault at depth, possibly reactivated as a Mesozoic normal fault (Reference 252; Reference 265; Reference 453). The Augusta fault is discussed in Subsection 2.5.1.1.4.3.

The greater than 20-mi-long, northeast-trending Upper Three Runs fault is restricted to basement rocks. Seismic reflection profiling shows that the Coastal Plain sediments are not offset or deformed by this fault (Reference 232; Reference 453). The Upper Three Runs fault is not expressed geomorphically, nor is microseismicity associated with this fault. Therefore, it is concluded that this fault is not a capable tectonic source within the site area. Neither the Crone and Wheeler (2000) compilation of Quaternary faults and tectonic features in the central and eastern United States, nor the Wheeler (2005) compilation update, identifies the Upper Three Runs fault as a potential Quaternary feature.

2.5.3.3 Correlation of Earthquakes With Capable Tectonic Sources

Seismicity within the VEGP site vicinity (25-mi radius) is shown in Figure 2.5-219. As shown on this figure, there is no spatial correlation of earthquake epicenters with known or postulated faults. No faults or geomorphic features within the site vicinity (25 mi radius) can be correlated with earthquakes. Based on review of existing literature, no reported historical earthquake epicenters have been associated with bedrock faults within a 25 mi radius of the VEGP site (Figure 2.5-219). None of these faults within 25 mi of the VEGP site are classified as capable tectonic sources.

In general, the South Carolina and Georgia portions of the Coastal Plain and Piedmont provinces exhibit a higher rate of seismicity than elsewhere in these provinces (Figure 2.5-221). This diffuse

earthquake activity is not concentrated or aligned with any mapped faults, nor is it associated with any known tectonic structures. [Figure 2.5-219](#) shows that no earthquakes of magnitude 3.0 or larger are known to have occurred within 25 mi of the site. However, several small events ($m_b < 3.0$) have occurred within the site vicinity.

The SRS seismic recording network, which consists of nine instruments located within and adjacent to the SRS, has been recording microseismicity in the VEGP site vicinity since it was installed in 1976. This local network recorded three small earthquakes (in 1985 [magnitude 2.6], 1988 [magnitude 2.0], and 1997 [magnitude 2.5]) and a small earthquake sequence in 2001–2002 within the boundaries of the SRS ([Reference 561](#)). These small SRS earthquakes, and also a 1993 event located north of the SRS in Aiken, have been studied in an effort to evaluate possible correlations with tectonic features ([Figure 2.5-219](#)).

The June 9, 1985, earthquake of local duration magnitude (M_D) 2.6 was located about 5 mi north of the northwest margin of the Dunbarton Basin ([Figure 2.5-219](#)). The depth of this event was initially determined to be approximately 0.6 mi (1 km) ([Reference 563](#)), and was later listed at a depth of 3.5 mi (5.8 km) ([Reference 561](#)). This earthquake had a focal plane solution that suggests either a sinistral component of slip on a northeast-striking plane or a dextral component of slip on a northwest-striking plane ([Reference 563](#)). The close location of the event to the northwest margin of the Dunbarton Basin and northeast strike of the sinistral nodal plane led Talwani et al. (1985) to associate this event with the northeast-striking basin border fault (later named the Pen Branch fault). However, Crone and Wheeler (2000) point out that the sinistral sense of slip from the fault plane solution is inconsistent for the Pen Branch fault given the northeast-southwest orientation of principal horizontal stress. Therefore, it is highly unlikely that this event is associated with the Pen Branch fault.

The August 5, 1988, earthquake of magnitude 2.0 was centered southeast of the Pen Branch fault within the Dunbarton Basin ([Figure 2.5-219](#)). The hypocenter of this event was located at a depth of about 1.5 mi (2.5 km) ([Reference 561](#)) and no focal mechanism solution could be obtained ([Reference 267](#)). Domoracki et al. (1999) suggested that this earthquake was associated with the Pen Branch fault. However, Stevenson and Talwani's (2004) more recent hypocenter location for this event suggests no spatial association with a known fault.

The August 8, 1993, Aiken, South Carolina, earthquake with a body wave magnitude estimated from Rayleigh surface waves (m_{blg}) of 3.2 was studied in detail by Stevenson and Talwani (1996), who determined that the event was located within a steep gravity gradient that they interpret to be the edge of a granitic pluton ([Figure 2.5-219](#)). The hypocenter of this event was located at a depth of about 6 mi (about 10 km) ([Reference 561](#)). The event is not spatially associated with a known fault.

The May 17, 1997, earthquake of magnitude 2.5 was located about 0.5 to 1 mi northwest of the Pen Branch fault ([Figure 2.5-219](#)). Given that this event had a depth of about 3 mi (5 km) ([Reference 561](#)), it is located in excess of 3 mi from the southeast-dipping Pen Branch fault.

The most recent activity, termed the Upper Three Runs earthquake sequence, included an October 8, 2001, main event of m_{blg} 2.6 centered near Upper Three Runs Creek and a series of seven very small aftershocks occurring through March 6, 2002, in a small area of 6.0 to 6.5 square km ([Reference 561](#)) ([Figure 2.5-219](#)). All events within this earthquake sequence occurred within depths of approximately 1.8 to 3 mi (3 to 5 km), with a positional uncertainty of about 1600 ft (about 500 m) due to the proximity of the local SRS seismic stations. Single event and composite focal mechanisms indicate a predominantly reverse motion on a fault plane oriented N25°W, 41°SW. A 3-D plot of hypocenters defined a fault plane of similar orientation ([Reference 561](#)).

Stevenson and Talwani (2004) examined gravity data and found a northeast-trending grain to the Bouguer gravity map. Upon further processing to derive a map of the first horizontal derivative of

gravity, they defined a small local northwest-trending ridge of gravity that they interpreted as the causative structure. The shallowness and small areal extent of the Upper Three Runs earthquake sequence, combined with the apparent association of a very small basement feature running counter to the regional structural trend, suggest that this earthquake activity is extremely localized and is not attributable to any regional features ([Reference 561](#)).

2.5.3.4 Ages of Most Recent Deformations

As presented in [Subsection 2.5.3.2](#), none of the four faults within 5 mi of the VEGP site exhibit evidence of Quaternary activity. The Pen Branch fault represents the northern bounding normal fault of the Mesozoic Dunbarton Basin, and this structure was reactivated as a Tertiary oblique-reverse fault. Borehole and seismic data provide no evidence for post-Eocene slip on the Pen Branch fault ([Reference 255](#)). Geomatrix (1993) concluded that the Pen Branch fault does not deform Quaternary fluvial terraces of the Savannah River within a resolution of 7 to 10 ft (2 to 3 m). The geomorphic evaluation of this same 350 ka to 1 Ma fluvial terrace surface performed as part of this ESP study demonstrates a lack of tectonic deformation within a resolution of about 3 ft (about 1 m) (described in [Subsection 2.5.1.2.4.3](#)).

The Ellenton fault was previously interpreted as a north-northeast-striking fault ([Reference 453](#)), but it does not appear in the most recent maps of subsurface SRS faults ([Reference 254](#), [Reference 255](#)) and likely does not exist.

The Steel Creek fault extends upward into Cretaceous units, but the uppermost extent of faulting remains unresolved ([Reference 453](#)). Geomatrix (1993) concluded that the Steel Creek fault does not deform Quaternary fluvial terraces of the Savannah River within a resolution of 7 to 10 ft (2 to 3 m).

The Upper Three Runs fault is restricted to basement rocks. Seismic reflection profiling revealed no evidence for this fault deforming overlying Coastal Plain sediments ([Reference 232](#); [Reference 453](#)).

2.5.3.5 Relationships of Tectonic Structures in the Site Area to Regional Tectonic Structures

The four faults identified within the site area (i.e., the Pen Branch, Ellenton, Steel Creek, and Upper Three Runs faults) are located on the SRS. Only one of these faults (the Pen Branch) is observed west of the Savannah River in Georgia. As described in [Subsection 2.5.3.6](#), none of the four faults within the site area is considered a capable tectonic feature.

2.5.3.5.1 Pen Branch Fault

The Pen Branch fault likely is the northern boundary fault of the Mesozoic Dunbarton Basin. During the Mesozoic, the fault accommodated crustal extension and thinning with a southeast-side-down normal sense of slip ([Reference 442](#); [Reference 265](#); [Reference 453](#)). Snipes et al. (1993) suggested that the southeastern margin of the Dunbarton Basin may also be bounded by a fault (the Martin fault), although Domoracki et al. (1999) suggested that the Dunbarton Basin is instead a half-graben bounded only by the Pen Branch fault to the north.

The Pen Branch fault was reactivated as a reverse or reverse-oblique fault during Cretaceous and into Tertiary time, with an up-to-the-southeast sense of slip ([Reference 559](#); [Reference 442](#); [Reference 255](#)). Stephenson and Stieve (1992) and Stieve and Stephenson (1995) suggested that the Pen Branch fault may sole into the shallow dipping Augusta fault (described in [Subsection 2.5.1.1.4.3](#)) or a Paleozoic/Mesozoic regional decollement at depth ([Figure 2.5-205](#)).

2.5.3.5.2 Ellenton Fault

The Ellenton fault as mapped by Stieve and Stephenson (1995) is a north-northwest striking fault located within the Dunbarton Basin between the Upper Three Runs and Pen Branch faults. The Ellenton fault orientation is roughly normal to the regional structural grain and to the other SRS faults and bears no clear relationship to regional structures. The Ellenton fault does not appear on the most recent SRS fault maps ([Reference 254](#), [Reference 255](#)) and likely does not exist.

2.5.3.5.3 Steel Creek Fault

This northeast-trending Steel Creek fault is roughly parallel to the regional structural grain and is located within the Dunbarton Basin. The Steel Creek fault is an up-to-the-northwest, secondary structure associated with the Pen Branch fault, with which it forms a horst structure within the basin ([Reference 453](#)).

2.5.3.5.4 Upper Three Runs Fault

The northeast-trending Upper Three Runs fault is roughly parallel to the regional structural grain and is restricted to basement rocks; seismic reflection profiles show that the fault does not offset Coastal Plain sediments ([Reference 232](#); [Reference 453](#)). The Upper Three Runs fault has been interpreted as an older (initially Paleozoic) fault, possibly reactivated as a Mesozoic normal fault ([Reference 252](#); [Reference 265](#); [Reference 453](#)). The Upper Three Runs fault possibly soles into the Augusta fault (described in [Subsection 2.5.1.1.4.3](#)) or a Paleozoic/Mesozoic regional decollement at depth ([Reference 453](#)) ([Figure 2.5-205](#)).

2.5.3.6 Characterization of Capable Tectonic Sources

Based on studies evaluated in the preceding sections, SNC concluded that there are no capable tectonic sources within 5 mi of the VEGP site. The Pen Branch fault, the nearest fault to the VEGP site, has undergone extensive study and multiple reviews by the NRC. All of these studies, including investigations as part of this ESP study, support the non-capable status of the Pen Branch fault as outlined below:

- NUREG-1137-8 concludes that the Pen Branch fault is not a capable fault and does not represent a hazard to the VEGP site. Similarly, other NRC reviews of the Pen Branch fault for facilities such as the Mixed Oxide Fuel (MOX) Fabrication Facility at SRS have also concluded that the Pen Branch fault is not a capable fault (NURERG-1821).
- The “association clause” of Appendix A 10 CFR 100.23 applies to this discussion as follows: Cumbest et al. (2000) noted that the Pen Branch fault shares characteristics with other Atlantic Coastal Plain faults that are considered non-capable. These characteristics include northeast-southwest strikes, small total offsets of Cenozoic strata in relation to fault age, slip histories that began in the Cretaceous, and offsets that decrease with decreasing age. Cumbest et al. (2000) argued that the abundance of shared characteristics between these faults implies that these faults are genetically related. Several of these faults have been shown to be non-capable. Therefore, Cumbest et al. (2000) concluded that the Pen Branch fault is likely non-capable as well.
- The Pen Branch fault is not exposed or expressed at the surface ([Reference 442](#); [Reference 453](#); [Reference 255](#)). Reconnaissance work and aerial photograph interpretation performed for the ESP study confirm that there is no exposure of the fault or geomorphic expression of potential Quaternary activity.

- Snipes et al. (1993) investigated a 10- to 20-ft-thick (3- to 6-m-thick) Quaternary light tan soil horizon in railroad cuts overlying the projected trend of the Pen Branch fault at the SRS. They observed no detectable offset of this unit. According to Snipes et al. (1993), the youngest horizon known from borehole studies to be faulted is the top of the Dry Branch Formation of Late Eocene age.
- Regional principal stress orientations based on stress-induced wellbore breakouts and hydraulically induced fracturing show that the maximum horizontal stress is parallel to the regional orientation of the Pen Branch fault, which makes “strike-slip faulting unlikely” and “reverse faulting essentially impossible” (Reference 388). The most-recent deformation observed for this fault in Tertiary sediments is reverse faulting.
- Geomatrix (1993) evaluated longitudinal profiles along Quaternary fluvial terraces of the Savannah River and concluded that no evidence of terrace surface warping or faulting exists within a resolution of 7 to 10 ft (2 to 3 m). Additionally, as part of the ESP study, local longitudinal terrace profiles across the now well-located Pen Branch fault support the earlier conclusion that no deformation is observed in the terrace remnant of the Ellenton terrace (estimated as 350 ka to 1 Ma) overlying the Pen Branch fault.
- As part of this ESP study, geomorphic analysis of the 350 ka to 1 Ma fluvial terrace overlying the surface projection of the Pen Branch fault at the SRS demonstrates the lack of tectonic deformation of this Quaternary geomorphic surface within a resolution of about 3 ft. The resolution of this study compared with the previous studies makes it by far the most definitive evidence for the non-capability of the Pen Branch fault both at the Savannah River Site and the VEGP site. Results are described in more detail in Subsection 2.5.1.2.4.3.

2.5.3.7 Designation of Zones of Quaternary Deformation Requiring Detailed Fault Investigation

No zones of quaternary deformation require detailed investigation within the site area.

2.5.3.8 Potential for Tectonic or Non-Tectonic Deformation at the Site

The potential for tectonic deformation at the site is negligible. There is, however, the evidence for past, and the potential for future, non-tectonic deformation at the site in the form of dissolution-induced collapse features. These conclusions are discussed in the following sections.

2.5.3.8.1 Potential for Tectonic Deformation at the Site

The potential for tectonic deformation at the site is negligible. The presence of the Pen Branch fault adjacent to the VEGP Units 3 and 4 footprint and beneath the monocline in the Blue Bluff Marl (Figures 2.5-242 and 2.5-245) suggests that past deformation of the Eocene strata has occurred in the form of non-brittle folding. However, this type of deformation associated with the non-capable Pen Branch fault is no longer active and will not impact the ground surface in the future. Since the original site studies in the early 1970s, no new information has been reported to suggest the existence of any Quaternary surface faults or capable tectonic sources within the site area.

2.5.3.8.2 Potential for Non-Tectonic Deformation at the Site

Several non-tectonic features are present in the site area. These include dissolution-induced collapse structures and clastic dikes. As described below, permanent ground deformation at the site may be produced by dissolution within the Utley Limestone, whereas clastic dikes are not potential sources of permanent ground deformation. Dissolution-related permanent ground deformation would

be mitigated at the site by the excavation and removal of the Utley Limestone during construction of the site.

Clastic dikes have been reported at the site and in the site vicinity (Reference 437; Reference 549; Reference 555; Reference 550). The origin of these features has been subject to considerable debate, but those on-site features described as “clastic dikes” likely were formed by soil weathering processes, as described in Subsection 2.5.3.8.2.2. NUREG-1137 concludes that no evidence exists that these features represent a safety issue for the plant, whatever their origin.

2.5.3.8.2.1 Dissolution Collapse Features

The potential for non-tectonic deformation at the site resulting from near-surface dissolution-induced collapse has long been recognized as a possibility and has been the subject of several studies e.g., (Reference 554, Reference 555). Bechtel (1984b) identified the presence of a variety of small-scale deformation structures in the walls of a garbage trench on the VEGP site within Tertiary Coastal Plain sediments (Figure 2.5-237). These structural features, including warped bedding, fractures, joints, minor offsets, and injected sand dikes, were interpreted as local phenomena related to dissolution of the underlying Utley Limestone and resultant plastic and brittle collapse of overlying Tertiary sediments (Reference 555) (Figures 2.5-363 and 2.5-364).

The dissolution origin for the warped bedding, fractures, small-scale faults, “clastic dikes,” and sand-injected dikes is interpreted largely from the observations and detailed documentation of these features in a large trench exposure that was over 900 ft long, 30 to 45 ft deep, and 25 to 40 ft across (Reference 555). The high concentration of these features within the trench and the spatial and kinematic relationships between different types of deformation features provide some of the best information regarding their origin. Field mapping efforts performed as part of the VEGP ESP application also identified “clastic dikes” within the VEGP site and surrounding site area, and similarly concluded these features are of a non-tectonic origin based on field observations.

The three-dimensional nature of the warped bedding, combined with the spatial and kinematic relationships of the small-scale faults and fractures along the margins of the more strongly warped depressions, clearly demonstrates a dissolution or sediment collapse origin. The highly irregular, discontinuous nature of folding is consistent with a non-tectonic dissolution origin and inconsistent with a tectonic origin, since there are no laterally persistent fold axes. For example, the upper contact of Unit F, a 1-to-2-ft-thick, moderately consolidated, laminated, red and yellow, silty fine sand, is folded into a highly irregular surface (Reference 555)(Figure 2.5-365). If this minor fold deformation was associated with the underlying Pen Branch fault, fold axes should be laterally persistent and parallel to the fault. The discontinuous nature of domes and depressions in an “egg carton” or “dimpled” pattern reflects the more random, non-tectonic process of dissolution (Figure 2.5-365).

Most of the small-scale faults have normal displacement toward or into the depressions, and a few exhibit minor reverse slip near the crests of some arches (Reference 555). These features are of limited dimensions and cannot be traced laterally across the width of the trench. The orientations of fractures and small faults are locally consistent with the limbs of the individual arches and depressions, but vary strongly from fold to fold. In some cases, such as shown in Figure 2.5-364, the small faults actually arc over the centers of some of the depressions. These field relationships all support an origin related to very localized settlement of the depressions resulting from dissolution and collapse of underlying strata.

The age of these dissolution features is poorly constrained; however, they are younger than the Eocene and Miocene host sediment and older than the overlying late Pleistocene or eolian sand of the Pinehurst Formation (Reference 555). No late Pleistocene or Holocene dissolution features have been identified at the site.

Anecdotal accounts provide additional evidence for the potential for dissolution-induced collapse at the site. The presence of a cave located near Mathes Pond, currently under water, and accounts of “soft zones” encountered in boreholes above the Blue Bluff Marl suggest the possibility of dissolution at the VEGP site.

Dissolution-induced collapse structures are not tectonic features, nor do they indicate regionally significant seismicity (Reference 555). NUREG-1137 concludes that no evidence exists that these features represent a safety issue for the plant. Dissolution collapse, however, represents a potential minor, non-tectonic surface deformation hazard in areas underlain by the Utley Limestone at the site. This hazard could be mitigated during construction through excavation and removal of the Utley Limestone to establish the foundation grade of the plant.

Not all depressions in the VEGP site area are the result of dissolution collapse. Carolina bays are non-tectonic, surficial geomorphic depressions that may resemble surface expression of dissolution collapse features. Carolina bays are commonly found throughout the VEGP site area and discussed in greater detail in Subsection 2.5.1.1.1. Unlike Carolina bays, surface depressions resulting from dissolution collapse are irregularly shaped and randomly oriented.

Pre-construction topographic maps of the VEGP site show several closed depressions at the site. Site reconnaissance performed for the ESP study shows that these depressions no longer exist and that they were likely destroyed by site excavations and activities. No present-day surface depressions were identified at the VEGP site as part of the ESP study.

2.5.3.8.2.2 Clastic Dikes

Clastic dikes are relatively planar, clay-filled features that typically flare out upward and are on the order of centimeters-to-decimeters wide and decimeters-to-meters long. Clastic dikes are widespread in the Coastal Plain of Georgia and South Carolina in the upper Miocene Barnwell and Hawthorne Formations. Despite the widespread occurrence of clastic dikes, however, their origin or origins are poorly understood. They have been variously attributed to seismic shaking or tectonic activity, to solution of underlying carbonate horizons and sediment collapse, and to weathering and soil-forming hypotheses [e.g., (Reference 437; (Reference 555); Reference 550)].

Clastic dikes on the VEGP site, in the site area, and on the SRS were described in detail by Alterman (1984), who noted feature dimensions, composition, grain size, and color, but did not propose a favored formation mechanism.

In describing clastic dikes exposed in the walls of a garbage trench more than 900 ft long located on the VEGP site, Bechtel (1984) differentiated two distinct classes of dikes: (1) “sand dikes” that resulted from plastic or liquid injection of loosely consolidated fine sand into overlying, fractured, relatively consolidated sediment, and (2) “clastic dikes” that resulted primarily from weathering and soil-forming processes preferentially enhanced along pre-existing fractures that formed during dissolution collapse. According to Bechtel (1984), the present geographic distribution of clastic dikes is controlled by the depth of weathering and paleosol development in the Coastal Plain sediments and by subsequent erosion of the land surface. Bechtel (1984) concluded that the dikes are primarily a weathering phenomenon that formed at least 10 ka to 100 ka. As part of the field reconnaissance performed for the ESP study, abundant “clastic dikes” have been observed in the site area that have characteristics consistent with a pedogenic or weathering origin, but no features were observed that can reasonably be interpreted to have formed as a result of injected sand. The field reconnaissance of “clastic dikes” exhibited the following primary characteristics, which were summarized by the Bechtel (1984) study of these features within a large trench exposure on the VEGP site:

1. The dikes are widely distributed through the region in deeply weathered clayey and silty sands of the Eocene Hawthorne and Barnwell Formations.

2. The dikes occur in nearly all exposures of the weathered profile but are rare in exposures of stratigraphically lower, less weathered sediment.
3. The dikes contain a central zone of bleached host rock bounded by a cemented zone of iron oxide. Some dikes contain a clay core.
4. Grain size analyses on samples indicate that the dike interval contains the same grain distribution as the host sediment with slightly more silt and clay (excluding clay core).
5. The dikes and associated mottling decrease downward in density and size. In most cases, the dikes taper downward and pinch out over a 5-to-15-ft distance.

NUREG-1137 concluded that no evidence exists that the clastic dikes represent a safety issue for the VEGP site. The SER suggests that the clastic dikes on the VEGP site may be non-tectonic, soft-sediment deformation features that formed 20 to 25 Ma.

In contrast to non-tectonic “clastic dikes,” Bartholomew et al. (2002) interpreted sand dike features found in the upper Eocene Tobacco Road Sand near Hancock Landing, Georgia, less than five mi north of the VEGP site, as evidence for strong paleoearthquakes probably associated with late Eocene to late Miocene earthquake activity possibly associated with the Pen Branch and/or Crackerneck faults. Bartholomew et al. (2002) describe sand dikes that cut across poorly bedded clay-rich strata and are filled with massive, medium to coarse sand.

However, the sand dikes identified by Bartholomew et al. (2002) are syndepositional due to the presence of marine animal burrows that cross cut the dikes. The formation of these dikes occurred during the late Eocene while the sediments were in a subaqueous marine environment ([Reference 550](#)). Whether these dikes of Bartholomew et al. (2002) formed as a result of seismic shaking or some other process related to soft sediment deformation (e.g., compaction and de-watering), these features are significantly older than Quaternary and, therefore, do not reflect geologically recent seismic activity.

2.5.4 Stability of Subsurface Materials and Foundations

This section presents information on the stability of subsurface materials and foundations at the VEGP site that may affect the proposed new unit's seismic Category 1 facilities. This geological, geophysical, geotechnical, and seismological information is developed and used as a basis to evaluate the stability of subsurface materials and foundations at the site. Field and laboratory test data was initially gathered during the ESP phase site investigation and subsequently augmented with field and laboratory data from a COL level investigation in support of the ESP limited work authorization (LWA) request.

Information presented in this section was developed from onsite geotechnical and geophysical investigations, a review of analysis and reports prepared for the existing VEGP units, and a review of geotechnical literature. Site specific reports prepared by Bechtel Power Corporation were included in this review; these reports addressed foundation investigation ([Reference 552](#)), backfill material investigations ([Reference 577](#), [Reference 578](#) and [Reference 581](#)), dynamic properties of the backfill ([Reference 579](#)), and the test fill program ([Reference 580](#)).

The ESP geotechnical field and laboratory investigation performed by MACTEC Engineering and Consulting, Inc. for the application was intended to enhance the understanding of the VEGP site and complement the existing geotechnical data developed for VEGP Units 1 and 2. The ESP geotechnical investigation data report is included as [Appendix 2.5A](#). Portions of this geotechnical data report were revised by MACTEC. A discussion of these revisions is provided in [Subsection 2.5.4.3.2.4](#). These revisions are reflected in [Appendix 2.5A](#). The ESP seismic reflection/refraction data report is included as [Appendix 2.5B](#).

A comprehensive site geotechnical field and laboratory investigation was performed by MACTEC to support the COL application. This investigation was conducted to augment the existing ESP geotechnical data and to further develop geotechnical data at specific proposed VEGP Units 3 and 4 structure locations and backfill borrow source locations. The COL investigation field work was substantially completed on April 20, 2007. The MACTEC geotechnical data report is included in [Appendix 2.5C](#). A test pad program was conducted in late 2007. A report on this effort is provided in [Appendix 2.5D](#).

2.5.4.1 Geologic Features

[Subsection 2.5.1.1](#) describes the regional geology, including regional physiography and geomorphology, regional geologic history, regional stratigraphy, and the regional tectonic setting. [Subsection 2.5.1.2](#) addresses site-specific geology and structural geology, including site physiography and geomorphology, site geologic history, site stratigraphy, site structural geology, and a site geologic hazard evaluation.

2.5.4.2 Properties of Subsurface Materials

Subsurface Uniformity

Soil structure interaction and foundation design are a function of the uniformity of the soil or rock below foundation. Although the design and analysis of the AP1000 is based on soil or rock conditions with uniform properties within horizontal layers, it includes provisions and design margins to accommodate many non-uniform sites. This subsection identifies the requirements for site investigation that may be used to demonstrate that:

- A site is “uniform” based on the criteria outlined in [Site Foundation Material Evaluation Criteria below](#). If the site can be demonstrated to be “uniform,” no further site specific analysis is required to qualify the site for the AP1000.

- A “non-uniform” site is acceptable to locate the AP1000 based on the criteria for acceptability outlined in [Site Foundation Material Evaluation Criteria below](#). Non-uniform sites may be shown to be acceptable as described in subsection 2.5.4.5.3.1 using site-specific evaluation as part of the Combined License application.

Considerations with respect to the materials underlying the nuclear island are the type of site, such as rock or soil, and whether the site can be considered uniform. If the site is non-uniform, the non-uniform soil characteristics, such as the location and profiles of soft and hard spots, should be considered. These considerations can be assessed with the information developed in response to Regulatory Guides 1.132 and 1.138. The geological investigations of [Subsections 2.5.1](#) and [2.5.7.5](#) provide information on the uniformity of the site, whether it may be geologically impacted, and whether the bedrock may be sloping or undulatory.

Site Foundation Material Evaluation Criteria

The AP1000 is designed for application at a site where the foundation conditions do not have extreme variation within the nuclear island footprint. This subsection provides criteria for evaluation of soil variability. The subsurface may consist of layers and these layers may dip with respect to the horizontal. If the dip is less than 20 degrees, the generic analysis using horizontal layers is applicable as described in NUREG/CR-0693 (Reference 2). The physical properties of the foundation medium may or may not vary systematically across a horizontal plane. The recommended methodology for checking uniformity is to calculate from the boring logs a series of “best-estimate” planes beneath the nuclear island footprint that define the top (and bottom) of each layer. The planes could represent stratigraphic boundaries, lithologic changes, and unconformities, but most important, they should represent boundaries between layers having different shear wave velocities. Shear wave velocity is the primary property used for defining uniformity of a site.

The distribution of bearing reactions under the basemat is a function of the subgrade modulus, which in turn is a function of the soil properties. The Combined License applicant shall demonstrate that the variation of subgrade modulus across the footprint is within the range considered for design of the nuclear island basemat. The farther that the non-uniform layer is located below the foundation, the less influence it has on the bearing pressures at the basemat. Lateral variability of the shear wave velocity at depths greater than 120 feet below grade (80 feet below the foundation) do not significantly affect the subgrade modulus.

Subsurface conditions should be evaluated by the Combined License applicant based on the geologic investigation in accordance with Regulatory Guide 1.132. Subsurface conditions should be evaluated within the nuclear island footprint and 40 feet beyond the boundaries of the nuclear island footprint at depths less than 120 feet below grade. Subsurface conditions may be considered uniform if the geologic and stratigraphic features can be correlated from one boring or sounding location to the next with relatively smooth variations in thicknesses or properties of the geologic units. An occasional anomaly or a limited number of unexpected lateral variations may occur. If a site can be classified as uniform, it qualifies for the AP1000 based on analyses and evaluations performed to support design certification without additional site-specific analyses.

As an example of sites that are considered uniform, the variation of soil properties in the material below the foundation to a depth of 120 feet below finished grade within the nuclear island footprint and 40 feet beyond the boundaries of the nuclear island footprint meets the criteria outlined below:

- The depth to a given layer indicated on each boring log may not fall precisely on the postulated “best-estimate” plane. The deviation of the observed layers from the “best-estimate” planes should not exceed 5 percent of the observed depths from the ground surface to the plane. If the deviation is greater than 5 percent, additional planes may be appropriate or additional borings may be required. This thereby diminishes the spacing.

- For a layer with a low strain shear wave velocity greater than or equal to 2500 feet per second, the layer should have approximately uniform thickness and should have a dip no greater than 20 degrees, and the shear wave velocity at any location within any layer should not vary from the average velocity within the layer by more than 20 percent.

Site-Specific Subsurface Uniformity Design Basis

Many sites that do not meet the above criteria for a uniform site are acceptable for the AP1000. The key attribute for acceptability of the site for an AP1000 is the bearing pressure on the underside of the basemat. A site having local soft or hard spots within a layer or layers does not meet the criteria for a uniform site. Non-uniform soil conditions may also require evaluation of the AP1000 seismic response as described in [Subsection 2.5.2](#).

As described in [Subsection 3.8.5](#), the nuclear island foundation is designed specifically for bearing pressures of 120 percent of those of the uniform soil properties case. Evaluation criteria are defined to evaluate sites that do not satisfy the site parameters directly. The design basis provided below is included to provide a clear specification of the design commitment and evaluation criteria required to demonstrate that a site-specific application satisfies AP1000 requirements. Application of the AP1000 to sites using this site-specific evaluation is not approved as part of the AP1000 design certification and the evaluation should be provided and reviewed as part of the Combined License application.

Rigid Basemat Evaluation

A site with nonuniform soil properties may be demonstrated to be acceptable by evaluation of the bearing pressures on the underside of a rigid rectangular basemat equivalent to the nuclear island. The soils identified in the site investigation may be included in a finite element model of the soil to analyze the effect of the lateral variability. When the variability identified at the site can be modeled in two dimensions (there is not significant variability in one horizontal direction), 2D analyses may be used. Where the variability occurs in both horizontal directions, a 3D analysis should be performed. Bearing pressures are calculated in a linear analysis for unit vertical load and overturning moments. For the site to be acceptable, the bearing pressures from this analysis need to be less than or equal to 120 percent of the bearing pressures calculated in similar analyses for a site having uniform soil properties.

Alternatively, the safe shutdown earthquake loads may be determined from a site-specific seismic analysis of the nuclear island using site-specific inputs as described in [Subsection 2.5.2](#). For the site to be acceptable, the bearing pressures from the site-specific analyses (with site-specific response and site-specific soil properties) need to be less than or equal to 120 percent of the bearing pressures calculated in similar rigid basemat analyses using the AP1000 design ground motion at a site having uniform soil properties.

Flexible Basemat Evaluation

For sites having bedrock close to the foundation level, the assumption of a rigid basemat may be overly conservative because local deformation of the basemat will reduce the effect of local soil variability. For such sites, a site-specific analysis may be performed using the AP1000 basemat model and methodology described in [Subsection 3.8.5](#). The soils may be represented by soil springs or by a finite element model of the soil depending on the type of variability identified at the site. The safe shutdown earthquake loads are those from the AP1000 design soil case representative of the site-specific soil. Alternatively, bearing pressures may be determined from a site-specific soil structure interaction analysis using site-specific inputs as described in [Subsection 2.5.2](#). For the site to be acceptable, the bearing pressures from the site-specific analyses, including static and dynamic loads, need to be less than the design bearing strength of each portion of the basemat.

2.5.4.2.1 Introduction

This section describes the static and dynamic engineering properties of the VEGP site subsurface materials. An overview of the subsurface profile and materials is given in [Subsection 2.5.4.2.2](#). The field investigations, described in [Subsection 2.5.4.3](#), are summarized in [Subsection 2.5.4.2.3](#). The descriptions of the subsurface materials provided in the following sections are based primarily on two recent field investigations, ESP and COL, and review of previous investigations. Within each section the ESP basis description is followed by the COL-basis description. The soils encountered during the ESP and COL subsurface investigations constitute alluvial and Coastal Plain deposits and can be placed in three groups for stability of subsurface materials and foundation purposes (i.e., for geotechnical purposes). These soils include, from top to bottom, sands with silt and clay (Group 1), clay marl (Group 2), and coarse-to-fine sand with interbedded thin seams of silt and/or clay (Group 3). The Upper Sand Stratum (Group 1 soils) will be completely removed and replaced with compacted structural fill prior to the construction of VEGP Units 3 and 4. The static and dynamic engineering properties of the three principal soil groups, along with the compacted structural fill, were determined by field investigation and laboratory testing. The laboratory tests and their results are summarized in [Subsection 2.5.4.2.4](#). The engineering properties of the subsurface materials are presented in [Subsection 2.5.4.2.5](#).

2.5.4.2.2 Description of Subsurface Materials

The site soils and bedrock are divided into five strata (Upper Sand Stratum, Marl Bearing Stratum, Lower Sand Stratum, Dunbarton Triassic Basin bedrock, and Paleozoic Crystalline bedrock), which correspond to the three soil groups mentioned in [Subsection 2.5.4.2.1](#) plus the two bedrock units:

- I. Upper Sand Stratum (Barnwell Group) – predominantly sands, silty sands, and clayey sands with occasional clay seams, soft zones, and shell zones. A shelly limestone (Utley Limestone) layer was encountered at the base of the Upper Sand Stratum or the top of the Blue Bluff Marl. The limestone contains shell zones, solution channels, cracks, and discontinuities. Severe fluid loss was observed in this layer during drilling for the ESP and COL subsurface investigations.
- II. Marl Bearing Stratum (Blue Bluff Marl or Lisbon Formation) - slightly sandy, cemented, overconsolidated, calcareous silt and clay with some shells and partially cemented, well indurated layers.
- III. Lower Sand Stratum (comprises several formations from the Still Branch just beneath the Blue Bluff Marl to the Cape Fear just above the Dunbarton Triassic Basin rock) – fine-to-coarse sand with interbedded silty clay and clayey silt.
- IV. Dunbarton Triassic Basin Rock – red sandstone, breccia, and mudstone, weathered through the upper 120 ft.
- V. Paleozoic Crystalline Rock – a competent rock with high shear wave velocities that underlies the non-capable Pen Branch Fault, which underlies the site.

These strata have been previously used as a means for classifying the soils and rock with regard to engineering properties, and are also used in this ESP SSAR.

The following sections provide brief descriptions of the subsurface materials, giving the soil and rock constituents, and their range of thickness encountered at the site. The information has been taken from the 14 borings and 10 cone penetrometer tests (CPT) performed during the ESP subsurface investigation. The locations of the ESP borings and CPTs are shown on [Figure 2.5-366](#). Reference is made, as appropriate, to borings performed for VEGP Units 1 and 2. For reference, the VEGP site

elevations in the areas explored range from about El. 219 to 256 ft msl, with a median of about El. 222 ft msl. It is noted that most of the VEGP ESP site is flat at about El. 220 ft msl with surrounding areas at higher elevations of about 250 ft msl. A finished plant grade of El. 220 ft msl is used for the new unit ESP analysis. The engineering properties are provided in [Subsection 2.5.4.2.5](#). [Figures 2.5-370, 2.5-372, and 2.5-373](#) provide illustrations of the subsurface conditions across the VEGP site observed in the ESP borings. A profile legend is provided as [Figure 2.5-369](#).

Information produced from 70 borings and 8 CPTs, located in the immediate area of the nuclear islands, from the COL subsurface investigation has also been used to develop the following descriptions of the subsurface materials. The locations of the explorations performed for the COL investigation are shown on [Figures 2.5-367 and 2.5-368](#). [Figures 2.5-371, 2.5-374, and 2.5-375](#) provide illustrations of the subsurface conditions across the Nuclear Islands (NIs) for Units 3 and 4, observed in the COL borings.

2.5.4.2.2.1 Upper Sand Stratum (Barnwell Group)

The ESP subsurface investigation ([Appendix 2.5A](#)) determined that the Upper Sand Stratum ranged in thickness from 78 to 157 ft beneath the ground surface at the completed boring locations. The wide range of thickness was due to two factors. First, three borings (B-1004, B-1005, and B-1006) were drilled from elevations about 30 ft higher than the remaining borings. Second, the top of the Blue Bluff Marl dips down toward the west and northwest portions of the VEGP site. The average thickness of the Upper Sand Stratum was 102 ft, and the median thickness was 94 ft at the ESP boring locations.

Field Standard Penetration Test (SPT) N-values obtained according to ASTM D 1586 ([Reference 568](#)) within the Upper Sand Stratum during the ESP subsurface investigation ranged from weight of rod (WOR) to 50 blows for 0-in. penetration (50/0"). The very high blow count values are indicative of zones containing the shelly limestone and shell hash. The average field SPT N-value was 25 blows per foot (bpf), and the median N-value was 21 bpf. These field values are uncorrected for hammer efficiency of the respective drill rig hammers used. Measurements of hammer energy were performed in borings B-1006 and B-1013. The measured energy transfer efficiency ranged from 65 to 87 percent, with an average value of 76 percent and a median value of 75 percent.

Selected samples recovered within the Upper Sand Stratum were submitted for laboratory testing, including percent fines, moisture content, and Atterberg Limits. The percent fines ranged from 3 to 60 percent, with an average value of 21 percent and a median value of 19 percent. The Plastic Limit ranged from 19 to 30, with an average value of 25 and a median value of 26. The Liquid Limit ranged from 43 to 97, with an average value of 62 and a median value of 53. The Plasticity Index ranged from 21 to 67, with an average value of 37 and a median value of 29. The natural moisture content of samples tested for Atterberg Limits ranged from 20 to 93 percent, with an average value of 63 percent and a median value of 70 percent.

Site geotechnical investigations for the existing units determined that the Upper Sand Stratum (Barnwell Group) is approximately 90 ft thick. A shelly limestone (Utley Limestone) is encountered at the base of this stratum and/or the top of the Blue Bluff Marl. The Upper Sand Stratum was determined to be susceptible to liquefaction during a seismic event equivalent to the safe shutdown earthquake (SSE) developed for VEGP Units 1 and 2. In addition, the underlying Utley limestone layer was determined to contain significant channeling, cracking, and other discontinuities. Therefore, it was considered necessary to remove both the Upper Sand Stratum and limestone layers before constructing VEGP Units 1 and 2. The standard penetration test data from previous studies indicate that the relative density of the Upper Sand Stratum is highly variable with a range from very loose to dense. Clay lenses encountered within the stratum ranged in consistency from soft to medium stiff.

Existing Units 1 and 2 unconsolidated undrained (UU) triaxial test results of samples within the Upper Sand Stratum indicate that the Mohr strength envelope of total stresses ranges from $c=2,100$ pounds per square foot (psf), $\phi=6^\circ$ to $c=440$ psf, $\phi=32^\circ$, depending on the clay and sand content within the sample. Likewise, previous consolidated undrained (CU) triaxial test results for samples within the Upper Sand Stratum indicate that the Mohr strength envelope ranges from $c=1,650$ psf, $\phi=17^\circ$ to $c=4,000$ psf, $\phi=25^\circ$ for total stress and $\phi'=33^\circ$ to $\phi'=34.5^\circ$ for effective stresses. Because of the large number of UU and CU triaxial tests previously performed on Upper Sand Stratum samples, and the fact that this stratum would be completely removed before constructing the ESP units, no new strength tests were performed during the ESP subsurface investigation.

The COL subsurface investigation, [Appendix 2.5C](#), with 70 borings located in the immediate area of the excavations for Units 3 and 4, was used to verify the characterization of the Upper Sand Stratum. From these data, the Upper Sand Stratum ranged in thickness from 81 to 97 feet with an average of 88 feet and a median thickness of 87 feet. One thousand four hundred and fourteen field SPT N-values were measured and ranged from WOR to 50/0" with a median of 18 bpf. Measurements of hammer energy were performed on each of the 12 drill rigs used for the COL investigation as presented in [Appendix 2.5C](#). One hundred and sixty-eight sieve analyses disclosed a range of 5 percent to 96 percent fines with an average value of 22 percent and a median value of 20 percent. Seventeen Atterberg Limits test results on samples from the clay lenses disclosed an average liquid limit of 72, an average plastic limit of 33, and an average calculated plasticity index of 39. The moist unit weight of 15 samples was calculated and ranged from 94 pcf to 124 pcf with an average of 113 pcf and a median value of 113 pcf. The specific gravity of two samples was calculated as 2.69 and 2.75. Results of CU triaxial tests indicate average shear strength values of $c=980$ psf, $\phi=18^\circ$ for total stress and $c'=260$ psf, $\phi=30^\circ$ for effective stress.

The design properties of the Upper Sand Stratum are provided in [Table 2.5-236](#) and were developed from laboratory and field test results from the ESP and COL investigations as previously described, and published engineering correlations.

2.5.4.2.2.2 Blue Bluff Marl (Lisbon Formation)

The ESP subsurface investigation ([Appendix 2.5A](#)) determined that the Blue Bluff Marl was found to range in thickness from 63 to 95 ft at three locations where the stratum was fully penetrated, with an average thickness of 76 ft and a median thickness of 69 ft. The typical thickness of the Blue Bluff Marl is illustrated on the subsurface profiles on [Figures 2.5-370, 2.5-372, and 2.5-373](#). The profiles on [Figures 2.5-370 and 2.5-372](#) also illustrate the downward dip of the top of the Blue Bluff Marl toward the west side of the VEGP site.

The data and laboratory test results from penetrations taken in the immediate area of the excavations for Units 3 and 4 for the COL subsurface investigation ([Appendix 2.5C](#)) were found to validate the ESP characterization of the Blue Bluff Marl except as noted in the following paragraphs. In the area of the excavations, the Blue Bluff Marl was penetrated at 42 of the 70 boring locations. The top of stratum elevation ranged from 122 ft to 140 ft with an average elevation of 132 ft. The thickness of the Blue Bluff Marl ranged from 60 ft to 77 ft with an average thickness of 67 ft and a median thickness of 68 ft. The representative thickness of the Blue Bluff Marl as determined by the COL borings is illustrated on the subsurface profile in [Figure 2.5-371](#).

Field SPT N-values obtained within the Blue Bluff Marl during the ESP subsurface investigation ranged from 26 bpf to 50 blows for 1-in. penetration (50/1"). The average field SPT N-value was 83 bpf, and the median N-value was 100+ bpf. As noted in the revised MACTEC ESP Data Report ([Appendix 2.5A](#)) fossiliferous limestone, cemented layers, and cemented nodules were encountered in the Blue Bluff Marl. The high blow counts are attributed to the presence of these cemented layers as evidenced by the angular, gravel-sized, carbonate particles recovered in the split barrel samples. SPT blow counts corresponding to less than 12 in. of sampler penetration were linearly extrapolated

to the 12 in. standard penetration. SPT blow counts that were linearly extrapolated to more than 100 bpf were truncated at 100 bpf when calculating SPT averages. The field values are uncorrected for hammer efficiency of the respective drill rig hammers used. It is noted that the 26 bpf value was measured near the bottom of the stratum in boring B-1002, and most measured values were above 50 bpf. Also, the SPT N-values did not suggest the presence of a likely weathered portion at the top of the stratum.

During the COL investigation, 742 SPT samples were taken in the Blue Bluff Marl. Field SPT N-values ranged from 13 bpf to 50/0" with a median value of 71 bpf. The field values are uncorrected for hammer efficiency of the respective drill rig hammers used. Many SPTs did not achieve the full sampler penetration (e.g., 50 blows/3"). These high blow counts were attributed to the presence of abundant, partially cemented, well indurated layers as described in the MACTEC COL Data Report ([Appendix 2.5C](#)). Most of the measured N-values were greater than 30 bpf indicating hard to very hard consistencies. In addition, SPT N-values appear to behave as expected, increasing with depth. None of the 742 measured SPT N-values was less than 10 bpf, which is twice as much as one of the criterion used to identify soft zones at the nearby Savannah River Site (SRS) site ($N < 5 \text{ bpf}$). A review of the borings logs did not reveal any layers below the Upper Sand stratum similar to the soft zones found at SRS. A summary of the SPT blow counts, corrected for hammer efficiency, collected from the borings within the power block is presented in [Figure 2.5-391](#).

Selected samples recovered within the Blue Bluff Marl during the ESP subsurface investigation were submitted for laboratory testing, including percent fines, moisture content, and Atterberg Limits. The percent fines ranged from 17.8 to 97.8 percent, with an average value of 48 percent and a median value of 41 percent. The plastic limit ranged from non-plastic (NP) to 51 percent, with an average value of 29 percent and a median value of 27 percent. The liquid limit ranged from NP to 99 percent, with an average value of 51 percent and a median value of 43 percent. The plasticity index ranged from NP to 58 percent, with an average value of 22 percent and a median value of 16 percent. The natural moisture content of samples tested for Atterberg Limits ranged from 14 to 67 percent, with an average value of 35 percent and a median value of 29 percent. In addition, 15 UU tests were performed on Blue Bluff Marl samples. The laboratory measured undrained shear strength ranged from 150 to 4,300 psf. The low end of measured values (150 psf) is lower than previously reported (260 psf) for VEGP Units 1 and 2, and the high end of measured values (4,300 psf) is significantly lower than previously reported (500,000 psf) for VEGP Units 1 and 2. The SPT N-values measured during the ESP and values previously measured in the laboratory for VEGP Units 1 and 2 support the use of a 10,000-psf design value. The reason for the sharp disagreement between the ESP laboratory values and previously reported undrained shear strength for the Blue Bluff Marl is severe sample disturbance due to sampling technique (pitcher sampler) and preparation of testing specimen. The SPT N-values measured during the ESP and values previously measured in the laboratory for VEGP Units 1 and 2 support the use of a 10,000-psf design value.

Selected samples of the Blue Bluff Marl collected during the COL investigation subsurface investigation were submitted for laboratory testing and included percent fines, moisture content, and Atterberg Limits. Sieve analyses tests were conducted on 90 representative samples that disclosed a range of fines from 29 percent to 98 percent, with an average value of 74 percent and a median value of 75 percent. Atterberg Limit tests were conducted on 92 representative samples and disclosed a liquid limit range from 34 to 112 percent, with an average value of 67 percent and a median value of 63 percent. The plastic limit ranged from 20 to 64 percent, with an average value of 34 percent and a median value of 33 percent. The calculated plasticity index ranged from 11 to 62 percent, with an average value of 33 percent and a median value of 30 percent. The natural moisture content of samples tested ranged from 14 to 62 percent, with an average value of 33 percent and a median value of 32 percent. The moist unit weight of 69 samples ranged from 95 pcf to 133 pcf with an average of 115 pcf and a median value of 115 pcf. The specific gravity of 8 samples was calculated and ranged from 2.61 to 2.66 with an average value of 2.64.

Site investigations for the existing units determined that the marl stratum (Blue Bluff Marl or Lisbon Formation) consists of hard, slightly sandy, cemented, overconsolidated, calcareous clay and ranges in thickness from approximately 60 ft to 100 ft. The comparative consistency of the Blue Bluff Marl ranges from hard to very hard. The materials are moderately brittle and resemble a calcareous claystone or siltstone. Previous seismic exploration within this stratum indicates a velocity interface approximately 15 ft beneath the top of the stratum. The upper 15 ft, a likely weathered portion, of the stratum recorded a compressive wave velocity of approximately 5,000 ft per second (fps), while the underlying material recorded a compressive wave velocity of approximately 7,000 fps. The static engineering properties of the Blue Bluff Marl stratum are summarized in [Table 2.5-236](#).

Previous laboratory results indicate the Blue Bluff Marl to be highly overconsolidated. Plasticity index values ranged from 2 to 70 with an average value of 25. Based on work by Skempton (1957), using the average PI value yields an s_u/p ratio of approximately 0.2, where s_u is undrained shear strength and p is the effective overburden pressure for a normally consolidated clay. An undrained shear strength of 16,000 psf was determined using the average value of shear strength test results which failed at less than 50,000 psf. However, given a shear strength (s_u) one can use the same relationship and compute p (in the case of an overconsolidated deposit, p would be equivalent to the preconsolidation pressure). Therefore, using the 16,000 psf value for undrained shear strength and a s_u/p ratio of 0.2, the preconsolidation pressure of the Blue Bluff Marl stratum was estimated to be 80,000 psf (an OCR of about 8). Settlements due to loadings from new structures would be small due to this high preconsolidation pressure, demonstrated by the settlement measurement for Units 1 and 2 as discuss in [Subsection 2.5.4.10.2](#).

The undrained shear strength of the Blue Bluff Marl was verified during the excavation for VEGP Units 1 and 2. Core samples of the Blue Bluff Marl were obtained and tested. The design value of $c = 10,000$ psf, $\phi = 0^\circ$ was found to be appropriately conservative. The average undrained shear strength of the core samples was 20,000 psf, and the lowest value obtained was 11,700 psf.

The heave of the Blue Bluff Marl stratum was monitored during the excavation for VEGP Units 1 and 2. Measurements were taken at nine locations at regular intervals. After excavation completion, an average heave of 1.25 in. was observed. Based on the heave measurements, the undrained Young's modulus, E , of the Blue Bluff Marl stratum was calculated to be 10,000 kips/ft², similar to values of E estimated from Menard pressuremeter and seismic velocity measurements during previous field investigations.

Strength tests were conducted in the laboratory during the COL investigation ([Appendix 2.5C](#)) on relatively undisturbed (intact) samples of the Blue Bluff Marl. Strength testing included 27 unconfined compression tests, 11 UU triaxial tests, and 27 CU triaxial tests. Eighteen consolidation tests were conducted. The UU and CU triaxial tests were conducted at various confining pressures. Test results disclosed that the shear strength of the BBM increased with increasing confining pressure, as expected. The Blue Bluff Marl is approximately located from a depth of 90 to 165 ft with a design ground water level at a depth of 55 feet. Based on this overburden condition, the range of confining pressures in the Blue Bluff Marl is between 6.5 ksf and 9.7 ksf. UU test results at a confining pressure of 8.1 ksf disclosed a minimum undrained shear strength of 1.7 ksf and a maximum of 11.7 ksf with an average value of 6.5 ksf. The CU test results disclosed a minimum undrained shear strength of 2.8 ksf and a maximum value of 32.2 ksf with an average value of 9.3 ksf in this range of confining pressure. Given that the Blue Blue Marl is characterized as an overconsolidated, calcareous clay, the undrained shear strength can be represented by considering the preconsolidation pressure. At a confining pressure of 16 ksf (the upper limit of the UU and CU test program) which represents approximately twice the in-situ confining pressure, UU test results disclosed an average undrained shear strength of 8.6 ksf and CU test results disclosed an average value of 14.9 ksf. The averaged undrained shear strength from the UU and CU tests is 11.8 ksf, which supports the design value of 10,000 psf used for VEGP Units 1 and 2.

Consolidation tests were conducted in the laboratory during the COL investigation (Appendix 2.5C) on 18 relatively undisturbed samples of the Blue Bluff Marl. The compression and recompression ratios were determined from the compression and recompression indices provided in the test results. Compression ratios ranged from 0.034 to 0.156 with an average value of 0.094. Recompression ratios ranged from 0.004 to 0.017 with an average of 0.010.

The static design properties of the Blue Bluff Marl stratum for VEGP Units 3 and 4 are provided in Table 2.5-236 and were developed from laboratory and field test results from ESP and COL subsurface investigations, available data from VEGP Units 1 and 2, as well as published engineering correlations.

A summary of the design dynamic shear modulus at strain levels of 10^{-4} percent, or lower, for the Blue Bluff Marl stratum, based on ESP investigation, is given in Table 2.5-238. Dynamic shear modulus values were computed from the in situ shear wave velocity measurements shown in Table 2.5-243. Additional in situ shear wave velocity measurements were taken during the COL investigation. These data, combined with ESP data as described in Subsection 2.5.4.7.1, are shown in Table 2.5-253.

2.5.4.2.2.3 Lower Sand Stratum

The ESP subsurface investigation (Appendix 2.5A) determined that the Lower Sand Stratum encompassed a number of geologic formations, including, listed in top to bottom order, the Still Branch, Congaree, Snapp, Black Mingo, Steel Creek, Gaillard/Black Creek, Pio Nono/Unnamed, and Cape Fear formations. The Lower Sand Stratum was fully penetrated at boring B-1003 and found to have a thickness of 900 ft at this location. Boring B-1003 also disclosed that the Lower Sand Stratum rests upon Dunbarton Triassic Basin rock. Typical depths are illustrated on the subsurface profile in Figure 2.5-372.

Field SPT N-values obtained to depths of about 300 ft within the Lower Sand Stratum during the ESP subsurface investigation ranged from 9 bpf to 50 blows for 4-in. penetration (50/4"). The average field SPT N-value was 59 bpf, and the median N-value was 47 bpf. These field values are uncorrected for hammer efficiency of the respective drill rig hammers used and comprise values measured mostly in the Still Branch Formation directly beneath the Blue Bluff Marl.

During the COL investigation, the Lower Sand Stratum was encountered in 42 of the COL borings with 36 nominal penetrations (one to 7 feet) and 6 substantial penetrations (84 to 263 feet) into this stratum. The maximum depth of penetration into the stratum was 263 ft in B-3001. One hundred and eleven field SPT N-values obtained in this stratum ranged from weight of hammer (WOH) to 50/1". The median field SPT N-value was 70 bpf. These field values are uncorrected for hammer efficiency of the respective drill rig hammers used and comprise values measured mostly in the Still Branch Formation directly beneath the Blue Bluff Marl. Nearly all of the N-values taken in the Lower Sand stratum are greater than 30 bpf indicating dense to very dense material. In addition, SPT N-values appear to behave as expected, increasing with depth. One N-value (B-4001, SS-38: WOH/18) taken in this stratum indicated very loose material. This sample was taken in the Still Branch Formation of the Lower Sand strata at an elevation of -41.5 to -43 feet. No recovery was obtained in the split barrel sample. An undisturbed sample (UD-11) was attempted prior to SS-38 from elevation -39.5 to -41.5 feet and no recovery was obtained in this sample. The material above this elevation was identified as light gray SAND (SP). The difficulty in sampling this material along with the weight of hammer reading in SS-38 is considered an anomaly and can be attributed to disturbed soil conditions at the bottom of the borehole. These conditions are likely the result of a hydrostatic pressure imbalance between the borehole and the in situ hydrostatic pressure. The resulting imbalance likely caused a quick condition to develop in the poorly graded sands at the sampling depth. Such quick conditions are difficult to sample, as evidenced by the lack of sample recovery in SS-38 and UD-11, as the now

disturbed poorly graded sand will flow out of the sampler. Besides this anomalous condition, no other evidence of soft zones or loose material was encountered in Lower Sand stratum.

ESP subsurface investigation selected samples recovered within the Lower Sand Stratum were submitted for laboratory testing, including percent fines, moisture content, and Atterberg Limits. The percent fines ranged from 3 to 80 percent, with an average value of 23.6 percent and a median value of 15 percent. The plastic limit ranged from NP to 38 percent, with average and median values of 30 percent. The liquid limit ranged from NP to 53 percent, with average and median values of 47 percent. The plasticity index ranged from NP to 19 percent, with average and median values of 17 percent. The natural moisture content for samples tested for Atterberg Limits ranged from 21 to 41 percent, with an average value of 30 percent and a median value of 28 percent. Samples with the higher percent fines and plasticity were from the silty clay and clayey silt layers in the Congaree and Snapp Formations within the Lower Sand Stratum.

Representative samples of the Lower Sand Stratum collected during the COL subsurface investigation were submitted for laboratory testing. Sieve analyses were conducted on 14 samples with a range from 5 to 70 percent fines, an average value of 23 percent, and a median value of 17 percent. The moist unit weight of 16 samples was calculated ranged from 113 pcf to 136 pcf with an average of 123 pcf and a median value of 122 pcf. The average specific gravity of four samples was calculated as 2.67. Results of CU triaxial tests indicate average shear strength values of $c=4,725$ psf, $\phi=26^\circ$ for total stress and $c'=215$ psf, $\phi'=36^\circ$ for effective stress.

During the COL investigation, alternating layers of fine-grained and coarse-grained soils were identified in the upper and lower portions of the Congaree Formation and in the upper portion of the Snapp Formation. These fine-grained soils were characterized as silts and clays and, where encountered, were on the order of 20 to 40 feet thick. The coarse-grained soils were characterized as silty to clayey, and poorly-graded sands. In boring B-3001, the fine-grained materials in the lower portion of the Congaree and the upper portion of the Snapp were on the order of 70 feet thick.

Site geotechnical investigations for the existing units determined that the Lower Sand Stratum consists of sands with interbedded silty clay or clayey silt. The thickness of this stratum was estimated to be 900 to 1,000 ft. SPT N-values obtained to depths of about 300 to 400 ft below grade during previous field investigations within the Lower Sand Stratum ranged from 70 to 100 bpf, indicative of a very dense material.

The static design properties of the Lower Sand Stratum for VEGP Units 3 and 4 are provided in [Table 2.5-236](#) and were developed from laboratory and field test results from ESP subsurface investigations, available data from VEGP Units 1 and 2, as well as published engineering correlations.

A summary of the design dynamic shear modulus at strain levels of 10^{-4} percent, or lower, for the Lower Sand Stratum, based on the ESP investigation, is given in [Table 2.5-238](#). Dynamic shear modulus values were computed from the in situ shear wave velocity measurements shown in [Table 2.5-243](#). Additional in situ shear wave velocity measurements were taken during the COL investigation. These data, combined with ESP data as described in [Subsection 2.5.4.7.1](#), are shown in [Table 2.5-228](#).

2.5.4.2.2.4 Dunbarton Triassic Basin Rock

The Dunbarton Triassic Basin Rock was cored at ESP borehole B-1003 only, and consisted of red sandstone, breccia, and mudstone, weathered through the upper 120 ft. The deepest COL borehole was advanced to a depth of 263 ft into the Lower Sand Stratum for a total depth of 420 ft and did not reach bedrock. Further details are provided in [Subsection 2.5.1](#). Because the rock

was too deep to be of any interest to foundation design, no laboratory tests were performed on the rock cores. Shear wave velocity was measured in the upper 274 ft of the rock profile, and these results were used to develop the shear wave velocity profile for site amplification that are presented in [Subsection 2.5.4.7.1](#).

2.5.4.2.2.5 Paleozoic Crystalline Rock

As indicated in [Figure 2.5-372](#), the VEGP site sits on over 1,000 feet of Coastal Plain sediments underlain by Triassic Basin sedimentary rock. Borehole B-1003 encountered the bottom of the Coastal Plain sediments and the start of a weathered section of the Triassic Basin at a depth of 1,049 feet. Under the part of Savannah River Site adjacent to the VEGP site, the southeast dipping Pen Branch fault separates the Triassic Basin rock from Paleozoic crystalline rock to the northwest ([Lee et al. 1997](#)). A seismic reflection survey in and around the VEGP site (shown in [Appendix 2.5B](#) and discussed in [Subsection 2.5.1.2.4.2](#)), has been interpreted to show the southwest continuation of the Pen Branch fault beneath the site and to indicate that the depth to the bottom of the Coastal Plain sediments is about 1,000 feet ([Figure 2.5-243](#)). This and interpretation of flexures within the older Coastal Plain sediments suggest that the Pen Branch fault lies below the area of the new containment units. Therefore, the information available implies that at some depth below the VEGP site the Paleozoic crystalline rock underlies the Triassic Basin rock.

2.5.4.2.2.6 Subsurface Profiles

[Figures 2.5-370](#), [2.5-372](#), and [2.5-373](#) illustrate typical subsurface profiles across the power block area proposed for the proposed VEGP Units 3 and 4 based on ESP borings. A profile legend is provided as [Figure 2.5-369](#). The locations of the borings used to develop profiles are shown in [Figure 2.5-366](#). [Figures 2.5-371](#), [2.5-374](#), and [2.5-375](#) illustrate typical subsurface profiles across the limited power block area proposed for VEGP Units 3 and 4 based on COL borings. The locations of the borings used to develop profiles are shown in [Figure 2.5-368](#). These profiles are discussed in [Subsection 2.5.4.5](#) with respect to excavation for the new units and in [Subsection 2.5.4.10.1](#) for bearing capacity considerations.

2.5.4.2.3 Field Investigations

The exploration programs performed previously for VEGP Units 1 and 2 are referenced, as warranted. The ESP and COL subsurface investigations are described in [Subsection 2.5.4.3](#). The boring logs from previous explorations are not included here; however, the locations of referenced borings from VEGP Units 1 and 2 are provided on [Figure 2.5-368](#). The borings and cone penetrometer tests from the ESP subsurface investigation program are summarized in [Table 2.5-244](#). Previous geophysical surveys and new geophysical surveys for the ESP investigation are described in [Subsection 2.5.4.4](#). Boring logs and CPT logs from the ESP field exploration are included in [Appendix 2.5A](#).

The exploration program for the COL subsurface investigation included borings, CPTs, seismic CPTs, geophysical surveys, and test pits. The boring, CPT, and test pit locations are summarized in [Table 2.5-245](#) and illustrated on [Figures 2.5-367](#) and [2.5-368](#). Geophysical surveys for the COL investigation are described in [Subsection 2.5.4.4](#). Boring logs, CPT logs, geophysical survey results, and test pit logs from the COL field exploration are included in [Appendix 2.5C](#).

Field investigations also included the construction and testing of a 20-foot thick below grade test pad using proposed borrow materials. This program was conducted to aid in evaluating the static and dynamic properties of the compacted backfill. Additional details of the program are provided in [Subsection 2.5.4.5.3](#). Results of this program are included in [Appendix 2.5D](#).

2.5.4.2.4 Laboratory Testing

2.5.4.2.4.1 Testing Overview

Numerous laboratory tests of soil samples were performed previously for VEGP Units 1 and 2, and new tests have been performed as part of the ESP and COL subsurface investigations. Previous test results are contained within Bechtel Power Corporation's Report on Foundation Investigations (Reference 552). The types and numbers of tests completed during the ESP subsurface investigation are shown in Table 2.5-239, and the test results are contained within the MACTEC report for the ESP subsurface investigation (Appendix 2.5A). A summary of all laboratory test results performed as part of the ESP subsurface investigation is provided in Table 2.5-241. The types and numbers of tests completed during the COL subsurface investigation are shown in Table 2.5-240 and the test results are contained within the MACTEC data report for the COL subsurface investigation (Appendix 2.5C). Results of resonant column torsional shear (RCTS) tests conducted on samples from the COL investigation are included in Attachment G of Appendix 2.5C. Laboratory tests, including RCTS, were also conducted as part of the Phase I test pad program and are included in Appendix 2.5D.

2.5.4.2.4.2 Laboratory Tests for the ESP Subsurface Investigation

Laboratory testing for the ESP investigation was performed in accordance with the guidance presented in Regulatory Guide 1.138, Laboratory Investigations of Soils for Engineering Analysis and Design of Nuclear Power Plants, US Nuclear Regulatory Commission, 2003 (RG 1.138). The laboratory work was performed under an approved quality program with work procedures developed specifically for the ESP application. Soil samples were shipped under Chain-of-Custody protection from the on-site storage area (described in Subsection 2.5.4.3.2) to the testing laboratory. Laboratory testing was performed at the MACTEC laboratories in Atlanta, Georgia.

The types and numbers of laboratory tests performed on the soil samples from the ESP exploration program are included on Table 2.5-239. The ESP tests focused primarily on verifying the basic properties of the Upper Sand Stratum, Blue Bluff Marl, and the upper formations in the Lower Sand Stratum.

The details and results of the laboratory testing are included in Appendix 2.5A. This appendix includes references to the industry standard used for each specific laboratory test. The results of the tests on soil samples are shown on Table 2.5-241.

2.5.4.2.4.3 Laboratory Tests for the COL Subsurface Investigation

Laboratory testing for the COL investigation was performed in accordance with the guidance presented in RG 1.138. The laboratory work was performed under an approved quality assurance program with work procedures developed specifically for the COL application. Soil samples were shipped using Chain-of-Custody tracking procedures from the on-site storage area (described in Subsection 2.5.4.3.3) to the testing laboratory. Laboratory tests were performed at various laboratories. RCTS tests were performed at the FUGRO laboratories in Houston, Texas. The details and results of the laboratory testing are included in Appendix 2.5C. This appendix includes references to the industry standard used for each specific laboratory test.

2.5.4.2.4.4 Laboratory Test for the Phase I Test Pad Program

Laboratory testing was conducted during construction of the test pad under an approved quality assurance program with work procedures developed specifically for the test pad program. An onsite laboratory was established to conduct most of the testing. Soil samples that were shipped to offsite laboratories were done so using Chain-of-Custody procedures. RCTS testing was

conducted offsite at laboratories in Houston, Texas and Austin, Texas. Details and results of the laboratory testing are included in [Appendix 2.5D](#).

2.5.4.2.5 Engineering Properties

The engineering properties for the Upper Sand, Blue Bluff Marl, Lower Sand Strata, and compacted structural fill, as provided in [Table 2.5-236](#), were derived from the ESP subsurface investigation and laboratory testing program and from previous VEGP site studies. A similar table, [Table 2.5-237](#), was derived from the COL investigation and Phase I test pad program. The COL data, used as the basis for these properties, was taken from the borings in the immediate vicinity of the combined NI (power block) excavation footprint. The engineering properties of the proposed borrow materials that were developed from the COL data are presented in [Subsection 2.5.4.5.3](#). The engineering properties for the structural backfill were derived from the COL investigation and the Phase I test pad program. The engineering properties developed from the ESP and COL subsurface investigation and laboratory testing programs and the Phase I test pad program ([Appendix 2.5A](#), [2.5C](#), and [2.5D](#), respectively) were similar to those obtained from the previous VEGP Units 1 and 2 field and laboratory testing programs.

Rock densities were derived from Tables 5-2 and 5-3 of ([Reference 548](#)) for crystalline and Triassic rock, respectively. Rock densities increased with depth from 2.75 gm/cc (171.6 pcf) to 3.42 gm/cc (213.4 pcf) in the crystalline rock, and from 2.53 gm/cc (157.9 pcf) to 3.42 gm/cc (213.4 pcf) in the Triassic rock.

The following sections briefly describe the sources and/or methods used to develop the selected properties shown in [Table 2.5-236](#) and [Table 2.5-237](#).

2.5.4.2.5.1 Rock Properties

The Recovery and Rock Quality Designations (RQD) are based on the results provided from the deep boring, B-1003. Rock coring was not performed during the previous investigations for VEGP Units 1 and 2. Geophysical testing at the deep boring, B-1003, extended for about 290 ft into the bedrock encountered at depth of 1,049 ft below the ground surface. The shear and compressional wave velocities are based on the suspension P-S velocity seismic test performed in borehole B-1003 as part of the ESP subsurface investigation ([Appendix 2.5A](#)). Laboratory strength testing of rock cores was not performed because the rock is deemed to be too deep to provide any additional useful engineering information.

2.5.4.2.5.2 Soil Properties

The properties of the soils underlying the site were developed from ESP and COL investigations, including laboratory testing programs, review of previous investigations for VEGP Units 1 and 2, and the Phase I test pad program. The following paragraphs describe the properties of the Upper Sand, Blue Bluff Marl, and Lower Sand Strata. The properties of the proposed compacted structural backfill are discussed in [Subsection 2.5.4.5.3](#).

Sieve analyses of 29 Upper Sand Stratum samples (including 1 fill sample), 28 Blue Bluff Marl samples, and 14 Lower Sand Stratum samples were performed as part of the ESP laboratory testing program ([Appendix 2.5A](#)).

The natural moisture content and Atterberg Limits of 4 Upper Sand Stratum, 20 Blue Bluff Marl, and 4 Lower Sand Stratum samples were determined as part of the ESP laboratory testing program. Design values shown on [Table 2.5-236](#) were taken as the average of these test results for the respective soil strata.

The COL laboratory testing program ([Appendix 2.5C](#)) included sieve analyses of 168 Upper Sand Stratum samples, 90 Blue Bluff Marl samples, and 14 Lower Sand Stratum samples. Atterberg Limits tests were conducted on 17 Upper Sand Stratum samples and 92 Blue Bluff Marl samples. Specific gravity measurements were made on two Upper Sand Stratum samples, 8 Blue Bluff Marl samples, and 4 Lower Sand Stratum samples.

The undrained shear strength of the Blue Bluff Marl bearing stratum was determined from laboratory test data, SPT N-values, and shear wave velocity measurement. Laboratory test data included unconsolidated undrained triaxial test and consolidated undrained triaxial test results from the ESP and COL investigations. Laboratory strength testing during previous investigations as well as during the construction of VEGP Units 1 and 2 were also reviewed.

The effective angle of internal friction of the Upper Sand Stratum was determined to be 34 degrees ([Reference 583](#)) from correlation with the average SPT N-value from the ESP investigation (based on $N_{60} = 25$ bpf). The N-value of 25 bpf represents the measured value of 20 bpf corrected to account for the higher automatic hammer efficiency measured in the field. This correction was made following the guidelines in ASTM D 6066 (1996). The median measured N-value from the COL investigation was 18 bpf, corresponding to a N_{60} -value of 25 bpf.

The effective angle of internal friction of the Lower Sand Stratum was determined to be 41 degrees ([Reference 583](#)) from correlation with the average SPT N-value from the ESP investigation (based on $N_{60} = 62$ bpf). The N-value of 62 bpf represents the measured value of 50 bpf corrected to account for the higher automatic hammer efficiency measured in the field. This correction was made following the guidelines in ASTM D 6066 (1996). The median measured N-value from the COL investigation was 70 bpf, corresponding to a N_{60} -value of 94 bpf.

Moist unit weights were measured in selected samples from the ESP laboratory testing program of the Blue Bluff Marl and Lower Sand Stratum. The unit weights of 15 Blue Bluff Marl samples ranged from 102 pounds per cubic foot (pcf) to 140 pcf, with an average of 120 pcf. Unit weights of three Lower Sand Stratum samples were 119.4 pcf, 121.7 pcf, and 128.3 pcf, with an average of 123 pcf.

The COL laboratory testing program included moist unit weight measurements of 15 samples in the Upper Sand Stratum, 69 in the Blue Bluff Marl, and 16 in the Lower Sand Stratum. The values in the Upper Sand Stratum ranged from 94 to 124 pcf with an average value of 113. The values in the Blue Bluff Marl ranged from 95 to 133 pcf with an average value of 115 pcf. The values in the Lower Sand Stratum ranged from 113 to 134 pcf with an average of 123 pcf.

The in situ moist unit weights of the Upper Sand Stratum, Blue Bluff Marl, and Lower Sand Stratum for VEGP Units 1 and 2 were 118 pcf, 119 pcf, and 117 pcf, respectively.

The design SPT N-value for the Upper Sand Stratum is taken as 25 bpf. This value is based on the ESP results reported in [Table 2.5-242](#) and includes correction for hammer efficiency. The results in [Table 2.5-242](#) show an average uncorrected field SPT N-value of 25 bpf and median value of 21 bpf. The design corrected N-value of 25 bpf corresponds to a field N-value of 20 bpf, which is lower than the average and median values. The median uncorrected field SPT N-value for the Upper Sands from the COL investigation was 18 bpf. SPT N values for VEGP Units 1 and 2 ranged from 2 to 60 bpf with an average of 30 bpf. The design value is within the range and near the average of the COL investigation and previous investigation values.

The design SPT N-value for the Blue Bluff Marl is taken as 100 bpf. This value is based on the results reported in [Table 2.5-242](#) and includes correction for hammer efficiency. The results in [Table 2.5-242](#) show an average uncorrected field SPT N-value of 83 bpf and median value of 100 bpf. The design corrected N-value of 100 bpf corresponds to a field N value of 80 bpf, which is lower than the average

and median values. The median uncorrected field SPT N-value for the Blue Bluff Marl from the COL investigation was 71 bpf ($N_{60}=95$ bpf). SPT N-values for VEGP Units 1 and 2 ranged from 10 to over 100 bpf with an average of over 100 bpf. The design value is within the range and near the median of the COL investigation and previous site investigation values.

The design SPT N-value for the Lower Sand Stratum is taken as 62 bpf. This value is based on the results reported in [Table 2.5-242](#) and includes correction for hammer efficiency. The results in [Table 2.5-242](#) show an average uncorrected field SPT N-value of 59 bpf and median value of 47 bpf. The design corrected N-value of 62 bpf corresponds to a field N-value of 50 bpf, which is lower than the average value and slightly higher than the median value. The median uncorrected field SPT N-value for the Lower Sands from the COL investigation was 70 bpf ($N_{60}=94$ bpf). SPT N-values for VEGP Units 1 and 2 ranged from 70 to 100+ bpf with an average of 100+ bpf. The design value is somewhat less than the previous site investigations range of values.

Shear wave velocities were measured by suspension P-S velocity tests and seismic CPTs during the ESP and COL subsurface investigations ([Appendix 2.5A](#) and [Appendix 2.5C](#), respectively). The suspension P-S velocity tests were performed in 5 boreholes for the ESP investigation, although only three of these tests extended into the Blue Bluff Marl and Lower Sand Strata. P-S velocity tests were performed in 6 boreholes for the COL investigation. Three seismic CPTs were performed in accordance with ASTM D 5778 (2000) for the ESP investigation and 8 for the COL investigation. Due to penetration resistance, the seismic CPT tests did not extend into the very hard underlying Blue Bluff Marl stratum. Further discussion of suspension P-S velocity and seismic CPT testing is provided in [Subsection 2.5.4.4](#).

A complete shear wave velocity profile was developed during the ESP investigation from the ground surface to about 300 ft into the Dunbarton Triassic Basin rock for a total depth of about 1,340 ft using both suspension P-S velocity and seismic CPT testing taken during the ESP investigation. Shear wave velocities within the Upper Sand Stratum ranged from about 570 fps to 3,310 fps. Shear wave velocities ranged from 1,060 fps to 4,260 fps within the Blue Bluff Marl stratum, 930 fps to 4,670 fps within the underlying Lower Sand Stratum, and 2,320 fps to 9,350 fps within the Dunbarton Triassic Basin. Shear wave velocity measurements were made to depths of up to 290 ft during previous investigations for VEGP Units 1 and 2. In addition, shear wave velocity data were reviewed from seven deep borings performed at the neighboring Savannah River Site. Typical shear wave velocity values were determined for the Upper Sand Stratum, Blue Bluff Marl, Lower Sand Stratum, and the Dunbarton Triassic Basin rock data based upon review of all the available data and are provided in [Table 2.5-243](#). Shear wave velocity values within the Lower Sand Stratum were determined for each of the geologic formations contained within. A more detailed discussion of shear wave velocity values and establishment of the shear wave velocity profile for site amplification are presented in [Subsection 2.5.4.7.1](#).

Shear wave velocity measurements were made during the COL investigation to a maximum depth of 420 feet. Shear wave velocities within the Upper Sand Stratum disclosed an average shear wave velocity of 940 fps. An average shear wave velocity of 2,050 fps was disclosed in the Blue Bluff Marl stratum. The shear wave velocity measurements in the Lower Sand stratum disclosed an average shear wave velocity of 1,750 fps. A more detailed discussion of shear wave velocity values and establishment of the shear wave velocity profile for site amplification are presented in [Subsection 2.5.4.7.1](#).

The high strain (i.e., in the range of 0.25 to 0.5 percent) elastic modulus values, tabulated in [Table 2.5-236](#), for the Upper Sand Stratum and Lower Sand Stratum have been derived using the relationship with the SPT N-value given in ([Reference 584](#)) The high strain elastic modulus for the Blue Bluff Marl stratum has been derived using the relationship with undrained shear strength given in ([Reference 584](#)). The shear modulus values have been obtained from the elastic modulus values using the relationship between elastic modulus, shear modulus, and Poisson's ratio ([Reference 583](#)).

The low strain (i.e., 10^{-4} percent) shear modulus, tabulated in [Table 2.5-238](#), for the Upper Sand Stratum has been derived from the average shear wave velocity of 940 fps. The low strain shear modulus of the Blue Bluff Marl stratum has been derived from the average shear wave velocity of 2,050 fps. The low strain shear modulus of the Lower Sand Stratum has been derived from the average shear wave velocity of 1,750 fps. The elastic modulus values have been obtained from the shear modulus values using the relationship between elastic modulus, shear modulus, and Poisson's ratio ([Reference 583](#)). The low strain shear modulus for the compacted backfill has been derived assuming an average shear wave velocity of 1,000 fps.

The values of unit coefficient of subgrade reaction are based on values for medium dense sand (Upper Sand Stratum), replaced as compacted structural fill, very-stiff-to-hard clay (Blue Bluff Marl), and dense-to-very-dense sand (Lower Sand Stratum) provided by Terzaghi (1955).

The earth pressure coefficients are Rankine values, assuming level backfill and a zero friction angle between the soil and the wall.

2.5.4.2.5.3 Chemical Properties

Chemical tests were not included in the ESP laboratory testing program. There were no aggressive chemical subsurface conditions identified in the license renewal aging management analysis of Unit 1 and 2 buried concrete ([Reference 594](#)). Chemical property testing of proposed backfill material (Upper Sand Stratum, switchyard borrow and Borrow Area 4) was conducted as part of the COL investigation. Laboratory tests included pH, chloride, and sulfate and were conducted on five split barrel samples from Upper Sand Stratum in the powerblock area; two bulk soil samples taken from test pits excavated in the switchyard borrow area; and three from bulk soil samples from Borrow Area 4. Average pH test results disclosed values of 6.8, 5.2 and 5.4 for the Upper sand, switchyard and Borrow Area 4, respectively, indicating the soil to be mildly corrosive ([Reference 565](#), [Reference 597](#)). Corresponding average chloride test results disclosed values of 188, 76 and 138 ppm indicating the soil is mildly corrosive ([Reference 565](#), [Reference 597](#)). Corresponding average sulfate test results disclosed values of 21, 9.8 and 16.3 ppm indicating the soil/concrete interaction will provide a mild exposure for sulfate attack ([Reference 564](#)). Tests were performed by Severn Trent Laboratories, Inc., working as a subcontractor to MACTEC. Test results are included in [Appendix 2.5C](#).

2.5.4.3 Exploration

[Subsection 2.5.4.3.1](#) summarizes previous subsurface investigation programs performed at the VEGP site, while [Subsection 2.5.4.3.2](#) describes the ESP subsurface investigation program and [Subsection 2.5.4.3.3](#) describes the COL subsurface investigation program.

2.5.4.3.1 Previous Subsurface Investigation Programs

Field investigations for VEGP Units 1 and 2 were initiated in January 1971. Field investigations consisted of borings, geophysical methods, and groundwater studies. Additional investigation was completed during excavation for VEGP Units 1 and 2 to verify and obtain further details concerning subsurface conditions in the power block area. A total of 474 borings and 60,000 ft of drilling were completed during these investigations. An additional 111 borings were completed after the initial investigations mentioned above for the following purposes: 41 borings were drilled to define soil conditions and lateral extent of the Blue Bluff Marl in the river facilities, 38 borings were drilled in the power block to collect samples of the Blue Bluff Marl and perform confirmatory testing, and 32 borings were drilled to collect subsurface data for the natural draft cooling tower foundation design. During the previous investigations, electric logging, natural gamma, density, neutron, caliper, and 3-D velocity logs (Birdwell) were performed at selected borings. Water pressure tests and Menard

pressuremeter tests were completed to determine properties of the Blue Bluff Marl bearing stratum. Fossil, mineral, or soluble carbonate tests were performed on recovered samples as warranted.

Geophysical methods were applied to supplement the test borings. The geophysical methods are described in [Subsection 2.5.4.4](#). For the previous investigations, a total of 28,400 ft of shallow refraction lines, 5,000 ft of deep refraction lines, and cross-hole velocities of subsurface were performed extending from the ground surface to a depth of 290 ft.

Twenty of the previously drilled borings for VEGP Units 1 and 2 fall within, or in the immediate proximity of, the proposed combined power block excavation footprint for the VEGP Units 3 and 4 site. The locations of these borings are provided in [Figure 2.5-368](#). Results of previous investigations are referenced as needed to support the subsurface data obtained during the ESP and COL subsurface investigations.

2.5.4.3.2 ESP Subsurface Investigation Program

The ESP subsurface investigation was performed during September through December 2005 over a substantial portion of the site enveloping the area that would contain the new reactors as well as the switchyard and the cooling towers for the proposed VEGP Units 3 and 4. This investigation consisted of exploration points that were located primarily to confirm the results obtained from the previous extensive investigations. Portions of the original ESP data report were revised as discussed in [Subsection 2.5.4.3.2.4](#).

The ESP exploration point locations are shown in [Figure 2.5-366](#). The exploration points from the ESP investigation are combined with selected boring locations from the previous investigations in [Figure 2.5-366](#).

The scope of work and the special methods used by the subsurface investigation contractor (MACTEC) and its subcontractors to collect data are listed below:

- Thirteen exploratory borings were drilled by MACTEC. Two of these borings (B-1002A and C-1005A) were drilled without sampling to allow suspension P-S velocity testing to be performed above zones of drilling fluid loss encountered in the Upper Sand Stratum above the Blue Bluff Marl.
- The efficiency of the automatic hammers employed by the two rotary drill rigs was determined by SPT energy measurements. These services were provided by GRL Engineers, Inc., of Cleveland, Ohio, working as a subcontractor to MACTEC.
- One continuous soil and rock coring borehole was completed at B-1003 by MACTEC.
- Ten CPTs were performed, including three down-hole seismic CPTs. These services were provided by Applied Research Associates (ARA) of South Royalton, Vermont, working as a subcontractor to MACTEC.
- In-situ hydraulic conductivity testing was performed by MACTEC (Section 8 of ASTM D 4044 2002) in 15 groundwater observation wells. Southern Company Services installed these wells and the report is in [Appendix 2.4A](#).
- Geophysical down-hole suspension P-S velocity logging was performed in five completed boreholes (B-1002, B-1002A, B-1003, B-1004, and C-1005A). These services were provided by GEOVision Geophysical Services (GEOVision) of Corona, California, working as a

subcontractor to MACTEC. GEOVision also performed caliper, natural gamma, resistivity, and spontaneous potential measurements in boreholes B-1002, B-1003, and B-1004, and a borehole deviation survey at B-1003.

- A topographic survey of all exploration points was performed by MACTEC.
- Laboratory testing of selected borehole samples was performed by MACTEC in its Atlanta, Georgia, laboratories.

The exploration program was performed following the guidelines in Regulatory Guide 1.132, *Site Investigations for Foundations of Nuclear Power Plants*, US Nuclear Regulatory Commission, 2003 (RG 1.132). The fieldwork was performed under an audited and approved quality program and work procedures developed specifically for the ESP application. The subsurface investigation and sample/core collection were directed by the MACTEC site manager, who was on site at all times during the field operations. A Bechtel geotechnical engineer or geologist, along with an SNC representative, was also on site during these operations. MACTEC's QA/QC expert made periodic visits to the site and was on site to audit MACTEC's subcontractors. The draft boring and well logs were prepared in the field by MACTEC geologists.

An on-site storage facility for soil samples and rock cores was established before the fieldwork began. Each sample and core was logged into an inventory system. Samples removed from the facility were noted in the sample inventory logbook. A Chain-of-Custody form was also completed for all samples removed from the facility.

Complete details and results of the exploration program appear in [Appendix 2.5A](#). The borings, CPTs, field permeability testing, and geophysical surveys are summarized below. The laboratory tests are summarized and the results discussed in [Subsection 2.5.4.2](#). The geophysical tests are summarized and the results discussed in [Subsection 2.5.4.4](#).

Additionally, a seismic reflection and refraction survey was performed at the site in early 2006 to collect data to help delineate the rock profile associated with the non-capable Pen Branch fault. The results of the seismic reflection and refraction survey are presented in [Appendix 2.5B](#) and interpreted results are discussed in [Subsection 2.5.1.2.4.2](#).

2.5.4.3.2.1 Borings and Samples/Cores

Thirteen borings (excluding B-1003) were drilled to depths ranging from 90 ft (C-1005A) to 304 ft (B-1004). The borings were advanced in the soil using mud-rotary drilling techniques and polymer and/or bentonite drilling fluids. [Table 2.5-244](#) provides a summary of the ESP boring and CPT locations and depths, and identifies geophysical testing performed in the boreholes.

The soil was sampled using an SPT sampler at continuous intervals to a 15-ft depth and at 5- or 10-ft intervals below 15 ft. The SPT was performed with automatic hammers and was conducted in accordance with ASTM D 1586 (1999). The recovered soil samples were visually described and classified by the onsite geologist in accordance with ASTM D 2488 (2000). A selected portion of the soil sample was placed in a glass sample jar with a moisture-proof lid. The sample jars were labeled, placed in boxes, and transported to the on-site storage area. Additionally, undisturbed samples of the Blue Bluff Marl (Lisbon Formation) were obtained using rotary pitcher samplers. Disturbed materials were removed from the upper and the lower ends of the tube, and both ends were trimmed square to establish an effective seal. Pocket penetrometer tests were taken on the trimmed lower end of the samples. Both ends of the sample were then sealed with hot microcrystalline wax and protected with plastic caps. Tubes were labeled and transported to the on-site storage area. [Table 2.5-246](#) provides a summary of undisturbed samples of the Blue Bluff Marl collected during the ESP subsurface investigation.

The energy transfer efficiency of the automatic SPT hammers used by the drill rigs was obtained using a PAK model pile driving analyzer for both drill rigs. Testing was performed at borings B-1006 and B-1013 from depth ranges of 5 to 20 ft, 30 to 50 ft, and 75 to 100 ft. Resultant energy transfer efficiency measurements ranged from 65 to 87 percent. The average energy transfer efficiency was 75 percent. [Table 2.5-247](#) provides the SPT hammer energy transfer efficiency results.

The continuous core boring, B-1003, was performed with a Christensen 94 mm wire line system. A Speedstar Quickdrill 275 drill rig was used. Casing was installed through the soil column to prevent cave-ins and to allow coring of rock at depths below 1,049 ft. Rock coring was performed using a HW-size, double-tube core barrel in accordance with ASTM D 2113 (1999). The recovered soil and rock core samples were placed in wooden core boxes, lined with plastic sheeting. The onsite geologist visually described the core, noting the presence of joints and fractures, and distinguishing natural breaks from mechanical breaks. The geologist also computed the percentage recovery and the RQD. The average core recovery was 77 percent for the entire borehole depth ([Appendix 2.5A](#)). Filled core boxes were transported to the on-site sample storage facility, where a photograph of each core was taken.

The boring logs and the photographs of the rock cores appear in [Appendix 2.5A](#). The soil materials encountered in the ESP borings are similar to those found in the previous borings conducted at the VEGP site.

2.5.4.3.2.2 Cone Penetrometer Tests

The CPTs were advanced in accordance with ASTM D 5778 (2000) using a 30 ton self-contained truck rig. Each CPT was advanced to refusal at depths ranging from 6 to 116.7 ft. using a Type 2 piezocone (shouldered). Shallow refusal was encountered at locations C-1001 and C-1009, and offset CPT tests were performed at locations C-1001A and C-1009A. All remaining CPT locations met refusal at or near the top of the Blue Bluff Marl bearing stratum. Down-hole seismic testing was performed at 5 ft intervals in CPTs C-1003, C-1005, and C-1009A (see [Subsection 2.5.4.4](#)) to measure the shear wave velocity in the Upper Sand Stratum. Pore pressure dissipation tests were performed at 68 ft and 79 ft depths in C-1003; 66 ft depth in C-1004; 56 ft, 73 ft, and 82 ft depths in C-1005; and 60 ft, 77 ft, 90 ft, and 99 ft depths in C-1009A.

The CPT logs, shear wave velocity results, and pore pressure versus time plots, for the dissipation tests, are contained in [Appendix 2.5A](#). CPT locations and depths are summarized in [Table 2.5-244](#).

2.5.4.3.2.3 In Situ Hydraulic Conductivity Testing

Fifteen observation wells were installed at the ESP project limits during May and June 2005, and a replacement observation well was installed in October 2005. Observation well details are provided in [Appendix 2.4A](#) and discussed in [Subsection 2.4.12](#).

Each well was developed by pumping. The well was considered developed when the pH and conductivity stabilized and the pumped water was reasonably free of suspended sediment. Permeability tests were then performed in each well in accordance with Section 8 of ASTM D 4044 (2002) using a procedure that is commonly termed the slug test method. Slug testing involves establishing a static water level, lowering a solid cylinder (slug) into the well to cause an increase in water level in the well, and monitoring the time rate for the well water to return to the pre-test static level. The slug is then rapidly removed to lower the water level in the well, and the time rate for the water to recover to the pre-test static level is again measured. Electronic transducers and data loggers were used to measure the water levels and times during the test.

Appendix 2.5A contains the well permeability test results and Appendix 2.4A contains the boring logs for the observation wells and the well installation records.

2.5.4.3.2.4 Sample Re-evaluation

The MACTEC ESP data report was revised on November 18, 2007, as provided in Appendix 2.5A. Revisions include changes to the elevation of the top of Utley Limestone, changes to borings logs, and additional laboratory data. Some material descriptions in the Blue Bluff Marl and Utley Limestone were revised to clarify the descriptors of the coarse grained fraction of the sample. The coarse grained fractions, previously described as gravel, upon re-examination of the samples were found to consist of angular, gravel-sized, carbonate particles and were attributed to the mechanical breakage of cemented nodules, shells, cemented limestone, and fossiliferous limestone by the split barrel sampler. The top of Utley Limestone was redefined in some of the ESP boreholes based on the identification criteria developed for the COL investigation program.

2.5.4.3.3 COL Subsurface Investigation Program

The COL subsurface investigation was performed by MACTEC from November 2006 through April 2007 over a large portion of the site, including the power block areas for VEGP Units 3 and 4, cooling towers, switchyard/borrow areas, haul road, intake structure, pumphouse, pipeline, and construction-related areas. The exploration points were located in accordance with the guidelines in RG 1.132. The following paragraphs describe the overall COL investigation program. Other portions of this document primarily address the portion of the COL investigation associated with safety-related structures, principally the combined footprint of the power block excavation.

The COL exploration point locations are shown on Figures 2.5-367 and 2.5-368. The scope of work and the methods used by the subsurface investigation contractor (MACTEC) and its subcontractors to collect data are listed below:

- A total of 174 exploratory borings were drilled across the site.
- Seventy-seven exploratory borings were drilled in the power block and cooling tower areas with the 3000 series conducted on the east side, Unit 3, and the 4000 series conducted on the west side, Unit 4. Continuous sampling was conducted in two of these borings, B-3013(C) and B-4013(C), to depths of 155 feet and 165 feet, respectively.
- Sixty-six borings in the 1100 series were drilled in the proposed switchyard, borrow, roadway, batch plant, intake, pumphouse, and other areas across the site.
- Thirty-one borings in the 5000 and 6000 series were drilled in the laydown, roadway, and other areas across the site.
- The efficiency of the automatic hammers employed by the 12 rotary drill rigs was determined by SPT energy measurements.
- Twenty-one CPTs utilizing a Type 2 piezocone were performed, including eight seismic CPTs taken in the power block areas. These services were provided by Gregg In-Situ, Inc., of Columbia, South Carolina, working as a subcontractor to MACTEC.
- Eight test pits were excavated in proposed borrow locations to obtain bulk samples for laboratory testing. The test pit excavations were logged by a MACTEC geologist.

- Geophysical down-hole suspension P-S velocity logging was performed in six completed boreholes, B-3001(DH), B-3002(DH), B-3003(DH), B-4001(DH), B-4002(DH), and B-4003(DH). These services were provided by GEOVision Geophysical Services (GEOVision) of Corona, California, working as a subcontractor to MACTEC. GEOVision also performed caliper, boring deviation, spontaneous potential, natural gamma, and resistivity measurements in these boreholes.
- Electrical resistivity testing was performed by MACTEC along 10 arrays across the site.
- Geophysical refraction microtremor (ReMi) testing was performed by MACTEC at four arrays.
- A horizontal and vertical survey of all exploration points was performed by Toole Surveying Company, Inc., working as a contractor to Southern Company Services.
- Laboratory testing of selected borehole samples was performed by MACTEC laboratories in Atlanta, Georgia and Charlotte North Carolina.
- RCTS testing was performed by FUGRO laboratories in Houston, Texas.

The exploration program was performed following the guidelines in RG 1.132. The fieldwork was performed under an audited and approved quality assurance program, along with approved work procedures developed specifically for the COL application. The subsurface investigation and sample/core collection were directed by the MACTEC site manager, who was on site at all times during the field operations. A Bechtel geotechnical engineer or geologist, along with an SNC representative, was also on site during these operations. MACTEC's QA/QC supervisor made periodic visits to the site, and additional QA/QC personnel visited the site to audit MACTEC's subcontractors. Draft boring logs were prepared in the field by MACTEC geologists and geotechnical engineers. A data report was also prepared by MACTEC as provided in [Appendix 2.5C](#).

An on-site storage facility for soil samples was established before the fieldwork began. Each sample was logged into an inventory system. Samples removed from the facility were noted in the sample inventory logbook. A Chain-of-Custody form was also completed for all samples removed from the facility.

2.5.4.3.3.1 Borings and Samples/Cores

One hundred and seventy-four borings were drilled to depths ranging from 21.5 ft to 420 ft. The borings were advanced in the soil using mud-rotary drilling methods and polymer and/or bentonite drilling fluids. [Table 2.5-245](#) provides a summary of the COL boring locations and depths.

The soil was sampled using an SPT sampler at intervals 2.5 ft within the upper 15 ft and thereafter at 5- or 10-ft intervals. The SPT was performed with automatic hammers and was conducted in accordance with ASTM D 1586 (1999). The recovered soil samples were visually described and classified by the onsite geologist or geotechnical engineer in accordance with ASTM D 2488 (2000). A selected portion of the soil sample was placed in a glass sample jar with a moisture-proof lid. The sample jars were labeled, placed in boxes, and transported to the on-site storage area. Additionally, relatively undisturbed samples were obtained. In the Upper Sand stratum, these samples were taken with the direct push method in accordance with ASTM D 1587. In the Blue Bluff Marl and Lower Sand strata these samples were taken using a Pitcher sampler, a double-tube core barrel sampler, due to the very hard/dense nature of the materials. Disturbed materials were removed from the upper and the lower ends of the tube, and both ends were trimmed square to establish an effective seal. Pocket penetrometer tests were taken on the

trimmed lower end of the samples. Both ends of the sample were then sealed with hot microcrystalline wax and protected with plastic caps. Tubes were labeled and transported to the on-site storage area.

Twelve drill rigs were used during the COL investigation. The energy transfer efficiency of the automatic SPT hammers was measured for each drill rig in accordance with ASTM D 4633 (2005). Resultant average energy transfer efficiency measurements ranged from 70.1 to 90.2 percent. [Table 2.5-248](#) provides a summary of the SPT hammer energy transfer efficiency results.

The boring logs are provided in [Appendix 2.5C](#). The soil materials encountered in the COL borings are similar to those found in the ESP borings and previous borings conducted at the VEGP site.

2.5.4.3.3.2 Cone Penetrometer Tests

Twenty-one CPTs for the COL investigation were advanced in accordance with ASTM D 5778 (2000) using a 20 ton self-contained truck rig mounted on a tracked ATV carrier. Each CPT was advanced to refusal (utilizing a Type 2 piezocone) which generally was encountered at or near the top of the Blue Bluff Marl bearing stratum. Eight of the 21 CPTs included seismic testing as discussed in [Subsection 2.5.4.4.3.2](#). These eight SCPTs were located in the power block and cooling tower areas of Units 3 and 4. Refusal depths encountered in these soundings ranged from 65.4 to 100.4 ft. The CPT logs, shear wave velocity results, and pore pressure versus time plots for dissipation test are contained in [Appendix 2.5C](#). CPT locations and depths are summarized in [Table 2.5-245](#).

2.5.4.3.3.3 Test Pits

Test pits were excavated at eight locations identified in proposed borrow areas using a track-mounted backhoe (Caterpillar 315L) capable of 12-foot reach. A MACTEC geologist logged the excavation by observing the walls of the excavation and collected representative bulk samples of the various material types. Glass jar samples were also obtained and sealed for moisture retention. The geologist prepared a Geotechnical Test Pit Log based on visual description of the excavated materials according to ASTM D 2488. The backhoe was used to backfill the test excavation using the excavated materials and the completion of logging and sample collection. The Geotechnical Test Pit Logs are included in [Appendix 2.5C](#). Test pit locations and elevations are summarized in [Table 2.5-245](#).

2.5.4.3.3.4 Resistivity

Field electrical resistivity testing was performed along 10 arrays in the proposed switchyards, the cooling towers, and the circulating water line areas of the site. The locations and array lengths were field adjusted to accommodate obstructions. Array locations are shown on [Figures 2.5-367](#) and [2.5-368](#). The Wenner four electrode method was used to perform the tests in accordance with ASTM G57 (2006). Electrode spacing ranged from 3 feet up to 300 feet in order to determine the soil resistivity at increasing depths. The resistivity data interpreted from the tests are contained [Appendix 2.5C](#).

2.5.4.4 Geophysical Surveys

[Subsection 2.5.4.4.1](#) summarizes previous geophysical investigations performed at the VEGP site; [Subsection 2.5.4.4.2](#) summarizes the VEGP site geophysical program for this ESP investigation; and [Subsection 2.5.4.4.3](#) summarizes the geophysical surveys performed for the COL

investigation program. Geophysical surveys were also performed for the Phase I test pad program and are summarized in Section 2.5.4.4.4.

2.5.4.4.1 Previous Geophysical Survey Programs

Field investigations that included geophysical methods for VEGP Units 1 and 2 were initiated in January 1971. Geophysical seismic refraction and cross-hole surveys were conducted at the site to evaluate the occurrence and characteristics of subsurface materials. The seismic refraction survey was used to determine depths to seismic discontinuities, based on measured compressive wave velocities. Shallow and deep refraction profiles were obtained throughout the site area, totaling 28,400 and 5,000 linear ft, respectively. The cross-hole seismic survey was conducted in the VEGP Units 1 and 2 power block area to determine in situ velocity data for both compressional and shear waves to a depth of 290 ft (82 ft below sea level) in bore holes 136, 146G, 148, 149, 151, and 154. In this procedure, three-component geophones were lowered into four of the bore holes to equal elevation levels. Energy was generated in a fifth bore hole, at the same elevation level, to determine cross-hole velocities. Boreholes spacing varied from a minimum of about 36 ft to a maximum of about 200 ft.

The seismic (compressional wave) velocities measured in the subsurface soils from depths of 0 to 290 ft ranged from 1,400 fps to 6,800 fps. The shear wave velocities measured in the subsurface soils from depths of 0 to 290 ft ranged from 600 to 1,800 fps. The Upper Sand Stratum, extending from a depth of 0 to 90 ft, has a compressional wave velocity range of 1,400 to 6,650 fps and a shear wave velocity range from 600 to 1,650 fps. The Blue Bluff Marl stratum (and underlying Lower Sand Stratum), extending from a depth of 90 to 290 ft, has a compressional wave velocity of 6,800 fps and shear wave velocities ranging from 1,600 to 1,800 fps. Young's Modulus and Shear Modulus were determined from these results. For the Upper Sand Stratum, Young's Modulus ranged from 0.2×10^5 to 2.0×10^5 pounds per square inch (psi), and Shear Modulus ranged from 0.8×10^4 to 6.8×10^4 psi. For the Blue Bluff Marl (and underlying Lower Sand Stratum), Young's Modulus was 2.3×10^5 psi, and Shear Modulus was 8.0×10^4 psi.

2.5.4.4.2 ESP Geophysical Surveys

Three down-hole seismic CPT tests and five suspension P-S velocity tests were performed during the VEGP site investigation, as described in [Subsection 2.5.4.3.2](#). In addition a seismic reflection and refraction survey was performed to image the subsurface and characterize the basement lithology and velocities beneath the VEGP site. This survey provided an image of the basement rock across the VEGP ESP site. The results of this survey are presented in [Appendix 2.5B](#) and the interpreted results are discussed in [Subsection 2.5.1.2.4.2](#). The incorporation of these results into the development of the rock shear wave velocity profile is described in [Subsection 2.5.4.7.1.2](#).

2.5.4.4.2.1 Suspension P-S Velocity Tests in Boreholes

Suspension P-S velocity testing was conducted in ESP borings B-1002, B-1002A, B-1003, B-1004, and C-1005A. Borings B-1002A and C-1005A did not extend below the Upper Sand Stratum. Details of the equipment used to create the seismic compressional and shear waves and to measure the seismic wave velocities are described in detail by Ohya (1986) and are also provided in [Appendix 2.5A](#). [Appendix 2.5A](#) also contains a detailed description of the results and the method used to compute the results. Because no ASTM standard is currently available for the suspension P-S velocity testing, a brief description is provided here. The suspension P-S velocity logging system uses a 23-ft (7-m) probe containing a source near the bottom, and two geophone receivers spaced 3.3 ft (1 m) apart, suspended by a cable. The probe is lowered into the borehole to a specified depth, where the source generates a pressure wave in the borehole fluid (drilling mud). The pressure wave is converted to seismic waves (P-wave and S-wave) at the borehole wall. Along the wall, at each receiver location, the P- and S-waves are converted back to pressure waves in the fluid and received

by the geophones, which send the data to the recorder on the surface. This procedure is typically repeated at every 1.65 ft (0.5 m) or 3.3 ft (1 m) as the probe is moved up the borehole. The elapsed time between arrivals of the waves at the geophone receivers is used to determine the average velocity of a 3.3-ft (1-m) high column of soil around the borehole. Source to receiver analysis is also performed for quality assurance. The results are summarized below.

The shear wave velocity was defined to the maximum explored depth of 1,338 ft ([Appendix 2.5A](#)). For the Upper Sand Stratum, shear wave velocities ranged from 590 to 3,300 fps, with an average value of 1,089 fps. For the Blue Bluff Marl, shear wave velocities ranged from 1,060 to 4,260 fps, with an average value of 2,354 fps. For the Lower Sand Stratum, shear wave velocities ranged from 930 fps to 4,670 fps, with an average value of 2,282 fps. Typical values for the shear wave velocities of each geologic formation contained within the Lower Sand Stratum are as follows: 1,700 fps for the Still Branch, 1,950 fps for the Congaree, 2,050 fps for the Snapp, 2,350 fps for the Black Mingo, 2,650 fps for the Steel Creek, 2,850 fps for the Gaillard/Black Creek, 2,870 fps for the Pio Nono, and 2,710 fps for the Cape Fear. The shear wave velocity in the portion of the Dunbarton Triassic Basin rock measured ranged from 2,320 to 9,350 fps. There was an upper weathered rock zone about 120 ft thick, where shear wave velocities increased linearly with depth at a very high rate. This high rate of linear increase with depth abated once shear wave velocities achieved values of about 5,300 fps, and shear wave velocities increased linearly with depth at a smaller rate. It is noted that sound rock with an average shear wave velocity of 9,200 fps was not encountered. However, enough data are available to linearly extrapolate to the sound rock horizon from the measurements.

The compressional wave was also defined to the maximum explored depth of 1,338 ft ([Appendix 2.5A](#)). For the Upper Sand Stratum, the compressional wave velocity ranged from 1,300 to 7,960 fps, with an average value of 2,572 fps. For the Blue Bluff Marl, compressional wave velocities ranged from 4,640 to 9,830 fps, with an average value of 6,793 fps. For the Lower Sand Stratum, compressional wave velocities ranged from 4,990 to 9,030 fps, with an average value of 6,610 fps. The compressional wave velocity in the Dunbarton Triassic Basin rock ranged from 7,300 to 18,360 fps.

Poisson's ratio was determined from the shear wave and compressional wave velocities ([Appendix 2.5A](#)). Poisson's ratio ranged from 0.09 to 0.49 within the Upper Sand Stratum, 0.33 to 0.48 within the Blue Bluff Marl, 0.32 to 0.49 within the Lower Sand Stratum, and 0.10 to 0.46 within the Dunbarton Triassic Basin.

2.5.4.4.2.2 Down-Hole Seismic Tests with Cone Penetrometer

The tests were performed at 5-ft intervals in ESP soundings C-1003, C-1005, and C-1009A. A seismic source, located on the surface, primarily generates shear waves and two geophones mounted horizontally inside near the bottom of the cone string record incoming seismic data. Measurements were only obtained at depths within the Upper Sand Stratum because all CPTs reached refusal at the top of the Blue Bluff Marl.

The shear wave speed and time of peak versus depth plots are included in [Appendix 2.5A](#). The shear wave velocities ranged from 572 to 1,317 fps, with an average value of 930 fps. These values were lower than those measured using the suspension P-S velocity technique and may reflect site variability.

2.5.4.4.2.3 Discussion and Interpretation of Results

Shear and compressional wave velocity measurements made during the ESP subsurface investigation were used as the basis for developing the recommended design values for each stratum that are provided in [Subsection 2.5.4.2](#). Results from seismic CPTs and suspension velocity logging were used to develop recommended values for the Barnwell Group. Because the seismic

CPTs could not penetrate into the Blue Bluff Marl, the recommended values for the Blue Bluff Marl and the Lower Sand Stratum are based on suspension velocity logging results only. No shear or compressional wave velocity measurements were made for the compacted fill during the ESP subsurface investigation. Recommended values for the compacted fill were initially based on data for existing VEGP Units 1 and 2 (Reference 496), as discussed in Subsection 2.5.4.7.1. Results from the COL investigation and Phase I test pad program were used to confirm the recommended values.

The profile of shear wave velocity versus depth for the subsurface strata is provided in Subsection 2.5.4.7.

2.5.4.4.3 COL Geophysical Surveys

Eight down-hole seismic CPT tests, six suspension P-S velocity tests, and four refraction microtremor testing (ReMi) arrays were performed during the COL site investigation. The results of these tests, with the exception of the ReMi data, are provided in Appendix 2.5C.

2.5.4.4.3.1 Suspension P-S Velocity Tests in Boreholes

Suspension P-S velocity testing was conducted in COL borings B-3001, B-3002, B-3003, B-4001, B-4002 and B-4003. Details of the equipment used to create the seismic compressional and shear waves and to measure the seismic wave velocities are described in detail by Ohya (1986) and are also provided in Appendix 2.5C. Appendix 2.5C also contains a detailed description of the results and the method used to compute the results. A summary of the results is provided in the following paragraphs.

The shear wave velocity was defined to the maximum explored depth of 420 ft. For the Blue Bluff Marl, shear wave velocities ranged from 1,267 to 2,984 fps, with an average value of 2,050 fps. For the Lower Sand Stratum, shear wave velocities ranged from 745 fps to 2,563 fps with average values for each geologic formation contained within the Lower Sand Stratum as follows: 1,621 fps for the Still Branch, 1,863 fps for the Congaree, and 1,871 fps for the Snapp.

Poisson's ratio was determined from the shear wave and compressional wave velocities and ranged from 0.40 to 0.48 with an average of 0.45.

2.5.4.4.3.2 Down-Hole Seismic Tests with Cone Penetrometer

The tests were performed at 0.6-ft intervals in COL soundings C-3001, C-3002, C-3003, C-3005, C-4001, C-4002, C-4003, and C-4005. A seismic source, located on the surface, primarily generates shear waves and two geophones mounted horizontally inside near the bottom of the cone string record incoming seismic data. Generally, the CPT soundings could not penetrate the dense/hard materials encountered in the Utley and/or Blue Buff Marl; therefore, the shear wave measurements were limited to the Upper Sand stratum. The penetration of the seismic CPT soundings ranged from 65.4 ft to 100.4 ft.

The shear wave speed and time of peak versus depth plots are included in Appendix 2.5C. The shear wave velocities measurements ranged from 435 to 3,802 fps. A summary plot of the COL average shear wave velocity profiles in the Upper Sand Strata is provided in Figure 2.5-377.

2.5.4.4.3.3 Refraction Microtremor Testing

ReMi testing was conducted at four arrays, two in the power block areas of the existing VEGP Units 1 and 2 and two in the footprint of proposed Units 3 and 4. The original intent of collecting these data was to establish the shear wave velocity characteristics of existing backfill at Units 1

and 2. During collection of the data, it was readily apparent that the frequency of the nearby operating plant equipment was interfering with the ReMi data. Unsuccessful attempts were made in the field to overcome this interference. SNC requested Dr. K Stokoe of the University of Texas-Austin to review the ReMi results. He expressed doubt that the test results truly represented the shear wave velocity profile. Therefore these data have not been considered in the COL geophysical survey and are not included in [Appendix 2.5C](#).

2.5.4.4.3.4 Geophysical Surveys in Compacted Fill

Geophysical surveys were conducted during construction (at three different levels) and upon completion of the 20-ft test pad in the Phase I test pad program in order to evaluate the shear wave profile in compacted fill. The SASW (Spectral Analysis of Surface Waves) method was used to determine shear wave velocity during various stages of construction and upon completion of construction. A more detailed description of this method and the measurements taken is provided in [Appendix 2.5D](#). The cross-hole method (ASTM D 4428) was also used to measure shear wave velocity through the fill. Upon completion of the test pad, 3 cased boreholes were installed through the 20-ft test pad, extending 20 feet below the test pad into native materials. Compressional and shear wave velocity measurements were made between the boreholes. Results from these geophysical tests, along with RCTS test results, were incorporated into the analysis to develop the shear wave velocity profile for the entire depth of backfill (approximately 90 feet) as discussed in [Subsection 2.5.4.7.1.1](#).

2.5.4.5 Excavation and Backfill

This section covers the following topics:

- The extent (horizontally and vertically) of anticipated safety-related excavations, fills, and slopes.
- Excavation methods and stability.
- Backfill design
- Backfill sources
- Quality control and ITAAC
- Construction dewatering impacts
- Retaining wall

2.5.4.5.1 Extent of Excavations, Fills, and Slopes

Within the VEGP Units 3 and 4 footprint ([Figure 2.5-366](#)) that will contain all safety-related structures, existing ground elevations are about El. 220 ft msl. The subsurface profiles in [Figures 2.5-370](#), [2.5-372](#), and [2.5-373](#) provide an impression of the grade elevation range across the VEGP ESP site. Plant grade for the proposed VEGP Units 3 and 4 will be at El. 220 ft msl. The base of the Nuclear Island foundations for the new units will be about El. 180 ft msl. This level corresponds to a depth of approximately 40 ft below final grade (below El. 220 ft msl), or approximately 50 to 60 ft above the top of the Blue Bluff Marl bearing stratum based on the borings completed during the ESP and COL subsurface investigations. Other foundations in the power block area will be placed at nominal depths near final grade.

Construction of the new units will require a substantial amount of excavation. The excavation will be necessary to completely remove the Upper Sand Stratum. Excavation total depth to the Blue Bluff Marl bearing stratum will range from approximately 80 to 90 ft below existing grade, based on the borings completed during the ESP and COL subsurface investigations. Deeper localized excavations will be required to remove shelly, porous, or weathered material that may be encountered near the top surface of the Blue Bluff Marl.

Seismic Category 1 backfill will be placed from the top of the Blue Bluff Marl to the bottom of the Nuclear Island (NI) foundation at a depth of about 40 ft below final grade. Seismic Category 2 backfill will be placed above the NI foundation level. The lateral extent of the Category 1 and 2 backfill is defined in [Figure 2.5-389](#). A retaining wall will be constructed along the perimeter of the NI as described in [Subsection 2.5.4.5.7](#) to facilitate backfilling and construction. Category 2 backfill will be placed behind the retaining wall to final grade or foundation elevation of non NI structures. Category 1 and 2 backfill material will meet the same criteria and consist of granular materials, selected from portions of the excavated Upper Sand Stratum and from other acceptable onsite borrow sources. Category 1 and 2 backfill material properties and source locations are described in more detail in [Subsections 2.5.4.5.3](#) and [2.5.4.5.4](#).

Engineered granular backfill (EGB) will be placed above the slopes, outside the specified lateral extent of the Category 1 and 2 backfill, as defined in [Figure 2.5-389](#). The areas where EGB will be placed will not affect the static or seismic performance of the safety-related facilities. The EGB will be well-compacted granular backfill meeting the following requirements;

- Compacted to a minimum of 95% of modified Proctor (ASTM D1557) maximum dry density value
- Consist of sands, silty sands and clayey sands (SP, SP-SM, SP-SC, SW, SW-SM, SW-SC, SC, SC-SM, or SM based on the Unified Soil Classification System (ASTM D2487)
- Has a maximum plasticity index (PI) of 25 and a maximum fines content (% passing the No. 200 sieve) of 35%.

Materials that exceed the limits for PI and fines content may be accepted on a case-by-case basis after an engineering evaluation has been performed.

2.5.4.5.2 Excavation Methods and Stability

Excavation for the nuclear island structures below grade may use either a sloping excavation or a vertical face as described in subsequent paragraphs. If sloping excavations are to be used on a soil site, the Combined License applicants must evaluate the 3D effects on the site response and perform site-specific SSI analyses using either or a combination of 2D or 3D SASSI models that reflect the sloping excavations. If backfill is to be placed adjacent to the exterior walls of the nuclear island, the Combined License applicant will provide information on the properties of backfill and its compaction requirements as described in [Subsection 2.5.4](#) and will evaluate its properties against those used in the seismic analyses described in [Subsection 3.7.2](#).

For the vertical face alternative, excavation in soil for the nuclear island structures below grade will establish a vertical face with lateral support of the adjoining undisturbed soil or rock. This vertical face will be covered by a waterproof membrane as described in subsection 3.8.5.1.1 and is used as the outside form for the exterior walls below grade of the nuclear island. Alternative methods include a soil nailing and mechanically stabilized earth (MSE) walls.

Excavation in the Upper Sand Stratum will be achieved with conventional excavating equipment. Excavation must adhere to OSHA regulations ([Reference 589](#)). The excavation will be open-cut,

with slopes no steeper than 2-horizontal to 1-vertical. Since the sandy soils can be highly erosive, even temporary slopes cut into the Upper Sand Stratum will be sealed and protected. Where insufficient space for open-cut slopes exists, vertical cuts will be supported with sheet pile or soldier pile and lagging walls. Dewatering will be required once the excavation progresses to depths beneath the groundwater table (approximately El. 150 to 155 ft in the excavation, based on the groundwater monitoring results contained in [Subsection 2.4.12](#)).

Temporary slopes will be graded as the excavation through the Upper Sand Stratum progresses. There are no permanent slopes in the NI area planned for the project that need to be considered for stability.

Possible weathered zones that may be encountered in the upper portion of the Blue Bluff Marl will be removed using conventional excavating equipment. These excavations will be sloped to facilitate placement of compacted structural fill, and the excavation areas will be thoroughly cleaned of loose materials before fill is placed.

2.5.4.5.2.1 Vertical Face Using Soil Nails

Soil nailing is a method of retaining earth in-situ. As the nuclear island excavation progresses vertically downward, holes are drilled horizontally into the adjoining undisturbed soil, a metal rod is inserted into the hole, and grout is pumped into each hole to fill the hole and to anchor the “nail” rod.

As each increment of the nuclear island excavation is completed, nominal eight to ten inch diameter holes are drilled horizontally through the vertical face of the excavation into adjacent undisturbed soil. These “nail” holes, spaced horizontally and vertically on five to six feet centers, are drilled slightly downward to the horizontal. A “nail”, normally a metal bar/rod, is center located for the full length of the hole. The nominal length of soil nails is 60 percent to 70 percent of the wall height, depending upon soil conditions. The hole is filled with grout to anchor the rod to the soil. A metal face plate is installed on the exposed end of the rod at the excavated wall vertical surface. Welded wire mesh is hung on the wall surface for wall reinforcement and secured to the soil nail face plates for anchorage. A 4,000 psi to 5,000 psi non-expansive pea gravel shotcrete mix is blown onto the wire mesh to form a nominal four to six inch thick soil retaining wall. Installation of the soil retaining wall closely follows the progress of the excavation and is from the top down, with each wire mesh-reinforced, shotcreted wall section being supported by the soil “nails” and the preceding elevations of soil nailed wall placements.

Soil nailing as a method of soil retention has been successfully used on excavations up to 55 feet deep on projects in the U.S. Soils have been retained for up to 90 feet in Europe. The state of California CALTRANS uses soil nailing extensively for excavations and soil retention installations. Soil nailing design and installation has a successful history of application which is evidenced by its excellent safety record.

The soil nailing method produces a vertical surface down to the bottom of the excavation and is used as the outside forms for the exterior walls below grade of the nuclear island. Concrete is placed directly against the vertical concrete surface of the excavation.

For methods of soil retention other than soil nailing, such as for excavation in rock, four to six inches of shotcrete are blown on to the vertical surface. The concrete for the exterior walls is placed against the shotcrete.

2.5.4.5.2.2 Vertical Face Using Mechanically Stabilized Earth Walls

Mechanically stabilized earth walls (MSE) are flexible retaining wall systems that use strip, grid, or sheet type of tensile reinforcements in the soil mass, and a discrete modular pre-cast concrete, which

is vertical. MSE walls function like, and are generally more economical than, conventional retaining walls. The tensile strength of the reinforcements and the slip at the interface of the reinforcement and the soil provide great internal stability to MSE walls. These walls may be used where the side soils have to be removed or the grade elevation needs to be raised. The walls and backfill are placed prior to construction of the nuclear island.

2.5.4.5.2.3 Mudmat

The mudmat provides a working surface prior to initiating the placement of reinforcement for the foundation mat structural concrete. The lower and upper mudmats are as follows:

- Lower mudmat — (6-inch layer) of un-reinforced concrete, with a minimum compressive strength of 2,500 psi. The lower mudmat will be used as the final dental concrete layer on the underlying foundation media.
- Upper mudmat — (6-inch layer) of un-reinforced concrete with a minimum compressive strength of 2,500 psi. This upper mudmat will support the chairs that, in turn, support the reinforcing steel.

The lower and upper mudmats are additionally described in [Subsection 3.8.5.1](#).

The waterproofing system is described in [Subsection 2.5.7.18](#) and [Subsection 3.8.5.1.1](#).

2.5.4.5.3 Backfill Design

The design of the Category 1 and Category 2 backfill for VEGP Units 3 and 4 was established through analysis and testing of the borrow material during the COL investigation, the Phase I test pad program, and previous site investigations. Selection and compaction requirements are discussed below.

Material selected for use as Category 1 and Category 2 backfill will be sand and silty sand and will meet the gradation requirements provided in [Table 2.5-257](#). Material that falls outside the gradation requirements in [Table 2.5-257](#) may be accepted on a case-by-case basis after an engineering evaluation has been performed to assess the overall impact of the material on the backfill design. Borrow material that does not meet the limits on the No. 200 sieve will not be accepted. A backfill specification will be developed to implement these requirements.

All Category 1 and Category 2 backfill will be compacted to a minimum of 95 percent of the maximum dry density, as determined by ASTM D 1557 (2002). Procedures will be developed to control all aspects of backfill placement including lift thickness, moisture conditioning, compaction, and testing. These procedures will result in a high quality, uniform, homogeneous backfill meeting all the requirements for supporting the AP1000 structures at the Vogtle site. The testing frequency for field density tests and ITAAC associated with backfill density and shear wave velocity are discussed in [Subsection 2.5.4.5.5](#).

The Phase I test pad program is complete and is documented in [Appendix 2.5D](#). The objective of this program was to establish site-specific design properties for the backfill, including density, compaction, gradation, and shear wave velocity, and to show that the backfill will satisfy the AP1000 standard plant design. The test pad was constructed below grade, was 20 ft deep, and was 20 ft x 60 ft in plan area. The test pad was constructed in the switchyard borrow area using methods similar to those used to construct the backfill for VEGP Units 1 and 2. The placement and compaction of the backfill were monitored and tested. Results of the test pad program demonstrated that the siting criterion for shear wave velocity of 1,000 fps at the NI foundation depth was achieved with the backfill material within the 20 ft thickness of the test pad.

The backfill properties were determined by evaluating field and laboratory results. Laboratory testing was conducted to measure density, moisture content, grain size, plasticity, shear, and shear modulus reduction and damping relationships. Field testing was conducted to measure density (compaction), shear wave velocity (SASW and cross-hole testing), and standard penetration resistance. Measured SPTs in the test fill (neglecting the upper four feet due to the lack of confining pressure) disclosed a median uncorrected N-value of 32 bpf (corrected for hammer efficiency, $N_{60} = 43$). A shear wave velocity profile was calculated based on field measurements of velocity in the test pad and in laboratory samples. This profile is discussed in [Subsection 2.5.4.7.1.1](#) and is presented in [Table 2.5-250](#). An average moist unit weight of 123 pcf was calculated. A drained internal angle of friction of 36° was determined from laboratory triaxial shear tests. Gradation requirements were developed based on the results of field and laboratory testing, including shear wave and compaction testing, from the COL investigation, test pad program, and results from previous investigations. These gradation requirements are presented [Table 2.5-257](#). Shear modulus reduction and damping relationships are presented in [Subsection 2.5.4.7.2](#). A summary of the engineering properties for compacted structural fill is presented in [Table 2.5-237](#).

A Phase II test pad program is scheduled for 2008. The purpose of this program will be to finalize the placement procedures and equipment. The program will use onsite material excavated from the switchyard borrow area. Test pad results will be used to finalize the details of the backfill construction program including construction methods, compaction methods and requirements, and testing protocol. These details will be incorporated into an earthwork specification and backfill placement procedures.

2.5.4.5.4 Backfill Sources

Sufficient sources of backfill have been identified on the Vogtle site through the boring and laboratory testing programs and analysis of their results as described below. Flowable fill may also be used as Category 2 backfill in small restricted areas where adequate compaction cannot be achieved or in large areas left open for relatively long periods, to minimize erosion or disturbance of underlying backfill. When flowable fill is used in large areas, it is limited to a total thickness of 1 foot or less. The flowable fill mix is designed to have similar strength characteristics as the compacted backfill.

Identified onsite sources of borrow material for the proposed backfill include acceptable materials from the Upper Sand stratum excavated from the power block and a borrow area (switchyard) north of the power block. An alternative borrow area is located about 4,000 feet north of the power block. This alternative location (Borrow Area 4) was also identified and investigated during construction of VEGP Units 1 and 2.

Approximately 3,900,000 cubic yards of material (including an allowance for ramps) will be excavated for the Units 3 and 4 power blocks. Approximately 3,600,000 cubic yards of material will be required to backfill these excavations, of which approximately 2,000,000 cubic yards of material must meet Category 1 and 2 requirements. Based on a review of the 70 SPT boring logs and laboratory test results on selected samples from the COL subsurface investigation, approximately 50 percent of the material excavated from the power block areas will qualify for reuse as Seismic Category 1 or 2 backfill. However, because a portion of the excavated material may be difficult to segregate, an estimated 30–50 percent of the excavated material is designated for borrow. This quantity accounts for approximately 1,200,000–2,000,000 cubic yards.

Additional backfill for the power blocks, approximately 1,600,000 cubic yards, is available from a borrow source located immediately north of the power blocks (Units 3 and 4 switchyard area). See [Figures 2.5-388](#) and [2.5-389](#) for plan and section views, respectively. The switchyard borrow

source was explored with 15 SPT borings and five test pits during the COL investigation. The engineering properties of these materials were evaluated with laboratory tests on disturbed, undisturbed, and bulk samples. The COL laboratory testing program ([Appendix 2.5C](#)) included sieve analyses of 27 samples that disclosed an average value of 15 percent fines and a median value of 15 percent. Based on the subsurface data, suitable backfill materials at the switchyard borrow source were identified. These materials were classified according to ASTM D 2488 as silty sands (SM) and poorly graded sands (SP). Clayey sands (SC) were also encountered in some samples. Compaction tests (ASTM D 1557) were conducted on five bulk samples taken from representative soils. Test results disclosed a range of 111 pcf to 125 pcf for the maximum dry density with an average value of 116 pcf.

If additional material is needed, an alternative borrow source is located about 4,000 feet north of the power block area, designated Borrow Area 4. It was explored with four SPT borings and three test pits during the COL investigation. This area was previously explored but not utilized during the design and construction of Units 1 and 2. Sieve analyses were conducted on 31 representative samples and disclosed values ranging from 7 percent to 43 percent fines content with an average value of 16. Compaction tests (ASTM D 1557) were conducted on five bulk samples taken from representative soils. Test results disclosed a range of 113 pcf to 121 pcf for the maximum dry density with an average value of 116 pcf. Based on the subsurface data, suitable backfill materials at Borrow Area 4 are located at the surface (approximate El. 246 ft) to a depth of 36 ft (approximate El. 210 ft) and the borrow area is estimated to contain approximately 1,200,000 cubic yards.

Other localized deposits of suitable material within the Barnwell Group of the Upper Sand stratum located within the VEGP Exclusion Area Boundary (EAB) ([Figure 1.1-202](#) outside of the above three borrow areas may be evaluated for use as borrow material. These additional borrow areas are limited to selected areas identified in NUREG 1872, Vol. 1, "Final Environmental Impact Statement for an Early Site Permit (ESP) at the Vogtle Electric Generating Plant Site," Table 4.3, as areas impacted by Vogtle 3 and 4 construction. These selected areas are described in NUREG 1872 as follows:

- Cooling Tower
- Temporary Parking
- Temporary Warehouse, Office, and Laydown
- Spoils Areas

In addition, three additional areas have been identified as containing suitable backfill material. These areas are identified as follows:

- Western portion of North Stockpile area (NOI 3, west)
- Borrow Area 1C (NOI 25)
- Railroad Borrow Area (NOI 28)

Deposits within these areas may be identified by review of existing boring data, additional informational borings or test pits, or excavation activities incidental to construction. The evaluation to use such material would include a geologic review of the materials, a laboratory testing program, and an engineering review of soil properties. This material would be designated as suitable for use as Category 1 and 2 backfill provided the evaluation concludes that the material meets the acceptance criteria contained in [Table 2.5-258](#). Once identified as suitable backfill, the material will be qualified and placed in accordance with all requirements for Category 1 and 2 backfill.

2.5.4.5.5 Quality Control and ITAAC

A quality assurance and quality control program for the backfill will be established to verify that the backfill has been constructed to the design requirements. A soil testing subcontractor, independent from the earthwork contractor, will be used to perform soil testing as part of the quality control program for backfill. The soil testing subcontractor will have an approved quality program.

The backfill quality control program will cover all aspects of the backfill testing program from qualification of the borrow material to confirmatory shear wave velocity testing of the as-placed backfill. Qualification of the borrow material will include soil classification tests, grain size distribution tests, and laboratory compaction (modified Proctor) tests. These tests will determine the acceptability of borrow material and optimum moisture content for compaction. Field density testing will be performed to verify compaction requirements are met as the backfill is placed. For limited earthwork, where fill is compacted with hand equipment, one density test will be conducted for every 2,000 square feet per foot of fill placed. For mass earthwork, the frequency of field density tests for both Category 1 and Category 2 backfill will be a minimum of one test per 500 cubic yards of compacted fill, with at least one test per lift. At least two density tests per lift will be located within the footprint directly beneath the Nuclear Island.

The backfill testing results, non-conformances related to backfill, and QA audits of backfill operations will be reviewed to determine if the as-built backfill meets the minimum 95% modified Proctor compaction requirement under the Seismic Category 1 structures. The results of this evaluation will be documented in a report to support the Inspection Test and Acceptance Criteria (ITAAC) identified in the Backfill ITAAC Table. Field density tests performed on backfill directly beneath the Nuclear Island will be used to demonstrate this ITAAC has been met.

Shear wave velocity testing will be performed on the completed backfill to confirm that the shear wave velocity, at the bottom of the NI foundation and below, is greater than or equal to 1,000 fps. Shear wave velocity will be measured using the SASW method. A report will be developed to document that the required shear wave velocity has been achieved to satisfy the ITAAC identified in the Backfill ITAAC Table.

Preliminary measurements of the shear wave velocity characteristics of the backfill will be made when backfill placement reaches the approximate elevation of the bottom of the NI foundation (El. 180 ft). SASW measurements will be taken within the NI footprint. In addition, representative SASW measurements will be taken at a minimum of three reference locations outside the NI footprint. SASW results for testing at this elevation will be used as supplemental information to document the backfill characteristics. The reference SASW locations will be selected so there will be minimal influence from structures that could impact the SASW testing (e.g., circulating water piping, Lampson Crane pad, MSE wall) when the backfill is at finish grade.

Upon completion of backfill to finish grade, SASW testing will be performed at the three reference locations outside of the NI footprint to determine the backfill shear wave velocity profile down to the top of the Blue Bluff Marl. The results of the SASW measurements made at finish grade will be used to document that the backfill shear wave velocity profile at the elevation of the bottom of the NI foundation and below is greater than or equal to 1,000 fps.

A second method of measuring shear wave velocity (e.g., cross-hole testing, seismic CPT) will be performed at one of the reference locations at finish grade. The results from this test will be compared to the SASW results for the same reference location to validate the SASW results. In the event that velocity measurements do not provide adequate evidence to support closure of the ITAAC, additional evaluations and testing may be performed.

The final report submitted to close the ITAAC will present the shear wave velocity profile for the completed backfill at the referenced locations and any supporting analysis or testing used to conclude that the ITAAC has been met. For each velocity profile, the shear wave velocity profile at the elevation of the bottom of the NI foundation and below will be compared to the required 1,000 fps.

Backfill ITAAC Table

Design Requirement	Inspections and Tests	Acceptance Criteria
Backfill material under Seismic Category 1 structures is installed to meet a minimum of 95 percent modified Proctor compaction.	Required testing will be performed during placement of the backfill materials.	A report exists that documents that the backfill material under Seismic Category 1 structures meets the minimum 95 percent modified Proctor compaction.
Backfill shear wave velocity is greater than or equal to 1,000 fps at the depth of the NI foundation and below.	Field shear wave velocity measurements will be performed when backfill placement is at the elevation of the bottom of the Nuclear Island foundation and at finish grade.	A report exists and documents that the as-built backfill shear wave velocity at the NI foundation depth and below is greater than or equal to 1,000 fps.

2.5.4.5.6 Control of Groundwater During Excavation

Construction dewatering is discussed in [Subsection 2.5.4.6.2](#). Since the Upper Sand Stratum soils can be highly erosive, sumps and ditches constructed for dewatering will be lined. The tops of excavations will be sloped back to prevent runoff down the excavated slopes during heavy rainfall.

2.5.4.5.7 Retaining Wall

A retaining wall will be constructed within each power block excavation to facilitate construction of the nuclear islands. This retaining wall, planned as a mechanically stabilized earth (MSE) wall, will be constructed around the perimeter of each NI and will permit backfilling of the excavations before construction of the NI foundations and substructure walls. The MSE wall will act as the exterior form for the foundation and substructure walls. Waterproofing will be placed on the surface of the precast concrete MSE wall facing panels before placing NI foundation and substructure wall concrete. ([Figure 2.5-390](#))

2.5.4.6 Groundwater Conditions

2.5.4.6.1 Groundwater Measurements and Elevations

Groundwater conditions at the site are discussed in detail in [Subsection 2.4.12](#), and only a summary is presented here. Groundwater is present in unconfined conditions in the Upper Sand Stratum and in confined conditions in the Lower Sand Stratum at the VEGP site. The Blue Bluff Marl is considered to be an aquiclude that separates the unconfined water table aquifer in the Upper Sand Stratum from the confined Tertiary aquifer in the Lower Sand Stratum. In the powerblock area, the groundwater generally occurs at a depth of about 65 to 70 ft below the existing ground surface.

Fifteen observation wells were installed at the site during June and July 2005, before the start of the ESP subsurface investigation program. Ten of these wells were installed in the unconfined aquifer, and five were installed in the confined Tertiary aquifer. Additionally, 22 existing wells were used as part of the groundwater monitoring program for the ESP study. Thirteen of these wells were installed in the unconfined water table aquifer, and nine were installed in the confined aquifer. The wells installed in the unconfined water table aquifer exhibit groundwater levels ranging from about El. 132

to El. 165.5 ft, while the wells installed in the confined aquifer exhibit groundwater levels ranging from about El. 82 to El. 128 ft. The logs and details of well installation and testing are contained in [Appendix 2.4A](#) and [Appendix 2.5A](#). Hydraulic conductivity (slug) tests were performed in the wells installed during the ESP field investigation, as described in [Subsection 2.5.4.3.2.3](#). Hydraulic conductivity (k) values for the unconfined water table aquifer in the Upper Sand Stratum, based on the slug test results, range from 4.4×10^{-5} to 9.3×10^{-4} cm/second, with a geometric mean of 1.75×10^{-4} cm/second. The hydraulic conductivity of the confined Teritary aquifer in the Lower Sand Stratum, based on the slug test results, ranges from 1.3×10^{-4} to 7.5×10^{-4} cm/second, with a geometric mean of 2.95×10^{-4} cm/second. Detailed descriptions of current groundwater conditions, as well as post-construction groundwater conditions are provided in [Subsection 2.4.12](#).

Groundwater levels at the site will require temporary dewatering of excavations extending below the water table during construction of new Units 3 and 4. Dewatering will be performed in a manner that will minimize drawdown effects on the surrounding environment and VEGP Units 1 and 2. Drawdown effects are expected to be limited to the VEGP site and to be negligible for VEGP Units 1 and 2. The relatively low permeability of the Upper Sand Stratum and underlying Blue Bluff Marl means that sumps and pumps should be sufficient for successful construction dewatering, as discussed in [Subsection 2.5.4.6.2](#).

The design groundwater level for VEGP Units 3 and 4 will be taken at El. 165 ft msl based on the results of groundwater monitoring performed during a period of 10 years prior to the ESP subsurface investigation, and during the ESP subsurface investigation, as discussed in [Subsection 2.4.12](#). This level corresponds to the design groundwater level for the existing VEGP Units 1 and 2. The static stability of the proposed structures based on this design groundwater level is discussed in [Subsection 2.5.4.10](#).

2.5.4.6.2 Construction Dewatering

Dewatering for all major excavations could be achieved by gravity-type systems. Due to the relatively impermeable nature of the Upper Sand Stratum, sump-pumping of ditches will be adequate to dewater the soil. These ditches will be advanced below the progressing excavation grade.

During construction of VEGP Units 1 and 2, the excavation materials were dewatered by a series of ditches oriented in an east-west direction. They were connected by a north-south ditch, which drained to a sump in the southwest corner of the excavation. The sump was equipped with four pumps each with a capacity of 500 gal./min to remove inflows from groundwater. Additional capacity was provided for the removal of inflows of storm water in the excavation.

Similar dewatering procedures will be implemented during the excavation for VEGP Units 3 and 4.

2.5.4.7 Response of Soil and Rock to Dynamic Loading

All new safety-related structures will be founded on the planned structural backfill, which will completely replace the existing Upper Sand Stratum soils. The seismic acceleration at the sound bedrock level will be amplified or attenuated up through the soil and rock column. To estimate this amplification or attenuation, the following data are required.

- Shear wave velocity profile of the soils and rock
- Variation with strain of the shear modulus and damping values of the soils
- Site-specific seismic acceleration-time history

In addition, an appropriate computer program is required to perform the analysis.

2.5.4.7.1 Shear Wave Velocity Profile

2.5.4.7.1.1 Soil Shear Wave Velocity Profile

Various measurements have been made at the VEGP ESP site to obtain estimates of the shear wave velocity in the soil. Measurements were also made at the site during the COL investigation to confirm ESP estimates of shear wave velocity in the soil.

All safety-related structures will be founded on the structural backfill that will be placed on top of the Blue Bluff Marl after complete removal of the Upper Sand Stratum. Shear wave velocity was not determined for the compacted backfill during the ESP subsurface investigation. Data for existing Units 1 and 2 is used ([Reference 496](#)) and the backfill shear wave velocity values are summarized in [Table 2.5-249](#).

During the COL investigation, shear wave velocity data for the compacted backfill was measured directly in the field during the Phase I test pad program. These data, with laboratory test data, were used to evaluate the shear wave velocity of the backfill. A summary of the Phase I test pad program, including a discussion of material properties, is included in [Subsection 2.5.4.5.3](#). The results of the test pad program are presented in [Appendix 2.5D](#). RCTS and other data from the COL investigation were also used to evaluate the shear wave velocity of the backfill. The RCTS data are presented in Attachment G of [Appendix 2.5C](#). Results of the COL investigation and Phase I test pad were used to develop the shear wave velocity profile of the backfill based on COL data. This profile is presented in [Table 2.5-250](#) and is in good agreement with the ESP backfill profile. Both of these profiles are included in the respective soil columns in [Figure 2.5-379](#).

[Figure 2.5-376](#) shows the shear wave velocity values measured in the subsurface soil and rock strata for the ESP subsurface exploration program using suspension P-S velocity and CPT down-hole seismic testing. [Figure 2.5-377](#) shows the shear wave velocity values measured in the Upper Sand Stratum using CPT down-hole seismic testing from COL data. The shear wave velocity profile shown in [Figure 2.5-378](#) is the profile interpreted from the results of the ESP data shown in [Figure 2.5-376](#) for strata below the Upper Sand Stratum, plus the shear wave velocity values for the backfill shown on [Table 2.5-249](#). The shear wave velocity values corresponding to the profile shown on [Figure 2.5-378](#) for the different soil strata encountered by the borings are provided in [Table 2.5-251](#).

The shear wave velocity profile developed from the ESP investigation and shown in [Figure 2.5-378](#) is used in the seismic amplification/attenuation analysis. The soil profile used consists of: Compacted backfill from 0 to 86 ft, Blue Bluff Marl from 86 to 149 ft, Lower Sand Stratum from 149 to 1,049 ft, Dunbarton Triassic Basin and Paleozoic Crystalline Rock below 1,049 ft.

During the COL investigation, shear wave velocity values were measured in the Blue Bluff Marl and the upper portions of the Lower Sand Stratum as previously described in [Subsection 2.5.4.4.3](#). These data included measurements in 6 boreholes, extending to a maximum depth of 420 feet below ground surface. Shear wave velocity values were measured in the Still Branch, Congaree, and Snapp Formations of the Lower Sand Stratum. These COL data (6 profiles) were combined with two ESP profiles (located in the powerblock area of Units 3 and 4) and averaged. The average shear wave profile for the this COL data set is shown on [Figure 2.5-379](#). This profile also reflects the average stratigraphy within the powerblock excavation footprints based on data from the COL borings. The shear wave velocity profile includes the shear wave velocity profile of the backfill that was developed during the Phase I test pad program. The profile below the COL data (below the upper portion of the Snapp formation)

incorporates the shear wave velocity data from the ESP profile. The COL profile consists of: compacted backfill from 0 to 88 ft, Blue Bluff Marl from 88 to 156 ft, Lower Sand Stratum from 156 to 1,058 ft, and Dunbarton Triassic Basin and Paleozoic Crystalline Rock below 1,058 ft. The ESP profile, shown on [Figure 2.5-378](#), is also illustrated on [Figure 2.5-379](#) for comparison purposes. [Figure 2.5-379](#) illustrates the relationship, including the similarity, between the two data sets. In general, within specific geologic formations, the two profiles demonstrate consistent shear wave velocity characteristics. The profile of the combined data set (COL) in the middle and upper portions of the Blue Bluff Marl is in good agreement with the ESP profile. At the lower portions of the Blue Bluff and in the Lower Sand Stratum, the COL profile exhibits slightly lower shear wave values than the ESP profile.

2.5.4.7.1.2 Rock Shear Wave Velocity Profile

As discussed in [Subsection 2.5.4.2.2](#), the VEGP ESP site sits on over 1,000 feet of Coastal Plain sediments underlain by Triassic Basin sedimentary rock, which in turn is underlain by Paleozoic crystalline rock (see [Figure 2.5-243](#)). For the purpose of subsequent site response analysis, for which input rock time histories must be inserted at a depth where the material shear-wave velocity is approximately 9,200 ft/s, it is necessary to know the shear-wave velocity profile and materials properties for the site down to the depth at which this velocity is encountered. Because the site overlies both Triassic Basin and Paleozoic crystalline rocks, it is necessary to consider effect of shear-wave velocities and material properties of both rock types and their geometries.

As indicated in [Figure 2.5-376](#), the shear-wave velocities measured at the top of the Triassic Basin, even through the weathered portion, do not reach the velocity of 9,200 ft/s. Inspection of available deep borehole shear-wave velocity at SRS ([Reference 596](#)) along with the B-1003 data [[Figure 2.5-380](#)], however, suggests the following character of rock shear-wave in the Triassic Basin:

- A weathered zone of ~200 feet thickness occurs at the top of the Triassic Basin, characterized by a steep shear-wave velocity gradient, where the shear-wave velocity rapidly increases with depth to a point where a relatively high shear-wave velocity, but less than 9,200 ft/s is reached;
- Below the weathered zone the shear-wave velocity increases with a gentler gradient within the unweathered rock;
- Considering the SRS data as a guide for shear-wave velocity within deep portions of the Triassic Basin, there are a range of gentle gradients and a range of shear-wave velocities for the top of the unweathered Triassic Basin that could be considered as a continuation of the site-specific profile presented by B-1003.

[Figure 2.5-244](#) indicates that the non-capable Pen Branch fault separates the Triassic Basin from the Paleozoic crystalline rocks. The structural geometry of these rock units and the fault, relative to the locations of boreholes B-1002 and B-1003 (approximate locations of the proposed nuclear units) and considering the velocity profiles shown in [Figure 2.5-380](#), a shear-wave velocity profile through the Triassic Basin would not likely reach 9,200 ft/s before encountering the Paleozoic crystalline rock. Several observations and studies at SRS [e.g., ([Reference 585](#), [Reference 586](#), [Reference 265](#))] indicate that the shear-wave velocity of the Paleozoic crystalline rock is at least 9,200 ft/s.

Therefore, to represent the variability of the depth at which the Paleozoic crystalline rock is encountered, with a shear-wave velocity of at least 9,200 ft/s, and the uncertainty of the shear-wave velocity gradient and velocity at the top of the unweathered Triassic Basin, six rock shear-wave velocity profiles were considered to comprise the base case used in the seismic amplification/attenuation analysis. [Figure 2.5-378](#) shows a plot of these six rock shear-wave velocity profiles and [Table 2.5-252](#), Part B presents their tabulation.

Figure 2.5-243 and Figure 2.5-380 suggest additional geometries for the shear-wave velocity profiles of the Triassic Basin and the Paleozoic crystalline rock that could impact site response. As interpreted in Figure 2.5-244, further to the northwest of the footprint of the project site the coastal Plain sediments would be underlain immediately by the Paleozoic crystalline rock. Conversely, further to the southeast of the footprint of the project, the Paleozoic crystalline rock is at such a depth that the shear-wave velocity gradient in the Triassic Basin would result in 9,200 ft/s being reached in the shear-wave velocity profile while still within the Triassic Basin. Close inspection of the DRB-9 shear-wave velocity profile in Figure 2.5-380 suggests a low-velocity zone at the bottom of the Triassic Basin at the encountering of the Pen Branch fault. Sensitivity analyses were performed that indicated that alternate shear-wave velocity models suggested by these observations result in insignificant variations in the site response, relative to the six profiles that were explicitly considered, as discussed above.

2.5.4.7.2 Variation of Shear Modulus and Damping with Shear Strain

2.5.4.7.2.1 Shear Modulus

2.5.4.7.2.1.1 ESP Analysis

The variation of soil shear modulus values of sands, gravels, and clays with shear strain is well-documented by researchers such as Seed and Idriss (1970); Seed et al. (1984); and Sun et al. (1988). This research, along with additional work, has been summarized by EPRI (Reference 515).

Shear modulus is derived from the respective unit weight and shear wave velocity of the soil strata with the following equation:

$$G_{\max} = \rho \cdot (V_s)^2 = \gamma \cdot (V_s)^2 / g \quad \text{Equation (20-27) on page 758 of Bowles (1982)}$$

Shear wave velocity data are shown on Table 2.5-251. Unit weight data are shown on Table 2.5-236. Values for shear modulus are tabulated during analysis with the SHAKE 2000 program (Reference 497), and the low strain values are also shown on Table 2.5-238 for the existing soils and rock, and on Table 2.5-249 for the compacted backfill.

From EPRI (Reference 515), the dynamic shear modulus reduction is derived in terms of depth for granular soils (Upper and Lower Sand Strata) and in terms of Plasticity Index (PI) for cohesive soils (Blue Bluff Marl).

The EPRI curves for sands (Reference 515, Figure 7.A-18) were used to derive the shear modulus reduction factors for the granular soil strata (compacted backfill and Lower Sand Stratum). The EPRI curves for clays (Reference 515, Figure 7.A-16) were used to derive the shear modulus reduction factors for the Lisbon Formation using PI = 25 percent. The shear modulus reduction factors are provided in Table 2.5-254 and Figure 2.5-381.

The shear modulus reduction factors developed for the neighboring SRS and contained in Lee (1996) were also used in the analysis. The SRS curves were selected based on their stratigraphic relationship to the Vogtle 3 and 4 site. The SRS curve labeled as Blue Bluff Marl in Table 2.5-256 and on Figure 2.5-383 is based on the Dry Branch Formation and the Santee Formation, the SRS stratigraphic equivalent to the Vogtle Blue Bluff Marl. Degradation curves for the compacted backfill were not developed for SRS. The mean site reduction site amplification factors using EPRI and SRS shear modulus degradation relationships were weighted equally as described in Subsection 2.5.2.5.1.2.1

2.5.4.7.2.1.2 COL Analysis

Site-specific dynamic shear modulus reduction curves were developed from RCTS test results on samples from the Blue Bluff Marl and Lower Sand strata as well as proposed borrow materials for the compacted backfill, taken during the COL investigation. Index testing was also conducted on these samples. Results of index and RCTS testing are included in Attachment G of [Appendix 2.5C](#).

In the Blue Bluff Marl, four relatively undisturbed samples (Pitcher samples) were tested. Two samples disclosed low plasticity indices (PI =26 and 27) while two disclosed high PI values (46 and 69). The shear modulus reduction data was plotted against shearing strain and overlain on the EPRI curves for clay ([Reference 515](#), Figure 7.A-16). The site specific data followed trends consistent with the EPRI relationships for PI. Site specific curves were derived for low PI material and high PI material based on the similarity of the EPRI PI curves.

In the Lower Sand Stratum, five relatively undisturbed samples (Pitcher samples) were tested. Three were identified as sand and two were identified as low plasticity clays. The shear modulus reduction data were plotted against shearing strain and overlain on the EPRI curves for depth for granular soils ([Reference 515](#), Figure 7.A-18). Note that RCTS data for the clayey samples were evaluated against the EPRI curves for clay; however, the damping relationships disclosed in these tests (as discussed later) were not consistent with the EPRI clay relationships. The site specific data followed trends consistent with the EPRI relationships for depth for granular soils. Site specific curves were derived for the sand and the clay materials in the Lower Sand stratum based on the similarity of the EPRI depth curves.

Five bulk samples from test pits in proposed borrow sources were identified for testing. Moisture-density (ASTM D 1557) and index testing were conducted on these samples. The fines content of these samples ranged from about 8 to 25 percent. RCTS tests were conducted on each bulk sample (using the same loading schedule) at two different levels of compaction (95% and 97% or 95% and 100%). The assigned confining pressures for the RCTS testing were determined based on representative depths throughout the proposed 90-ft column of backfill. Test results disclosed little variation based on the level of compaction. The shear modulus reduction data was plotted against shearing strain and overlaid on the EPRI curves for depth for granular soils ([Reference 515](#), Figure 7.A-18). Test results for samples at low confining pressures disclosed similar trends, as did test results for samples at higher confining pressures. The site specific data followed trends consistent with the EPRI relationships for depth for granular soils. Site specific damping curves for borrow material were developed for samples under low confining pressure (depths less than 25 ft) and for samples under higher confining pressures (greater than 25 ft) based on the similarity of the EPRI curves for depth for granular soils.

Site specific shear modulus reduction curves developed from the RCTS testing of COL samples are provided in [Table 2.5-255](#) and [Figure 2.5-382](#). These data were used to evaluate the site response as described in [Subsection 2.5.2.9.3](#)

2.5.4.7.2.2 Damping

2.5.4.7.2.2.1 ESP Analysis

The publications cited above address the variation of soil damping with cyclic shear strain as well as the variation of shear modulus with shear strain.

From EPRI ([Reference 515](#)), the damping ratio is derived in terms of depth for granular soils (Upper and Lower Sand Strata) and in terms of PI for cohesive soils (Blue Bluff Marl).

The EPRI curves for sands (Reference 515, Figure 7.A-19) were used to derive the damping ratios for the granular soil strata (compacted backfill and Lower Sand Stratum). The EPRI curves for clays (Reference 515, Figure 7.A-17) were used to derive the damping ratios for the Lisbon Formation using PI = 25 percent. The damping ratios are provided in Table 2.5-254 and Figure 2.5-384.

The damping ratio values developed for the neighboring SRS and contained in Lee (1996) were also used in the analysis. The SRS curves were selected based on their stratigraphic relationship to the Vogtle 3 and 4 site. The SRS curve labeled as Blue Bluff Marl in Table 2.5-256 and on Figure 2.5-386 is based on the Dry Branch Formation and the Santee Formation, the SRS stratigraphic equivalent to the Vogtle Blue Bluff Marl. Degradation curves for the compacted backfill were not developed for SRS. The mean site reduction site amplification factors using EPRI and SRS shear modulus degradation relationships were weighted equally as described in Subsection 2.5.2.5.1.2.1.

2.5.4.7.2.2.2 COL Analysis

Site-specific damping curves were developed from RCTS test results on samples from the Blue Bluff Marl and Lower Sand strata as well as proposed borrow materials for the compacted backfill, as similarly described in Subsection 2.5.4.7.2.1.2.

The RCTS damping relationships for the Blue Bluff Marl samples were plotted and overlain on the EPRI curves for clay (Reference 515, Figure 7.A-17). The site specific data followed trends consistent with the EPRI damping relationships for PI. Site specific curves were derived for low PI material and high PI material based on the similarity of the EPRI PI curves.

The RCTS damping relationships for the Lower Sand Stratum samples were plotted against shearing strain and overlain on the EPRI curves for depth for granular soils (Reference 515, Figure 7.A-19). The damping relationships for the clayey samples were evaluated against EPRI curves for clay; however, these data disclosed lower damping values at lower shear strains. Instead the RCTS data were more closely aligned with the EPRI relationships with depth for granular soils. The site specific data for both sand and clay samples followed trends consistent with the EPRI relationships for depth for granular soils. Therefore, site specific damping curves were derived for the sand and the clay materials in the Lower Sand stratum based on the similarity of the EPRI curves for depth for granular soils.

The RCTS damping relationships for the proposed borrow sources were plotted against shearing strain and overlain on the EPRI curves for depth for granular soils (EPRI TR-102293 1993, Figure 7.A-19). Test results for samples at low confining pressures disclosed similar trends, as did test results for samples at higher confining pressures. The site specific data followed trends consistent with the EPRI relationships for depth for granular soils. Site specific damping curves for borrow material were developed for samples under low confining pressure (depths less than 25 ft) and for samples under higher confining pressures (greater than 25 ft) based on the similarity of the EPRI curves for depth for granular soils.

Site specific damping curves developed from the RCTS testing of COL samples are provided in Table 2.5-255 and Figure 2.5-385. These data were used to evaluate the site response as described in Subsection 2.5.2.9.3.

After randomization, the damping curves were cut off at 15 percent damping ratio per NUREG-0800, Section 3.7.2 (1996).

2.5.4.7.3 Soil/Rock Column Amplification/Attenuation Analysis

The SHAKE2000 (Reference 497) computer program was used to compute the site dynamic responses for the soil/rock profiles described in Subsection 2.5.4.7.1. The computation was performed in the frequency domain using the complex response method. Subsection 2.5.2.5 describes in detail the soil/rock column amplification/attenuation analysis based on the ESP soil column.

SHAKE2000 uses an equivalent linear procedure to account for the non-linearity of the soil by employing an iterative procedure to obtain values for shear modulus and damping that are compatible with the equivalent uniform strain induced in each sublayer. At the outset of the analysis, a set of properties (based on the values of shear modulus and damping presented in Subsection 2.5.4.7.1, and total unit weight) was assigned to each sublayer of the soil profile. The analysis was conducted using these properties, and the shear strain induced in each sublayer was calculated. The shear modulus and damping ratio for each sublayer was then modified based on the shear modulus and damping ratio versus strain relationships presented in Subsection 2.5.4.7.2. The analysis was repeated until strain-compatible modulus and damping values were achieved.

2.5.4.7.4 Two-Dimensional Effects Site Response Analysis (Bathtub Model)

The model for the site dynamic response analysis as described in Subsection 2.5.2.5 depicted the backfill above the Blue Bluff Marl as a continuum. The model did not account for the extent of the excavation and backfill and any impacts the Upper Sands have on the site response. These impacts were evaluated by considering the site response with the Upper Sands in place and with these materials replaced with backfill. The average shear wave profile of the Upper Sands as developed from the COL data, as shown on Figure 2.5-377, was used to characterize shear wave velocity of the Upper Sands. A discussion of this analysis and results are presented in Subsection 2.5.2.9.2.

2.5.4.7.5 Comparison of ESP vs. COL Soil Column

Subsurface data were collected and evaluated at the site during two distinct phases referred to as the ESP investigation and COL investigation (including the Phase 1 test pad program) as presented in Subsection 2.5.4.3. The ESP investigation was limited in scope and broad in areal coverage; whereas the COL investigation was more focused in coverage (to the power block area) and extensive in scope. Subsurface data, including shear wave velocity, from the ESP investigation were taken from widely spaced borings. One of these boreholes (B-1003) extended through the entire soil column (over 1,000 ft) and into the underlying sedimentary rock of the Triassic Basin. Subsurface data from VEGP Units 1 and 2 and other regional sources were also evaluated. Soil non-linearity curves obtained from EPRI and the nearby Savannah River Site (SRS) were assigned based on soil type and depth. The resulting ESP soil column was used in the amplification/attenuation analysis in Subsection 2.5.2.5.

The COL investigation provided numerous additional subsurface data specific to the powerblock areas of Units 3 and 4. The COL investigation was taken to exploration depths of 420 ft. ESP data taken within the powerblock areas were compiled with the COL data to develop the COL soil column. These data included averaged shear wave velocities, averaged strata thicknesses and densities. A thick clay layer (approximately 70 ft) encountered in the Lower Sands, as discussed in Subsection 2.5.4.2.2.3, was incorporated into the COL soil column as shown on Figure 2.5-379. Site specific soil non-linearity curves for the various strata, including the clay soils in the Lower Sands, were developed from RCTS testing of representative COL samples and are included in the COL soil column. These data were discussed in Subsection 2.5.4.7.2 and are presented in Figures 2.5-382 (G/Gmax curves) and 2.5-385 (damping ratio curves). Site specific dynamic properties of the

compacted backfill were developed during the COL laboratory testing program and the Phase 1 test pad program and are included in the COL soil column.

The stratification and shear wave velocity profiles for the ESP and COL soil columns are presented in [Figure 2.5-379](#). The offset in soil stratification between the soil columns reflects refinements due to the additional data collected during the COL investigation. The stratification of the ESP soil column is based on the deep boring, B-1003. The stratification of the COL soil column is based on numerous additional borings in the power block areas. The data disclosed thicker near surface strata as compared with boring B-1003. No additional stratification or shear wave velocity data below the top of the Snapp Formation in the Lower Sands were collected during the COL investigation; therefore, the COL soil column stratification and shear wave velocity profiles between the Snapp Formation and the top of the Triassic Basin bedrock were carried over from the ESP soil column with the same strata thicknesses but slightly shifted in depth to match the thicker near surface strata. Comparison of the two shear wave velocity profiles indicates good agreement between the data sets. Trends within the strata are consistent.

Comparisons of the soil non-linearity curves used for ESP and COL are presented in the attached [Figures 2.5-392 through 2.5-397](#). [Figures 2.5-392, 2.5-393, and 2.5-394](#) illustrate the normalized shear modulus vs. shear strain curves for compacted backfill, Blue Bluff Marl, and Lower Sands, respectively. [Figures 2.5-395, 2.5-396, and 2.5-397](#) illustrate the soil damping vs. shear strain curves for the same strata. The figures include both the site specific curves developed during the COL investigation and the EPRI and SRS model curves assigned during the ESP investigation. The COL site specific data for the Lower Sands includes non-linearity curves for both sand and clay materials in this stratum. Generally the figures suggest that the subsurface soils behave more linearly (provide a smaller reduction in shear modulus and less damping) than the models used for the ESP investigation.

The COL soil column, including shear wave velocity and site specific non-linearity relationships as described here, was used in the site response sensitivity analysis to evaluate the effects of the COL data with the ESP data as described in [Subsection 2.5.2.9.3](#).

2.5.4.7.6 MSE Backfill Shear Wave Velocity Profile

As discussed in [Subsection 2.5.4.5.7](#), an MSE wall is planned to facilitate construction of the Nuclear Island. This wall, as shown on [Figure 2.5-390](#), will be founded at the NI foundation level and will consist of wall facing panels and tensile elements embedded in the backfill behind the wall face. During construction, the backfill immediately behind the wall face, for a distance of about 5 feet, will likely be compacted with smaller, potentially hand-operated, compactors and in thinner lifts to achieve the compaction criteria of at least 95 percent of the maximum dry density modified Proctor value (ASTM D 1557). Beyond this wall face zone, the backfill will be compacted as part of the mass earthwork operation utilizing larger self-propelled compaction equipment. Owing to the likely different compaction procedures and the presence of the MSE wall face, the shear wave velocity profile of the backfill in the 5 ft wall face zone may be reduced. To investigate the effect of this possibility, a reduced velocity profile for the full height of the wall (MSE best estimate) was used in a soil structure interaction analysis, as presented in [Appendix 2.5E](#). The results show that there are no differences in the seismic structural responses from the potentially reduced shear wave velocity profile behind the MSE wall.

2.5.4.8 Liquefaction Potential

The AP1000 design has not been evaluated for a site where there is a liquefaction potential of the soil below the nuclear island.

Soil liquefaction is a process by which loose, saturated, granular deposits lose a significant portion of their shear strength due to pore pressure buildup resulting from cyclic loading, such as that caused by an earthquake. Soil liquefaction occurrence (or lack thereof) depends on geologic age, state of soil saturation, density, gradation, plasticity, and earthquake intensity and duration. Soil liquefaction can occur, leading to foundation bearing failures and excessive settlements, when all of the following criteria are met:

1. Design ground acceleration is high.
2. Soil is saturated (i.e., close to or below the water table).
3. Site soils are sands or silty sands in a loose or medium dense condition.

The naturally occurring Upper Sand Stratum soils at the VEGP site meet these three criteria. These soils consist of sands with varying fines content. An approximate 30-ft depth of the Upper Sand Stratum occurs beneath the groundwater table at a depth of 60 ft beneath the ground surface. The average corrected SPT N-value within the Upper Sand Stratum was 25 bpf, indicating a medium dense condition. The underlying Blue Bluff Marl soils are significantly cohesive; although some seams of coarse-grained materials are present. The Lower Sand Stratum is sufficiently dense and deep. Liquefaction is not a concern within these strata; although the liquefaction potential of the coarse-grained materials in the Blue Bluff Marl will be discussed. The liquefaction potential of the Upper Sand Stratum will also be discussed.

During construction of VEGP Units 1 and 2, the entire portion of the Upper Sand Stratum was removed and replaced with engineered fills due to susceptibility to liquefaction. A similar excavation will be executed for VEGP Units 3 and 4.

Regulatory Guide 1.198, *Procedures and Criteria for Assessing Seismic Soil Liquefaction at Nuclear Power Plant Sites*, US Nuclear Regulatory Commission, November 2003 (RG 1.198) is used as a guide for liquefaction analysis presented herein.

2.5.4.8.1 Acceptable Factor of Safety Against Liquefaction

RG 1.198 states that factors of safety (FS) ≤ 1.1 against liquefaction are considered low, FS ≈ 1.1 to 1.4 are considered moderate, and FS ≥ 1.4 are considered high. The Committee of Earthquake Engineering of the National Research Council (NRC/NAP 1985) states:

There is no general agreement on the appropriate margin (factor) of safety, primarily because the degree of conservatism thought desirable at this point depends upon the extent of the conservatism already introduced in assigning the design earthquake. If the design earthquake ground motion is regarded as reasonable, a safety factor of 1.33 to 1.35...is suggested as adequate. However, when the design ground motion is excessively conservative, engineers are content with a safety factor only slightly in excess of unity.

2.5.4.8.2 Previous Liquefaction Analyses

The liquefaction potential of the Upper Sand Stratum was previously evaluated using the standard penetration test blow counts obtained during the investigations for VEGP Units 1 and 2 and the simplified procedure of Seed and Idriss. This evaluation indicated that the Upper Sand Stratum below the groundwater table was susceptible to liquefaction when subjected to the maximum SSE acceleration of 0.2g developed for VEGP Units 1 and 2. Based on this evaluation, the Upper Sand Stratum was removed to an approximate elevation of 130 to 135 ft in the VEGP Units 1 and 2 power block area. Select sand and silty sand compacted to 97 percent of the maximum density determined by ASTM D 1557 was placed from the top of the Blue Bluff Marl stratum to the design elevation of the

various power block structures with the exception of an area north of the turbine building. The liquefaction potential of compacted backfill in the power block area was evaluated, and the analysis indicated a factor of safety against liquefaction on the order of 1.9 to 2.0. The analysis was done utilizing cyclic strength data (PSAR data) obtained from tests on specimens of compacted backfill.

During the investigations for borrow sources for VEGP Units 1 and 2, additional dynamic data (borrow source data) were obtained to supplement the cyclic strength data for the compacted fill. Cyclic triaxial tests were performed on compacted specimens of sands obtained from stockpiles and borrow areas. The cyclic stress ratios versus the number of cycles to 2.5 percent total strain (initial liquefaction) showed that the stress ratios for the cleaner sands were substantially lower than for silty sands. In the liquefaction analysis performed using the PSAR data, stress ratios for the cleaner sands were used to obtain the safety factor against liquefaction. Therefore, the cyclic stress ratios for the cleaner sands obtained during investigations for borrow material were compared with values obtained during the PSAR investigations. A comparison of the two test data (PSAR data versus borrow source data) indicates that the PSAR data represent a lower bound of test values. If the liquefaction analysis were performed using the upper bound values (borrow source data), a factor of safety higher than 1.9 to 2.0 would have been obtained for the design SSE conditions.

From the discussion presented above for the VEGP Units 1 and 2, it is concluded that there exists an adequate factor of safety against liquefaction for the compacted backfill.

2.5.4.8.3 Liquefaction Analyses Performed for the ESP Application

2.5.4.8.3.1 Liquefaction Analyses of the Upper Sands

Based on previous investigations and excavation completed for the existing VEGP Units 1 and 2 and their proximity to proposed VEGP Units 3 and 4, the Upper Sand Stratum will be completely removed and replaced with select compacted non-liquefiable fills back to the plant grade within the footprint of the planned power block.

Because select compacted non-liquefiable fills will be used to replace the Upper Sand Stratum in the power block area of proposed VEGP Units 3 and 4, no liquefaction study was performed for this ESP investigation.

2.5.4.8.3.2 Liquefaction Analyses of the Blue Bluff Marl

The Blue Bluff Marl is identified as a cemented, overconsolidated, calcareous fine-grained material (silt and clay), and thus exhibits high factor of safety against liquefaction. However, some lenses of silty fine sand were encountered during the COL investigation. Due to the presence of these materials, a review of the liquefaction potential of the Blue Bluff Marl is presented in the following paragraphs.

The present state-of-the-art considers an evaluation of data from SPT, CPT, and shear wave velocity (V_s) measurements, with the method employing SPT measurements being the most well-developed and well-recognized. Initially, a measure of the stress imparted to the soils by the ground motion is calculated, referred to as the cyclic stress ratio (CSR). Then, a measure of the resistance of soils to the ground motion is calculated, referred to as the cyclic resistance ratio (CRR). And finally, a factor of safety (FOS) against liquefaction is calculated as the ratio of the resisting stress, CRR, to the driving stress, CSR. Details of the liquefaction methodology and the relationships for calculating CSR, CRR, FOS, and other intermediate parameters such as the stress reduction coefficient (r_d), the magnitude scaling factor (MSF), the K_σ correction factor accounting for liquefaction resistance with increasing confining pressure, and a host of other correction factors, can be found in (Reference 606). A MSF of 1.11 was used in the analyses, based on the selected earthquake magnitude. A review of the results of liquefaction potential analyses

using the available SPT and Vs data (CPT data was unavailable) for the Blue Bluff Marl in the power block are of Units 3 and 4 follows.

2.5.4.8.3.2.1 Liquefaction Potential Based on SPT Data

SPT N_{60} -values versus elevation are presented on [Figure 2.5-391](#) for the 70 borings taken in the power block area of Units 3 and 4 for the COL investigation. With the assumption of clean sand (i.e., fines content, FS = 5%), the results show that most of the coarse-grained soil samples have corrected SPT blow counts, N_1 or $(N_1)_{60}$, greater than 30, indicating non-liquefiable. Among eight of the soil soils that are analyzed, only three of them are potentially liquefiable, with calculated factors of safety (FS) against liquefaction 1.43, 1.75, and 2.19. In all cases, the FS against liquefaction in the Blue Bluff Marl was greater than 1.1.

2.5.4.8.3.2.2 Liquefaction Potential Based on Shear Wave Velocity Data

Shear wave velocity (V_s) data measured in the Blue Bluff Marl by P-S logging in six borings taken in the power block for the COL investigation were evaluated for liquefaction potential. The shear wave velocity values were corrected for overburden (V_{s1}) following recommendations in ([Reference 606](#)). The calculated V_{s1} values ranged from 253 meters/second to 508 m/s. The relationship between V_{s1} , CRR, and liquefaction potential presented by ([Reference 606](#)), suggests that the Blue Bluff Marl is non-liquefiable based these calculated values.

2.5.4.8.3.3 Liquefaction Analyses of the Compacted Backfill

The backfill will be compacted to a minimum of 95 percent of the maximum dry density as determined by ASTM D 1557. The Phase I test pad program ([Appendix 2.5D](#)) was conducted to evaluate backfill properties. Borrow sources and quantities have been identified as summarized in [Subsection 2.5.4.5.3](#). Field and laboratory testing was conducted on these materials. Results from the testing of borrow sources and the test pad program including measured N -values and shear wave velocities are consistent with the results from Units 1 and 2. Figure 16 of [Appendix 2.5D](#) provides a plot of $N_{1(60)}$ vs depth and demonstrates an average $N_{1(60)}$ value (below a depth of 2 feet) equal to or greater than 40 bpf. In addition, the shear wave velocity profile for the backfill, as presented in [Table 2.5-250](#), demonstrates a shear wave velocity greater than 1,000 fps below a depth of 30 feet. Therefore, as determined for Units 1 and 2 and presented in [Subsection 2.5.4.8.2](#) for the design basis earthquake, liquefaction is not a concern.

2.5.4.8.4 Liquefaction Conclusions

Based on the foregoing sections on the analysis of liquefaction potential, the following conclusions are made:

- Only the Upper Sand Stratum below the groundwater table falls into the gradation and relative density categories where liquefaction would be considered possible.
- The Upper Sand Stratum was completely removed and replaced with compacted structural fill before construction of the existing VEGP Units 1 and 2. The same approach will be used before construction of the proposed VEGP Units 3 and 4.
- The liquefaction potential of the compacted structural fill, consisting of materials and methods similar to VEGP Units 1 and 2 is not a concern.
- The Blue Bluff Marl is primarily cohesive but has some lenses of coarse-grained materials. These materials were found to have an adequate factor of safety against liquefaction (greater than 1.1).

2.5.4.9 Earthquake Design Basis

The site ground motion response spectra (GMRS) is derived and discussed in detail in [Subsection 2.5.2.6](#). The Operating Basis Earthquake (OBE) is discussed in [Subsection 2.5.2.8](#).

2.5.4.10 Static Stability

All safety-related structures will be founded on the structural backfill that will be placed on top of the Blue Bluff Marl after complete removal of the Upper Sand Stratum. The base of the Containment and Auxiliary Building foundations for VEGP Units 3 and 4 will be about El. 180 ft msl. This level corresponds to a depth of 40 ft below final grade (below El. 220 ft msl), or 50 to 60 ft above the top of the Blue Bluff Marl bearing stratum based on the borings completed during the ESP and COL subsurface investigations. Other foundations in the power block area will be placed at depths of about 4 ft below final grade. The following sections on bearing capacity and settlement focus on these two scenarios.

Based on the results of the ESP and COL investigations and the Phase I test pad program, the soils supporting the NIs do not exhibit extreme variations in subgrade stiffness and the site can be considered uniform according to ([Reference 603](#)). As presented in [Subsection 2.5.4.2.2.2](#), the subsurface data disclosed a nearly even top of Blue Bluff Marl (varying from El. 122 ft to El. 140 ft over the length of the excavation footprints) with relatively uniform thickness and consistent engineering properties. The earthwork specification for the compacted backfill will be developed after the completion of the Phase II test pad program which is expected to finalize the placement procedures and material types. The Phase I test pad program considered materials and placement procedures consistent with Units 1 and 2. Test results disclosed consistent engineering properties including density, shear wave velocity, and N-values as presented in [Subsection 2.5.4.5.3](#).

A coefficient of friction of 0.45 against concrete can be expected for the sand and silty sand compacted backfill material. A site-specific stability evaluation was conducted by Westinghouse. Results are presented in [Appendix 2.5E](#).

2.5.4.10.1 Bearing Capacity

The maximum bearing reaction determined from the 3D SASSI analyses described in Appendix 3G is less than 35,000 lb/ft² under all combined loads, including the safe shutdown earthquake. The maximum dynamic bearing demand of 35 ksf occurs under the west edge of the shield building and is primarily due to the response to the east-west component of the earthquake. The east edge of the nuclear island lifts off the soil. The Combined License applicant will verify that the site-specific allowable soil bearing capacities for static and dynamic loads at the site will exceed the static and dynamic bearing demand given in [Table 2.0-201](#).

The evaluation of the allowable capacity of the soil is based on the properties of the underlying materials, including appropriate laboratory test data to evaluate strength, and considering local site effects, such as fracture spacing, variability in properties, and evidence of shear zones. The allowable bearing capacity should provide a factor of safety appropriate for the design load combination, including safe shutdown earthquake loads.

If the shear wave velocity or the allowable bearing capacity is outside the range evaluated for AP1000 design certification, a site-specific evaluation can be performed using the AP1000 basemat model and methodology described in subsection 3.8.5. The safe shutdown earthquake loads are those from the AP1000 analyses described therein. Alternatively, bearing pressures may be determined from a site-specific analysis using site-specific inputs. For the site to be acceptable, the

bearing pressures from the site-specific analyses, including static and dynamic loads, need to be less than the capacity of each portion of the basemat.

All structures in the power block footprint will be founded on the structural backfill compacted to a minimum of 95% (ASTM D 1557) as presented in [Subsection 2.5.4.5](#). The structural backfill will be about 90 ft thick in the power block area. The Nuclear Island will be founded at a depth of about 40 ft below grade (about 50 ft of structural backfill beneath the foundations). Other structures will be founded at an approximate depth of 4 ft below grade. The allowable static bearing capacity values are calculated with Terzaghi's bearing capacity equations. An internal angle of friction of 36° was used for the compacted backfill as developed from field and laboratory testing of borrow materials during the Phase I test pad program ([Appendix 2.5D](#)) and the COL investigation ([Appendix 2.5C](#)). The influence of the Blue Bluff Marl on the allowable bearing pressure was evaluated using procedures outlined by Vesic (1975). With a factor of safety of 3.0 (ASCE 1994), site conditions provide an allowable bearing pressure of 34 ksf under static loading conditions for the Nuclear Island, which is greater than the required 8.6 ksf (WEC CCC-004). An internal friction angle of 34° was used to calculate the allowable bearing capacity values for foundations placed on compacted fills at depths of about 4 ft below finished grade as provided in [Figure 2.5-387](#).

The allowable bearing capacity of the structural backfill under the Nuclear Island for dynamic loading conditions was also evaluated using Terzaghi's bearing capacity equation for local shear (Peck et al. 1974) and Soubra's method with seismic bearing capacity factors ([Reference 595](#)) using Terzaghi's bearing capacity equation for general shear with an internal friction angle of 36°. To simulate the potential for higher edge pressures during dynamic loading, three foundation widths were considered (10, 25, and 50 ft) corresponding to 10, 25, and 50 percent of the width of the Nuclear Island basemat. The results from these two methods compared well, with Terzaghi's approach for local shear providing more conservative values. The computed average ultimate capacities of the three widths (10, 25, and 50 ft) were 89, 100, and 119 ksf, respectively. A width of 25 ft and a factor of safety of 2.25 (ASCE 1994) were used for site specific conditions providing an allowable bearing pressure greater than 42 ksf under dynamic loading conditions for the Nuclear Island. This value is greater than the required 35 ksf for dynamic bearing (WEC SC2-065) as well as the Vogtle site specific maximum dynamic demand (for the ESP soil profile as described in [Appendix 2.5E](#)) of 18 ksf.

The bearing capacity of the structural backfill was also evaluated in terms of the ratio of the ultimate bearing capacity to the structure demand. This capacity over demand (C/D) ratio provides an alternative measure of the margin of safety against bearing failure. These C/D ratios were evaluated for the static and dynamic demand conditions as provided by Westinghouse (WEC CCC-004 and WEC SCE-065), as well as the maximum dynamic demand from the Vogtle site specific seismic evaluation ([Appendix 2.5E](#)). The results are given below:

Condition	Static	Dynamic	Site-Specific Dynamic
Ultimate Capacity (C), ksf	102	100 ^a	100 ^a
Demand (D), ksf	8.6 ^b	35 ^c	18 ^d
C/D	11.9	2.9	5.6
a. Based on a reduced foundation width of 25 feet to account for higher edge pressures during a seismic event. b. APP-1000-CCC-004, Rev. 0, Nuclear Island - Stability Evaluation. c. APP-1000-S2C-065, Rev. 0, Nuclear Island Stick Model Analysis at Soil Sites. d. Based on analysis using ESP profile in Appendix 2.5E .			

The C/D ratios are higher than those typically used for standard practice. While these results do not take into account settlement of the structures, the significant margin suggests that settlements will be minimal and within the design requirements (WEC SC2-065). A further discussion of settlement is provided in [Subsection 2.5.4.10.2](#).

The results of settlement analyses are presented in [Subsection 2.5.4.10.2](#).

2.5.4.10.2 Settlement Analysis

The AP1000 does not rely on structures, systems, or components located outside the nuclear island to provide safety-related functions. Differential settlement between the nuclear island foundation and the foundations of adjacent buildings does not have an adverse effect on the safety-related functions of structures, systems, and components. Differential settlement under the nuclear island foundation could cause the basemat and buildings to tilt. Much of this settlement occurs during civil construction prior to final installation of the equipment. Differential settlement of a few inches across the width of the nuclear island would not have an adverse effect on the safety-related functions of structures, systems, and components. [Table 2.5-1](#) provides guidance to the Combined License applicant on predictions of absolute and differential settlement that are acceptable without further evaluation. The predicted settlements will cover the periods before construction begins through the construction phase, and for the subsequent plant operating period or otherwise justified. The predicted settlements will be based on conservative assumptions of soil properties. If the predicted settlements exceed the limits of [Table 2.5-1](#), a detailed evaluation and construction plan will be described by the Combined License applicant. During construction and plant operation at a soil site, settlements would be measured and compared to the predicted settlement values and any exceedances would require additional investigation.

Alternatives for the additional evaluations are provided as follows:

1. Evaluate the impact of the elevated estimated settlement values on the critical components of the AP1000 including, but not limited to, piping spanning between the nuclear island and the adjacent structures, the equipment support pads, the construction gap between the nuclear island and adjacent buildings, and the stresses on the basemat (along with influences to the underlying soil).
2. Submit a construction sequence to control the predicted settlement behavior. A revised sequence should follow the specific schedule to distribute construction loads as necessary in order to obtain acceptable values. Depending on soil conditions, a significant amount of the settlement could occur during construction and can be controlled through the construction sequence.
3. Provide a uniform excavation and engineered backfill to manage static building rotation and differential settlement between the nuclear island and adjacent structures.
4. Implement an active settlement monitoring system throughout the entire construction sequence as well as a long-term (plant operation) plan. By monitoring the settlement throughout construction, the Combined License applicant will be able to modify the construction sequences of adjacent buildings to conform to the site's settlement characteristics and minimize differential settlement. For soil sites, the potential heave or rebound of the excavation bottom, the effect of dewatering, and the effect of foundation loading during construction should be monitored by the Combined License applicant. The monitoring system shall consist of three primary elements as follows:

- Piezometers to measure pore pressures in a soil layer prone to consolidation type settlement. Vibrating wire piezometers are preferred for this purpose because they are adequately sensitive and responsive and easily record positive and negative changes on a real time basis.
- Settlement monuments placed directly on concrete, preferably on the mudmat for early construction monitoring and on the corners of the structures at grade once the mudmat monuments have been covered by backfill to be used for long-term monitoring. Monuments at grade are to be accessible with conventional surveying equipment.
- Settlement telltales if monuments are not practical or if fills are used over consolidation type soils and it is necessary to monitor settlement of the consolidation type in-situ soils independent of the consolidation of the engineered fill soil. Most soil sites will not need this particular form of monitoring.

Develop graphs and plots of the field measurements to:

- Show movement (settlement or heave) versus time.
- Estimate construction loads versus time.
- Measure ground water levels from the dewatering activities versus time.

This data should be maintained during construction and post-construction as needed depending on the field measurement results.

For the large mat foundations that support the major power plant structures, general considerations based on previous site experience (Reference 582) indicate that the total settlement can exceed the suggested limit of 2 in. encountered in the geotechnical literature (Peck et al. 1974). Settlement monitoring of VEGP Units 1 and 2 (Reference 582) disclosed foundation settlements ranging from 2.7 to 3.2 in. for the containment buildings, versus calculated/design values of 4.0 to 4.3 in. Similar results were obtained for the control building (measured settlements ranging from 1.1 to 1.9 inches versus calculated/design values of 3.2 to 3.4 in.), auxiliary building (measured settlements ranging from 2.9 to 3.3 in. versus calculated/design values of 4.4 to 4.6 in.), and the NSCW towers (measured settlements ranging from 2.5 to 3.6 in. versus calculated/design values of 4.5 to 4.8 in.). The ratio of measured to predicted settlement for these structures ranged from less than 0.5 to about 0.75, indicating that the subsurface soils were generally stiffer than anticipated.

Similarly, the measured differential settlements between mats of Units 1 and 2 (Reference 582), which can affect pipe connections, was generally within the suggested limit of $\frac{3}{4}$ in. encountered in the geotechnical literature (Reference 590). The measured differential settlements within structures of Units 1 and 2 were smaller than the design limit of $\frac{1}{670}$ (Reference 582).

It is noted that settlements reported for Units 1 and 2 (Reference 582) were essentially elastic, i.e., they took place during construction. This reflects the elastic nature of the compacted backfill, the heavily overconsolidated Blue Bluff Marl, and the underlying Lower Sand Stratum.

For footings that support smaller plant components, the total settlement can be limited to 1 inch, while the differential settlement between footings can be limited to $\frac{1}{2}$ in. (Reference 590).

The general approach used for Units 1 and 2 consisted of estimating total and differential settlements for powerblock structures and using them as design values. A detailed settlement monitoring program was established, and measured settlements were compared with the design values. Re-analysis and/or corrective measures were employed if measured settlements exceeded design

or trigger values. An additional strategy consisted of installing pipes as late in the construction schedule as practicable and installing pipe supports only when construction of the structure that the pipe was connected to was essentially complete.

Laboratory consolidation tests were conducted on relatively undisturbed samples from the Blue Bluff Marl and the Lower Sand strata collected during the COL investigation. These results are included in [Appendix 2.5C](#), and they confirm the elastic behavior and very stiff and dense nature of the Blue Bluff Marl and Lower Sand strata. A test fill program has been performed (Subsection 2.5.4.5.8) to assess properties of compacted backfill. The results confirm the very dense nature, similar to Units 1 and 2, of the fill and the expected performance under load.

A detailed settlement analysis was performed at the VEGP Early Site Permit Application phase for Units 3 and 4 utilizing similar elastic properties used for the analysis of Units 1 and 2. The analysis incorporated excavation, dewatering, and a timeline of construction to estimate, as much as practical, mat displacement time histories. The results showed that for the assumed loads, predicted total settlements range from about 2 to 3 inches, with a tilt of approximately $\frac{1}{4}$ inch in 50 feet, and a differential settlement between structures of less than 1 inch ([Reference 599](#)). In addition, predicted heave due to foundation excavation ranges from about 1 to 2 $\frac{1}{2}$ inches ([Reference 599](#)). As expected, the results were similar to movements measured for Units 1 and 2.

A subsequent analysis was performed to address changes to the construction sequence in [Subsection 3.8.5.4.2](#) ([Reference 607](#)). This analysis concluded that settlement is within the requirements of [Table 2.5-1](#).

2.5.4.10.2.1 Displacement Monitoring

An instrumentation plan will be developed to monitor heave in the subsurface soils due to excavation, change in pore pressures due to excavation and dewatering, and settlement due to construction of the structures. The detailed plan to be developed will include displacement monitoring at depth in order to estimate and confirm moduli of the subsurface soils. Estimates of unloading (excavation) and loading will be made to correlate movement with load and to update the movement time histories discussed in [Subsection 2.5.4.10.2](#).

The instrumentation will be monitored on a regular basis and will include conventional survey, electronic instrumentation, and where practical, remote telemetry. Particular emphasis will be placed on differential movement and tilt of the structures.

2.5.4.10.3 Lateral Earth Pressure

The development of lateral earth pressures, static and dynamic (seismic), against the below-grade walls of safety-related structures is expected to be minimized with the construction of the mechanically stabilized earth (MSE) walls. As described in [Subsection 2.5.4.5.7](#), the MSE walls are constructed adjacent to the Nuclear Island (NI) to facilitate the placement of backfill in the powerblock excavation. This bottom-up construction occurs prior to construction of the NI, and the MSE walls serve as the outside form for the NI below-grade walls. Although the MSE walls are expected to relieve much of the static lateral earth pressures exerted on the below-grade walls, over time these pressures may be transferred to the below-grade structure. Thus, the evaluation of site-specific lateral earth pressures for safety-related structures does not consider any influence from the MSE walls and full at-rest lateral earth pressures are assumed.

Site-specific static lateral earth pressures, assuming frictionless vertical walls and horizontally placed backfill, are evaluated using Rankine's theory for active, at-rest, and passive conditions ([Reference 201](#)). The earth pressure coefficients, $k_a = 0.26$, $k_o = 0.4$, and $k_p = 3.9$ are based on a

drained friction angle of 36 degrees for the compacted structural fill as presented in [Table 2.5-237](#). The at-rest earth pressure coefficient, k_o , for the compacted structural fill against the NI below grade walls is conservatively taken as 0.5.

The evaluation of site-specific lateral earth pressures includes the influence from surcharges. A vertical areal surcharge of 2,500 psf is used. This pressure conservatively represents construction loading prior to construction of adjacent buildings and subsequent adjacent permanent building loads. The vertical areal surcharge of 2,500 psf equates to a lateral surcharge pressure of 1,250 psf, which exceeds the AP1000 maximum lateral static plus dynamic design surcharge pressures.

Close-in compaction (behind the MSE wall) with a heavy vibratory roller is also considered. Lateral earth pressures increase as a result of compaction. These pressures are controlled at the construction stage by limiting the size of compaction equipment and its proximity to the walls. The influence of compaction was evaluated based on the characteristics of the vibratory compactor used for the Phase 1 Test Pad program ([Appendix 2.5D](#)). Compaction induced lateral earth pressures under at-rest conditions were evaluated using procedures developed by Duncan, et. al. ([Reference 203](#)). The inclusion of compaction-induced pressures is conservative given that these pressures will be exerted on the MSE wall prior to construction of the below-grade NI walls.

Site-specific seismic lateral earth pressures are evaluated for at-rest conditions using ASCE 4-98 ([Reference 202](#)). The site-specific ground acceleration at a frequency of 100 hertz for the Vogtle 3 and 4 site is taken as 0.266g ([Subsection 2.5.2.6](#), [Table 2.5-233](#) and [Figure 2.5-307](#)).

Hydrostatic pressures, attributed to the groundwater level, exert lateral pressure on below-grade structures. At the VEGP Units 3 and 4 site, in the power block areas, the design groundwater elevation of 165 ft msl, as noted in [Subsection 2.4.12](#), is about 15 feet below the NI basemat elevation of approximately 180 ft msl. The post construction water level, as identified in [Appendix 2.4B](#), will also be well below the basemat elevation. Since the groundwater level is located well below the basemat, hydrostatic forces will not be exerted on the below-grade walls and hydrostatic pressures are not considered in the site-specific evaluation of lateral earth pressure for the NI.

In summary, [Figure 2.5-201](#) presents the site-specific total at-rest lateral earth pressures for the below grade NI rigid walls. This diagram was developed assuming level ground surface, a post construction groundwater level below the basemat elevation (no hydrostatic pressure), an areal surcharge pressure of 2,500 psf, and compaction-induced pressure increases. [Figure 2.5-202](#) presents the comparison of the site-specific total at-rest lateral earth pressure distribution compared to the AP1000 DCD design envelope in both the N-S and E-W directions. In both cases, the site-specific at-rest earth pressure is enveloped by the DCD design earth pressure envelopes by significant margins.

2.5.4.11 Design Criteria

Applicable geotechnical-related design criteria are discussed in various sections and are summarized below.

[Subsection 2.5.4.8](#) specifies that the acceptable factor of safety against liquefaction of site soils should be ≥ 1.1 in accordance with Regulatory Guide 1.198.

Bearing capacity criteria are presented in [Subsection 2.5.4.10](#). A minimum factor of safety of 3 is used when applying bearing capacity equations. This factor of safety is also applied against breakout failure due to uplift forces on buried piping. For soils, this factor of safety can be reduced to 2.25 when dynamic or transient loading conditions apply ([Reference 566](#)).

Subsection 2.5.5.2 specifies that the minimum acceptable long-term static factor of safety against slope stability failure is 1.5 and that the minimum acceptable long-term seismic factor of safety against slope stability failure is 1.1 (**Reference 601**).

Appendix 2.5E describes the site-specific analyses that have been performed to show the acceptability of the AP1000 plant at the Vogtle site.

2.5.4.12 Techniques to Improve Subsurface Conditions

For the ESP investigation, ground improvement techniques were not considered beyond the removal and replacement of the Upper Sand Stratum. Likewise, no additional ground improvement methods are being considered based on the COL investigation. The Phase I test pad program (**Appendix 2.5D**) presents the field and test results of the materials and methods that are currently planned for the backfill to replace the Upper Sand Stratum. For areas outside the power block excavation, surficial ground can be improved through densification with heavy vibratory rollers. Other ground improvement methods and the use of piles will be considered as warranted.

The development of lateral earth pressures, static and dynamic (seismic), against the below-grade walls of safety-related structures is expected to be minimized with the construction of the mechanically stabilized earth (MSE) walls. As described in **Subsection 2.5.4.5.7**, the MSE walls are constructed adjacent to the Nuclear Island (NI) to facilitate the placement of backfill in the powerblock excavation. This bottom-up construction occurs prior to construction of the NI, and the MSE walls serve as the outside form for the NI below-grade walls. Although the MSE walls are expected to relieve much of the static lateral earth pressures exerted on the below-grade walls, over time these pressures may be transferred to the below-grade structure. Thus, the evaluation of site-specific lateral earth pressures for safety-related structures does not consider any influence from the MSE walls and full at-rest lateral earth pressures are assumed.

Site-specific static lateral earth pressures, assuming frictionless vertical walls and horizontally placed backfill, are evaluated using Rankine's theory for active, at-rest, and passive conditions (**Reference 201**). The earth pressure coefficients, $k_a = 0.26$, $k_o = 0.4$, and $k_p = 3.9$ are based on a drained friction angle of 36 degrees for the compacted structural fill as presented in **Table 2.5-237**. The at-rest earth pressure coefficient, k_o , for the compacted structural fill against the NI below grade walls is conservatively taken as 0.5.

The evaluation of site-specific lateral earth pressures includes the influence from surcharges. A vertical areal surcharge of 2,500 psf is used. This pressure conservatively represents construction loading prior to construction of adjacent buildings and subsequent adjacent permanent building loads. The vertical areal surcharge of 2,500 psf equates to a lateral surcharge pressure of 1,250 psf, which exceeds the AP1000 maximum lateral static plus dynamic design surcharge pressures.

Close-in compaction (behind the MSE wall) with a heavy vibratory roller is also considered. Lateral earth pressures increase as a result of compaction. These pressures are controlled at the construction stage by limiting the size of compaction equipment and its proximity to the walls. The influence of compaction was evaluated based on the characteristics of the vibratory compactor used for the Phase 1 Test Pad program (**Appendix 2.5D**). Compaction induced lateral earth pressures under at-rest conditions were evaluated using procedures developed by Duncan, et. al. (**Reference 203**). The inclusion of compaction-induced pressures is conservative given that these pressures will be exerted on the MSE wall prior to construction of the below-grade NI walls.

Site-specific seismic lateral earth pressures are evaluated for at-rest conditions using ASCE 4-98 (**Reference 202**). The site-specific ground acceleration at a frequency of 100 hertz for the Vogtle 3 and 4 site is taken as 0.266g (**Subsection 2.5.2.6**, **Table 2.5-233** and **Figure 2.5-310**).

Hydrostatic pressures, attributed to the groundwater level, exert lateral pressure on below-grade structures. At the VEGP Units 3 and 4 site, in the power block areas, the design groundwater elevation of 165 ft msl, as noted in [Subsection 2.4.12](#), is about 15 feet below the NI basemat elevation of approximately 180 ft msl. The post construction water level, as identified in [Appendix 2.4B](#), will also be well below the basemat elevation. Since the groundwater level is located well below the basemat, hydrostatic forces will not be exerted on the below-grade walls and hydrostatic pressures are not considered in the site-specific evaluation of lateral earth pressure for the NI.

In summary, [Figure 2.5-201](#) presents the site-specific total at-rest lateral earth pressures for the below grade NI rigid walls. This diagram was developed assuming level ground surface, a post construction groundwater level below the basemat elevation (no hydrostatic pressure), an areal surcharge pressure of 2,500 psf, and compaction-induced pressure increases. [Figure 2.5-202](#) presents the comparison of the site-specific total at-rest lateral earth pressure distribution compared to the AP1000 DCD design envelope in both the N-S and E-W directions. In both cases, the site-specific at-rest earth pressure is enveloped by the DCD design earth pressure envelopes by significant margins.

2.5.4.13 Heavy Lift Derrick Counterweight and Ring Foundation

The ring foundation for the heavy lift derrick (HLD) and counterweight are abandoned in place below grade following construction of Units 3 and 4. The HLD rails are removed from the ring foundation after construction of Units 3 and 4. The (HLD) counterweight and ring foundation are shown on [Figure 2.5-203](#).

The top of the HLD counterweight and ring foundation concrete is located at approximately elevation 215 ft MSL, which is five feet below the nominal site grade of 220 ft MSL. The HLD counterweight and ring foundation are not visible following the installation of the roads, drainage provisions, and ground surface cover.

The HLD counterweight and ring foundation are below the surface drainage system provisions and do not affect the runoff for the local PMP flood event discussed in [Subsection 2.4.2.3](#). The HLD counterweight and ring foundation are located above the design ground water elevation of 165 ft MSL, and do not impact the hydrological analyses described in [Subsections 2.4.12](#) and [2.4.13](#).

The safety-related portion of the excavations is filled with Category 1 backfill to the NI basemat and with Category 2 backfill to grade. The side slopes are filled with engineered granular backfill (EGB), which is non-safety related and does not affect the static or seismic performance of the safety-related structures.

As shown on [Figure 2.5-203](#), the HLD counterweight and ring foundation does not extend into the safety-related backfill of either Unit 3 or Unit 4. The ring foundation does extend into the EGB backfill of the excavations for both Unit 3 and Unit 4. The counterweight overall depth is approximately 28 ft, and is below the EGB backfill of the excavation for Unit 4. Subsection 3.7.1.1.1 provides the results of the evaluation which confirms that the presence of the HLD counterweight and ring foundation has no effect on the site specific seismic analyses.

2.5.5 Stability of Slopes

2.5.5.1 Review of Existing Slopes

The location of VEGP Units 3 and 4 will be atop a bluff on the southwest bank of the Savannah River. The new units will be located to the west of the existing Units 1 and 2 as described in [Section 1.2](#). The ground is flat to gently rolling and at approximately the same grade elevation of the existing units (220 ft msl). There are no existing slopes or embankments near the proposed location of Units 3 and 4; therefore, no dynamic slope stability analysis was performed for VEGP Units 3 and 4.

2.5.5.2 New Slopes

There is no planned permanent slope that would adversely affect, either directly or indirectly, any of the safety-related structures that would be built for the new AP1000 Units 3 and 4. Site grading for construction of the new units would result in non-safety-related permanent cut and fill slopes. Permanent cut slopes would have heights of the order of 50 feet or less, and would be located to the north and west of the new switchyard area, several hundred feet away from planned or existing safety-related structures. Permanent fill slopes would have heights of the order of 20 ft or less, and would be located to the south and west of the new cooling tower area, several hundred feet away from planned or existing safety-related structures.

Construction excavation cut slopes would be required in the new AP1000 power block area where soils above the Blue Bluff Marl would be removed and replaced with compacted structural fill. The construction excavation cut slopes would be temporary during the construction period only. Also, these excavation slopes would be sufficiently far away from the existing VEGP Unit 1 and 2 safety-related structures, and therefore, would not adversely affect, directly or indirectly, any of the existing safety-related structures.

The proposed permanent non-safety-related slopes will be analyzed for dynamic and static conditions during the design stage. The minimum acceptable factors of safety against stability failure of permanent slopes are 1.5 for long-term static conditions and 1.1 for long-term seismic conditions (USACE 2003). The construction excavation cut slopes will be analyzed for static conditions during the design stage. The minimum acceptable factor of safety against stability failure of excavation slopes is 1.3, based on what was used for Units 1 and 2. These analyses will be performed to ensure that these slopes will not pose a hazard to the public. Such analyses are not part of this document.

2.5.6 Embankments and Dams

2.5.6.1 Review of Existing Embankments and Dams

There are no earth, rock or earth and rock fill embankments required for plant flood protection or for impounding cooling water required for the operation of the plant.

Figure 1.1-202 shows the locations of three existing non-safety-related impoundments at the VEGP site. They are:

- Mallard Pond located to the north of the proposed switchyard
- Debris Basin Dam #1 located to the southeast of the proposed AP1000 cooling towers
- Debris Basin Dam #2 located to the southwest of the proposed AP1000 cooling towers

These impoundments are not used for plant flood protection or for impounding cooling water required for the operation of the plant. However, brief descriptions of these impoundments are provided here.

The proposed finished grade elevation for the new AP1000 units is approximately 220 ft msl. The pool level in Mallard Pond is below El. 125 ft msl. In the event of a dam breach at Mallard Pond, the water would drain to the north and away from the proposed new units. The pool levels in Debris Basin Dams #1 and #2 are below El. 150 ft msl, and in the event of a dam breach, the water would drain to the south and away from the proposed new units.

2.5.6.2 New Embankments and Dams

No new embankments or dams would be constructed at the site for flood protection or for impounding cooling water required to operate the new AP1000 units. The proposed finished grade elevation for the new AP1000 units is approximately 220 ft msl. This site finished grade elevation is much higher than the probable maximum flood (PMF) elevation discussed in Subsection 2.4.3 and the dam break level discussed in Subsection 2.4.4. Therefore, no new embankments or dams would be required to be constructed at the site for flood protection. Also, the new AP1000 units use cooling towers, and makeup water would be pumped from the Savannah River. Therefore, no new embankments or dams would be required to be constructed at the site for impounding cooling water required to operate the new AP1000 units.

In summary, no embankments and dams are required to be addressed in this section.

2.5.7 Combined License Information

2.5.7.1 Basic Geologic and Seismic Information

Regional and site-specific geological, seismological, and geophysical information as well as conditions caused by human activities are addressed in Subsections 2.5.1, 2.5.2, and 2.5.4.

2.5.7.2 Seismic and Tectonic Characteristics Information

Site-specific information related to the vibratory ground motion aspects of the site and region are addressed in Subsections 2.5.2 and 2.5.4.

2.5.7.3 Geoscience Parameters

Site-specific seismic analyses are addressed in Subsections 2.5.2 and 2.5.4.

2.5.7.4 Surface Faulting

Surface and subsurface geological, seismological, and geophysical information related to the potential for surface or near-surface faulting affecting the site is addressed in Subsection 2.5.3.

2.5.7.5 Site and Structures

Site-specific information regarding the underlying site conditions and geologic features is addressed in Subsection 2.5.4.

2.5.7.6 Properties of Underlying Materials

The properties of the foundation soils for design of the nuclear island basemat are addressed in Subsection 2.5.4.

2.5.7.7 Excavation and Backfill

Seismic Category I excavations, fills, and slopes are addressed in Subsection 2.5.4.

2.5.7.8 Ground Water Conditions

Groundwater conditions are addressed in Subsection 2.5.4.

2.5.7.9 Liquefaction Potential

Liquefaction potential is addressed in Subsection 2.5.4.

2.5.7.10 Bearing Capacity

The allowable soil bearing capacities for static and dynamic loads are addressed in Subsection 2.5.4.

2.5.7.11 Earth Pressures

The static and dynamic lateral earth pressures and hydrostatic groundwater pressures acting on plant safety-related facilities are addressed in Subsection 2.5.4.

2.5.7.12 Soil Properties for Seismic Analysis of Buried Pipes

The AP1000 does not utilize safety-related buried piping. No additional information is required on soil properties.

2.5.7.13 Static and Dynamic Stability of Facilities

Soil characteristics affecting the stability of the nuclear island are addressed in [Subsection 2.5.4](#).

2.5.7.14 Subsurface Instrumentation

Instrumentation for monitoring the performance of the foundations of the nuclear island is addressed in [Subsection 2.5.4](#) and [Appendix 2.5E](#).

2.5.7.15 Stability of Slopes

The static and dynamic stability of soil and rock slopes, the failure of which could adversely affect the nuclear island, is addressed in [Subsection 2.5.5](#).

2.5.7.16 Embankments and Dams

The static and dynamic stability of embankments and dams, the failure of which could adversely affect the nuclear island, is addressed in [Subsection 2.5.6](#).

2.5.7.17 Settlement of Nuclear Island

Settlement of the nuclear island foundation and adjacent buildings is addressed in [Subsection 2.5.4](#).

2.5.7.18 Waterproofing System

The waterproofing system used for the foundation mat (mudmat) and below grade exterior walls exposed to flood and groundwater under seismic Category I structures is addressed in [Subsections 3.8.5.1 and 3.4.1.1.1.1](#).

2.5.8 References

1. American Concrete Institute (ACI), "Building Code Requirements for Structural Concrete," ACI 318-02.
2. NUREG/CR-0693, "Seismic Input and Soil Structure Interaction," February 1979.
3. APP-GW-GLR-115, "Effect of High Frequency Seismic Content on SSCs," Westinghouse Electric Company LLC.
201. Lambe, T.W. and R.V. Whitman, *Soil Mechanics*, John Wiley & Sons, Inc., New York, NY, 1969.
202. ASCE 4-98 (2000), *Seismic Analysis of Safety-Related Nuclear Structures and Commentary*, ASCE, Reston, VA, 2000.
203. Duncan, J.M., G.W. Williams, A.L. Sehn and R.B. Seed, "Closure of 'Estimation of Earth Pressures due to Compaction'", *Journal of Geotechnical Engineering*, ASCE, New York, NY, 119(7):1172-1177, July, 1993.
204. **(Aadland and Bledsoe 1990)** Aadland, R. K., and Bledsoe, H. W., Classification of hydrostratigraphic units at the Savannah River Site, South Carolina: USDOE Report, WSRC-RP-90-987, Westinghouse Savannah River Co., Westinghouse Savannah River Laboratory, Aiken, S.C., 15 p., 1990.
205. **(Amick 1990)** Amick, D. C., Paleoliquefaction investigations along the Atlantic Seaboard with emphasis on the prehistoric earthquake chronology of coastal South Carolina, unpub. Ph.D. dissertation, University of South Carolina, 1990.
206. **(Amick et al. 1990b)** Amick, D., Maurath, G., and Gelinas, R., Characteristics of seismically induced liquefaction sites and features located in the vicinity of the 1886 Charleston, South Carolina earthquake: *Seismological Research Letters*, v. 61, no. 2, p. 117-130, 1990.
207. **(Amick et al. 1990c)** Amick, D., Gelinas, R., Maurath, G., Cannon, R., Moore, D., Billington, E., and Kemppinen, H., Paleoliquefaction features along the Atlantic Seaboard: U.S. Nuclear Regulatory Commission Report, NUREG/CR-5613, 1990.
208. **(Anderson 1990)** Anderson, E. E., The Seismotectonics of the Savannah River Site: The Results of a Detailed Gravity Survey, unpub. Masters thesis, University of South Carolina, Columbia, South Carolina, 248 p., 1990.
209. **(Austin et al. 1990)** Austin, J. A., Stoffa, P. L., Phillips, J. D., Oh, J., Sawyer, D. S., Purdy, G. M., Reiter, E., and Makris, J., Crustal structure of the southeast Georgia embayment-Carolina trough: preliminary results of a composite seismic image of a continental suture (?) and a volcanic passive margin: *Geology*, v. 18, p. 1023-1027, 1990.
210. **(Bakun and Hopper 2004)** Bakun, W. H., and Hopper, M. G., Magnitudes and locations of the 1811-1812 New Madrid, Missouri, and the 1886 Charleston, South Carolina, earthquakes: *Bulletin of the Seismological Society of America*, v. 94, no. 1, p. 64-75, 2004.
211. **(Bechtel 1982)** Bechtel Power Corporation, Vogtle Electric Generating Plant, Studies of Postulated Millett Fault, October 1982.

- 212. **(Bechtel 1989)** Bechtel, Field review of geologic conditions near the Vogtle site relative to possible extension of the postulated “Pen Branch fault” into Georgia, report prepared for Georgia Power Company, 195 p., September 15 1989.
- 213. **(Behrendt and Yuan 1987)** Behrendt, J. C. and Yuan, A., The Helena Banks strike-slip (?) fault zone in the Charleston, South Carolina, earthquake area; results from a marine, high-resolution, multichannel, seismic-reflection survey: Geological Society of America Bulletin, v. 98, no. 5, p. 591-601, 1987.
- 214. **(Behrendt et al. 1981)** Behrendt, J. C., Hamilton, R. M., Ackermann, H. D., and Henry, V. J., Cenozoic faulting in the vicinity of the Charleston, South Carolina, 1886 earthquake: Geology, v. 9, no. 3, p. 117-122, 1981.
- 215. **(Behrendt et al. 1983)** Behrendt, J. C., Hamilton, R. M., Ackermann, H. D., Henry, V. J., and Bayer, K. C., Marine multichannel seismic-reflection evidence for Cenozoic faulting and deep crustal structure near Charleston, South Carolina: U. S. Geological Survey Professional Paper 1313-J, p. J1-J29, 1983.
- 216. **(Berkman 1991)** Berkman, E., High resolution seismic survey - Pen Branch fault – Savannah River Site, South Carolina: Emerald Exploration Consultants, Inc. report, Austin, TX, 89 p., 210 fig., 1991.
- 217. **(Bickford et al. 1986)** Bickford, M. E., Van Schmus, W. R., and Zietz, I., Proterozoic history of the mid-continent region of North America: Geology, v. 14, p. 492-496, 1986.
- 218. **(Bobyarchick 1981)** Bobyarchick, A. R., The eastern Piedmont fault system and its relationship to Alleghanian tectonics in the southern Appalachians: Journal of Geology, v. 89, p. 335-347, 1981.
- 219. **(Bollinger 1977)** Bollinger, G. A., Reinterpretation of the intensity data for the 1886 Charleston, South Carolina, earthquake: in Rankin, D.W. (ed.), Studies Related to the Charleston, South Carolina, Earthquake of 1886- A Preliminary Report: U.S. Geological Survey Professional Paper 1028, p. 17-32, 1977.
- 220. **(Bollinger 1992)** Bollinger, G. A., Specification of source zones, recurrence rates, focal depths, and maximum magnitudes for earthquakes affecting the Savannah River Site in South Carolina: U. S. Geological Survey Bulletin, 1992.
- 221. **(Bollinger and Sibol 1985)** Bollinger, G. A. and Sibol, M. S., Seismicity, seismic reflection studies, gravity and geology of the Central Virginia seismic zone: part I - Seismicity, Geological Society of America Bulletin, v. 96, p. 49-57, 1985.
- 222. **(Bollinger and Wheeler 1988)** Bollinger, G. A. and Wheeler, R. L., The Giles County, Virginia, seismic zone - seismological results and geological interpretations, U. S. Geological Survey Professional Paper 1355, 1988.
- 223. **(Bollinger et al. 1991)** Bollinger, G. A., Johnston, A. C., Talwani, P., Long, L. T., Shedlock, K. M., Sibol, M. S., and Chapman, M. C., Seismicity of the Southeastern United States; 1698-1986 in Neotectonics of North America, Decade Map Volume to Accompany the Neotectonic Maps (D. B. Slemmons, E. R. Engdahl, M. D. Zoback, D. B. Blackwell, eds.), p. 291-308, 1991.

-
224. **(Bollinger et al. 1992)** Bollinger, G.A., Sibol, M.S., and Chapman, M.C., Maximum magnitude estimation for an intraplate setting – Example: the Giles County, Virginia, seismic zone: *Seismological Research Letters*, v. 63, no. 2, p. 139, 1992.
225. **(Bramlett 1989)** Bramlett, K. W., *Geology of the Johnston-Edgefield Area, S. C., and Its Regional Implications*: unpub. M.S. thesis University of South Carolina, Columbia, SC, 1989.
226. **(Bramlett et al. 1982)** Bramlett, K. W., Secor, D. T., and Prowell, D. C., “The Belair Fault: A Cenozoic Reactivation Structure in the Eastern Piedmont”, *Geological Society of America Bulletin*, vol. 93, pp. 1109-1117, 1982.
227. **(Brooks and Sassaman 1990)** Brooks, M. J. and Sassaman, K. E., Point bar geoarchaeology in the Upper Coastal Plain of the Savannah River Valley, S. C., a case study, in Lasca N. P., and Donahue, J., (eds., *Archaeological Geology of North America: Geological Society of America Centennial Special Publications No. 4*, p. 183 – 197, 1990.
228. **(Bryant and McCracken 1964)** Bryant, J. P. and McCracken, R. J., Properties of soils and sediments of the Carolina Bays: *Journal of the Elisha Mitchell Scientific Society*, v. 80, no. 2, North Carolina Academy of Science, Durham, NC, 1964.
229. **(Bukry 2001)** Bukry, D., Late Campanian (Zone CC22) coccoliths from the Millhaven Core, Screven county, Georgia: in Edwards, Lucy, E. (editor), *Geology and paleontology of five cores from Screven and Burke counties, eastern Georgia*: United States Geological Survey Professional Paper 1603, p. D1-D4, 2001.
230. **(Butler 1979)** Butler, J. R., The Carolina Slate Belt in North Carolina and Northeastern South Carolina: A Review: *Geological Society of America Abstracts with Program*, v. 11, p. 172, 1979.
231. **(Bybell 2001)** Bybell, M. L., Calcareous nannofossil biostratigraphy of Cenozoic sediments from the Millhaven Core, Screven county, Georgia: in Edwards, Lucy, E. (editor), *Geology and paleontology of five cores from Screven and Burke counties, eastern Georgia*: United States Geological Survey Professional Paper 1603, p. F1-F13, 2001.
232. **(Chapman and DiStefano 1989)** Chapman, W. L. and DiStefano, M. P., Savannah River Plant Seismic Survey, 1987-88: Conoco Inc., Seismic Acquisition Section, Research Report 1809-005-006-1-89, p. 110, 1989.
233. **(Chapman and Krimgold 1994)** Chapman, M. C., and Krimgold, F., Seismic hazard assessment for Virginia, Virginia Tech Seismological Laboratory, Department of Geological Sciences, February 1994.
234. **(Chapman et al. 1997)** Chapman, M. C., Powell, C. A., Vlahovic, G. and Sibol, M. S., A statistical analysis of earthquake focal mechanisms and epicenter locations in the eastern Tennessee seismic zone, *Bulletin of the Seismological Society of America*, v. 87, no. 6, p. 1522-1536, 1997.
235. **(Chapman et al. 2002a)** Chapman, M.C., Munsey, J.W., Powell, C.A., Whisner, S.C., and Whisner, J., The Eastern Tennessee seismic zone – summary after 20 years of network monitoring: *Seismological Research Letters*, v. 73, no. 2, p. 245, 2002.

-
236. **(Christopher 1982)** Christopher, R. A., Palynostratigraphy of the basal Cretaceous units of the eastern Gulf and southern Atlantic Coastal Plains, in Arden, D.D., Beck, B.F., and Morrow, Eleanore, eds., Proceedings; Second symposium on the geology of the southeastern coastal plain: Georgia Geologic Survey Information Circular 53, p. 10–23, pls. 1–3, 1982.
237. **(Christopher et al. 1979)** Christopher, R. A., Owens, J. P., and Sohl, N. F., Late Cretaceous palynomorphs from the Cape Fear Formation of North Carolina: Southeastern Geology, v. 20, no. 3, p. 145–159, 1979.
238. **(Clarke et al. 1985)** Clarke, J. S., Brooks, R., and Faye, R. E., Hydrogeology of the Dublin and Midville aquifer systems of east central Georgia: Georgia Geologic Survey Information Circular 74, 62 p., 1985.
239. **(Clarke et al. 1994)** Clarke, J. S., Falls, W. F., Edwards, L. E., Frederiksen, N. O., Bybell, L. M., Gibson, T. G., and Litwin, R. J., Geologic, hydrologic and water-quality data for a multi-aquifer system in coastal plain sediments near Millers Pond, Burke County, Georgia, 1992–93: Georgia Geologic Survey Information Circular 96, 34 p., 1 pl. in pocket, 1994.
240. **(Colman 1983)** Colman, S. M., Progressive changes in the morphology of fluvial terraces and scarps along the Rappahannock River, Virginia: Earth Surface Processes and Landforms, v. 8, p. 201 – 212, 1983.
241. **(Colquhoun and Johnson 1968)** Colquhoun, D. J., and Johnson, Jr., H. S. Tertiary Sea-Level Fluctuation in South Carolina: Paleogeography, Paleoclimatology, Paleoecology. v. 5, pp. 105-126, 1968.
242. **(Colquhoun and Steel 1985)** Colquhoun, D. J. and Steele, K. B., Chronostratigraphy and Hydrostratigraphy of the Northwestern South Carolina Coastal Plain: Annual Cooperative Grant Agreement No. 13040 R-83-591, Project No. G868-05, Interim Technical Report to Water Resources Research Institute, Clemson University, Clemson, South Carolina, p. 15, 1985.
243. **(Colquhoun et al. 1983)** Colquhoun, D. J., Woollen, I. D., Van Nieuwenhuise, D. S., Padgett, G. G., Oldham, R. W., Boylan, D. C., Bishop, J. W., and Howell, P. D. Surface and subsurface stratigraphy, structure and aquifers of the South Carolina Coastal Plain: SCDHEC Report ISBN 0-9613154-0-7, 78 p., 1983.
244. **(Committee for Gravity Anomaly Map of North America 1987)** Committee for the Gravity Anomaly Map of North America, Gravity anomaly map of North America, continent-scale map, 1:5,000,000 scale, Geological Society of America, Boulder, CO, 1987.
245. **(Cook et al. 1979)** Cook, F. A., Albaugh, D. S., Brown, L. D., Kaufman, S., Oliver, J. E., Hatcher, R. D. Jr., Thin-skinned tectonics in the crystalline southern Appalachians: COCORP seismic reflection profiling of the Blue Ridge and Piedmont. Geology, vol. 7, p. 563-567, 1979.
246. **(Cook et al. 1981)** Cook, F.A., L.D. Brown, S. Kaufman, J.E. Oliver, and T.A. Petersen, COCORP seismic profiling of the Appalachian orogen beneath the Coastal Plain of Georgia, Geological Society of America Bulletin, v. 92, no. 10, p. 738-748, 1981.
-

- 247. **(Cooke 1936)** Cooke, C. W., Geology of the Coastal Plain of South Carolina: U.S. Geological Survey Bulletin 867, 196 p., 1936.
- 248. **(Cooke 1954)** Cooke, C. W., Carolina bays and the shapes of eddies: U. S. Geological Survey Professional Paper 254-I, p. 195 - 206, 1954.
- 249. **(Coruh et al. 1987)** Coruh, C., Costain, J. K., Hatcher, Jr., R.D. Pratt, T.L., Williams, R. T., Phinney R. A., Results from regional vibroseis profiling: Appalachian ultradeep core hole site study: Geophysical Journal of the Royal Astronomical Society, v. 89, p. 473-474, 1987.
- 250. **(Coruh et al. 1988)** Coruh, C., Bollinger, G. A., and Costain, J. K., Seismogenic structures in the central Virginia seismic zone, Geology, v. 16, p. 748-751, 1988.
- 251. **(Crone and Wheeler 2000)** Crone, A. J., and Wheeler, R. L., Data for Quaternary faults, liquefaction features, and possible tectonic features in the Central and Eastern United States, east of the Rocky Mountain Front: U. S. Geological Survey Open-File Report 00-260, 2000.
- 252. **(Cumbest and Price 1989b)** Cumbest, R. J., and Price, V., Continued extension of the Dunbarton Basin: an explanation for faulting in the coastal plain of South Carolina: Savannah River Company, Report WSRC-RP-89-1263, 1989.
- 253. **(Cumbest et al. 1992)** Cumbest, R. J., Price, V. and Anderson, E. E., 1992, Gravity and Magnetic Modeling of the Dunbarton Triassic Basin, South Carolina, Southeastern Geology, v. 33, no.1, p. 37-51, 1992.
- 254. **(Cumbest et al. 1998)** Cumbest, R. J., Stephenson, D. E., Wyatt, D. E., and Maryak, M., Basement surface faulting and topography for Savannah River site and vicinity: Westinghouse Savannah River Company, Technical Report 98-00346, 1998.
- 255. **(Cumbest et al. 2000)** Cumbest, R. J., Wyatt, D. E., Stephenson, D. E., and Maryak, M., Comparison of Cenozoic faulting at the Savannah River site to fault characteristics of the Atlantic Coast fault province: implications for fault capability: Westinghouse Savannah River Company, Technical Report 2000-00310, 2000.
- 256. **(Dahlen 1981)** Dahlen, F. A., Isostasy and the ambient state of stress in the oceanic lithosphere: Journal of Geophysical Research, v. 86, no. B9, p. 7801-7807, 1981.
- 257. **(Dallmeyer et al. 1986)** Dallmeyer, R. D., Wright, J. E., Secor, D. T., Jr., and Snoke, A. W., Character of the Alleghenian Orogeny in the Southern Appalachians: Part II. geochronological constraints on the tectonothermal evolutions of the Eastern Piedmont in South Carolina: Geological Society of America Bulletin. v. 97, pp. 1329-1344, 1986.
- 258. **(Daniels 1974)** Daniels, D. L., Geologic Interpretation of Geophysical Maps, Central Savannah River Area, South Carolina and Georgia, U.S. Geological Survey, Geophysical Investigation Map GP-893, 1974.
- 259. **(Daniels 2005)** Daniels, D. L., South Carolina Aeromagnetic and Gravity Maps and Data: A Web Site for Distribution of Data, U.S. Geological Survey Open-File Report 2005-1022 (<http://pubs.usgs.gov/of/2005/1022/>), 2005.

-
260. **(Davis 1980)** Davis, G.J., 1980, The southwestern extension of the Middleton-Lowndesville cataclastic zone in the Greensboro, Georgia, area and its regional implications: M.S. thesis, University of Georgia, 151 p., 1980.
261. **(Dennehy et al. 1988)** Dennehy, K. F., Prowell, D. C., and McMahon, P. B., Geohydrology of the Defense Waste Processing Facility and vicinity, Savannah River Plant, South Carolina, U.S. Geological Survey Water Resources Investigation, WRI 88-4221, 90 p., 1988.
262. **(Dennis 1991)** Dennis, A.J., Is the central Piedmont suture a low-angle normal fault?: *Geology*, v. 19, p. 1081-1084, 1991.
263. **(Dennis et al. 2004)** Dennis, A. J., Shervais, J. W., Mauldin, J., Maher, H. D., Jr., and Wright, J. E., Petrology and geochemistry of Neoproterozoic volcanic arc Terranes beneath the Atlantic Coastal Plain, Savannah River Site, South Carolina: *Geological Society of America Bulletin*, v. 116, no. 5-6, p. 572-593, 2004.
264. **(Dillon and Popenoe 1988)** Dillon, W. P., and Popenoe, P., The Blake Plateau Basin and Carolina Trough, in Sheridan, R.E., and J. A. Grow (eds.), *The Geology of North America*, v. I-2, The Atlantic Continental Margin: US., DNAG Publication, Vol. I-1, Geological Society of America, Boulder, Colorado. p. 291-328, 1988.
265. **(Domoracki 1994)** Domoracki, W. J., A geophysical investigation of geologic structure and regional tectonic setting at the Savannah River Site, South Carolina, excerpts from a doctoral dissertation in preparation at Virginia Polytechnic Institute: Westinghouse Savannah River Company, WSRC-TR-94-0317, 1994.
266. **(Domoracki 1995)** Domoracki, W., A Geophysical Investigation of Geologic Structure and Regional Tectonic Setting at the Savannah River Site, South Carolina, unpub. Ph.D dissertation, Virginia Polytechnic Institute and State University, Blacksburg, Virginia, 1995.
267. **(Domoracki et al. 1999)** Domoracki, W. J., Stephenson, D. E., Coruh, C., and Costain, J. K., Seismotectonic structures along the Savannah River Corridor, South Carolina, USA: *Journal of Geodynamics*, v. 27, no. 1, p. 97-118, 1999.
268. **(Dutton 1889)** Dutton, C. E., The Charleston earthquake of August 31, 1886: U.S. Geological Survey, Ninth annual report 1887-88, 1889.
269. **(Edwards 2001)** Edwards, L., Dinocyst biostratigraphy of Tertiary sediments from five cores from Screven and Burke counties, Georgia: in Edwards, Lucy, E. (ed.), *Geology and paleontology of five cores from Screven and Burke counties, eastern Georgia*: U.S. Geological Survey Professional Paper 1603, p. G1-G5, 2001.
270. **(Edwards et al. 2001)** Edwards, L., Frederiksen, N. O., Bybell, L. M., Gibson, T. G., Gohn, G. S., Self-Trail, J. M., Litwin, R. J., Overview of the biostratigraphy and paleoecology of sediments from five cores from Screven and Burke counties, Georgia: in Edwards, Lucy, E. (editor, *Geology and paleontology of five cores from Screven and Burke counties, eastern Georgia*: U.S. Geological Survey Professional Paper 1603, p. B1-B19, 2001.
271. **(EPRI 1986a)** Electric Power Research Institute (EPRI), *Seismic Hazard Methodology for the Central and Eastern United States, Tectonic Interpretations*. 1986.
-

-
272. **(Fallaw and Price 1992)** Fallaw, W. C. and Price, Van, (eds.), Geological Investigations of the Central Savannah River Area, South Carolina, and Georgia: Carolina Geological Society Field Trip Guidebook for 1992, p. 112, 1992.
273. **(Fallaw and Price 1995)** Fallaw, W. C., and Price, V., Stratigraphy of the Savannah River Site and vicinity: Southeastern Geology, v. 35, no. 1, p. 21-58, 1995.
274. **(Fallaw et al. 1990a)** Fallaw, W. C., Price, Van., and Thayer, P. A., Stratigraphy of the Savannah River Site, South Carolina: Proceedings of the Second Bald Head Island Conference on Coastal Plains Geology, November 6-11, 1990, Addendum, p. 1-4, 1990.
275. **(Fallaw et al. 1990b)** Fallaw, W. C., Price, V., and Thayer, P.A., Effects of varying degrees of marine influence on tertiary sediments in southwestern South Carolina: Geological Society of America Abstracts with Programs v. 22 no. 7 p A45, 1990.
276. **(Fallaw et al. 1992)** Fallaw, W. C., Price, V., and Thayer, P.A., Stratigraphy of the Savannah River Site, South Carolina in Zullo, V. A., Harris, W. B., and Price, V., (eds.), Savannah River region: transition between the Gulf and Atlantic Coastal Plains, Proceedings of the second Bald Head Island Conference on Coastal Plains geology: University of North Carolina at Wilmington and the U.S. Department of Energy, p. 29-32, 1992.
277. **(Fallaw et al. 1995)** Fallaw, W. C., Snipes, D. S., Hodges, R. A., Price, V., and Temples, T. J., Facies changes in middle Eocene sediments, southwestern coastal plain of South Carolina. Geological Society of America, Southeastern Section, 44th annual meeting, Abstracts with Programs - Geological Society of America, v. 27, no. 2, p. 52, 1995.
278. **(Falls and Prowell 2001)** Falls, W. F., and Prowell, D. C., Stratigraphy and depositional environments from five cores from Screven and Burke counties, Georgia: in Edwards, Lucy, E. (ed.), Geology and paleontology of five cores from Screven and Burke counties, eastern Georgia: United States Geological Survey Professional Paper 1603, p. A1-A20, 2001.
279. **(Farrar 1985)** Farrar, S. S., Tectonic evolution of the easternmost Piedmont, North Carolina: Geological Society of America Bulletin, v. 96, p.362-380, 1985.
280. **(Faye and Prowell 1982)** Faye, R. E., and Prowell, D. C., Effects of Late Cretaceous and Cenozoic faulting on the geology and hydrology of the coastal plain near the Savannah River, Georgia and South Carolina: U.S. Geological Survey Open-File Report 82-0156, 1982.
281. **(Frankel et al. 1996)** Frankel, A., Barnhard, T., Perkins, D., Leyendecker, E. V., Dickman, N., Hanson, S., and Hopper, M., National seismic-hazard maps: documentation, U.S.Geological Survey. Open-File Report 96-532, 1996.
282. **(Frankel et al. 2002)** Frankel, A. D., Petersen, M. D., Mueller, C. S., Haller, K. M., Wheeler, R. L., Leyendecker, E. V., Wesson, R. L., Harmensen, S. C., Cramer, C. H., Perkins, D. M., and Rukstales, K. S., Documentation for the 2002 update of the national seismic hazard maps: U. S. Geological Survey Open-File Report 02-420, 2002.
283. **(Frederiksen 2001)** Frederiksen, N. O., Pollen biostratigraphy of lower Tertiary sediments from five cores from Screven and Burke counties, Georgia: in Edwards, Lucy, E. (ed.), Geology and paleontology of five cores from Screven and Burke counties, eastern Georgia: U.S. Geological Survey Professional Paper 1603, p. H1-H21, 2001.
-

-
284. **(Frederiksen et al. 2001)** Frederiksen, N. O., Edwards, L. E., Litwin, R. J., Palynomorph biostratigraphy and paleoecology of upper Cretaceous sediments from four cores from Screven and Burke counties, Georgia: in Edwards, Lucy, E. (ed.), *Geology and paleontology of five cores from Screven and Burke counties, eastern Georgia*: U.S. Geological Survey Professional Paper 1603, p. C1-C32, 2001.
285. **(Froelich and Olsen 1984)** Froelich, A. J. and Olsen, P.E., Newark Supergroup, a revision of the Newark Group in eastern North America: U. S. Geological Survey Bulletin 1537A, pp A55-A58, 1984.
286. **(Fullagar and Bartholomew 1983)** Fullagar, P.D., and Bartholomew, M. J., Rubidium-strontium ages of the Watauga River, Cranberry, and Crossing Knob gneisses, northwestern North Carolina, in Lewis, S. E., ed., *Geological investigations in the Blue Ridge of northwestern North Carolina: 1983 Guidebook for the Carolina Geological Society*, North Carolina Division of Land Resources, Article 11, 29 p., 1983.
287. **(Fullagar and Butler 1979)** Fullagar, P. D., and Butler, J. R., 325 to 265 m.yr. old granitic plutons in the Piedmont of the Southeastern Appalachians: *American Journal of Science*, v. 279, pp. 161-185, 1979.
288. **(Fullagar and Odom 1973)** Fullagar, P.D., and Odom, A. L., Geochronology of Precambrian gneisses in the Blue Ridge province of northwestern North Carolina and adjacent parts of Virginia and Tennessee: *Geological Society of America Bulletin*, v.84, p.3065-3080, 1973.
289. **(Fullagar et al. 1979)** Fullagar, P.D., Hatcher, R. D., Jr., and Merschat, C. E., 1200 m.y.-old gneisses in the Blue ridge province of North and South Carolina: *Southeastern Geology*, v.20, p. 69-78, 1979.
290. **(Gamble et al. 1977b)** Gamble, E. E., Daniels, R. B., and Wheeler, W. H., The Goldsboro Ridge, an enigma: *Southeastern Geology*, v. 12, p. 151 – 158, 1977.
291. **(Gangopadhyay and Talwani 2005)** Gangopadhyay, A. and Talwani, P., Fault intersections and intra plate seismicity in Charleston South Carolina: insights from a 2-d numerical model, *Current Science*, v. 88, no. 10, 2005.
292. **(Geomatrix 1993)** Geomatrix Consultants, "Preliminary Quaternary and Neotectonic Studies": Savannah River Site, South Carolina, Report prepared for Lawrence Livermore National Laboratory and Westinghouse Savannah River Company, February 1993.
293. **(Glover et al. 1980)** Glover, L., III, Poland, F. B., Tucker, R. D. and Bourland, W. C., Diachronous Paleozoic mylonites and structural heredity of Triassic-Jurassic basins in Virginia: *Geological Society of America Abstracts with Programs*. v. 12, p. 178, 1980.
294. **(Gohn 2001)** Gohn, G. S., Ostracode biostratigraphy of Upper Campanian (Cretaceous marine sediments from the Millhaven Core, Screven county, Georgia: in Edwards, Lucy, E. (ed.), *Geology and paleontology of five cores from Screven and Burke Counties, eastern Georgia*: United States Geological Survey Professional Paper 1603, p. E1-E11, 2001.
295. **(Goldsmith et al. 1988)** Goldsmith, R., Milton, D. J. and Horton, J. W. Jr., *Geologic map of the Charlotte 10 X 20 quadrangle, North Carolina and South Carolina*: U. S. Geological Survey Miscellaneous Investigations Series Map I-1251-E, 1:250,000 scale, 1988.
-

- 296. **(Gore 1986)** Gore, P. J. W., Depositional framework of a Triassic rift basin: The Durham and Sanford sub-basins of the Deep River basin, North Carolina, in Textoris, D.A., ed., Society of Economic Paleontologists and Mineralogists Field Guidebook, Third annual Midyear Meeting, Raleigh, North Carolina, p. 53-115, 1986.
- 297. **(Griffin 1979)** Griffin, V.S., Jr., Geology of the Abbeville East, Abbeville West, Latimer, and Lowndesville quadrangles, South Carolina: South Carolina Geological Survey MS-24, 55p., 1979.
- 298. **(Grow et al. 1988)** Grow, J. A., K.D. Klitgord, J. S. Schlee, Structure and evolution of Baltimore Canyon trough: in Sheridan, R.E., and J. A. Grow (ed.), The Atlantic Continental Margin: US., DNAG Publication, Vol. I-1, Geological Society of America, Boulder, Colorado, p. 269-290, 1988.
- 299. **(Guccione 2005)** Guccione, M. J., Late Pleistocene and Holocene paleoseismology of an intraplate seismic zone in a large alluvial valley, the New Madrid Seismic Zone, central USA, Tectonophysics, v. 408, p. 236-264, 2005.
- 300. **(Hamilton et al. 1983)** Hamilton, R. M., Behrendt, J. C., and Ackermann, H. D., Land multichannel seismic-reflection evidence for tectonic features near Charleston, South Carolina, Studies Related to the Charleston, South Carolina, Earthquake of 1886- Tectonics and Seismicity, U.S. Geologic Survey Professional Paper 1313-I, p. I1-I18, 1983.
- 301. **(Hanson et al. 1993)** Hanson, K. L., Bullard, T. F., de Wit, M. W., and Stieve, A. L., Applications of Quaternary stratigraphic, soil-geomorphic, and quantitative geomorphic analyses to the evaluation of tectonic activity and landscape evolution in the upper Coastal Plain, S. C., Proceedings, 4th DOE Natural Phenomena Hazards Mitigation Conference, Atlanta, Georgia, v. 2, p. 672 – 681, 1993.
- 302. **(Harris and Zullo 1992)** Harris, W. B., and Zullo, V. A., Sequence stratigraphy of Paleocene and Eocene deposits in the Savannah River region, in Zullo, V. A., Harris, W. B., and Price, V., eds., Savannah River region; transition between the Gulf and Atlantic Coastal Plains: Proceedings of the Second Bald Head Island Conference on Coastal Plains Geology, Hilton Head Island, November 6–11, 1990, p. 134–142, 1992.
- 303. **(Harrison and McDougall 1980)** Harrison, T. M., and McDougall, I., Investigations of an intrusive contact, northwest Nelson, New Zealand-I. Thermal, chronological and isotopic constraints: Geochimica et Cosmochimica Acta, v. 44, p. 1985-2003, 1980.
- 304. **(Hatcher 1971)** Hatcher, R. D., Jr., Stratigraphic, petrologic, and structural evidence favoring a thrust solution to the Brevard problem: American Journal of Science, v. 270, p. 177-202, 1971.
- 305. **(Hatcher 1972)** Hatcher, R. D., Jr., Developmental model for the southern Appalachians: Geological Society of America Bulletin, v. 83, p. 2735-2760, 1972.
- 306. **(Hatcher 1978)** Hatcher, R. D. Jr., Tectonics of the western Piedmont and Blue Ridge, southern Appalachians: review and speculation: American Journal of Science, vol. 278, p. 276-304, 1978.
- 307. **(Hatcher 1987)** Hatcher, R.D., Jr., Tectonics of the southern and central Appalachain internides. Annual Review of Earth and Planetary Sciences, 15, pages 337-362, 1987.

-
308. **(Hatcher and Butler 1979)** Hatcher, R. D. Jr., and Butler, J. R., Guidebook for southern Appalachian field trip in the Carolinas, Tennessee, and northeastern Georgia: International Geologic Correlation Program Project 27, University of North Carolina, Chapel Hill, 117p., 1979.
309. **(Hatcher and Edelman 1987)** Hatcher, R.D., Jr., and Edelman, S.H., Macro-scale partitioning in the southern and central Appalachians: Thrusting and strike-slip as products of Alleghanian collision: Geological Society of America Abstracts with Programs, v. 19, p. 89, 1987.
310. **(Hatcher and Goldberg 1991)** Hatcher, R. D., Jr., and Goldberg, S. A., The Blue Ridge geologic province; in Horton, J. W., Jr., and Zullo, V. A. (eds.), The Geology of the Carolinas: Carolina Geological Society 50th Anniversary Volume, p.11-35, 1991.
311. **(Hatcher et al. 1977)** Hatcher, R. D., Jr., Howell, D. E., and Talwani, P., Eastern Piedmont Fault System: speculations on its extent: Geology, v. 5, pp. 636-640, 1977.
312. **(Hatcher et al. 1986a)** Hatcher, R. D., Jr., Costello, J. O., S. H. Edelman, The Smokies Foothills duplex and possible significance of the Guess Creek fault: A corollary to the mapping of King and Neuman: Geological Society of America Abstracts with Programs, v.; 18, p. 226, 1986.
313. **(Hatcher et al. 1986b)** Hatcher, R. D., Jr., Hopson, J. L., Edelman, S. H., Liu, A., McClellan, E. A., Stieve, A. L., Detailed Geologic Map of the Appalachian Ultradeep Core Hole (ADCOH Region: New Constraints on the Structure of the Southern Appalachian Internides: Geological Society of America Abstracts with Programs, v. 18, p. 631, 1986.
314. **(Hatcher et al. 1988)** Hatcher, R. D., Jr., Hooper, R. J., Heyn T., McConnell, K. I., and Costello, J. O., Geometric and time relations of thrusts in the crystalline southern Appalachians: in Mitra, G., and Wojtal, S., (eds.), Geometry and mechanisms of Appalachian thrusting, with special reference to the Appalachians: Geological Society of America Special Paper 222, p. 185-196, 1988.
315. **(Hatcher et al. 1990)** Hatcher, R. D., Jr., Osberg, P. H., Drake, A. A., Jr., Robinson, P., and Thomas, W. A., Tectonic Map of the U. S. Appalachians, Plate 1, in Hatcher, R. D., Jr., Thomas, W. A., and Viele, G. W., (eds.), The Appalachian-Ouachita orogen in the United States: Boulder, Colorado, Geological Society of America, The Geology of North America, v. F-2, scale 1/2,500,000, 1990.
316. **(Hatcher et al. 1994)** Hatcher, R. D., Jr., Colquhoun, D. J., Secor, D. T., Cook, F. A., Dillon, W. P., Klitgord, K. D., Popenoe, P., Merschat, C. E., Wiener, L. E., Milici, R. C., Nelson, A. E., Sheridan, R. E., and Snoke, A. W., Continent-ocean transect E5 - Cumberland Plateau (North American Craton) to Blake Plateau Basin: Geological Society of America, scale 1:500,000, 1994.
317. **(Hatcher et al. 1996)** Hatcher, R. D., Jr., Carter, M. W., Clark, G. M., and Mills, H. H., Large landslides in western Blue Ridge of Tennessee and North Carolina: Normal mass-wasting phenomena, products of late Pleistocene climates, or smoking gun for earthquake(s) in East Tennessee?: Geological Society of America Abstracts with Programs, v. 28, no. 7, p. A-299, 1996.

318. **(Hatcher et al. 2002)** Hatcher, R.D., Jr., An Inner Piedmont primer, in Hatcher, R.D., Jr., and Bream, B.R., (eds.), Inner Piedmont geology in the South Mountains-Blue Ridge Foothills and the southwestern Brushy Mountains, central-western North Carolina: North Carolina Geological Survey, Carolina Geological Society annual field trip guidebook, p. 1-18, 2002.
319. **(Hatcher et al. 2005)** Hatcher, R.D., Jr., Merschat, A. J. and Thigpen, J. R. Blue Ridge Primer, in Hatcher, R.D., Jr., and Merschat, A.J. (eds.), Blue Ridge Geology Geotraverse East of the Great Smoky Mountains National Park, Western North Carolina: North Carolina Geological Survey, Carolina Geological Society Annual Field Trip Guidebook, p. 1-24, 2005.
320. **(Hauser 1993)** Hauser, E. C., Grenville foreland thrust belt hidden beneath the eastern U.S. mid-continent: *Geology*, v. 21, p. 61-64, 1993.
321. **(Henry 1995)** Henry, V. J., Summary of results of a seismic survey of the Savannah river adjacent to the Savannah River Plant Site, Burke County, Georgia, Georgia Geologic survey project report 24, 22 p., 1995.
322. **(Heyn 1988)** Heyn, T., Geology of the hinge zone of the Sauratown Mountains anticlinorium, North Carolina, in Hatcher, R.D., Jr., (ed.), Structure of the Sauratown Mountains window, North Carolina: Carolina Geological Society Guidebook, p. 20-50, 1988.
323. **(Hooper and Hatcher 1988)** Hooper, R. J., and Hatcher, R. D., Jr., The Pine Mountain Terrane, a complex window in the Georgia and Alabama Piedmont- Evidence from the eastern termination: *Geology*, v. 16, p. 307-310, 1988.
324. **(Hopson 1989)** Hopson, J. L., Structure, stratigraphy, and petrogenesis of the Lake Burton mafic-ultramafic complex, in Fritz, W. J., Hatcher, R. D., Jr., and Hopson, J.L. (eds.), Georgia Geological Society Guidebook, v. 9, p. 93-100, 1989.
325. **(Hopson et al. 1989)** Hopson, J. L., Hatcher, R. D. Jr., and Stieve, A. L., Geology of the eastern Blue Ridge of northeast Georgia and the adjacent Carolinas, in Fritz, W. J., Hatcher, R. D., Jr., and Hopson, J. L., Georgia Geological Society Guidebook, v. 9, p. 1 – 38, 1989.
326. **(Horton 1981)** Horton, J. W., Jr., Shear zone between the Inner Piedmont and Kings Mountain belts in the Carolinas: *Geology*, v. 9, p. 28-33, 1981.
327. **(Horton and McConnell 1991)** Horton, J. W. Jr., and McConnell, K. I., The Western Piedmont, in Horton, J. W., Jr., and Zullo, V. A. (eds.), The Geology of the Carolinas: Carolina Geological Society 50th Anniversary Volume, p. 36-48, 1991.
328. **(Horton et al. 1989)** Horton, J. W., Drake, A. A., and Rankin, D. W., 1989, Tectonstratigraphic Terranes and their Paleozoic boundaries in the central and southern Appalachians, Geological Society of America, Special Paper 230, p. 213-245, 1989.
329. **(Horton et al. 1991)** Horton, J.W., Drake, A.A., Rankin, D.W., and Dallmeyer, R.D., Preliminary Tectonstratigraphic Terrane map of the central and southern Appalachians, U.S. Geological Survey, Miscellaneous Investigation Series, scale 1:2,000,000, 1991.

- 330. **(Hough et al. 2000)** Hough, S. E., Armbruster, J. G., Seeber, L., and Hough, S. E., On the Modified Mercalli intensities and magnitudes of the 1811-1812 New Madrid earthquakes: *Journal of Geophysical Research*, v. 105, no. B10, p. 23, 839-23,864, 2000.
- 331. **(Howard et al. 2005)** Howard, C. S., Charleton, J. E., and McCarney, K. J., New geologic synthesis of the Dreher Shoals and Carolina Terranes, Lake Murray and Saluda Dam, Columbia, SC: *Geological Society of America Abstracts with Programs*, v. 37, no. 2, p. 36, 2005.
- 332. **(Huddlestun and Hetrick 1978)** Huddlestun, P. F. and Hetrick, J. H., Stratigraphy of the Tobacco Road Sand—A New Formation: *Georgia Geologic Survey Bulletin* 93, pp. 56-77, 1978.
- 333. **(Huddlestun and Hetrick 1985)** Huddlestun, P. F. and Hetrick, J. H., Upper Eocene stratigraphy of central and eastern Georgia: *Georgia Geologic Survey Bulletin* 95, 78 p, 1985.
- 334. **(Huddlestun and Summerour 1996)** Huddlestun, P. F., and Summerour, J. H., The lithostratigraphic framework of the uppermost Cretaceous and lower Tertiary of eastern Burke County, Georgia: *Georgia Geologic Survey Bulletin* 127, 94 p., 1996.
- 335. **(Humphreys and Coblenz in review)** Humphreys, E. D., and Coblenz, D. D., North America dynamics and western U.S. tectonics: manuscript submitted to *Reviews of Geophysics*, in review.
- 336. **(Hutchinson and Klitgord 1986)** Hutchinson, D. R., and Klitgord, K. D., Evolution of Rift Basins on the Continental Margin off Southern New England, in Manspeizer, Warren, (ed.), *Triassic-Jurassic Rifting: North America and Africa*: American Association of Petroleum Geologists Memoir, 1986.
- 337. **(Iverson and Smithson 1983)** Iverson, W. P., and Smithson, S. B., Reprocessing and reinterpretation of COCORP southern Appalachian profiles: *Earth and Planetary Science Letters*, v. 62, p. 75-90, 1983.
- 338. **(Johnson 1942)** Johnson, D. W., *The origins of Carolina bays*: New York, Columbia University Press, 341 p., 1942.
- 339. **(Johnston 1996)** Johnston, A. C., Seismic moment assessment of earthquake in stable continental regions - III. New Madrid 1811-1812, Charleston 1886 and Lisbon 1755: *Geophysical Journal International*, v. 126, p. 314-344, 1996.
- 340. **(Johnston and Reinbold 1985)** Johnston, A. C., and Reinbold, D. J., A basement block model for southern Appalachian seismicity: *Geological Society of America Abstracts with Programs*, v. 17, no. 2, p. 97, 1985.
- 341. **(Johnston and Schweig 1996)** Johnston, A. C., and Schweig, E. G., The enigma of the New Madrid earthquakes of 1811-1812: *Annual Review of Earth and Planetary Sciences*, v. 24, p. 339-384, 1996.
- 342. **(Johnston et al. 1985)** Johnston, A. C., Reinbold, D. J., and Brewer, S. I., Seismotectonics of the southern Appalachians: *Bulletin of the Seismological Society of America*, v. 75, no. 1, p. 291-312, 1985.

-
343. **(Johnston et al. 1994)** Johnston, A. C., Coopersmith, K. J., Kanter, L. R., and Cornell, C. A., The earthquakes of stable continental regions, volume I: assessment of large earthquake potential, Final Report TR-102261-V1, prepared for Electric Power Research Institute, 1994.
344. **(Kaczorowski 1976)** Kaczorowski, R. T., Origin of the Carolina bays, in Hayes, M. O., and Kana, T. W. (eds.), Terrigenous clastic depositional environments: Technical report No. 11-CRD, Coastal Research Division, Department of Geology, University of South Carolina, Columbia, p. II-16 to II-36, 1976.
345. **(Kanter 1994)** Kanter, L. R., Tectonic interpretation of Stable Continental Crust in : The Earthquakes of Stable Continental Regions, prepared by Johnston; A.C.; Coppersmith, K.J. Kanter, L.R., and Cornell, C.A., Electric Power Research Institute, pp. 2.1 - 2.98, 1994.
346. **(Keen and Haworth 1985)** Keen, C.E., and Haworth, R.T., DNAG Transect D-3: Rifted continental margin off Nova Scotia: Offshore eastern Canada: Geological Society of America, Centennial Continent/Ocean Transect #4, Boulder, Colorado, 1985.
347. **(Kelson et al. 1996)** Kelson, K. I., Simpson, G. D., van Arsdale, R. B., Haraden, C. C., and Lettis, W. R., Multiple late Holocene earthquakes along the Reelfoot fault, central New Madrid seismic zone, Journal of Geophysical Research, v. 101, no. B3, p. 6151-6170, 1996.
348. **(Kidd 1996)** Kidd, N. B., Determination of the hydraulic properties of coastal plain aquifers at Millers Pond and Millhaven, east-central Georgia: Clemson, S.C., Clemson University, M.S. thesis, 153 p., 1996.
349. **(King 1955)** King, P. B., A geologic cross section across the southern Appalachians, an outline of the geology in the segment in Tennessee, North Carolina, and South Carolina, in Russell, R.J., (ed.), Guides to southeastern geology: Geological Society of America Annual Meeting, p. 332-373, 1955.
350. **(King 1964)** King, P. B., Geology of the central Great Smoky Mountains: Tennessee: U. S. Geological Survey Professional Paper 340-C, 148 p., 1964.
351. **(King 1971)** King, P. B., Systematic Pattern of Triassic Dikes in the Appalachian Region, Second Report: U.S. Geological Survey Professional Paper 759-D, 1971.
352. **(King and Beikman 1974)** King, P.B., and Beikman H.M., Geologic Map of the United States (exclusive of Alaska and Hawaii): U.S. Geological Survey, 3 map sheets, 1:250,000 scale, 1974.
353. **(King and Zietz 1978)** King, E. R., and Zietz, I., The New York-Alabama lineament: geophysical evidence for a major crustal break in the basement beneath the Appalachian basin: Geology, v. 6, p. 312-318, 1978.
354. **(King et al. 1968)** King, P. B., Neuman, R. B., and Hadley, J. B., Geology of the Great Smoky Mountains National Park, Tennessee and North Carolina: U. S. Geological Survey Professional Paper 587, 23 p., 1968.

- 355. **(Klitgord and Schouten 1986)** Klitgord, K. D., and Schouten, H., Plate kinematics of the central Atlantic: in Vogt, P.R., and Tucholke, B.E., (eds.), The Geology of North America, Vol M: The Western North Atlantic Region, DNAG Publication, Geological Society of America, Boulder, Colorado, pp. 351-378, 1986.
- 356. **(Klitgord et al. 1988)** Klitgord, K. D., Hutchinson, D. R., Schouten, H., US Atlantic continental margin: structural and tectonic framework: in Sheridan, R.E., and J. A. Grow (eds.), The Atlantic Continental Margin: US., DNAG Publication, Vol. I-1, Geological Society of America, Boulder, Colorado, pp. 19-25, 1988.
- 357. **(Knight 1993)** Knight, J. P., Transmittal of GSB/HGEB Staff Review of Vogtle Fault Investigation Report, Studies of Postulated Millett Fault, NRC internal memorandum for T. M. Novak, January 26, 1993, 4 p., 1993.
- 358. **(Lennon 1986)** Lennon, G., Identification of a northwest trending seismogenic graben near Charleston, South Carolina, U. S. Nuclear Regulatory Commission Report, NUREG/CR-4075, 43 p., 1986.
- 359. **(Lindholm 1978)** Lindholm, R. C., Triassic-Jurassic Faulting in Eastern North America--A Model Based on Pre-Triassic Structures: Geology, v. 6, pp. 365-368, 1978.
- 360. **(Logan and Euler 1989)** Logan, W. R., and Euler, G. M., Geology and ground-water resources of Allendale, Bamberg, and Barnwell Counties and part of Aiken County, South Carolina: South Carolina Water Resources Commission Report 155, 113 p., 1989.
- 361. **(Long and Chapman 1977)** Long L.T., and Chapman, J.W., Jr., Bouguer gravity map of the Summerville-Charleston, South Carolina epicentral zone and tectonic implications, in Rankin, D.W. (editor), Studies related to the Charleston, South Carolina earthquake of 1886 – A preliminary report: U. S. Geological Survey Professional Paper 1028, p 151-166, 1977.
- 362. **(Luetgert et al. 1994)** Luetgert, J. H., Benz, H. M., and Madabhushi, S., Crustal structure beneath the Atlantic Coastal Plain of South Carolina: Seismological Research Letters, vol 65, no. 2., p. 180-191, 1994.
- 363. **(Madabhushi and Talwani 1990)** Madabhushi, S., and Talwani, P., Composite fault plane solutions of recent Charleston, South Carolina, earthquakes: Seimological Research Letters, v. 61, no. 3-4, p. 156, 1990.
- 364. **(Madabhushi and Talwani 1993)** Madabhushi, S., and Talwani, P., Fault plane solutions and relocations of recent earthquakes in Middleton Place-Summerville Seismic Zone near Charleston, South Carolina: Bulletin of the Seismological Society of America, v. 83, no. 5, p. 1442-1466, 1993.
- 365. **(Maher 1978)** Maher, H. D. "Stratigraphy and Structure of the Belair and Kiokee Belts near Augusta, Georgia," in Snoke, A.W. (ed.), Geological Investigations of the Eastern Piedmont, Southern Appalachians: Carolina Geological Society Field Trip Guidebook South Carolina Geological Survey, pp. 47-54, 1978.
- 366. **(Maher 1979)** Maher, H.D., Jr., Stratigraphy, metamorphism, and structure of the Kiokee and Belair belts near Augusta, Georgia, MS thesis: Columbia, South Carolina, University of South Carolina, 94 p., 1979.

-
367. **(Maher 1987)** Maher, H. D., Kinematic history of mylonitic rocks from the Augusta fault zone, South Carolina and Georgia: *American Journal of Science*, v. 287, p. 795-816, 1987.
368. **(Maher et al. 1991)** Maher, H. D., Sacks, P.E., and Secor, D. T., Jr., The eastern Piedmont of South Carolina, in Horton, Jr., J.W. and Zullo, V.A. (eds.), *The Geology of the Carolinas*, University of Tennessee Press, Knoxville, p. 93-108, 1991.
369. **(Maher et al. 1992)** Maher, H. D., Jr., Sacks, P., Secor, D., and Wright, J., Magmatic softening in the orogenic hinterlands southern Appalachian Piedmont, Georgia: *Geological Society of America Abstracts with Programs*, v.24, no.2, 1992.
370. **(Maher et al. 1994)** Maher, H. D., Dallmeyer, R. D., Secor, D. T., Jr., and Sacks, P. E., 40-Ar/39-Ar constraints on chronology of August fault zone movement and late Alleghanian extension, southern Appalachian piedmont, South Carolina and Georgia: *American Journal of Science*, v. 294, p. 428-448, 1994.
371. **(Manspeizer et al. 1978)** Manspeizer, W., Puffer, J. H., and Cousminer, H. L., Separation of Morocco and Eastern North America: A Triassic-Liassic Stratigraphic Record: *Geological Society of America Bulletin*. v. 89, pp. 901-920, 1978.
372. **(Marine 1974a)** Marine, I. W., Geohydrology of buried Triassic basin at Savannah River Plant, South Carolina: *American Association of Petroleum Geologists Bulletin*, v. 58, p. 1825-1837, 1974.
373. **(Marine 1974b)** Marine, I. W., Geohydrology of the buried Triassic basin at the Savannah River Plant: *Groundwater*, vol. 2, 96 pp., 1974.
374. **(Marine and Siple 1974)** Marine, I. W., and Siple, G. E., Buried Triassic basin in the central Savannah River area, South Carolina and Georgia: *Geological Society of America Bulletin*, v. 85, p. 311-320, 1974.
375. **(Markewich 1985)** Markewich, H. W., Geomorphic evidence for Pliocene - Pleistocene uplift in the area of the Cape Fear Arch, North Carolina, in Morisawa, M., and Hock, J. T. (eds.), *Tectonic Geomorphology: Proceedings of the 15th Annual Binghampton Geomorphology Symposium*, Allen and Unwin, Boston, Massachusetts, P. 279 - 297, 1985.
376. **(Markewich and Christopher 1982)** Markewich, H. W., and Christopher, R. A., Pleistocene and Holocene fluvial history of Uphapee Creek, Macon County, Alabama: *U. S. Geological Survey Bulletin* 1522, 16 p., 1982.
377. **(Marple and Talwani 1993)** Marple, R. T., and Talwani, P., Evidence for possible tectonic upwarping along the South Carolina coastal plain from an examination of river morphology and elevation data: *Geology*, v. 21, p. 651-654, 1993.
378. **(Marple and Talwani 2000)** Marple, R. T., and Talwani P., Evidence for a buried fault system in the coastal plain of the Carolinas and Virginia; implications for neotectonics in the Southeastern United States: *Geological Society of America Bulletin*, v. 112, no. 2, p. 200-220, 2000.
379. **(Marshak and Mitra 1988)** Marshak, S. and Mitra, G., Basic Methods of Structural Geology: Prentice Hall, Englewood Cliffs, New Jersey, 446p., 1988.
-

-
380. **(McBride 1991)** McBride, J. H., Constraints on the Structure and Tectonic Development of the Early Mesozoic South Georgia Rift, Southeastern United States; Seismic Reflection Data Processing and Interpretation: Tectonics, v. 10, no. 5, pp. 1065-1083, 1991.
381. **(McCarney et al. 2005)** McCarney, K. J., Charleton, J. E., and Howard, C. S., Brittle features mapped along a shear zone at Saluda Dam, central South Carolina: Geological Society of America Abstracts with Programs, v. 37, no. 2, p. 5, 2005.
382. **(McClelland 1987)** McClelland, S. A., Surface and subsurface stratigraphy of Cretaceous and younger strata along the Savannah River from southern Richmond County through Burke County, Georgia: Columbia, S.C., University of South Carolina, M.S. thesis, 123 p., 1987.
383. **(McConnell 1988)** McConnell, K. I., Geology of the Sauratown Mountains anticlinorium: Vienna and Pinnacle 7.5 minute quadrangles, in Hatcher, R.D., Jr., (ed.), Structure of the Sauratown Mountains window, North Carolina: Carolina Geological Society Guidebook, p. 51-66, 1988.
384. **(McConnell 1994)** McConnell, D. A., Fixed-hinge, basement-involved fault-propagation folds, Wyoming: Geological Society of America Bulletin, v. 106, p. 1583-1593, 1994.
385. **(Melton and Schriever 1933)** Melton, I. A., and Schriever, W., the Carolina “bays” - are they meteorite scars?: Journal of Geology, v. 41, p. 52 - 66, 1933.
386. **(Mittwede et al. 1987)** Mittwede, S. K., Odegard, M., and Sharp, W. E., Major chemical characteristics of the Hammett Grove meta-igneous suite, northeastern South Carolina: Southeastern Geology, v. 28, no. 1, p. 49 - 63, 1987.
387. **(Mixon et al. 1989)** Mixon, R. B., Berquist, C. R., Jr., Newell, W. L., and Johnson, G. H., Geologic map of the Coastal Plain and adjacent parts of the Piedmont, Virginia: U. S. Geological Survey Miscellaneous Investigations Map I-2033, 2 pls., scale 1:250,000, 1989.
388. **(Moos and Zoback 2001)** Moos, D., and Zoback, M. D., In situ stress measurements in the NPR Hole, Volume I – results and interpretations: Final Report submitted to Westinghouse Savannah River Company, WSRC-TR-2001-00499, DOE Contract No. DE-AC09-96SR18500, 41 p., 2001.
389. **(Nelson and Zietz 1981)** Nelson, A. E., and Zietz, I., The Clingman Lineament: aeromagnetic evidence for a major discontinuity in the North American basement: Geological Society of America Abstracts with Programs, v. 13, no. 1, p. 31, 1981.
390. **(Nelson et al. 1985)** Nelson, K. D., Arnow, J. A., McBride, J. H., Willemin, J. H., Huang, J., Zheng, L., and Oliver, J. E., New COCORP Profiling in the Southeastern United States. Part I: Late Paleozoic Suture and Mesozoic Rift Basin: Geology, v. 13, pp. 714-718, 1985.
391. **(Nelson et al. 1987)** Nelson, A. E., Horton, J. W., Jr., and Clarke, J. W., Generalized Tectonic Map of the Greenville 10 X 20 quadrangle, Georgia, South Carolina, and North Carolina: U. S. Geological Survey Miscellaneous Field Studies Map MF-1898, scale 1:250,000, 1987.

-
392. **(Neuman and Nelson 1965)** Neuman, R.B. and Nelson, W. H., Geology of the western Great Smoky Mountains, Tennessee: U. S. Geological Survey Professional Paper 349-D, 81 p., 1965.
393. **(Noel et al. 1988)** Noel, J. R., Spariosu D., J., and Dallmeyer, R. D., Paleomagnetism and 40 Ar/39Ar ages from the Carolina slate belt, Albemarle, North Carolina: Implications for Terrane amalgamation: *Geology*, v. 16, p.64-68, 1988.
394. **(Nystrom et al. 1990)** Nystrom, P. G., Willoughby, R. H., and Dockery, D. T., III, Claibornian Stratigraphy of the Savannah River Site and Surrounding Area: in Zullo, V. A., Harris, W. B., and Price, Van, (eds.), 1990, Savannah River Region: Transition between the Gulf and Atlantic Coastal Plains: Proceedings of the second Bald Head Island Conference on Coastal Plains Geology, Hilton Head Island, November 6-11, pp. 56-61, 1990.
395. **(O'Connor and Prowell 1976)** O'Connor, B. J., and Prowell, D. C., The geology of the Belair fault zone and basement rocks of the Augusta Georgia area: *Georgia Geological Society Guidebook* 16, p. 21-32, 1976.
396. **(Obermeier and McNulty 1998)** Obermeier, S. F., and McNulty, W. E., Paleoliquefaction evidence for seismic quiescence in central Virginia during the late middle Holocene time: *Eos Transactions of the American Geophysical Union*, v. 79, no. 17, p. S342, 1998.
397. **(Obermeier and Pond 1999)** Obermeier, S. F., and Pond, E. C., Issues in using liquefaction features for paleoseismic analysis: *Seismological Research Letters*, v. 70, no. 1, p. 34-58, 1999.
398. **(Obermeier et al. 1985)** Obermeier, S. F., Gohn, G. S., Weems, R. E., Gelinas, R. L., and Rubin, M., Geologic evidence for recurrent moderate to large earthquakes near Charleston, South Carolina: *Science*, v. 227, no. 4685, p. 408-411, 1985.
399. **(Obermeier et al. 1990)** Obermeier, S. F., Jacobson, R. B., Smoot, J. P., Weems, R. E., Gohn, G. S., Monroe, J. E., and Powars, D. S., Earthquake-induced liquefaction features in the coastal setting of South Carolina and in the fluvial setting of the New Madrid seismic zone: U. S. Geological Survey Professional Paper 1504, p. 44, 1990.
400. **(Olsen 1978)** Olsen, P.E., On the use of the term Newark for Triassic and early Jurassic rocks of eastern North America: *Newsletters on Stratigraphy*, v. 7, p. 90-95, 1978.
401. **(Olsen and Schlische 1988)** Olsen, P.E., and Schlische, R. W., Unraveling the rules of rift basins: *Geological Society of America Abstracts with Programs*, v. 20, p. A123, 1988.
402. **(Olsen et al. 1991)** Olsen, P. E., Froelich, A. J., Daniels, D. L.; Smoot, J. P., and Gore, P. J. W., Rift basins of early Mesozoic age: in Horton, J.W., Jr., and Zullo, V.A. (eds.), *The Geology of the Carolinas*, University of Tennessee Press, Knoxville, pp.142-170, 1991.
403. **(Parsons Brinckerhoff 1973)** Parsons, Brinckerhoff, Quade, and Douglas, Inc., Bedrock Waste Storage Project, Triassic Basin Fault Probing Program Report, Du Pont de Nemours and Co., Savannah River Plant, Aiken, South Carolina, 1973.
404. **(Petersen et al. 1984)** Petersen, T. A., Brown, L. D., Cook, F. A., Kaufman, S., and Oliver, J. E., Structure of the Riddleville Basin from COCORP Seismic Data and Implications for Reactivation Tectonics: *Journal of Geology*, vol. 92, pp. 261-271, 1974.
-

-
405. **(Petty et al. 1965)** Petty, A. J., Petrafeso, F. A., and Moore, F. C., Jr., Aeromagnetic map of the Savannah River Plant Area, South Carolina and Georgia: U.S. Geological Survey Geophysical Investigations Map GP-489, scale 1:250,000, 1965.
406. **(Poag and Valentine 1988)** Poag, C. W., and Valentine, P.C., Mesozoic and Cenozoic stratigraphy of the US Atlantic continental shelf and slope. in Sheridan, R.E., and Grow, J. A. (eds.), The Atlantic Continental Margin: US., DNAG Publication, Vol. I-1, Geological Society of America, Boulder, Colorado, p. 67- 85, 1988.
407. **(Powell et al. 1994)** Powell, C. A., Bollinger, G. A., Chapman, M. C., Sibol, M. S., and Johnston, A. R., A seismotectonic model for the 300 km-long eastern Tennessee seismic zone, Science, v. 264, p. 686-688, 1994.
408. **(Preston and Brown 1964)** Preston, C.D., and Brown, C.Q., Geologic section along a Carolina bay, Sumter County, S.C., Southeastern Geology, v. 6, no. 1, p. 21-29, 1964.
409. **(Price et al. 1989)** Price, V., Steele, J., and Stieve, A., Pen Branch Fault Investigation Program Plan, ESS-SRL-89-395, 1989.
410. **(Prouty 1952)** Prouty, W. F., Carolina bays and their origins: Geological Society of America Bulletin, v. 63, p. 167 – 224, 1952.
411. **(Prowell 1988)** Prowell, D. C., Cretaceous and Cenozoic tectonism on the Atlantic Coastal Margin, in Sheridan, R. E. and Grow, J. A. (eds.), The geology of North America, the Atlantic Continental Margin, Geological Society of America, v. I-2, p. 557 - 564, 1988.
412. **(Prowell 1996)** Prowell, D. C., Geologic map of the Savannah River site, Aiken, Allendale, and Barnwell Counties, South Carolina: U. S., Geological Survey, Miscellaneous Field Studies map MF-2300, 1996.
413. **(Prowell 2005)** Prowell, D.C., Personal Communication, 2005.
414. **(Prowell and O'Connor 1978)** Prowell, D. C., and O'Connor, B. J., Belair fault zone: evidence of Tertiary fault displacement in eastern Georgia: Geology, v. 6, p. 681-684, 1978.
415. **(Prowell et al. 1975)** Prowell, D. C., O'Connor, B. J., and Rubin, M., Preliminary evidence for Holocene movement along the Belair fault zone near Augusta, Georgia: U. S. Geological Survey Open File Report 75-680, p. 15, 1975.
416. **(Prowell et al. 1985a)** Prowell, D. C., Christopher, R. A., Edwards, L. E., Bybell, L. M., and Gill, H. E., Geologic section of the updip Coastal Plain from central Georgia to western South Carolina: U.S. Geological Survey Miscellaneous Field Studies, Map MF-1737, 1985.
417. **(Prowell et al. 1985b)** Prowell, D. C., Edwards, L. E., and Frederiksen, N. O., The Ellenton Formation in South Carolina, A Revised Age Designation from Cretaceous to Paleocene: United States Geological Survey Bulletin 1605-A, 1985.
418. **(Rast and Kohles 1986)** Rast, N., and Kohles, K.M., The origin of the Ocoee Supergroup: American Journal of Science, v. 286, p 593-616, 1986.
-

-
419. **(Ratcliffe 1971)** Ratcliffe, N. M., The Ramapo Fault System in New York and Adjacent Northern New Jersey: A Case of Tectonic Heredity, Geological Society of America Bulletin. v. 82, pp. 125-142, 1971.
420. **(Richardson and Reding 1991)** Richardson, R. M., and Reding, L. M., North American Plate dynamics: Journal of Geophysical Research, v. 96, no. B7, p. 12,201-12,223, 1991.
421. **(Rozen 1981)** Rozen, R.W., The Middleton-Lowndesville cataclastic zone in the Elberton East quadrangle, Georgia, in Horton, J.W., Jr., Butler, J.R., and Milton, D.M., (eds.), Geological investigations of the Kings Mountain belt and adjacent areas in the Carolinas: Carolina Geological Society Guidebook, p. 174-180, 1981.
422. **(Sacks and Dennis 1987)** Sacks, P. E., and Dennis, A. J., The Modoc Zone-D2 (Early Alleghenian in the Eastern Appalachian Piedmont, South Carolina and Georgia: : in Secor, D.T., Jr. (ed.), Anatomy of the Alleghenian Orogeny as Seen from the Piedmont of South Carolina and Georgia, Carolina Geological Society Field Trip Guidebook., South Carolina Geological Survey, pp. 19-34, 1987.
423. **(Sacks and Secor 1990)** Sacks, P. E., and Secor, D. T., Jr., Delamination in collisional orogens: Geology, v. 18, p. 999-1002, 1990.
424. **(Sacks et al. 1987)** Sacks, P. E., Maher, H.D., Jr., and Secor, D. T., The Burks Mountain belt of ultramafic rocks in the Kiokee belt, southern Appalachian Piedmont: Geological Society of America Abstracts with Programs, v. 19, p.127, 1987.
425. **(Samson et al. 1990)** Samson, S., Palmer, A.R., and Secor, D. T., Jr., Biogeographical significance of Cambrian trilobites from the Carolina Slate Belt: Geological Society of America Bulletin, v. 102, p. 1459-1470, 1990.
426. **(Savage 1982)** Savage, H., Jr., The mysterious Carolina bays: Columbia University Press, 121 p., 1982.
427. **(Schlische 2003)** Schlische, R. W., Progress in understanding the structural geology, basin evolution, and tectonic history of the eastern North America rift system: in LeTourneau, P.M., and Olsen, P.E. (eds.), The Great Rift Valleys of Pangea in Eastern North America--Volume 1--Tectonics, Structure, and Volcanism, Columbia University Press, New York, p. 21-64, 2003.
428. **(Schlische and Olsen 1990)** Schlische, R. W. and Olsen, P.E., Quantitative filling model for continental extensional basins with application to the early Mesozoic rifts of eastern North America: Journal of Geology, v. 98, p. 135-155, 1990.
429. **(Secor 1987)** Secor, D. T., Jr., Regional Overview - Anatomy of the Alleghenian Orogeny as Seen from the Piedmont of South Carolina and Georgia: Carolina Geological Society Field Trip Guidebook. ed., D. T. Secor, Jr., South Carolina Geological Survey, pp. 1-18, 1987.
430. **(Secor et al. 1983)** Secor, D. T., Jr., Samson, S. L., Snoke, A. W., and Palmer, A. R., Confirmation of Carolina Slate Belt as an Exotic Terrane: Science, v. 221, pp. 649-651, 1983.

-
431. **(Secor et al. 1986a)** Secor, D.T. Jr., Snoke, A.W., Bramlett, K.W., Costello, O.P., and Kimbrell, O.P., Character of the Alleghanian orogeny in the southern Appalachians Part I. – Alleghanian deformation in the eastern Piedmont of South Carolina: Geological Society of America Bulletin, v. 97, p. 1319-1328, 1986.
432. **(Secor et al. 1986b)** Secor, D.T., Jr., Snoke, A.W., and Dallmeyer, R.D., Character of the Alleghanian orogeny in the southern Appalachians: Part III. Regional tectonic relations: Geological Society of America Bulletin, v.97, p. 1345-1353, 1986.
433. **(Seeber and Armbruster 1981)** Seeber, L., and Armbruster, J. G., The 1886 Charleston, South Carolina earthquake and the Appalachian detachment: Journal of Geophysical Research, v. 86, no. B9, p. 7874-7894, 1981.
434. **(Seeber and Armbruster 1988)** Seeber, L., and Armbruster, J. G., Seismicity along the Atlantic seaboard of the U.S.; Intraplate neotectonics and earthquake hazard: in R. E. Sheridan and J. A. Grow (eds.) The Atlantic Continental Margin: U.S., The Geology of North America, vol. I-2, Geological Society of America, Boulder Colorado, p. 564-582, 1988.
435. **(Sheridan et al. 1993)** Sheridan, R. E., Musser, D. L., Glover, L., Talwani, P., Ewing, J. I., Holbrook, W. S., Purdy, G. M., Hawman, R., and Smithson, S., Deep seismic reflection data of EDGE U.S. mid-Atlantic continental-margin experiment: implications for Appalachian sutures and Mesozoic rifting and magmatic underplating: Geology, v. 21, p. 563-567, 1993.
436. **(Shumaker 2000)** Shumaker, R. C., The New York-Alabama lineament: an early Iapetian wrench fault?: American Association of Petroleum Geologists Bulletin, v. 84, no. 4, p. 1393, 2000.
437. **(Siple 1967)** Siple, G. E., Geology and Ground Water of the Savannah River Plant and Vicinity, South Carolina, U.S. Geological Survey Water Supply, Paper no. 1841, p. 113, 1967.
438. **(Sloan 1908)** Sloan, Earle, Catalogue of mineral localities of South Carolina: South Carolina Geological Survey, ser. 4, Bulletin 2, p. 449-453, 1908.
439. **(Smith 1931)** Smith, L. L., Solution depressions in sandy sediments of the Coastal Plain in South Carolina: Journal of Geology, v. 39, p. 641-652, 1931.
440. **(Smoot 1985)** Smoot, J. P., The closed-basin hypothesis and its use in facies analysis of the Newark Supergroup, in Robinson, G. R., Jr., and Froelich, A.J., (eds.), Proceedings of the second US Geological Survey workshop on the early Mesozoic basins of the eastern US: United States Geological Survey Circular 946, p. 4-10, 1985.
441. **(Snipes et al. 1989)** Snipes, D.S., Fallaw, W.C., and Price, V., Jr., The Pen Branch fault: documentation of late Cretaceous and Tertiary faulting in the coastal plain of South Carolina (DRAFT): Westinghouse Savannah River Company draft report, 44 p., January 8, 1989.
442. **(Snipes et al. 1993a)** Snipes, D. S., Fallaw, W. C., Price, V., Jr., and Cumbest, R. J., 1993, The Pen Branch Fault: Documentation of late Cretaceous-Tertiary faulting in the Coastal Plain of South Carolina: Southeastern Geology, v. 33, no. 4, p. 195-218, 1993.

-
443. **(Snipes et al. 1993b)** Snipes, D. S., Hodges, R. A., Warner, R. D., Fallaw, W. C., Price, V. Jr., Cumbest, R. J., and Logan, W. R., The Martin Fault: Southeastern boundary of the early Mesozoic Dunbarton Basin, Abstract with Programs, Geological Society of America Annual Meeting, Boston, MA, 1993.
444. **(Snoke and Frost 1990)** Snoke, A. W., and Frost, B. R., Exhumation of high pressure pelitic schist, Lake Murray Spillway, South Carolina: Evidence for crustal extension during Alleghanian strike-slip faulting: *American Journal of Science*, v. 290 p.853-881, 1990.
445. **(Snoke et al. 1980)** Snoke, A. W., S. A. Kish, and D. T. Secor, J, Deformed Hercynian granitic rocks from the Piedmont of South Carolina: *American Journal of Science*. v. 280, pp. 1018-1034, 1980.
446. **(Sohl and Owens 1991)** Sohl, N. F., and Owens, J. P., Cretaceous stratigraphy of the Carolina Coastal Plain, in Horton, J. W., Jr., and Zullo, V. A., (eds.), *Geology of the Carolinas*: Knoxville, Tenn., University of Tennessee Press, p. 191-220, 1991.
447. **(Soller 1988)** Soller, D. R., *Geology and tectonic history of the lower Cape Fear River valley, southeastern North Carolina*: U.S. Geological Survey, Professional Paper 1466-A, 60 p., 1988.
448. **(Soller and Mills 1991)** Soller, D. R., and Mills, H.H., Surficial geology and geomorphology, in Horton, , J. W., Jr., and Zullo, V. A., *The Geology of the Carolinas*, Carolina Geological Society Fiftieth Anniversary Volume, University of Tennessee Press, Knoxville, pp. 290-308, 1991.
449. **(Steele 1985)** Steele, K.B., Lithostratigraphic correlation of Cretaceous and younger strata of the Atlantic Coastal Plain province within Aiken, Allendale and Barnwell Counties, South Carolina: Columbia, S.C., University of South Carolina, M.S. thesis, 174 p., 1985.
450. **(Steltenpohl 1988)** Steltenpohl, M.G., Kinematics of the Towaliga, Bartletts Ferry, and Goat Rock fault zones, Alabama: The late Paleozoic dextral shear system in the southernmost Appalachians: *Geology*, v. 16, p. 852-888, 1988.
451. **(Stephenson and Stieve 1992)** Stephenson, D. E., and Stieve, A., Structural model of the basement in the central Savannah River area, South Carolina and Georgia, Westinghouse Savannah River Company Technical Report 92-120, 1992.
452. **(Stevenson 1982)** Stevenson, A. C., Geomorphic history of a portion of the Savannah River flood plain, Barnwell County, South Carolina: Master of Science Thesis, University of South Carolina, 108 p., 1982.
453. **(Stieve and Stephenson 1995)** Stieve, A.L., and Stephenson, D. E., Geophysical evidence for post Late Cretaceous reactivation of basement structures in the central Savannah River area, *Southeastern Geology*, v 35., no.1, p. 1-20, 1995.
454. **(Stieve et al. 1994)** Stieve, A., Coruh, C., and Costain, J., Confirmatory drilling project final report (U): Westinghouse Savannah River Company Report WSRC-RP-94-013, 298 p., 1994.

-
455. **(Summerour et al. 1998)** Summerour, J. H., Shapiro, E. A., and Huddlestun, P. F., An investigation of Tritium in the Gordon and other aquifers in Burke County, Georgia – Phase II: Georgia Department of Natural Resources, Georgia Geologic Survey Information Circular 102, 12 p., 1998.
456. **(Suppe and Medwedeff 1990)** Suppe, J., and Medwedeff, D. A., Geometry and kinematics of fault-propagation folding: *Eclogae Geol. Helv.*, v. 83, no. 3, p. 409-454, 1990.
457. **(Talwani 1982)** Talwani, P., An internally consistent pattern of seismicity near Charleston, South Carolina: *Geology*, v. 10, no. 12, p. 654-658, 1982.
458. **(Talwani 1999)** Talwani, P., Fault geometry and earthquakes in continental interiors: *Tectonophysics*, v. 305, no. 1-3, p. 371-379, 1999.
459. **(Talwani 2000)** Talwani, P., Macroscopic effects of the 1886 Charleston earthquake, A compendium of field trips of South Carolina Geology, South Carolina Geological Survey, 2000.
460. **(Talwani and Katuna 2004)** Talwani, P. and Katuna M., Macroseismic effects of the 1886 Charleston earthquake: Carolina Geological Society field trip guidebook, p. 18, 2004.
461. **(Talwani and Schaeffer 2001)** Talwani, P., and Schaeffer, W. T., Recurrence rates of large earthquakes in the South Carolina coastal plain based on paleoliquefaction data: *Journal of Geophysical Research*, v. 106, no. B4, p. 6621-6642, 2001.
462. **(Tarr and Rhea 1983)** Tarr, A. C., and Rhea, B. S., Seismicity near Charleston, South Carolina, March 1973 to December 1979, in Gohn, G. S., (ed.), *Studies Related to the Charleston, South Carolina Earthquake of 1886: Tectonics and Seismicity*, U.S. Geological Survey Professional Paper 1313, p. R1-R17, 1983.
463. **(Tarr et al. 1981)** Tarr, A. C., Talwani, P., Rhea, S., Carver, D., and Amick, D., Results of recent South Carolina seismological studies: *Bulletin of the Seismological Society of America*, v. 71, no. 6, p. 1883-1902, 1981.
464. **(Thom 1970)** Thom, B. G., Carolina bays in Horry and Marion counties, South Carolina: *Geological Society of America Bulletin*, v. 18, p.783-814, 1970.
465. **(Turcotte and Schubert 2002)** Turcotte, D. L., and Schubert, G., *Geodynamics*: Cambridge, UK, Cambridge University Press, 2002.
466. **(Tuttle et al. 2002)** Tuttle, M. P., Schweig, E. S., III, Sims, J. D., Lafferty, R. H., Wolf, L. W., and Haynes, M. L., The earthquake potential of the New Madrid seismic zone: *Bulletin of the Seismological Society of America*, v. 92, no. 6, p. 2080-2089, 2002.
467. **(Tuttle et al. 2005)** Tuttle, M. P., Schweig, E. S., Campbell, J., Thomas, P. M., Sims, J. D., and Lafferty, R. H., Evidence for New Madrid earthquakes in A. D. 300 and 2350 B. C., *Seismological Research Letters*, v. 76, no. 4, p. 489-501, 2005.
468. **(USACE 1952)** U.S. Army Corps of Engineers, Charleston District. *Geologic-Engineering Investigations, Savannah River Plant*. DPWR-52, E.I. du Pont de Nemours and Company, Savannah River Plant, Aiken, SC, 1952.

- 469. **(Van Arsdale 2000)** Van Arsdale, R. B., Displacement history and slip rate on the Reelfoot fault of the New Madrid seismic zone, *Engineering Geology*, v. 55, p. 219-226, 2000.
- 470. **(Van Arsdale et al. 1995)** Van Arsdale, R. B., Kelson, K. I., and Lurnsden, C. H., Northern extension of the Tennessee Reelfoot scarp into Kentucky and Missouri, *Seismological Research Letters*, v. 66, no. 5, p. 57-62, 1995.
- 471. **(Van Schmus et al. 1996)** Van Schmus, W. R., Bickford, M. E., and Turek, A., Proterozoic geology of the east-central Midcontinent basin: in van der Pluijm, B.A., and Catacosinos, P. A., (eds.), *Basement and Basins of Eastern North America*, Geological Society of America Special Paper 308, Boulder, CO, p. 7-32, 1996.
- 472. **(Veatch and Stephenson 1911)** Veatch, Otto, and Stephenson, L.W., Preliminary report on the coastal plain of Georgia: *Georgia Geologic Survey Bulletin* 26, 446 p., 1911.
- 473. **(Vick et al. 1987)** Vick, H. K., Channell, J. E. T., and Opdyke, N.D., Ordovician docking of the Carolina slate belt: Paleomagnetic data: *Tectonics*, v.6, p.573-583, 1987.
- 474. **(Waddell et al. 1995)** Waddell, M. G., Keith, J. F., and Domoracki, W. J., High-resolution seismic characterization: GGS-1, Burke County, Georgia, *Earth Sciences and Resources Institute, ESRI-USC Technical Report 95-F129-1*, University of South Carolina, Columbia, 20 p., 1995.
- 475. **(Weems 1998)** Weems, R. E., Newly recognized en echelon fall lines in the Piedmont and Blue Ridge provinces of North Carolina and Virginia, with a discussion of their possible ages and origins: *U.S. Geological Survey Open-File Report 98-0374*, 52 p., 1998.
- 476. **(Weems and Lewis 2002)** Weems, R. E., and Lewis, W. C., Structural and tectonic setting of the Charleston, South Carolina, region; evidence from the Tertiary stratigraphic record: *Geological Society of America Bulletin*, v. 114, no. 1, p. 24-42, 2002.
- 477. **(Weems et al. 1997)** Weems, R. E., Lemon, E. M., Jr., and Nelson, M. S., *Geology of the Pringletown, Ridgeville, Summerville, and Summerville Northwest 7.5-minute quadrangles, Berkeley, Charleston, and Dorchester counties, South Carolina: Miscellaneous Investigations Series*, U. S. Geological Survey, 1997.
- 478. **(Wehr and Glover 1985)** Wehr, F., and Glover, L., III, Stratigraphy and tectonics of the Virginia-North Carolina Blue Ridge: Evolution of a late Proterozoic-Early Paleozoic hinge zone: *Geological Society of America Bulletin*, v. 96, p. 285-295, 1985.
- 479. **(Wentworth and Mergner-Keefer 1983)** Wentworth, C.M., and Mergner-Keefer, M., Regenerate faults of the southeastern United States, in Gohn, G. S. (ed.), *Studies related to the Charleston, South Carolina, earthquake of 1886: Tectonics and seismicity*, U.S. Geological Survey Professional Paper 1313, pp. S1-S20, 1983.
- 480. **(Wheeler 1995)** Wheeler, R. L., Earthquakes and the cratonward limit of Iapetan faulting in eastern North America, *Geology*, v. 23, p. 105-108, 1995.
- 481. **(Wheeler 1996)** Wheeler, R. L., Earthquakes and the southeastern boundary of the intact Iapetan margin in eastern North America: *Seismological Research Letters*, v. 67, p. 77-83, 1996.

-
482. **(Wheeler 2005)** Wheeler, R. L., Known or suggested Quaternary tectonic faulting, Central and Eastern United States; new and updated assessments for 2005: U. S. Geological Survey Open-File Report 2005-1336, 2005.
483. **(Wheeler and Crone 2001)** Wheeler, R. L., and Crone, A. C., Known and suggested Quaternary faulting in the mid-continent United States: Engineering Geology, v. 62, p. 51-78, 2001.
484. **(Wheeler and Johnston 1992)** Wheeler, R. L., and Johnston, A. C., Geologic implications of earthquake source parameters in central and eastern North America: Seismological Research Letters, v. 63, no. 4, p. 491-505, 1992.
485. **(White et al. 2000)** White, D. J., Forsyth, D. A., Asudeh, I., Carr, S. D., Wu, H., Easton, R. M., and Mereu, M., A seismic-based cross-section of the Grenville orogen in southern Ontario and western Quebec: Canadian Journal of Earth Science, v. 37, p. 183-192, 2000.
486. **(Wildermuth and Talwani 2001)** Wildermuth, E., and Talwani, P., A detailed gravity survey of a pull-apart basin in northeast South Carolina: Geological Society of America – Abstracts with Programs, v. 33, no. 6, p. 240, 2001.
487. **(Withjack et al. 1998)** Withjack, M. O., Schlische, R. W., and Olsen, P. E., Diachronous rifting, drifting, and inversion on the passive margin of central eastern North America: an analog for other passive margins: American Association of Petroleum Geologists Bulletin, v. 82, no. 5A, p. 817-835, 1998.
488. **(Wyatt 2000)** Wyatt, D. E., Natural phenomena hazards (NPH) design criteria and other characterization information for the mixed oxide (MOX) fuel fabrication facility at Savannah River Site, Westinghouse Savannah River Company Technical Report WSRC-TR-2000-00454, 418 p., 2000.
489. **(Wyatt and Harris 2000)** Wyatt, D. E., and Harris, L. D., Savannah River Site environmental remediations systems in unconsolidated upper coastal plain sediments-stratigraphic and structural consideration, Carolina Geological Society Field Trip Guidebook, Westinghouse Savannah River Company Document WSRS-MS-2000-00606, 2000.
490. **(Zoback 1992)** Zoback, M. L., Stress field constraints on intraplate seismicity in eastern North America: Journal of Geophysical Research, v. 97, no. B8, p. 11,761-11,782, 1992.
491. **(Zoback and Zoback 1989)** Zoback, M. L., and Zoback, M. D., Tectonic stress field of the coterminous United States, in Pakiser, L.C. and Mooney, W.D., (eds.), Geophysical Framework of the Continental United States: Geological Society of America Memoir 172, p. 523-539, 1989.
492. **(Abrahamson and Silva 1997)** Abrahamson, N. N., A. and W. J. Silva. "Empirical response spectral attenuation relations for shallow crustal earthquakes," Bull. Seism. Soc. Am., Empirical Response Spectral Attenuation Relations for Shallow Crustal Earthquakes, Seismological Research Letters, v. 68, n. 1, 94-127, Jan/Feb 1997.

-
493. **(ANSS 2005)** The Advanced National Seismic System catalog is website: <http://quake.geo.berkeley.edu/anss/catalog-search.html>. Catsearch.16391.txt, 27 pages, downloaded on June 3, 2005.
 494. **(ASCE 2005)** American Society of Civil Engineers, “Seismic Design Criteria for Structures, Systems, and Components in Nuclear Facilities”, ASCE/SEI 43-05, 2005.
 495. **(Atkinson and Boore 1995)** Atkinson, G. M. and D. M. Boore, Ground-Motion Relations for Eastern North America. Bull. Seism. Soc. Am., v. 85, n. 1, 17-30 (1995).
 496. **(Bechtel 1984)** Bechtel Power Corporation, Seismic Analysis Report, Vogtle Nuclear Generating Plant Units 1 and 2, October 1984.
 497. **(Bechtel 2000)** Bechtel Corporation, *Theoretical and User’s Manual for SHAKE 2000*, prepared by N Deng and F Ostadan, San Francisco, CA, 2000.
 498. **(Bechtel 2006d)** Lindvall, S. C. and Hartleb, R. D., Update of Charleston Seismic Source and Integration with EPRI Source Models, Bechtel engineering study report 25144-006-V14-CY06-00006, revision 001, 2006.
 499. **(Behrendt et al 1988)** Behrendt, J. C., Klitgord, K. D., and Hutchinson, D. R., Reactivated Boundary Fault Zones of Buried Early Mesozoic Basins as Possible Sources of Seismicity in the Charleston, S.C. Region: Abstracts with Programs - Geological Society of America Southeastern Section, v. 20, no. 4, p. 253, 1988.
 500. **(Bollinger et al. 1985)** Bollinger, G. A., Chapman, M. C., Sibol, M. S., and Costain, J. K., An analysis of earthquake focal depths in the southeastern U. S., Geophysical Research Letters, v. 12, no. 11, p. 785-788, 1985.
 501. **(Bronk Ramsey 1995)** Bronk Ramsey, C., Radiocarbon calibration and analysis of stratigraphy: the OxCal program, Radiocarbon, v. 37, no. 2, p. 425-430, 1995.
 502. **(Bronk Ramsey 2001)** Bronk Ramsey, C., Development of the radiocarbon program OxCal: Radiocarbon, v. 43, no. 2A, p. 355-363, 2001.
 503. **(Chapman 2005b)** Chapman, M., Personal Communication, 2005.
 504. **(Chapman and Talwani 2002)** Chapman, M. C. and Talwani. P., Seismic Hazard Mapping for Bridge and Highway Design in South Carolina, South Carolina Department of Transportation Report, 2002.
 505. **(Chapman et al. 2002)** Chapman, M. C., Munsey, J. W., Powell, C. A., Whisner, S. C., and Whisner J., The Eastern Tennessee Seismic Zone - Summary after 20 Years of Network Monitoring: Seismological Research Letters, v. 73, no. 2, p. 245, 2002.
 506. **(Costantino, 1996)** Costantino, C. J. (1996). Recommendations for Uncertainty Estimates in Shear Modulus Reduction and Hysteretic Damping Relationships. Published as an appendix in Silva, W. J., N. Abrahamson, G. Toro and C. Costantino (1997). “Description and validation of the stochastic ground motion model.” Report Submitted to Brookhaven National Laboratory, Associated Universities, Inc. Upton, New York 11973, Contract No. 770573.
 507. **(Cornell 1968)** Cornell, C. A., Engineering Seismic Risk Analysis, Bulletin of the Seismological Society of America, v. 58, no. 5, p. 1583-1606, 1968.
-

- 508. **(Cornell and Winterstein 1988)** Cornell, C. A. and Winterstein, S. R., Temporal and Magnitude Dependence in Earthquake Recurrence Models, Bulletin of the Seismological Society of America, v. 79, p. 1522-1537, 1988.
- 509. **(Cramer 2001)** Cramer, C. H., A Seismic Hazard Uncertainty Analysis for the New Madrid Seismic Zone, Engineering Geology, v. 62, p. 251-266, 2001.
- 510. **(Ellsworth et al. 1999a)** Ellsworth, W. L., Matthews, M. V., Nadeau, R. M., Nishenko, S. P., Reasenberg, P. A., and Simpson, R. W., A Physically-Based Earthquake Recurrence Model for Estimation of Long-Term Earthquake Probabilities, U.S. Geological Survey Open-File Report 99-522, 22p., 1999.
- 511. **(EPRI NP-4726 1986)** Electric Power Research Institute (EPRI), Volumes 5–10, Seismic Hazard Methodology for the Central and Eastern United States, Tectonic Interpretations, July 1986.
- 512. **(EPRI NP-4726-A 1988)** Seismic Hazard Methodology for the Central and Eastern United States, Volume 1, Part 2: Methodology (Revision 1). EPRI NP-4726-A, Rev. 1, dated November 1988.
- 513. **(EPRI NP-6452-D 1989)** Electric Power Research Institute (EPRI), EQHAZARD Primer, Prepared by Risk Engineering for Seismicity Owners Group and EPRI, June 1989.
- 514. **(EPRI NP-6395-D 1989)** Probabilistic seismic hazard evaluation at nuclear plant sites in the central and eastern United States, resolution of the Charleston Earthquake issue, EPRI Rept. 6395-D, Palo Alto, CA, April 1989.
- 515. **(EPRI TR-102293 1993)** Electric Power Research Institute. "Guidelines for Determining Design Basis Ground Motions." Volume 5: Quantification of Seismic Source Effects. EPRI Report TR-102293, Project 3302, Final Report, November 1993.
- 516. **(EPRI 1009684 2004)** Electric Power Research Institute, CEUS Ground Motion Project Final Report, Elec. Power Res. Inst, Technical Report 1009684, dated December 2004.
- 517. **(Fletcher et al. 1978)** Fletcher, J. B., Sbar, M. L., and Sykes, L. R., Seismic Trends and Travel-time Residuals in Eastern North America and Their Tectonic Implications: Geological Society of America Bulletin, v. 89, p. 1656-1676, 1978.
- 518. **(Grant and Sieh 1994)** Grant, L. B. and Sieh, K., Paleoseismic Evidence of Clustered Earthquakes on the San Andreas Fault in the Carrizo Plain, California, Journal of Geophysical Research, v. 99, n. B4, p. 6819-6841, 1994.
- 519. **(Lee 1996)** Lee, R., "Investigations of Nonlinear Dynamic Properties at the Savannah River Site," *Report No. WSRC-TR-96-0062, Rev. 1*, Aiken, SC, 1996.
- 520. **(Lee 2001)** Lee, R.C., "Development of MFFF-Specific Vertical-to-Horizontal Seismic Spectral Ratios," Report No. WSRC-TR-2001-00342, Rev. 0, Westinghouse Savannah River Co., Aiken, SC, 2001.
- 521. **(Marple and Talwani 1990)** Marple, R. T., and Talwani, P., Field investigations of the Woodstock Lineament: Seismological Research Letters, v. 61, no. 3-4, p. 156, 1990.

-
522. **(Marple and Talwani 2004)** Marple, R. T. and Talwani, P., Proposed Shenandoah Fault and East Coast-Stafford Fault System and Their Implications for Eastern U. S. Tectonics, *Southeastern Geology*, v. 43, no. 2, p. 57-80, 2004.
523. **(Martin and Clough 1994)** Martin, J. R. and Clough, G. W., Seismic Parameters from Liquefaction Evidence, *Journal of Geotechnical Engineering*, v. 120, no. 8, p. 1345-1361, 1994.
524. **(Matthews et al. 2002)** Matthews, M. V., Ellsworth, W. L., and Reasenber, P. A., A Brownian model for recurrent earthquakes, *Bulletin of the Seismological Society of America*, v. 92, p. 2233-2250, 2002.
525. **(McGuire et al. 2001)** McGuire, R.K., W. J. Silva, and C. J. Costantino. Technical Basis for Revision of Regulatory Guidance on Design Ground Motions, Hazard- and Risk-Consistent Ground Motion Spectra Guidelines. prepared for Nuclear Regulatory Commission, NUREG/CR-6728, 2001.
526. **(McGuire et al. 2002)** McGuire, R. K., W. J. Silva, and C. J. Costantino, Technical Basis for Revision of Regulatory Guidance on Design Ground Motions: Development of Hazard- & Risk-Consistent Seismic Spectra for Two Sites, Revision 0, prepared for Nuclear Regulatory Commission, NUREG/CR-6769, 2002.
527. **(NIST/SEMATECH 2006)** NIST/SEMATECH, e-Handbook of Statistical Methods, <http://www.itl.nist.gov/div898/handbook/>, accessed 11 January 2006.
528. **(Obermeier 1996)** Obermeier, S., Liquefaction-induced features: in *Paleoseismology*, J. McCalpin (ed.), Academic Press, San Diego, p. 331-396, 1996.
529. **(Obermeier 2005)** Obermeier, S., personal communication, September 2, 2005.
530. **(Obermeier et al. 1989)** Obermeier, S. F., Weems, R. E., Jacobson, R. B., and Gohn, G. S., Liquefaction evidence for Repeated Holocene Earthquakes in the Coastal Region of South Carolina, *Annals of the New York Academy of Sciences*, v. 558, p. 183-195, 1989.
531. **(Rockwell et al. 2000)** Rockwell, T. K., Lindvall, S., Herzberg, M., Murbach, D., Dawson, T., and Berger, G., Paleoseismology of the Johnson Valley, Kickapoo, and Homestead Valley faults: clustering of earthquakes in the Eastern California shear zone, *Bulletin of the Seismological Society of America*, v. 90, no. 5, p. 1200-1236, 2000.
532. **(Savage 1991)** Savage, J. C., Criticism of Some Forecasts of the National Earthquake Evaluation Council, *Bulletin of the Seismological Society of America*, v. 81, n. 3, p. 862-881, 1991.
533. **(Savy et al. 2002)** Savy, J. B., Foxall, W., Abrahamson, N., and Bernreuter, D., Guidance for Performing Probabilistic Seismic Hazard Analysis for a Nuclear Plant Site: Example Application to the Southeastern United States, U.S. Nuclear Regulatory Commission, NUREG/CR-6607, 2002.
534. **(Seeber and Armbruster 1981)** Seeber, L., and Armbruster, J. G., The 1886 Charleston, South Carolina earthquake and the Appalachian detachment: *Journal of Geophysical Research*, v. 86, no. B9, p. 7874-7894, 1981.

-
535. **(SEUSSN 2005)** The South Eastern United States Seismic Network catalog is available from the Virginia Tech Seismic Observatory FTP site: <http://www.geol.vt.edu/outreach/vtso/anonftp/catalog/susn2003cat.txt>, (266 pages), Susn2003cat.txt, bulletin.txt and catalog.txt, downloaded on June 3, 2005.
536. **(Sieh et al. 1989)** Sieh, K., Stuiver, M., and Brillinger, D., A More Precise Chronology of Earthquakes Produced by the San Andreas fault in Southern California, *Journal of Geophysical Research*, v. 94, n. B1, p. 603-623, 1989.
537. **(Smith and Talwani 1985)** Smith, W. A., and Talwani, P., Preliminary interpretation of a detailed gravity survey in the Bowman and Charleston, S.C. seismogenic zones: Abstracts with Programs - Geological Society of America southeastern section, v. 17, no. 2, p. 137, 1985.
538. **(SSHAC 1997)** SSHAC, Recommendations for Probabilistic Seismic Hazard Analysis: Guidance on Uncertainty and Use of Experts, Prepared by Senior Seismic Hazard Analysis Committee (SSHAC), NUREG/CR-6372, 1997.
539. **(Sykes 1978)** Sykes, L. R., Intraplate Seismicity, Reactivation of Preexisting Zones of Weakness, Alkaline Magmatism, and Other Tectonism Postdating Continental Fragmentation: *Reviews of Geophysics*, v. 16, p. 621-688, 1978.
540. **(Talwani 2005)** Talwani, P., Personal Communication, September 8, 2005.
541. **(Toro 1996)** Toro, G. R. (1996). Probabilistic Models of Site Velocity Profiles for Generic and Site-Specific Ground-Motion Amplification Studies. Published as an appendix in Silva, W. J., N. Abrahamson, G. Toro and C. Costantino (1997). "Description and validation of the stochastic ground motion model." Report Submitted to Brookhaven National Laboratory, Associated Universities, Inc. Upton, New York 11973, Contract No. 770573.
542. **(Toro 1997)** Toro, G.R. (1997). Probabilistic Models of Site Velocity Profiles at the Savannah River Site, Aiken, South Carolina. Report by Risk Engineering, Inc. to Pacific Engineering and Analysis, April. Published as an appendix in Lee, R.C.; Maryak, M.E.; and McHood, M.D. 1997. SRS Seismic Response Analysis and Design Basis Guidelines. WSRC-TR-97-0085, Rev. 0. Aiken, South Carolina: Westinghouse Savannah River Company.
543. **(Toro 2005)** Toro, G.R. (2005). Site-Wide Probabilistic Model of Shear-Wave Velocity Profiles at the Savannah River Site, Aiken, South Carolina. Report by Risk Engineering, Inc. to Bechtel Savannah River Co., October.
544. **(Tuttle 2001)** Tuttle, M. P., The Use of Liquefaction Features in Paleoseismology: Lessons Learned in the New Madrid Seismic Zone, central United States, *Journal of Seismology*, v. 5, p. 361-380, 2001.
545. **(Wells and Coppersmith 1994)** Wells D.L. and K.J. Coppersmith. New Empirical Relationships Among Magnitude, Rupture Length, Rupture Width, Rupture Area, and Surface Displacement," *Bulletin Seismological Society of America*, 84, 4, 974-1002, August 1994.
546. **(WGCEP 1995)** Working Group on California Earthquake Probabilities, Seismic Hazards in Southern California: Probable earthquakes, 1994 to 2024, *Bulletin of the Seismological Society of America*, v. 85, p. 379-439, 1995.
-

-
547. **(WGCEP 2003)** Working Group on California Earthquake Probabilities, Earthquake Probabilities in the San Francisco Bay region: 2002-2031, U. S. Geological Survey Open-File Report 03-2134, 2003.
548. **(WSRC 1998)** General SRS Strain Compatible Soil Properties for 1886 Charleston Earthquake (U), Calculation K-CLC-G-0060, McHood, M.D, October 29, 1998.
549. **(Alterman 1984)** Alterman, I., Summary of visit to examine clastic dikes near Vogtle, June 21–22, 1984, US Nuclear Regulatory Commission docket nos. 50-424 and 50- 425, 26 pp., 1984.
550. **(Bartholomew et al. 2002)** Bartholomew, M.J., Brodie, B.M., Willoughby, R.H., Lewis, S.E., and Syms, F.H., Mid-Tertiary paleoseismites: syndepositional features and section restoration used to indicate paleoseismicity, Atlantic coastal plain, South Carolina and Georgia, Geological Society of America Special Paper 359, pp. 63–74, 2002.
551. **(Bechtel 1974a)** Crane, D., Report of marl investigation – Alvin W. Vogtle nuclear plant, Bechtel Power Corporation – Geotechnical Services, 11 pp. + attachments, 1974.
552. **(Bechtel 1974b)** Bechtel Power Corporation, Report on foundation investigations for Alvin W. Vogtle nuclear power plant, v. 1 and 2, prepared for Southern Services, Inc., and Georgia Power Company, file no. 25144-006-T14-CY06-00006, 1974.
553. **(Bechtel 1978e)** Bechtel Incorporated, Report on stratigraphic irregularities exposed in the auxiliary building excavation – Alvin W. Vogtle nuclear power plant, prepared for Southern Services, Inc., and Georgia Power Company, 12 pp., 1978.
554. **(Bechtel 1981)** Bechtel Power Corporation, Report on joints in marl near cooling tower 2A, 10 pp., 1981.
555. **(Bechtel 1984b)** Bechtel Power Corporation – Geology Group, Geologic evaluation of trench exposure – Vogtle electric generating plant, 43 pp., 1984.
556. **(McDowell and Houser 1983)** McDowell, R.C. and Houser, B.B., Map showing distribution of small-scale deformation structures in part of the upper coastal plain of South Carolina and adjacent Georgia, US Geological Survey, misc. field studies map MF-1538, 1:250,000 scale, 1983.
557. **(Nelson 1989)** Nelson, J.S., A review of seismic reflection data – postulated Pen Branch fault area, Savannah River project, report prepared for Bechtel Civil and Minerals, 8 pp. + attachments, 1989.
558. **(Prowell 1994a)** Prowell, D.C., Preliminary geologic map of the Barnwell 30' x 60' quadrangle, South Carolina and Georgia, US Geological Survey Open-File Report 94-673, 1:100,000 scale, 1994.
559. **(Stephenson and Chapman 1988)** Stephenson, D.S. and Chapman, W.L., Structure associated with the buried Dunbarton basin, South Carolina from recent seismic data: Geological Society of America – Abstracts with Programs, v. 20, p. 318, 1988.
560. **(Stevenson and Talwani 1996)** Stevenson, D.A., and Talwani, P., Aiken earthquake of August, 1993, Seismological Research Letters, v. 67, pp. 43-50, 1996.

- 561. **(Stevenson and Talwani 2004)** Stevenson, D. and Talwani, P., 2001–2002 Upper Three Runs sequence of earthquakes at the Savannah River site, South Carolina, *Seismological Research Letters*, v. 75, pp. 107–116, 2004.
- 562. **(Stieve et al. 1991)** Stieve, A., Stephenson, D.E., and Aadland, R.K., Pen Branch fault program: consolidated report on the seismic reflection surveys and the shallow drilling (U), Westinghouse Savannah River Company Technical Report WSRC-TR-91-87, 48 pp., 1991.
- 563. **(Talwani et al. 1985)** Talwani, P., Rawlins, J., and Stephenson, D.E., The Savannah River plant, South Carolina earthquake of June 09, 1985 and its tectonic setting, *Earthquake Notes*, v. 56, pp. 101–106, 1985.
- 564. **(ACI 1994)** American Concrete Institute (1994). *Manual of Concrete Practice, Part 1, Materials and General Properties of Concrete*.
- 565. **(API 1991)** American Petroleum Institute (1991). "Cathodic Protection of Aboveground Petroleum Storage Tanks," *API Recommended Practice No. 651, Washington D.C.*
- 566. **(ASCE 1994)** American Society of Civil Engineers, *Bearing Capacity of Soils*, Technical Engineering and Design Guide, 1994.
- 567. **(ASTM D 1557 2002)** ASTM International, *Standard Test Methods for Laboratory Compaction Characteristics of Soil Using Modified Effort (56,000 ft-lbf/ft³ (2,700 kN-m/m³))*, ASTM D 1557, Conshohocken, PA, 2002.
- 568. **(ASTM D 1586 1999)** ASTM International, *Standard Test Method for Penetration Test and Split-Barrel Sampling of Soils*, ASTM D 1586 Conshohocken, PA, 1999.
- 569. **(ASTM D 2113 1999)** ASTM International, *Standard Practice for Rock Core Drilling and Sampling of Rock for Site Investigation*, ASTM D 2113, Conshohocken, PA, 1999.
- 570. **(ASTM D 2488 2000)** ASTM International, *Standard Practice for Description and Identification of Soils (Visual-Manual Procedure)*, ASTM D 2488, Conshohocken, PA, 2000.
- 571. **(ASTM D 4044 2002)** ASTM International, *Standard Test Method (Field Procedure) for Instantaneous Change in Head (Slug) Tests for Determining Hydraulic Properties of Aquifers*, ASTM D 4044, Conshohocken, PA, 2002.
- 572. **(ASTM D 4428 2000)** ASTM International, *Standard Test Method for Crosshole Seismic Testing*, ASTM D 4428, Conshohocken, PA, 2000.
- 573. **(ASTM D 4633 2005)** ASTM International, *Standard Test Method for Energy Measurements for Dynamic Penetrometers*, ASTM D 4633, Conshohocken, PA, 2005.
- 574. **(ASTM D 5778 2000)** ASTM International, *Standard Test Method for Performing Electronic Friction Cone and Piezocone Penetration Testing of Soils*, ASTM D 5778, Conshohocken, PA, 2000.
- 575. **(ASTM D 6066 1996)** ASTM International, *Standard Practice for Determining the Normalized Penetration Resistance of Sands for Evaluation of Liquefaction Potential*, ASTM D 6066, Conshohocken, PA, 1996.

-
576. **(ASTM G 57 2006)** ASTM International, *Standard Test Method Field Measurements of Soil Resistivity Using the Wenner Four-Electrode Method*, ASTM G 57, Conshohocken, PA, 2006.
577. **(Bechtel 1978a)** Bechtel Power Corporation, Report on Backfill Material Investigations, Alvin W. Vogtle Nuclear Project, January 1978.
578. **(Bechtel 1978b)** Bechtel Power Corporation, Report on Backfill Material Investigations, Alvin W. Vogtle Nuclear Project, Addendum No. 1, October 1978.
579. **(Bechtel 1978c)** Bechtel Power Corporation, Report on Dynamic Properties for Compacted Backfill, Alvin W. Vogtle Nuclear Project, February 1978.
580. **(Bechtel 1978d)** Bechtel Power Corporation, Test Fill Program, Phase II, Alvin W. Vogtle Nuclear Project, October 1978.
581. **(Bechtel 1979)** Bechtel Power Corporation, Report on Backfill Material Investigations, Alvin W. Vogtle Nuclear Project, Addendum No. 2, November 1979.
582. **(Bechtel 1986)** Bechtel Power Corporation, VEGP Report on Settlement, Vogtle Nuclear Generating Plant Units 1 and 2, August 1986.
583. **(Bowles 1982)** Bowles, J.E., *Foundation Analysis and Design*, Third Edition, McGraw-Hill Book Company, New York, 1982.
584. **(Davie and Lewis 1988)** Davie, J.R. and Lewis, M.R., "Settlement of Two Tall Chimney Foundations," *Proceedings, Second International Conference on Case Histories in Geotechnical Engineering*, St. Louis, MO, June 1988.
585. **(Geovision 1999)** Geovision, Inc. (1999). Suspension velocity measurements at the Savannah River Site, GCB-8. Report 9211-01, prepared for Exploration Resources, dated March 26, 1999.
586. **(Lee et al. 1997)** Lee, R.C., M.E. Maryak, and M.D. McHood. "SRS Seismic Response Analysis and Design Basis Guidelines," *Report No. WSRC-TR-97-0085, Rev. 0*, Westinghouse Savannah River Co., Savannah River Site, Aiken, SC, 1997.
587. **(NRC/NAP 1985)** National Research Council, *Liquefaction of Soils During Earthquakes*, Committee on Earthquake Engineering, National Academy Press, Washington, D.C. 1985.
588. **(Ohya 1986)** Ohya, S., "In Situ P and S Wave Velocity Measurement," *Proceedings of In Situ '86*, ASCE, New York, NY, 1986.
589. **(OSHA 2000)** Occupational Safety and Health Administration (OSHA), 29 CFR Part 1926, *Safety and Health Regulations for Construction*, 2000.
590. **(Peck et al. 1974)** Peck, R.B., Hanson, W.E., and Thornburn, T.H., *Foundation Engineering*, Second Edition, John Wiley and Sons, Inc., New York, 1974.
591. **(Seed and Idriss 1970)** Seed, H.B., and Idriss, I.M., *Soil Moduli and Damping Factors for Dynamic Response Analyses*, Report No. UCB/EERC-70/10, University of California, Berkeley, December 1970.
-

-
592. **(Seed et al. 1984)** Seed, H.B., Wong, R.T., Idriss, I.M., and Tokimatsu, K., *Moduli and Damping Factors for Dynamic Analyses of Cohesionless Soils*, Report No. UCB/EERC-84/14, University of California, Berkeley, September 1984.
593. **(Skempton 1957)** Skempton, A. W., "Discussion of the Planning and Design of the New Hong Kong Airport," *Proceedings of the Institution of Civil Engineers*, Vol. 7, pp. 305-307, 1957.
594. **(SNC 2007)** Vogtle Electric Generating Plant Units 1 and 2, Application for License Renewal, Southern Nuclear Operating Company, June 27, 2007.
595. **(Soubra 1999)** Soubra, Abudul-Hamid, "Upper-Bound Solutions for Bearing Capacity of Foundations," *Journal of Geotechnical and Geoenvironmental Engineering*, Vol. 125 No. 1, ASCE Publications, Reston, VA, pp. 59-68.
596. **(SRS 2005)** Birdwell elastic properties logs for SRS boreholes DRB-9, DRB-10, and DRB-11. per. comm. Frank Syms, Savannah River Site, August 26, 2005.
597. **(STS 1990)** STS Consultants, Inc. (1990). "Reinforced Soil Structures, Vol. 1, Design and Construction Guidelines," *FHWA Report No. FHWA-RD-89-043*, McLean, VA.
598. **(Sun et al. 1988)** Sun, J.I., Golesorkhi, R., and Seed, H.B., *Dynamic Moduli and Damping Ratios for Cohesive Soils*, Report No. UCB/EERC-88/15, University of California, Berkeley, August 1988.
599. **(Rizzo 2008)** "Report No. 05-3423-R1. Rev 0, Foundation Mats Settlements Vogtle AP1000 Foundations," Paul C. Rizzo Associates, Inc., Monroeville, PA, March 2008.
600. **(Terzaghi 1955)** Terzaghi, K., "Evaluation of Coefficients of Subgrade Reaction," *Geotechnique*, Volume 5, 1955.
601. **(USACE 2003)** U.S. Army Corps of Engineers, *Engineering and Design - Slope Stability*, EM 1110-2-1902, Office of the Chief of Engineers, Dept. of the Army, 2003.
602. **(Vesic 1975)** Vesic, A.S., *Bearing Capacity of Shallow Foundations*, in *Foundation Engineering Handbook*, H.F. Winterkorn and H-Y Fang, Editors, Van Nostrand Reinhold Company, New York, 1975.
603. **(WEC 2008)** "RAI-TR85-SEB1-31," Westinghouse Electric Company LLC., Pittsburgh, PA, February 2008.
604. **(WEC CCC-004)** APP-1000-CCC-004, Rev. 0, *Nuclear Island - Stability Evaluation*.
605. **(WEC SC2-065)** APP-1000-S2C-065, Rev. 0, *Nuclear Island Stick Model Analysis at Soil Sites*.
606. **(Youd et al. 2001)** Youd, T. L., Idriss, I. M., Andrus, R. D., Arango, I., Castro, G., Christian, J. T., Dobry, R., Liam Finn, W. D., Harder, L. F., Jr., Hynes, M. E., Ishihara, K., Koester, J. P., Laio, S. S. C., Marcuson, III, W. F., Martin, G. R., Mitchell, J. K., Moriwaki, Y., Power, M. S., Robertson, P. K., Seed, R. B., Stokoe, II, K. H. (2001). "Liquefaction resistance of soils: Summary report from the 1996 NCEER and 1998 NCEER/NSF workshops on evaluation of liquefaction resistance of soils", *Journal of Geotechnical and Geoenvironmental Engineering*, 127(10), pp. 817-833.
-

607. SV0-GW-GEF-004, Rev. 0, Settlement Sensitivity Evaluation of Construction Sequence to Support SB Course 7 Panel Installation.

Table 2.5-1
Limits of Acceptable Settlement Without Additional Evaluation

Differential Across Nuclear Island Foundation Mat	Total for Nuclear Island Foundation Mat	Differential Between Nuclear Island and Turbine Building⁽¹⁾	Differential Between Nuclear Island and Other Buildings⁽¹⁾
1/2 inch 50 ft	6 inches	3 inches	3 inches

Note:

1. Differential settlement is measured at the center of the nuclear island and the center of the adjacent structures.

Table 2.5-201
Definitions of Classes Used in the Compilation of Quaternary Faults, Liquefaction Features, and Deformation in the Central and Eastern United States

Class Category	Definition
Class A	Geologic evidence demonstrates the existence of a Quaternary fault of tectonic origin, whether the fault is exposed for mapping or inferred from liquefaction to other deformational features.
Class B	Geologic evidence demonstrates the existence of a fault or suggests Quaternary deformation, but either (1) the fault might not extend deeply enough to be a potential source of significant earthquakes, or (2) the currently available geologic evidence is too strong to confidently assign the feature to Class C but not strong enough to assign it to Class A.
Class C	Geologic evidence is insufficient to demonstrate (1) the existence of tectonic fault, or (2) Quaternary slip or deformation associated with the feature.
Class D	Geologic evidence demonstrates that the feature is not a tectonic fault or feature; this category includes features such as demonstrated joints or joint zones, landslides, erosional or fluvial scarps, or landforms resembling fault scarps, but of demonstrable non-tectonic origin.

Source: Crone and Wheeler 2000; Wheeler 2005

Table 2.5-202 (Sheet 1 of 2)
Earthquakes 1985–2005, Update to the EPRI (NP-4726-A 1988)
Seismicity Catalog with $E_m \geq 3.0$, Within a 30° to 37° N, 78° to 86° W
Latitude-Longitude Window, Incorporating the 200 mi (320 km) Radius Site Region

Year	Mo	Dy	Hr	Mn	Sec	Lat	Lon	Z(km)	Int	Emb	Smb	Rmb
1985	12	22	0	56	5.0	35.701	-83.720	13.4		3.25	0.30	3.35
1986	1	7	1	26	43.3	35.610	-84.761	23.1		3.06	0.30	3.17
1986	2	13	11	35	45.6	34.755	-82.943	5.0		3.50	0.10	3.51
1986	3	13	2	29	31.4	33.229	-83.226	5.0	4	3.30	0.25	3.37
1986	7	11	14	26	14.8	34.937	-84.987	13.0	6	3.80	0.10	3.81
1986	9	17	9	33	49.5	32.931	-80.159	6.7	4	3.30	0.25	3.37
1987	3	16	13	9	26.8	34.560	-80.948	3.0		3.06	0.30	3.17
1987	3	27	7	29	30.5	35.565	-84.230	18.5	6	4.20	0.10	4.21
1987	7	11	0	4	29.5	36.105	-83.816	25.1	5	3.79	0.10	3.80
1987	7	11	2	48	5.9	36.103	-83.819	23.8	4	3.43	0.10	3.44
1987	9	1	23	2	49.4	35.515	-84.396	21.1		3.06	0.30	3.17
1987	9	22	17	23	50.1	35.623	-84.312	19.4	5	3.50	0.10	3.51
1987	11	27	18	58	29.3	36.852	-83.110	26.8	5	3.50	0.10	3.51
1987	12	12	3	53	28.8	34.244	-82.628	5.0		3.00	0.10	3.01
1988	1	9	1	7	40.6	35.279	-84.199	12.2	4	3.30	0.25	3.37
1988	1	23	1	57	16.4	32.935	-80.157	7.4	5	3.50	0.25	3.57
1988	2	16	15	26	54.8	36.595	-82.274	4.0	4	3.30	0.10	3.31
1988	2	18	0	37	45.4	35.346	-83.837	2.4	4	3.50	0.10	3.51
1989	6	2	5	4	34.0	32.934	-80.166	5.8	4	3.30	0.25	3.37
1990	8	17	21	1	15.9	36.934	-83.384	0.6	5	4.00	0.10	4.01
1990	11	13	15	22	13.0	32.947	-80.136	3.4	5	3.50	0.10	3.51
1991	6	2	6	5	34.9	32.980	-80.214	5.0	5	3.50	0.25	3.57
1991	9	24	7	21	7.0	35.701	-84.117	13.3	4	3.30	0.10	3.31
1991	10	30	14	54	12.6	34.904	-84.713	8.1		3.06	0.30	3.17
1992	1	3	4	21	23.9	33.981	-82.421	3.3	5	3.50	0.25	3.57
1992	8	21	16	31	56.1	32.985	-80.163	6.5	6	4.10	0.10	4.11
1993	1	15	2	2	50.9	35.039	-85.025	8.1	4	3.30	0.10	3.31
1993	7	12	4	48	20.8	36.035	-79.823	5.0	4	3.30	0.10	3.31
1993	8	8	9	24	32.4	33.597	-81.591	8.5	5	3.50	0.10	3.51
1994	2	12	2	40	24.5	36.800	-82.000	5.0		3.42	0.41	3.61
1994	4	5	22	22	0.4	34.969	-85.491	24.3	5	3.50	0.10	3.51
1994	4	16	20	10	12.2	35.752	-83.968	1.8	5	3.50	0.25	3.57
1995	3	11	8	15	52.3	36.959	-83.133	1.0		3.80	0.10	3.81
1995	3	11	9	50	4.4	36.990	-83.180	1.0		3.30	0.10	3.31
1995	3	18	22	6	20.8	35.422	-84.941	26.0		3.25	0.30	3.35
1995	4	17	13	46	0.0	32.997	-80.171	8.4	6	3.90	0.10	3.91
1995	6	26	0	36	17.1	36.752	-81.481	1.8	5	3.40	0.10	3.41
1995	7	5	14	16	44.7	35.334	-84.163	10.0	4	3.70	0.10	3.71
1995	7	7	21	1	3.0	36.493	-81.833	10.0	4	3.06	0.10	3.08
1996	4	19	8	50	14.0	36.981	-83.018	0.0		3.90	0.10	3.91
1997	5	19	19	45	35.8	34.622	-85.353	2.7	4	3.06	0.10	3.08
1997	7	19	17	6	34.4	34.953	-84.811	2.8	4	3.61	0.10	3.62

Table 2.5-202 (Sheet 2 of 2)
Earthquakes 1985–2005, Update to the EPRI (NP-4726-A 1988)
Seismicity Catalog with $E_m \geq 3.0$, Within a 30° to 37° N, 78° to 86° W
Latitude-Longitude Window, Incorporating the 200 mi (320 km) Radius Site Region

Year	Mo	Dy	Hr	Mn	Sec	Lat	Lon	Z(km)	Int	Emb	Smb	Rmb
1997	7	30	12	29	25.3	36.512	-83.547	23.0	5	3.80	0.10	3.81
1998	4	13	9	56	15.6	34.471	-80.603	6.6	5	3.90	0.10	3.91
1998	6	5	2	31	3.9	35.554	-80.785	9.4		3.34	0.10	3.35
1998	6	17	8	0	23.9	35.944	-84.392	11.3	5	3.60	0.10	3.61
1999	1	17	18	38	5.1	36.893	-83.799	1.0	3	3.06	0.27	3.15
2000	1	18	22	19	32.2	32.920	-83.465	19.2	5	3.50	0.10	3.51
2001	3	7	17	12	23.8	35.552	-84.850	6.8	3	3.20	0.10	3.21
2001	3	21	23	35	34.9	34.847	-85.438	0.0	3	3.16	0.27	3.24
2001	6	11	18	27	54.3	30.226	-79.885	10.0		3.33	0.41	3.53
2001	7	26	5	26	46.0	35.971	-83.552	14.3	3	3.25	0.10	3.26
2002	11	8	13	29	3.2	32.422	-79.950	3.9		3.50	0.41	3.69
2002	11	11	23	39	29.7	32.404	-79.936	2.4		4.23	0.41	4.42
2003	3	18	6	4	24.2	33.689	-82.888	5.0		3.50	0.41	3.69
2003	4	29	8	59	38.1	34.445	-85.620	9.1	6	4.70	0.10	4.71
2003	5	2	10	48	43.5	34.512	-85.604	10.0		3.01	0.41	3.20
2003	5	5	10	53	49.9	33.055	-80.190	11.4		3.06	0.30	3.17
2003	7	13	20	15	17.0	32.335	-82.144	5.0		3.58	0.41	3.77
2004	7	20	9	13	14.4	32.972	-80.248	10.3		3.17	0.41	3.37
2004	9	17	15	21	43.6	36.932	-84.006	1.2		3.66	0.41	3.85

Table 2.5-203 (Sheet 1 of 2)
Summary of Bechtel Seismic Sources

Source	Description	Pa ¹	Mmax (m _B) and Wts. ²	Smoothing Options and Wts. ³	Inter- dependencies ⁴	New Information to Suggest Change in Source:		
						Geometry? ⁵	Mmax? ⁶	RI? ⁷
<u>Sources within 200 mi (320 km) that contribute to 99% of hazard</u>								
H	Charleston Area	0.50	6.8 [0.20] 7.1 [0.40] 7.4 [0.40]	1 [0.33] 2 [0.34] 4 [0.33]	P(H N3)=0.15	Yes ⁸	Yes ⁸	Yes ⁸
N3	Charleston Faults	0.53	6.8 [0.20] 7.1 [0.40] 7.4 [0.40]	1 [0.33] 2 [0.34] 4 [0.33]	P(N3 H)=0.16	Yes ⁸	Yes ⁸	Yes ⁸
BZ4	Atlantic Coastal Region	1.00	6.6 [0.10] 6.8 [0.40] 7.1 [0.40] 7.4 [0.10]	1 [0.33] 2 [0.34] 3 [0.33]	Background; P _B =1.00	No	No	No
BZ5	S. Appalachians	1.00	5.7 [0.10] 6.0 [0.40] 6.3 [0.40] 6.6 [0.10]	1 [0.33] 2 [0.34] 3 [0.33]	Background; P _B =1.00	No	No	No
F	S.E. Appalachians	0.35	5.4 [0.10] 5.7 [0.40] 6.0 [0.40] 6.6 [0.10]	1 [0.33] 2 [0.34] 4 [0.33]	ME with G; ME with 13, 15, 16, 17	No	No	No
G	NW South Carolina	0.35	5.4 [0.10] 5.7 [0.40] 6.0 [0.40] 6.6 [0.10]	1 [0.33] 2 [0.34] 4 [0.33]	ME with F; ME with 13, 15, 16, 17	No	No	No
<u>Other Sources within 200 mi (320 km) that do not contribute to 99% of hazard</u>								
13	Eastern Mesozoic Basins	0.10	5.4 [0.10] 5.7 [0.40] 6.0 [0.40] 6.6 [0.10]	1 [0.33] 2 [0.34] 4 [0.33]	no overlap with H or N3; ME with all sources in BZ5	No	No	No
24	Bristol Trends	0.25	5.7 [0.10] 6.0 [0.40] 6.3 [0.40] 6.6 [0.10]	1 [0.33] 2 [0.34] 4 [0.33]	ME with 19, 25, 25A	No	No	No
15	Rosman Fault	0.05	5.4 [0.10] 5.7 [0.40] 6.0 [0.40] 6.6 [0.10]	1 [0.33] 2 [0.34] 4 [0.33]	ME with all other sources	No	No	No

Table 2.5-203 (Sheet 2 of 2)
Summary of Bechtel Seismic Sources

Source	Description	Pa ¹	Mmax (m _b) and Wts. ²	Smoothing Options and Wts. ³	Inter- dependencies ⁴	New Information to Suggest Change in Source:		
						Geometry? ⁵	Mmax? ⁶	RI? ⁷
16	Belair Fault	0.05	5.4 [0.10]	1 [0.33]	ME with all other sources	No	No	No
			5.7 [0.40]	2 [0.34]				
			6.0 [0.40]	4 [0.33]				
			6.6 [0.10]					

1 Pa = probability of activity; (from EPRI NP-6452-D 1989)

2 Maximum Magnitude (Mmax) and weights (wts.); (from EPRI NP-6452-D 1989)

3 Smoothing options are defined as follows (from EPRI NP-6452-D 1989):

1 = constant a, constant b (no prior b);

2 = low smoothing on a, high smoothing on b (no prior b);

3 = low smoothing on a, low smoothing on b (no prior b);

4 = low smoothing on a, low smoothing on b (weak prior of 1.05).

Weights on magnitude intervals are [1.0, 1.0, 1.0, 1.0, 1.0, 1.0, 1.0].

4 ME = mutually exclusive; PD = perfectly dependent

5 No, unless (1) new geometry proposed in literature or (2) new seismicity pattern

6 No, unless (1) new data suggests Mmax exceeds or differs significantly from the EPRI Mmax distribution or (2) exceeded by historical seismicity.

7 RI = recurrence interval; assumed no change if no new paleoseismic data or rate of seismicity has not significantly changed

8 Replace this source with the Updated Charleston Seismic Source (UCSS) Model

Table 2.5-204 (Sheet 1 of 2)
Summary of Dames & Moore Seismic Sources

						New Information to Suggest Change in Source:		
Source	Description	Pa ¹	Mmax (m _b) and Wts. ²	Smoothing Options and Wts. ³	Interdependencies ⁴	Geometry? ⁵	Mmax? ⁶	RI? ⁷
<i>Sources within 200 mi (320 km) that contribute to 99% of hazard</i>								
54	Charleston Seismic Zone	1.00	6.6 [0.75] 7.2 [0.25]	1 [0.22] 2 [0.08] 3 [0.52] 4 [0.18]	none	Yes ⁸	Yes ⁸	Yes ⁸
52	Charleston Mesozoic Rift	0.46	4.7 [0.75] 7.2 [0.25]	3 [0.75] 4 [0.25]	ME with 47 thru 50, 65; ME with 52	No	No	No
53	S. Appalachian Mobile Belt (Default Zone)	0.26	5.6 [0.80] 7.2 [0.20]	1 [0.75] 2 [0.25]	Default for 47 thru 52, 65	No	No	No
41	S. Cratonic Margin (Default Zone)	0.12	6.1 [0.80] 7.2 [0.20]	1 [0.75] 2 [0.25]	Default for 42, 43, and 46	No	No	No
20	S. Coastal Margin	1.00	5.3 [0.80] 7.2 [0.20]	1 [0.75] 2 [0.25]	none	No	No	No
<i>Other Sources within 200 mi (320 km) that do not contribute to 99% of hazard</i>								
4	Appalachian Fold Belts	0.35	6.0 [0.80] 7.2 [0.20]	1 [0.75] 2 [0.25]	ME with 4A, 4B, 4C, 4D	No	No	No
4A	Kink in Fold Belt	0.65	5.0 [0.75] 7.2 [0.25]	3 [0.75] 4 [0.25]	ME with 4	No	No	No
49	Jonesboro Basin	0.28	6.0 [0.75] 7.2 [0.25]	3 [0.75] 4 [0.25]	PD with 47, 48, 50, 51, 65; ME with 52	No	No	No
50	Buried Triassic Basins	0.28	6.0 [0.75] 7.2 [0.25]	3 [0.75] 4 [0.25]	PD with 47, 48, 49, 51, 65; ME with 52	No	No	No
51	Florence Basin	0.28	6.0 [0.75] 7.2 [0.25]	3 [0.75] 4 [0.25]	PD with 47 thru 50, 65; ME with 52	No	No	No

Table 2.5-204 (Sheet 2 of 2)
Summary of Dames & Moore Seismic Sources

Source	Description	Pa ¹	Mmax (m _b) and Wts. ²	Smoothing Options and Wts. ³	Interdependencies ⁴	New Information to Suggest Change in Source:		
						Geometry? ⁵	Mmax? ⁶	RI? ⁷
65	Dunbarton Triassic Basin	0.28	5.9 [0.75] 7.2 [0.25]	3 [0.75] 4 [0.25]	PD with 47 thru 51; ME with 52	No	No	No
C01	Combination zone 4-4A- 4B-4C-4D	NA	6.0 [0.80] 7.2 [0.20]	1 [0.75] 2 [0.25]	NA	No	No	No

1 Pa = probability of activity; (from EPRI NP-6452-D 1989)

2 Maximum Magnitude (Mmax) and weights (wts.); (from EPRI NP-6452-D 1989)

3 Smoothing options are defined as follows (from EPRI NP-6452-D 1989)

1 = No smoothing on a, no smoothing on b (strong prior of 1.04);

2 = No smoothing on a, no smoothing on b (weak prior of 1.04);

3 = Constant a, constant b (strong prior of 1.04);

4 = Constant a, constant b (weak prior of 1.04).

Weights on magnitude intervals are [0.1, 0.2, 0.4, 1.0, 1.0, 1.0, 1.0]

4 ME = mutually exclusive; PD = perfectly dependent

5 No, unless (1) new geometry proposed in literature or (2) new seismicity pattern

6 No, unless (1) new data suggests Mmax exceeds or differs significantly from the EPRI Mmax distribution or (2) exceeded by historical seismicity.

7 RI = recurrence interval; assumed no change if no new paleoseismic data or rate of seismicity has not significantly changed

8 Replace this source with the Updated Charleston Seismic Source (UCSS) Model

Table 2.5-205 (Sheet 1 of 2)
Summary of Law Engineering Seismic Sources

Source	Description	Pa ¹	Mmax (_{mb}) and Wts. ²	Smoothing Options and Wts. ³	Inter- dependencies ⁴	New Information to Suggest Change in Source:		
						Geometry? ⁵	Mmax? ⁶	RI? ⁷
<u>Sources within 200 mi (320 km) that contribute to 99% of hazard</u>								
35	Charleston Seismic Zone	0.45	6.8 [1.00]	2a [1.00]	Overlaps 8 and 22	Yes ⁸	Yes ⁸	Yes ⁸
17	Eastern Basement	0.62	5.7 [0.20] 6.8 [0.80]	1b [1.00]	none	No	No	No
22	Reactivated E. Seaboard Normal	0.27	6.8 [1.00]	2a [1.00]	ME with 8 and 21; overlaps 24, 35, and 39	No	No	No
108	Brunswick, NC Background	1.00	4.9 [0.50] 5.5 [0.30] 6.8 [0.20]	2a [1.00]	Background; P _B =0.42	No	No	No
C09	Mesozoic Basins (8 - Bridged)	NA	6.8 [1.00]	2a [1.00]	NA	No	No	No
C10	8-35	NA	6.8 [1.00]	2a [1.00]	NA	No	No	No
C11	22 - 35	NA	6.8 [1.00]	2a [1.00]	NA	No	No	No
M33	Mafic Pluton	0.43	6.8 [1.00]	5 [1.00]	none	No	No	No
M36	Mafic Pluton	0.43	6.8 [1.00]	5 [1.00]	none	No	No	No
M37	Mafic Pluton	0.43	6.8 [1.00]	5 [1.00]	none	No	No	No
M38	Mafic Pluton	0.43	6.8 [1.00]	5 [1.00]	none	No	No	No
M39	Mafic Pluton	0.43	6.8 [1.00]	5 [1.00]	none	No	No	No
M40	Mafic Pluton	0.43	6.8 [1.00]	5 [1.00]	none	No	No	No
M41	Mafic Pluton	0.43	6.8 [1.00]	5 [1.00]	none	No	No	No
M42	Mafic Pluton	0.43	6.8 [1.00]	5 [1.00]	none	No	No	No
<u>Other Sources within 200 mi (320 km) that do not contribute to 99% of hazard</u>								
217	Eastern Basement Background	1.00	4.9 [0.50] 5.7 [0.50]	1b [1.00]	Background; P _B =0.29; same geometry as 17	No	No	No

Table 2.5-205 (Sheet 2 of 2)
Summary of Law Engineering Seismic Sources

Source	Description	Pa ¹	Mmax (m _b) and Wts. ²	Smoothing Options and Wts. ³	Inter- dependencies ⁴	New Information to Suggest Change in Source:		
						Geometry? ⁵	Mmax? ⁶	RI? ⁷
107	Eastern Piedmont	1.00	4.9 [0.30] 5.5 [0.40] 5.7 [0.30]	1a [1.00]	Background; P _B =0.42	No	No	No
GC13	22 - 24 - 35	NA	6.8 [1.00]	2a [1.00]	NA	No	No	No
GC12	22 - 24	NA	6.8 [1.00]	2a [1.00]	NA	No	No	No
8	Mesozoic Basins	0.27	6.8 [1.00]	a and b values calculated for C09	ME with 22; overlaps with 35	No	No	No

1 Pa = probability of activity; (from EPRI NP-6452-D 1989)

2 Maximum Magnitude (Mmax) and weights (wts.); (from EPRI NP-6452-D 1989)

3 Smoothing options are defined as follows: (from EPRI NP-6452-D 1989)

1a = High smoothing on a, constant b (strong prior of 1.05);

1b = High smoothing on b, constant b (strong prior of 1.00);

1c = High smoothing on a, constant b (strong prior of 0.95);

1d = High smoothing on a, constant b (strong prior of 0.90);

1e = High smoothing on a, constant b (strong prior of 0.70);

2a = Constant a, constant b (strong prior of 1.05);

2c = Constant a, constant b (strong prior of 0.95);

2d = Constant a, constant b (strong prior of 0.90).

Weights on magnitude intervals are all 1.0 for above options.

3a = High smoothing on a, constant b (strong prior of 1.05).

Weights on magnitude intervals are [0.0, 1.0, 1.0, 1.0, 1.0, 1.0, 1.0] for option 3a.

4 ME = mutually exclusive; PD = perfectly dependent

5 No, unless (1) new geometry proposed in literature or (2) new seismicity pattern

6 No, unless (1) new data suggests Mmax exceeds or differs significantly from the EPRI Mmax distribution or (2) exceeded by historical seismicity.

7 RI = recurrence interval; assumed no change if no new paleoseismic data or rate of seismicity has not significantly changed

8 Replace this source with the Updated Charleston Seismic Source (UCSS) Model

Table 2.5-206 (Sheet 1 of 2)
Summary of Rondout Seismic Sources

Source	Description	Pa ¹	Mmax (m _b) and Wts. ²	Smoothing Options and Wts. ³	Interdependencies ⁴	New Information to Suggest Change in Source:		
						Geometry? ⁵	Mmax? ⁶	RI? ⁷
<i>Sources within 200 mi (320 km) that contribute to 99% of hazard</i>								
24	Charleston	1.00	6.6 [0.20] 6.8 [0.60] 7.0 [0.20]	1 [1.00] (a=-0.710, b=1.020)	none	Yes ⁸	Yes ⁸	Yes ⁸
26	South Carolina	1.00	5.8 [0.15] 6.5 [0.60] 6.8 [0.25]	1 [1.00] (a=-1.390, b=0.970)	none	No	No	No
<i>Other Sources within 200 mi (320 km) that do not contribute to 99% of hazard</i>								
49	Appalachian	1.00	4.8 [0.20] 5.5 [0.60] 5.8 [0.20]	2 [1.00]	Background; P _B =1.00	No	No	No
C01	Background 49	NA	4.8 [0.20] 5.5 [0.60] 5.8 [0.20]	3 [1.00]	none	No	No	No
C09	49+32	NA	4.8 [0.20] 5.5 [0.60] 5.8 [0.20]	3 [1.00]	none	No	No	No
50	Grenville	1.00	4.8 [0.20] 5.5 [0.60] 5.8 [0.20]	2 [1.00]	Background; P _B =1.00	No	No	No
C02	Background 50	NA	4.8 [0.20] 5.5 [0.60] 5.8 [0.20]	3 [1.00]	does not contain 12 or 13	No	No	No
C07	50 (02) + 12	NA	4.8 [0.20] 5.5 [0.60] 5.8 [0.20]	3 [1.00]	none	No	No	No
25	Southern Appalachians	0.99	6.6 [0.30] 6.8 [0.60] 7.0 [0.10]	1 [1.00] (a=-0.630, b=1.150)	none	No	No	No

Table 2.5-206 (Sheet 2 of 2)
Summary of Rondout Seismic Sources

Source	Description	Pa ¹	Mmax (m _b) and Wts. ²	Smoothing Options and Wts. ³	Interdependencies ⁴	New Information to Suggest Change in Source:		
						Geometry? ⁵	Mmax? ⁶	RI? ⁷
27	Tennessee-VA Border Zone	0.99	5.2 [0.30] 6.3 [0.55] 6.5 [0.15]	1 [1.00] (a=-1.120, b=0.930)	none	No	No	No

1 Pa = probability of activity; (from EPRI NP-6452-D 1989)

2 Maximum Magnitude (Mmax) and weights (wts.); (from EPRI NP-6452-D 1989)

3 Smoothing options are defined as follows: (from EPRI NP-6452-D 1989)

1, 6, 7, 8 = a, b values as listed above, with weights shown;

3 = Low smoothing on a, constant b (strong prior of 1.0);

5 = a, b values as listed above, with weights shown.

4 ME = mutually exclusive; PD = perfectly dependent

5 No, unless (1) new geometry proposed in literature or (2) new seismicity pattern

6 No, unless (1) new data suggests Mmax exceeds or differs significantly from the EPRI Mmax distribution or (2) exceeded by historical seismicity.

7 RI = recurrence interval; assumed no change if no new paleoseismic data or rate of seismicity has not significantly changed

8 Replace this source with the Updated Charleston Seismic Source (UCSS) Model

Table 2.5-207 (Sheet 1 of 3)
Summary of Weston Seismic Sources

Source	Description	Pa ¹	Mmax (m _b) and Wts. ²	Smoothing Options and Wts. ³	Interdependencies ⁴	New Information to Suggest Change in Source:		
						Geometry? ⁵	Mmax? ⁶	RI? ⁷
<i>Sources within 200 mi (320 km) that contribute to 99% of hazard</i>								
25	Charleston Seismic Zone	0.99	6.6 [0.90] 7.2 [0.10]	1b [1.00]	none	Yes ⁸	Yes ⁸	Yes ⁸
26	South Carolina	0.86	6.0 [0.67] 6.6 [0.27] 7.2 [0.06]	1b [1.00]	none	No	No	No
104	Southern Coastal Plain	1.00	5.4 [0.24] 6.0 [0.61] 6.6 [0.15]	1a [0.20] 2a [0.80]	Background; P _B =1.00	No	No	No
C19	103-23-24	NA	5.4 [0.26] 6.0 [0.58] 6.6 [0.16]	1a [1.00]	NA	No	No	No
C20	104-22	NA	6.0 [0.85] 6.6 [0.15]	1a [0.30] 2a [0.70]	NA	No	No	No
C21	104-25	NA	5.4 [0.24] 6.0 [0.61] 6.6 [0.15]	1a [0.30] 2a [0.70]	NA	No	No	No
C23	104-22-26	NA	5.4 [0.80] 6.0 [0.14] 6.6 [0.06]	1a [0.50] 2a [0.50]	NA	No	No	No
C24	104-22-25	NA	5.4 [0.80] 6.0 [0.14] 6.6 [0.06]	1a [0.50] 2a [0.50]	NA	No	No	No
C26	104-28BCDE-22	NA	5.4 [0.24] 6.0 [0.61] 6.6 [0.15]	1a [0.30] 2a [0.70]	NA	No	No	No
C27	104-28BCDE-22-25	NA	5.4 [0.30] 6.0 [0.70]	1a [0.70] 2a [0.30]	NA	No	No	No

Table 2.5-207 (Sheet 2 of 3)
Summary of Weston Seismic Sources

Source	Description	Pa ¹	Mmax (m _b) and Wts. ²	Smoothing Options and Wts. ³	Interdependencies ⁴	New Information to Suggest Change in Source:		
						Geometry? ⁵	Mmax? ⁶	RI? ⁷
C33	26-25		6.6 [0.90] 7.2 [0.10]	1b [1.00]	NA	No	No	No
C35	104-28BE-25	NA	5.4 [0.24] 6.0 [0.61] 6.6 [0.15]	1a [0.20] 1b [0.80]	NA	No	No	No
<i>Other Sources within 200 mi (320 km) that do not contribute to 99% of hazard</i>								
C22	104-26	NA	5.4 [0.24] 6.0 [0.61] 6.6 [0.15]	1a [0.30] 1b [0.70]	NA	No	No	No
C34	104-28BE-26	NA	5.4 [0.24] 6.0 [0.61] 6.6 [0.15]	1a [0.20] 1b [0.80]	NA	No	No	No
C25	104-28BCDE	NA	5.4 [0.24] 6.6 [0.61] 6.6 [0.15]	1a [0.30] 2a [0.70]	NA	No	No	No
C28	104-28BCDE-22-26	NA	5.4 [0.30] 6.0 [0.70]	1a [0.70] 2a [0.30]	NA	No	No	No
28B	Zone of Mesozoic Basin	0.26	5.4 [0.65] 6.0 [0.25] 6.6 [0.10]	1b [1.00]	PD with 28C, 28D, and 28E	No	No	No
C01	28A thru E	NA	5.4 [0.65] 6.0 [0.25] 6.6 [0.10]	1b [1.00]	NA	No	No	No
103	Southern Appalachians	1.00	5.4 [0.26] 6.0 [0.58] 6.6 [0.16]	1a [0.20] 2a [0.80]	Background; P _B =1.00	No	No	No
C17	103-23	NA	5.4 [0.26] 6.0 [0.58] 6.6 [0.16]	1a [0.70] 2a [0.30]	NA	No	No	No
C18	103-24	NA	5.4 [0.26] 6.0 [0.58] 6.6 [0.16]	1a [0.70] 1b [0.30]	NA	No	No	No

Table 2.5-207 (Sheet 3 of 3)
Summary of Weston Seismic Sources

Source	Description	Pa ¹	Mmax (m _b) and Wts. ²	Smoothing Options and Wts. ³	Interdependencies ⁴	New Information to Suggest Change in Source:		
						Geometry? ⁵	Mmax? ⁶	RI? ⁷
28D	Zone of Mesozoic Basin	0.26	5.4 [0.65] 6.0 [0.25] 6.6 [0.10]	1b [1.00]	PD with 28B, 28C, and 28E	No	No	No
28E	Zone of Mesozoic Basin	0.26	5.4 [0.65] 6.0 [0.25] 6.6 [0.10]	1b [1.00]	PD with 28B, 28C, and 28D	No	No	No
102	Appalachian Plateau	1.00	5.4 [0.62] 6.0 [0.29] 6.6 [0.09]	1a [0.20] 2a [0.80]	Background; P _B =1.00	No	No	No
24	New York-Alabama- Clingman	0.90	5.4 [0.26] 6.0 [0.58] 6.6 [0.16]	1b [1.00]	Contained in 103	No	No	No

1 Pa = probability of activity; (from EPRI NP-6452-D 1989)

2 Maximum Magnitude (Mmax) and weights (wts.); (from EPRI NP-6452-D 1989)

3 Smoothing options are defined as follows: (from EPRI NP-6452-D 1989)

1a = Constant a, constant b (medium prior of 1.0);

1b = Constant a, constant b (medium prior of 0.9);

1c = Constant a, constant b (medium prior of 0.7);

2a = Medium smoothing on a, medium smoothing on b (medium prior of 1.0);

2b = Medium smoothing on a, medium smoothing on b (medium prior of 0.9);

2c = Medium smoothing on a, medium smoothing on b (medium prior of 0.7).

4 ME = mutually exclusive; PD = perfectly dependent

5 No, unless (1) new geometry proposed in literature or (2) new seismicity pattern

6 No, unless (1) new data suggests Mmax exceeds or differs significantly from the EPRI Mmax distribution or (2) exceeded by historical seismicity.

7 RI = recurrence interval; assumed no change if no new paleoseismic data or rate of seismicity has not significantly changed

8 Replace this source with the Updated Charleston Seismic Source (UCSS) Model

Table 2.5-208 (Sheet 1 of 2)
Summary of Woodward-Clyde Seismic Sources

Source	Description	Pa ¹	Mmax (m _b) and Wts. ²	Smoothing Options and Wts. ³	Interdependencies ⁴	New Information to Suggest Change in Source:		
						Geometry? ⁵	Mmax? ⁶	RI? ⁷
<i>Sources within 200 mi (320 km) that contribute to 99% of hazard</i>								
30	Charleston (includes NOTA)	0.573	6.8 [0.33] 7.3 [0.34] 7.5 [0.33]	2 [0.10] 3 [0.10] 4 [0.10] 5 [0.10] 9 [0.60] (a = -1.005, b = 0.852)	ME with 29, 29A	Yes ⁸	Yes ⁸	Yes ⁸
29	S. Carolina Gravity Saddle (Extended)	0.122	6.7 [0.33] 7.0 [0.34] 7.4 [0.33]	2 [0.25] 3 [0.25] 4 [0.25] 5 [0.25]	ME with 29A, 29B, and 30	Yes ⁸	Yes ⁸	Yes ⁸
29A	SC Gravity Saddle No. 2 (Combo C3)	0.305	6.7 [0.33] 7.0 [0.34] 7.4 [0.33]	2 [0.25] 3 [0.25] 4 [0.25] 5 [0.25]	ME with 29, 29B, and 30	Yes ⁸	Yes ⁸	Yes ⁸
29B	SC Gravity Saddle No. 3 (NW Portion)	0.183	5.4 [0.33] 6.0 [0.34] 7.0 [0.33]	2 [0.25] 3 [0.25] 4 [0.25] 5 [0.25]	ME with 29, 29A	No	No	No
	Vogtle Background		5.8 [0.33] 6.0 [0.34] 6.6 [0.33]		None	No	No	No
<i>Other Sources within 200 mi (320 km) that do not contribute to 99% of hazard</i>								
31	Blue Ridge Combo	0.024	5.9 [0.33] 6.3 [0.34] 7.0 [0.33]	2 [0.25] 3 [0.25] 4 [0.25] 5 [0.25]	ME with 31A	No	No	No

Table 2.5-208 (Sheet 2 of 2)
Summary of Woodward-Clyde Seismic Sources

Source	Description	Pa ¹	Mmax (m _b) and Wts. ²	Smoothing Options and Wts. ³	Interdependencies ⁴	New Information to Suggest Change in Source:		
						Geometry? ⁵	Mmax? ⁶	RI? ⁷
31A	Blue Ridge	0.211	5.9 [0.33]	2 [0.25]	ME with 31	No	No	No
	Combination -		6.3 [0.34]	3 [0.25]				
	Alternate		7.0 [0.33]	4 [0.25]				
	Configuration			5 [0.25]				

1 Pa = probability of activity; (from EPRI NP-6452-D 1989)

2 Maximum Magnitude (Mmax) and weights (wts.); (from EPRI NP-6452-D 1989)

3 Smoothing options are defined as follows: (from EPRI NP-6452-D 1989)

1 = Low smoothing on a, high smoothing on b (no prior);

2 = High smoothing on a, high smoothing on b (no prior);

3 = High smoothing on a, high smoothing on b (moderate prior of 1.0);

4 = High smoothing on a, high smoothing on b (moderate prior of 0.9);

5 = High smoothing on a, high smoothing on b (moderate prior of 0.8);

6 = Low smoothing on a, high smoothing on b (moderate prior of 1.0);

7 = Low smoothing on a, high smoothing on b (moderate prior of 0.9);

8 = Low smoothing on a, high smoothing on b (moderate prior of 0.8).

Weights on magnitude intervals are all 1.0

9 = a and b values as listed.

4 ME = mutually exclusive; PD = perfectly dependent

5 No, unless (1) new geometry proposed in literature or (2) new seismicity pattern

6 No, unless (1) new data suggests Mmax exceeds or differs significantly from the EPRI Mmax distribution or (2) exceeded by historical seismicity.

7 RI = recurrence interval; assumed no change if no new paleoseismic data or rate of seismicity has not significantly changed

8 Replace this source with the Updated Charleston Seismic Source (UCSS) Model

Table 2.5-209
Summary of USGS Seismic Sources (Frankel et al. 2002)

Source	Mmax (Mw) and Wts.	Largest Mmax Value Considered by USGS		
		Mw	mb ¹	
<u>Sources within 200 mi (320 km)</u>				
Extended Margin Background	7.5 [1.00]	7.5	7.2	
Charleston	6.8 [0.20] 7.1 [0.20] 7.3 [0.45] 7.5 [0.15]	7.5	7.2	
Eastern Tennessee	7.5 [1.00]	7.5	7.2	
<u>Selected Sources Beyond 200 mi (320km)</u>				
New Madrid	7.3 [0.15] 7.5 [0.20] 7.7 [0.50] 8.0 [0.15]	8.0	7.5	
Stable Craton Background	7.0 [1.00]	7.0	6.9	

1 m_b converted from Mw using average of Atkinson and Boore (1995), Frankel et al (1996), and EPRI (TR-102293 1993) relations

Table 2.5-210
Chapman and Talwani (2002) Seismic Source Zone Parameters

Charleston Characteristic Sources		Mean Recurrence		Mmax ²	
				m _{blg}	M
Charleston Area Source		550 years	nr	7.1 [.2] 7.3 [.6] 7.5 [.2]	
ZRA Fault Source (Zone of River Anomalies)		550 years	nr	7.1 [.2] 7.3 [.6] 7.5 [.2]	
Ashley River-Woodstock Fault Source (modeled as 3 parallel faults)		550 years	nr	7.1 [.2] 7.3 [.6] 7.5 [.2]	
Non-Characteristic Background Sources		a ¹	b ¹	m _{blg}	M
1.	Zone1	0.242	0.84	6.84	7.00
2.	Zone2	-0.270	0.84	6.84	7.00
3.	Central Virginia	1.184	0.64	6.84	7.00
4.	Zone4	0.319	0.84	6.84	7.00
5.	Zone5	0.596	0.84	6.84	7.00
6.	Piedmont and Coastal Plain	1.537	0.84	6.84	7.00
6a.	Pied&CP NE	0.604	0.84	6.84	7.00
6b.	Pied&CP SW	1.312	0.84	6.84	7.00
7.	South Carolina Piedmont	2.220	0.84	6.84	7.00
8.	Middleton Place	1.690	0.77	6.84	7.00
9.	Florida and continental margin	1.371	0.84	6.84	7.00
10.	Alabama	1.800	0.84	6.84	7.00
11.	Eastern Tennessee	2.720	0.90	6.84	7.00
12.	Southern Appalachian	2.420	0.84	6.84	7.00
12a.	Southern Appalachian North	2.185	0.84	6.84	7.00
13.	Giles County, VA	1.070	0.84	6.84	7.00
14.	Central Appalachians	1.630	0.84	6.84	7.00
15.	Western Tennessee	2.431	1.00	6.84	7.00
16.	Central Tennessee	2.273	1.00	6.84	7.00
17.	Ohio-Kentucky	2.726	1.00	6.84	7.00
18.	West VA-Pennsylvania	2.491	1.00	6.84	7.00
19.	USGS (1996) gridded seismicity rates and b value	nr ³	0.95	6.84	7.00

1 a and b values in terms of m_{blg} magnitude, reported in Chapman and Talwani (2002).

2 Mmax range for characteristic events was designed to "represent the range of magnitude estimates of the 1886 Charleston shock proposed by Johnston (1996)" (Chapman and Talwani, 2002, p. 12). Square brackets indicate weights assigned to characteristic magnitudes. For non-characteristic background events, a truncated form of the exponential probability density function was used (Chapman and Talwani, 2002, p. 6-7).

3 nr = not reported

Table 2.5-211
Local Charleston-Area Tectonic Features

Name of Feature	Evidence	Key References
Adams Run fault	subsurface stratigraphy	Weems and Lewis (2002)
Ashley River fault	microseismicity	Talwani (1982, 2000) Weems and Lewis (2002)
Appalachian detachment (decollement)	gravity & magnetic data seismic reflection & refraction	Cook <i>et al.</i> (1979, 1981) Behrendt <i>et al.</i> (1981, 1983) Seeber and Armbruster (1981)
Blake Spur fracture zone	oceanic transform postulated to extend westward to Charleston area	Fletcher <i>et al.</i> (1978) Sykes (1978) Seeber and Armbruster (1981)
Bowman seismic zone	microseismicity	Smith and Talwani (1985)
Charleston fault	subsurface stratigraphy	Colquhoun <i>et al.</i> (1983) Lennon (1986) Talwani (2000) Weems and Lewis (2002)
Cooke fault	seismic reflection	Behrendt <i>et al.</i> (1981, 1983) Hamilton <i>et al.</i> (1983) Wentworth and Mergner-Keefer (1983) Behrendt and Yuan (1987)
Drayton fault	seismic reflection	Hamilton <i>et al.</i> (1983) Behrendt <i>et al.</i> (1983) Behrendt and Yuan (1987)
East Coast fault system/ Zone of river anomalies (ZRA)	geomorphology seismic reflection microseismicity	Marple and Talwani (1993) Marple and Talwani (2000, 2004)
Gants fault	seismic reflection	Hamilton <i>et al.</i> (1983) Behrendt and Yuan (1987)
Garner-Edisto fault	subsurface stratigraphy	Colquhoun <i>et al.</i> (1983)
Helena Banks fault zone	seismic reflection	Behrendt <i>et al.</i> (1981, 1983) Behrendt and Yuan (1987)
Middleton Place-Summerville seismic zone	microseismicity	Tarr <i>et al.</i> (1981) Madabhushi and Talwani (1993)
Sawmill Branch fault	microseismicity	Talwani and Katuna (2004)
Summerville fault	microseismicity	Weems <i>et al.</i> (1997)
Woodstock fault	geomorphology microseismicity	Talwani (1982, 1999, 2000) Marple and Talwani (1990, 2000)

Note: Those tectonic features identified following publication of the EPRI teams' reports (post-1986) are highlighted by **bold-face** type.

Table 2.5-212
Geographic Coordinates (Latitude and Longitude) of Corner Points
of Updated Charleston Seismic Source (UCSS) Geometries

Source Geometry	Longitude	Latitude
	(decimal degrees)	(decimal degrees)
A	-80.707	32.811
A	-79.840	33.354
A	-79.527	32.997
A	-80.392	32.455
B	-81.216	32.485
B	-78.965	33.891
B	-78.3432	33.168
B	-80.587	31.775
B'	-78.965	33.891
B'	-78.654	33.531
B'	-80.900	32.131
B'	-81.216	32.485
C	-80.397	32.687
C	-79.776	34.425
C	-79.483	34.351
C	-80.109	32.614

Table 2.5-213
Comparison of Post-EPRI NP-6395-D 1989 Magnitude Estimates
for the 1886 Charleston Earthquake

Study	Magnitude Estimation Method	Reported Magnitude Estimate	Assigned Weights	Mean Magnitude (M)
Johnston <i>et al.</i> (1994)	worldwide survey of passive-margin, extended-crust earthquakes	M 7.56 ± 0.35 ^a	--	7.56
Martin and Clough (1994)	geotechnical assessment of 1886 liquefaction data	M 7 - 7.5	--	7.25
Johnston (1996)	isoseismal area regression, accounting for eastern North America anelastic attenuation	M 7.3 ± 0.26	--	7.3
Chapman and Talwani (2002) (South Carolina Department of Transportation)	consideration of available magnitude estimates	M 7.1	0.2	7.3
		M 7.3	0.6	
		M 7.5	0.2	
Frankel <i>et al.</i> (2002) (USGS National seismic hazard mapping project)	consideration of available magnitude estimates	M 6.8	0.20	7.2
		M 7.1	0.20	
		M 7.3	0.45	
		M 7.5	0.15	
Bakun and Hopper (2004)	isoseismal area regression, including empirical site corrections	M_I 6.4 - 7.2 ^b	--	6.9 ^c

Notes:

^a Estimate from Johnston *et al.* (1994) Chapter 3.

^b 95% confidence interval estimate; M_I (intensity magnitude) is considered equivalent to **M** (Bakun and Hopper, 2004).

^c Bakun and Hopper's (2004) *preferred* estimate.

Table 2.5-214
Comparison of Talwani and Schaeffer (2001) and UCSS Age Constraints
on Charleston-Area Paleoliquefaction Events

Liquefaction Event	Event Age (YBP) ^b	Talwani and Schaeffer (2001) ^a				(this study) Event Age (YBP) ^{b, c, d}
		scenario 1		scenario 2		
		Source	M	Source	M	
1886 A.D.	64	Charleston	7.3	Charleston	7.3	64
A	546 ± 17	Charleston	7+	Charleston	7+	600 ± 70
B	1,021 ± 30	Charleston	7+	Charleston	7+	1,025 ± 25
C	1,648 ± 74	Northern	6+	--	--	--
C'	1,683 ± 70	--		Charleston	7+	1,695 ± 175
D	1,966 ± 212	Southern	6+	--	--	--
E	3,548 ± 66	Charleston	7+	Charleston	7+	3,585 ± 115
F	5,038 ± 166	Northern	6+	Charleston	7+	--
F'	--	--	--	--	--	5,075 ± 215
G	5,800 ± 500	Charleston	7+	Charleston	7+	--

Notes:

^a Modified after Talwani and Schaeffer's (2001) Table 2.

^b Years before present, relative to 1950 A.D.

^c Event ages based upon our recalibration of radiocarbon (to 2-sigma using OxCal 3.8 (Bronk Ramsey, 1995; 2001) data presented in Talwani and Schaeffer's (2001) Table 2.

^d See Table B-1 for recalibrated 2-sigma sample ages and Table B-2 for 2-sigma age constraints on paleoliquefaction events.

Table 2.5-215
Seismic Sources Used for Each 1986 EPRI Team

Earth Science Team	Sources used
Bechtel	F, G, H, ,N3,BZ4, BZ5
Dames & Moore	20, 41, 52, 53, 54
Law Engineering	17, 22, 35, 108, C09, C10, C11, M33, M36, M37, M38, M39, M40, M41, M42
Rondout Associates	24, 26
Woodward-Clyde Cons.	29, 29A, 29B, 30, 32
Weston Geophysical Corp.	25, 26, 104, C19, C20, C21, C23, C24, C26, C27, C33, C35

Table 2.5-216
Comparison of Seismic Hazard at VEGP ESP

Mean Hazard Comparison			
PGA	EPRI-SOG	REI 2005	
<u>cm/s²</u>	<u>hazard</u>	<u>hazard</u>	<u>% diff</u>
50	8.15E-04	8.23E-04	0.97%
100	2.23E-04	2.26E-04	1.48%
250	2.84E-05	2.91E-05	2.29%
500	4.04E-06	4.21E-06	4.11%
700	1.36E-06	1.42E-06	4.71%
1000	3.82E-07	4.02E-07	5.10%
Median Hazard Comparison			
PGA	EPRI-SOG	REI 2005	
<u>cm/s²</u>	<u>hazard</u>	<u>hazard</u>	<u>% diff</u>
50	5.65E-04	5.75E-04	1.84%
100	1.43E-04	1.45E-04	1.05%
250	1.99E-05	2.16E-05	8.69%
500	2.53E-06	2.63E-06	3.95%
700	7.86E-07	8.13E-07	3.41%
1000	2.05E-07	2.19E-07	6.73%
85% Hazard Comparison			
PGA	EPRI-SOG	REI 2005	
<u>cm/s²</u>	<u>hazard</u>	<u>hazard</u>	<u>% diff</u>
50	1.49E-03	1.32E-03	-11.54%
100	4.16E-04	3.67E-04	-11.71%
250	4.96E-05	4.79E-05	-3.51%
500	7.01E-06	7.16E-06	2.15%
700	2.44E-06	2.46E-06	0.61%
1000	6.98E-07	7.08E-07	1.42%

Table 2.5-217
Hard Rock Mean UHS Results (in g) for VEGP ESP

Mean annual frequency of exceedance	Spectral frequency						
	PGA	25 Hz	10 Hz	5 Hz	2.5 Hz	1 Hz	0.5 Hz
10^{-4}	0.214	0.551	0.399	0.317	0.223	0.101	0.0653
5×10^{-5}	0.288	0.762	0.532	0.412	0.294	0.134	0.0924
10^{-5}	0.559	1.54	0.983	0.728	0.512	0.235	0.185
5×10^{-6}	0.747	2.06	1.28	0.914	0.635	0.294	0.241
10^{-6}	1.48	4.09	2.33	1.54	1.02	0.465	0.423

Table 2.5-218
**Computed and Recommended Mbar and Dbar Values Used
for Development of High and Low Frequency Target Spectra**

<i>High Frequency (5-10 Hz)</i>				
	10^{-4}	10^{-5}	10^{-6}	Recommended Values
Mbar (Mw)	5.5	5.6	5.6	5.6
Dbar (km)	17.7	11.5	9.1	12
<i>Low Frequency (1-2.5 Hz)</i>				
	10^{-4}	10^{-5}	10^{-6}	Recommended Values
Mbar (Mw)	7.2	7.2	7.2	7.2
Dbar (km)	136.5	134.3	132.9	130

Table 2.5-219
Candidate High-Frequency (M5.6, R = 12km)
Time Histories for Spectral Matching

Earthquake	Date	Mw	Station	Distance (km)	Vs30m (m/s)
Saguena	11/25/88	5.9	GSC Site 16	51.9	“???”
San Francisco	03/22/57	5.28	Golden Gate Park	11.13	874.0
Coyote Lake	08/06/79	5.74	Gilroy Array #1	10.67	1428.0
Mammoth Lakes-09	06/11/80	4.85	USC McGee Creek	7.49	684.9
Coalinga-04	07/09/83	5.18	Sulphur Baths (temp)	14.47	617.4
Coalinga-05	07/22/83	5.77	Sulphur Baths (temp)	13.40	617.4
Morgan Hill	04/24/84	6.19	Gilroy - Gavilan Coll.	14.84	729.7
Morgan Hill	04/24/84	6.19	Gilroy Array #1	14.91	1428.0
N. Palm Springs	07/08/86	6.06	Silent Valley - Poppet Flat	17.03	684.9
Whittier Narrows-01	10/01/87	5.99	Mt Wilson - CIT Seis Sta	22.73	821.7
Whittier Narrows-02	10/04/87	5.27	Mt Wilson - CIT Seis Sta	18.74	821.7
Anza-02	10/31/01	4.92	Anza - Pinyon Flat	12.37	724.9
Anza-02	10/31/01	4.92	Anza - Tripp Flats Training	24.73	684.9
Anza-02	10/31/01	4.92	Idyllwild - Keenwild Fire Sta.	29.07	845.4
Gilroy	05/14/02	4.90	Gilroy - Gavilan Coll.	2.82	729.7

Table 2.5-220
Candidate Low-Frequency (M7.2, R = 130 km)
Time Histories for Spectral Matching

Earthquake	Date	Mw	Station	Distance (km)	Vs30m (m/s)
San Fernando	02/09/1971	6.61	Isabella Dam (Aux Abut)	130.98	684.9
Loma Prieta	10/18/1989	6.93	SF-Rincon Hill	74.14	873.1
Loma Prieta	10/18/1989	6.93	So. San Francisco, Sierra Pt.	63.15	1020.6
Loma Prieta	10/18/1989	6.93	Yerba Buena Island	75.17	659.8
Northridge	01/17/1994	6.69	Rancho Cucamonga-Deer Canyon	79.99	821.7
Northridge	01/17/1994	6.69	Wrightwood-Jackson Flat	64.66	821.7
Kobe	01/16/1995	6.90	OKA	86.94	609.0
Kocaeli	08/17/1999	7.51	Bursa Sivil	65.53	659.6
Chi-Chi	09/20/1999	7.62	ILA031	83.31	649.3
Kobe	01/16/1995	6.90	MZH	70.26	609.0
Hector Mine	10/16/1999	7.13	Anza-Pinyon Flat	89.98	724.9
Hector Mine	10/16/1999	7.13	Anza-Tripp Flats Training	102.40	684.9
Hector Mine	10/16/1999	7.13	Banning-Twin Pines Road	83.43	684.9
Hector Mine	10/16/1999	7.13	Heart Bar State Park	61.21	684.9
Hector Mine	10/16/1999	7.13	Seven Oaks Dam Project Office	87.20	659.6

Table 2.5-221
Site Response Analyses Performed

Probability (per year) ->	10 ⁻⁴		10 ⁻⁵		10 ⁻⁶				Total No. Analyses
Time Histories Analyzed ->	30 High Freq.	30 Low Freq.	30 High Freq.	30 Low Freq.	30 High Freq.	30 Low Freq.			
Randomized Soil Columns (EPRI) ->	60	60	60	60	60	60			360
Randomized Soil Columns (SRS) ->	60	60	60	60	60	60			360
									720

Table 2.5-222
Amplification Factors as a Function of Input Hard Rock Motion at Top of Blue Bluff Marl
(depth 86 feet), as Developed from Site Response Analysis using SRS and EPRI Soil
Degradation Models, for High-frequency Rock Motions

-		10^{-4}		10^{-5}		10^{-6}			
-		Hard rock input motion	mean amp. factors	Hard rock input motion	mean amp. factors	Hard rock input motion	mean amp. factors		
Freq, Hz		EPRI	SRS		EPRI	SRS		EPRI	SRS
100	0.294	1.18	1.20	0.703	0.979	0.920	1.60	0.766	0.620
76	0.400	0.903	0.930	0.957	0.740	0.695	2.17	0.571	0.462
60	0.499	0.769	0.799	1.19	0.606	0.573	2.71	0.456	0.369
50	0.595	0.697	0.722	1.42	0.531	0.500	3.23	0.386	0.313
40	0.631	0.775	0.819	1.51	0.553	0.523	3.43	0.379	0.306
30	0.655	0.961	1.02	1.57	0.664	0.626	3.63	0.398	0.319
25	0.647	1.14	1.21	1.55	0.812	0.768	3.71	0.446	0.354
20	0.615	1.33	1.39	1.47	0.991	0.937	3.34	0.579	0.453
16.5	0.575	1.47	1.52	1.38	1.133	1.07	3.13	0.705	0.560
13.4	0.521	1.67	1.69	1.25	1.312	1.23	2.83	0.875	0.685
12.2	0.494	1.78	1.81	1.18	1.417	1.33	2.69	0.953	0.754
10	0.438	1.81	1.82	1.05	1.600	1.50	2.38	1.15	0.928
8.1	0.377	2.19	2.18	0.902	1.747	1.65	2.05	1.34	1.09
7	0.339	2.30	2.26	0.811	1.984	1.87	1.84	1.47	1.21
6	0.298	2.05	2.03	0.713	2.096	1.93	1.62	1.68	1.38
5	0.257	2.11	2.08	0.615	2.022	1.88	1.40	1.90	1.56
4	0.212	2.56	2.54	0.507	2.300	2.16	1.15	2.09	1.70
3.3	0.175	2.88	2.81	0.419	2.687	2.51	0.952	2.42	2.00
2.5	0.131	3.16	3.05	0.314	3.089	2.83	0.713	2.78	2.33
2	0.101	2.49	2.38	0.242	2.651	2.38	0.549	2.96	2.39
1.5	0.064	3.22	3.12	0.154	3.193	2.86	0.350	3.28	2.48
1	0.035	2.34	2.30	0.0828	2.542	2.41	0.188	3.00	2.55
0.8	0.024	2.63	2.59	0.0563	2.695	2.55	0.128	2.95	2.54
0.7	0.0187	3.15	3.10	0.0447	3.141	2.97	0.101	3.31	2.86
0.61	0.0148	3.80	3.78	0.0354	3.842	3.69	0.0804	4.02	3.52
0.5	0.0109	3.40	3.43	0.0260	3.597	3.59	0.0590	4.00	3.81
0.33	0.00525	2.19	2.19	0.0126	2.269	2.25	0.0286	2.52	2.40
0.25	0.00314	1.98	1.97	0.00751	2.059	2.00	0.0171	2.24	2.07
0.15	0.00106	2.06	2.04	0.00254	2.149	2.05	0.00577	2.37	2.06
0.1	0.000370	2.27	2.23	0.000890	2.341	2.18	0.00201	2.43	2.06

Table 2.5-223
Amplification Factors as a Function of Input Hard Rock Motion at Top of Blue Bluff Marl
(depth 86 feet), as Developed from Site Response Analysis using SRS and EPRI Soil
Degradation Models, for Low-frequency Rock Motions

		10^{-4}		10^{-5}		10^{-6}			
		Hard rock input motion		Hard rock input motion		Hard rock input motion			
		mean amp. factors		mean amp. factors		mean amp. factors			
Freq, Hz		EPRI	SRS	EPRI	SRS	EPRI	SRS		
100	0.224	1.31	1.25	0.517	1.111	0.896	1.03	0.931	0.591
76	0.305	0.987	0.942	0.704	0.828	0.667	1.40	0.692	0.439
60	0.380	0.802	0.765	0.878	0.660	0.532	1.74	0.550	0.349
50	0.453	0.695	0.662	1.047	0.557	0.449	2.08	0.462	0.293
40	0.483	0.677	0.644	1.115	0.532	0.428	2.22	0.437	0.277
30	0.506	0.764	0.73	1.168	0.529	0.417	2.32	0.417	0.264
25	0.505	0.90	0.86	1.167	0.570	0.440	2.32	0.422	0.266
20	0.493	1.07	1.02	1.139	0.653	0.492	2.26	0.445	0.276
16.5	0.476	1.21	1.16	1.101	0.762	0.57	2.19	0.481	0.293
13.4	0.453	1.41	1.34	1.046	0.877	0.66	2.08	0.536	0.316
12.2	0.440	1.49	1.42	1.017	0.943	0.71	2.02	0.571	0.335
10	0.413	1.61	1.54	0.954	1.151	0.87	1.90	0.68	0.389
8.1	0.381	1.91	1.82	0.880	1.343	1.05	1.75	0.83	0.46
7	0.359	2.09	1.96	0.830	1.534	1.23	1.65	0.97	0.55
6	0.334	1.99	1.88	0.771	1.734	1.35	1.53	1.12	0.66
5	0.307	1.97	1.89	0.709	1.804	1.38	1.41	1.36	0.78
4	0.275	2.46	2.37	0.635	1.967	1.62	1.26	1.57	0.93
3.3	0.246	2.90	2.78	0.569	2.443	2.05	1.13	1.94	1.21
2.5	0.209	3.29	3.05	0.483	2.813	2.29	0.960	2.43	1.61
2	0.181	2.34	2.16	0.418	2.817	2.24	0.831	2.82	1.82
1.5	0.137	3.30	3.07	0.318	3.124	2.29	0.632	3.19	1.70
1	0.0917	2.27	2.21	0.214	2.697	2.42	0.423	3.70	2.32
0.8	0.0768	2.67	2.56	0.193	2.754	2.41	0.405	3.26	2.42
0.7	0.0703	3.25	3.10	0.184	3.233	2.80	0.397	3.50	2.48
0.61	0.0652	4.00	3.90	0.177	3.933	3.43	0.390	3.94	2.71
0.5	0.0590	3.66	3.72	0.167	4.107	4.01	0.382	4.75	3.46
0.33	0.0317	1.97	2.00	0.0901	2.219	2.30	0.206	2.85	2.96
0.25	0.0209	1.64	1.65	0.0592	1.726	1.75	0.136	2.05	2.06
0.15	0.0095	1.36	1.36	0.0270	1.395	1.39	0.0617	1.55	1.54
0.1	0.0047	1.30	1.29	0.0134	1.321	1.31	0.0307	1.45	1.40

Table 2.5-224
Amplification Factors as a Function of Input Hard Rock Motion at 40-ft Depth Horizon (FIRS), as Developed from Site Response Analysis using SRS and EPRI Soil Degradation Models, for High-Frequency Rock Motions

10 ⁻⁴				10 ⁻⁵			10 ⁻⁶					
Hard rock input motion		mean amp. factors		Hard rock input motion		mean amp. factors		Hard rock input motion		mean amp. factors		
Freq, Hz		EPRI	SRS		EPRI	SRS		EPRI	SRS		EPRI	SRS
100	0.294	1.13	1.17	0.703	0.874	0.874	1.60	0.608	0.568			
76	0.400	0.851	0.885	0.957	0.655	0.655	2.17	0.452	0.422			
60	0.499	0.706	0.739	1.19	0.527	0.528	2.71	0.361	0.336			
50	0.595	0.627	0.660	1.42	0.451	0.453	3.23	0.304	0.283			
40	0.631	0.687	0.733	1.51	0.457	0.458	3.43	0.292	0.272			
30	0.655	0.826	0.89	1.57	0.516	0.516	3.63	0.291	0.269			
25	0.647	0.99	1.07	1.55	0.621	0.626	3.71	0.310	0.284			
20	0.615	1.19	1.27	1.47	0.776	0.778	3.34	0.390	0.358			
16.5	0.575	1.34	1.42	1.38	0.919	0.92	3.13	0.480	0.444			
13.4	0.521	1.56	1.63	1.25	1.102	1.10	2.83	0.609	0.554			
12.2	0.494	1.71	1.78	1.18	1.216	1.22	2.69	0.675	0.617			
10	0.438	1.76	1.82	1.05	1.430	1.43	2.38	0.85	0.795			
8.1	0.377	2.08	2.15	0.902	1.575	1.59	2.05	1.03	0.96			
7	0.339	2.19	2.23	0.811	1.780	1.80	1.84	1.15	1.09			
6	0.298	2.05	2.08	0.713	1.916	1.89	1.62	1.34	1.27			
5	0.257	2.22	2.24	0.615	1.966	1.94	1.40	1.57	1.49			
4	0.212	2.76	2.82	0.507	2.335	2.33	1.15	1.79	1.68			
3.3	0.175	3.09	3.16	0.419	2.777	2.79	0.952	2.12	2.03			
2.5	0.131	3.30	3.34	0.314	3.160	3.16	0.713	2.52	2.47			
2	0.101	2.56	2.56	0.242	2.702	2.65	0.549	2.68	2.57			
1.5	0.064	3.26	3.26	0.154	3.162	3.04	0.350	2.96	2.61			
1	0.035	2.35	2.37	0.0828	2.510	2.50	0.188	2.72	2.61			
0.8	0.024	2.64	2.64	0.0563	2.655	2.62	0.128	2.71	2.57			
0.7	0.0187	3.15	3.14	0.0447	3.097	3.03	0.101	3.03	2.86			
0.61	0.0148	3.79	3.82	0.0354	3.773	3.72	0.0804	3.72	3.51			
0.5	0.0109	3.40	3.46	0.0260	3.556	3.63	0.0590	3.76	3.81			
0.33	0.00525	2.18	2.21	0.0126	2.237	2.28	0.0286	2.35	2.40			
0.25	0.00314	1.98	2.00	0.00751	2.015	2.03	0.0171	2.06	2.06			
0.15	0.00106	2.08	2.10	0.00254	2.102	2.10	0.00577	2.15	2.07			
0.1	0.000370	2.31	2.33	0.000890	2.295	2.27	0.00201	2.18	2.08			

Table 2.5-225
Amplification Factors as a Function of Input Hard Rock Motion at 40-ft Depth Horizon
(FIRS), as Developed from Site Response Analysis Using SRS and EPRI Soil Degradation
Models, for Low-Frequency Rock Motions

		10^{-4}			10^{-5}			10^{-6}		
		Hard rock input motion		mean amp. factors	Hard rock input motion		mean amp. factors	Hard rock input motion		mean amp. factors
Freq, Hz		EPRI	SRS		EPRI	SRS		EPRI	SRS	
100	0.224	1.26	1.25	0.517	0.978	0.888	1.03	0.715	0.549	
76	0.305	0.947	0.942	0.704	0.728	0.661	1.40	0.531	0.408	
60	0.380	0.762	0.759	0.878	0.581	0.527	1.74	0.422	0.324	
50	0.453	0.653	0.647	1.047	0.489	0.443	2.08	0.354	0.272	
40	0.483	0.629	0.623	1.115	0.462	0.418	2.22	0.333	0.255	
30	0.506	0.682	0.67	1.168	0.450	0.405	2.32	0.319	0.244	
25	0.505	0.78	0.77	1.167	0.467	0.415	2.32	0.321	0.246	
20	0.493	0.93	0.92	1.139	0.520	0.453	2.26	0.334	0.254	
16.5	0.476	1.08	1.07	1.101	0.600	0.52	2.19	0.355	0.267	
13.4	0.453	1.28	1.27	1.046	0.701	0.59	2.08	0.388	0.286	
12.2	0.440	1.38	1.37	1.017	0.758	0.65	2.02	0.411	0.301	
10	0.413	1.51	1.50	0.954	0.943	0.80	1.90	0.48	0.344	
8.1	0.381	1.77	1.76	0.880	1.101	0.96	1.75	0.56	0.40	
7	0.359	1.96	1.92	0.830	1.271	1.14	1.65	0.66	0.48	
6	0.334	1.94	1.91	0.771	1.464	1.28	1.53	0.78	0.57	
5	0.307	2.02	2.01	0.709	1.594	1.37	1.41	0.96	0.69	
4	0.275	2.59	2.60	0.635	1.835	1.67	1.26	1.15	0.84	
3.3	0.246	3.06	3.09	0.569	2.292	2.16	1.13	1.45	1.10	
2.5	0.209	3.37	3.33	0.483	2.617	2.44	0.960	1.83	1.51	
2	0.181	2.38	2.35	0.418	2.661	2.43	0.831	2.11	1.69	
1.5	0.137	3.29	3.19	0.318	2.871	2.35	0.632	2.46	1.61	
1	0.0917	2.26	2.26	0.214	2.517	2.45	0.423	3.00	2.21	
0.8	0.0768	2.65	2.59	0.193	2.605	2.42	0.405	2.75	2.30	
0.7	0.0703	3.23	3.13	0.184	3.075	2.80	0.397	2.98	2.35	
0.61	0.0652	3.97	3.92	0.177	3.766	3.43	0.390	3.40	2.59	
0.5	0.0590	3.64	3.74	0.167	3.953	4.01	0.382	4.18	3.32	
0.33	0.0317	1.96	2.00	0.0901	2.158	2.29	0.206	2.59	2.87	
0.25	0.0209	1.63	1.65	0.0592	1.688	1.75	0.136	1.88	2.01	
0.15	0.0095	1.35	1.36	0.0270	1.372	1.39	0.0617	1.46	1.51	
0.1	0.0047	1.29	1.30	0.0134	1.295	1.31	0.0307	1.36	1.38	

Table 2.5-226
Amplification Factors as a Function of Input Hard Rock Motion at Ground Surface (GMRS),
as Developed from Site Response Analysis Using SRS and EPRI Soil Degradation Models,
for High-Frequency Rock Motions

-		10 ⁻⁴		10 ⁻⁵		10 ⁻⁶			
-	Hard rock input motion	mean amp. factors		Hard rock input motion	mean amp. factors		Hard rock input motion	mean amp. factors	
Freq, Hz		EPRI	SRS		EPRI	SRS		EPRI	SRS
100	0.294	1.22	1.26	0.703	0.849	0.847	1.60	0.540	0.510
76	0.400	0.915	0.945	0.957	0.634	0.632	2.17	0.401	0.379
60	0.499	0.743	0.768	1.19	0.508	0.506	2.71	0.319	0.301
50	0.595	0.640	0.665	1.42	0.428	0.427	3.23	0.268	0.253
40	0.631	0.664	0.694	1.51	0.415	0.414	3.43	0.254	0.240
30	0.655	0.775	0.82	1.57	0.434	0.434	3.63	0.244	0.230
25	0.647	0.96	1.02	1.55	0.495	0.495	3.71	0.245	0.232
20	0.615	1.25	1.33	1.47	0.627	0.629	3.34	0.289	0.274
16.5	0.575	1.42	1.50	1.38	0.777	0.78	3.13	0.344	0.326
13.4	0.521	1.68	1.75	1.25	0.950	0.96	2.83	0.420	0.397
12.2	0.494	1.86	1.93	1.18	1.071	1.08	2.69	0.469	0.444
10	0.438	1.95	2.02	1.05	1.307	1.31	2.38	0.61	0.585
8.1	0.377	2.38	2.46	0.902	1.517	1.53	2.05	0.76	0.72
7	0.339	2.55	2.60	0.811	1.793	1.81	1.84	0.88	0.85
6	0.298	2.40	2.44	0.713	2.013	1.98	1.62	1.09	1.06
5	0.257	2.55	2.57	0.615	2.136	2.10	1.40	1.39	1.33
4	0.212	3.09	3.17	0.507	2.554	2.55	1.15	1.71	1.62
3.3	0.175	3.37	3.45	0.419	3.010	3.03	0.952	2.16	2.07
2.5	0.131	3.49	3.53	0.314	3.336	3.33	0.713	2.72	2.67
2	0.101	2.66	2.66	0.242	2.804	2.75	0.549	2.93	2.79
1.5	0.064	3.32	3.32	0.154	3.208	3.08	0.350	3.20	2.79
1	0.035	2.37	2.40	0.0828	2.528	2.52	0.188	2.83	2.69
0.8	0.024	2.65	2.66	0.0563	2.656	2.62	0.128	2.75	2.59
0.7	0.0187	3.17	3.16	0.0447	3.088	3.02	0.101	3.06	2.88
0.61	0.0148	3.80	3.82	0.0354	3.761	3.71	0.0804	3.74	3.51
0.5	0.0109	3.40	3.46	0.0260	3.538	3.61	0.0590	3.77	3.80
0.33	0.00525	2.20	2.23	0.0126	2.236	2.27	0.0286	2.37	2.40
0.25	0.00314	2.01	2.02	0.00751	2.027	2.04	0.0171	2.09	2.07
0.15	0.00106	2.14	2.17	0.00254	2.130	2.13	0.00577	2.21	2.13
0.1	0.000370	2.41	2.44	0.000890	2.339	2.32	0.00201	2.26	2.15

Table 2.5-227
Amplification Factors as a Function of Input Hard Rock Motion at Ground Surface (GMRS),
as Developed from Site Response Analysis Using SRS and EPRI Soil Degradation Models,
for Low-Frequency Rock Motions

-	10^{-4}			10^{-5}			10^{-6}		
-	Hard rock input motion	mean amp. factors		Hard rock input motion	mean amp. factors		Hard rock input motion	mean amp. factors	
Freq, Hz		EPRI	SRS		EPRI	SRS		EPRI	SRS
100	0.224	1.33	1.33	0.517	0.957	0.871	1.03	0.662	0.527
76	0.305	1.002	0.997	0.704	0.713	0.648	1.40	0.492	0.392
60	0.380	0.803	0.799	0.878	0.568	0.516	1.74	0.391	0.311
50	0.453	0.680	0.676	1.047	0.478	0.434	2.08	0.328	0.261
40	0.483	0.654	0.648	1.115	0.450	0.409	2.22	0.308	0.245
30	0.506	0.687	0.68	1.168	0.434	0.395	2.32	0.294	0.234
25	0.505	0.77	0.76	1.167	0.442	0.401	2.32	0.296	0.235
20	0.493	0.95	0.94	1.139	0.478	0.429	2.26	0.305	0.242
16.5	0.476	1.12	1.11	1.101	0.541	0.48	2.19	0.320	0.253
13.4	0.453	1.33	1.32	1.046	0.625	0.55	2.08	0.343	0.270
12.2	0.440	1.44	1.42	1.017	0.676	0.60	2.02	0.359	0.281
10	0.413	1.62	1.60	0.954	0.838	0.74	1.90	0.40	0.315
8.1	0.381	1.95	1.94	0.880	1.008	0.91	1.75	0.47	0.36
7	0.359	2.18	2.14	0.830	1.205	1.10	1.65	0.55	0.42
6	0.334	2.17	2.13	0.771	1.434	1.28	1.53	0.65	0.51
5	0.307	2.25	2.23	0.709	1.600	1.39	1.41	0.81	0.62
4	0.275	2.82	2.84	0.635	1.883	1.72	1.26	1.00	0.77
3.3	0.246	3.26	3.30	0.569	2.360	2.23	1.13	1.28	1.05
2.5	0.209	3.50	3.45	0.483	2.658	2.48	0.960	1.72	1.47
2	0.181	2.43	2.39	0.418	2.662	2.43	0.831	2.06	1.66
1.5	0.137	3.30	3.20	0.318	2.845	2.33	0.632	2.43	1.58
1	0.0917	2.26	2.25	0.214	2.481	2.42	0.423	2.92	2.16
0.8	0.0768	2.64	2.58	0.193	2.564	2.39	0.405	2.66	2.24
0.7	0.0703	3.21	3.11	0.184	3.031	2.77	0.397	2.90	2.30
0.61	0.0652	3.96	3.90	0.177	3.716	3.39	0.390	3.30	2.53
0.5	0.0590	3.62	3.73	0.167	3.903	3.96	0.382	4.08	3.26
0.33	0.0317	1.95	1.99	0.0901	2.136	2.27	0.206	2.53	2.83
0.25	0.0209	1.63	1.65	0.0592	1.673	1.73	0.136	1.84	1.98
0.15	0.0095	1.35	1.36	0.0270	1.362	1.38	0.0617	1.43	1.49
0.1	0.0047	1.29	1.29	0.0134	1.287	1.30	0.0307	1.35	1.37

Table 2.5-228
Spectral Accelerations (SA, in g) for Hard Rock Conditions and for Hypothetical
Outcrop of Highest Competent In Situ Layer (Top of Blue Bluff Marl)

Freq	Hard Rock spectral accel, g			Soil spectral accel, g		
	10^{-4}	10^{-5}	10^{-6}	10^{-4}	10^{-5}	10^{-6}
100	0.214	0.559	1.480	0.255	0.531	1.025
76	0.293	0.777	2.059	0.268	0.558	1.063
60	0.394	1.057	2.802	0.311	0.629	1.167
50	0.464	1.257	3.334	0.333	0.656	1.180
40	0.517	1.416	3.758	0.423	0.778	1.310
30	0.545	1.511	4.011	0.545	0.984	1.452
25	0.551	1.540	4.090	0.646	1.217	1.636
20	0.522	1.419	3.685	0.723	1.390	1.925
16.5	0.493	1.309	3.330	0.758	1.474	2.139
13.4	0.456	1.176	2.914	0.784	1.523	2.299
12.2	0.438	1.115	2.727	0.800	1.553	2.349
10	0.399	0.983	2.330	0.722	1.522	2.405
8.1	0.375	0.904	2.071	0.831	1.551	2.517
7	0.359	0.852	1.909	0.801	1.658	2.574
6	0.339	0.792	1.728	0.671	1.601	2.650
5	0.317	0.728	1.540	0.612	1.306	2.665
4	0.287	0.659	1.369	0.694	1.190	2.419
3.3	0.259	0.595	1.213	0.735	1.335	2.350
2.5	0.223	0.512	1.020	0.706	1.300	2.184
2	0.193	0.445	0.886	0.440	1.153	2.036
1.5	0.152	0.352	0.698	0.484	0.952	1.705
1	0.101	0.235	0.465	0.226	0.597	1.396
0.8	0.091	0.230	0.489	0.237	0.595	1.388
0.7	0.083	0.220	0.481	0.264	0.664	1.436
0.61	0.076	0.207	0.462	0.299	0.761	1.535
0.5	0.065	0.185	0.423	0.238	0.745	1.741
0.33	0.038	0.107	0.245	0.075	0.242	0.712
0.25	0.026	0.072	0.166	0.042	0.126	0.341
0.15	0.012	0.033	0.075	0.016	0.046	0.116
0.1	0.006	0.016	0.036	0.007	0.021	0.051

Table 2.5-229
Spectral Accelerations (SA, in g) for Hard Rock Conditions
and for Hypothetical Outcrop at 40-ft Depth Horizon (FIRS)

Freq	Hard Rock spectral accel, g			Soil spectral accel, g		
	10 ⁻⁴	10 ⁻⁵	10 ⁻⁶	10 ⁻⁴	10 ⁻⁵	10 ⁻⁶
100	0.214	0.559	1.480	0.246	0.489	0.870
76	0.293	0.777	2.059	0.254	0.509	0.900
60	0.394	1.057	2.802	0.287	0.563	0.986
50	0.464	1.257	3.334	0.302	0.575	0.991
40	0.517	1.416	3.758	0.372	0.658	1.074
30	0.545	1.511	4.011	0.473	0.788	1.134
25	0.551	1.540	4.090	0.566	0.961	1.214
20	0.522	1.419	3.685	0.656	1.120	1.396
16.5	0.493	1.309	3.330	0.699	1.230	1.562
13.4	0.456	1.176	2.914	0.744	1.319	1.714
12.2	0.438	1.115	2.727	0.778	1.374	1.777
10	0.399	0.983	2.330	0.713	1.398	1.901
8.1	0.375	0.904	2.071	0.803	1.442	2.068
7	0.359	0.852	1.909	0.775	1.539	2.145
6	0.339	0.792	1.728	0.673	1.512	2.261
5	0.317	0.728	1.540	0.637	1.265	2.346
4	0.287	0.659	1.369	0.745	1.163	2.164
3.3	0.259	0.595	1.213	0.796	1.324	2.093
2.5	0.223	0.512	1.020	0.747	1.289	1.902
2	0.193	0.445	0.886	0.457	1.133	1.690
1.5	0.152	0.352	0.698	0.492	0.918	1.418
1	0.101	0.235	0.465	0.227	0.580	1.208
0.8	0.091	0.230	0.489	0.238	0.579	1.233
0.7	0.083	0.220	0.481	0.265	0.647	1.282
0.61	0.076	0.207	0.462	0.299	0.743	1.381
0.5	0.065	0.185	0.423	0.238	0.731	1.592
0.33	0.038	0.107	0.245	0.075	0.239	0.670
0.25	0.026	0.072	0.166	0.042	0.124	0.322
0.15	0.012	0.033	0.075	0.016	0.045	0.112
0.1	0.006	0.016	0.036	0.007	0.020	0.049

Table 2.5-230
Spectral Accelerations (SA, in g) for Hard Rock Conditions
and for Ground Surface Motions (GMRS)

Freq	Hard Rock spectral accel, g			Soil spectral accel, g		
	10^{-4}	10^{-5}	10^{-6}	10^{-4}	10^{-5}	10^{-6}
100	0.214	0.559	1.480	0.266	0.474	0.777
76	0.293	0.777	2.059	0.272	0.492	0.803
60	0.394	1.057	2.802	0.300	0.541	0.877
50	0.464	1.257	3.334	0.306	0.545	0.879
40	0.517	1.416	3.758	0.356	0.595	0.942
30	0.545	1.511	4.011	0.440	0.662	0.959
25	0.551	1.540	4.090	0.547	0.762	0.976
20	0.522	1.419	3.685	0.686	0.905	1.050
16.5	0.493	1.309	3.330	0.739	1.042	1.132
13.4	0.456	1.176	2.914	0.802	1.140	1.205
12.2	0.438	1.115	2.727	0.846	1.213	1.256
10	0.399	0.983	2.330	0.789	1.279	1.379
8.1	0.375	0.904	2.071	0.920	1.390	1.542
7	0.359	0.852	1.909	0.892	1.551	1.662
6	0.339	0.792	1.728	0.767	1.586	1.861
5	0.317	0.728	1.540	0.709	1.335	2.076
4	0.287	0.659	1.369	0.812	1.197	2.060
3.3	0.259	0.595	1.213	0.849	1.365	2.060
2.5	0.223	0.512	1.020	0.775	1.309	1.893
2	0.193	0.445	0.886	0.466	1.134	1.654
1.5	0.152	0.352	0.698	0.494	0.910	1.397
1	0.101	0.235	0.465	0.227	0.572	1.178
0.8	0.091	0.230	0.489	0.237	0.570	1.197
0.7	0.083	0.220	0.481	0.263	0.638	1.250
0.61	0.076	0.207	0.462	0.297	0.734	1.346
0.5	0.065	0.185	0.423	0.237	0.722	1.556
0.33	0.038	0.107	0.245	0.075	0.236	0.657
0.25	0.026	0.072	0.166	0.042	0.123	0.317
0.15	0.012	0.033	0.075	0.016	0.045	0.110
0.1	0.006	0.016	0.036	0.007	0.020	0.049

Table 2.5-231
Amplitudes (g) for the Hypothetical Outcrop of Highest Competent
In Situ Layer (Top of Blue Bluff Marl)

	Soil amplitudes				raw	smoothed
Freq	10 ⁻⁴	10 ⁻⁵	AR	DF2	SSE	SSE
100	0.255	0.531	2.08	1.08	0.275	0.275
76	0.268	0.558	2.08	1.08	0.289	0.295
60	0.311	0.629	2.02	1.05	0.328	0.326
50	0.333	0.656	1.97	1.03	0.344	0.366
40	0.423	0.778	1.84	0.978	0.423	0.435
30	0.545	0.984	1.80	0.962	0.545	0.551
25	0.646	1.217	1.88	0.995	0.646	0.646
20	0.723	1.390	1.92	1.01	0.732	0.725
16.5	0.758	1.474	1.95	1.02	0.774	0.764
13.4	0.784	1.523	1.94	1.02	0.800	0.795
12.2	0.800	1.553	1.94	1.02	0.816	0.803
10	0.722	1.522	2.11	1.09	0.787	0.787
8.1	0.831	1.551	1.87	0.989	0.831	0.789
7	0.801	1.658	2.07	1.07	0.860	0.773
6	0.671	1.601	2.39	1.20	0.807	0.758
5	0.612	1.306	2.13	1.10	0.673	0.748
4	0.694	1.190	1.71	0.924	0.694	0.724
3.3	0.735	1.335	1.82	0.967	0.735	0.710
2.5	0.706	1.300	1.84	0.977	0.706	0.706
2	0.440	1.153	2.62	1.30	0.571	0.580
1.5	0.484	0.952	1.96	1.03	0.499	0.480
1	0.226	0.597	2.65	1.31	0.295	0.295
0.8	0.237	0.595	2.51	1.25	0.297	0.297
0.7	0.264	0.664	2.51	1.25	0.332	0.332
0.61	0.299	0.761	2.55	1.27	0.379	0.379
0.5	0.238	0.745	3.13	1.50	0.356	0.356
0.33	0.0750	0.242	3.23	1.53	0.115	0.115
0.25	0.0420	0.126	3.00	1.44	0.0606	0.0606
0.15	0.0158	0.0458	2.90	1.41	0.0222	0.0222
0.1	0.00718	0.0207	2.88	1.40	0.0100	0.0100

Table 2.5-232
FIRS Amplitudes (g) for the Hypothetical Outcrop at 40-ft Depth Horizon

Freq	Soil amplitudes		AR	DF2	raw	smoothed
	10 ⁻⁴	10 ⁻⁵			FIRS	FIRS
100	0.246	0.489	1.99	1.04	0.255	0.255
76	0.254	0.509	2.00	1.05	0.266	0.270
60	0.287	0.563	1.96	1.03	0.295	0.293
50	0.302	0.575	1.90	1.00	0.304	0.325
40	0.372	0.658	1.77	0.946	0.372	0.381
30	0.473	0.788	1.67	0.903	0.473	0.480
25	0.566	0.961	1.70	0.916	0.566	0.566
20	0.656	1.120	1.71	0.92	0.656	0.649
16.5	0.699	1.230	1.76	0.94	0.699	0.697
13.4	0.744	1.319	1.77	0.95	0.744	0.734
12.2	0.778	1.374	1.77	0.95	0.778	0.749
10	0.713	1.398	1.96	1.03	0.733	0.733
8.1	0.803	1.442	1.80	0.958	0.803	0.749
7	0.775	1.539	1.99	1.04	0.805	0.745
6	0.673	1.512	2.25	1.15	0.771	0.745
5	0.637	1.265	1.99	1.04	0.662	0.748
4	0.745	1.163	1.56	0.857	0.745	0.737
3.3	0.796	1.324	1.66	0.902	0.796	0.753
2.5	0.747	1.289	1.72	0.928	0.747	0.747
2	0.457	1.133	2.48	1.24	0.567	0.582
1.5	0.492	0.918	1.87	0.99	0.492	0.478
1	0.227	0.580	2.55	1.27	0.288	0.288
0.8	0.238	0.579	2.44	1.22	0.291	0.291
0.7	0.265	0.647	2.45	1.23	0.325	0.325
0.61	0.299	0.743	2.49	1.24	0.372	0.372
0.5	0.238	0.731	3.07	1.47	0.350	0.350
0.33	0.075	0.239	3.18	1.52	0.114	0.114
0.25	0.042	0.124	2.96	1.43	0.060	0.060
0.15	0.016	0.045	2.88	1.40	0.022	0.022
0.1	0.007	0.020	2.85	1.39	0.010	0.010

Table 2.5-233
SSE Amplitudes (g) for the Ground Surface (GMRS)

- Freq	Soil amplitudes		- AR	- DF2	raw SSE	smoothed SSE
	10 ⁻⁴	10 ⁻⁵				
100	0.266	0.474	1.78	0.95	0.266	0.266
76	0.272	0.492	1.81	0.96	0.272	0.277
60	0.300	0.541	1.80	0.96	0.300	0.297
50	0.306	0.545	1.78	0.95	0.306	0.321
40	0.356	0.595	1.67	0.905	0.356	0.365
30	0.440	0.662	1.50	0.832	0.440	0.452
25	0.547	0.762	1.39	0.783	0.547	0.547
20	0.686	0.905	1.32	0.75	0.686	0.670
16.5	0.739	1.042	1.41	0.79	0.739	0.737
13.4	0.802	1.140	1.42	0.80	0.802	0.789
12.2	0.846	1.213	1.43	0.80	0.846	0.809
10	0.789	1.279	1.62	0.88	0.789	0.789
8.1	0.920	1.390	1.51	0.835	0.920	0.818
7	0.892	1.551	1.74	0.93	0.892	0.815
6	0.767	1.586	2.07	1.07	0.823	0.814
5	0.709	1.335	1.88	1.00	0.709	0.814
4	0.812	1.197	1.47	0.818	0.812	0.787
3.3	0.849	1.365	1.61	0.877	0.849	0.802
2.5	0.775	1.309	1.69	0.912	0.775	0.775
2	0.466	1.134	2.43	1.22	0.569	0.589
1.5	0.494	0.910	1.84	0.98	0.494	0.481
1	0.227	0.572	2.52	1.26	0.285	0.285
0.8	0.237	0.570	2.41	1.21	0.287	0.287
0.7	0.263	0.638	2.42	1.22	0.321	0.321
0.61	0.297	0.734	2.47	1.24	0.367	0.367
0.5	0.237	0.722	3.05	1.46	0.347	0.347
0.33	0.0747	0.236	3.16	1.51	0.113	0.113
0.25	0.0419	0.123	2.95	1.42	0.0597	0.0597
0.15	0.0157	0.0451	2.86	1.39	0.0219	0.0219
0.1	0.00718	0.0204	2.84	1.38	0.00992	0.00992

Table 2.5-234
Conversion Between Body-Wave (m_b) and Moment (M) Magnitudes

Convert	To	Convert	To
m_b	M	M	m_b
4.00	3.77	4.00	4.28
4.10	3.84	4.10	4.41
4.20	3.92	4.20	4.54
4.30	4.00	4.30	4.66
4.40	4.08	4.40	4.78
4.50	4.16	4.50	4.90
4.60	4.24	4.60	5.01
4.70	4.33	4.70	5.12
4.80	4.42	4.80	5.23
4.90	4.50	4.90	5.33
5.00	4.59	5.00	5.43
5.10	4.69	5.10	5.52
5.20	4.78	5.20	5.61
5.30	4.88	5.30	5.70
5.40	4.97	5.40	5.78
5.50	5.08	5.50	5.87
5.60	5.19	5.60	5.95
5.70	5.31	5.70	6.03
5.80	5.42	5.80	6.11
5.90	5.54	5.90	6.18
6.00	5.66	6.00	6.26
6.10	5.79	6.10	6.33
6.20	5.92	6.20	6.40
6.30	6.06	6.30	6.47
6.40	6.20	6.40	6.53
6.50	6.34	6.50	6.60
6.60	6.49	6.60	6.66
6.70	6.65	6.70	6.73
6.80	6.82	6.80	6.79
6.90	6.98	6.90	6.85
7.00	7.16	7.00	6.91
7.10	7.33	7.10	6.97
7.20	7.51	7.20	7.03
7.30	7.69	7.30	7.09
7.40	7.87	7.40	7.15
7.50	8.04	7.50	7.20
		7.60	7.26
		7.70	7.32
		7.80	7.37
		7.90	7.43
		8.00	7.49

Table 2.5-235
Summary of Bedrock Faults Mapped Within the 5-Mile VEGP Site Radius

Fault Name	Proximity to VEGP Site (mi)	Length (mi/km)	Orientation	Sense of Slip	Relationship to Dunbarton Basin	Evidence for Non-Capability
Pen Branch	On site	>20/>30	NE	SE up, reverse	NW border (normal) fault, reactivated as reverse	a, b, c, d
Ellenton	~4	~4/~6.5	NNW	E down, unknown	Unknown; located NW of basin	b, c, e
Steel Creek	~2	>11/>18	NNE	NW up, reverse	Secondary structure forming horst with Pen Branch	b, c, d
Upper Three Runs	~5	>20/>30	NE-NNE	Unknown	Unknown; located NW of basin	b, c, f

Note: Fault locations based on Cumbest et al. (1998), Stieve and Stephenson (1995), and work performed as part of this ESP study

- a Seismic reflection and borehole data show lack of post-Eocene slip (NUREG-1137-8; Cumbest et al. 2000)
- b Lack of geomorphic expression
- c Lack of seismicity associated with fault
- d Quaternary fluvial terraces of Savannah River overlying projection of fault appear undeformed (Geomatrix 1993)
- e Fault does not appear in most recent SRS fault maps (Cumbest et al. 1998, 2000)
- f No disruption to base of Coastal Plain section (pre-Cretaceous age) (Stieve and Stephenson 1995)

Table 2.5-236
Static Engineering Properties of Subsurface Materials (ESP)

Parameter ⁽¹⁾	Stratum			
	Upper Sand	Compacted Structural Fill	Blue Bluff Marl	Lower Sand
Range of Thickness, feet	79 to 124	79 to 124	63 to 95	900
Average thickness, feet	92	92	76	900
USCS symbol	SP/SM/SC/ML	SP/SM/SC	CL/ML	SP/SM/ML
Natural moisture content (ω), %	N/A	N/A	35	N/A
Unit weight (pcf)	115	123 (moist) 133 (saturated)	115	115
Atterberg Limits				
Liquid limit (LL), %	N/A ⁽²⁾	N/A	51	N/A
Plastic limit (PL), %	N/A	N/A	26	N/A
Plasticity index (PI), %	N/A	N/A	25	N/A
Measured SPT N-value, bpf	20	N/A	80	50
Adjusted SPT N60-value, bpf	25	N/A	100	62
Strength properties				
Undrained shear strength (c_u), ksf	—	0	10	0
Internal friction angle (ϕ'), degrees	34	34	0	34
Elastic modulus (high strain) (E_s), ksf	900	1,500	10,000	10,800 ⁽³⁾ 13,500 ⁽⁴⁾
Shear modulus (high strain) (G_s), ksf	350	600	3,500	4,200 ⁽³⁾ 5,200 ⁽⁴⁾
Shear modulus (low strain) (G_{max}), ksf	3,088	3,820	20,475	20,538
Coefficient of Subgrade Reaction (k_1), tcf	N/A	300	N/A	N/A
Earth Pressure Coefficients				
Active (K_a)	N/A	0.3	N/A	N/A
Passive (K_p)	N/A	3.5	N/A	N/A
At Rest (K_0)	N/A	0.5	N/A	N/A
Coefficient of Sliding	N/A	0.45	N/A	N/A
Poisson's Ratio	0.09–0.49 ⁽⁵⁾		0.33–0.48	0.32–0.49
Notes.				
(1) The values tabulated above are for use as a design guideline only. Reference should be made to specific boring and CPT logs and laboratory test results for appropriate modifications at specific design locations.				
(2) N/A indicates that the properties were not measured or are not applicable.				
(3) This value applies between depths of 0 to 100 ft below the bottom of the Blue Bluff Marl.				
(4) This value applies between depths of 100 to 300 ft below the bottom of the Blue Bluff Marl.				
(5) Values not determined during COL investigation, retain ESP values.				

Table 2.5-237
Static Engineering Properties of Subsurface Materials (COL)

Parameter ⁽¹⁾	Stratum			
	Upper Sand	Compacted Structural Fill	Blue Bluff Marl	Lower Sand ⁽⁵⁾
Range of Thickness, feet	82 to 94	82 to 94	60 to 77	900
Average thickness, feet	88	88	68	900
USCS symbol	SP/SM/SC/ML	SP/SM	CL/CH/ML/MH	SP/SM/ML/CL
Natural moisture content (ω), %	N/A	N/A	32	N/A
Unit weight (pcf)	113	123 (moist) 133 (saturated)	115	120
Atterberg Limits				
Liquid limit (LL), %	N/A ⁽²⁾	N/A	63	N/A
Plastic limit (PL), %	N/A	N/A	33	N/A
Plasticity index (PI), %	N/A	N/A	30	N/A
Measured SPT N-value, bpf	18	32	71	50
Adjusted SPT N_{60} -value, bpf	25	43	95	62
Strength properties				
Undrained shear strength (c_u), ksf	—	-	10	—
Internal friction angle (ϕ'), degrees	34	36	0	34
Elastic modulus (high strain) (E_s), ksf	900	1,500	9,000	10,800 ⁽³⁾ 13,500 ⁽⁴⁾
Shear modulus (high strain) (G_s), ksf	350	520	3,000	4,200 ⁽³⁾ 5,200 ⁽⁴⁾
Shear modulus (low strain) (G_{max}), ksf	3,100	3,800	15,000	20,538
Coefficient of Subgrade Reaction (k_1), tcf	N/A	1,000	N/A	N/A
Earth Pressure Coefficients				
Active (K_a)	N/A	0.26	N/A	N/A
Passive (K_p)	N/A	3.9	N/A	N/A
At Rest (K_0)	N/A	0.4	N/A	N/A
Coefficient of Sliding	N/A	0.45	N/A	N/A
Poisson's Ratio	0.09–0.49 ⁽⁵⁾	0.24–0.45	0.43	0.32–0.49

Notes.

(1) The values tabulated above are for use as a design guideline only. Reference should be made to specific boring and CPT logs and laboratory test results for appropriate modifications at specific design locations.

(2) N/A indicates that the properties were not measured or are not applicable.

(3) This value applies between depths of 0 to 100 ft below the bottom of the Blue Bluff Marl.

(4) This value applies between depths of 100 to 300 ft below the bottom of the Blue Bluff Marl.

(5) Values not fully evaluated during COL investigation, ESP values retained.

Table 2.5-238
Design Dynamic Shear Modulus (ESP)

Geologic Formation	Depth (ft)	Elevation (ft)	G_{max} (ksf)
Upper Sand Stratum (Barnwell Group)	0 to 16	223 to 207	7,000
	16 to 41	207 to 182	2,286
	41 to 58	182 to 165	2,580
	58 to 86	165 to 137	2,893
Blue Bluff Marl (Lisbon Formation)	86 to 92	137 to 131	6,978
	92 to 97	131 to 126	10,321
	97 to 102	126 to 121	15,750
	102 to 105	121 to 118	10,321
	105 to 111	118 to 112	17,286
	111 to 123	112 to 100	19,723
	123 to 149	100 to 74	25,080
Lower Sand Stratum	149 to 156	74 to 67	14,286
(Still Branch)	156 to 216	67 to 7	9,723
(Congaree)	216 to 331	7 to -108	13,580
(Snapp)	331 to 438	-108 to -215	15,009
(Black Mingo)	438 to 477	-215 to -254	19,723
(Steel Creek)	477 to 587	-254 to -364	25,080
(Gaillard/Black Creek)	587 to 798	-364 to -575	29,009
(Pio Nono)	798 to 858	-575 to -635	29,418
(Cape Fear)	858 to 1,049	-635 to -826	26,229
Dunbarton Triassic Basin	1,049		

Note: Gmax was calculated using g from Table 2.5-236, and the shear wave velocity values from Table 2.5-243.

Table 2.5-239
Types and Numbers of Laboratory Tests Completed for the ESP Application

Type of Test	Number of Tests Performed
Grain size	61
Unit Weight	31
Natural Moisture Content	75
Atterberg Limits	27
UU Triaxial (1-point)	15

Table 2.5-240
Types and Numbers of Completed Laboratory Tests
in the Powerblock Footprint for the COL Investigation

Type of Test	Number of Tests Performed
Moisture Content	113
Wash #200	272
Unit Weight	100
Atterberg Limits	109
Chemical Analysis	5
Unconfined Compression	27
Unconsolidated Undrained Triaxial	11
Consolidated Undrained Triaxial	27
1-D Consolidation	18
Resonant Column Torsional Shear	19

Table 2.5-241 (Sheet 1 of 4)
Summary of Laboratory Tests Performed on Selected Soils Samples from ESP Borings

SAMPLE DETAILS						SOIL TESTING							
Boring No.	Top Depth (ft)	Length (ft)	Type	Formation	SPT N-value (bpf)	% Fines	γ (pcf)	ω_N (%)	PL (%)	LL (%)	PI (%)	USCS Classification	UU s_u (ksf)
B-1002	7.5	1.5	SS	Fill	20	9.4		6.2					
	18.5	1.5	SS	Barnwell	19	37.1		24.4					
	28.5	1.5	SS	Barnwell	8	24.9		31.8					
	33.5	1.5	SS	Barnwell	6	31.6		58.8					
	38.5	1.5	SS	Barnwell	7			92.8	27	48	21		
	53.5	1.5	SS	Barnwell	8	10.5		42.9					
	63.5	1.5	SS	Barnwell	13	7.2		29.3					
	73.5	1.5	SS	Barnwell	12	10		24.5					
	83.5	1.5	SS	Barnwell	9	6.1		27.6					
	92.0	2.5	UD-Upper	Lisbon	N/A	67.2	103.6	52.1	50	83	33	MH	1.15
			UD-Middle				102.4						3.35
	103.5	2.5	UD	Lisbon	N/A	35.9	114.3	56.6	22	34	12	CL	
							114.5	26.5					2.4
	113.5	2.5	UD	Lisbon	N/A	33.8	132.8	25.5	19	29	10	SC	
							132.9	16.3					2.15
	123.5	2.5	UD	Lisbon	N/A	24.5	140.2	13.5	17	22	5	GC-GM	
	133.5	2.0	UD	Lisbon	N/A	96.6	118.0	28.6	26	40	14	CL	
							118.1	29.8					2.4
	153.5	1.5	SS	Lisbon	27	39.4		23.3	21	34	13	ML	
	188.5	1.5	SS	Still Branch	9	6.6		40.7	NP	NP	NP	SM	
	238.5	1.5	SS	Congaree	77	12.3		18.5					
B-1003	15	5	C	Barnwell	N/A	20.9		13.4					
	35	5	C	Barnwell	N/A	29.8		42.1					
	55	5	C	Barnwell	N/A	13.4		17.5					
	75	5	C	Barnwell	N/A	8.2		32.3					

Table 2.5-241 (Sheet 2 of 4)
Summary of Laboratory Tests Performed on Selected Soils Samples from ESP Borings

SAMPLE DETAILS						SOIL TESTING							
Boring No.	Top Depth (ft)	Length (ft)	Type	Formation	SPT N-value (bpf)	% Fines	γ (pcf)	ω_N (%)	PL (%)	LL (%)	PI (%)	USCS Classification	UU s_u (ksf)
B-1003	88	5	C	Lisbon	N/A	33.4		67.4	42	93	51	SM	
	93	2.5	UD-1	Lisbon	N/A	40.6	115.7	30.6	32	54	22	SM	
							115.8	29.5					4.3
	104.7	2	C	Lisbon	N/A	31.7	111.5	40.6	51	83	32	SM	
	121.7	5	C	Lisbon	N/A	42.5	122.5	28.0	NP	NP	NP	SM	
	141.7	5	C	Lisbon	N/A	34.2	126.1	25.9	28	46	18	SM	
B-1003	165.7	5	C	Still Branch	N/A	5.4	121.7	23.6	NP	NP	NP	SP-SM	
	185.7	5	C	Still Branch	N/A	16.4		32.3					
	205.7	5	C	Still Branch	N/A	21.4		39.3					
	240.7	5	C	Congaree	N/A	10.9		23.2					
	280.7	5.0	C	Congaree	N/A	14.2		23.2					
	315.7	5.0	C	Congaree	N/A	79.8		32.7	24	43	19	CL	
							119.4	31.0					
	350.7	5.0	C	Snapp	N/A	78.5	128.3	21.3	22	41	19	ML	
	400.7	5.0	C	Snapp	N/A	15.8		18.9					
	450.7	5.0	C	Black Mingo	N/A	15.9		28.6					
	496.7	5.0	C	Steel Creek	N/A	13.2		26.4					
B-1004	9.0	1.5	SS	Barnwell	13	24.4		13.8					
	12.0	1.5	SS	Barnwell	12	23.1		14.5					
	23.5	1.5	SS	Barnwell	8	14.9		18.5					
	43.5	1.5	SS	Barnwell	4	60.0		46.2	24	58	34	ML	
	53.5	1.5	SS	Barnwell	7	41.0		62.9					
	68.5	1.5	SS	Barnwell	6	19.9		24.1					
	83.5	1.5	SS	Barnwell	6	11.5		28.8					
	123.5	1.5	SS	Barnwell	5	19.2		19.7	19	43	24	GM	

Table 2.5-241 (Sheet 3 of 4)
Summary of Laboratory Tests Performed on Selected Soils Samples from ESP Borings

SAMPLE DETAILS						SOIL TESTING							
Boring No.	Top Depth (ft)	Length (ft)	Type	Formation	SPT N-value (bpf)	% Fines	γ (pcf)	ω_N (%)	PL (%)	LL (%)	PI (%)	USCS Classification	UU s_u (ksf)
B-1004	144.0	1.5	UD-Upper	Lisbon	N/A	46.3	105.1	44.6	38	59	21	SM	
							105.2	52.0					0.15
			UD-Middle				114.2	29.8					0.8
	153.5	1.5	UD	Lisbon	N/A	41.7		30.1	27	43	16	SM	
							117.4	25.2					
							119.3	28.7					3.75
	163.5	2.5	UD-Upper	Lisbon	N/A	58.3		25.1	37	55	18	MH	
							117.4	30.2					1.05
			UD-Middle				125.6	24.5					1.2
	177.0	2.5	UD-Upper	Lisbon	N/A	41.7	124.7	20.8	22	31	9	SM	
							124.6	22.4					0.8
			UD-Middle				131.8	39.2					1.9
B-1004	188.5	2.0	UD	Lisbon	N/A	75.2	120.4	29.0	24	41	17	CL	
							120.6	28.4					4.0
	198.5	2.0	UD	Lisbon	N/A	34.5	128.1	26.2	21	31	10	SM	
							128.2	21.7					3.0
B-1006	7.5	1.5	SS	Barnwell	3	7.3		3.8					
	33.5	1.5	SS	Barnwell	13	26.1		19.7					
	58.5	1.5	SS	Barnwell	W HAMM	58.3		92.8	30	97	67	CH	
	68.5	1.5	SS	Barnwell	W HAMM	3.1		25.4					
	88.5	1.5	SS	Barnwell	W HAMM	15.7		51.9					
	108.5	1.5	SS	Barnwell	42	21.5		22.0					
	123.5	1.5	SS	Lisbon	50/2"	64.1		53.7	43	99	56	MH	

Table 2.5-241 (Sheet 4 of 4)
Summary of Laboratory Tests Performed on Selected Soils Samples from ESP Borings

SAMPLE DETAILS						SOIL TESTING							
Boring No.	Top Depth (ft)	Length (ft)	Type	Formation	SPT N-value (bpf)	% Fines	γ (pcf)	ω_N (%)	PL (%)	LL (%)	PI (%)	USCS Classification	UU s_u (ksf)
B-1010	7.5	1.5	SS	Barnwell	27	7.8		5.7					
	33.5	1.5	SS	Barnwell	23	17.0		18.9					
	58.5	1.5	SS	Barnwell	19	13.3		27.3					
	73.5	1.5	SS	Barnwell	6	23.9		30.8					
	98.5	1.5	SS	Lisbon	77	91.3		49.9	47	94	58	CH	

Legend:

NP = non-plastic

ω_N = natural moisture content

γ = unit weight

% Finer = % finer than the #200 sieve

PL = plastic limit

LL = liquid limit

PI = plasticity index

UU s_u = undrained strength from UU triaxial test

SS = split spoon or split barrel sample

UD = undisturbed sample

UD-Upper = test specimen taken from top of UD sample

UD-Middle = test specimen taken from middle of UD sample

C = soil core

W HAMM = weight of hammer (sampler penetrated at least 18" under the weight of the hammer, no blows applied by the hammer)

Table 2.5-242
Summary of SPT N-Values Measured at the ESP Borings

Boring Number	Measured SPT N-value (blows/ft) for Different Formations		
	Upper Sand Stratum (Barnwell Group)	Blue Bluff Marl (Lisbon Formation)	Lower Sand Stratum
B-1001	47, 32, 22, 22, 22, 23, 21, 23, 23, 37, 13, 10, 7, 5, 6, 12, 13, 30, 11, 37, 36, 47, WOR, 50/5"	50/5", 50/4", 51, 50/4", 50/6", 50/4", 50/5"	Not measured
B-1002	30, 67, 28, 33, 19, 10, 8, 6, 7, 12, 22, 8, 11, 13, 18, 12, 10, 9	77/11", 68/7", 54, 72, 50/2", 78/8", 65, 40, 27	46, 26, 50/4", 40, 9, 43, 32, 41, 50, 77
B-1004	21, 24, 25, 16, 16, 13, 19, 12, 14, 10, 8, 17, 13, 14, 4, 5, 7, 7, 18, 6, 5, 9, 5, 5, 17, 11, 16, 20, 18, 34, 5, 9, 50/5"	77, 50/4", 50/0", 50/3", 50/3", 77, 79, 50/5", 50/4", 70/10", 81, 78, 58	79/10", 35, 50/5", 95, 47, 104
B-1005	27, 29, 26, 15, 11, 11, 10, 17, 13, 19, 17, 19, 11, 7, WOH, 37, 17, 34, 28, 25, 50/1", 56, 37, 69, 46, 54, 57, 33, 31, 37, 95, 30, 32, 50/4", 80/9", 39	50/5", 50/4"	Not measured
B-1006	19, 20, 15, 9, 2, 3, 4, 8, 10, 11, 30, 24, 17, 13, 10, 2, 8, 7, WOH, 9, WOH, WOH, 13, 7, WOH, 14, 19, 28, 42, 50	50/5", 50/2"	Not measured
B-1007	30, 32, 10, 10, 8, 14, 23, 20, 27, 26, 31, 25, 23, 15, 15, 24, 21, 26, 36, 37, 27, 36, 18, 13	50/2", 50/3", 45, 50/2", 50/5", 50/4", 74	Not measured
B-1008	19, 30, 53, 67, 34, 31, 19, 24, 30, 36, 30, 20, 17, 17, 25, 18, 22, 33, 39, 22, 25, 50/5", 50/4", 50/5"	46, 65, 53, 71/9", 50/3", 50/3", 50/4"	Not measured
B-1009	19, 37, 42, 44, 20, 21, 27, 21, 20, 30, 29, 35, 19, 31, 37, 42, 23, 13, 27, 32, 20, 8, 10, 40, 24	51, 50/5"	Not measured
B-1010	13, 18, 29, 24, 20, 27, 9, 13, 18, 29, 72, 23, 27, 23, 30, 26, 15, 34, 19, 6, 28, 6, 20, 10, 15, 21	67, 50/4"	Not measured
B-1011	8, 7, 11, 10, 14, 15, 15, 20, 13, 44, 42, 12, 25, 48, 28, 41, 37, 49, 60, 40, 50/0", 50/4"	69, 74, 50/3", 50/1", 36	Not measured
B-1013	9, 14, 26, 26, 12, 26, 26, 33, 9, 22, 16, 41, 16, 34, 22, 25, 21, 28, 12, 26, 15, 8, 18, 36, 13, 26	50/2", 76	Not measured
Range:	WOR-50/0"	27-50/1"	9-50/4"
Average:	25	83	59
Median	21	100	47

NOTES:

- ^a SPT blow counts will be adjusted to reflect the measured hammer efficiencies.
- ^b WOR means that the sampler penetrated 18" or more under weight of the rods, and WOH means that the sampler penetrated 18" or more under weight of the rods and hammer. These values were taken as zero when calculating the average.
- ^c SPT blow counts linearly extrapolated to more than 100 bpf were truncated at 100 bpf when calculating the average.
- ^d SPT N-values shown for the Barnwell Group exclude measurements in the fill layers encountered at borings B-1001, B-1002, B-1004, and B-1005.

Table 2.5-243
Typical Shear Wave Velocity Values for Existing Strata (ESP)

Geologic Formation	Depth (ft)	Elevation (ft)	V_s (fps)
Upper Sand Stratum (Barnwell Group)	0 to 16	223 to 207	1,400
	16 to 41	207 to 182	800
	41 to 58	182 to 165	850
	58 to 86	165 to 137	900
Blue Bluff Marl (Lisbon Formation)	86 to 92	137 to 131	1,400
	92 to 97	131 to 126	1,700
	97 to 102	126 to 121	2,100
	102 to 105	121 to 118	1,700
	105 to 111	118 to 112	2,200
	111 to 123	112 to 100	2,350
	123 to 149	100 to 74	2,650
Lower Sand Stratum	149 to 156	74 to 67	2,000
(Still Branch)	156 to 216	67 to 7	1,650
(Congaree)	216 to 331	7 to -108	1,950
(Snapp)	331 to 438	-108 to -215	2,050
(Black Mingo)	438 to 477	-215 to -254	2,350
(Steel Creek)	477 to 587	-254 to -364	2,650
(Gaillard/Black Creek)	587 to 798	-364 to -575	2,850
(Pio Nono)	798 to 858	-575 to -635	2,870
(Cape Fear)	858 to 1,049	-635 to -826	2,710
Dunbarton Triassic Basin	1,049	-826	2,710
	1,093	-870	5,300
	1,323	-1,100	7,800

Table 2.5-244
Summary of ESP Borings and CPTs

Boring Number	Plant Coordinates		State Coordinates		Elevation (ft msl)	Depth (ft)
	Northing	Easting	Northing	Easting		
	(ft)	(ft)	(ft)	(ft)		
B-1001	7,662	6,220	1,142,662	620,220	221.64	123.9
B-1002 ^{a,b}	7,999	6,985	1,142,999	620,985	221.98	260
B-1002A ^{a,d}	7,986	6,986	1,142,986	620,986	222.27	105
B-1003 ^{a,b,c}	7,974	7,890	1,142,974	621,890	223.21	1338
B-1004 ^{a,b}	7,985	6,131	1,142,985	620,131	249.78	304
B-1005	8,992	6,155	1,143,992	620,155	253.14	164.3
B-1006	8,810	7,343	1,143,810	621,343	255.95	124.2
B-1007	7,662	7,120	1,142,662	621,120	221.02	125
B-1008	7,671	7,996	1,142,671	621,996	219.51	124.3
B-1009	6,001	6,361	1,141,001	620,361	220.39	98.9
B-1010	6,000	7,280	1,141,000	621,280	218.60	104.3
B-1011	8,741	8,378	1,143,741	622,378	219.38	100
B-1013	5,976	8,272	1,140,976	622,272	218.62	105
C-1005A ^{a,d}	7,990	8,179	1,142,990	622,179	223.66	90
CPT Number	Plant Coordinates		State Coordinates		Elevation (ft msl)	Depth (ft)
	Northing	Easting	Northing	Easting		
	(ft)	(ft)	(ft)	(ft)		
C-1001A	8,028	6,356	1,143,028	620,356	248.57	116.7
C-1002	7,668	6,575	1,142,668	620,575	222.13	78.5
C-1003 ^{e,f}	7,669	7,478	1,142,669	621,478	219.80	80
C-1004 ^f	7,646	8,362	1,142,646	622,362	220.82	77
C-1005 ^{e,f}	7,995	8,175	1,142,995	622,175	223.81	82
C-1006	8,001	7,262	1,143,001	621,262	222.80	74
C-1007	8,271	8,055	1,143,271	622,055	222.81	81.7
C-1008	8,268	6,931	1,143,268	620,931	221.30	76
C-1009A ^{e,f}	5,980	6,798	1,140,980	620,798	218.93	99
C-1010	6,008	7,754	1,141,008	621,754	219.06	96

^a Location of suspension P-S velocity logging.

^b Location of caliper, natural gamma, resistivity, and spontaneous potential measurements.

^c Location of borehole deviation survey.

^d Boreholes drilled without sampling to allow the performance of suspension P-S velocity logging above the zone of drilling fluid loss.

^e Location of seismic CPT.

^f Location of pore pressure dissipation tests.

Note: State Plane Coordinates are from NAD27 Georgia East state grid system. Plant coordinates are converted from the following formula:

Plant North + 1,135,000 = State North

Plant East + 614,000 = State East

Table 2.5-245 (Sheet 1 of 6)
Summary of COL Borings, CPTs, and Test Pits

Boring Number	Plant Coordinates		State Coordinates		Elevation (ft, msl)	Depth (ft)
	Northing (ft)	Easting (ft)	Northing (ft)	Easting (ft)		
B-1105	9,168	6,003	1,144,168	620,003	257.89	148.8
B-1107	9,154	6,916	1,144,154	620,916	266.66	150.0
B-1108	9,214	7,273	1,144,214	621,273	273.56	149.8
B-1109	9,180	7,581	1,144,180	621,581	276.48	150.0
B-1110	9,171	8,011	1,144,171	622,011	265.14	150.0
B-1111	9,213	8,334	1,144,213	622,334	224.90	150.0
B-1112	9,223	8,691	1,144,223	622,691	213.74	23.0
B-1112A	9,219	8,561	1,144,219	622,561	227.14	150.0
B-1113	8,901	6,217	1,143,901	620,217	249.99	170.0
B-1116	8,894	7,265	1,143,894	621,265	261.82	138.5
B-1117	8,891	7,628	1,143,891	621,628	263.89	149.3
B-1118	8,886	8,008	1,143,886	622,008	257.91	149.4
B-1119	8,888	8,334	1,143,888	622,334	223.57	150.0
B-1120	8,893	8,558	1,143,893	622,558	227.18	149.8
B-1121	8,576	6,216	1,143,576	620,216	241.33	150.0
B-1123	8,575	6,922	1,143,575	620,922	241.27	150.0
B-1124	8,628	7,422	1,143,628	621,422	241.21	150.0
B-1125	8,587	7,628	1,143,587	621,628	240.97	150.0
B-1126	8,568	7,980	1,143,568	621,980	219.88	150.0
B-1127	8,573	8,332	1,143,573	622,332	219.67	150.0
B-1128	8,573	8,682	1,143,573	622,682	218.26	73.0
B-1128A	8,574	8,685	1,143,574	622,685	217.92	148.8
B-1129	8,278	7,894	1,143,278	621,894	221.84	100.0
B-1130	7,483	8,250	1,142,483	622,250	217.46	99.2
B-1131	8,173	7,823	1,143,173	621,823	222.18	98.6
B-1132	7,614	7,450	1,142,614	621,450	218.73	100.0
B-1133	7,969	7,451	1,142,969	621,451	221.20	100.0
B-1134	8,283	7,104	1,143,283	621,104	222.04	100.0
B-1136	8,178	7,023	1,143,178	621,023	221.65	100.0
B-1138	8,470	5,193	1,143,470	619,193	215.82	100.0
B-1139	7,290	7,027	1,142,290	621,027	216.68	150.0
B-1140	7,290	7,824	1,142,290	621,824	216.58	150.0
B-1142	9,417	6,650	1,144,417	620,650	224.69	100.0
B-1146	10,428	8,272	1,145,428	622,272	240.04	98.6
B-1148	10,538	9,237	1,145,538	623,237	218.94	100.0
B-1150	10,467	10,235	1,145,467	624,235	170.69	100.0
B-1152	10,582	11,227	1,145,582	625,227	117.05	100.0
B-1153	10,569	11,673	1,145,569	625,673	103.58	100.0
B-1154	10,664	12,216	1,145,664	626,216	95.08	98.8

Table 2.5-245 (Sheet 2 of 6)
Summary of COL Borings, CPTs, and Test Pits

Boring Number	Plant Coordinates		State Coordinates		Elevation (ft, msl)	Depth (ft)
	Northing (ft)	Easting (ft)	Northing (ft)	Easting (ft)		
B-1155	12,390	10,936	1,147,390	624,936	84.95	150.0
B-1156	12,302	10,572	1,147,302	624,572	85.70	99.2
B-1157	12,210	11,062	1,147,210	625,062	86.77	150.0
B-1158	10,195	12,669	1,145,195	626,669	88.74	149.5
B-1159	12,286	10,955	1,147,286	624,955	88.70	150.0
B-1161	12,363	10,862	1,147,363	624,862	86.10	150.0
B-1162	12,235	10,815	1,147,235	624,815	85.55	200.0
B-1163	12,171	10,939	1,147,171	624,939	85.95	150.0
B-1164	11,995	10,519	1,146,995	624,519	220.50	150.0
B-1166	12,453	9,962	1,147,453	623,962	203.40	100.0
B-1168	12,688	9,468	1,147,688	623,468	202.20	100.0
B-1170	12,424	8,954	1,147,424	622,954	223.29	98.9
B-1172	11,983	8,539	1,146,983	622,539	249.49	100.0
B-1174	11,476	8,228	1,146,476	622,228	225.81	100.0
B-1176	10,876	8,195	1,145,876	622,195	221.48	35.0
B-1176A	10,879	8,197	1,145,879	622,197	221.51	100.0
B-1185	9,717	8,232	1,144,717	622,232	226.78	148.9
B-1186	9,712	4,819	1,144,712	618,819	277.51	178.8
B-1187	9,710	5,260	1,144,710	619,260	277.68	150.0
B-1189	9,460	4,997	1,144,460	618,997	279.98	150.0
B-1191	9,302	5,491	1,144,302	619,491	260.30	150.0
B-1192	9,217	4,841	1,144,217	618,841	243.17	179.5
B-1193	9,091	5,278	1,144,091	619,278	254.11	178.8
B-1194	12,505	7,630	1,147,505	621,630	199.35	50.0
B-1195	12,575	8,478	1,147,575	622,478	220.60	50.0
B-1196	12,287	8,018	1,147,287	622,018	217.52	50.0
B-1197	11,875	8,004	1,146,875	622,004	245.60	50.0
B-3001(DH)	7,600	7,800	1,142,600	621,800	218.40	420.0
B-3002(DH)	7,600	7,872	1,142,600	621,872	218.89	249.9
B-3002A	7,598	7,879	1,142,598	621,879	218.83	21.5
B-3003(DH)	7,600	7,727	1,142,600	621,727	218.29	250.0
B-3004	7,447	7,867	1,142,447	621,867	218.51	160.0
B-3005	7,718	7,749	1,142,718	621,749	219.20	155.0
B-3006	7,426	7,925	1,142,426	621,925	217.59	155.0
B-3007	7,719	7,877	1,142,719	621,877	220.78	159.8
B-3008	7,425	7,773	1,142,425	621,773	217.86	155.0
B-3009	7,484	7,957	1,142,484	621,957	217.85	153.9
B-3010	7,635	8,025	1,142,635	622,025	219.69	160.0
B-3011	7,777	8,025	1,142,777	622,025	220.57	165.0
B-3012	7,773	7,912	1,142,773	621,912	220.40	159.3
B-3013(C)	7,843	7,825	1,142,843	621,825	220.51	155.0

Table 2.5-245 (Sheet 3 of 6)
Summary of COL Borings, CPTs, and Test Pits

Boring Number	Plant Coordinates		State Coordinates		Elevation (ft, msl)	Depth (ft)
	Northing (ft)	Easting (ft)	Northing (ft)	Easting (ft)		
B-3014	7,799	7,749	1,142,799	621,749	220.26	158.7
B-3015	7,957	7,824	1,142,957	621,824	221.78	150.0
B-3016	7,978	7,913	1,142,978	621,913	222.48	150.0
B-3017	8,034	7,750	1,143,034	621,750	222.10	150.0
B-3018	7,738	8,116	1,142,738	622,116	219.80	155.0
B-3019	7,977	8,167	1,142,977	622,167	222.42	153.8
B-3020	7,978	8,075	1,142,978	622,075	222.44	149.4
B-3021	8,070	8,033	1,143,070	622,033	223.19	154.5
B-3022	8,070	7,873	1,143,070	621,873	223.86	150.0
B-3023	8,061	7,680	1,143,061	621,680	222.81	150.5
B-3024	7,906	7,400	1,142,906	621,400	220.16	150.0
B-3025	7,460	7,425	1,142,460	621,425	218.21	150.0
B-3026	7,290	7,404	1,142,290	621,404	215.76	149.2
B-3027	7,059	7,423	1,142,059	621,423	218.80	150.0
B-3028	6,867	7,409	1,141,867	621,409	220.12	150.0
B-3029	6,882	7,804	1,141,882	621,804	220.13	149.9
B-3030	6,700	7,800	1,141,700	621,800	221.99	150.0
B-3031	6,399	8,042	1,141,399	622,042	222.70	150.0
B-3032	6,158	7,710	1,141,158	621,710	220.05	149.5
B-3033	6,405	7,715	1,141,405	621,715	222.26	149.3
B-3034	6,400	7,915	1,141,400	621,915	224.67	149.2
B-3035	7,729	7,675	1,142,729	621,675	219.34	150.5
B-3036	7,442	7,676	1,142,442	621,676	217.87	155.0
B-3037	8,057	7,769	1,143,057	621,769	222.94	150.0
B-3038	6,883	7,543	1,141,883	621,543	220.76	98.9
B-3039	7,918	7,754	1,142,918	621,754	219.17	150.0
B-4001(DH)	7,600	7,000	1,142,600	621,000	218.88	399.9
B-4002(DH)	7,600	7,072	1,142,600	621,072	219.06	250.0
B-4003(DH)	7,600	6,927	1,142,600	620,927	218.99	249.8
B-4004	7,460	7,047	1,142,460	621,047	218.45	150.0
B-4005	7,715	6,949	1,142,715	620,949	221.13	164.9
B-4006	7,720	7,076	1,142,720	621,076	220.98	165.0
B-4007	7,426	7,125	1,142,426	621,125	217.90	170.0
B-4008	7,424	6,974	1,142,424	620,974	218.08	169.4
B-4009	7,486	7,157	1,142,486	621,157	217.91	164.9
B-4010	7,668	7,249	1,142,668	621,249	219.09	160.0
B-4011	7,773	7,236	1,142,773	621,236	219.08	150.0
B-4013(C)	7,843	7,020	1,142,843	621,020	222.24	165.0
B-4014	7,832	6,950	1,142,832	620,950	220.74	158.6
B-4015	7,773	7,115	1,142,773	621,115	220.11	155.0
B-4016	7,996	7,113	1,142,996	621,113	221.23	149.6

Table 2.5-245 (Sheet 4 of 6)
Summary of COL Borings, CPTs, and Test Pits

Boring Number	Plant Coordinates		State Coordinates		Elevation (ft, msl)	Depth (ft)
	Northing (ft)	Easting (ft)	Northing (ft)	Easting (ft)		
B-4017	8,035	6,950	1,143,035	620,950	220.94	150.0
B-4018	7,735	7,316	1,142,735	621,316	220.30	160.0
B-4019	7,976	7,371	1,142,976	621,371	221.76	160.0
B-4020	7,969	7,280	1,142,969	621,280	222.79	89.4
B-4020A	7,974	7,280	1,142,974	621,280	222.56	165.0
B-4021	8,093	7,247	1,143,093	621,247	224.55	150.0
B-4022	8,081	7,074	1,143,081	621,074	220.71	148.7
B-4023	8,062	6,880	1,143,062	620,880	220.71	150.0
B-4024	7,905	6,602	1,142,905	620,602	223.80	150.0
B-4025	7,510	6,625	1,142,510	620,625	220.80	150.0
B-4026	7,330	6,598	1,142,330	620,598	221.54	150.0
B-4027	7,180	6,633	1,142,180	620,633	217.73	150.0
B-4028	6,984	6,588	1,141,984	620,588	219.57	150.0
B-4029	6,875	6,700	1,141,875	620,700	220.28	150.0
B-4030	6,677	6,698	1,141,677	620,698	222.35	150.3
B-4031	6,400	6,975	1,141,400	620,975	222.13	150.0
B-4032	6,118	6,795	1,141,118	620,795	220.24	38.5
B-4032A	6,124	6,795	1,141,124	620,795	220.22	150.0
B-4033	6,398	6,349	1,141,398	620,349	219.93	149.4
B-4034	6,376	6,795	1,141,376	620,795	222.79	150.0
B-4035	7,729	6,876	1,142,729	620,876	220.52	164.8
B-4036	7,457	6,876	1,142,457	620,876	218.05	170.0
B-5001	11,177	7,808	1,146,177	621,808	218.99	150.0
B-5002	11,340	7,808	1,146,340	621,808	241.53	150.0
B-5003	11,387	7,575	1,146,387	621,575	227.94	148.7
B-5004	11,548	7,568	1,146,548	621,568	236.61	149.8
B-6002	9,134	5,627	1,144,134	619,627	247.90	150.0
B-6003	8,925	5,423	1,143,925	619,423	229.76	179.4
B-6004	8,718	5,473	1,143,718	619,473	231.59	150.0
B-6005	8,718	5,874	1,143,718	619,874	242.59	178.8
B-6006	8,070	6,302	1,143,070	620,302	248.22	50.0
B-6007	7,731	6,302	1,142,731	620,302	222.28	50.0
B-6008	10,444	8,676	1,145,444	622,676	240.11	150.0
B-6009	9,774	7,748	1,144,774	621,748	246.04	100.0
B-6010	8,893	7,059	1,143,893	621,059	263.39	169.3
B-6011	9,558	7,262	1,144,558	621,262	244.00	120.0
B-6012	9,257	6,481	1,144,257	620,481	194.20	120.0
B-6013	8,170	3,235	1,143,170	617,235	251.14	50.0
B-6014	8,168	4,281	1,143,168	618,281	209.79	50.0
B-6015	8,166	5,318	1,143,166	619,318	221.52	50.0
B-6018	7,909	4,367	1,142,909	618,367	204.66	50.0

Table 2.5-245 (Sheet 5 of 6)
Summary of COL Borings, CPTs, and Test Pits

Boring Number	Plant Coordinates		State Coordinates		Elevation (ft, msl)	Depth (ft)
	Northing (ft)	Easting (ft)	Northing (ft)	Easting (ft)		
B-6019	7,133	4,344	1,142,133	618,344	163.94	50.0
B-6020	7,634	5,556	1,142,634	619,556	221.48	130.0
B-6021	7,186	5,103	1,142,186	619,103	209.80	120.0
B-6022	7,225	6,040	1,142,225	620,040	216.23	90.0
B-6023	6,553	5,178	1,141,553	619,178	202.77	50.0
B-6024	6,546	5,998	1,141,546	619,998	216.07	50.0
B-6025	5,519	5,190	1,140,519	619,190	172.69	50.0
B-6026	5,538	5,900	1,140,538	619,900	215.46	50.0
B-6027	10,779	12,145	1,145,779	626,145	96.65	75.0
B-6028	10,611	12,062	1,145,611	626,062	95.70	50.0
B-6029	12,772	9,967	1,147,772	623,967	85.41	50.0
B-6030	12,588	10,223	1,147,588	624,223	88.37	50.0
CPT Number	Plant Coordinates		State Coordinates		Elevation (ft, msl)	Depth (ft)
	Northing (ft)	Easting (ft)	Northing (ft)	Easting (ft)		
C-1101	9,357	6,185	1,144,357	620,185	265.76	71.4
C-1102	9,424	7,333	1,144,424	621,333	267.61	51.4
C-1103	10,012	8,037	1,145,012	622,037	236.52	27.4
C-1104	10,602	8,747	1,145,602	622,747	230.19	77.1
C-1105	10,483	9,734	1,145,483	623,734	200.57	50.2
C-1106	10,534	10,748	1,145,534	624,748	138.02	20.0
C-1107	12,234	10,202	1,147,234	624,202	211.92	71.0
C-1108	12,628	9,753	1,147,628	623,753	200.89	59.6
C-1109	12,622	9,172	1,147,622	623,172	209.79	72.5
C-1110	12,199	8,740	1,147,199	622,740	242.39	72.3
C-1111	11,753	8,346	1,146,753	622,346	250.69	32.2
C-3001(S)	7,611	7,727	1,142,611	621,727	218.37	70.1
C-3002(S)	7,607	7,873	1,142,607	621,873	218.89	67.9
C-3003(S)	6,772	7,802	1,141,772	621,802	221.38	82.0
C-3004	6,542	7,807	1,141,542	621,807	223.25	72.7
C-3005(S)	6,267	7,792	1,141,267	621,792	221.27	101.1
C-4001(S)	7,600	6,919	1,142,600	620,919	218.87	74.2
C-4002(S)	7,600	7,064	1,142,600	621,064	219.08	82.2
C-4003(S)	6,785	6,708	1,141,785	620,708	221.16	82.5
C-4004	6,543	6,598	1,141,543	620,598	219.99	77.1
C-4005(S)	6,250	6,594	1,141,250	620,594	220.01	90.2

Table 2.5-245 (Sheet 6 of 6)
Summary of COL Borings, CPTs, and Test Pits

Test Pit Number	Plant Coordinates		State Coordinates		Elevation (ft, msl)	Depth (ft)
	Northing (ft)	Easting (ft)	Northing (ft)	Easting (ft)		
TP-B-1108	9,312	7,146	1,144,312	621,146	264.14	12.2
TP-B-1117	8,967	7,628	1,143,967	621,628	269.50	9.0
TP-B-1121	8,592	6,402	1,143,592	620,402	241.17	14.0
TP-B-1125	8,604	7,686	1,143,604	621,686	240.61	11.0
TP-B-1185	9,634	8,242	1,144,634	622,242	225.17	11.0
TP-B-1194	12,501	7,708	1,147,501	621,708	202.73	11.5
TP-B-1195	12,648	8,363	1,147,648	622,363	212.15	8.0
TP-B-1197	11,874	8,075	1,146,874	622,075	245.94	11.0

(DH) - Location of suspension P-S velocity logging and/or geophysical measurements.

(S) - Location of seismic CPT.

(C) – Borings with continuous sampling

Note: State Plane Coordinates are from NAD27 Georgia East state grid system. Plant coordinates are converted from the following formula:

Plant North + 1,135,000 = State North

Plant East + 614,000 = State East

Plant vertical datum is NGVD29, for this study msl = NGVD29

Table 2.5-246
Summary of Undisturbed Samples of the Blue Bluff Marl (ESP)

Boring Number	Sample Number	Depth at Top of Sample (ft)	Length of Sample (in.)
B-1002	UD-1	92.0	30
B-1002	UD-2	103.5	30
B-1002	UD-3	113.5	30
B-1002	UD-4	123.5	30
B-1002	UD-5	133.4	30
B-1003	UD-1	92.0	30
B-1004	UD-1	144.0	18
B-1004	UD-2	148.5	18
B-1004	UD-3	163.5	30
B-1004	UD-4	177.0	30
B-1004	UD-5	188.5	30
B-1004	UD-6	198.5	30

Table 2.5-247
Summary of SPT Hammer Energy Transfer Efficiency from ESP Investigation

Borehole and Sample Number	Energy Transfer Efficiency (%)
B1013-SS5	65
B1013-SS8	70
B1013-SS10	68
B1013-SS13	71
B1013-SS14	72
B1013-SS15	73
B1008-SS26	79
B1008-SS27	75
B1008-SS28	75
B1006-SS7	71
B1006-SS8	74
B1006-SS10	77
B1006-SS15	85
B1006-SS16	86
B1006-SS17	87
B1006-SS26	83
B1006-SS27	80
B1006-SS28	82
Range:	65-87
Average:	76
Median:	75

Table 2.5-248
Summary of SPT Hammer Energy Transfer Efficiency from COL Investigation

Hammer Serial No.	Rig Type	Number of Measurements	Min. ETR (%)	Max. ETR (%)	Avg. ETR (%)	Hammer Correction (Ce)
100	Diedrich D-50 ATV	6	69.1	75.1	72.4	1.21
165952	CME 850 ATV	7	78.9	90.0	83.4	1.39
200587	CME 75 Truck	5	83.7	86.6	84.2	1.40
211797	CME 75 Truck	3	75.1	80.3	77.6	1.29
219505	CME 55 Truck	3	67.1	80.6	70.1	1.17
219907	CME 75 Truck	3	76.6	84.6	80.2	1.34
270256	CME 85 Truck	5	77.7	88.0	82.5	1.38
311025	CME 55 Truck	4	88.3	92.6	90.2	1.50
328848	CME 750 ATV	3	83.1	85.1	84.0	1.40
331145	CME 55LC Truck	5	85.7	90.0	88.4	1.47
337153	CME 550 ATV	4	76.0	87.7	82.0	1.37
XO2958	CME 850 ATV	3	78.0	79.4	78.9	1.32

Table 2.5-249
Estimated Shear Wave Velocity and Dynamic Shear Modulus
Values for the Compacted Backfill (ESP)

Depth (ft)	Vs(1) (fps)	Gmax(2) (ksf)
0 to 6	573	1,255
6 to 10	732	2,049
10 to 14	811	2,510
14 to 18	871	2,898
18 to 23	927	3,280
23 to 29	983	3,694
29 to 36	1040	4,130
36 to 43	1092	4,553
43 to 50	1137	4,940
50 to 56	1175	5,274
56 to 63	1209	5,588
63 to 71	1232	5,796
71 to 79	1253	6,001
79 to 86	1273	6,186
(1) From Figure 6-1 of Bechtel (1984). (2) Gmax were calculated using γ from Table 2.5-236.		

Table 2.5-250
Shear Wave Velocity Values for the Compacted Backfill (COL)

Depth (ft)	Vs (fps)
0	550
5	724
10	832
20	975
30	1064
40	1130
50	1183
60	1228
70	1267
80	1302
85	1318
86.5	1327
88	1327

Table 2.5-251
Shear Wave Velocity Values for Site Amplification Analysis
Part A: Soil Shear-Wave Velocities (ESP)

Geologic Formation	Depth (feet)	V_s (fps)
Compacted Backfill	0 to 6	573
	6 to 10	732
	10 to 14	811
	14 to 18	871
	18 to 23	927
	23 to 29	983
	29 to 36	1,040
	36 to 43	1,092
	43 to 50	1,137
	50 to 56	1,175
	56 to 63	1,209
	63 to 71	1,232
	71 to 79	1,253
	79 to 86	1,273
Blue Bluff Marl (Lisbon Formation)	86 to 92	1,400
	92 to 97	1,700
	97 to 102	2,100
	102 to 105	1,700
	105 to 111	2,200
	111 to 123	2,350
	123 to 149	2,650
Lower Sand Stratum (Still Branch)	149 to 156	2,000
	156 to 216	1,650
(Congaree)	216 to 331	1,950
(Snapp)	331 to 438	2,050
(Black Mingo)	438 to 477	2,350
(Steel Creek)	477 to 587	2,650
(Gaillard/Black Creek)	587 to 798	2,850
(Pio Nono)	798 to 858	2,870
(Cape Fear)	858 to 1,049	2,710
Dunbarton Triassic Basin & Paleozoic Crystalline Rock	> 1,049	see Table 2.5-252, Part B

Table 2.5-252
Shear Wave Velocity Values for Site Amplification Analysis
Part B: Rock Shear-Wave Velocities - Six Alternate Profiles

	Vs (ft/s)	
Depth (ft)	Gradient #1	Gradient #2
1,049 to 1,100	4,400	4,400
1,100 to 1,150	5,650	5,650
1,150 to 1,225	6,650	6,650
1,225 to 1,337.5	7,600	7,600
1,337.5 to 1,402.5	8,000	8,700
1,402.5 to 1,405	8,005	8,703
1,405 to 1,525	8,059	8,739
> 1,525	9,200	9,200

Rock Vs profile corresponding to the location midway between B-1002 and B-1003.

	Vs (ft/s)	
Depth (ft)	Gradient #1	Gradient #2
1,049 to 1,100	4,400	4,400
1,100 to 1,150	5,650	5,650
1,150 to 1,225	6,650	6,650
1,225 to 1,337.5	7,600	7,600
1,337.5 to 1,450	8,000	8,700
1,450 to 1,550	8,090	8,760
1,550 to 1,650	8,180	8,820
1,650 to 1,750	8,270	8,880
1,750 to 1,830	8,360	8,940
1,830 to 1,900	8,414	8,976
> 1,900	9,200	9,200

Rock Vs profile corresponding to the location of B-1003.

	Vs (ft/s)	
Depth (ft)	Gradient #1	Gradient #2
1,049 to 1,100	4,400	4,400
1,100 to 1,150	5,650	5,650
1,150 to 1,225	6,650	6,650
1,225 to 1,337.5	7,600	7,600
1,337.5 to 1,450	8,000	8,700
1,450 to 1,550	8,090	8,760
1,550 to 1,650	8,180	8,820
1,650 to 1,750	8,270	8,880
1,750 to 1,850	8,360	8,940
1,850 to 1,950	8,450	9,000
1,950 to 2,050	8,540	9,060
2,050 to 2,127.5	8,630	9,120
2,127.5 to 2,155	8,679.5	9,153
2,155 to 2,275	8,733.5	9,189
> 2,275	9,200	9,200

Table 2.5-253
Shear Wave Velocity Values for Site Amplification Analysis
Part A: Soil Shear-Wave Velocities (COL Soil Column)

Geologic Formation	Depth (feet) (ft)	V_s (fps) (fps)
Compacted Backfill	0	550
	5	724
	10	832
	20	975
	30	1064
	40	1130
	50	1183
	60	1228
	70	1267
	80	1302
	85	1318
	86.5	1327
	88	1327
Blue Bluff Marl (Lisbon Formation)	88 to 96	1,341
	96 to 102	1,747
	102 to 110	1,988
	110 to 122	2,300
	122 to 156	2,541
Lower Sand Stratum (Still Branch)	156 to 164	1,820
	164 to 220	1,560
(Congaree)	220 to 236	1,757
	236 to 280	2,000
	280 to 328	1,926
	328 to 340	1,727
(Snapp)	340 to 447	2,050
(Black Mingo)	447 to 486	2,350
(Steel Creek)	486 to 596	2,650
(Gaillard/Black Creek)	596 to 807	2,850
(Pio Nono)	807 to 867	2,870
(Cape Fear)	867 to 1,059	2,710

Table 2.5-254
Summary of Modulus Reduction and Damping Ratio Values – EPRI-Base

Shear Strain (%)	0-20 ft (Compacted Backfill)		20-50 ft (Compacted Backfill)		50-86 ft (Compacted Backfill)		86-149 ft (Blue Bluff Marl)		149-215.7 ft (Lower Sand Stratum-Still Branch Formation)		Between 215.7 and 500 ft (Lower Sand Stratum below Still Branch)		Soil between 500 ft and top of rock (about 1,000 ft) (Deep Sands)	
	G/G _{max}	Damping Ratio	G/G _{max}	Damping Ratio	G/G _{max}	Damping Ratio	G/G _{max}	Damping Ratio	G/G _{max}	Damping Ratio	G/G _{max}	Damping Ratio	G/G _{max}	Damping Ratio
0.0001	1	1.4	1	1.2	1	1	1	1.4	1	0.8	1	0.7	1	0.6
0.00032	1	1.5	1	1.2	1	1	1	1.4	1	0.9	1	0.8	1	0.6
0.001	0.98	1.8	0.99	1.4	1	1.2	0.99	1.5	1	1	1	0.8	1	0.6
0.00316	0.914	2.8	0.946	2.1	0.97	1.64	0.96	2	0.98	1.33	0.988	1.12	0.99	0.81
0.01	0.75	5	0.82	3.6	0.87	2.8	0.84	2.9	0.9	2.2	0.93	1.8	0.95	1.2
0.03162	0.509	9.3	0.608	7	0.68	5.49	0.63	6	0.74	4.36	0.791	3.53	0.852	2.5
0.1	0.27	15.3	0.36	12.4	0.43	10.2	0.36	11.4	0.5	8.6	0.57	7.1	0.65	5.3
0.3162	0.116	21.9	0.165	19.1	0.22	16.5	0.16	17	0.27	14.61	0.321	12.78	0.41	10.27
1	0.04	27	0.06	24.9	0.09	22.9	0.06	19.4	0.12	21.2	0.15	19.3	0.2	16.7

Table 2.5-255
Summary of Modulus Reduction and Damping Ratio Values – Site Specific

Stratum	Backfill				Blue Bluff Marl				Lower Sands			
Sub strata	<25ft		≥25ft		Low PI		High PI		Sands		Clay (Congaree/ Snapp)	
Shear Strain (%)	G/Gmax	Damping Ratio	G/Gmax	Damping Ratio	G/Gmax	Damping Ratio	G/Gmax	Damping Ratio	G/Gmax	Damping Ratio	G/Gmax	Damping Ratio
0.00010	1	0.97	1	0.62	1	1.44	1	1	1	0.62	1	0.86
0.00032	1	1.05	1	0.62	1	1.56	1	1.05	1	0.62	1	0.87
0.00100	0.998	1.05	1	0.7	1	1.67	1	1.32	1	0.7	1	0.93
0.00359	0.942	1.44	0.975	0.89	0.96	2.34	0.9965	1.71	0.997	0.89	0.99	1.21
0.01019	0.826	2.26	0.902	1.3	0.867	3.23	0.97	2.3	0.954	1.32	0.928	1.8
0.03170	0.603	4.55	0.748	2.6	0.673	5.75	0.88	3.97	0.858	2.6	0.8	3.62
0.10000	0.355	8.97	0.495	5.64	0.395	10.63	0.679	6.715	0.649	5.59	0.56	7.54
0.30690	0.172	14.94	0.269	10.65	0.187	16.39	0.433	11.115	0.411	10.65	0.327	13
0.65313	0.089	19.38	0.158	14.73	0.1	19.08	0.2785	14.545	0.263	14.68	0.198	17.42
1.00000	0.072	22.12	0.117	17.11	0.068	19.12	0.217	15.77	0.209	17.11	0.154	19.87

Table 2.5-256
Summary of Modulus Reduction and Damping Ratio Values – SRS-Based

Cyclic Shear Strain (%)	Blue Bluff Marl		Shallow Sand (<300 ft)		Deep Sand (>300 ft)	
	G/G _{max}	Damping Ratio	G/G _{max}	Damping Ratio	G/G _{max}	Damping Ratio
0.0001	1	0.8	1	0.6	1	0.5
0.0002	1	0.8	1	0.6	1	0.5
0.0003	1	0.8	1	0.7	1	0.5
0.0005	1	0.8	1	0.7	1	0.5
0.001	0.99	0.9	0.99	0.8	0.995	0.6
0.002	0.98	1.1	0.98	1	0.99	0.7
0.003	0.965	1.2	0.96	1.1	0.985	0.8
0.005	0.94	1.5	0.93	1.4	0.96	0.9
0.01	0.89	2.1	0.87	2.2	0.92	1.4
0.02	0.8	3.3	0.77	3.5	0.85	2.2
0.03	0.72	4.3	0.69	4.7	0.78	3
0.05	0.61	6.1	0.57	6.7	0.69	4.5
0.1	0.43	9.6	0.4	10.4	0.53	7.3
0.2	0.28	13.1	0.25	14.8	0.36	11.2
0.3	0.205		0.18		0.27	13.8
0.5	0.13	19	0.12	21	0.18	
0.7	0.1		0.09		0.14	
1	0.08		0.07	27	0.1	23

Table 2.5-257
Acceptable Gradation Envelope for Compacted Backfill

Sieve No.	Opening Size (mm)	Percent Passing	
		Minimum	Maximum
4	4.75	97	100
10	2.00	95	100
20	0.85	85	98
40	0.425	50	95
60	0.25	17	80
100	0.15	7	50
140	0.106	4	28
200	0.075	3	25

Table 2.5-258
**Criteria for Evaluation of Borrow Material from Outside of the Three Designated Category
 1 and 2 Borrow Areas**

Parameter	Acceptance Criteria
Location	Exclusion Area Boundary (Figure 1.1-202)
Geological Origin	Barnwell Group
Soil Classification	SP, SP-SM or SM
Maximum Dry Density (Modified Proctor)	Engineering Evaluation
Fines Content, Percent passing on a #200 Sieve	3% Minimum 25% Maximum
Gradation	Table 2.5-257 and associated text in Subsection 2.5.4.5.3

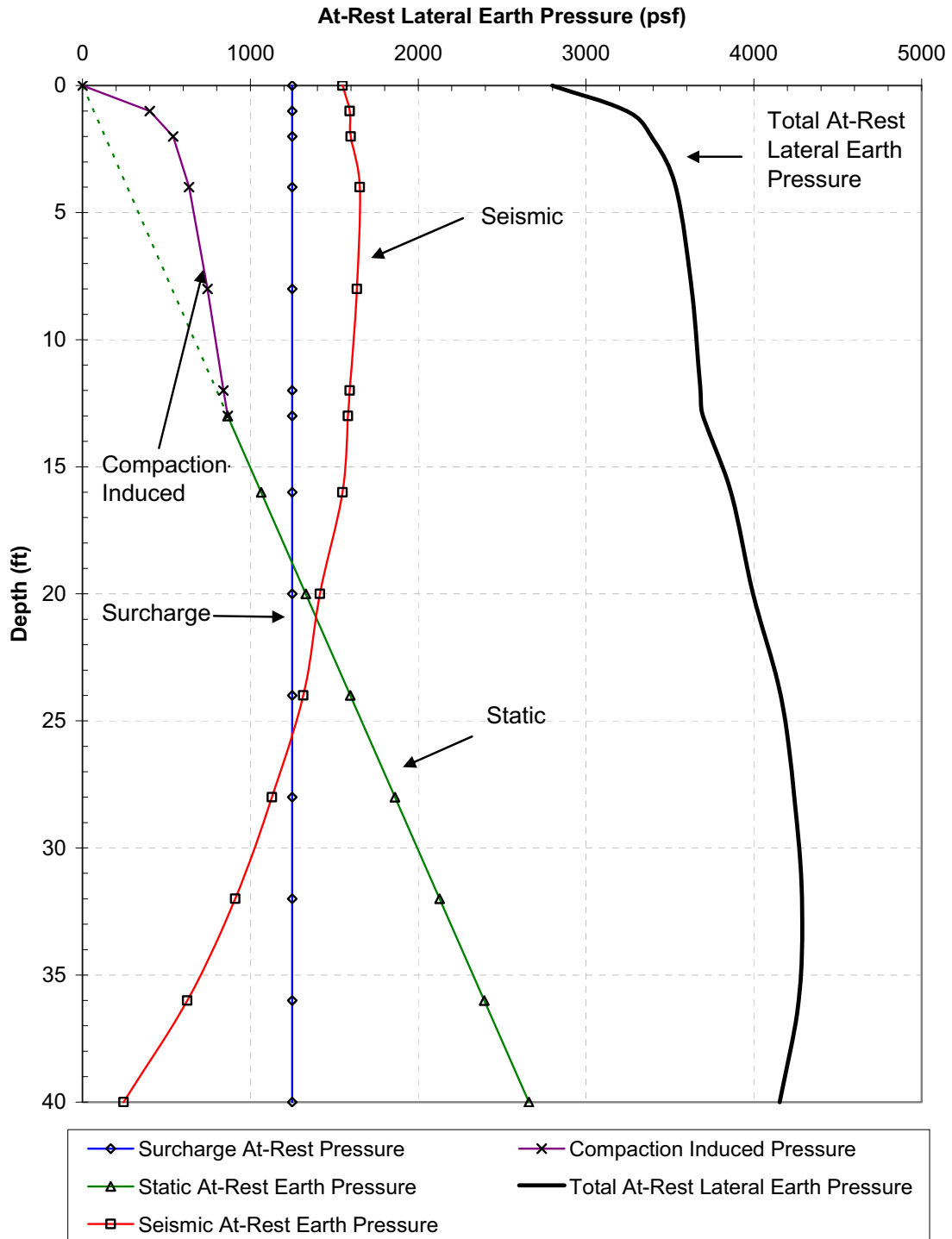


Figure 2.5-201
Vogtle Site-Specific At-Rest Lateral Earth Pressure Diagrams
for Rigid Below Grade Nuclear Island (NI) Walls

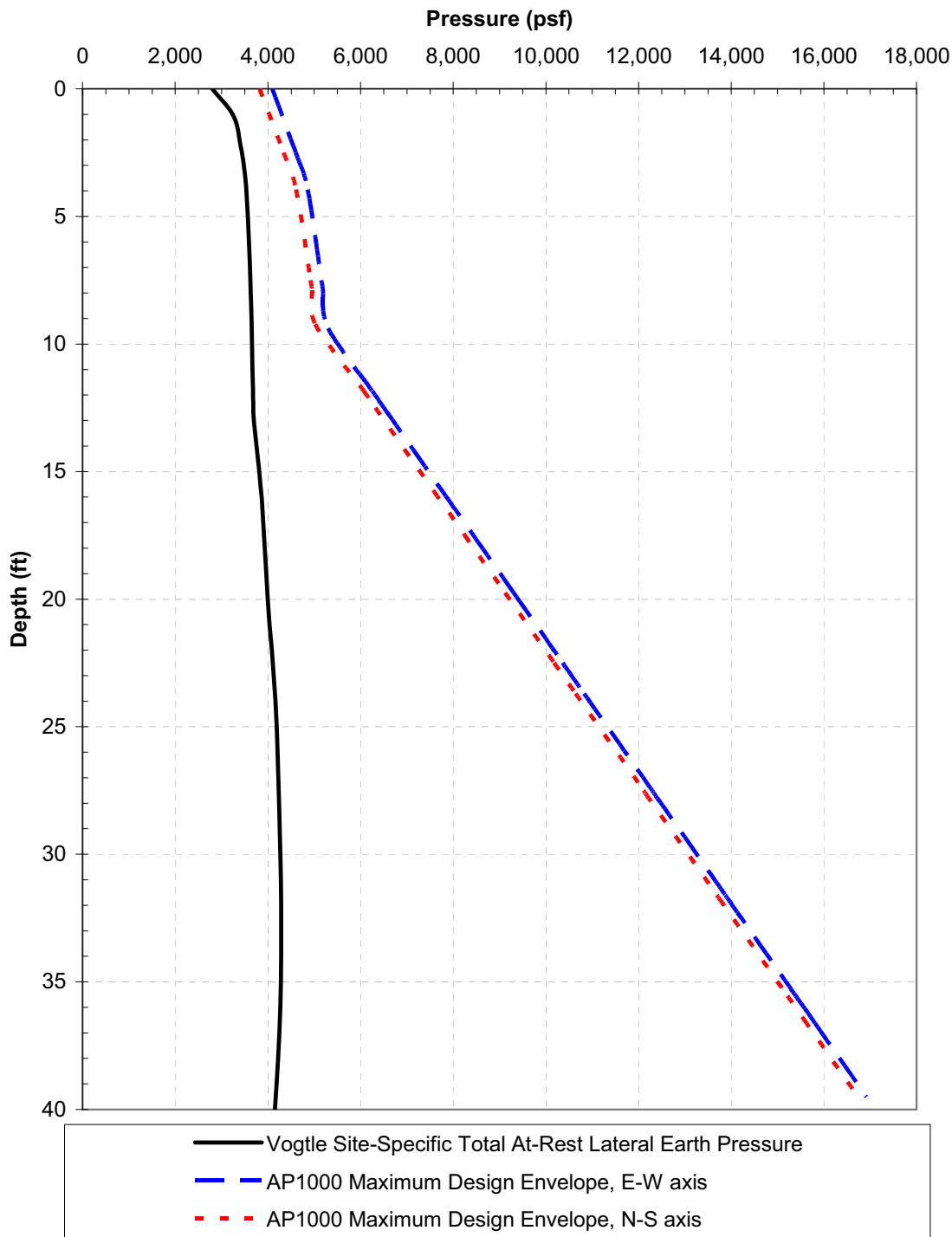


Figure 2.5-202
Comparison of Vogtle Site-Specific Total At-Rest Lateral Earth Pressure Diagrams and AP1000 Maximum Design Envelopes

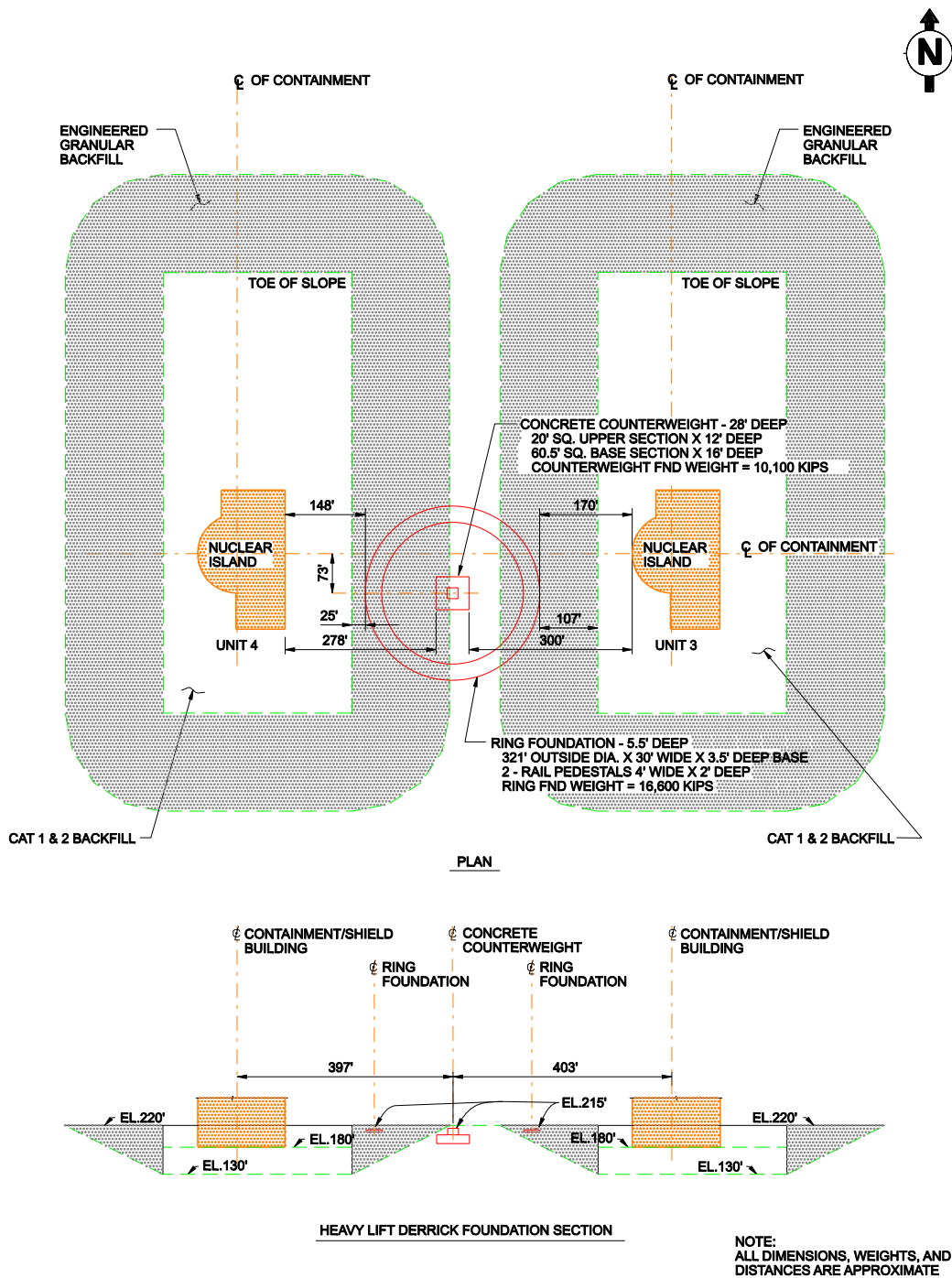


Figure 2.5-203
Heavy Lift Derrick Foundation Location

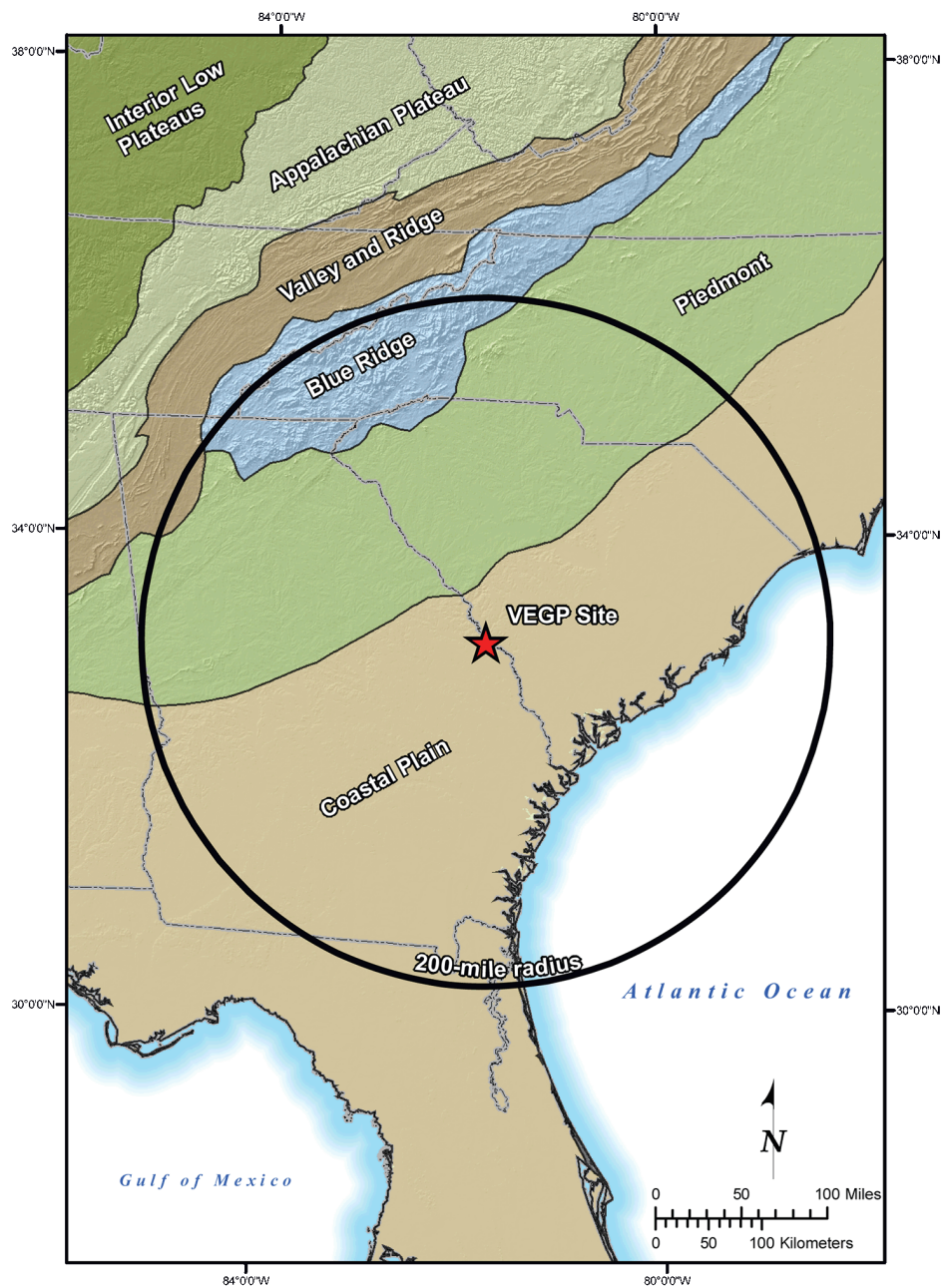


Figure 2.5-204
Physiographic Provinces of the Southeastern United States

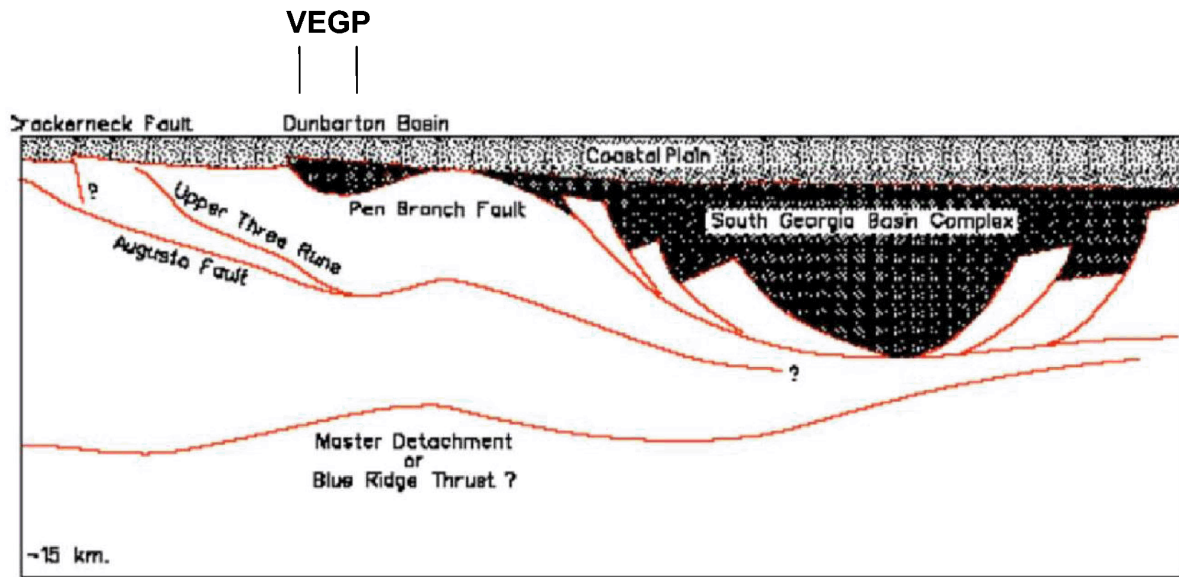


Figure 2.5-205
Conceptual Section Linking Dunbarton Basin with South Georgia Basin Complex

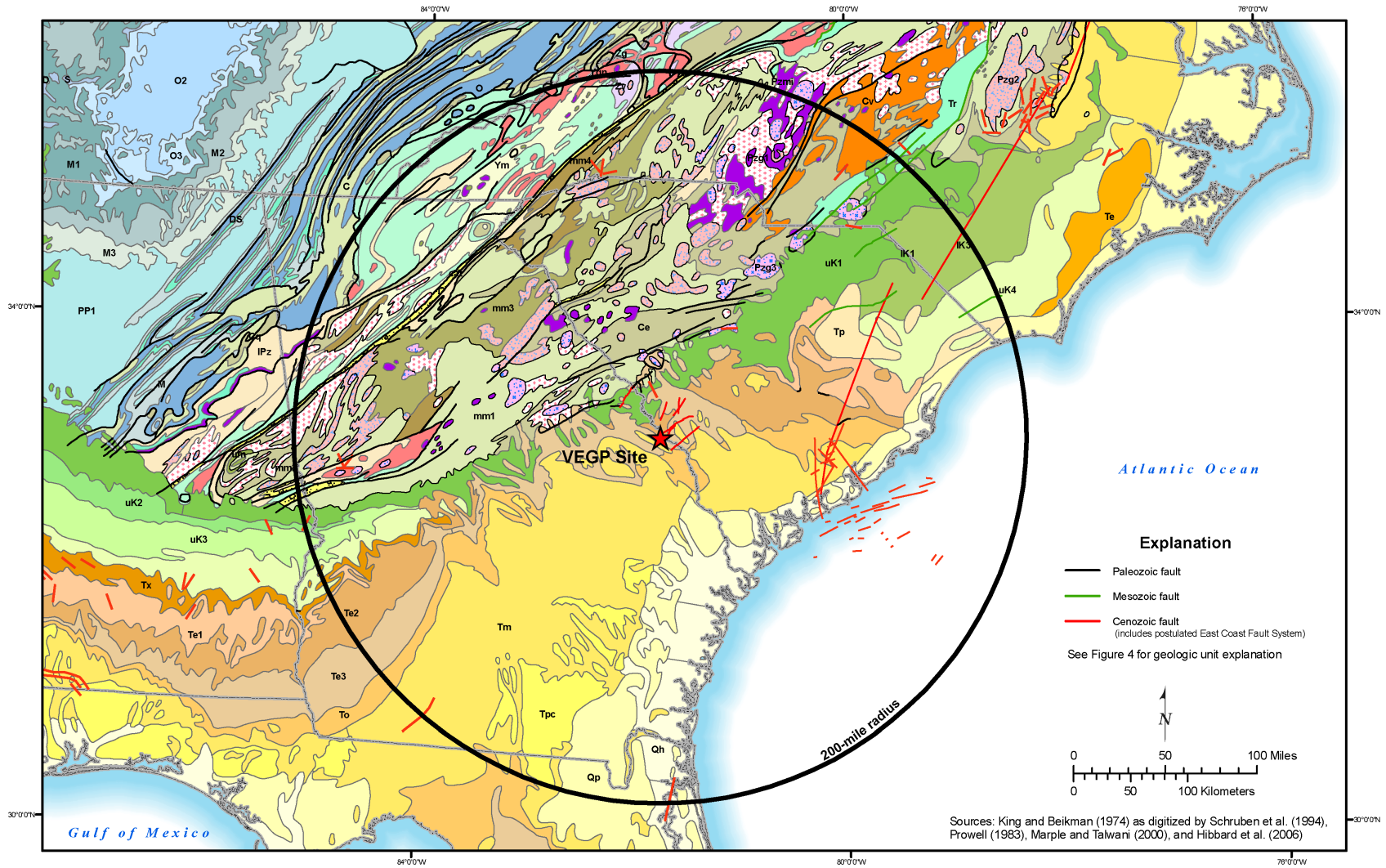


Figure 2.5-206
Regional Geologic Map (200-Mile Radius)

Explanation

Vogtle 200-mile geology
King and Beikman (1974) unit descriptions

Qh	Holocene	Pzmi	Paleozoic mafic intrusives
Qp	Pleistocene	Pzg3	Upper Paleozoic granitic rocks
Tp	Pliocene	Pzg2	Middle Paleozoic granitic rocks
Tpc	Pliocene continental	Pzg1	Lower Paleozoic granitic rocks
Tm	Miocene	Ygn	Orthogneiss
To	Oligocene	Ym	Paragneiss and schist
Te	Eocene	Z	sedimentary rocks
Te1	Eocene Wilcox Group	Zg	granitic rocks
Te2	Eocene Claiborne Group	Zv	volcanic rocks
Te3	Eocene Jackson Group	cat	Cataclastic rocks
Tx	Paleocene	mm1	felsic paragneiss and schist
uK1	Woodbine and Tuscaloosa groups	mm2	mafic paragneiss
uK2	Austin and Eagle Ford Groups	mm3	migmatite
uK3	Taylor Group	mm4	felsic orthogneiss
uK4	Navarro Group	um	Ultramafic rocks
IK1	Trinity group		
IK3	Washita Group		
Tr	Triassic		
PP1	Atokan and Morrowan Series		
M	Mississippian		
M1	Osagean and Kinderhookian Series		
M2	Meramecian Series		
M3	Chesterian Series		
D	Devonian		
DS	Devonian and Silurian		
S	Silurian		
O	Ordovician		
O2	Middle Ordovician (Mohawkian)		
O3	Upper Ordovician (Cincinnatian)		
C	Cambrian		
Ce	Cambrian eugeosynclinal		
Cq	basal Lower Cambrian clastic rocks		
Cv	Cambrian volcanics		
IPz	Lower Paleozoic		

Figure 2.5-207
Regional Geologic Map (200-Mile Radius) Explanation

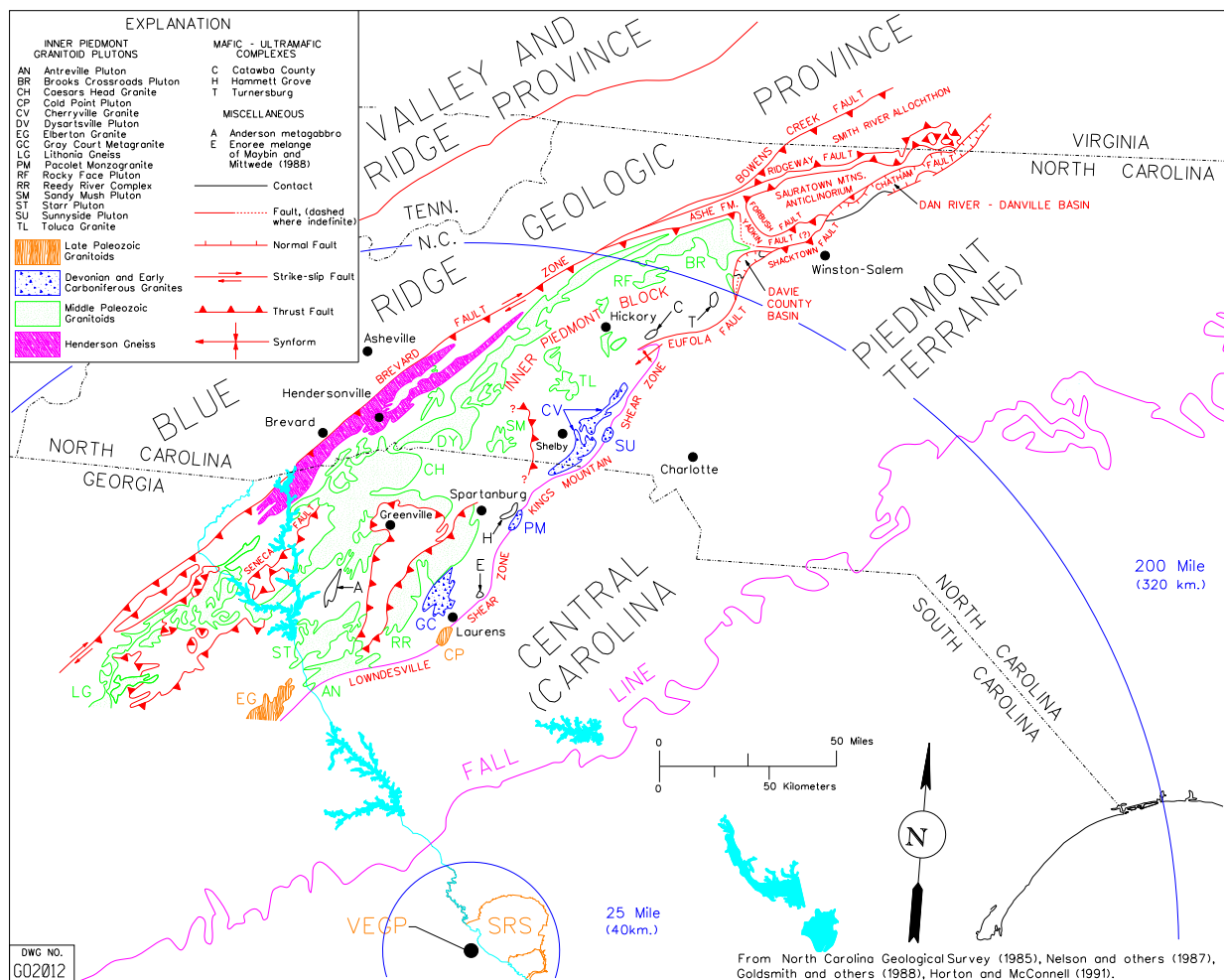


Figure 2.5-208
Simplified Geologic Map of Western Piedmont Terrane
in Relation to Blue Ridge and Carolina Terranes

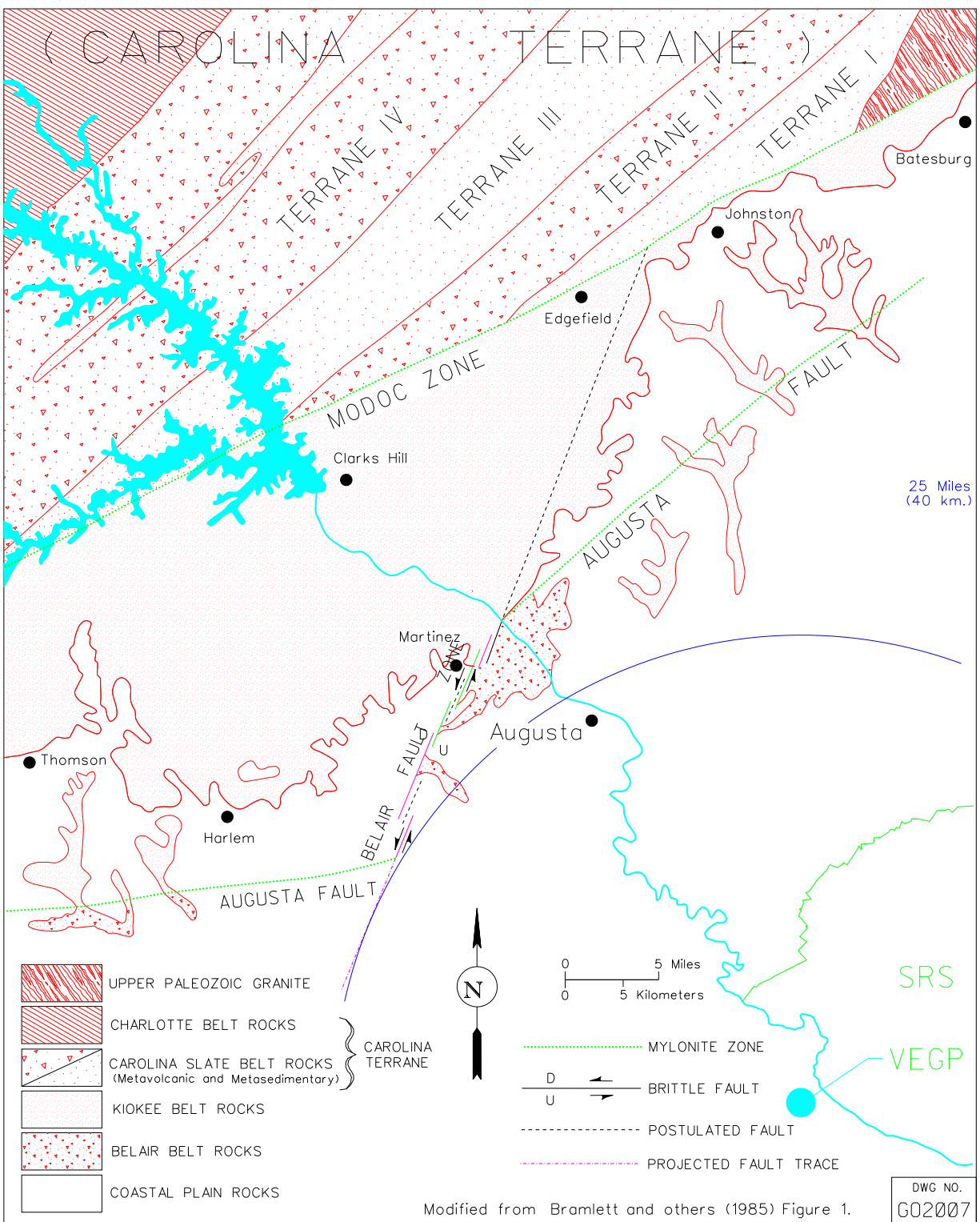


Figure 2.5-209
Map of Carolina Terrane and Modoc Zone

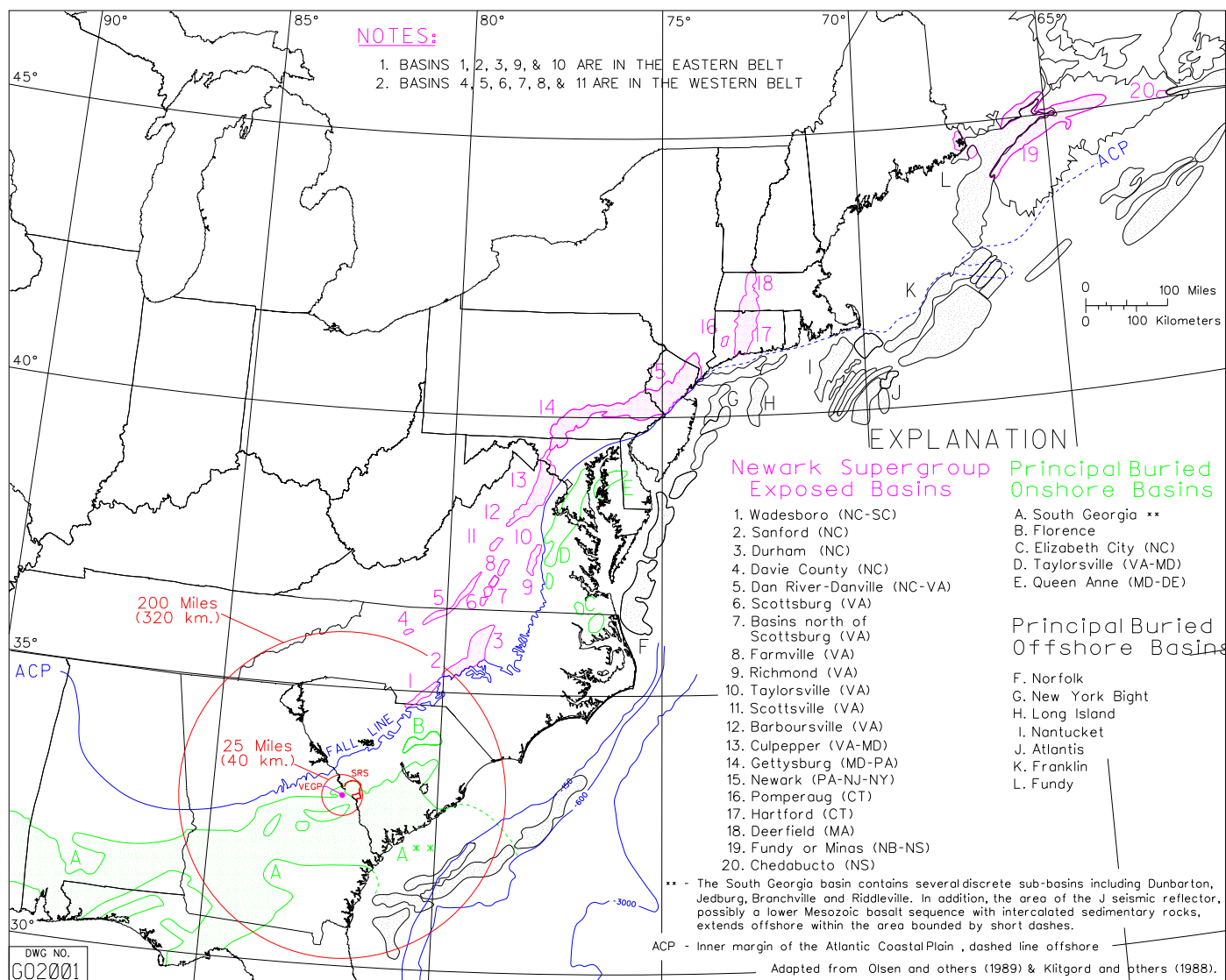


Figure 2.5-210
Triassic Basins in the Eastern United States

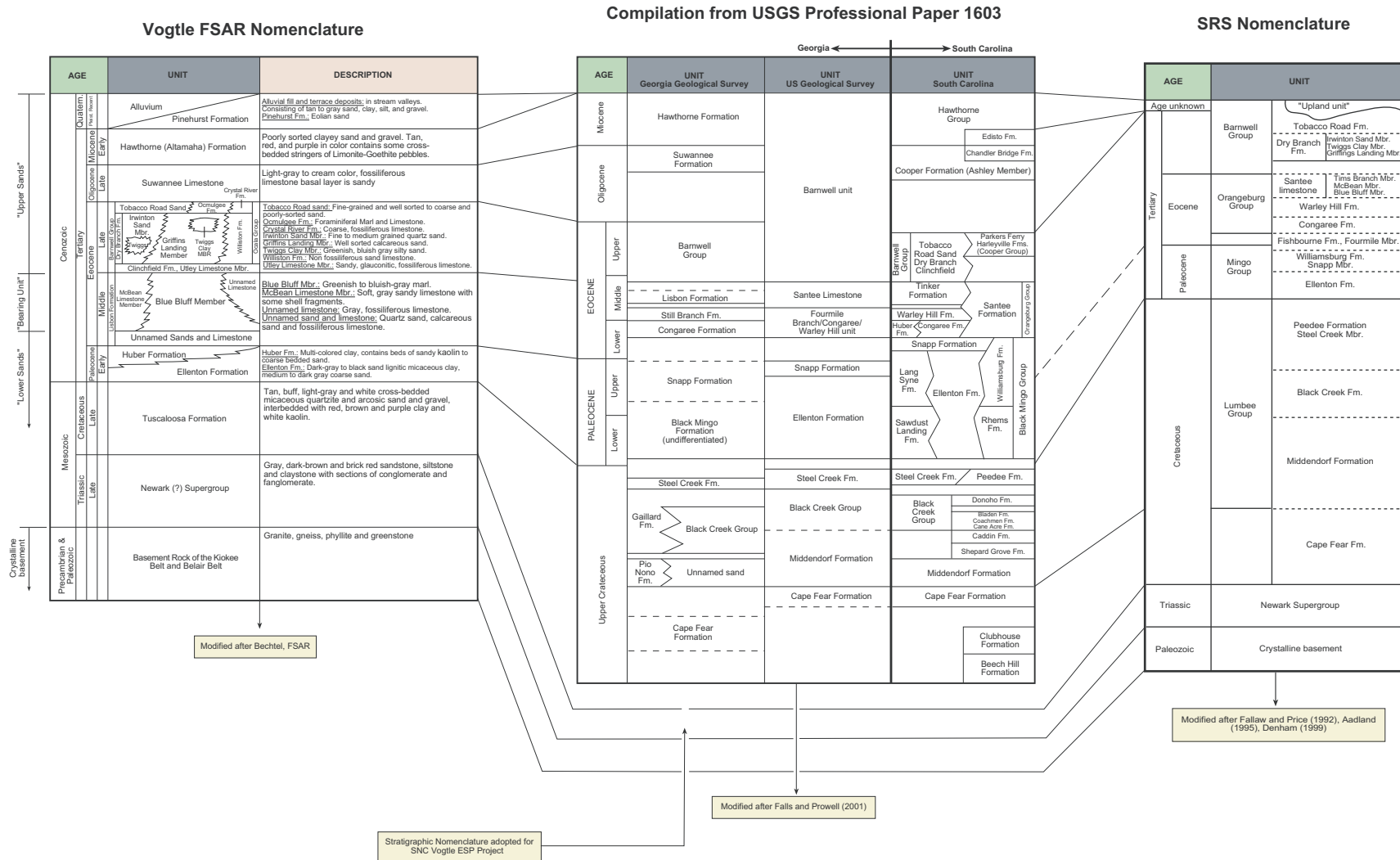


Figure 2.5-211
Stratigraphic Correlation Chart

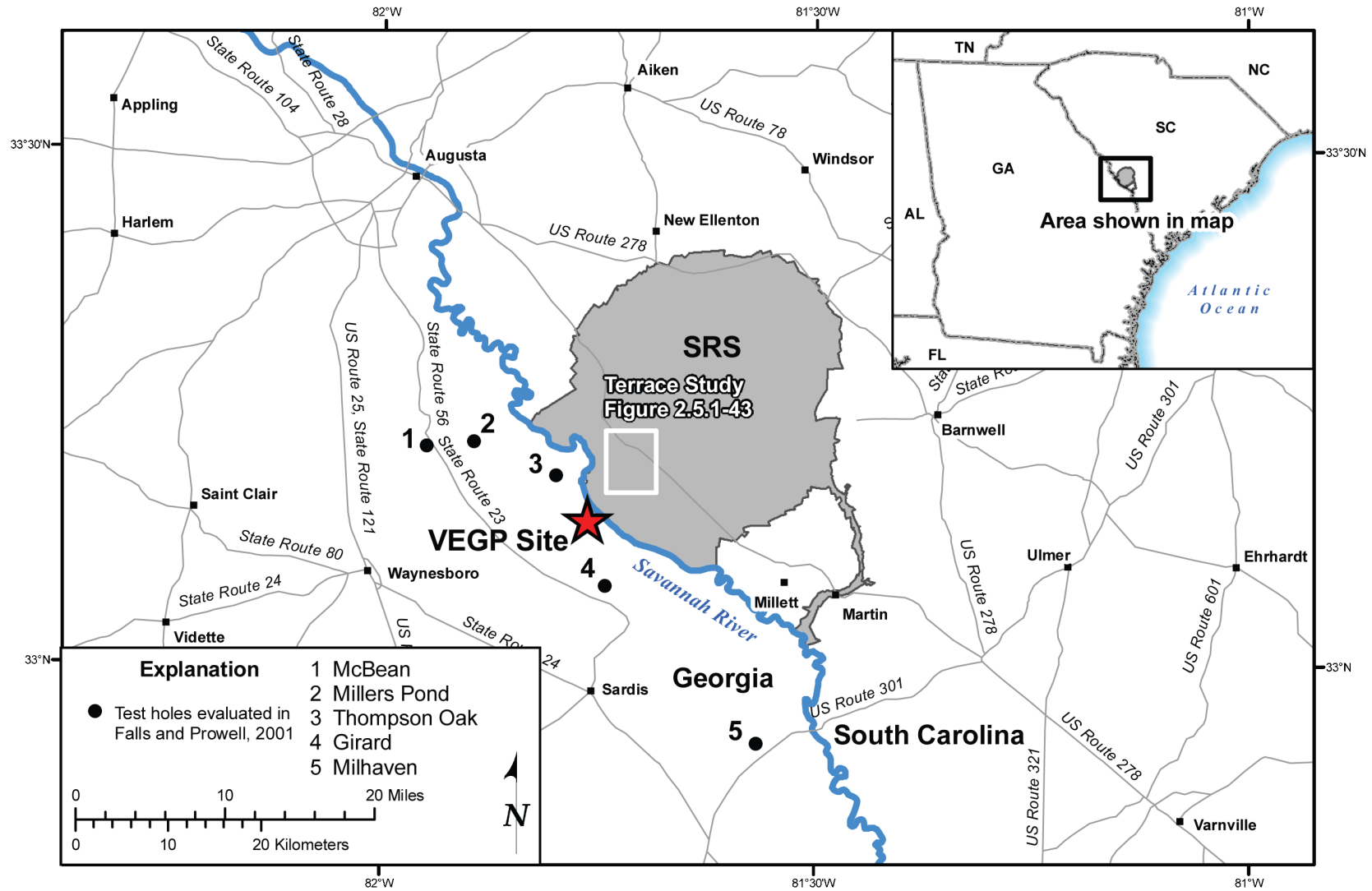
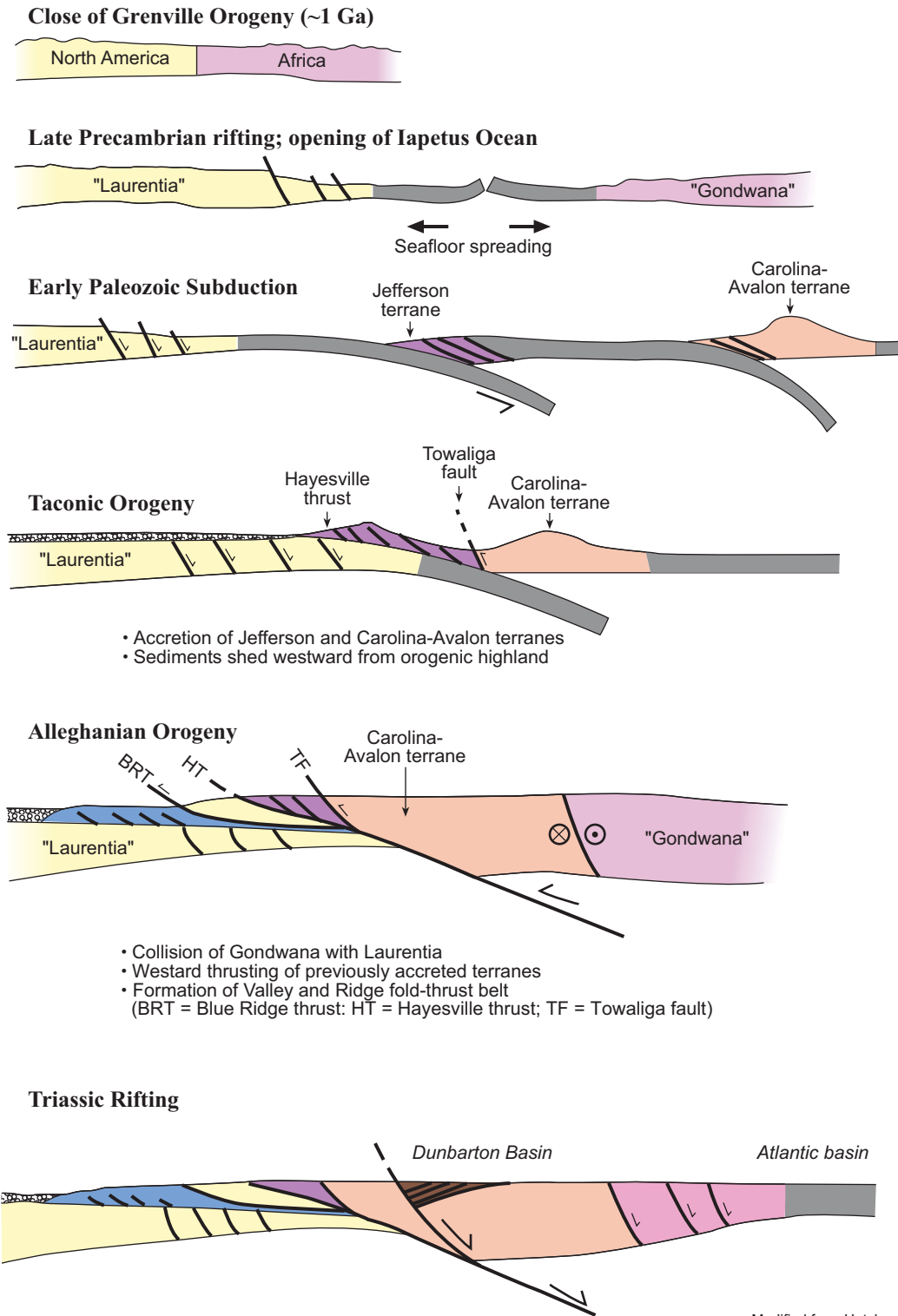


Figure 2.5-212
Location Map Showing SRS Boundary and VEGP Site



Modified from Hatcher, 1987

Figure 2.5-213
Evolution of the Appalachian Orogen

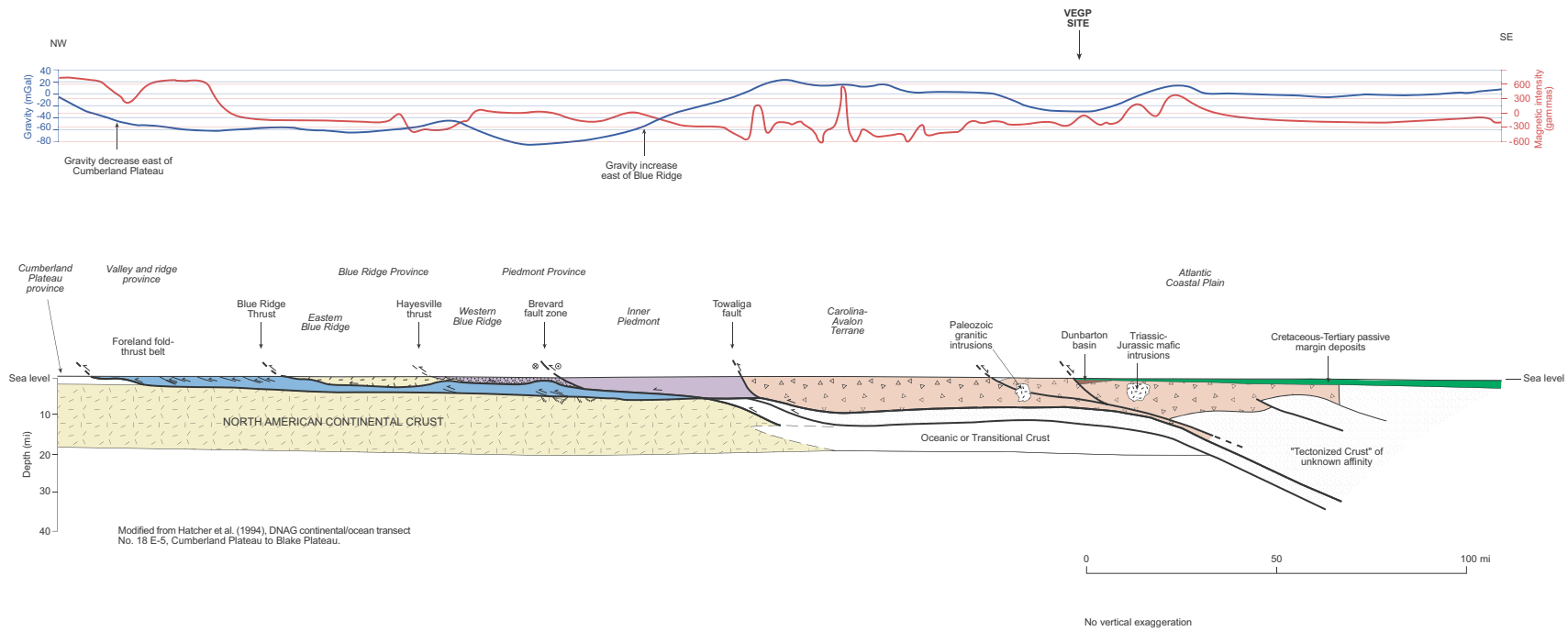


Figure 2.5-214
Regional Cross Section – DNAG E-5

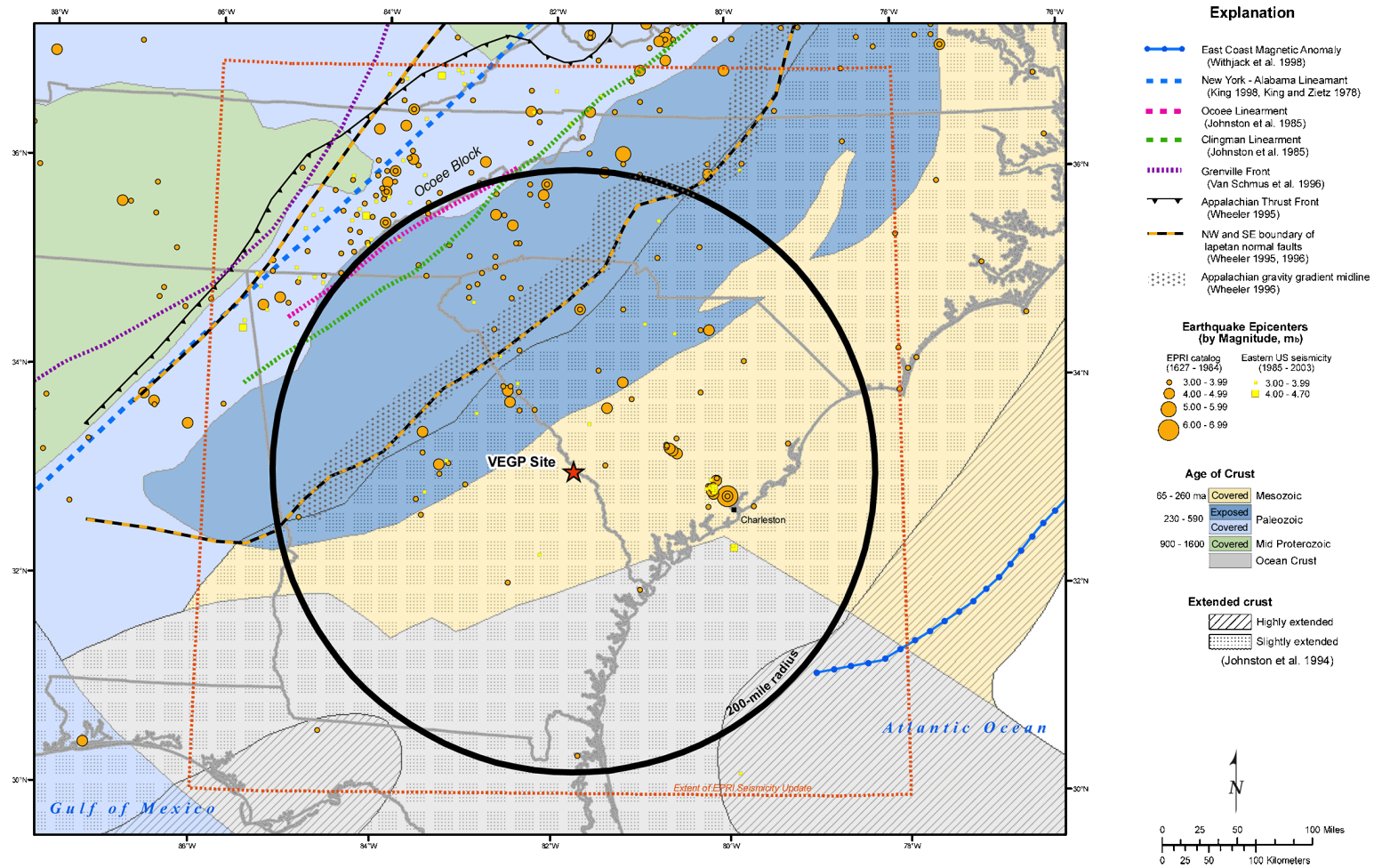


Figure 2.5-215
Tectonic Features of the Southeastern United States

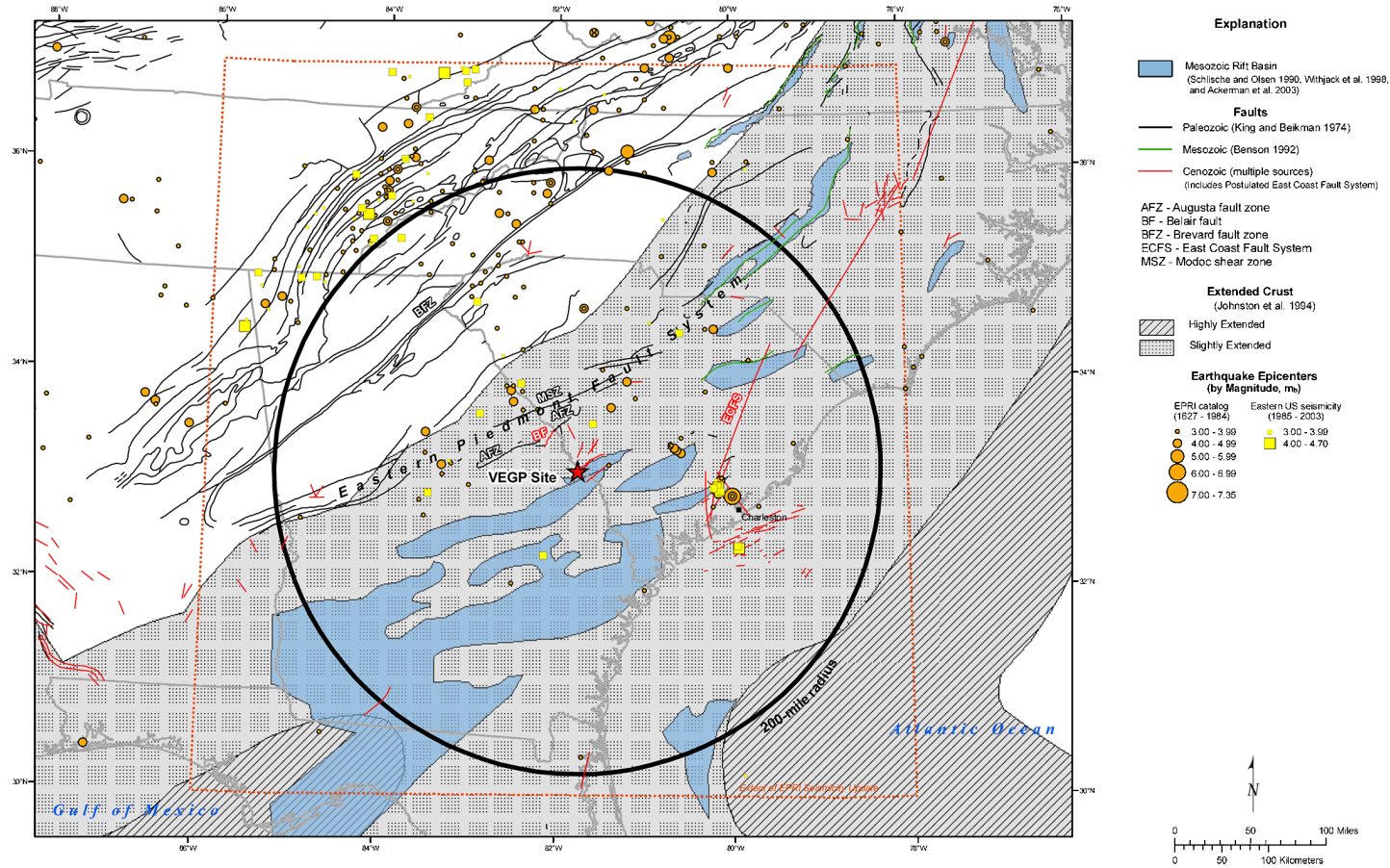


Figure 2.5-216
Regional Tectonic Features Map (200-Mile Radius)

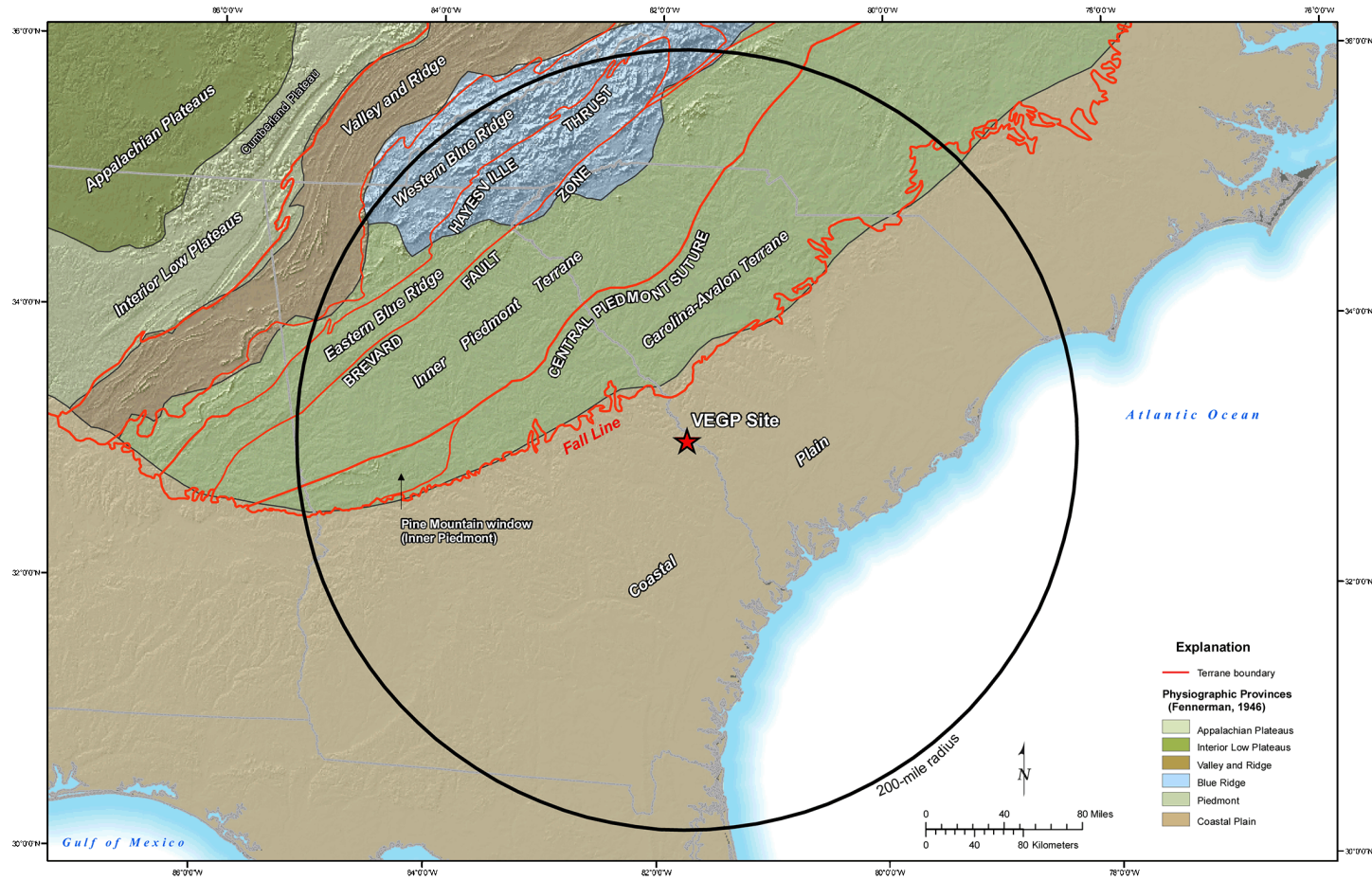
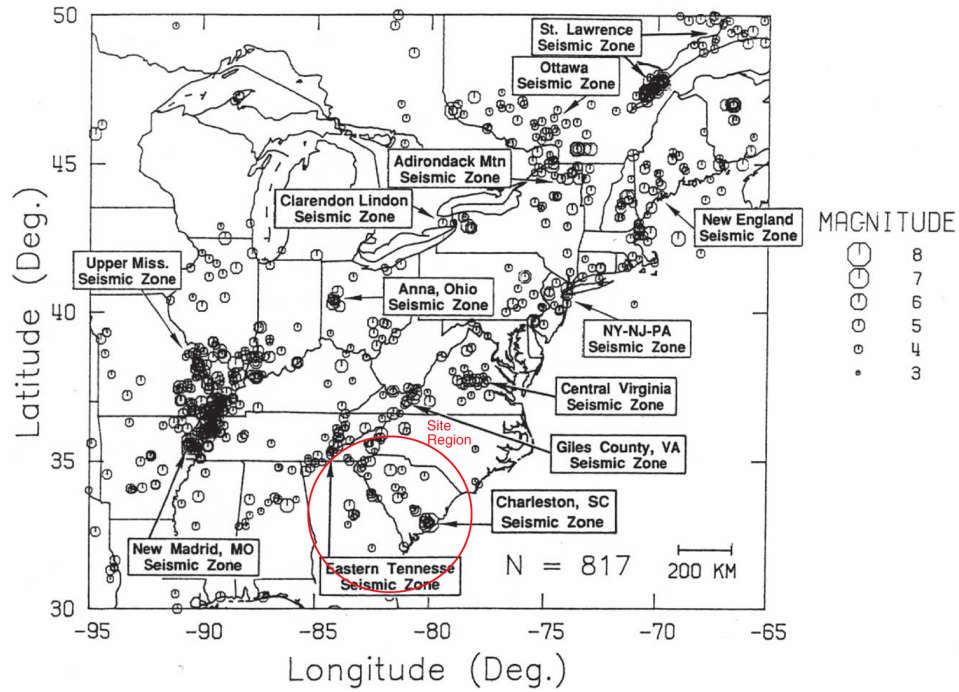


Figure 2.5-217
Terrains and Physiographic Provinces of Site Region



Source: Bollinger et al. 1992

Figure 2.5-218
Seismic Source Zones and Seismicity in Central and Eastern North America

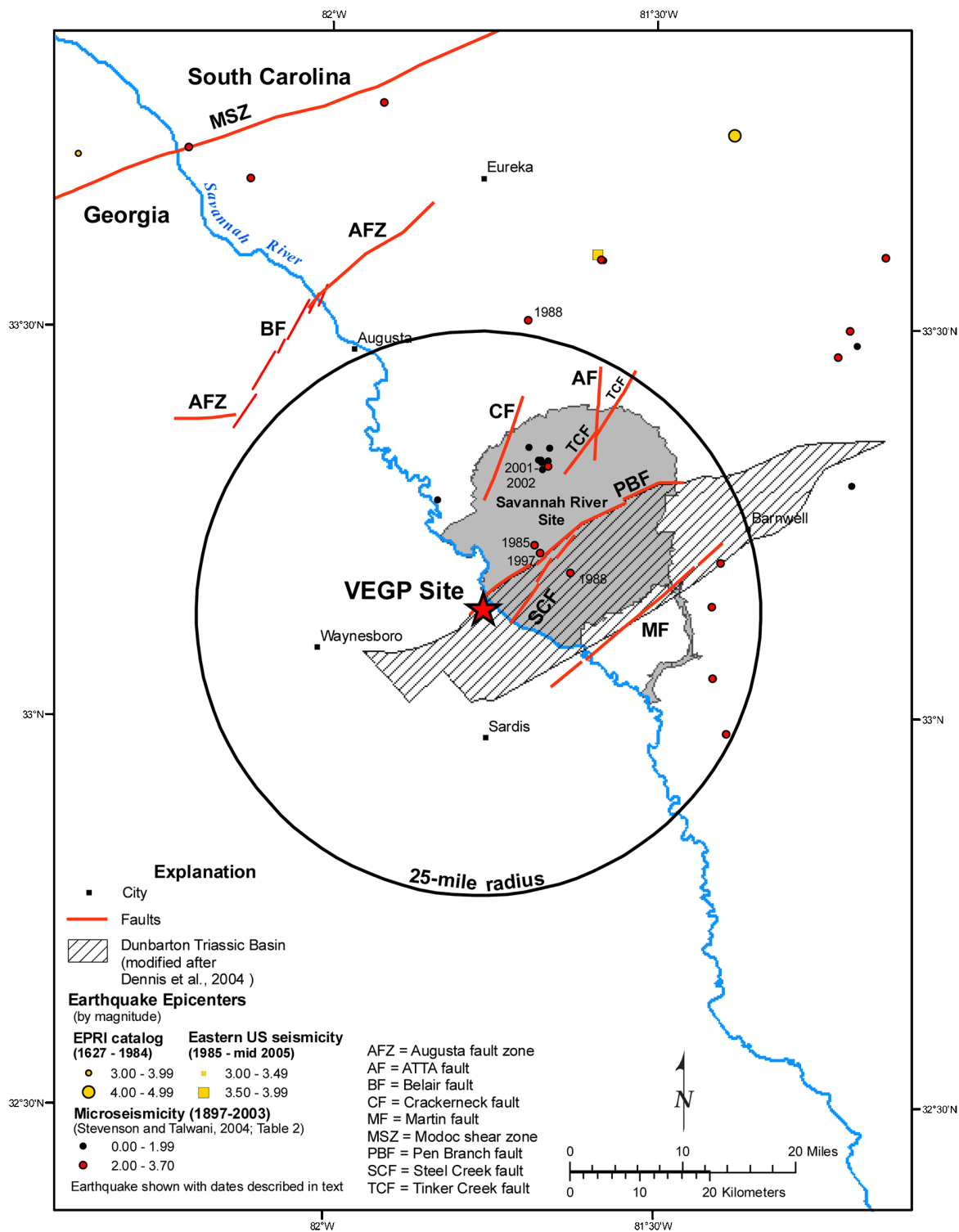
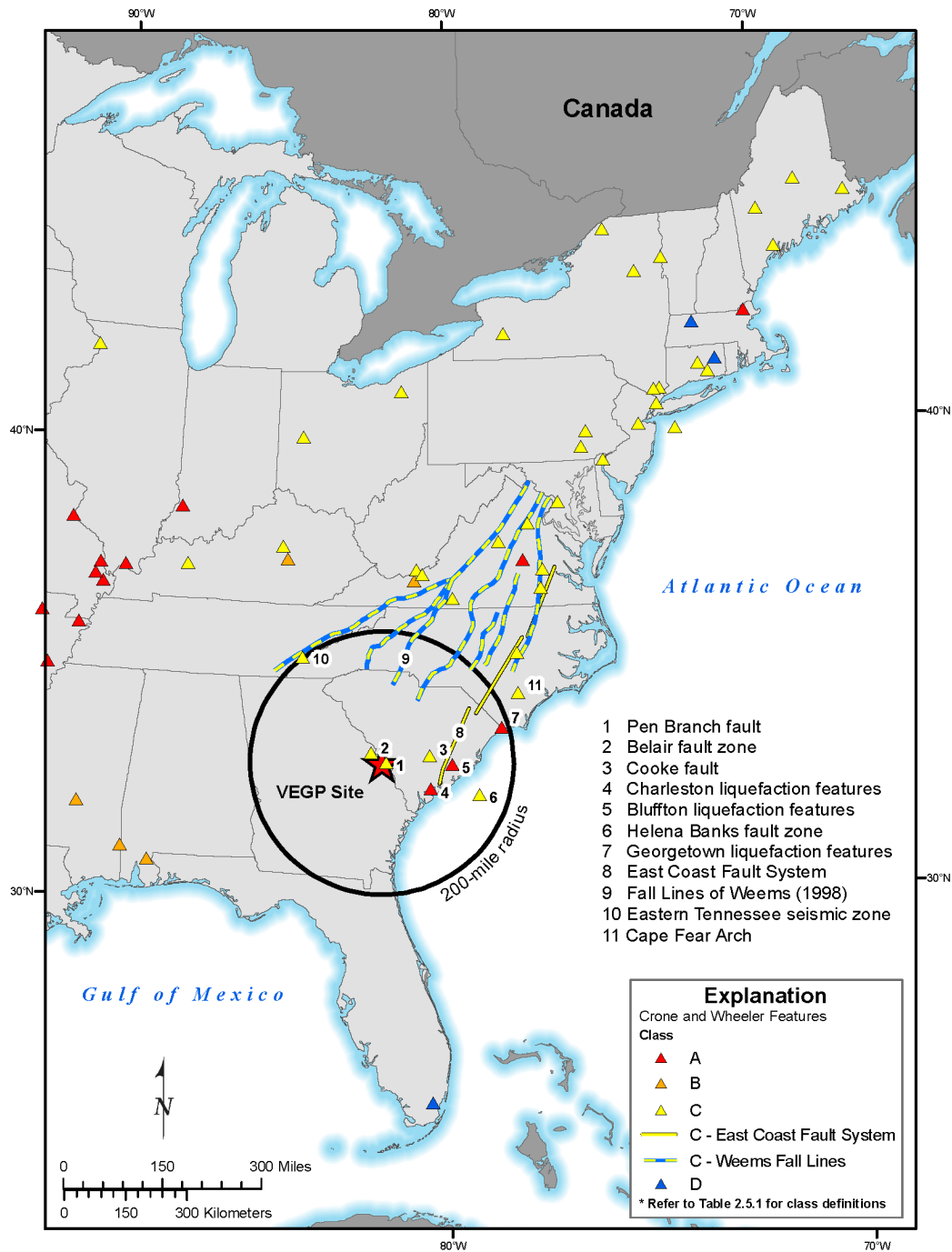


Figure 2.5-219
Site Vicinity Tectonic Features and Seismicity



Source: Crone and Wheeler (2000), Wheeler (2005)

Figure 2.5-220
Potential Quaternary Features Map

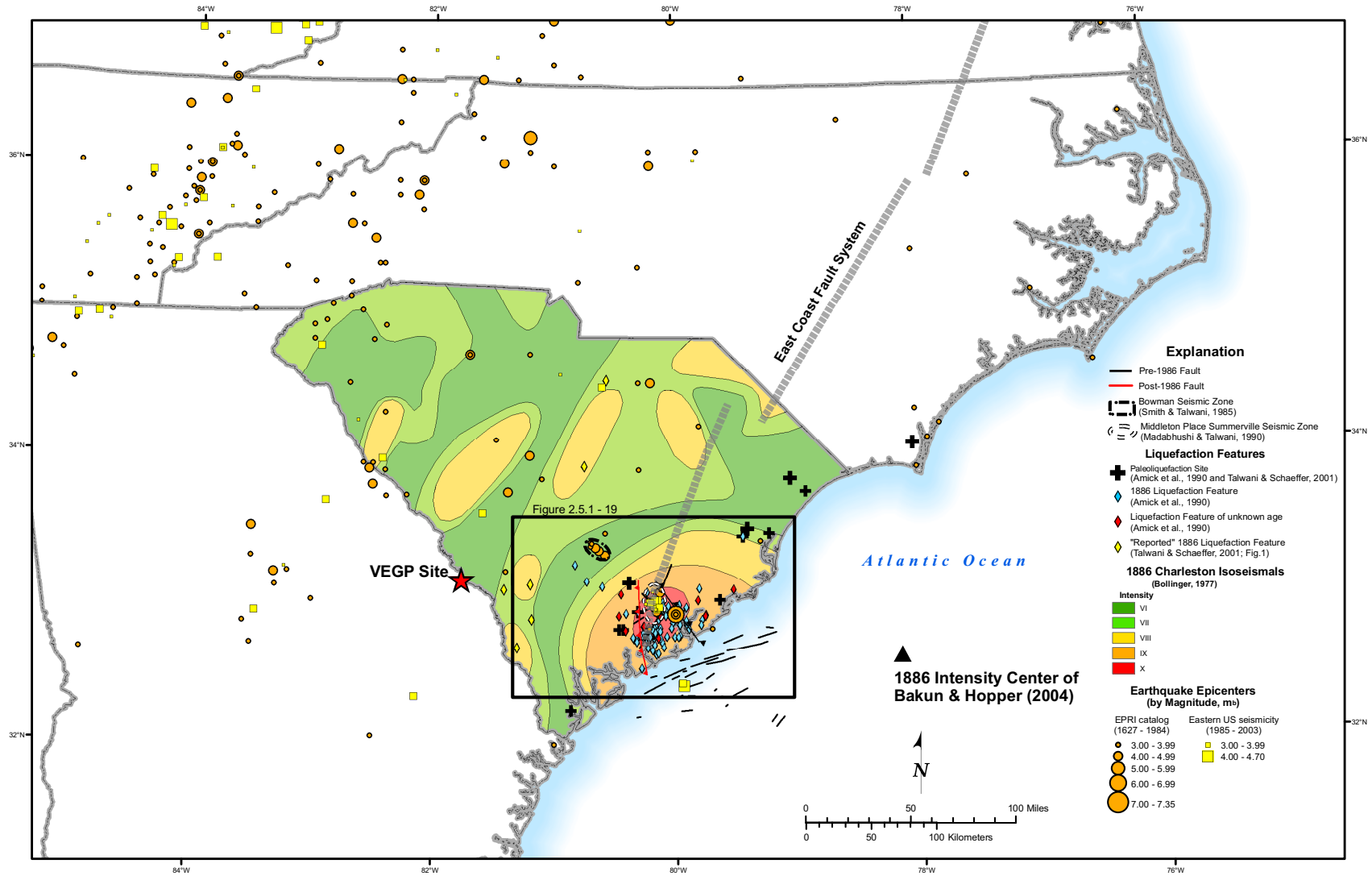


Figure 2.5-221
Regional Charleston Tectonic Features

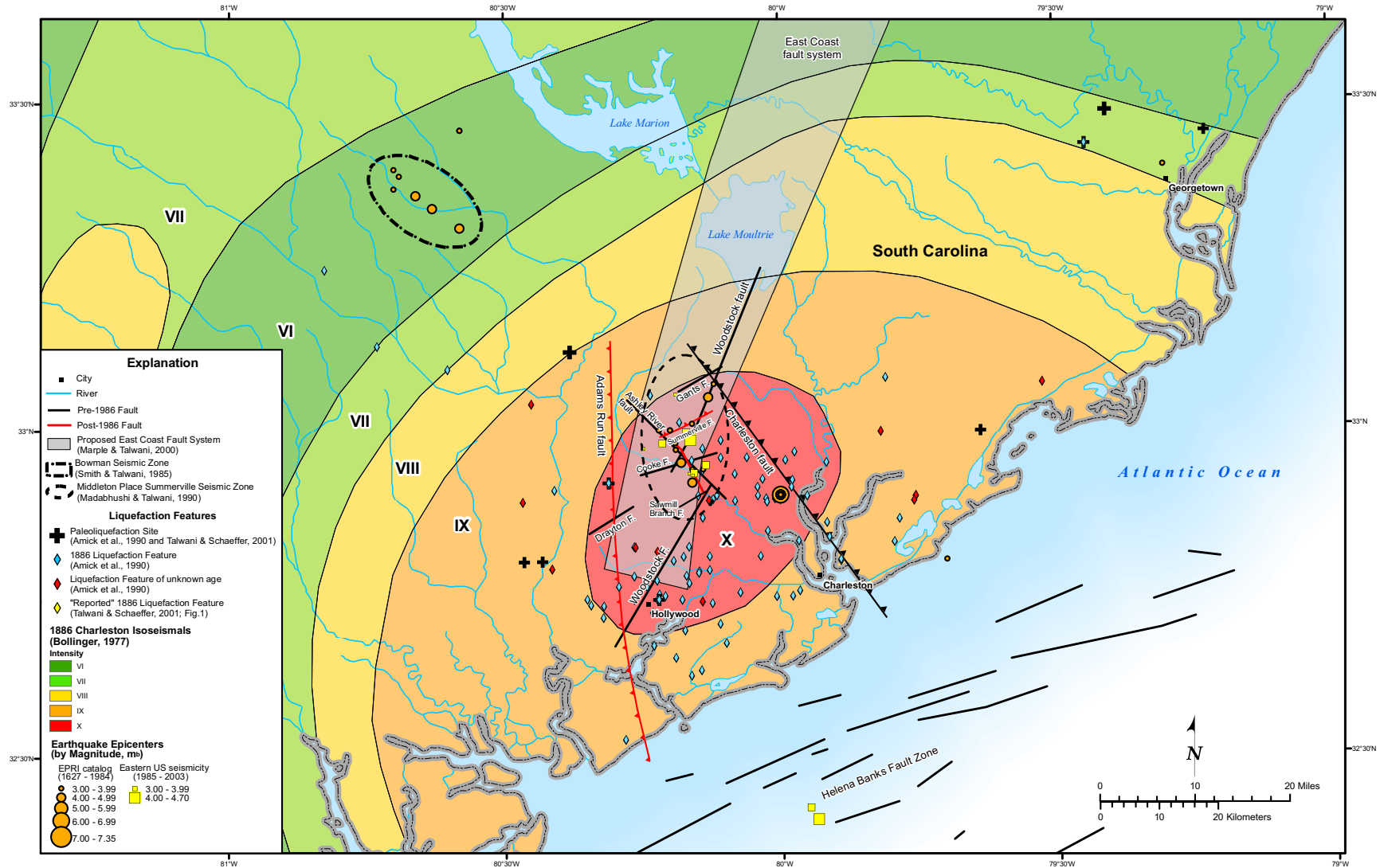


Figure 2.5-222
Local Charleston Tectonic Features

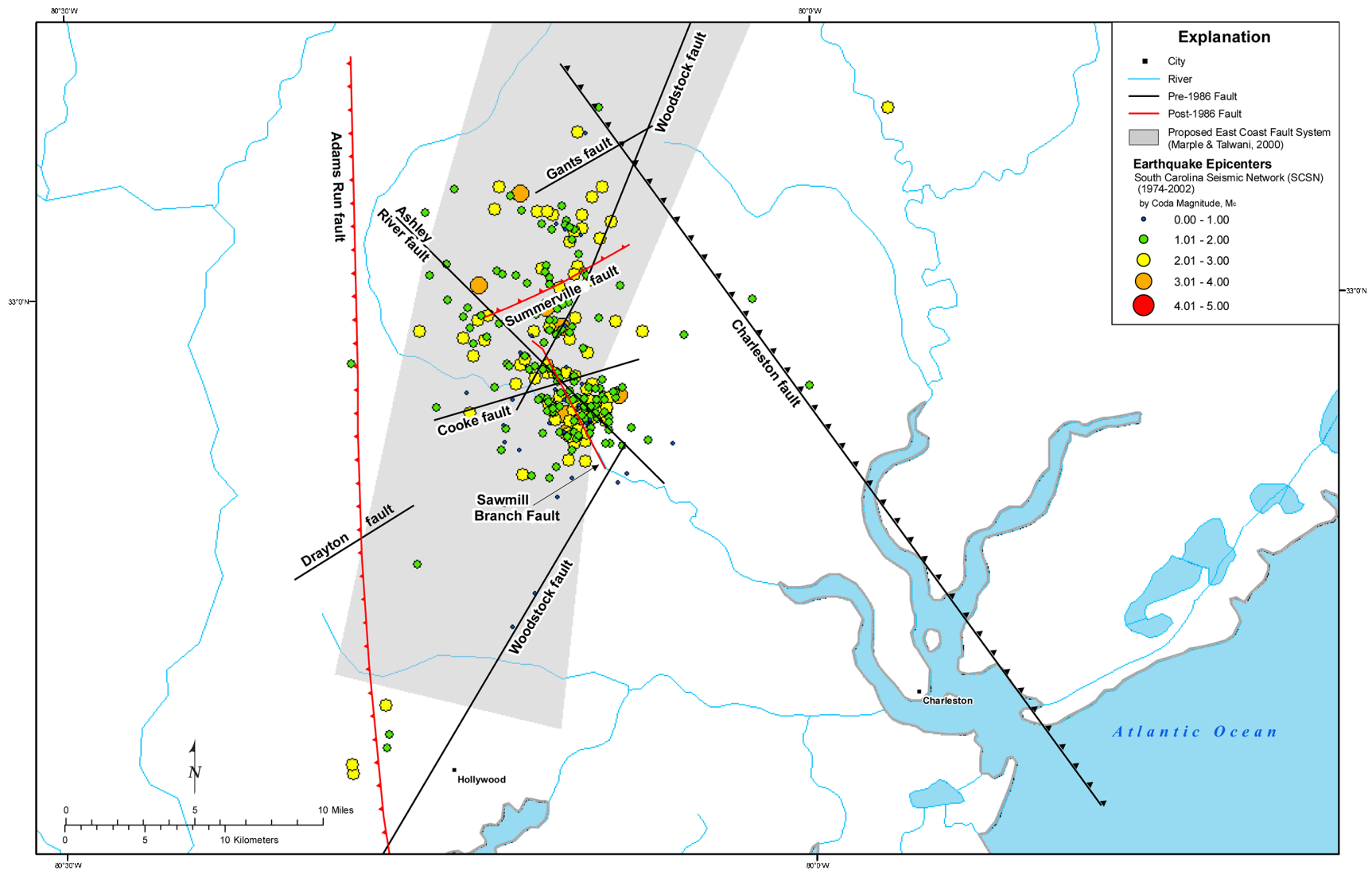
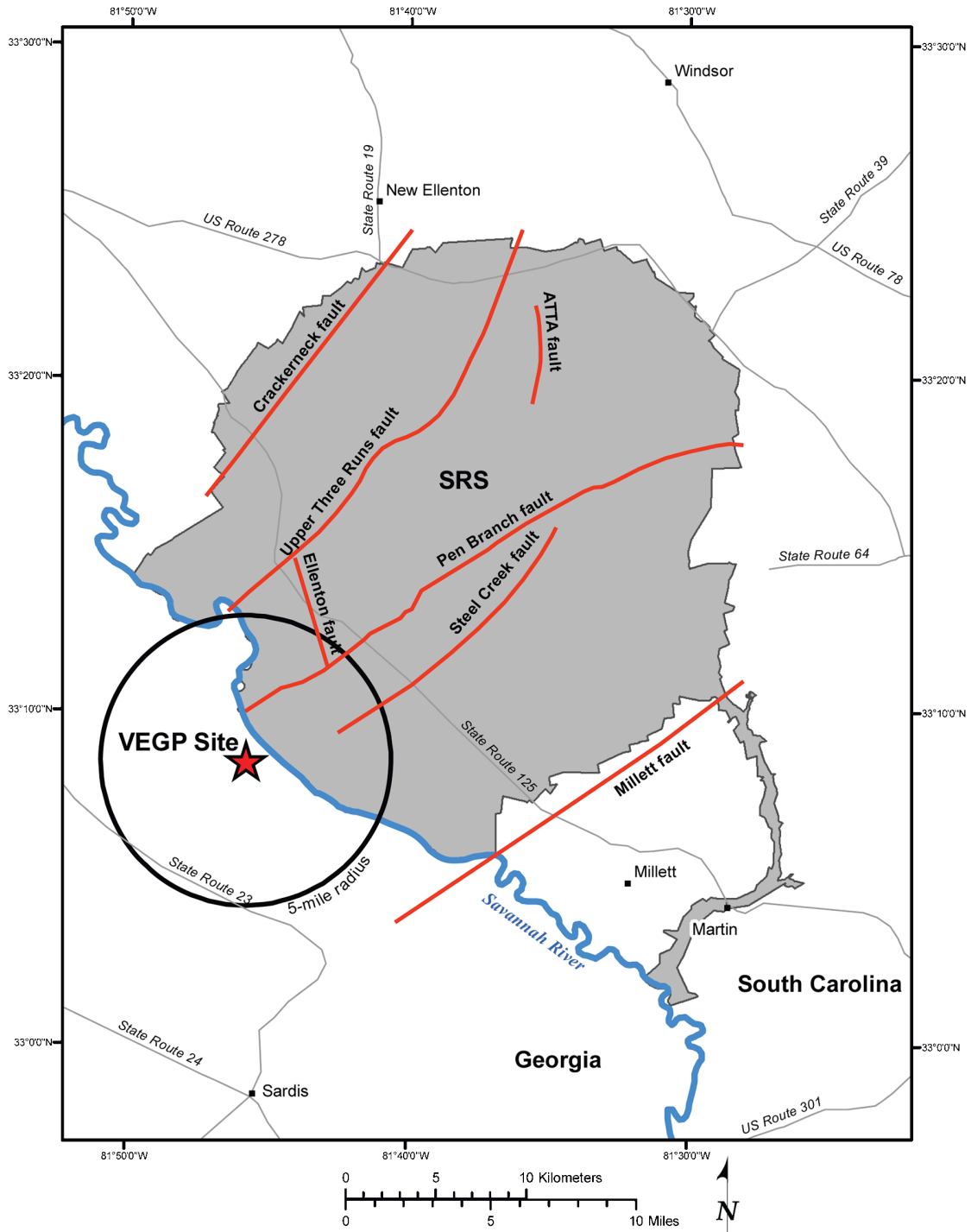
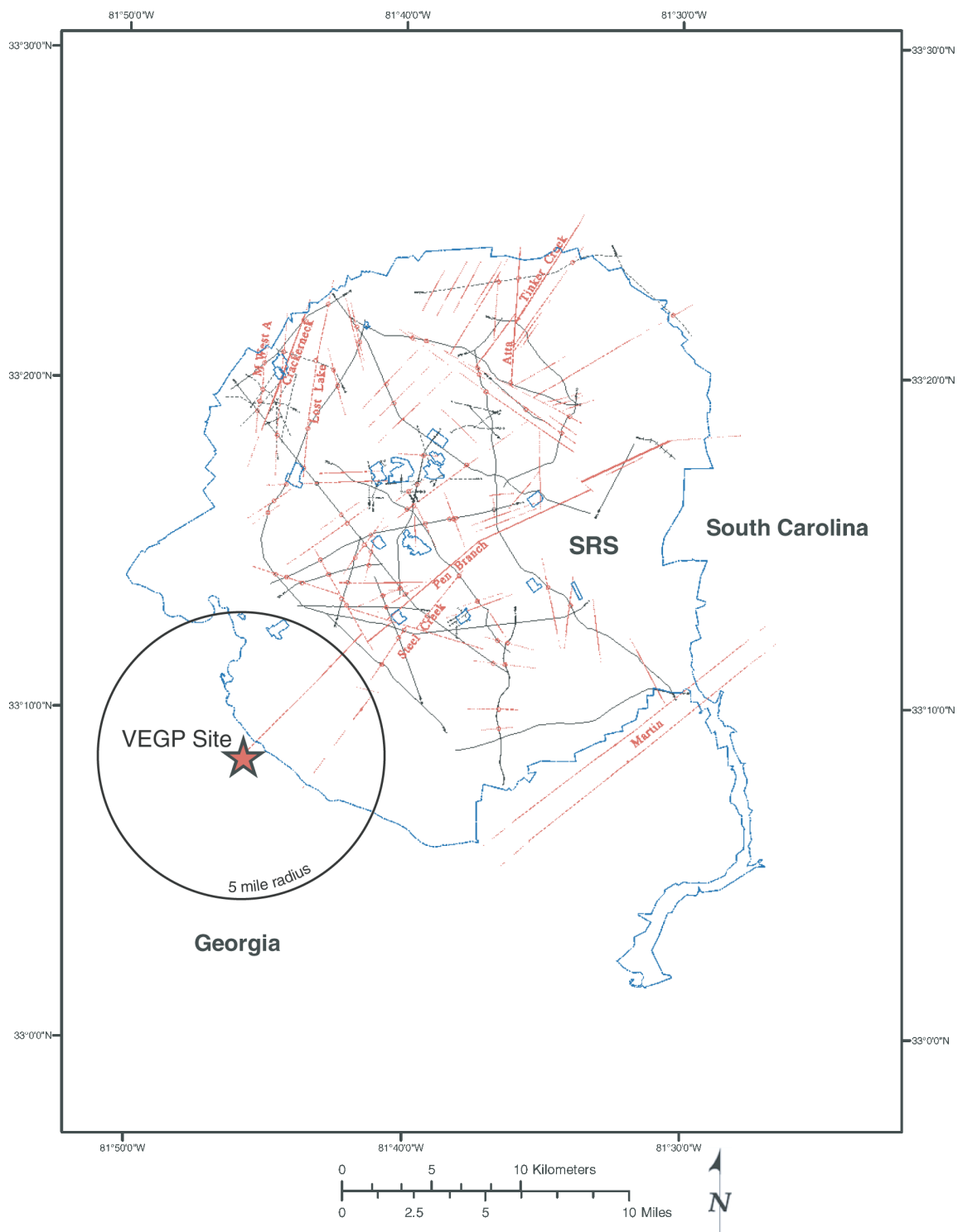


Figure 2.5-223
Local Charleston Seismicity



Source: Stieve and Stephenson 1995

Figure 2.5-224
SRS Faults from Stieve and Stephenson (1995)



Source: Cumbest et al. 1998

Figure 2.5-225
SRS Faults from Cumbest et al. (1998)

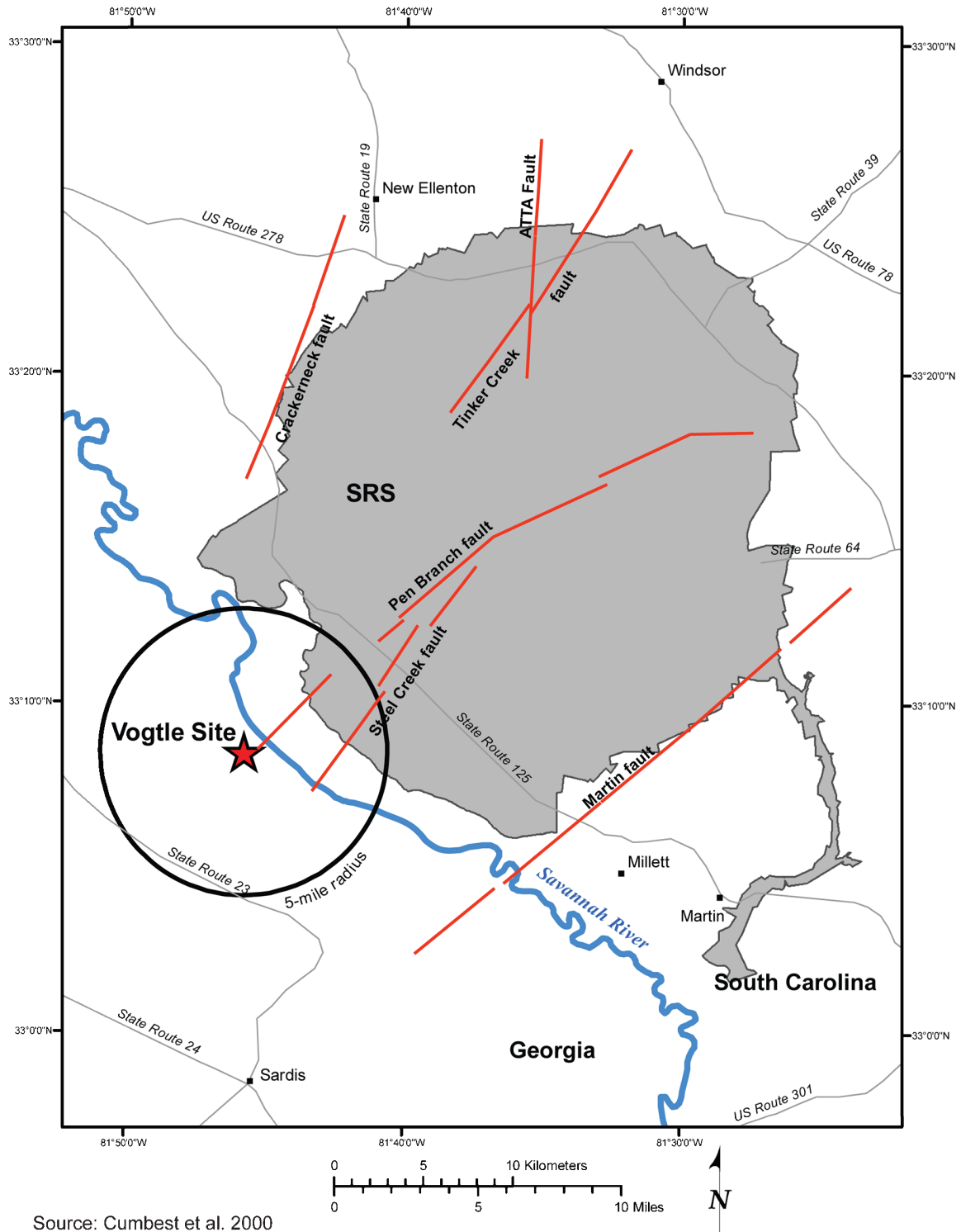


Figure 2.5-226
SRS Faults—First-Order Faults of Cumbe et al. (2000)



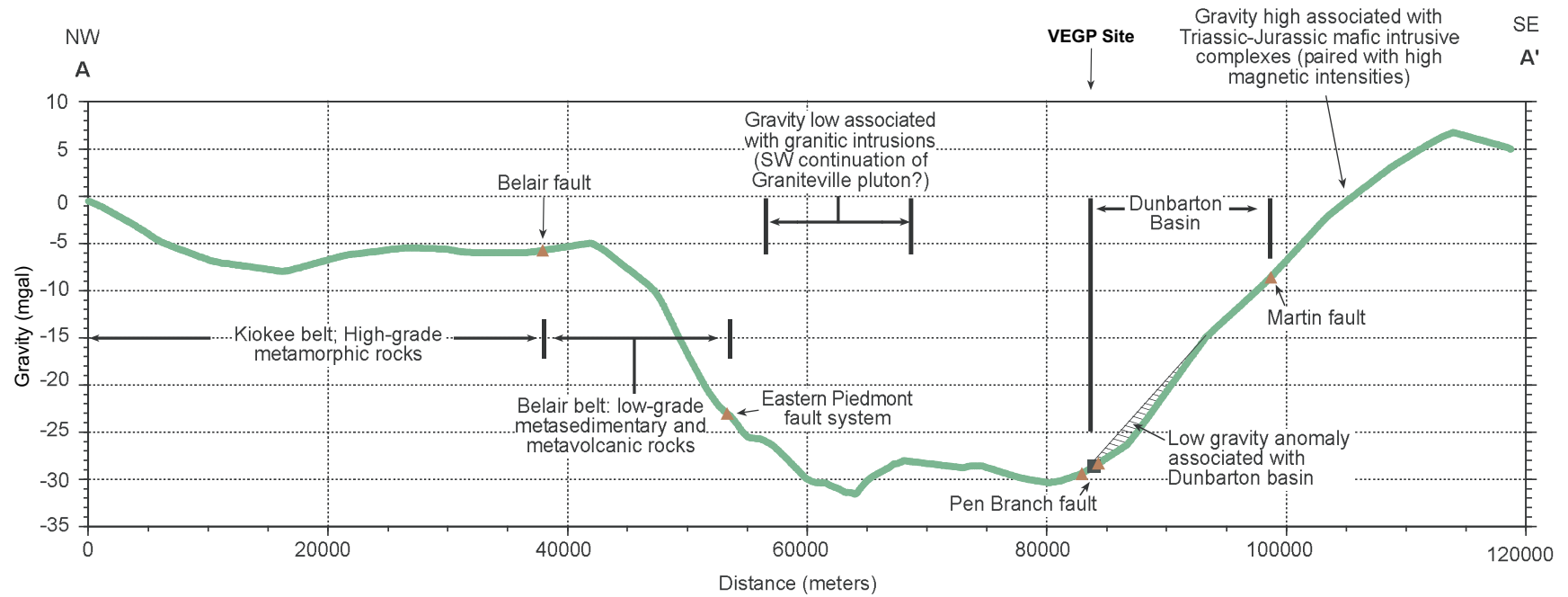


Figure 2.5-228
Northwest–Southeast Gravity Profile Through the VEGP Site

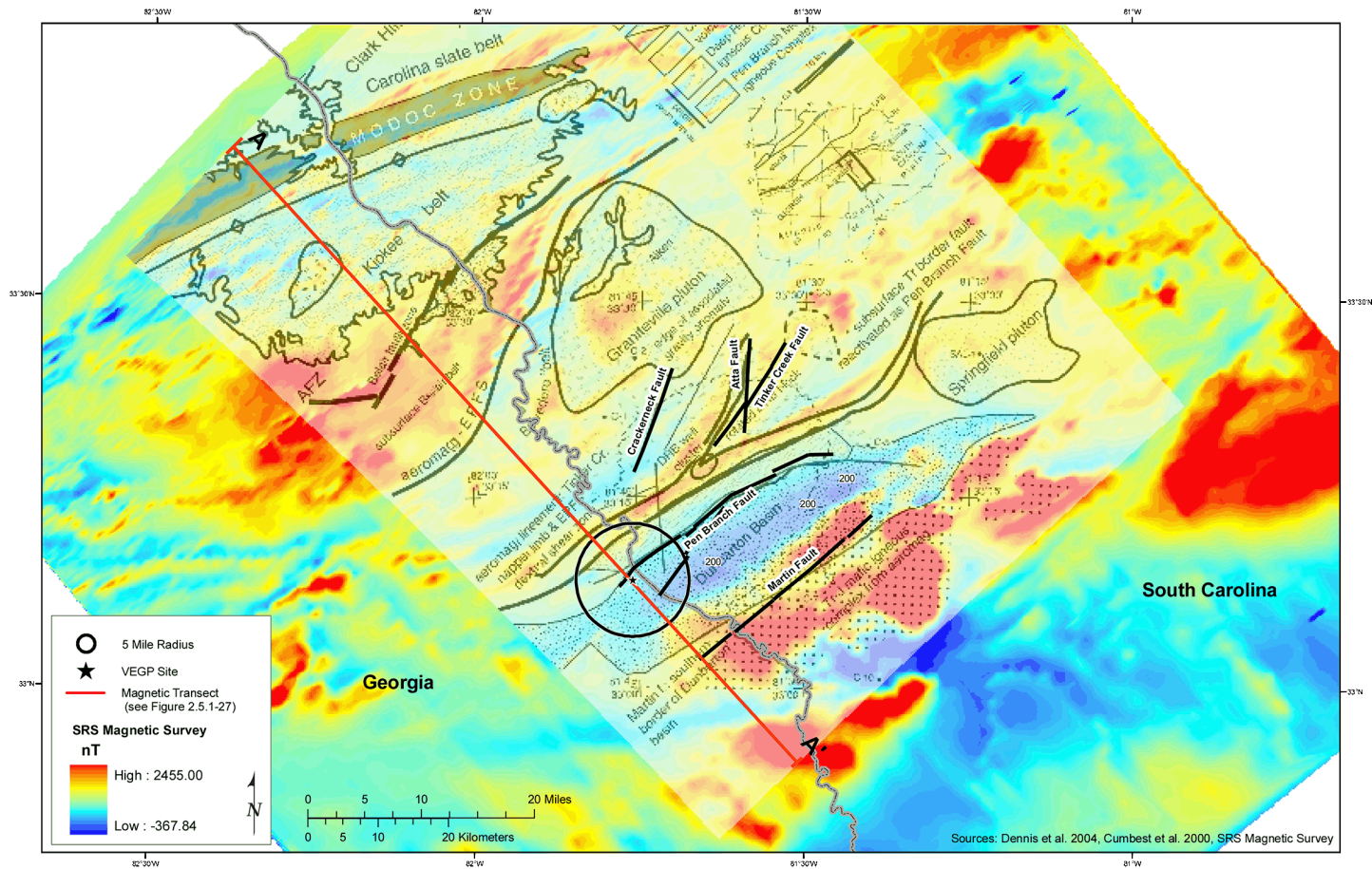


Figure 2.5-229
Magnetic Field in the Vicinity of the VEGP Site

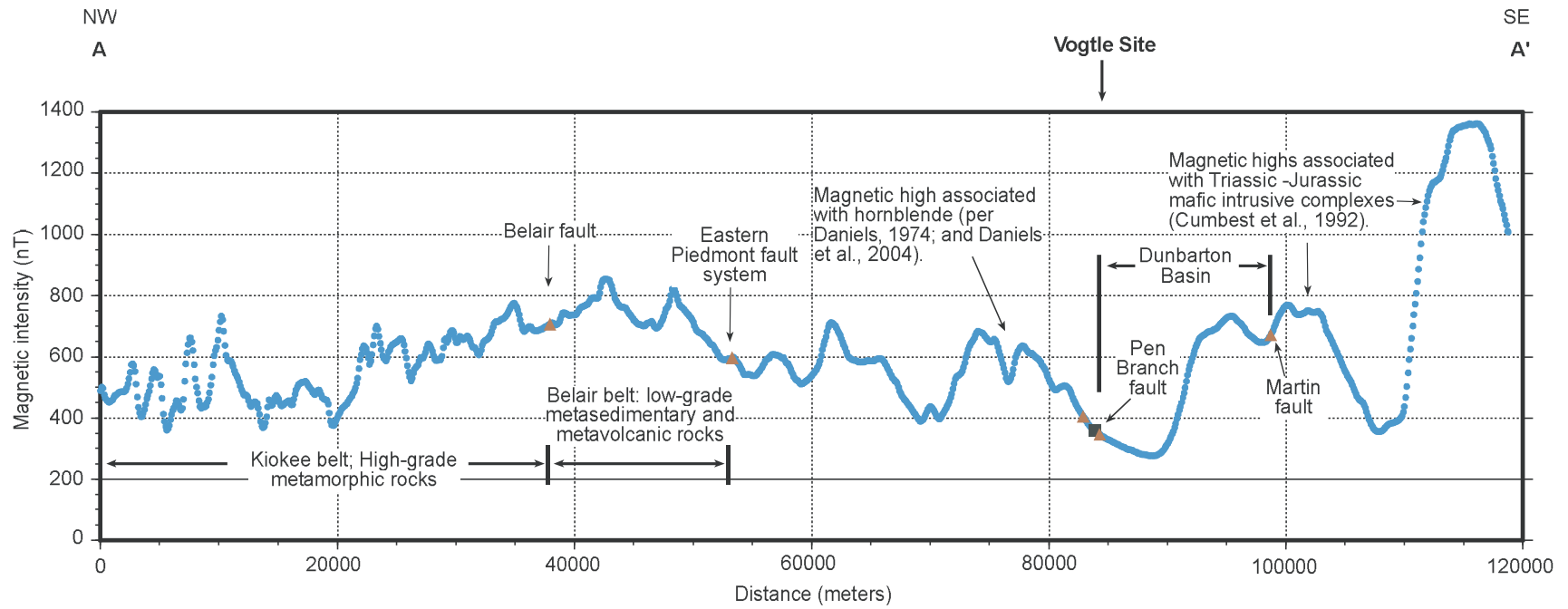
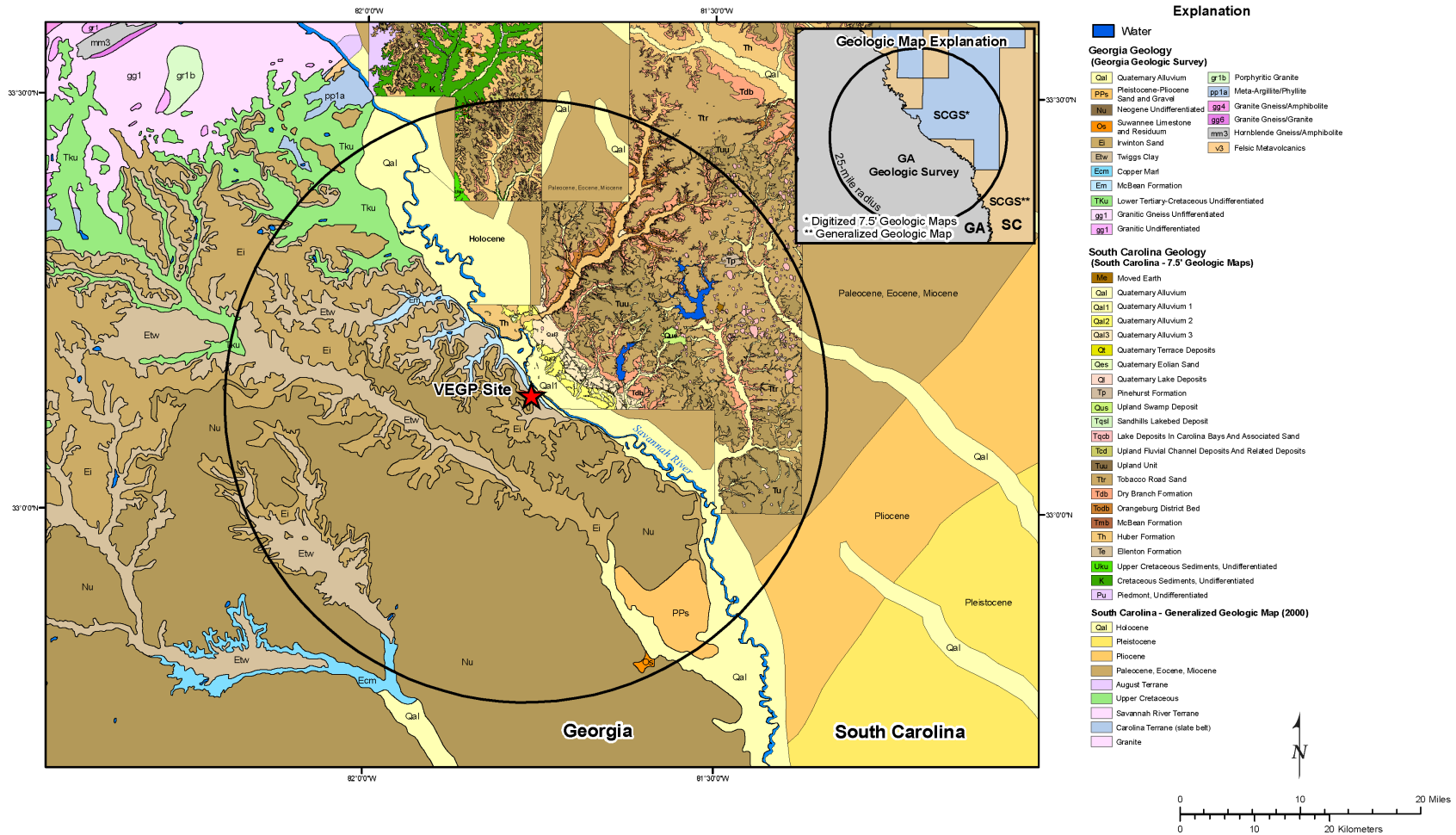


Figure 2.5-230
Northwest–Southeast Profile of Magnetic Intensity Through the VEGP Site



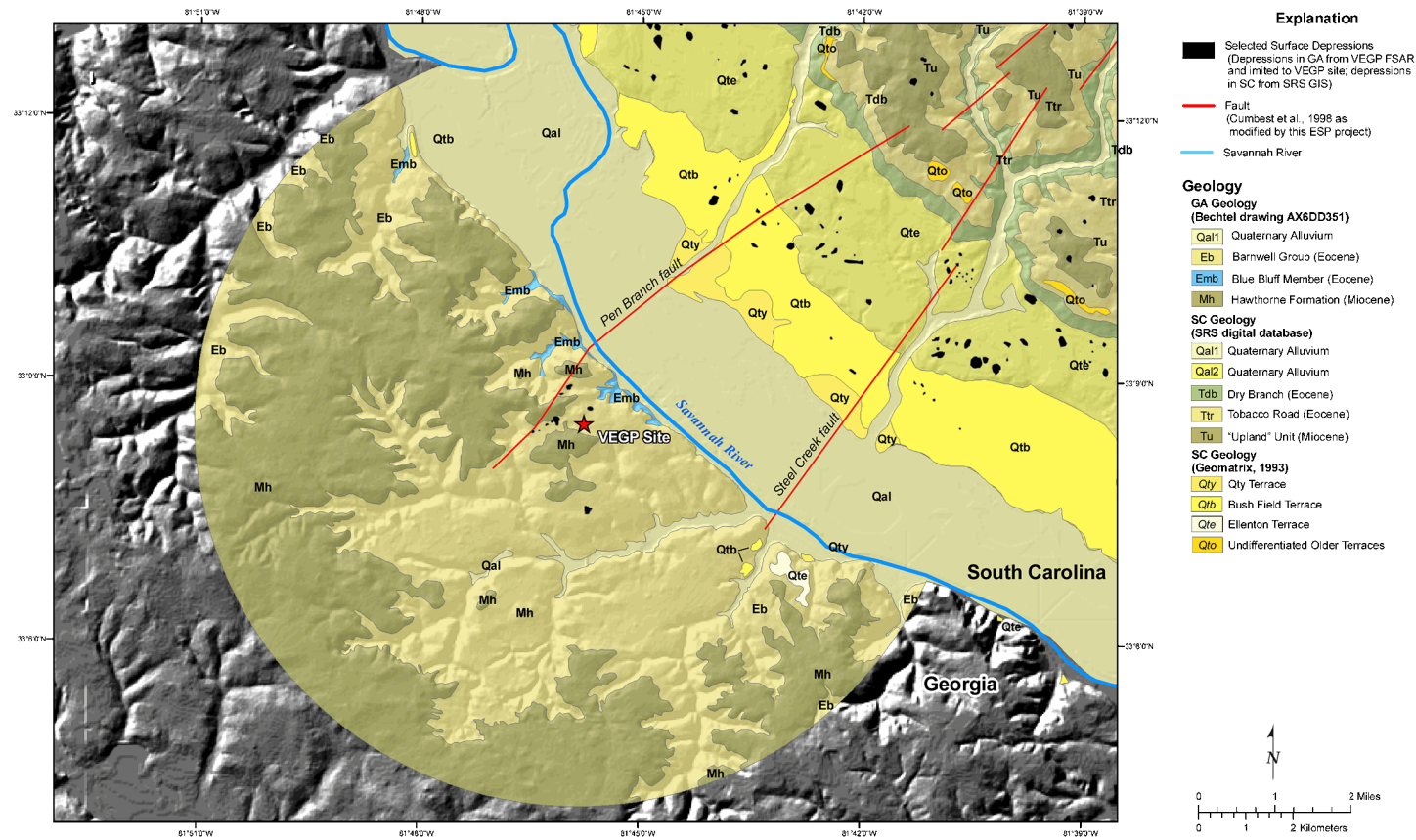


Figure 2.5-232
Site Area Geologic Map (5-Mile Radius)

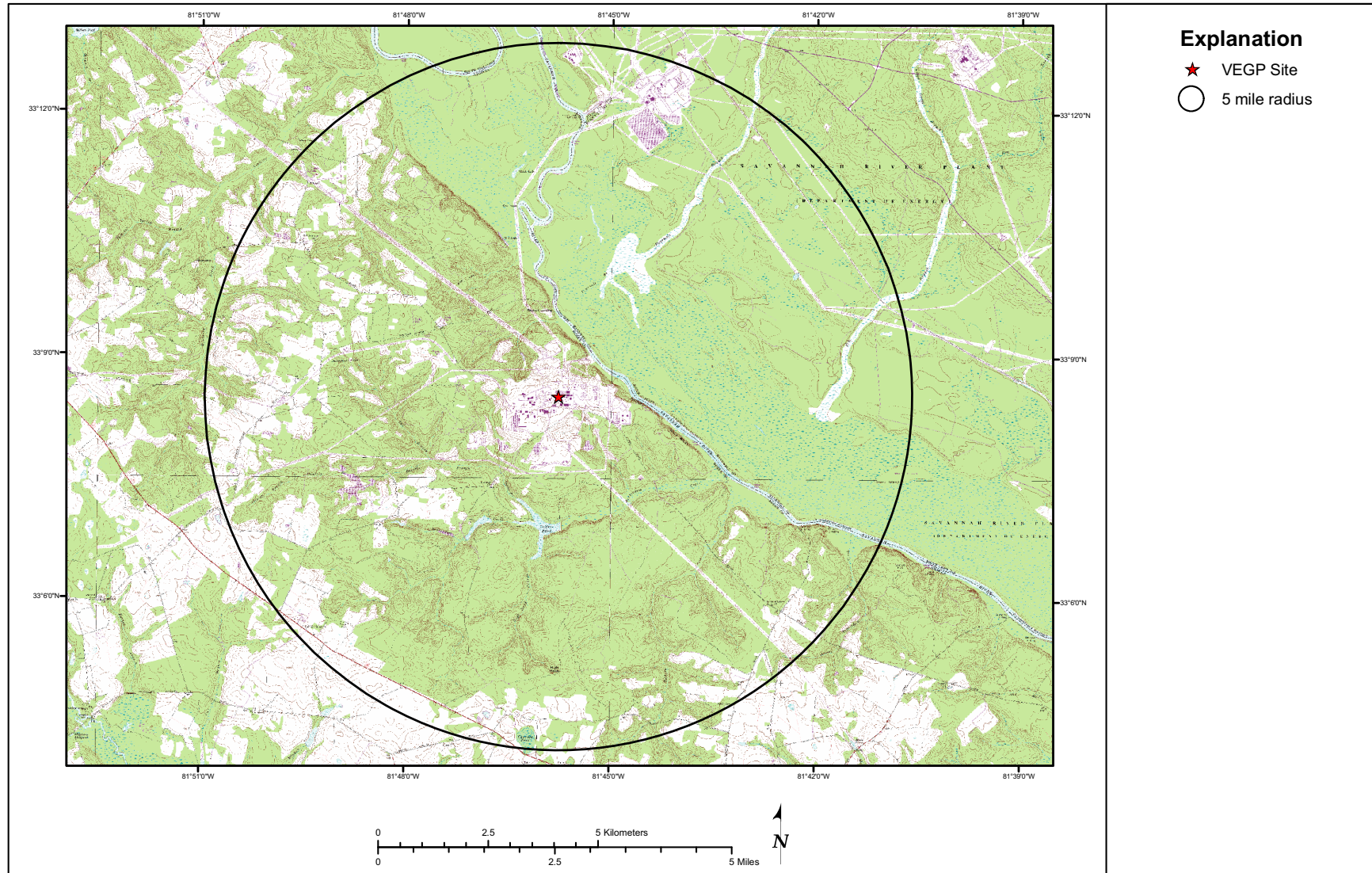


Figure 2.5-233
Site Area Topographic Map (5-Mile Radius)

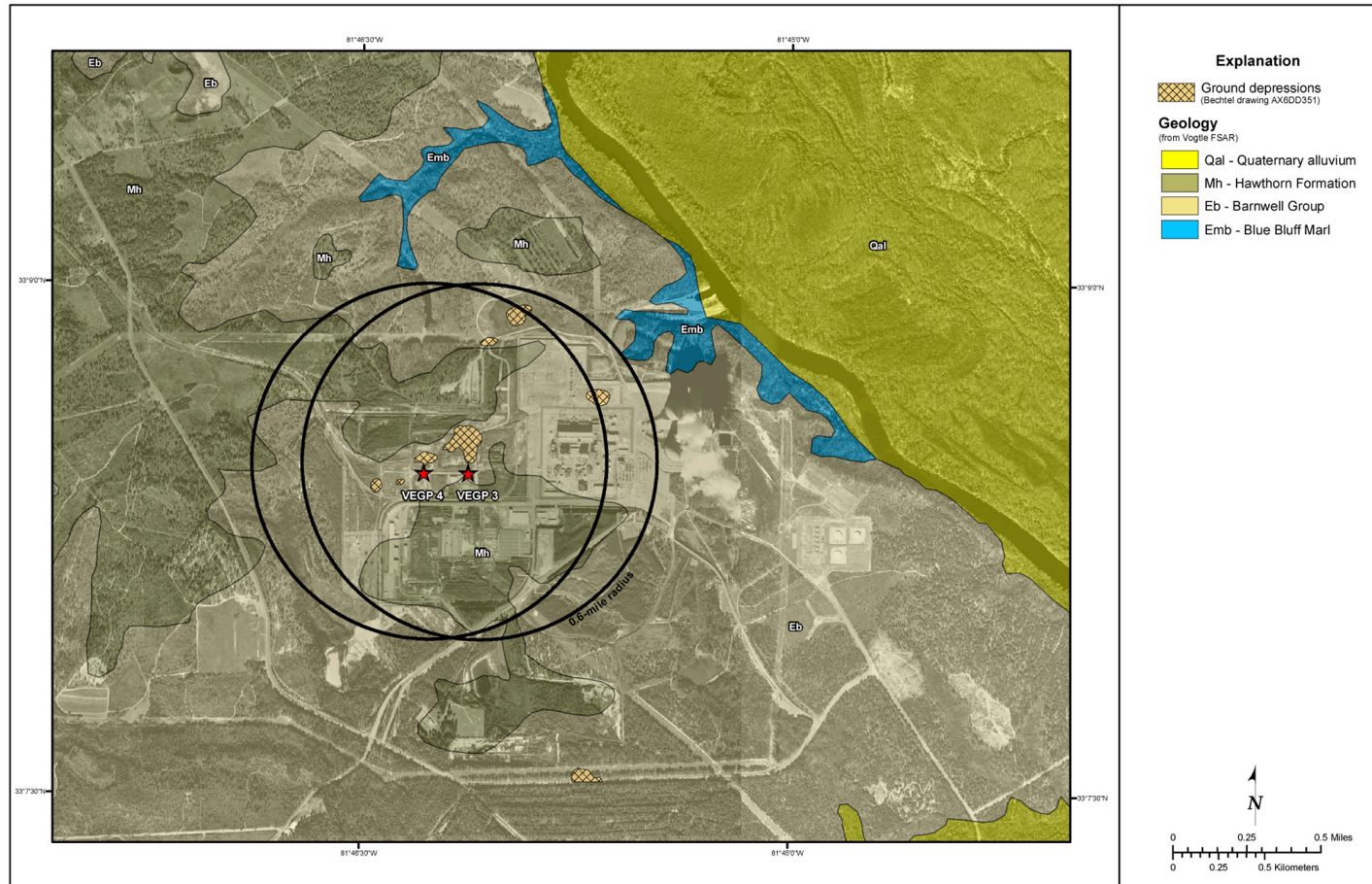


Figure 2.5-234
Site Geologic Map (0.6-Mile Radius)

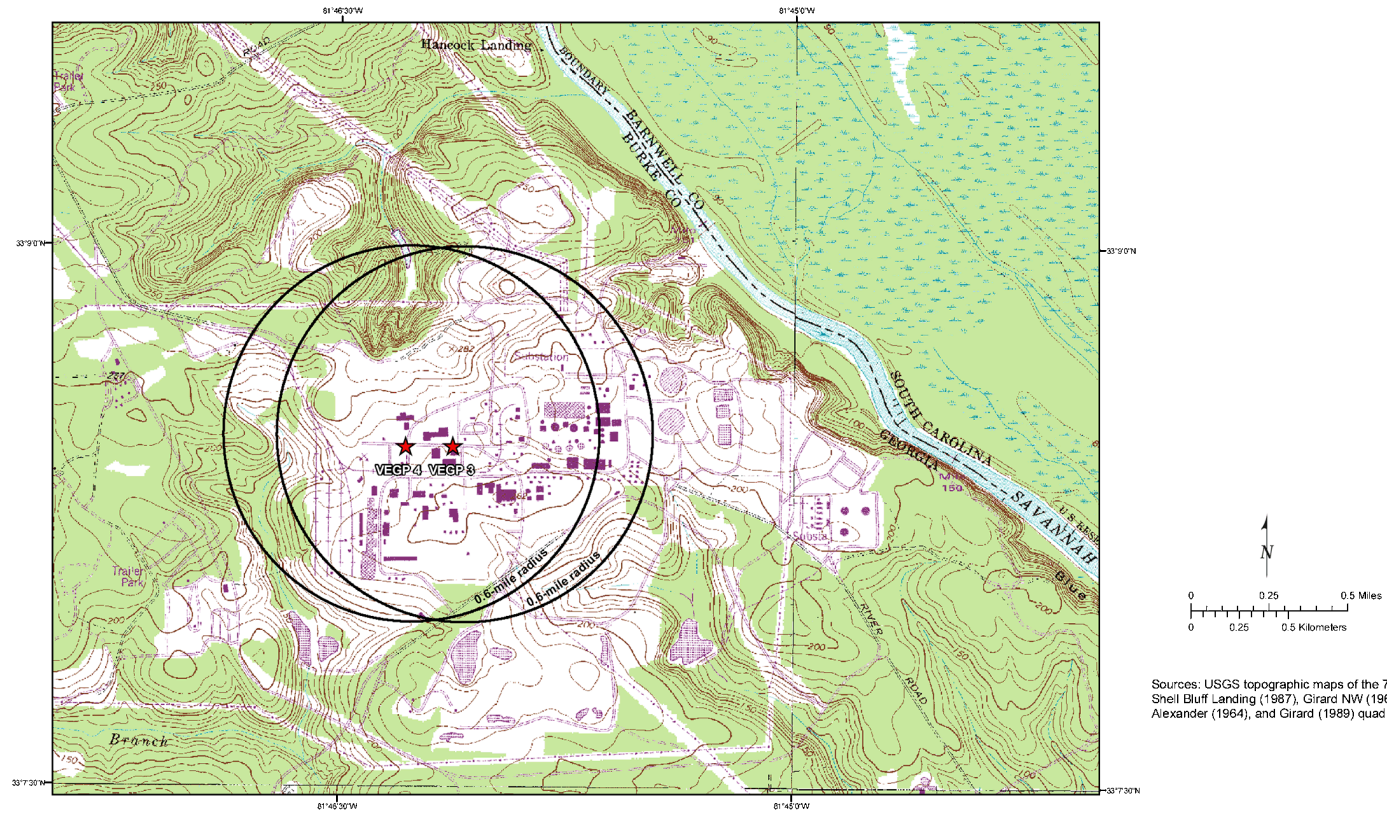


Figure 2.5-235
Site Topographic Map (0.6-Mile Radius)

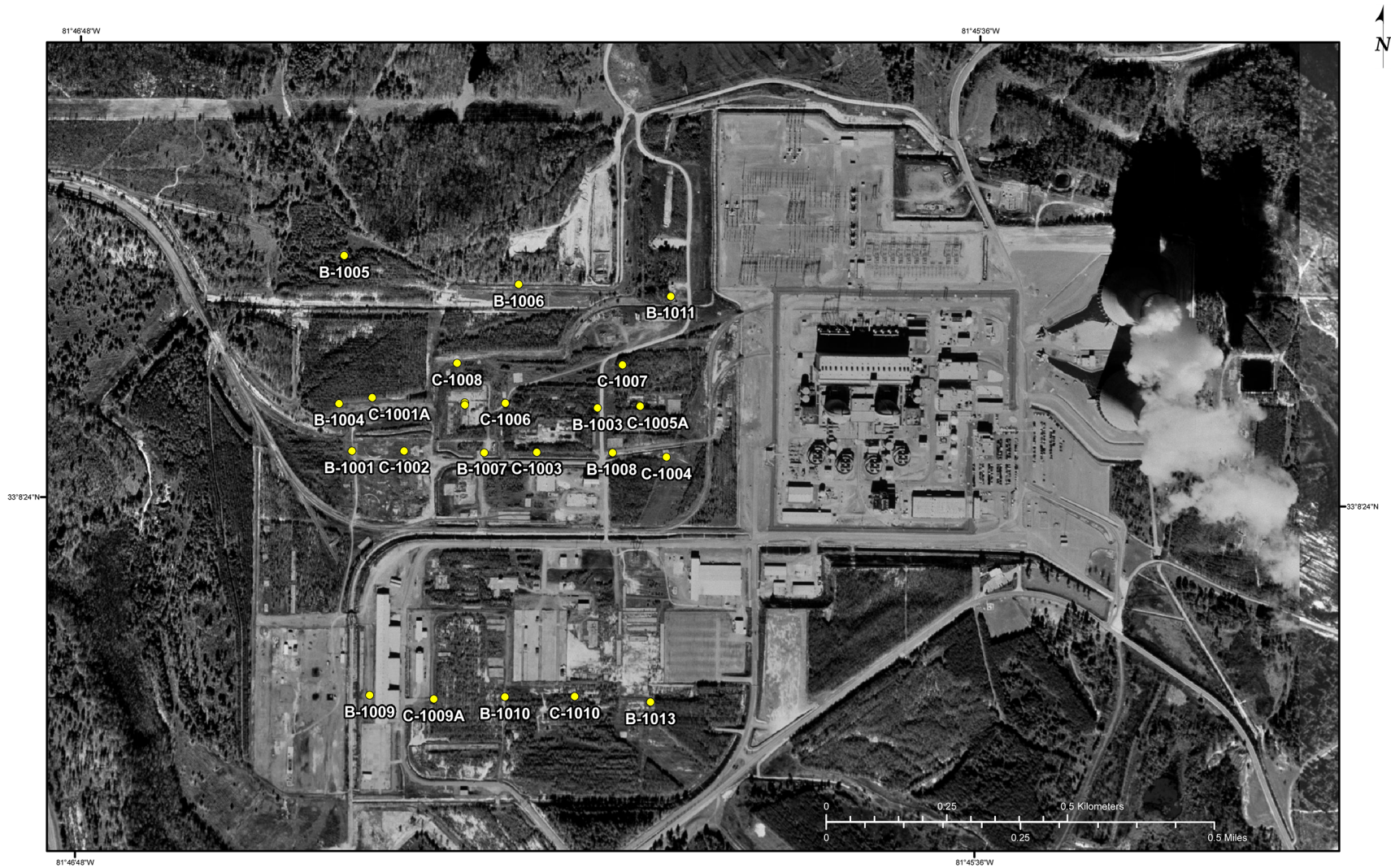


Figure 2.5-236
Site Borings Location Map

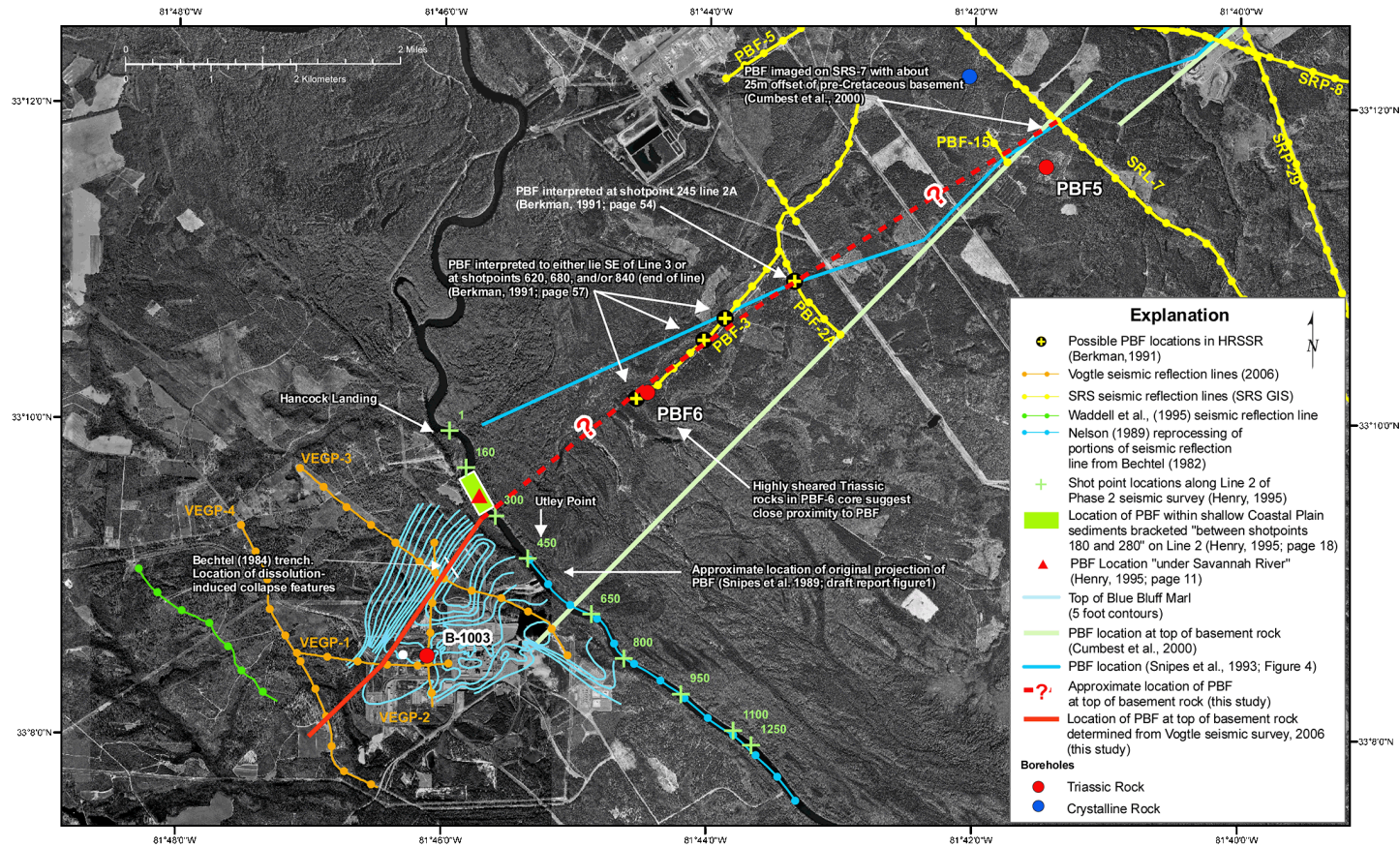


Figure 2.5-237
Location of Pen Branch Fault

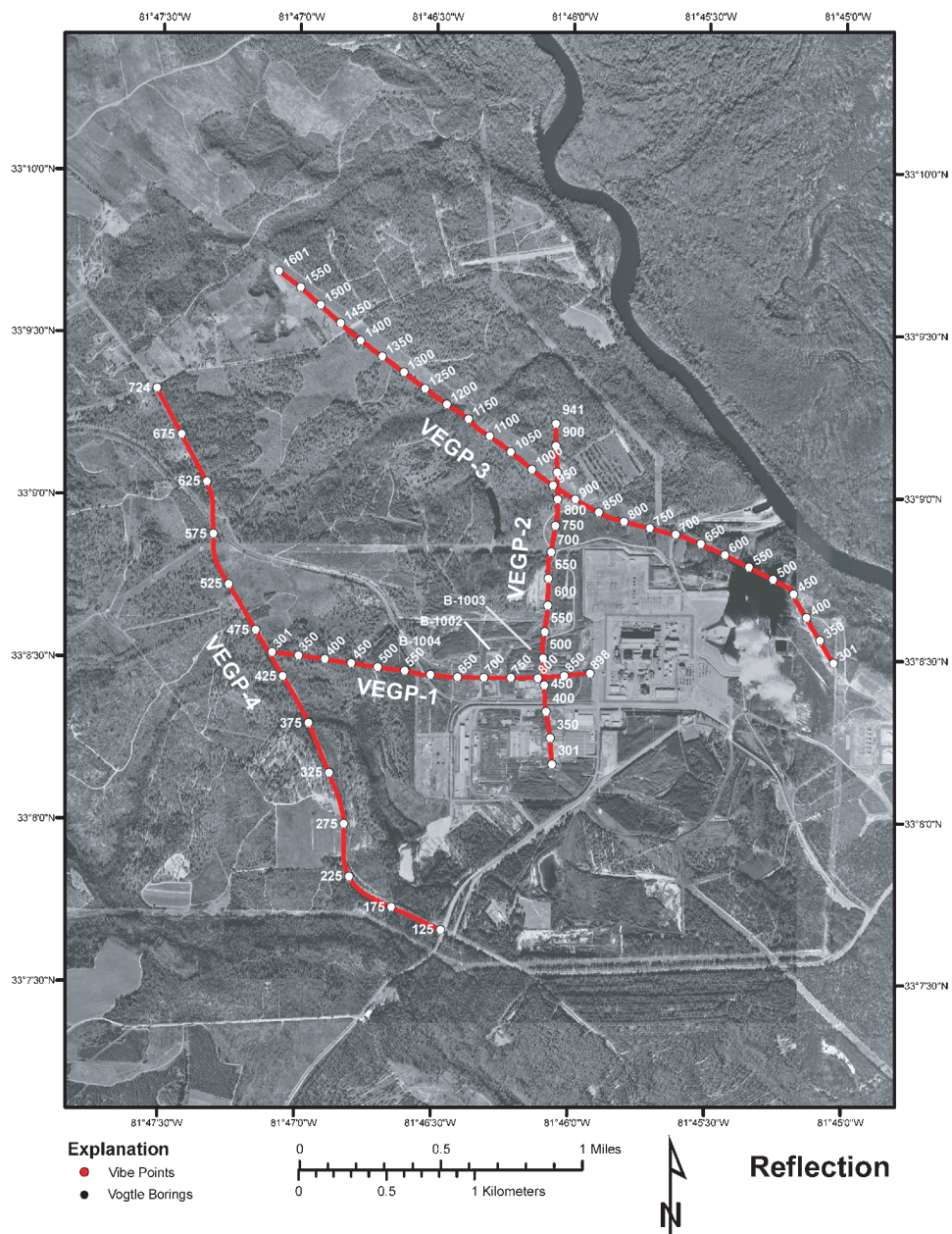


Figure 2.5-238
Seismic Reflection Array

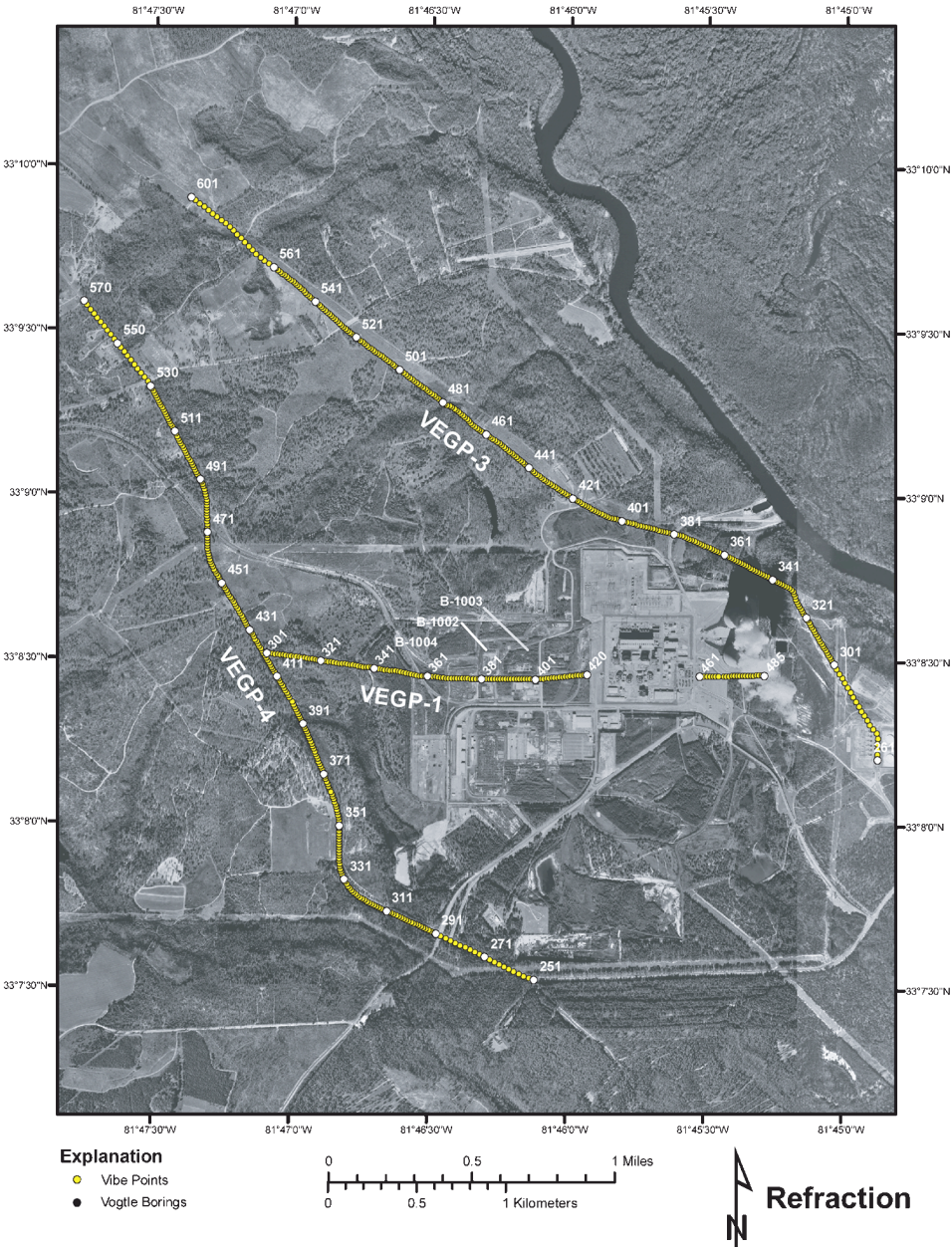


Figure 2.5-239
Seismic Refraction Array

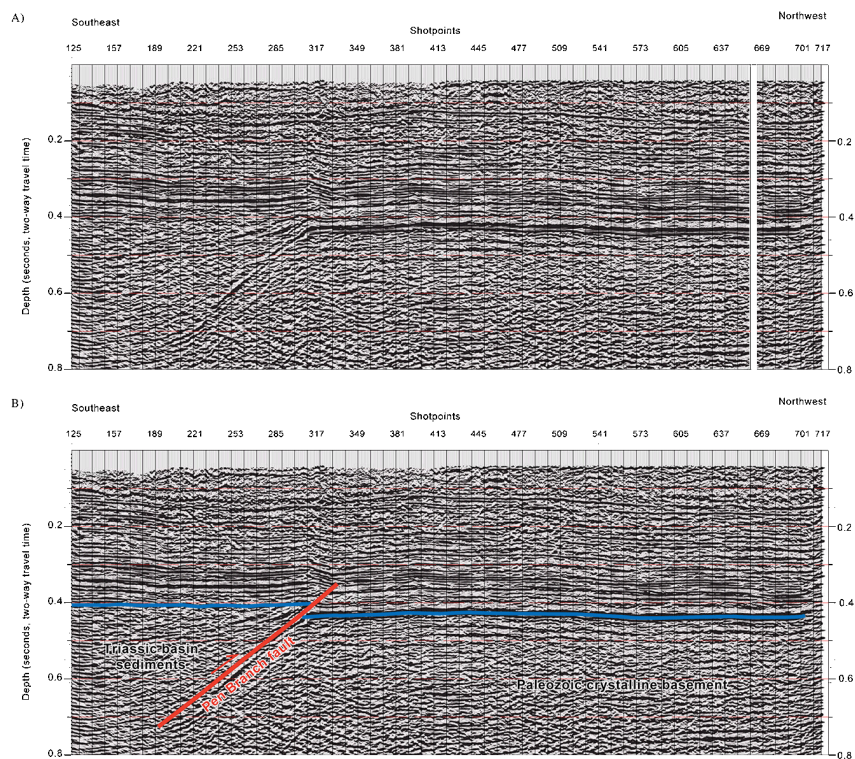
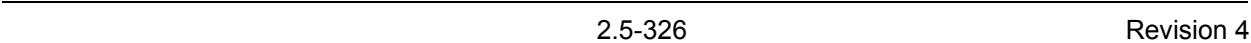


Figure 2.5-240
(A) Seismic Reflection Line 4 (Time Section; Display Velocity = 12,000 fps)
(B) Interpretation (Blue Line Represents Top of Basement)

AGE				UNIT	DEPTH (FT)	ELEVATION (FT MSL)
Cenozoic	TerTiary	Eocene	Upper	Barnwell Group • Tobacco Road Sand • Dry Branch Formation • Clinchfield Formation ○ Utley Limestone Member	Ground surface 74	+218 +144
			Middle	Claiborne Group • Lisbon Formation ○ Blue Bluff Member • Still Branch Sand • Congaree Formation	88 173 216	+130 +50 +7
			Lower			
		Paleocene	Upper	• Snapp Formation • Black Mingo Formation	331 438	-108 -215
			Lower			
Mesozoic	Cretaceous	Upper		• Steel Creek Formation • Gaillard Formation/ Black Creek Formation • Pio Nono Formation / Unnamed Sand • Cape Fear Formation	477 587 798 858	-254 -364 -575 -635
	Triassic			Triassic (Dunbarton) basin	1049 Boring terminated at 1338	-826

Note: The site stratigraphic column is based primarily on cored boring B-1003. The data on the Utley Limestone and Blue Bluff Marl have been revised based on more extensive data from the ESP and COL borings.

Figure 2.5-241
Site Stratigraphic Column



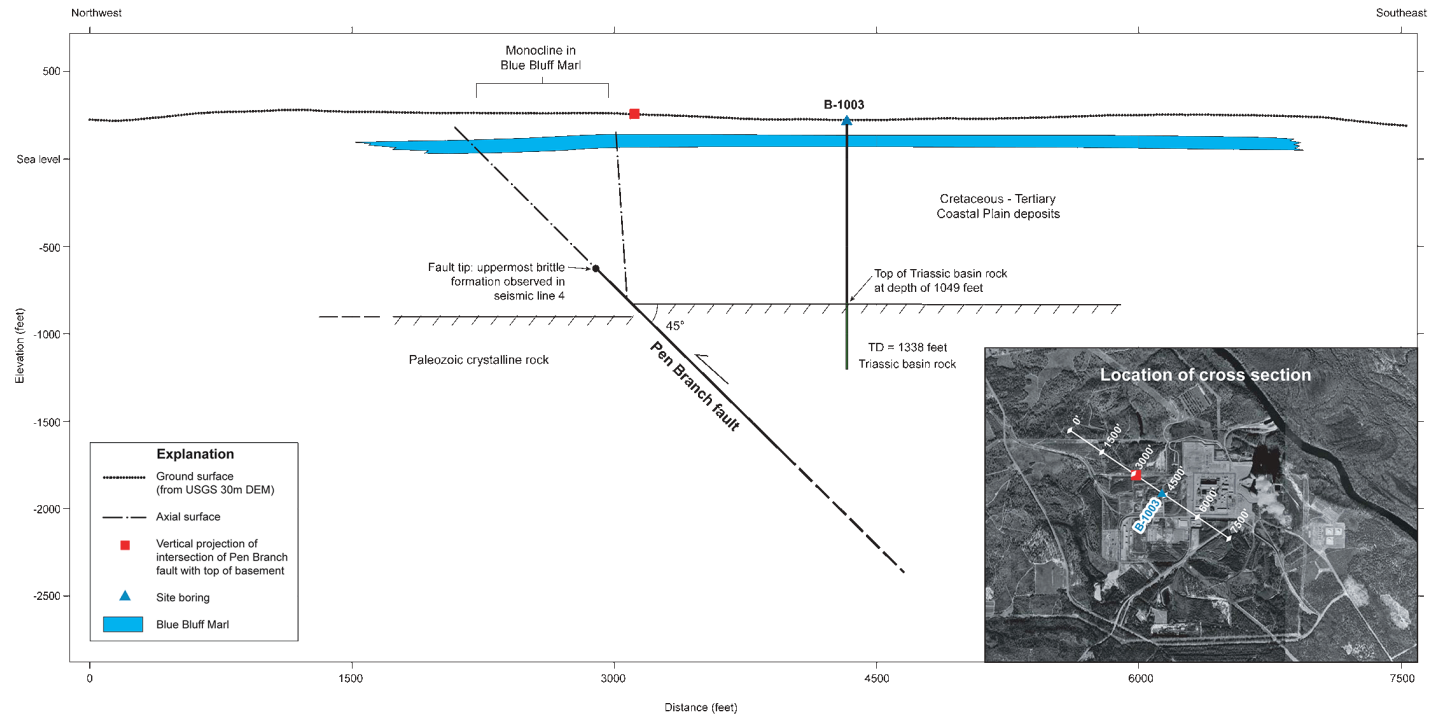


Figure 2.5-243
Northwest–Southeast Cross Section Showing Pen Branch Fault Beneath VEGP Site

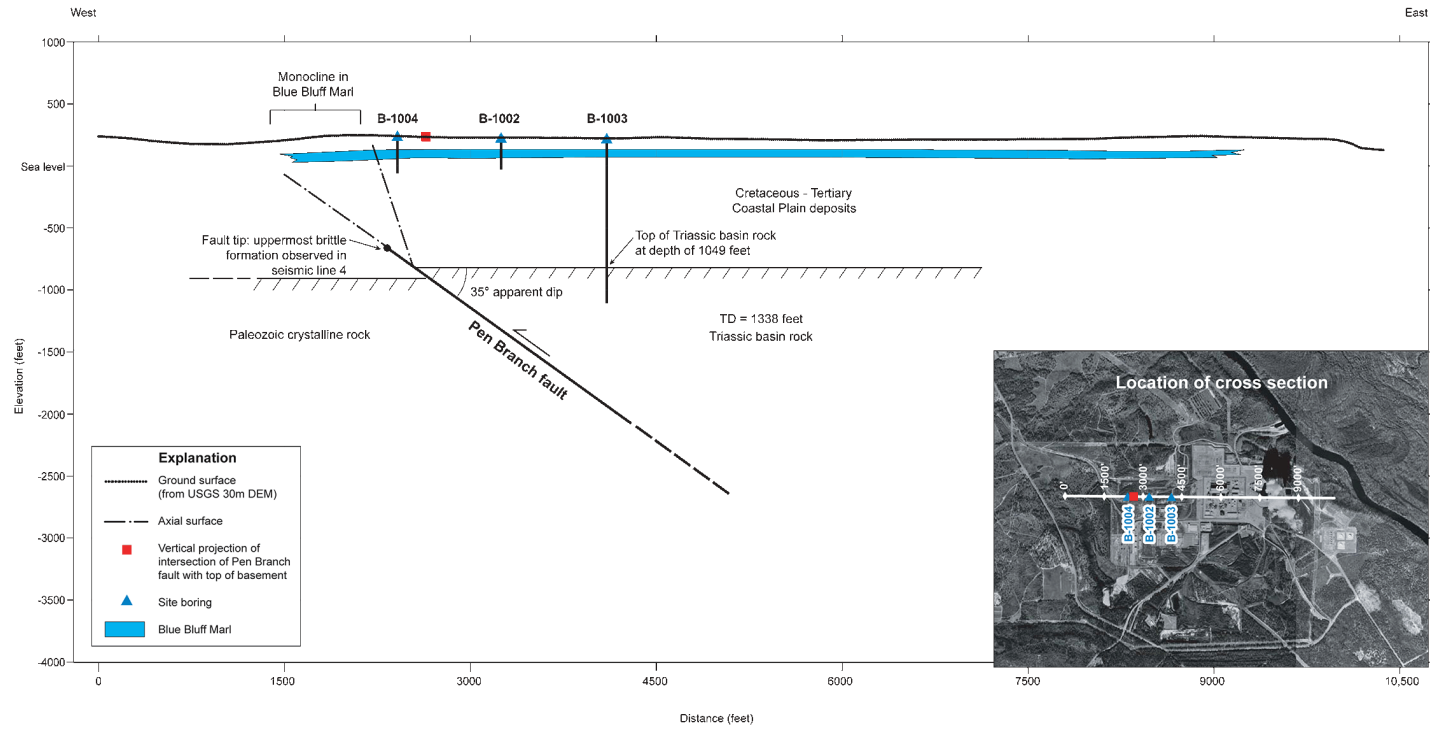


Figure 2.5-244
East–West Cross Section Showing Pen Branch Fault Beneath VEGP Site

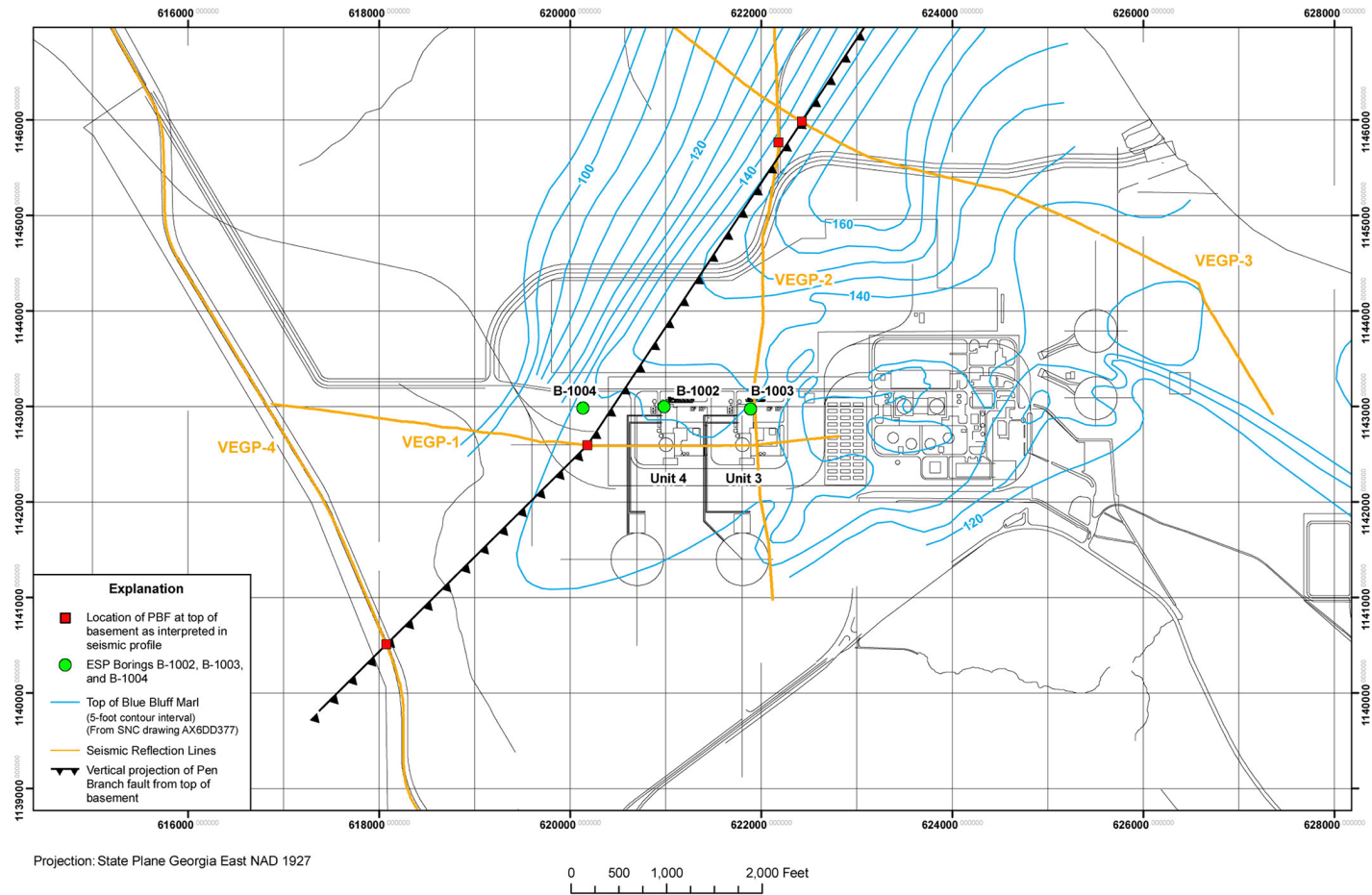


Figure 2.5-245
VEGP Site Plant Layout

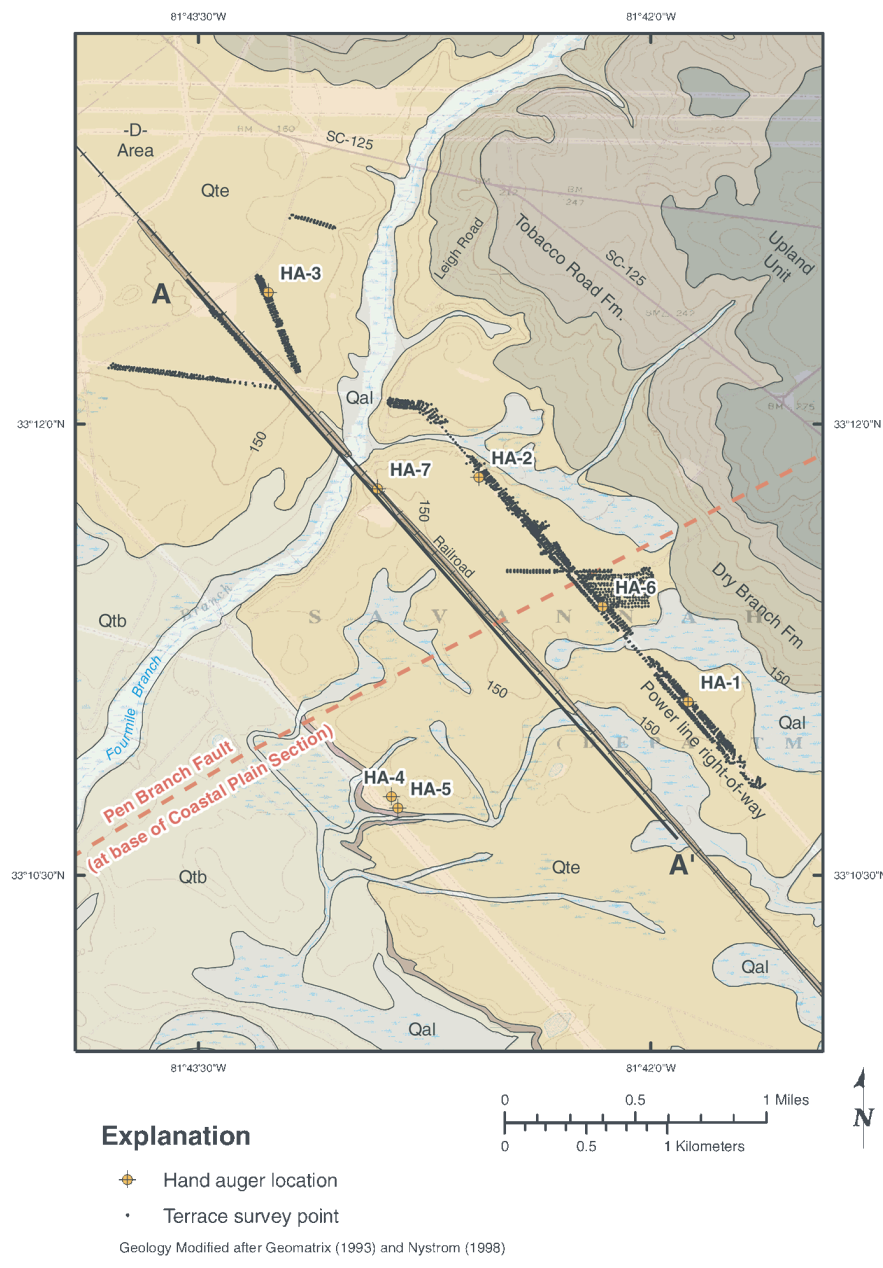


Figure 2.5-246
Geologic Map of Qte Terrace Study Area

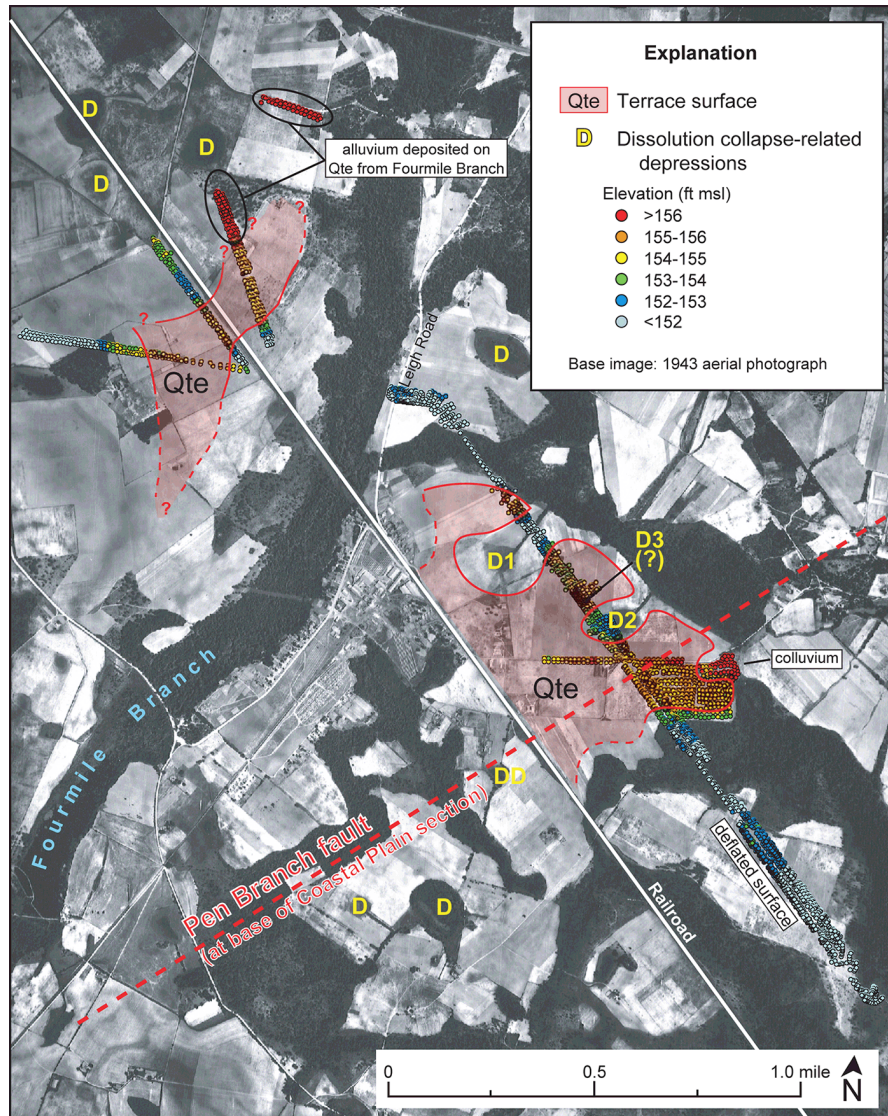


Figure 2.5-247
Geomorphic Map Showing Best-Preserved Remnants of Qte
Terrace Surface (Red Shading) in Study Area at the SRS.
Yellow Ds Indicate Dissolution Collapse-Related Depressions.
Base Image is 1943 Aerial Photograph.

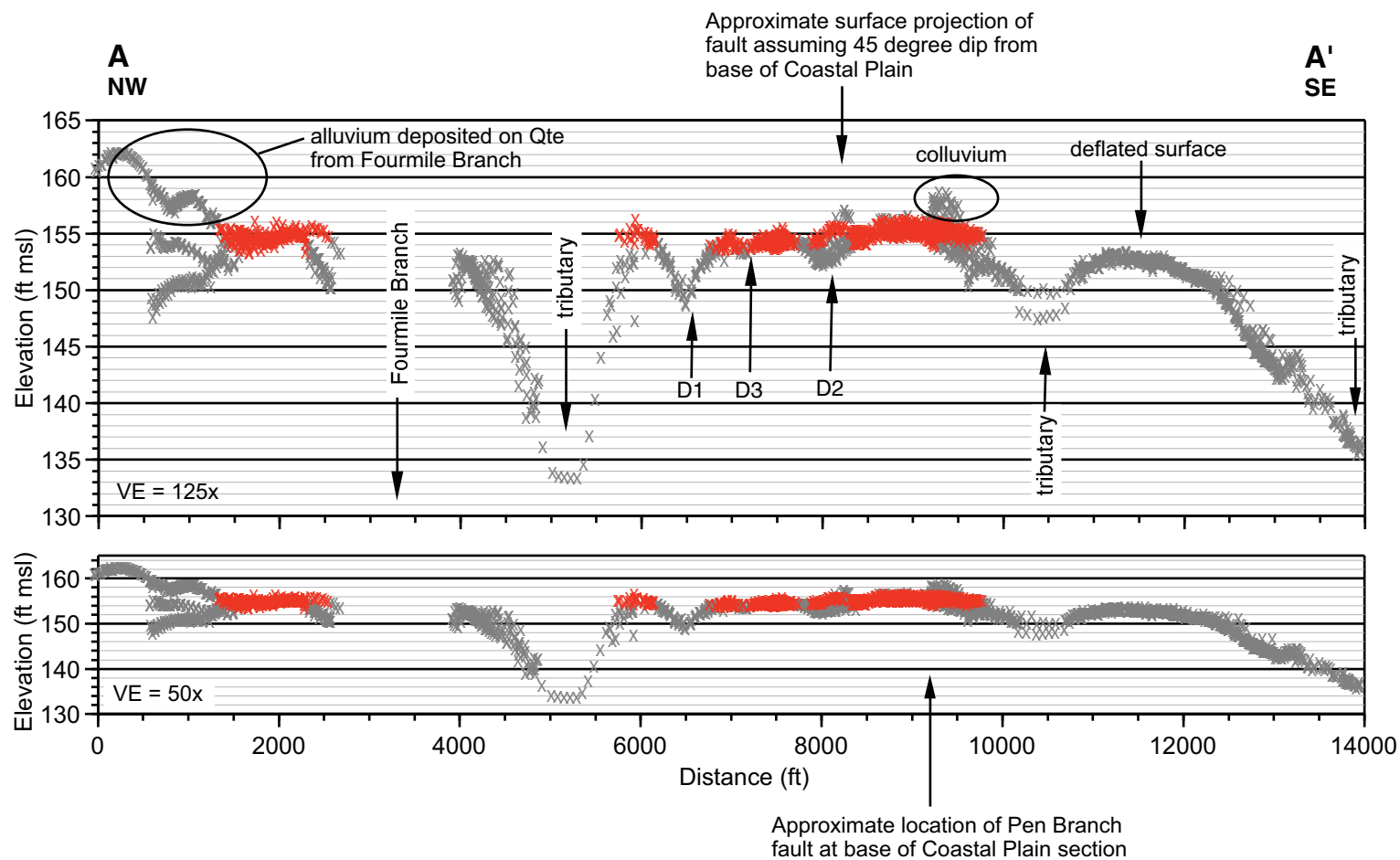


Figure 2.5-248
Longitudinal Profile A-A' from SRS Qte Terrace Surface. Points Interpreted as Representing the Best-Preserved Remnant of the Qte Surface are Shown in Red, all Other Points that Do Not Represent the Terrace Surface are Shown in Gray.

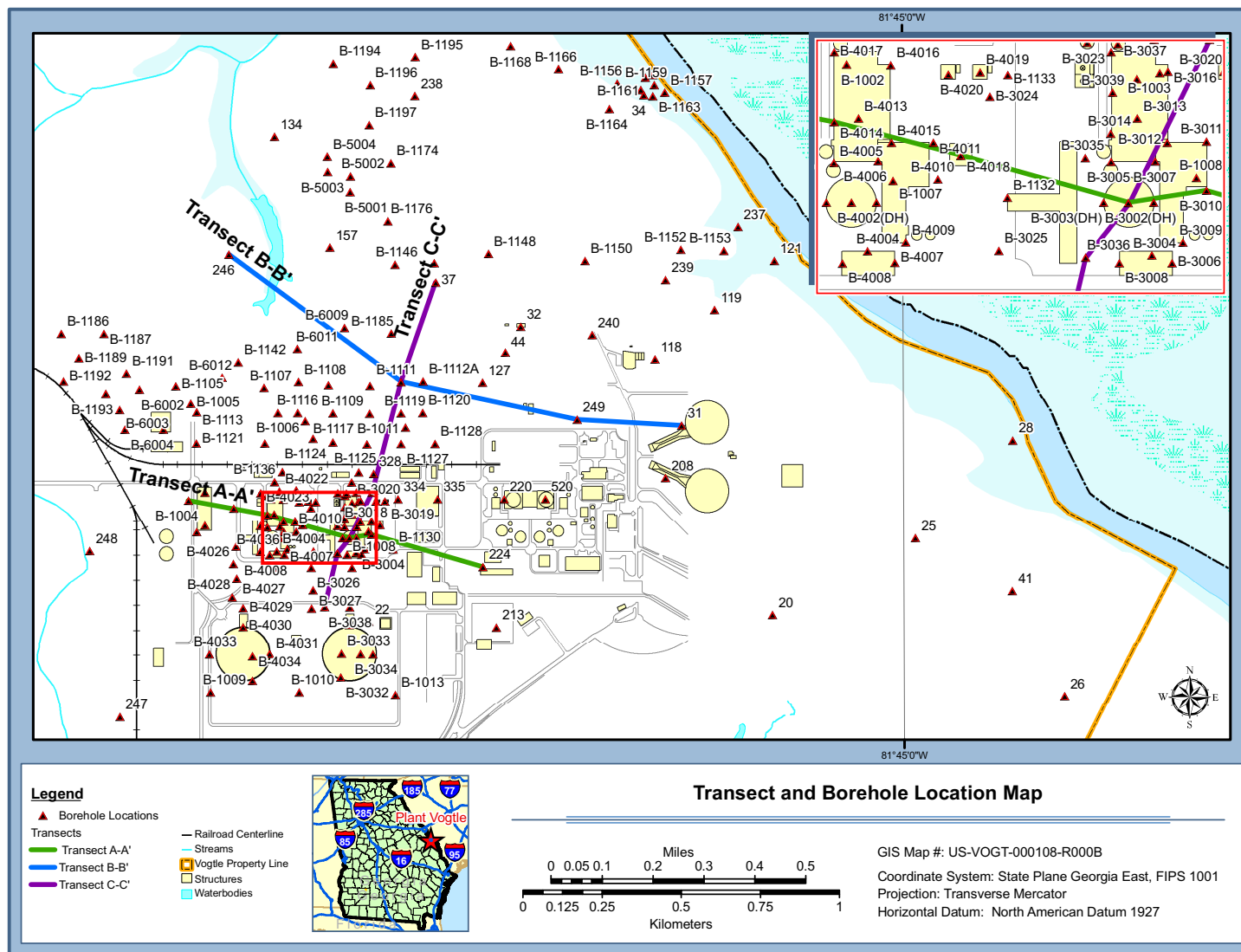


Figure 2.5-249
Transect and Borehole Location Map

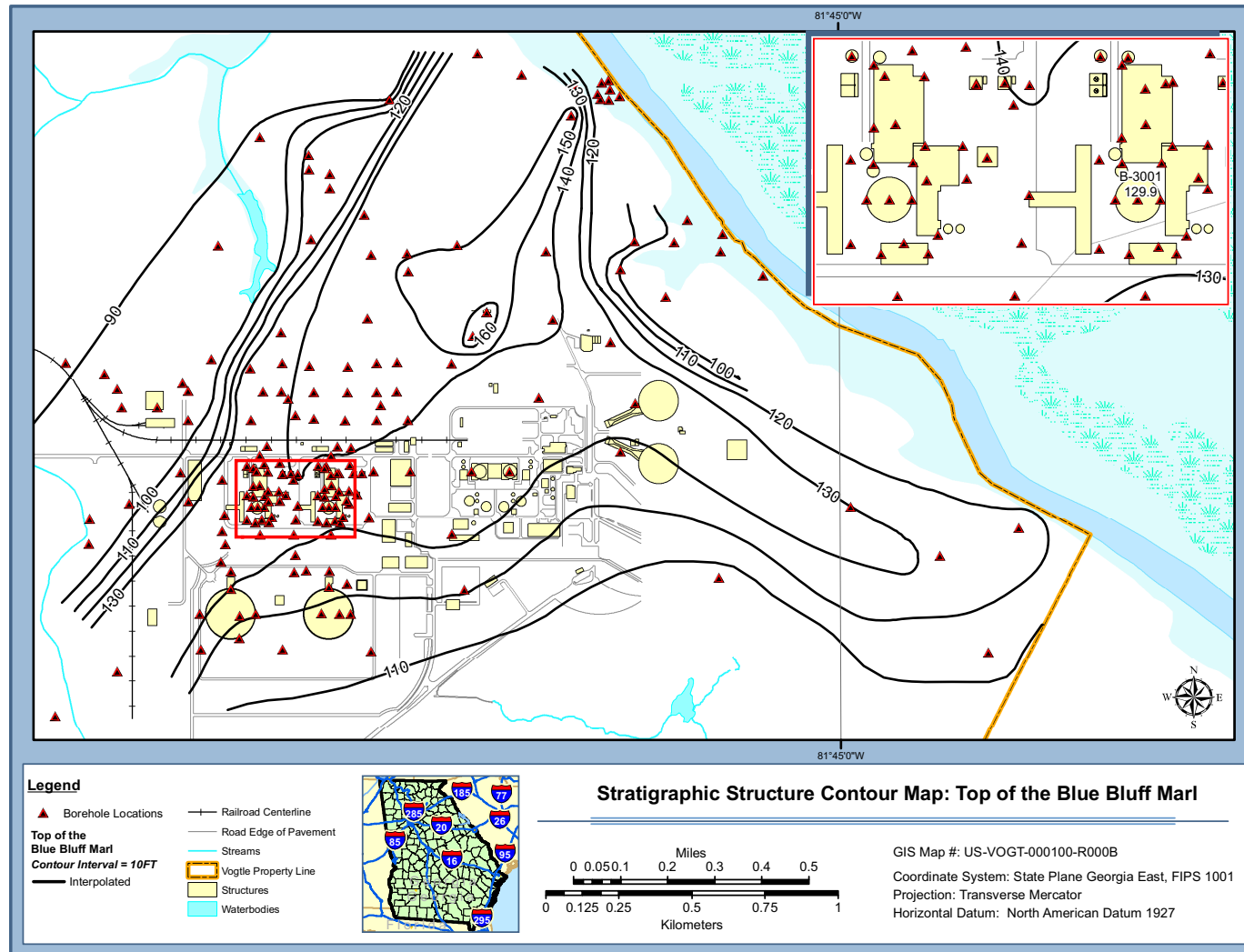


Figure 2.5-250
Stratigraphic Structure Contour Map: Top of Blue Bluff Marl

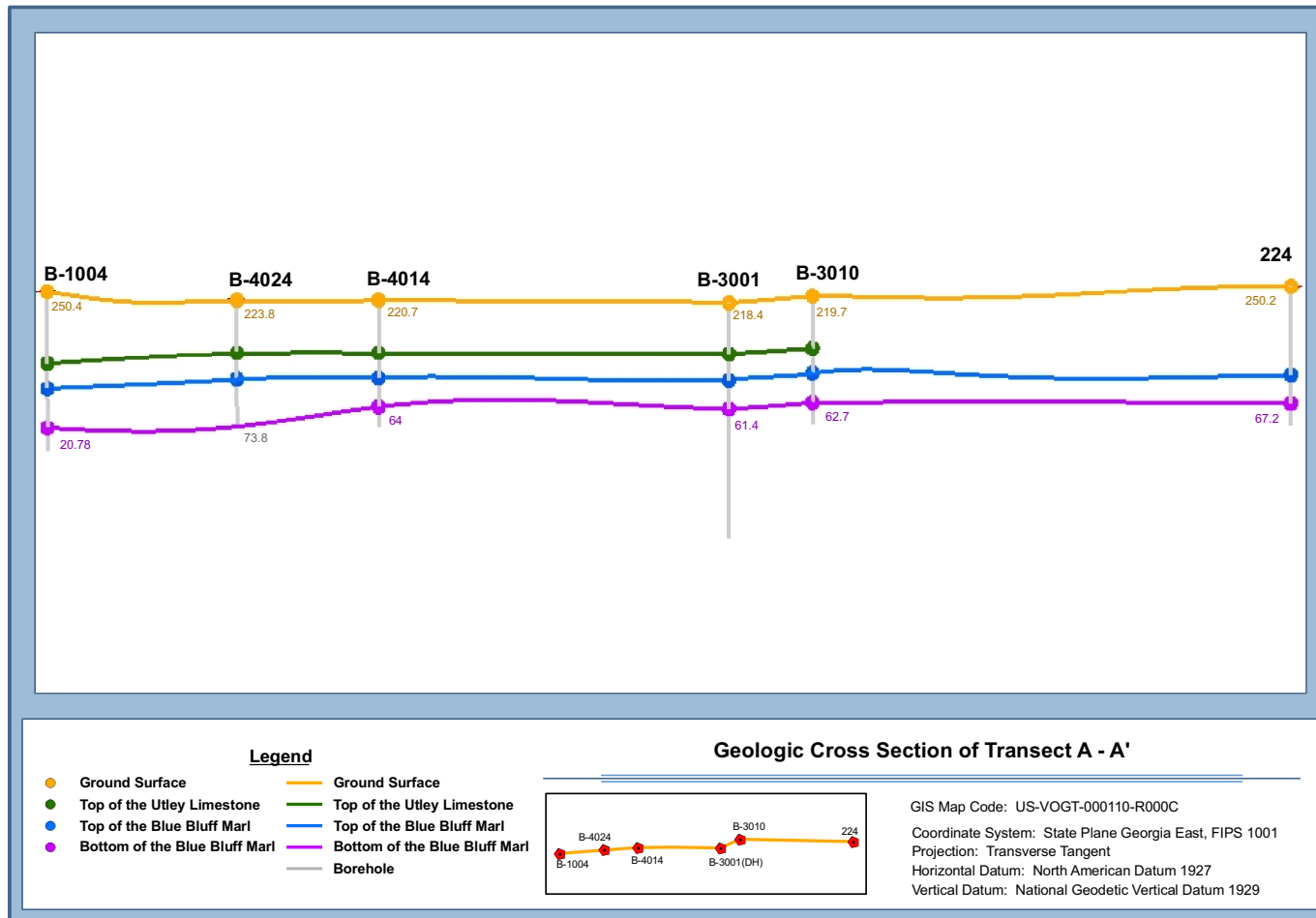


Figure 2.5-251
Geologic Cross section of Transect A-A'

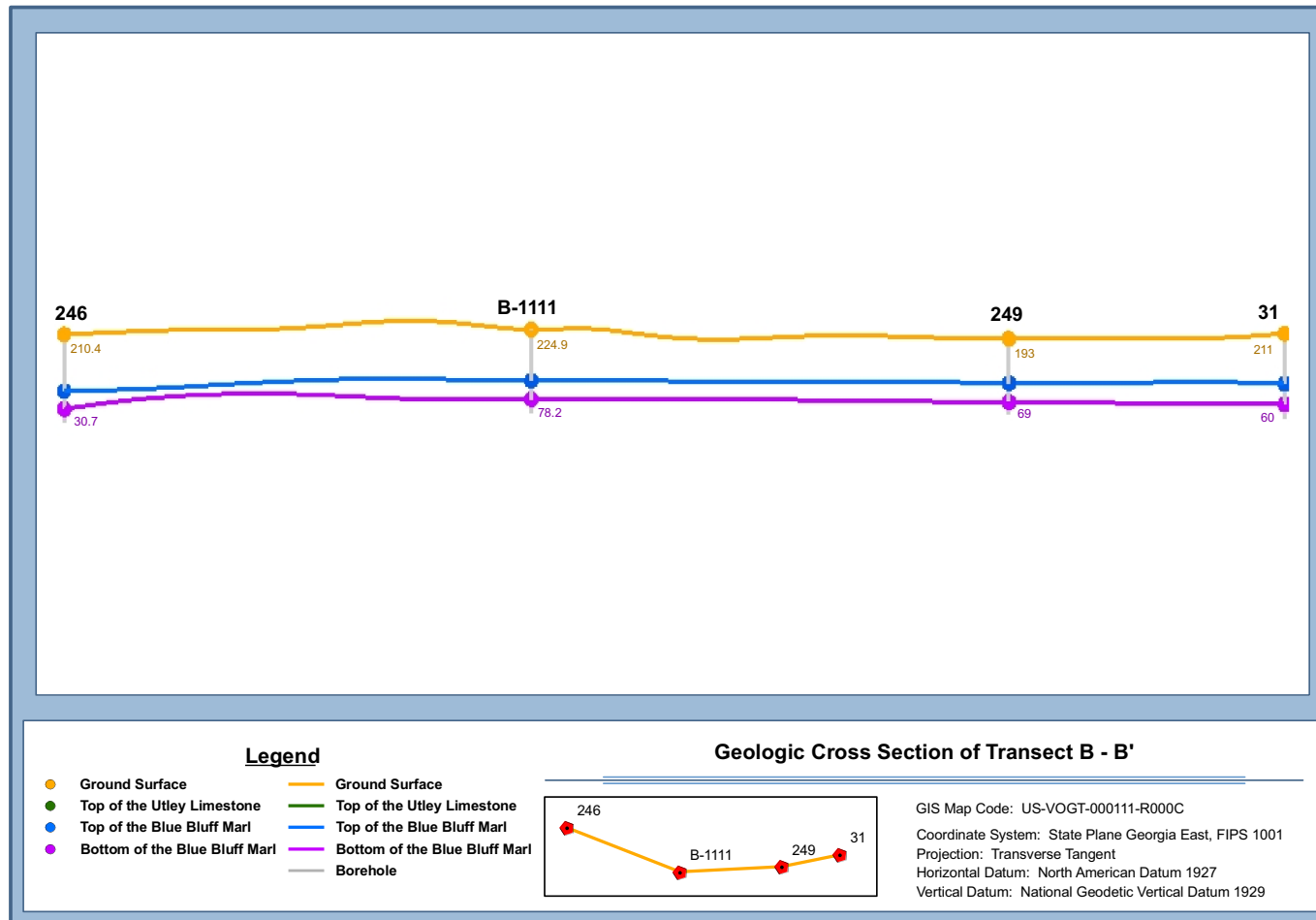


Figure 2.5-252
Geologic Cross Section of Transect B-B'

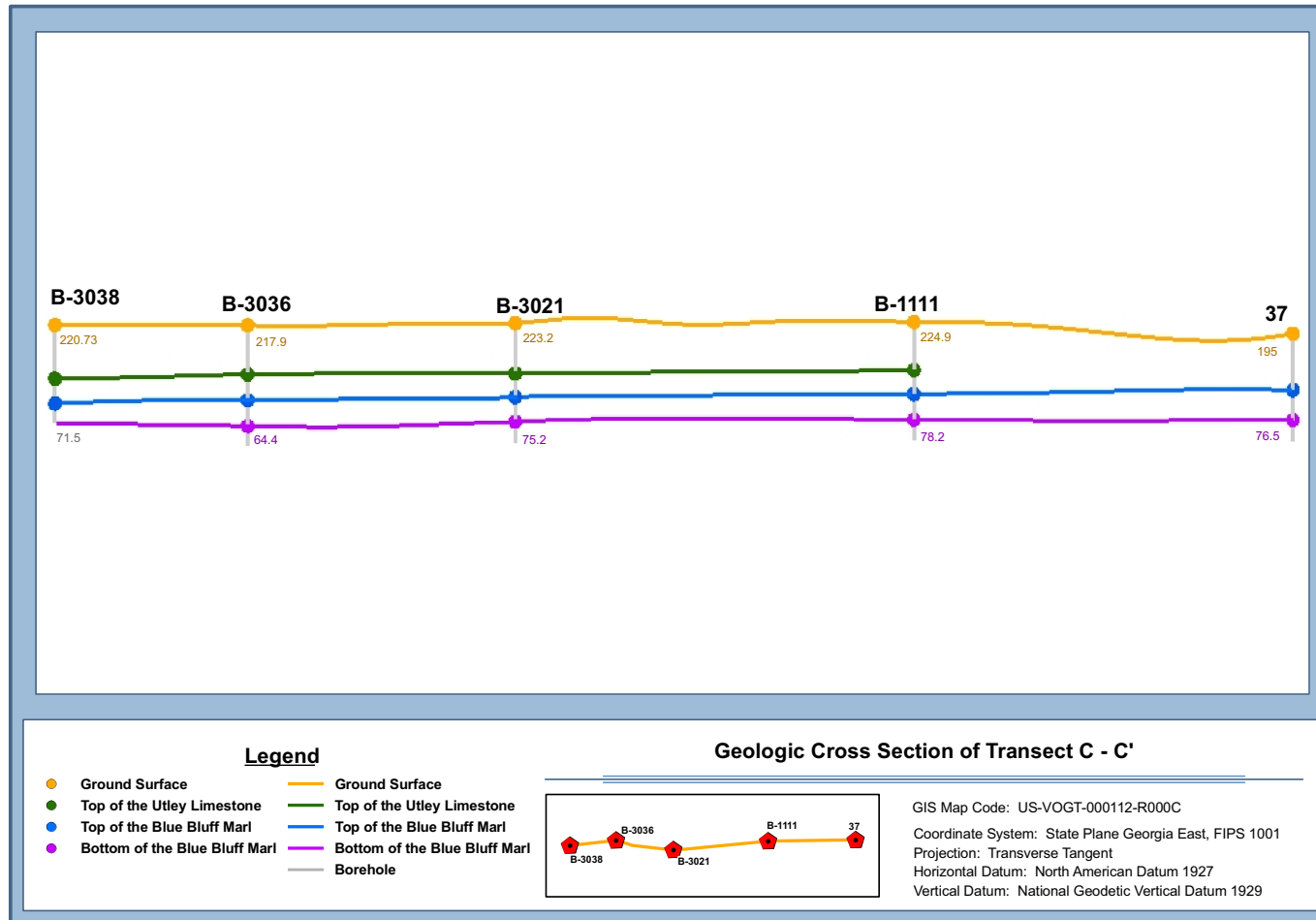


Figure 2.5-253
Geologic Cross Section of Transect C-C'

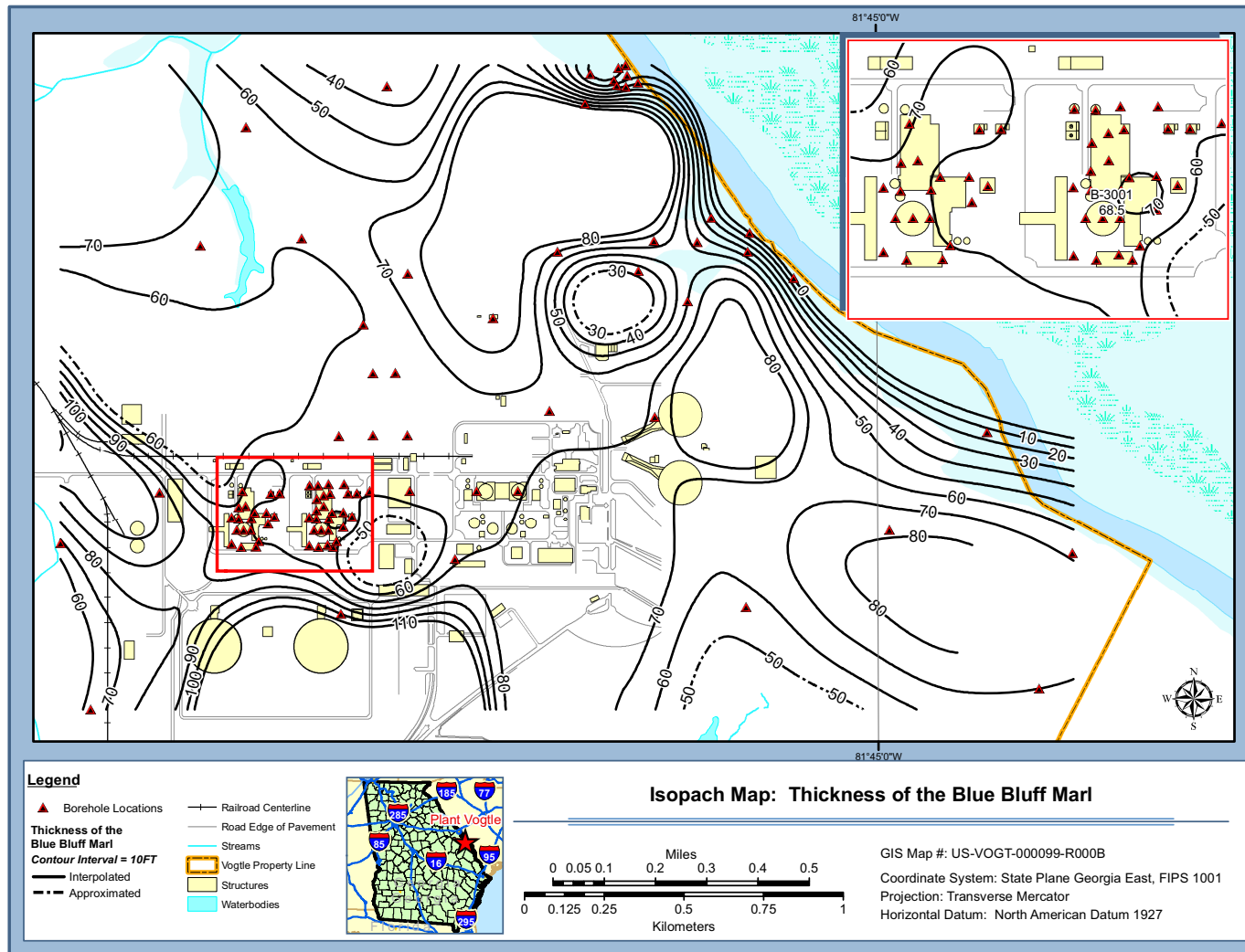


Figure 2.5-254
Isopach Map: Thickness of the Blue Bluff Marl

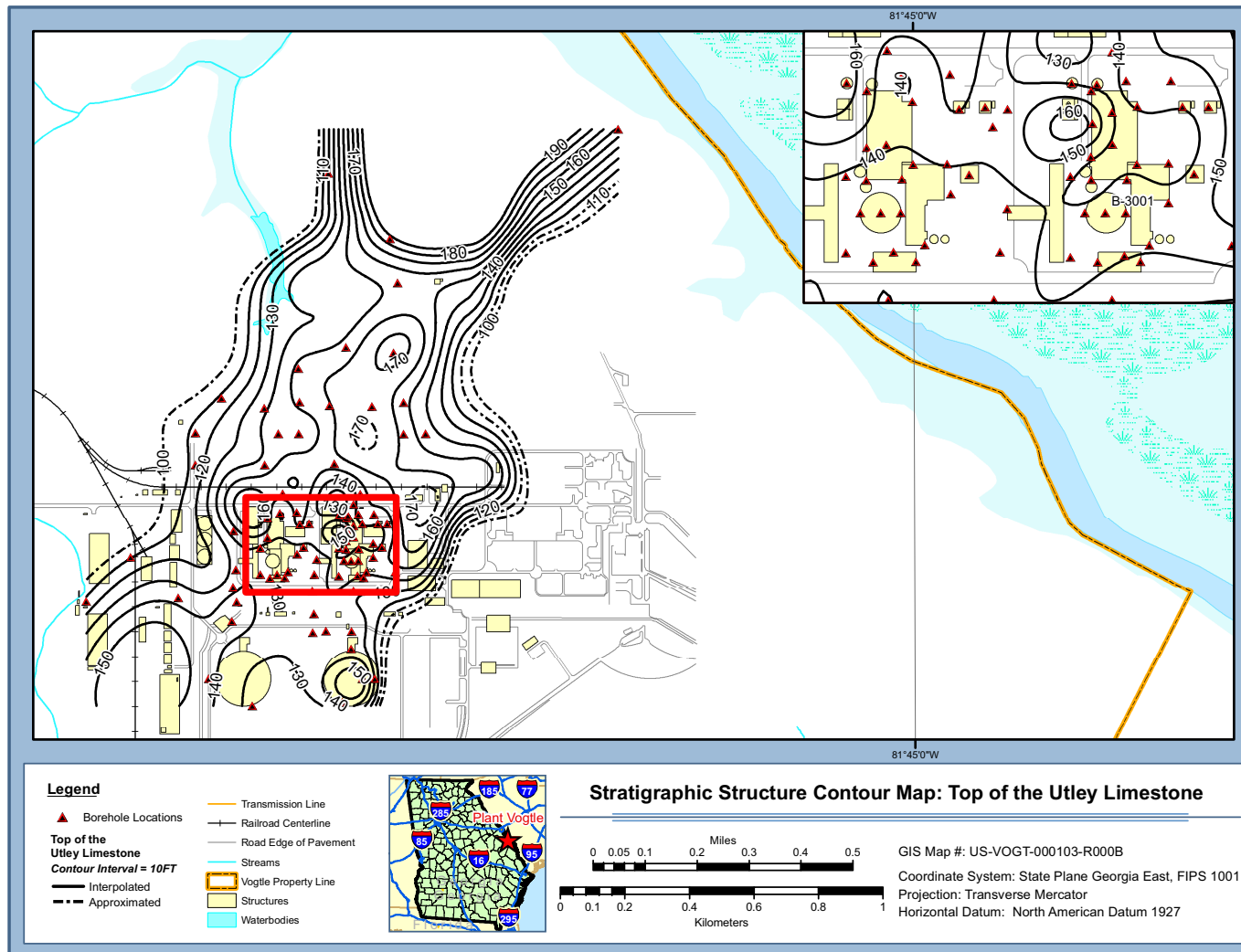


Figure 2.5-255
Stratigraphic Structure Contour Map: Top of the Utley Limestone

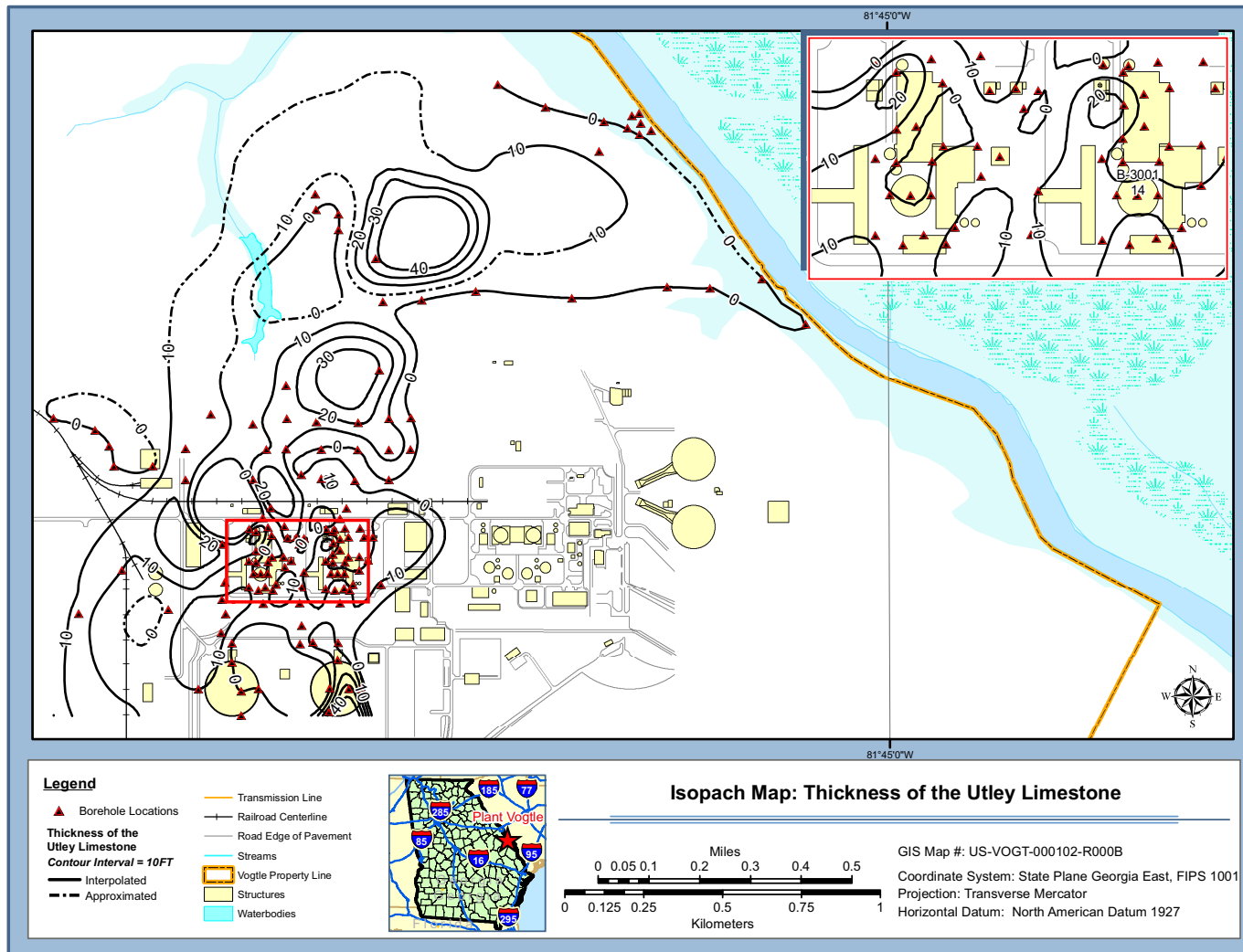


Figure 2.5-256
Isopach Map: Thickness of the Utley Limestone

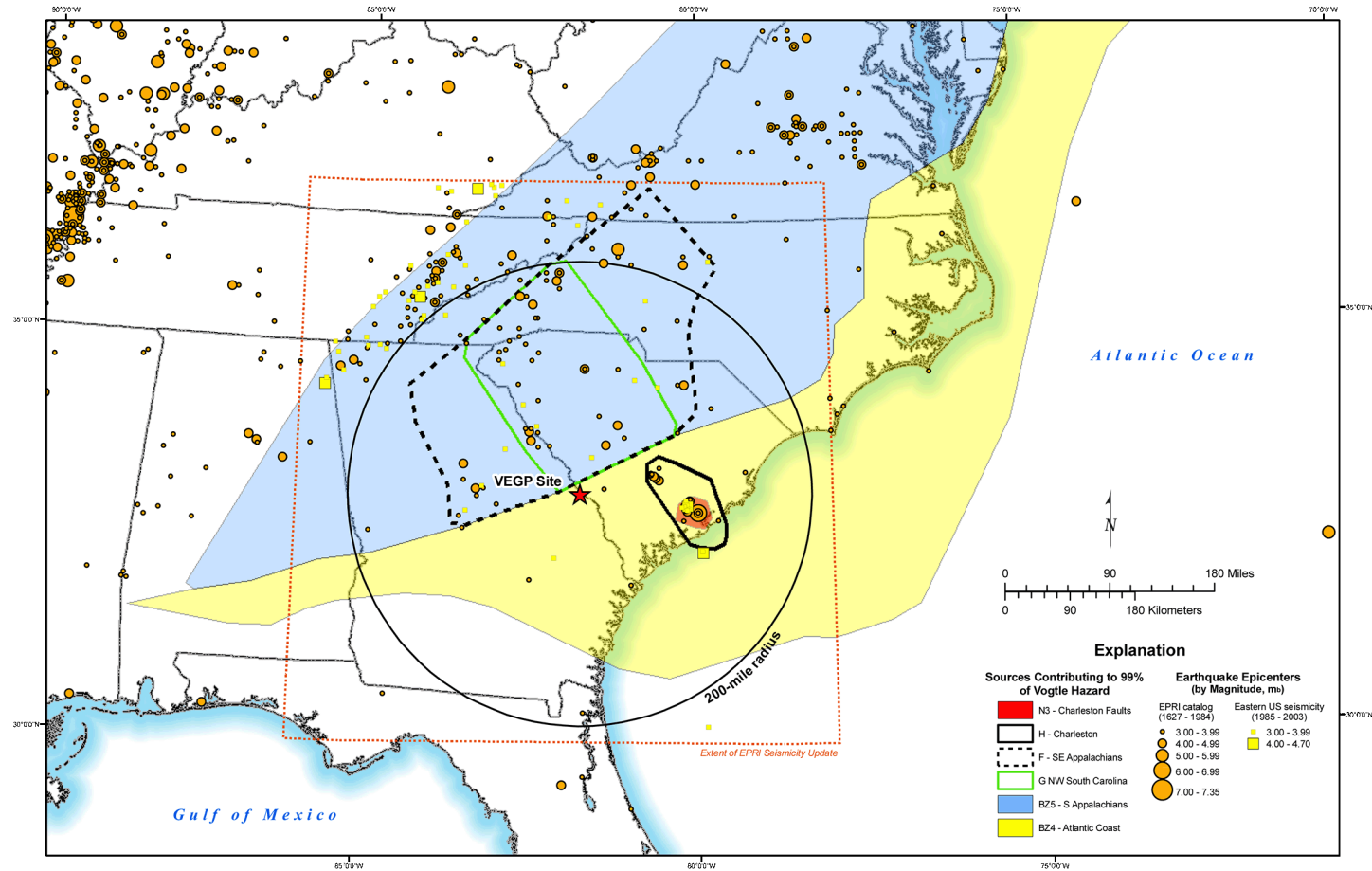


Figure 2.5-257
Bechtel EPRI Zones

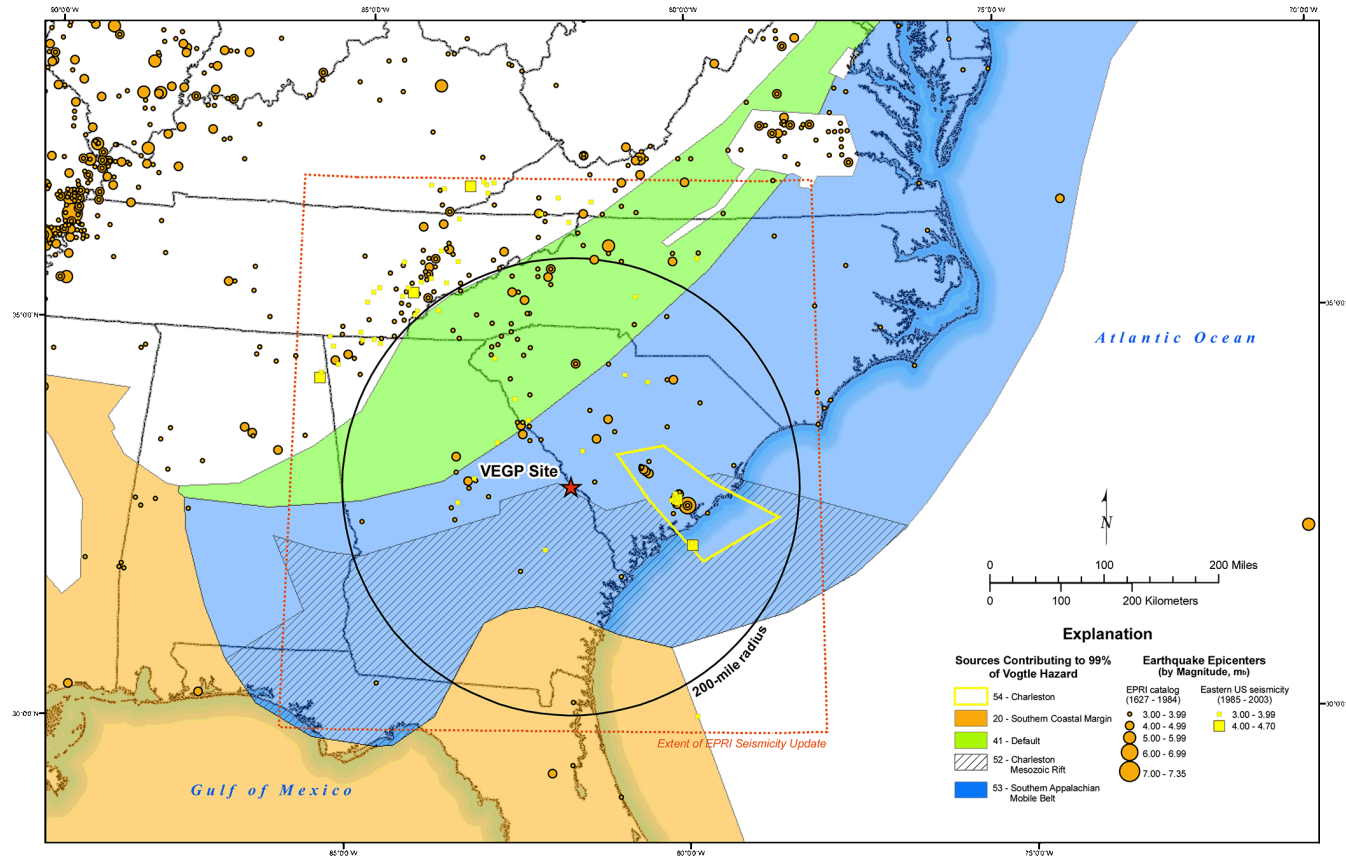


Figure 2.5-258
Dames and Moore EPRI Zones

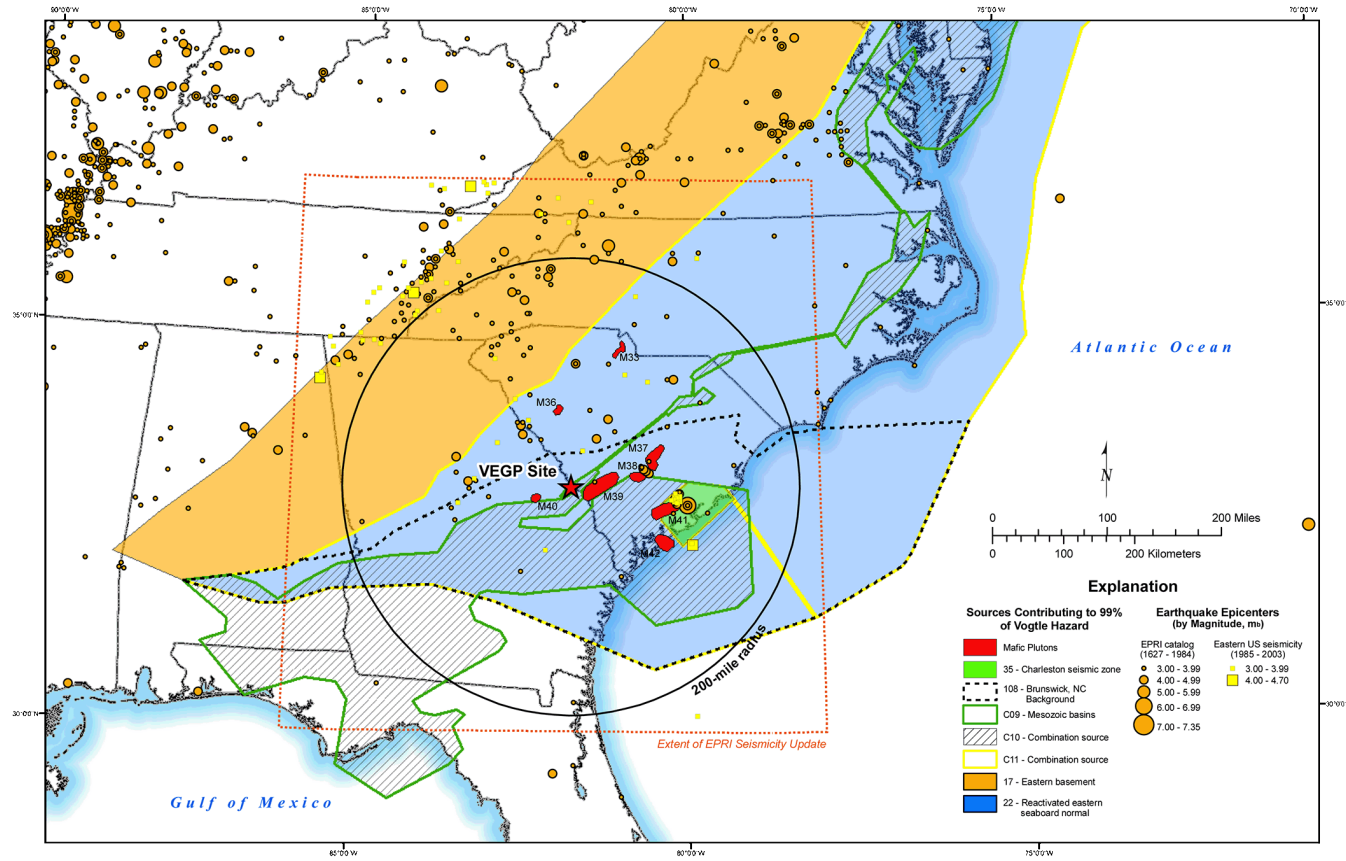


Figure 2.5-259
Law EPRI Zones

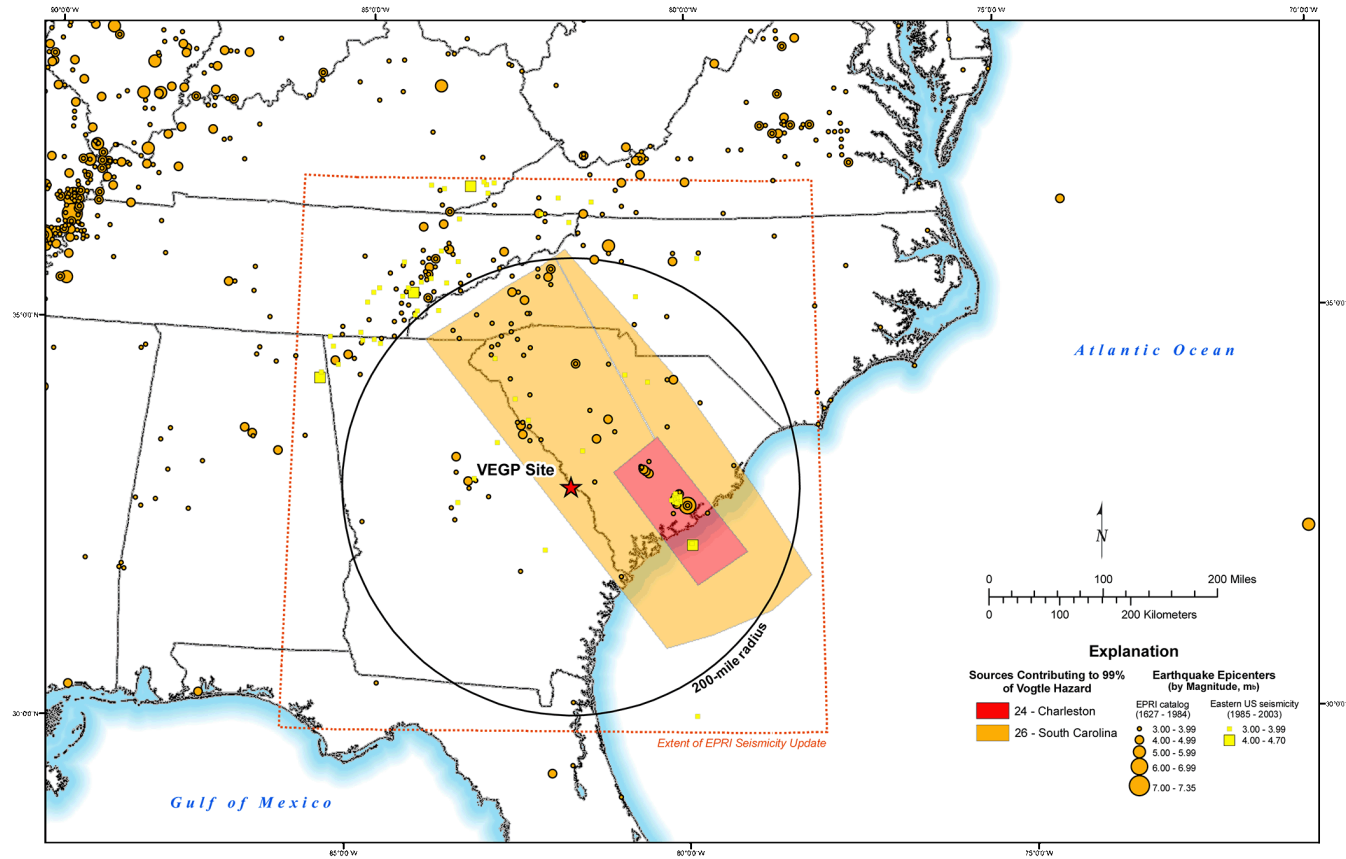


Figure 2.5-260
Rondout EPRI Zones

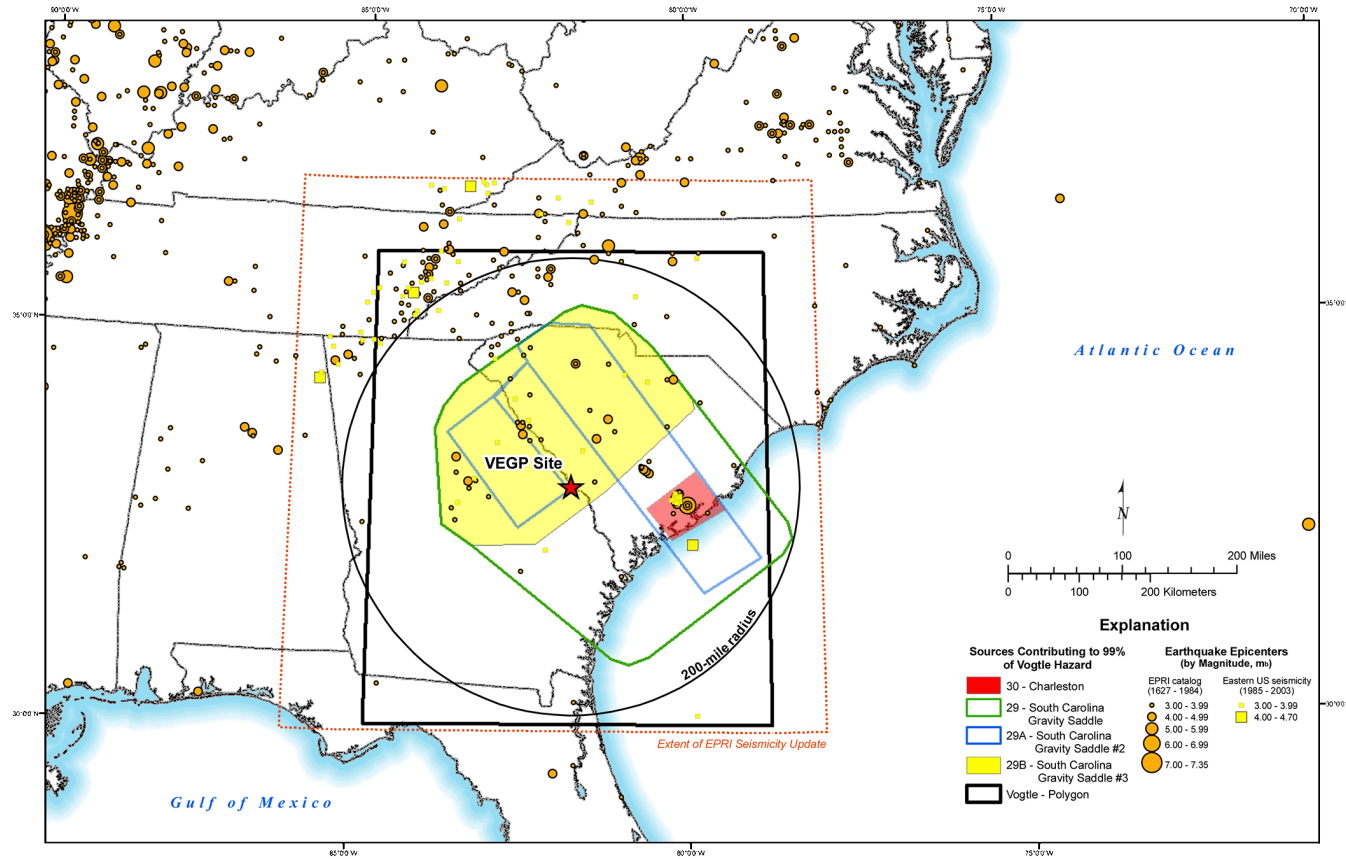


Figure 2.5-261
Woodward-Clyde EPRI Zones

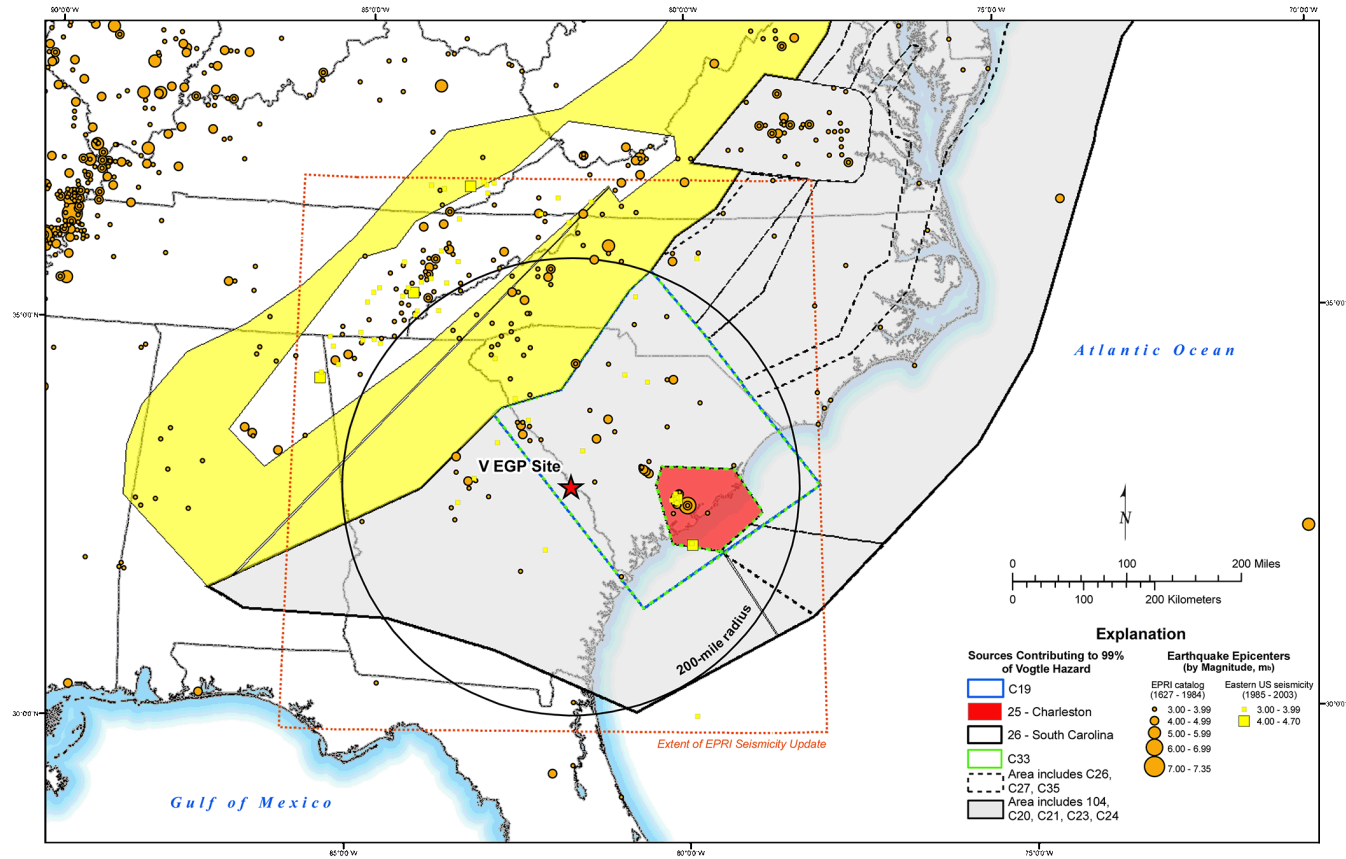


Figure 2.5-262
Weston EPRI Zones

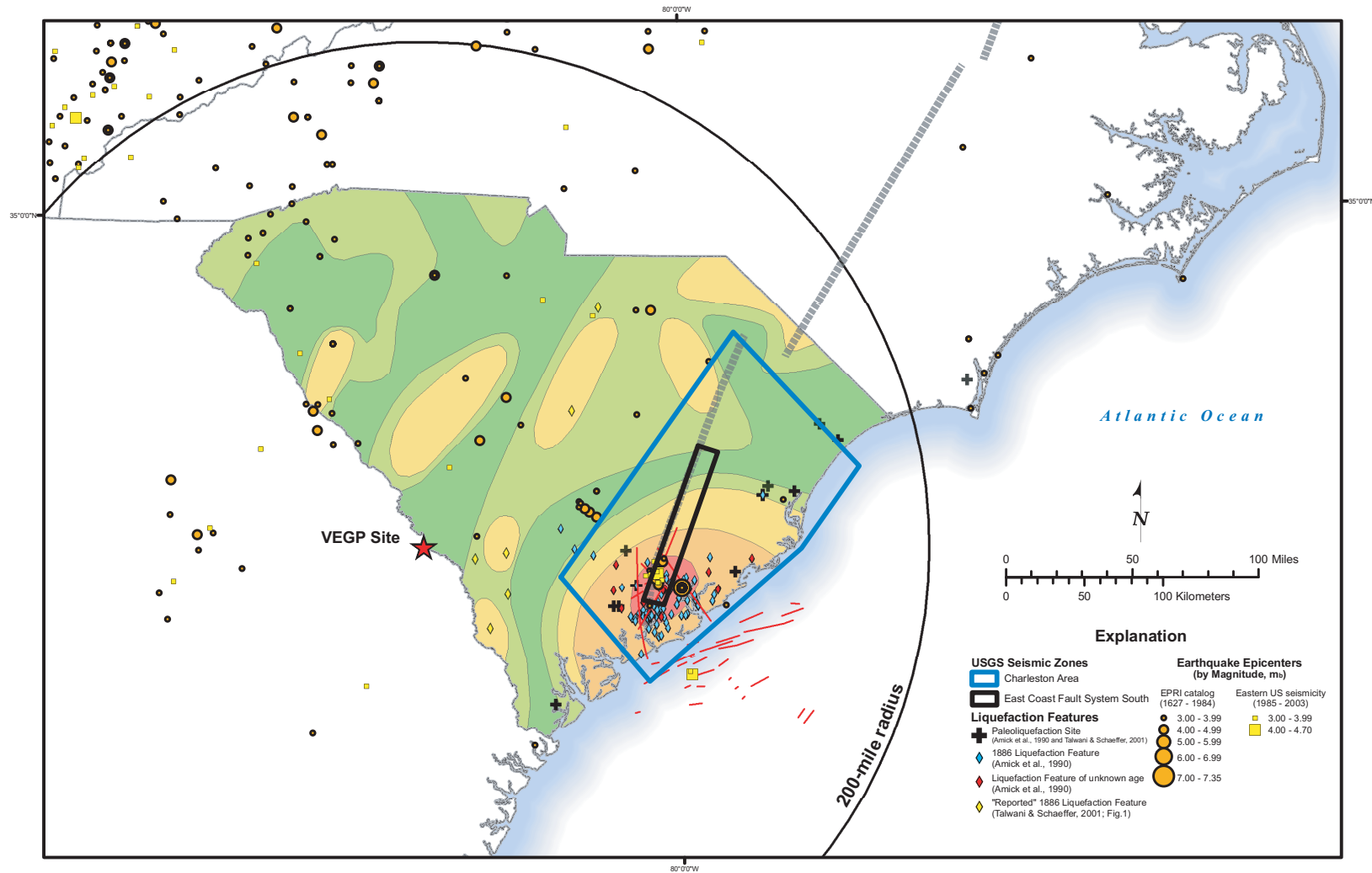


Figure 2.5-263
USGS Model

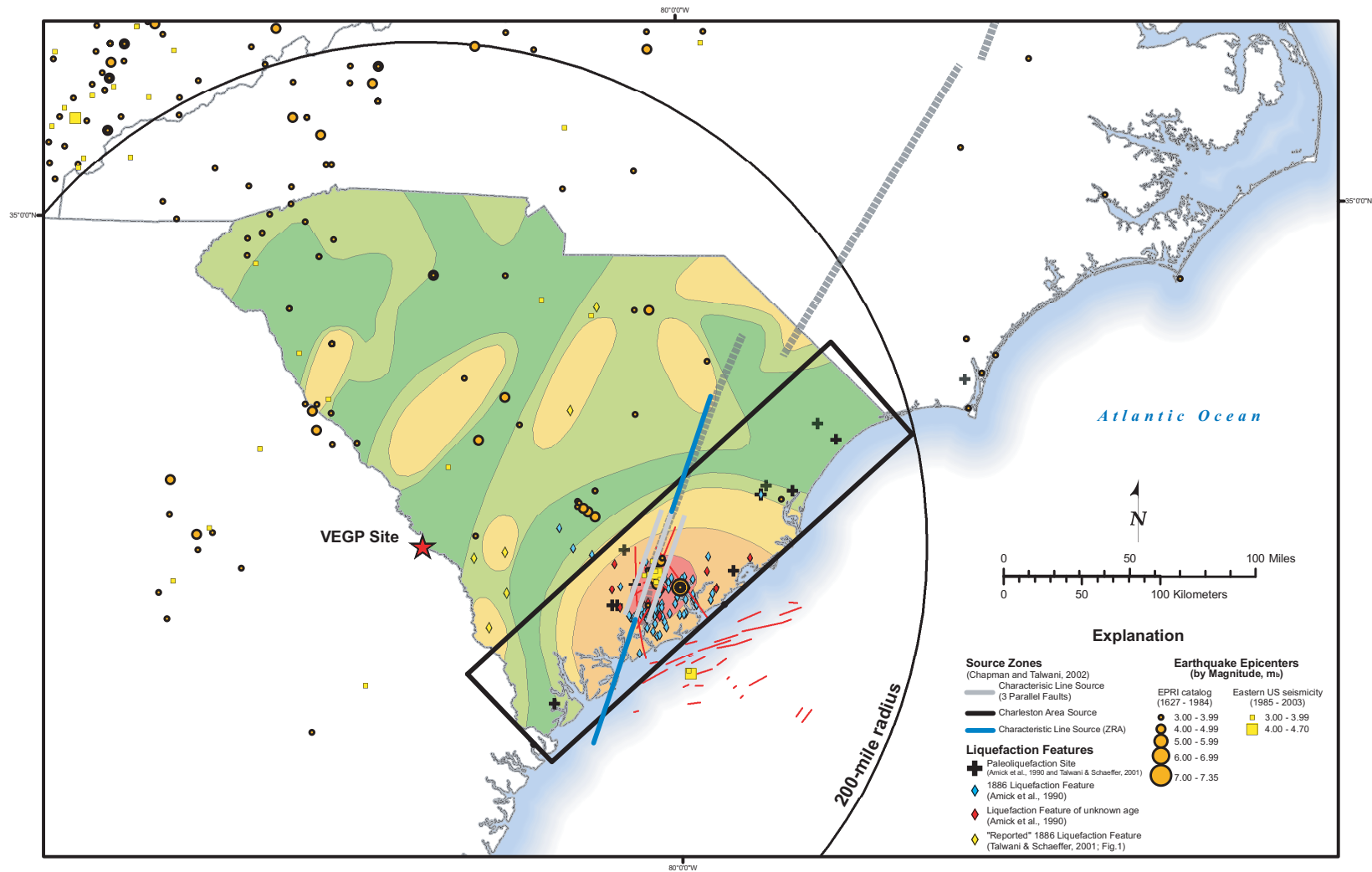


Figure 2.5-264
SCDOT Model

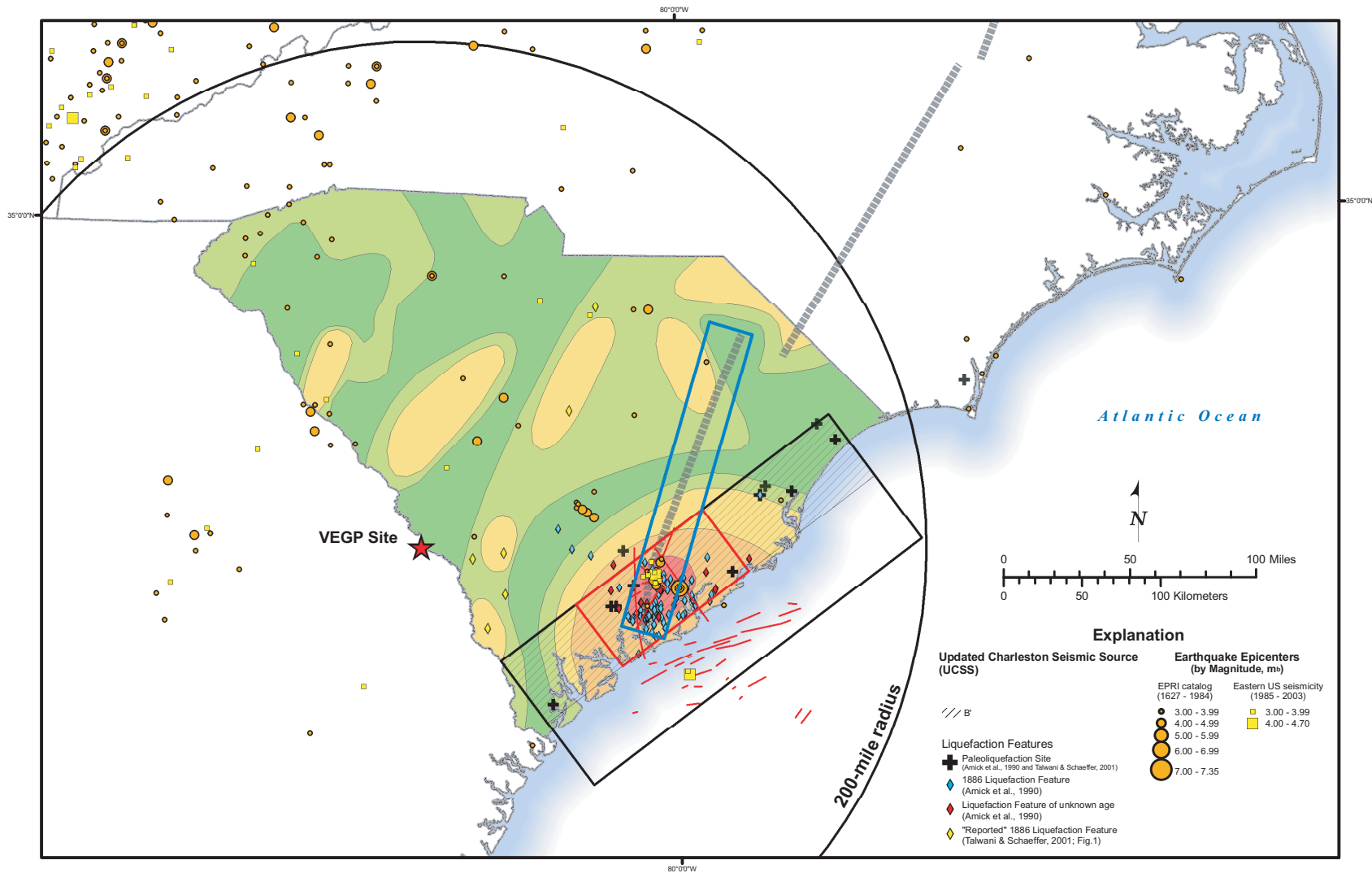


Figure 2.5-265
UCSS Map

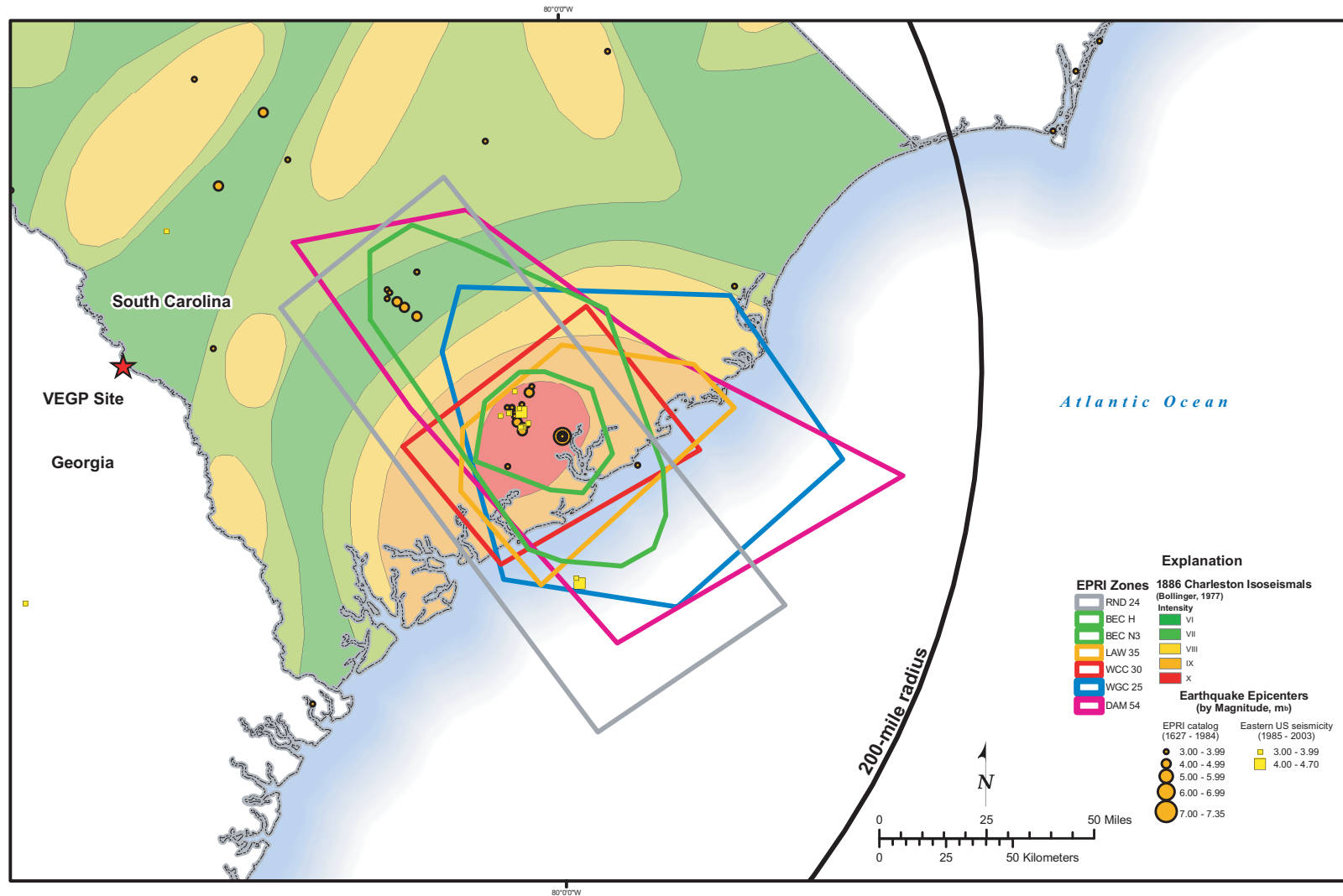


Figure 2.5-266
EPRI All Charleston Map

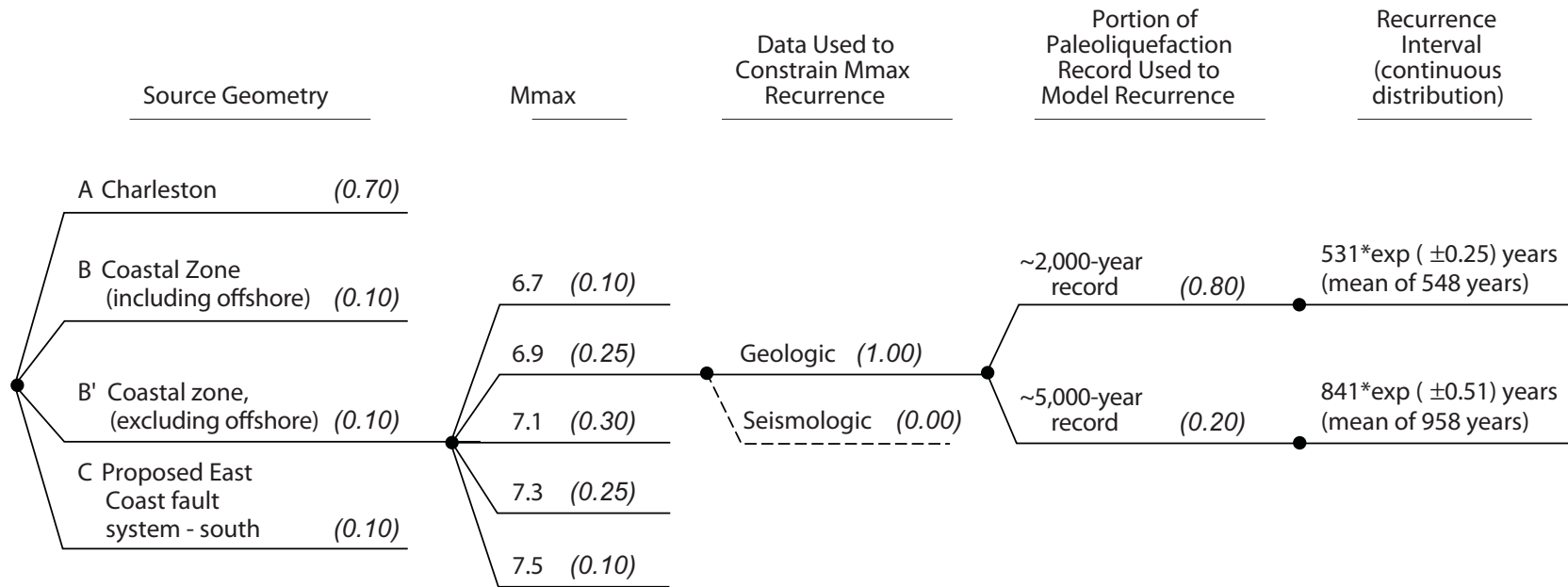
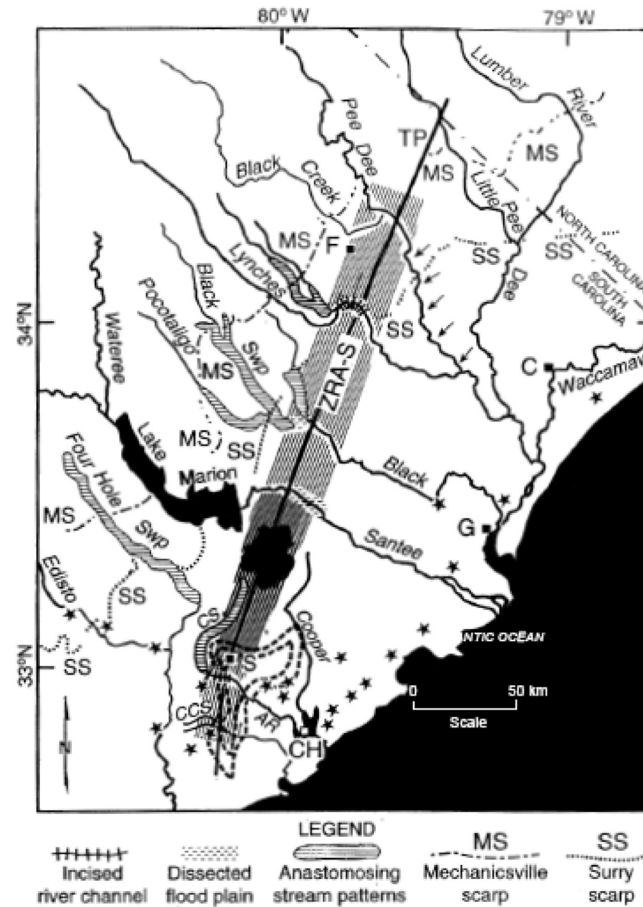


Figure 2.5-267
Updated Charleston Seismic Source (USGS) Logic Tree
with Weights for each Branch Shown in Italics



Map of ZRA-S from Marple and Talwani (2000). Figure shows southern zone of river anomalies (ZRA-S; striped area), anastomosing stream patterns, pre 1886 sandblow sites (stars), and topographic profile (TP, bold line) approximately along the ZRA-S axis. Arrows along Pee Dee River denote reach flowing against southwest valley wall. Closed dashed contours near Summerville are highest-intensity isoseismals of the 1886 Charleston, South Carolina, earthquake (from Dutton, 1889). Abbreviations are as follows: AR - Ashley River; C - Conway; CCS - Caw Caw Swamp; CH - Charleston; CS - Cypress Swamp; F - Florence; G - Georgetown; LM - Lake Moultrie; MS - Mechanicsville littoral scarp; S - Summerville; SS - Surry littoral scarp.

Figure 2.5-268
Map of ZRA-S from Marple and Talwani (2000)

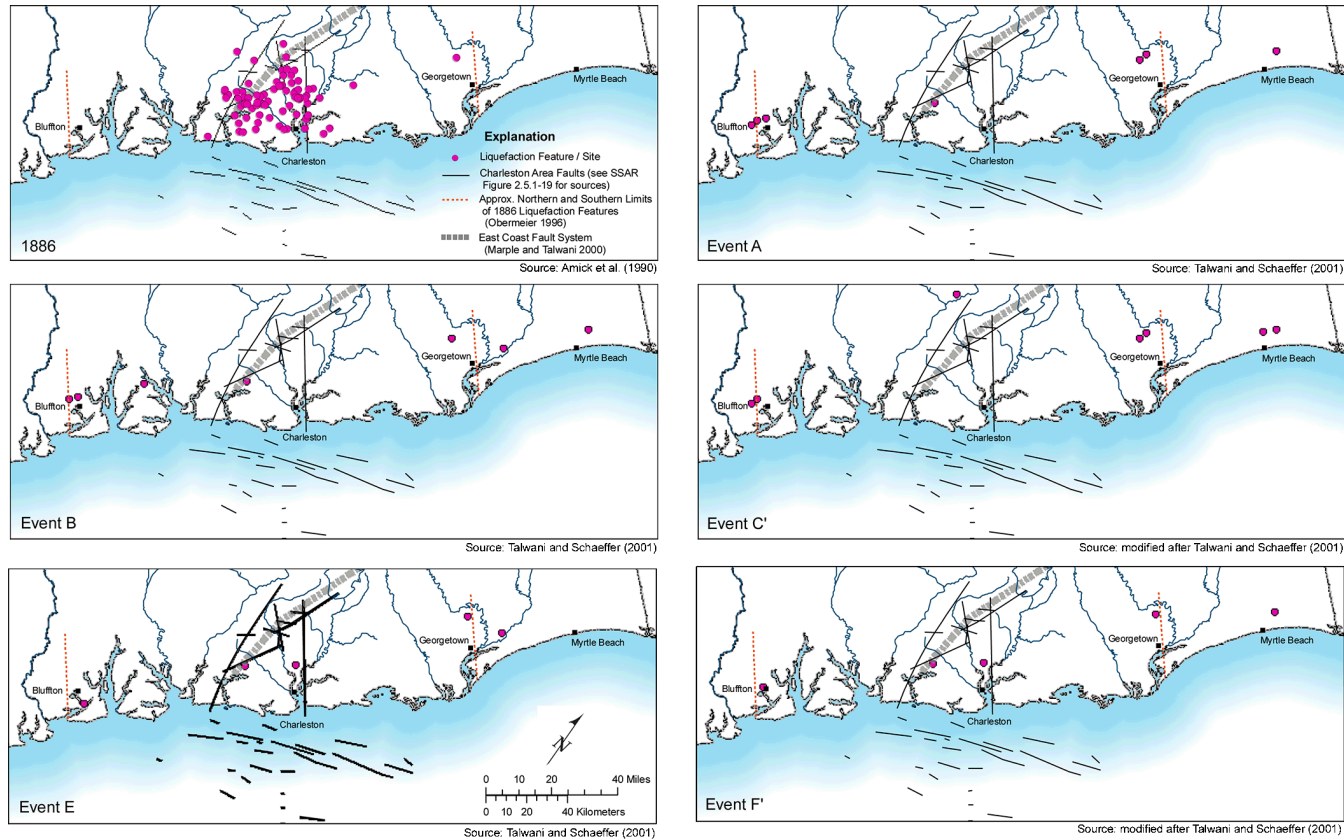


Figure 2.5-269
Geographic Distribution of Liquefaction Features
Associated with Charleston Earthquakes

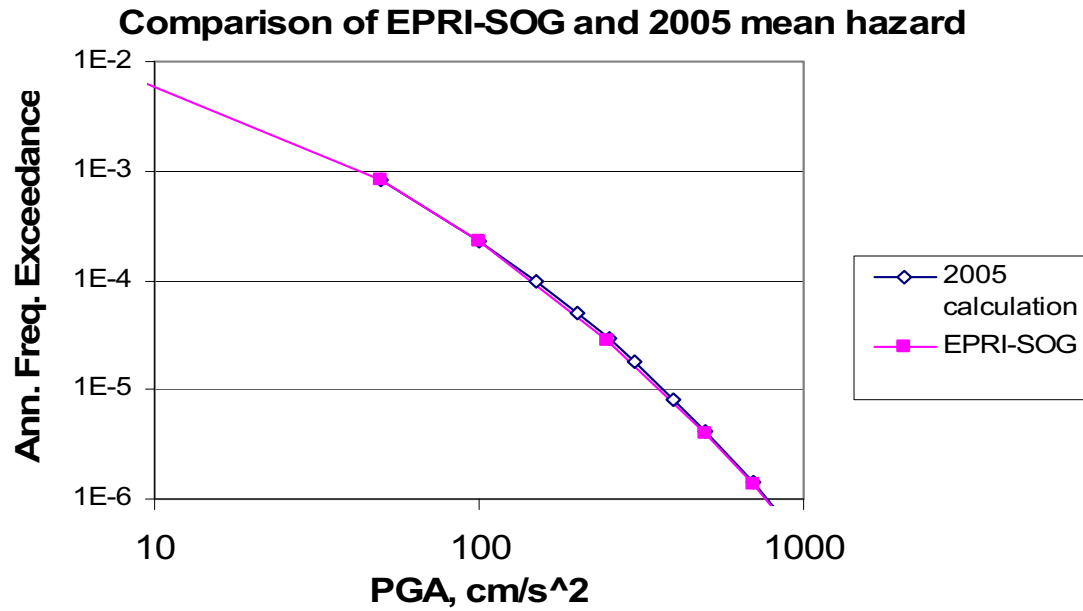


Figure 2.5-270
PGA Mean Seismic Hazard Curves for
Current (2005) Calculation and for EPRI-SOG

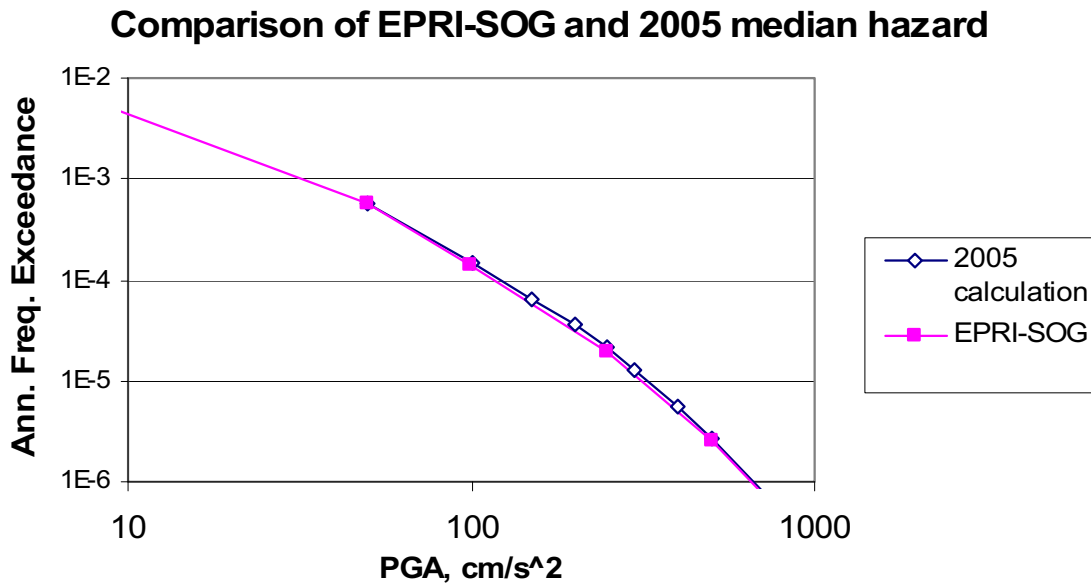


Figure 2.5-271
PGA Median Seismic Hazard Curves for
Current (2005) Calculation and for EPRI-SOG

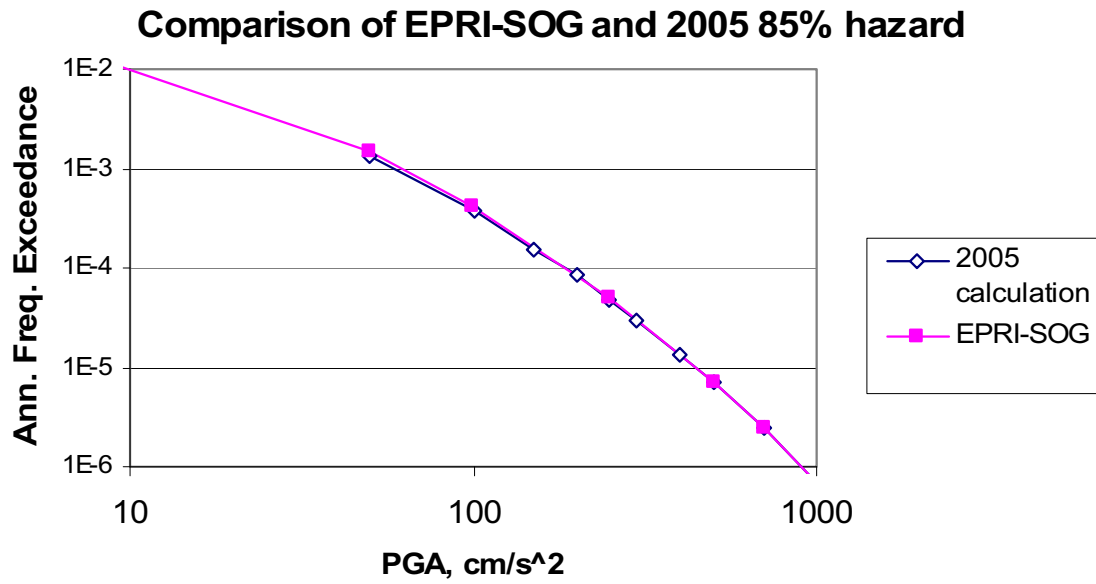


Figure 2.5-272
PGA 85 Percent Seismic Hazard Curves
for Current (2005) Calculation and for EPRI-SOG

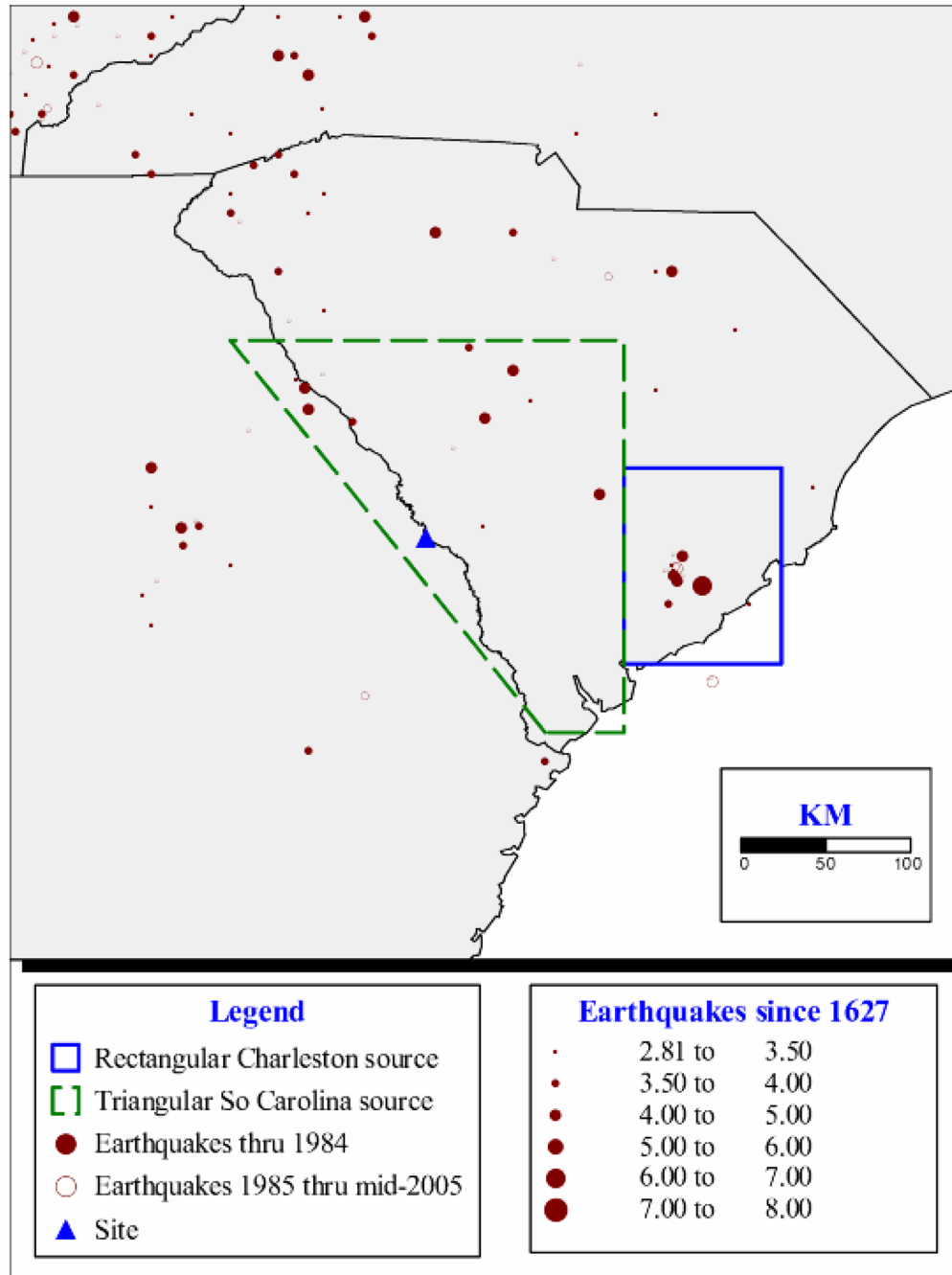


Figure 2.5-273
Map Showing Two Areas Used To Examine
Effect of New Seismicity Information

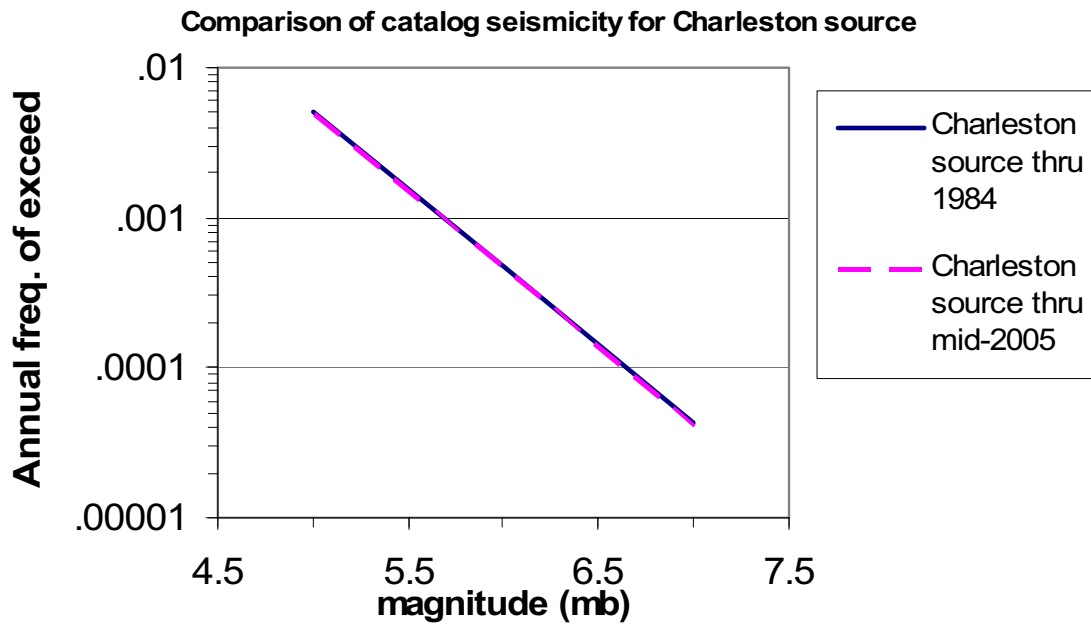


Figure 2.5-274
Comparison of Recurrence Rates for Rectangular Charleston Source

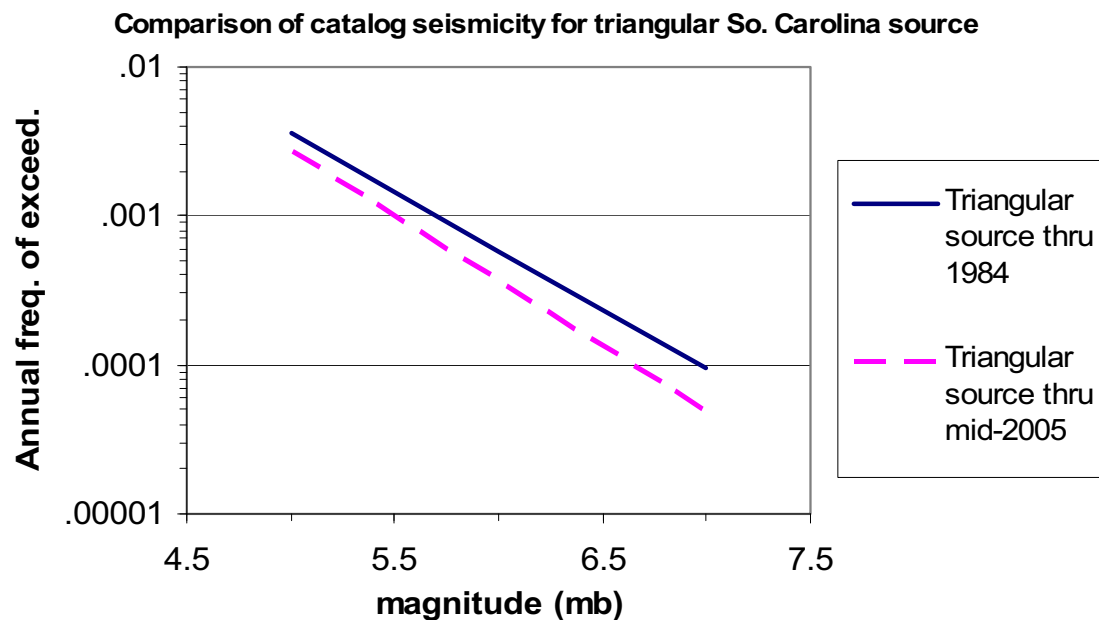


Figure 2.5-275
Comparison of Recurrence Rates for Triangular South Carolina Source

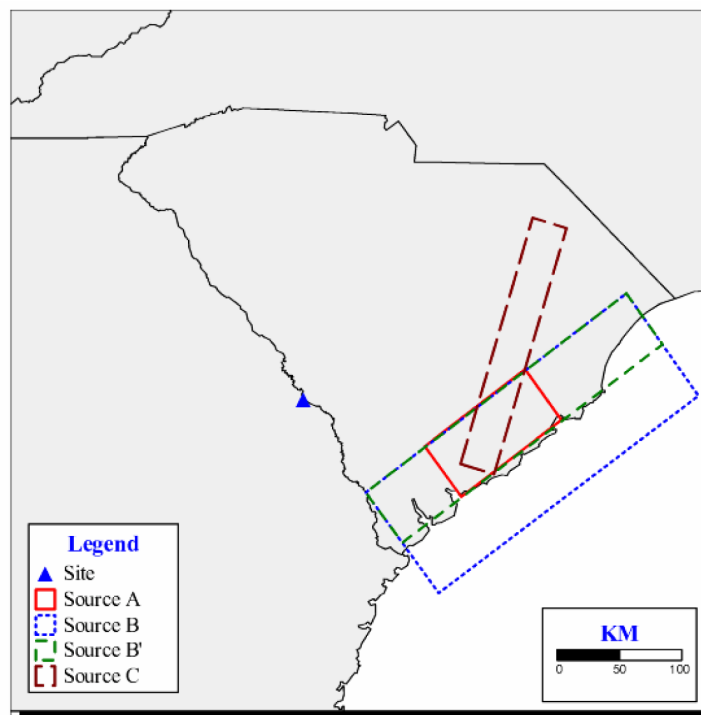


Figure 2.5-276
Geometry of Four New Charleston Sources

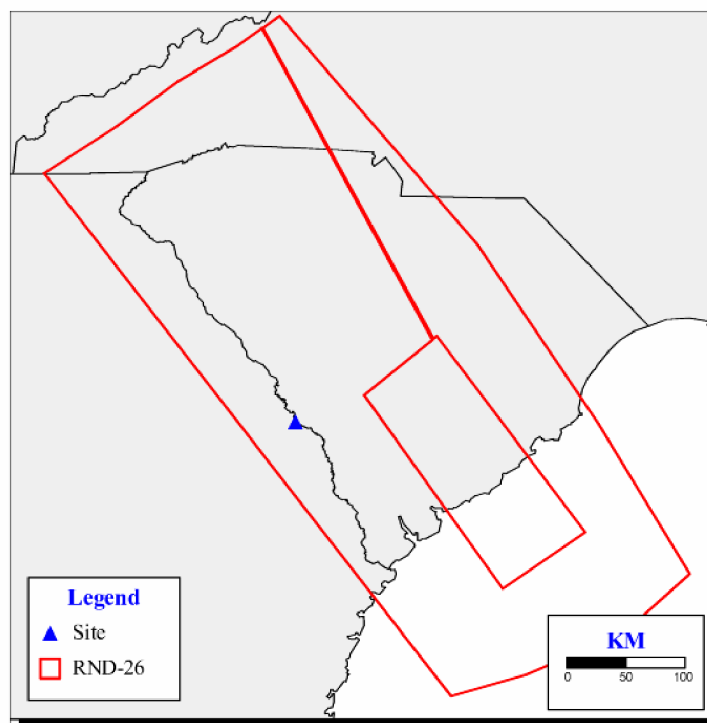


Figure 2.5-277
Original Rondout Source 26

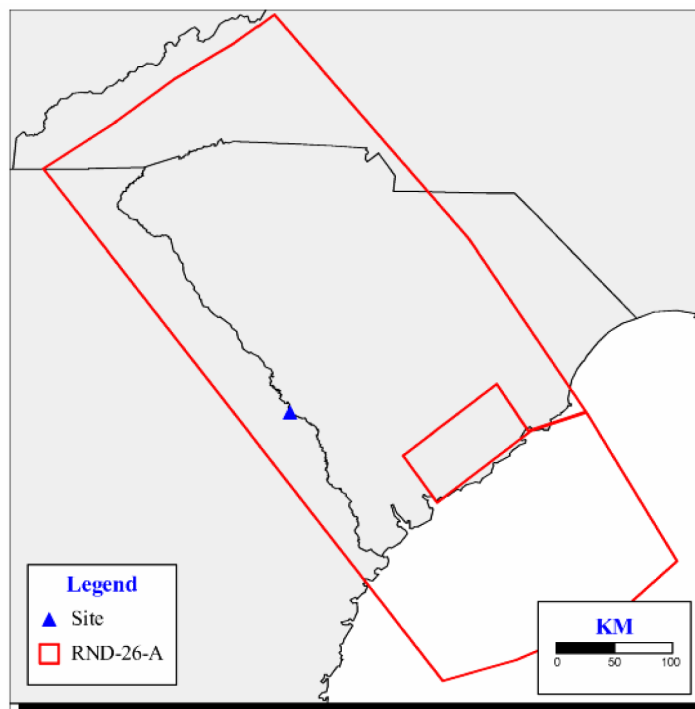


Figure 2.5-278
New Rondout Source 26-A that Surrounds Charleston Source A

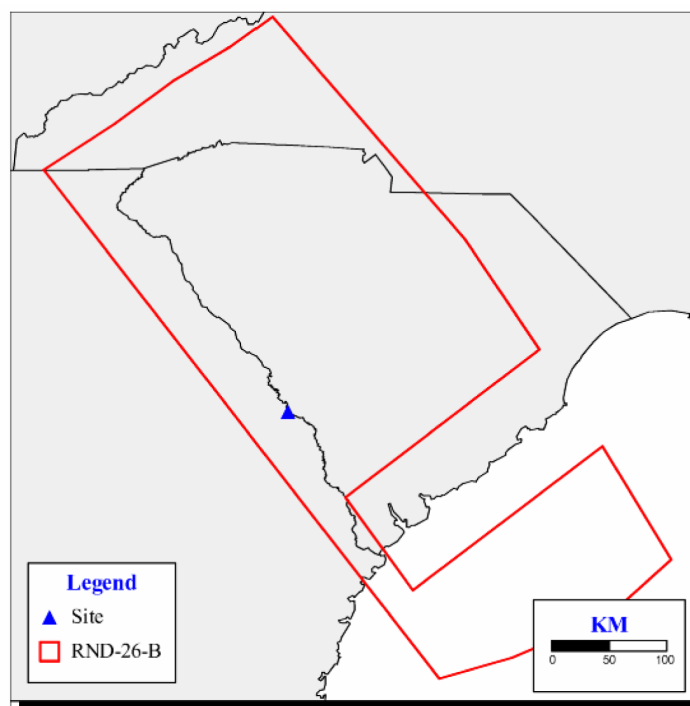


Figure 2.5-279
New Rondout Source 26-B that Surrounds Charleston Source B

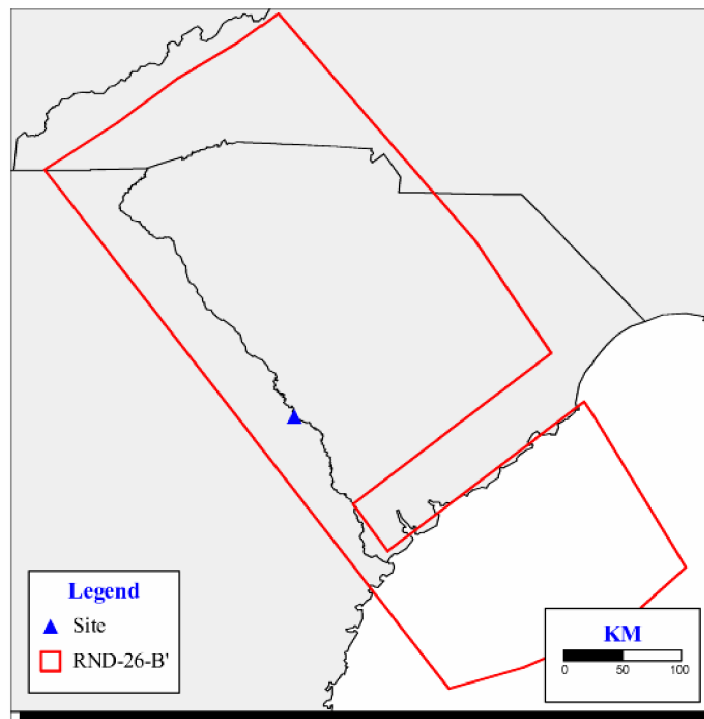


Figure 2.5-280
New Rondout Source 26-B' that Surrounds Charleston Source B

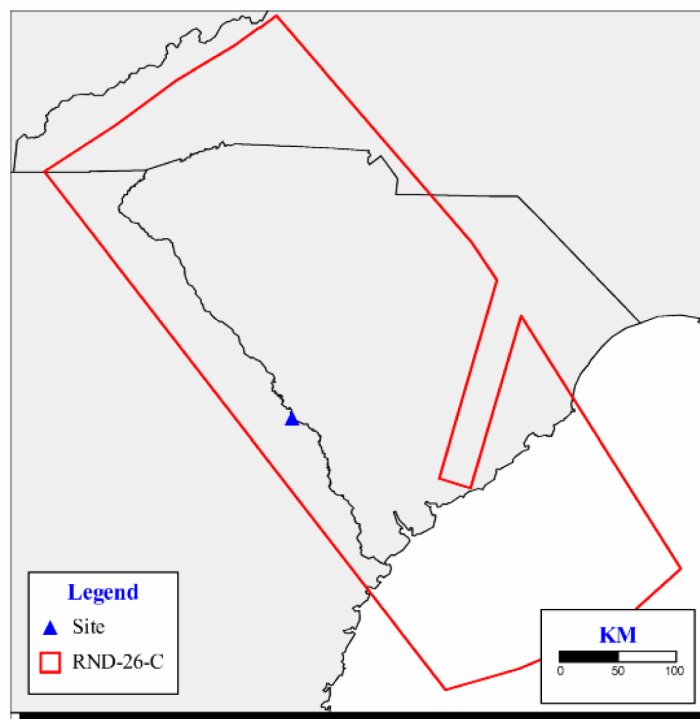


Figure 2.5-281
New Rondout Source 26-C that Surrounds Charleston Source C

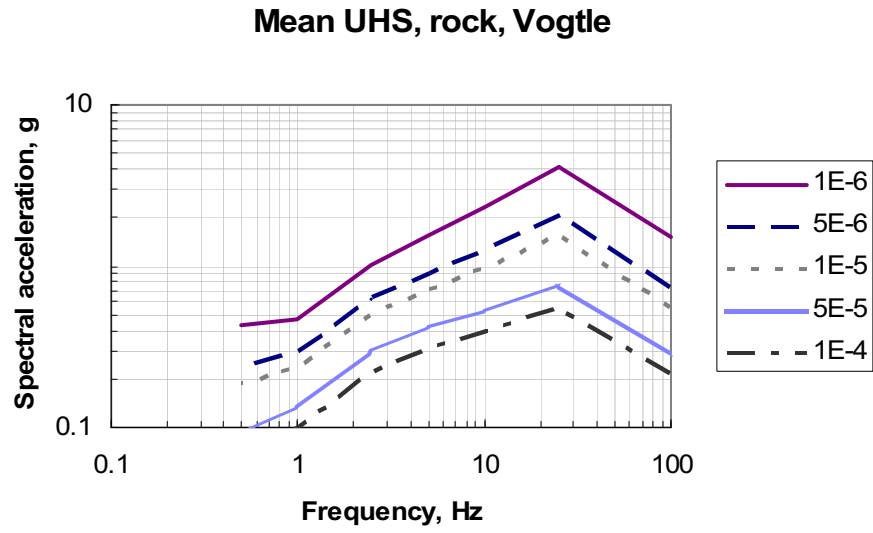


Figure 2.5-282

Mean Uniform Hazard Spectra, Hard Rock Conditions, for VEGP ESP

High Frequency, $1.0\text{e-}4$

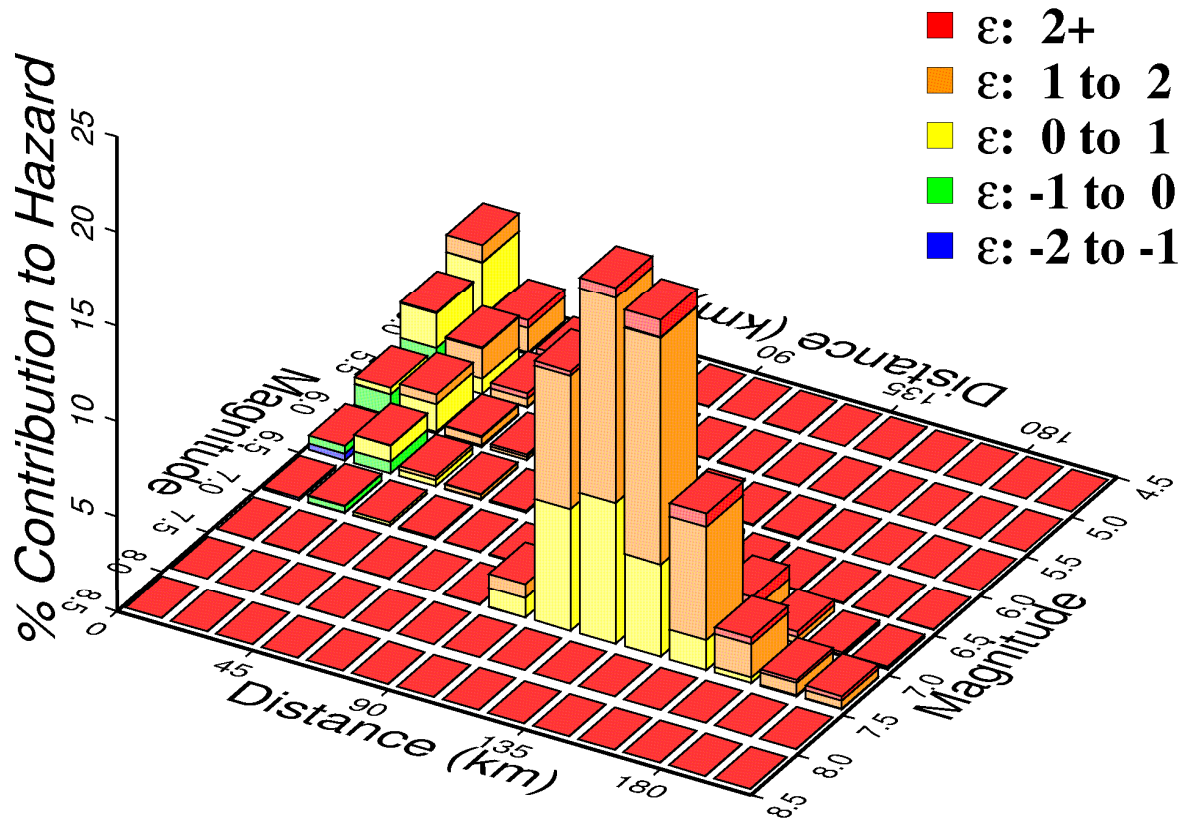


Figure 2.5-283
Hard Rock Magnitude-Distance Deaggregation for High Frequencies,
 10^{-4} Mean Annual Frequency of Exceedance

Low Frequency, 1.0e-4

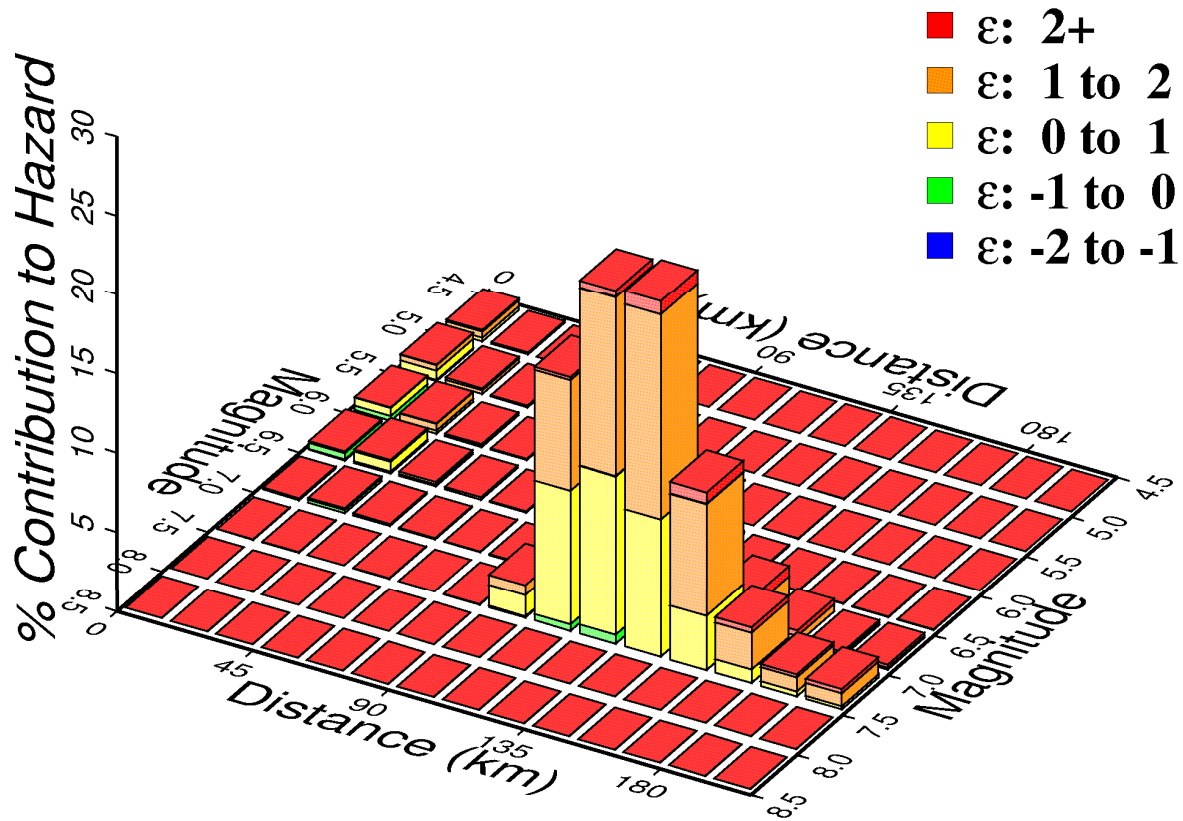


Figure 2.5-284
Hard Rock Magnitude-Distance Deaggregation for Low Frequencies,
 10^{-4} Mean Annual Frequency of Exceedance

High Frequency, 1.0×10^{-5}

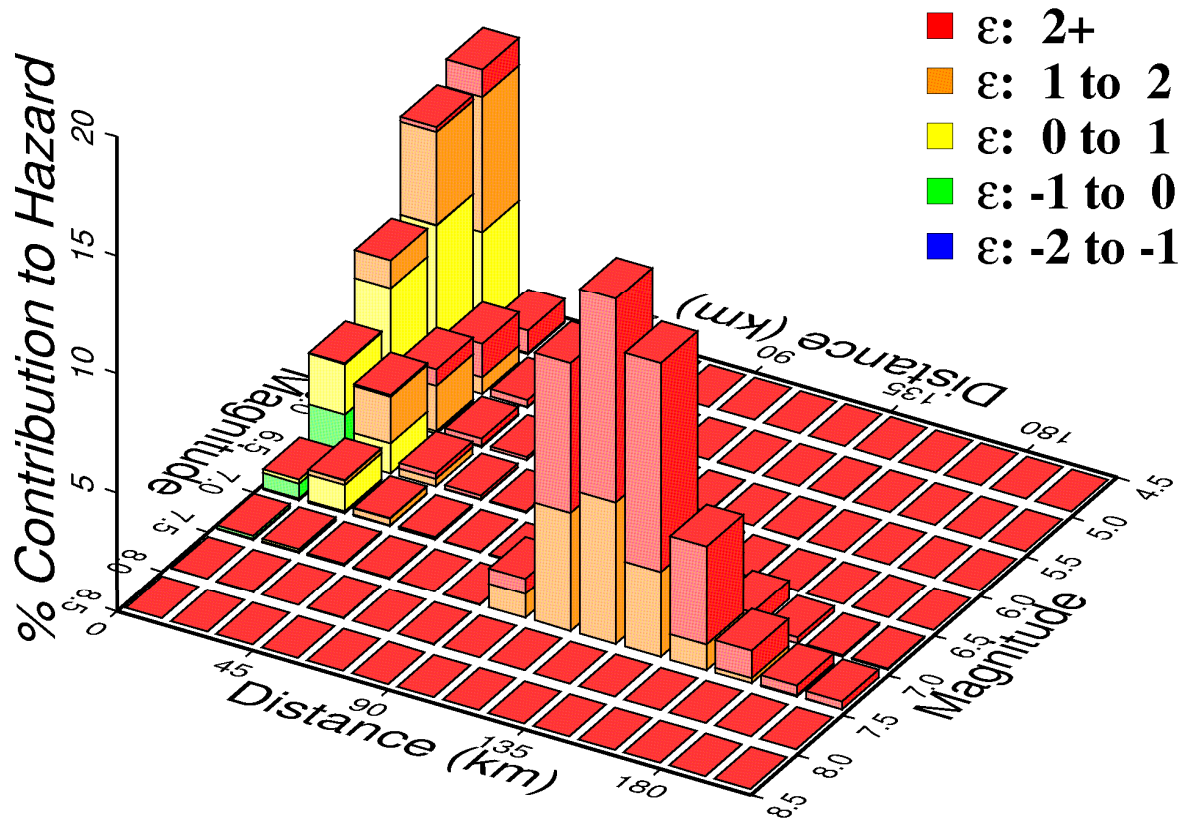


Figure 2.5-285
Hard Rock Magnitude-Distance Deaggregation for High Frequencies,
 10^{-5} Mean Annual Frequency of Exceedance

Low Frequency, $1.0\text{e-}5$

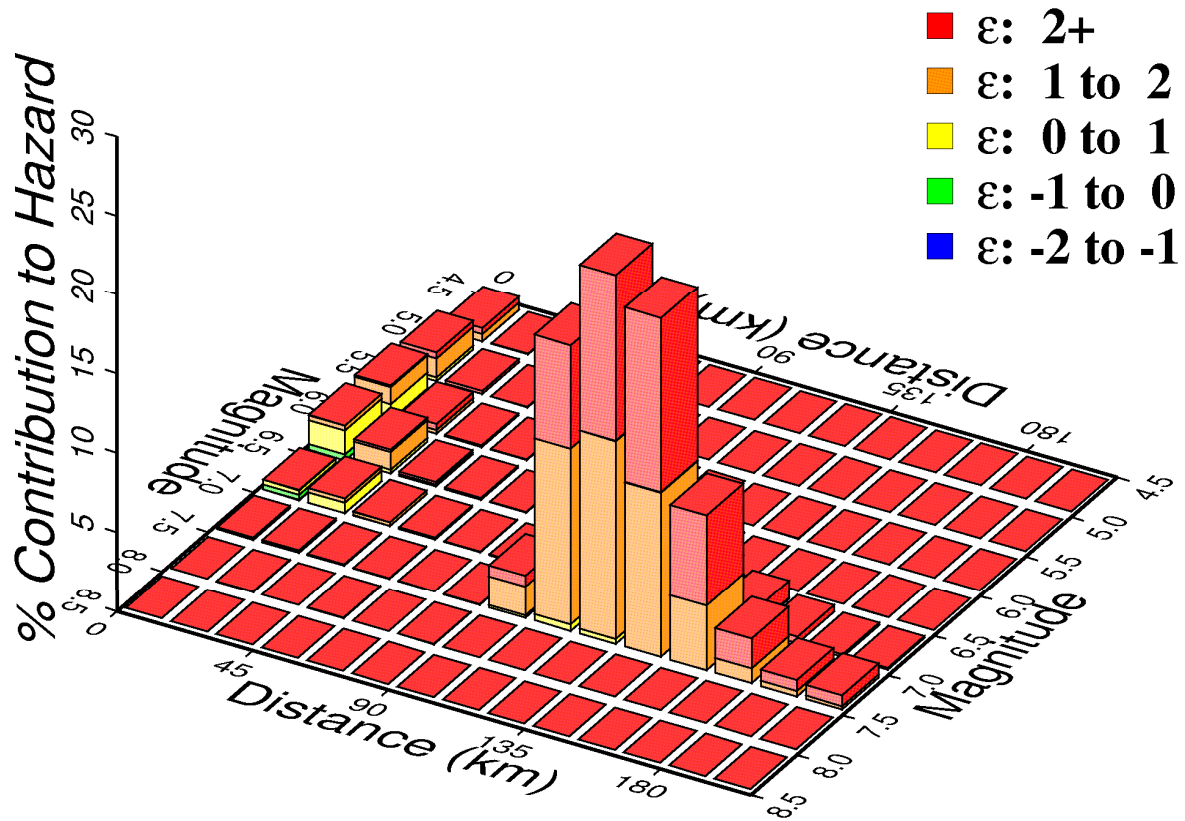


Figure 2.5-286
Hard Rock Magnitude-Distance Deaggregation For Low Frequencies,
 10^{-5} Mean Annual Frequency of Exceedance

High Frequency, $1.0\text{e-}6$

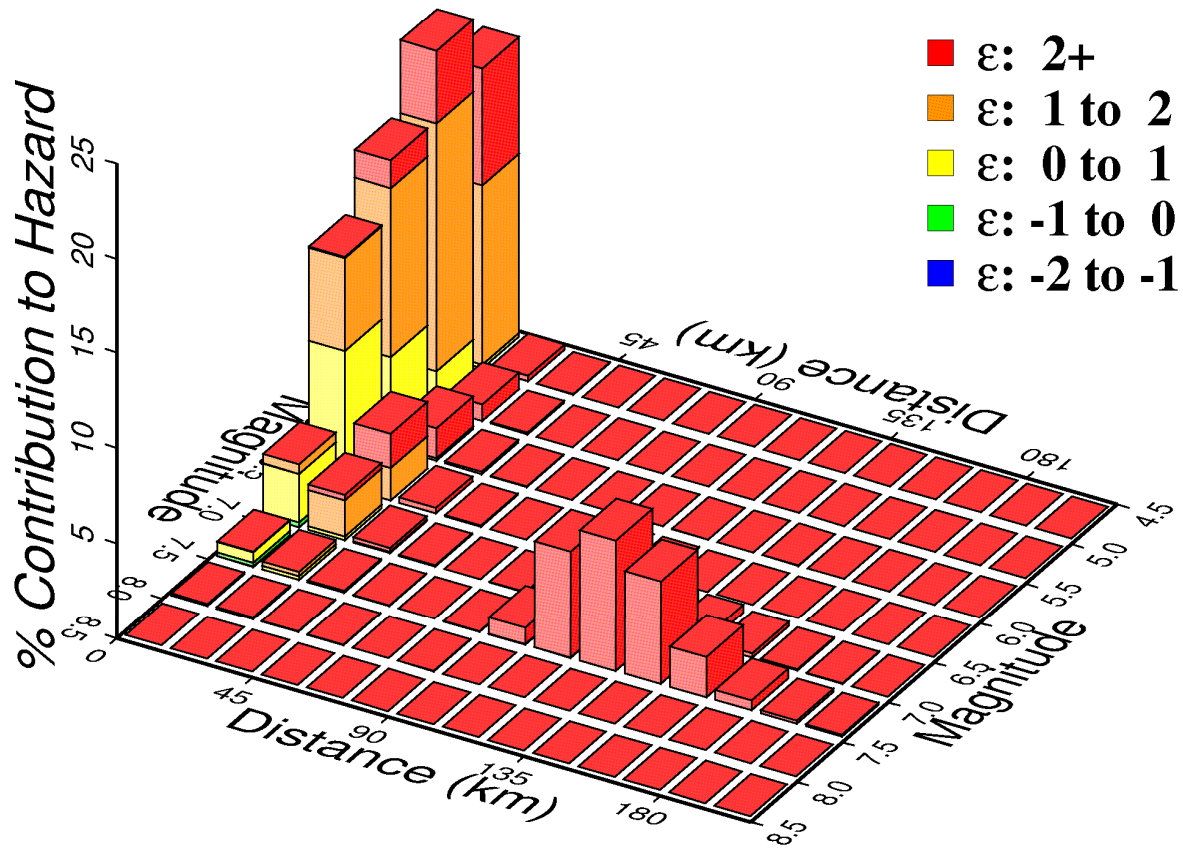


Figure 2.5-287
Hard Rock Magnitude-Distance Deaggregation for High Frequencies,
 10^{-6} Mean Annual Frequency of Exceedance

Low Frequency, 1.0e-6

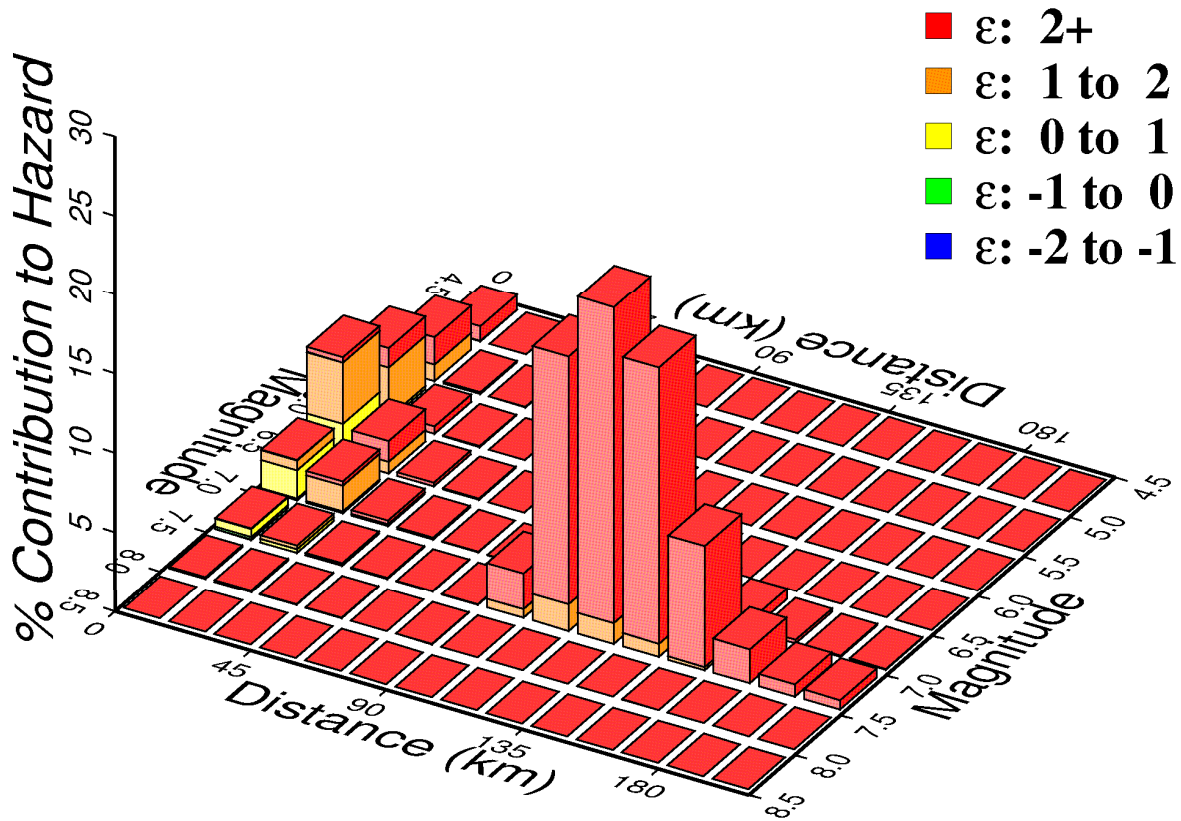


Figure 2.5-288
Hard Rock Magnitude-Distance Deaggregation for Low Frequencies,
 10^{-6} Mean Annual Frequency of Exceedance

High-frequency magnitude (Mw) deaggregations

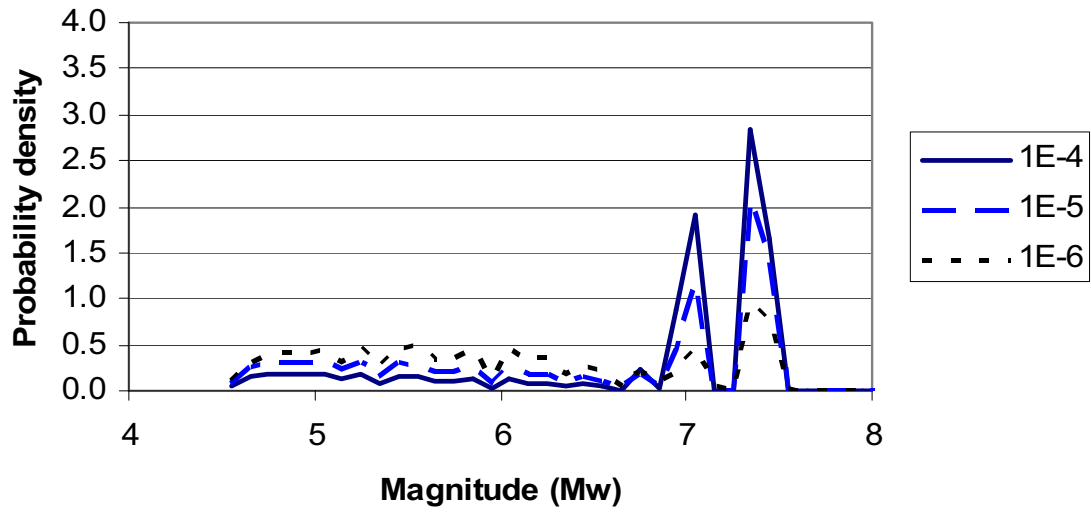


Figure 2.5-289
Magnitude Deaggregation for High Frequencies
for Three Mean Annual Frequencies of Exceedance

Low-frequency magnitude (Mw) deaggregations

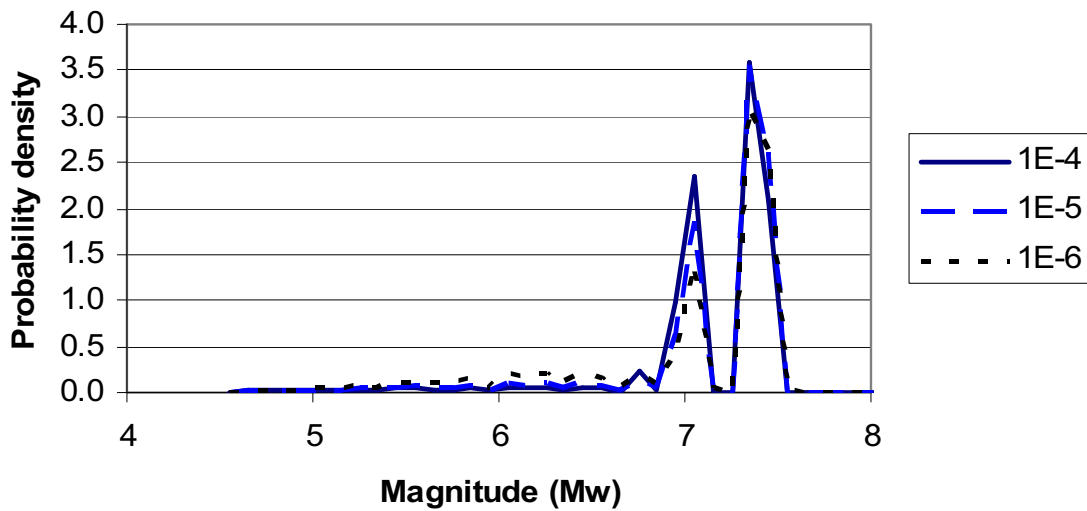


Figure 2.5-290
Magnitude Deaggregation for Low Frequencies
for Three Mean Annual Frequencies of Exceedance

High-frequency distance deaggregations

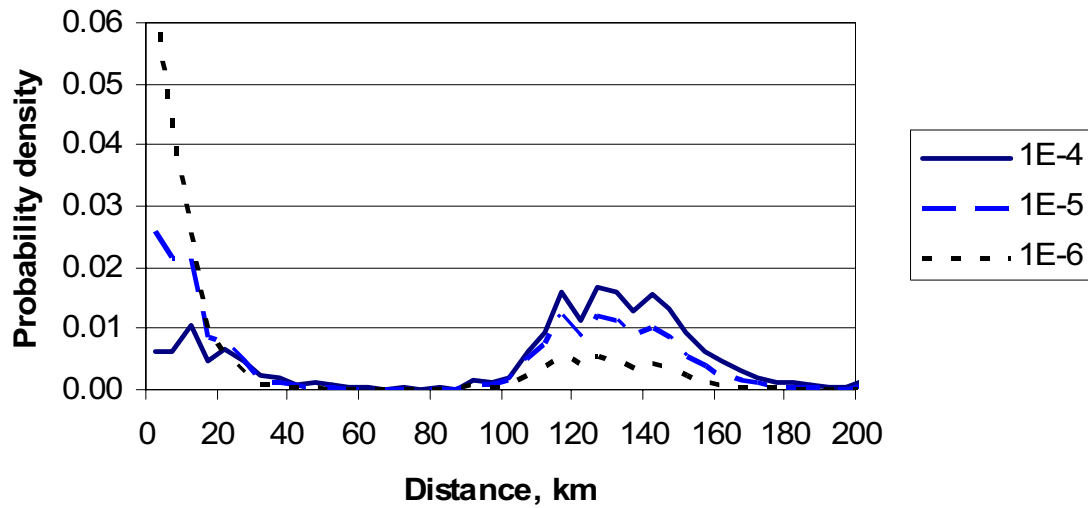


Figure 2.5-291
Hard Rock Distance Deaggregation for High Frequencies
for Three Mean Annual Frequencies of Exceedance

Low-frequency distance deaggregations

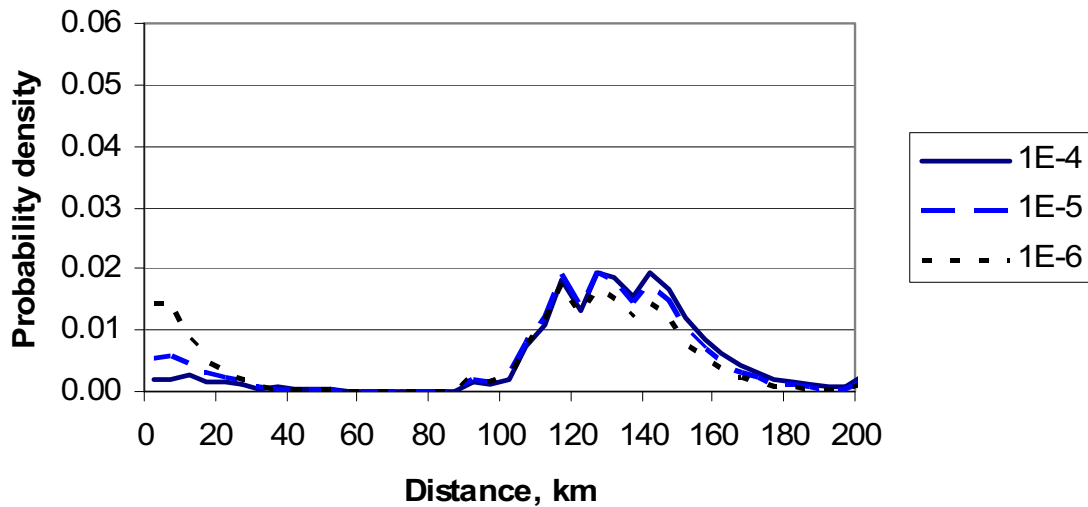


Figure 2.5-292
Hard Rock Magnitude Deaggregation for Low Frequencies
for Three Mean Annual Frequencies of Exceedance

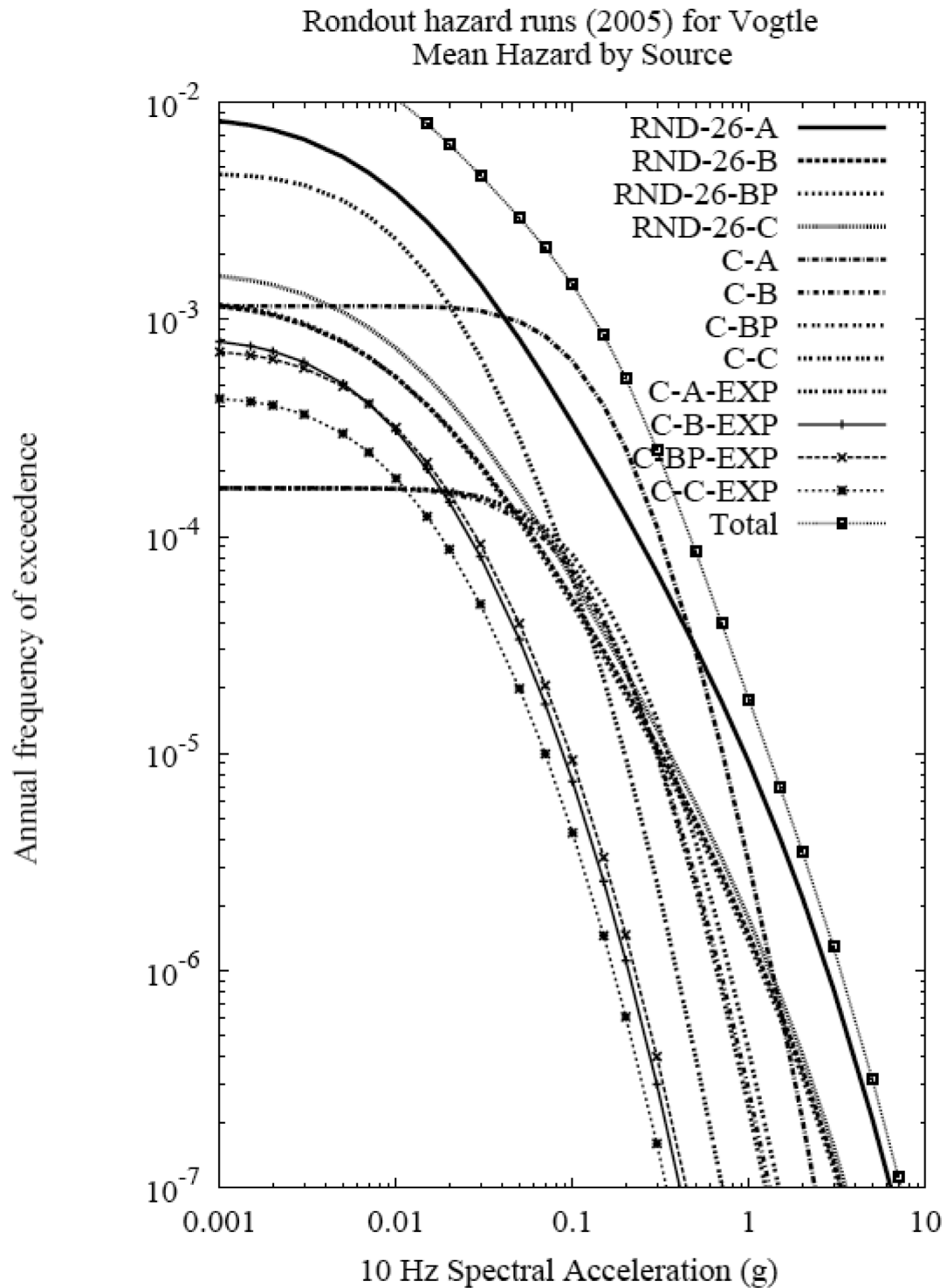


Figure 2.5-293
10 Hz Hard Rock Seismic Hazard Curves
by Seismic Source for Rondout Team

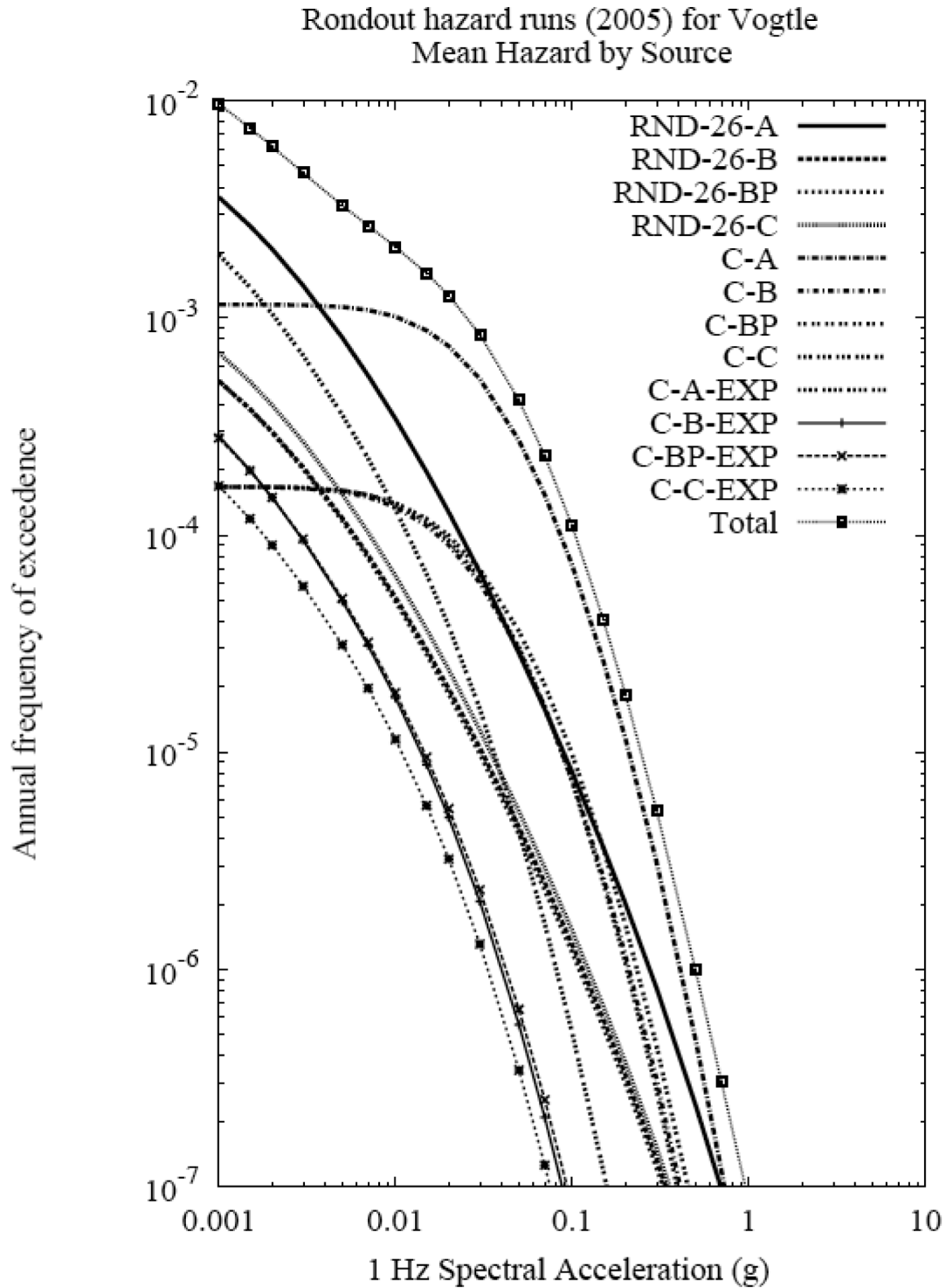
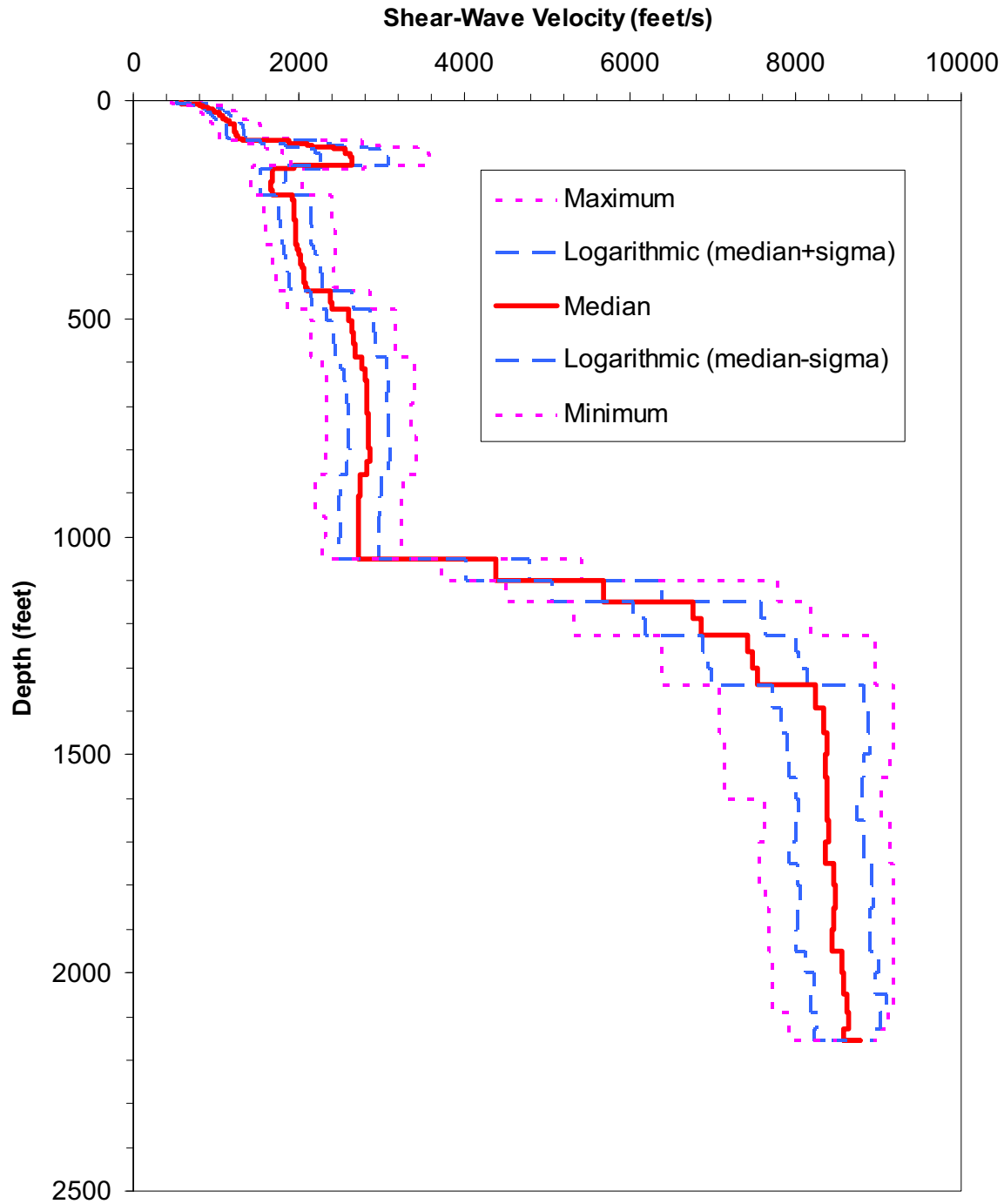


Figure 2.5-294
1 Hz Hard Rock Seismic Hazard Curves
by Seismic Source for the Rondout Team



Note: Statistics do not include the velocities on the crystalline bedrock.

Figure 2.5-295
Summary Statistics Calculated from the
60 Shear-Wave Velocity Profiles

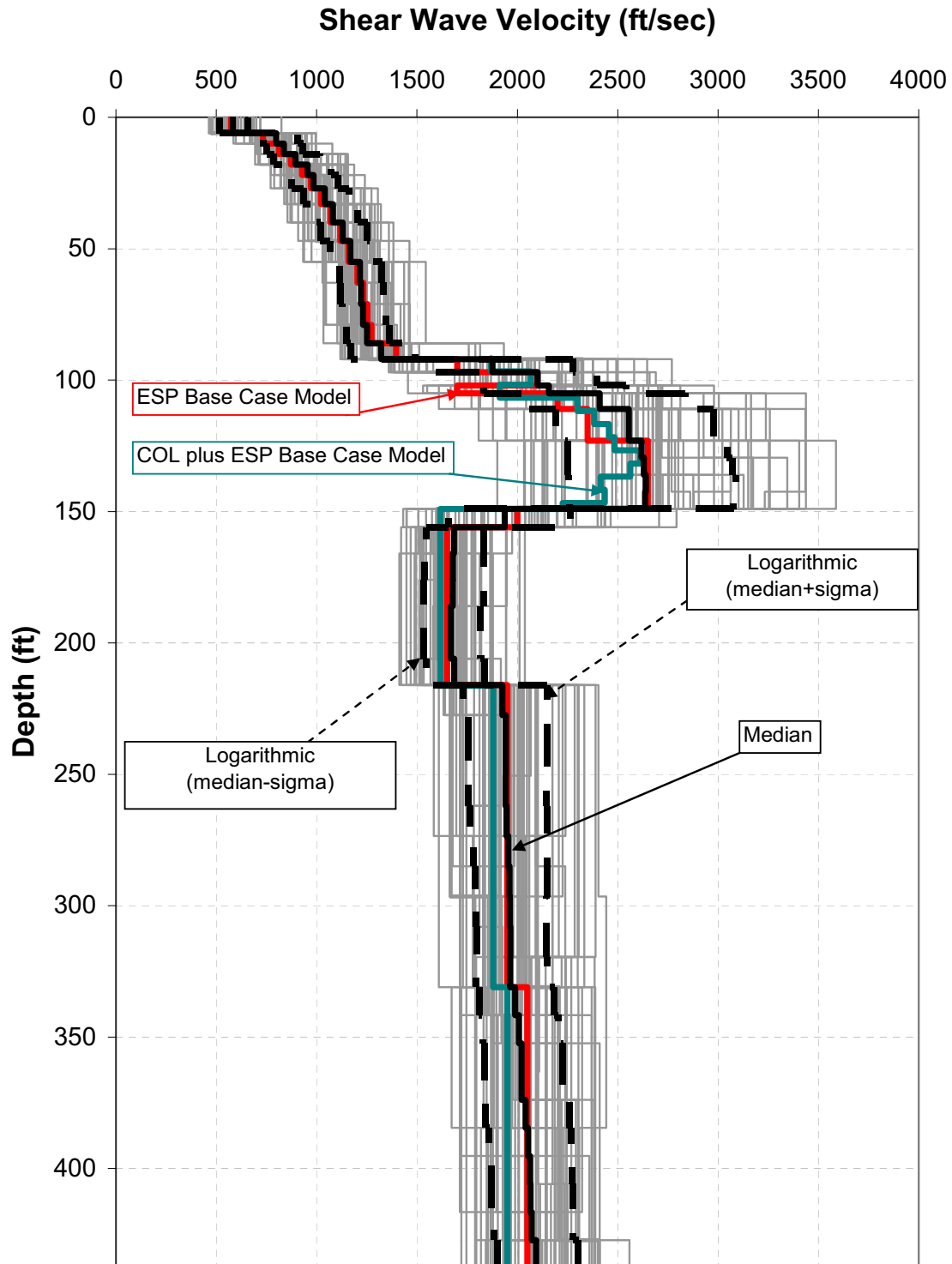


Figure 2.5-296
ESP and COL plus ESP Soil Models

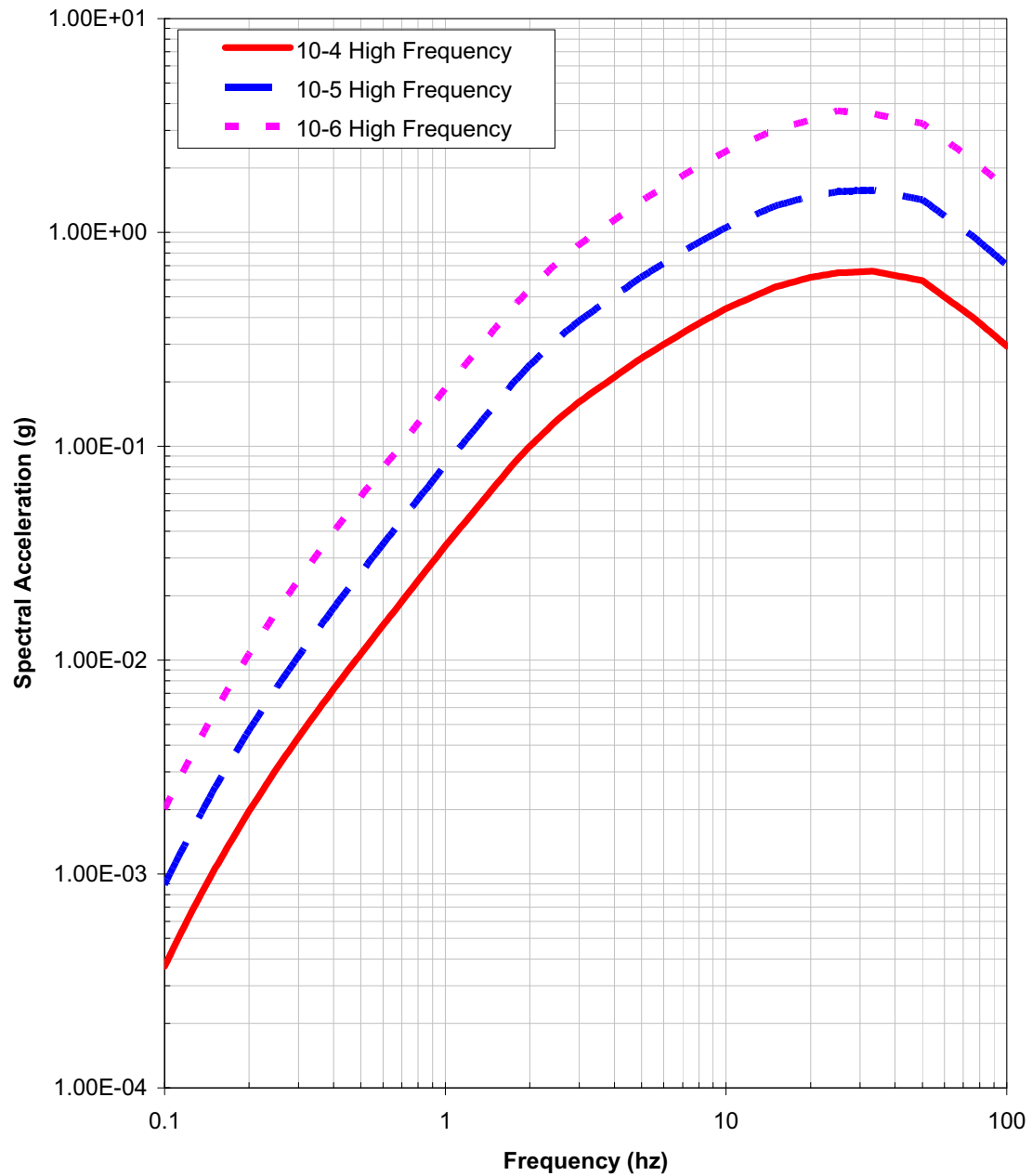
SNC Targets: High Frequency Spectra

Figure 2.5-297
High Frequency Hard Rock Target Spectra for the
Three Annual Probability Levels of 10⁻⁴, 10⁻⁵, and 10⁻⁶

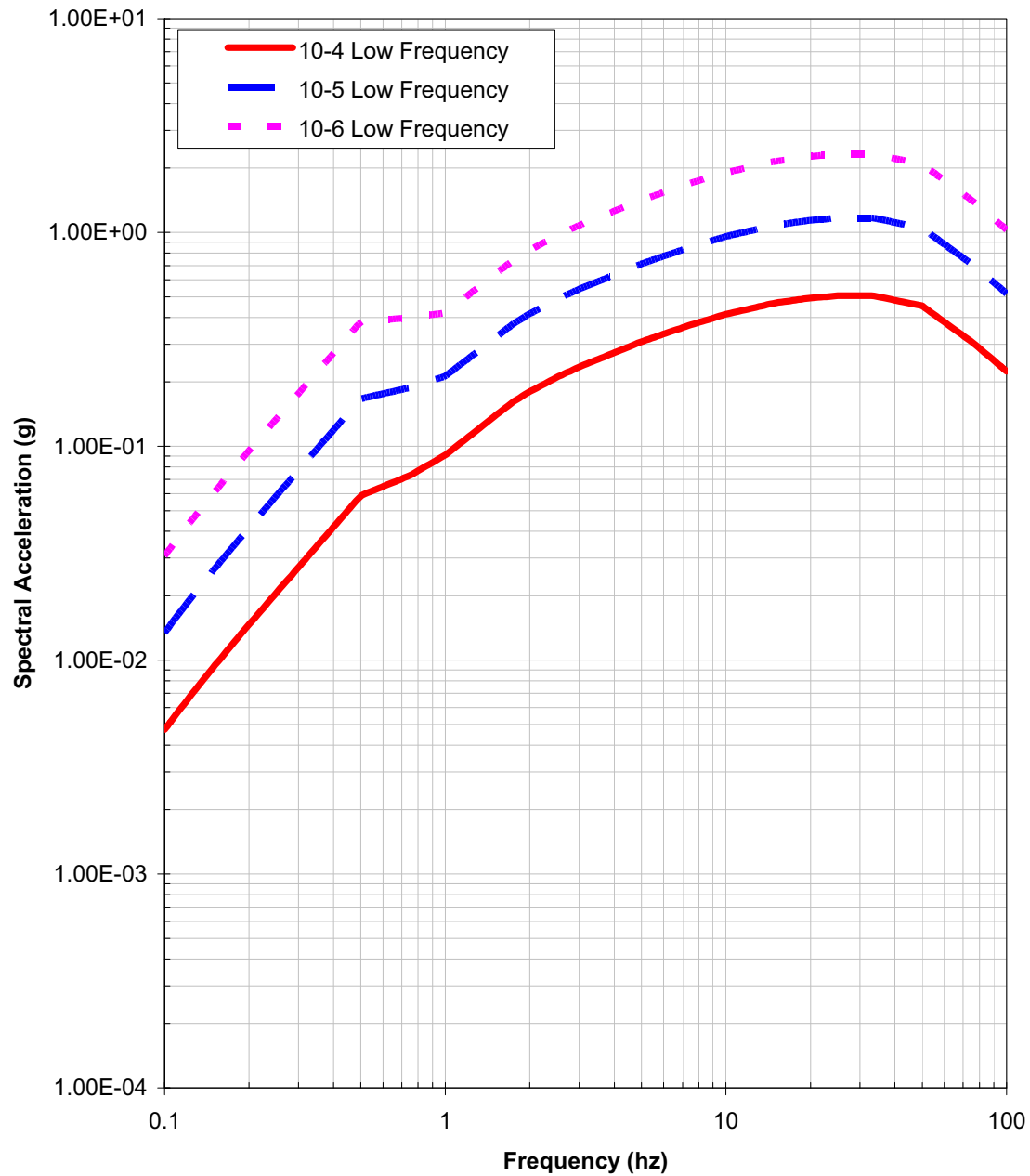
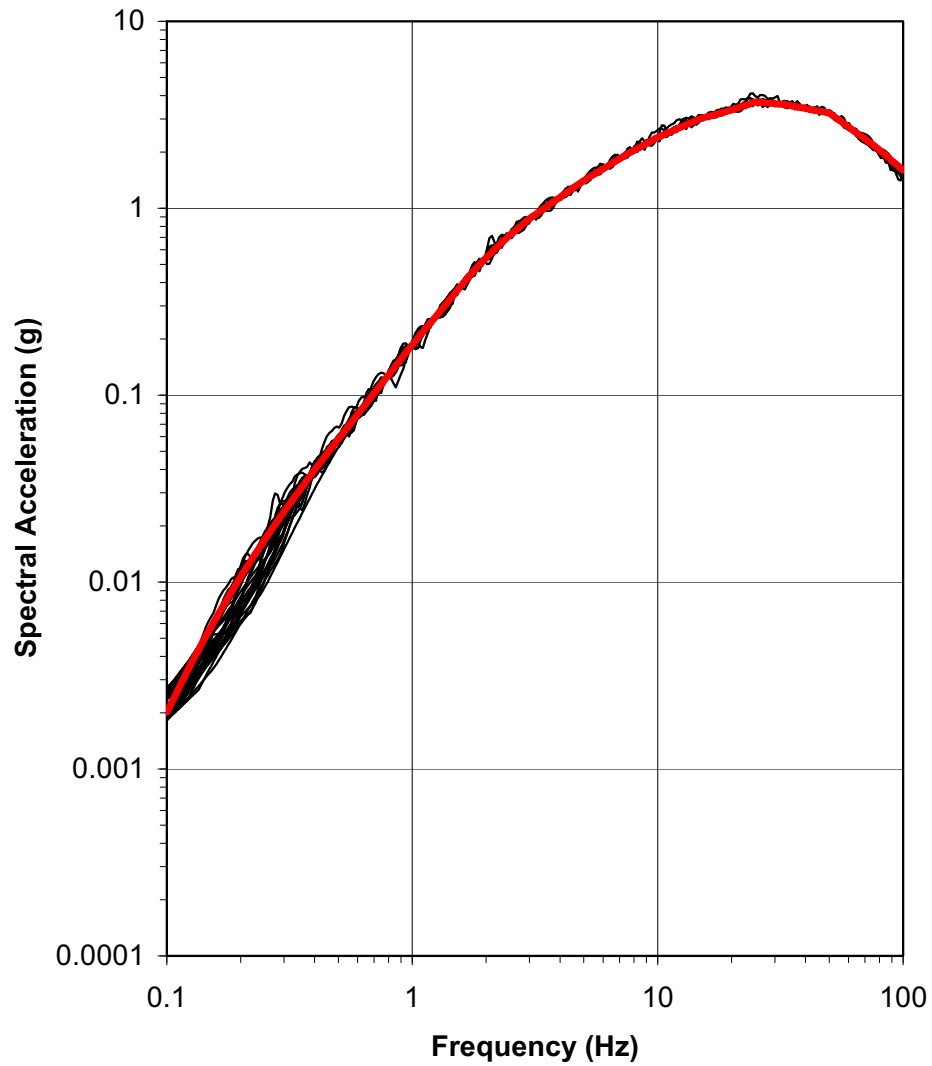
SNC Targets: Low Frequency Spectra

Figure 2.5-298
Low Frequency Hard Rock Target Spectra
for the Three Annual Probability Levels of 10^{-4} , 10^{-5} , and 10^{-6}

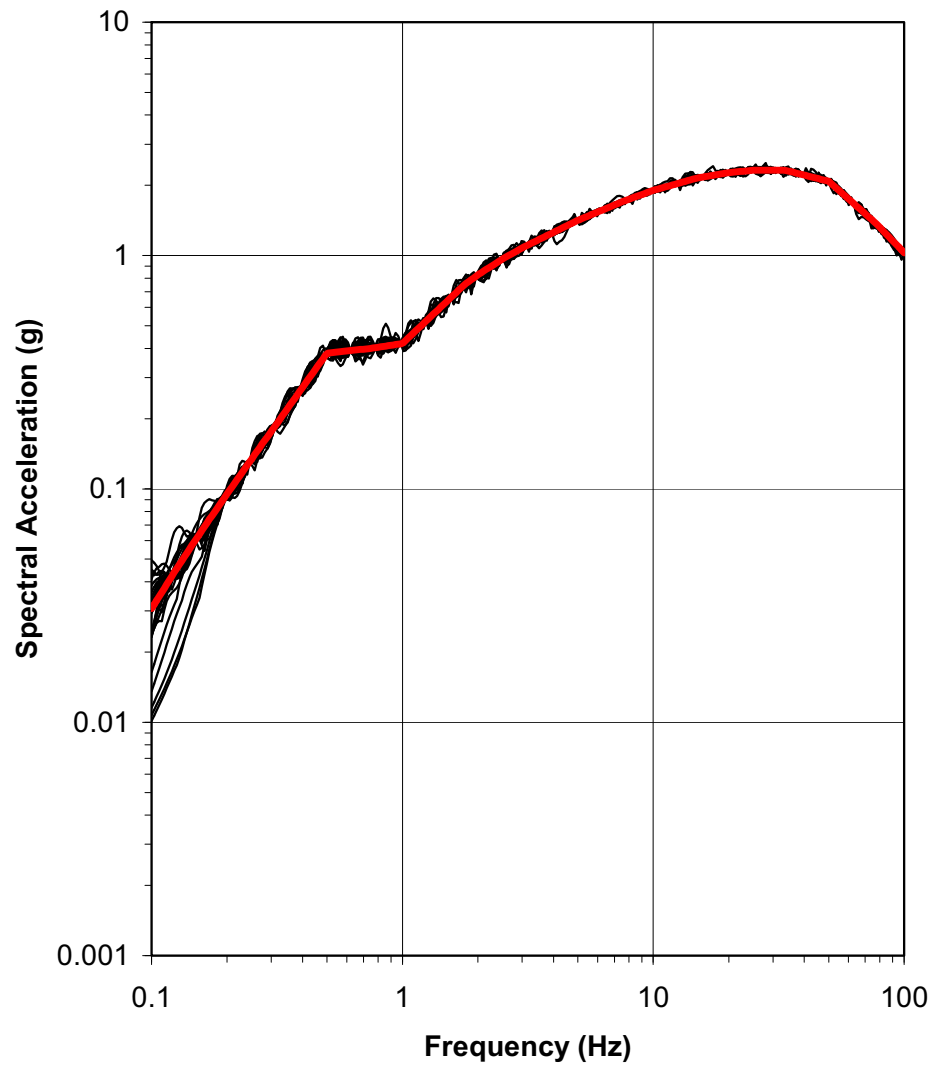
Spectral-Matched Time History Spectra: RP6HF



Note: Heavy red line is the target spectrum and thin black lines are the individual matches.

Figure 2.5-299
High Frequency (10^{-6}) Match for the 30 Time Histories

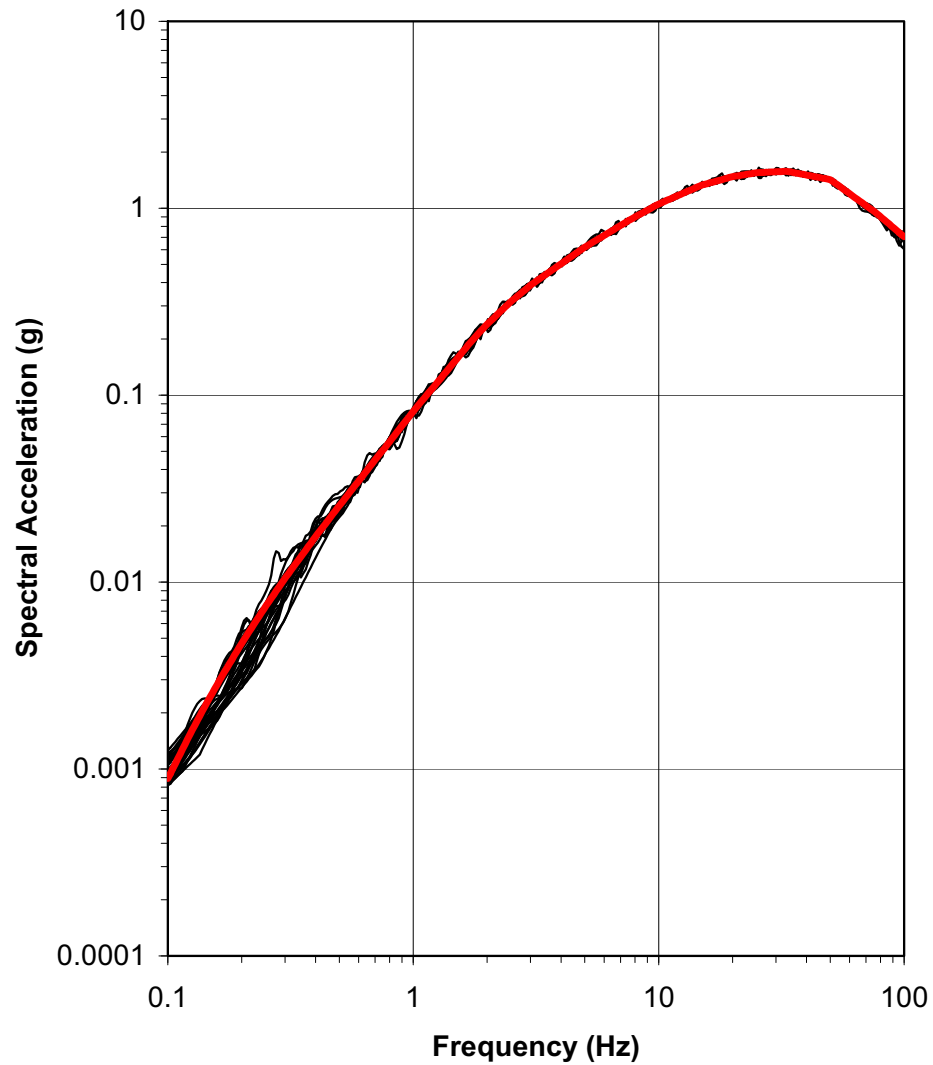
Spectral-Matched Time History Spectra: RP6LF



Note: Heavy red line is the target spectrum and thin black lines are the individual matches.

Figure 2.5-300
Low Frequency (10^{-6}) Match for the 30 Time Histories

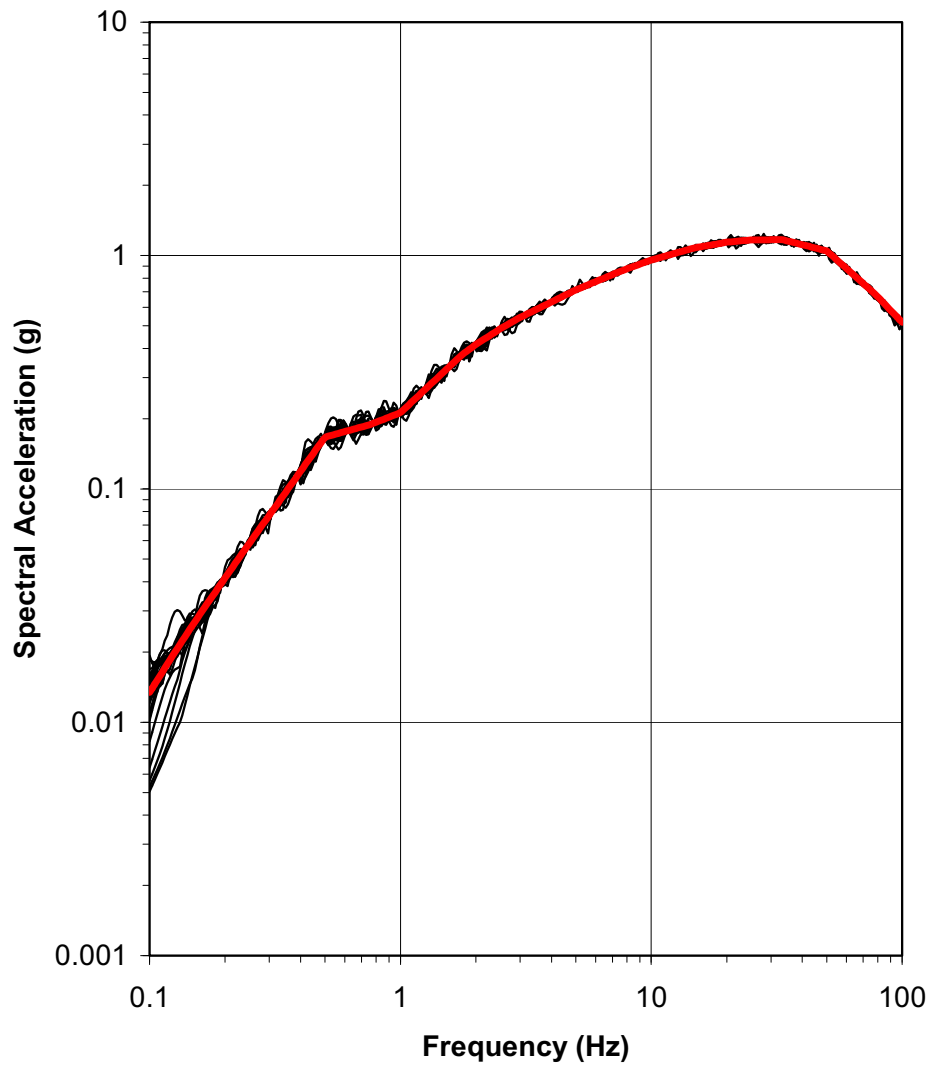
Spectral-Matched Time History Spectra: RP5HF



Note: Heavy red line is the target spectrum and thin black lines are the individual matches.

Figure 2.5-301
High Frequency (10^{-5}) Match for the 30 Time Histories

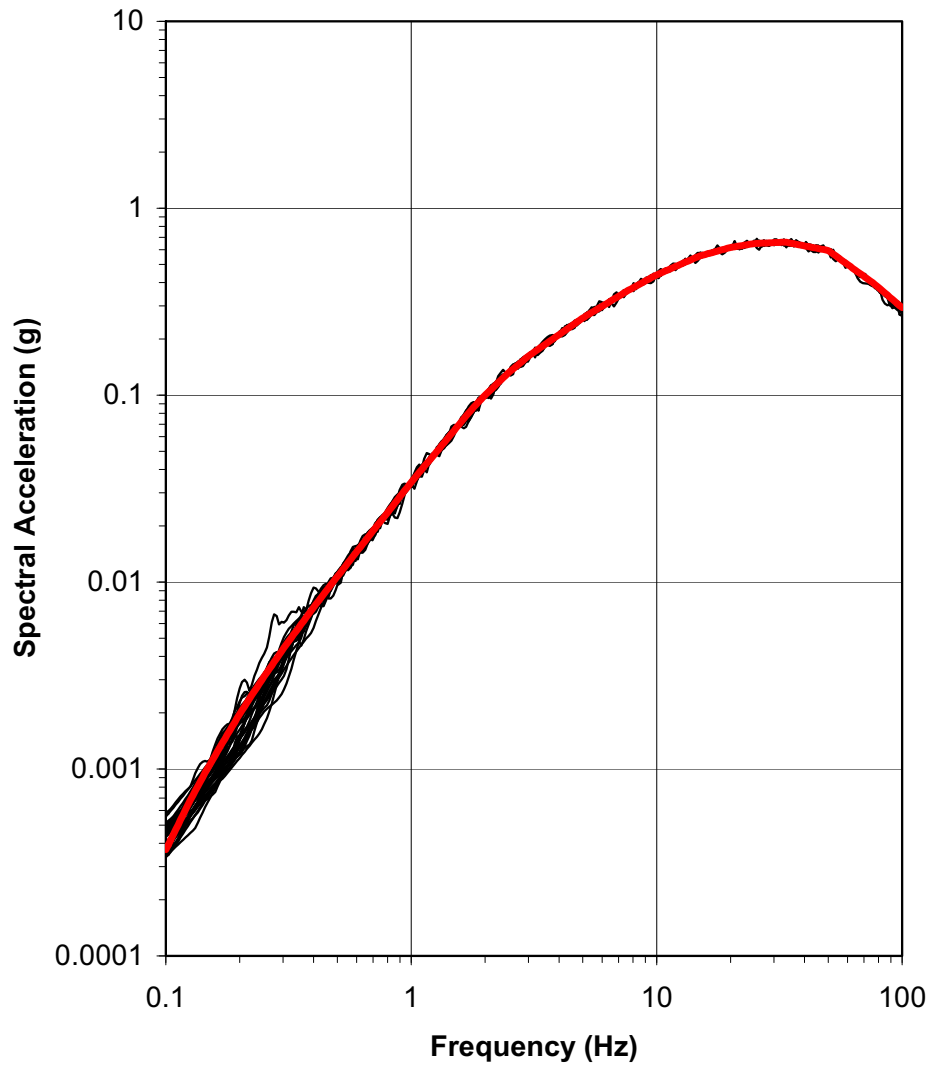
Spectral-Matched Time History Spectra: RP5LF



Note: Heavy red line is the target spectrum and thin black lines are the individual matches.

Figure 2.5-302
Low Frequency (10^{-5}) Match for the 30 Time Histories

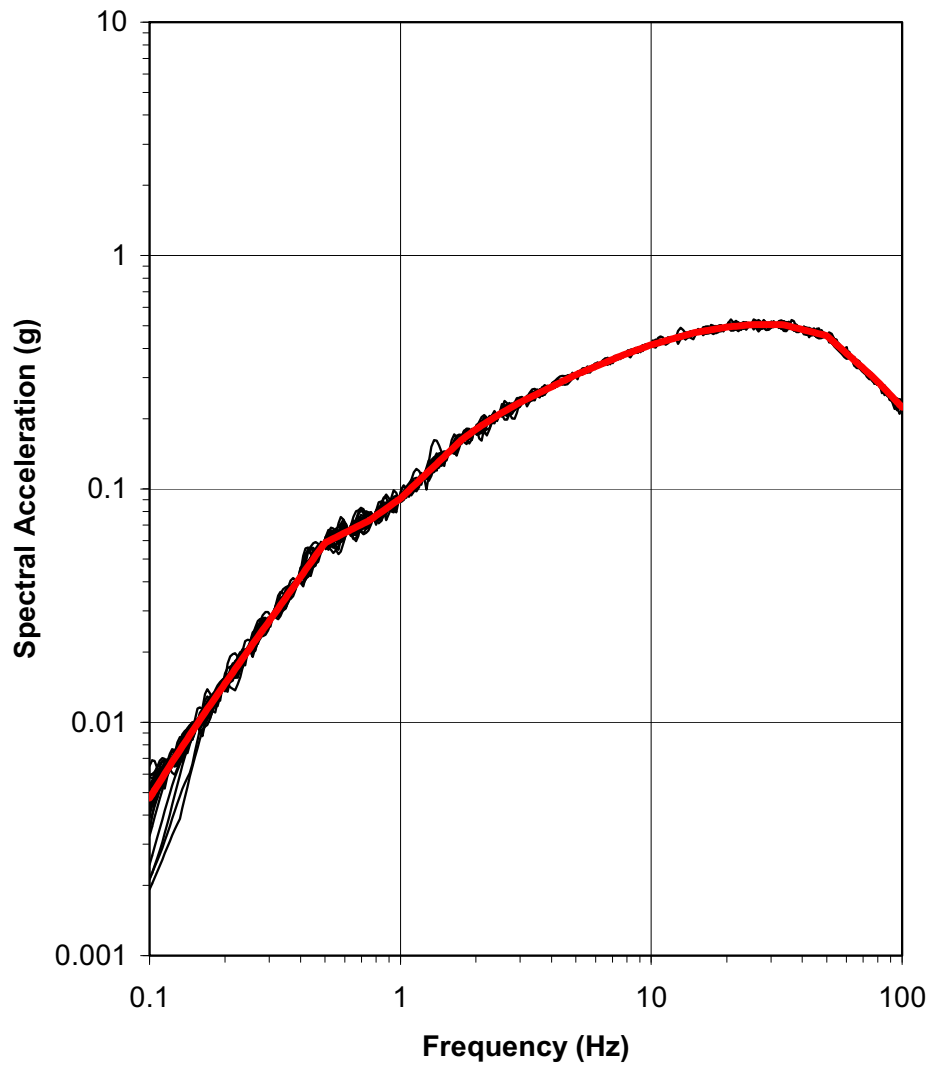
Spectral-Matched Time History Spectra: RP4HF



Note: Heavy red line is the target spectrum and thin black lines are the individual matches.

Figure 2.5-303
High Frequency (10^{-4}) Match for the 30 Time Histories

Spectral-Matched Time History Spectra: RP4LF



Note: Heavy red line is the target spectrum and thin black lines are the individual matches.

Figure 2.5-304
Low Frequency (10^{-4}) Match for the 30 Time Histories

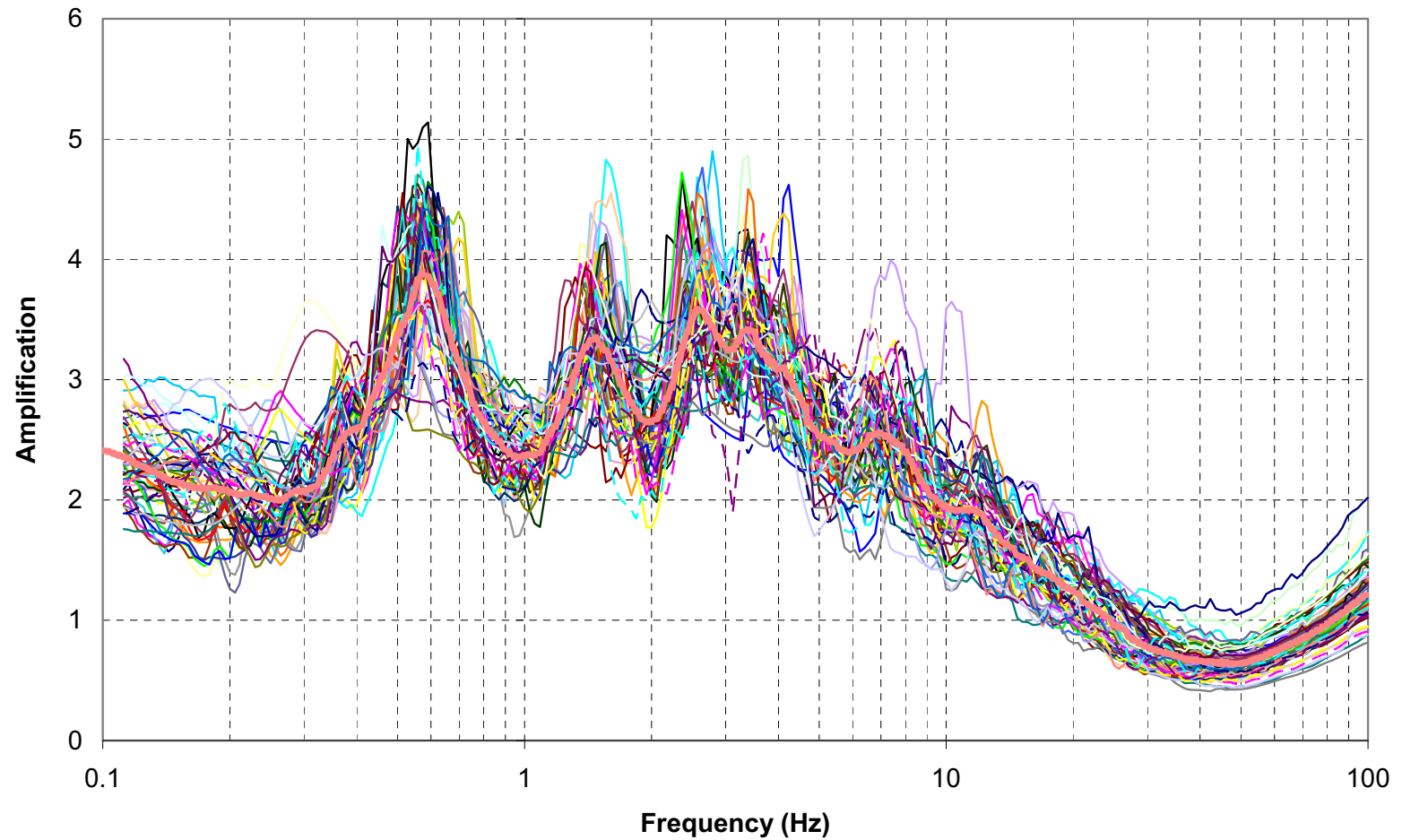


Figure 2.5-305
Typical Results of Spectral Amplification at 86-ft Depth (Top of Blue Bluff Marl)
Using EPRI Degradation Curves for High Frequency Time Histories
of 10^{-4} MAFE Input Motion Level

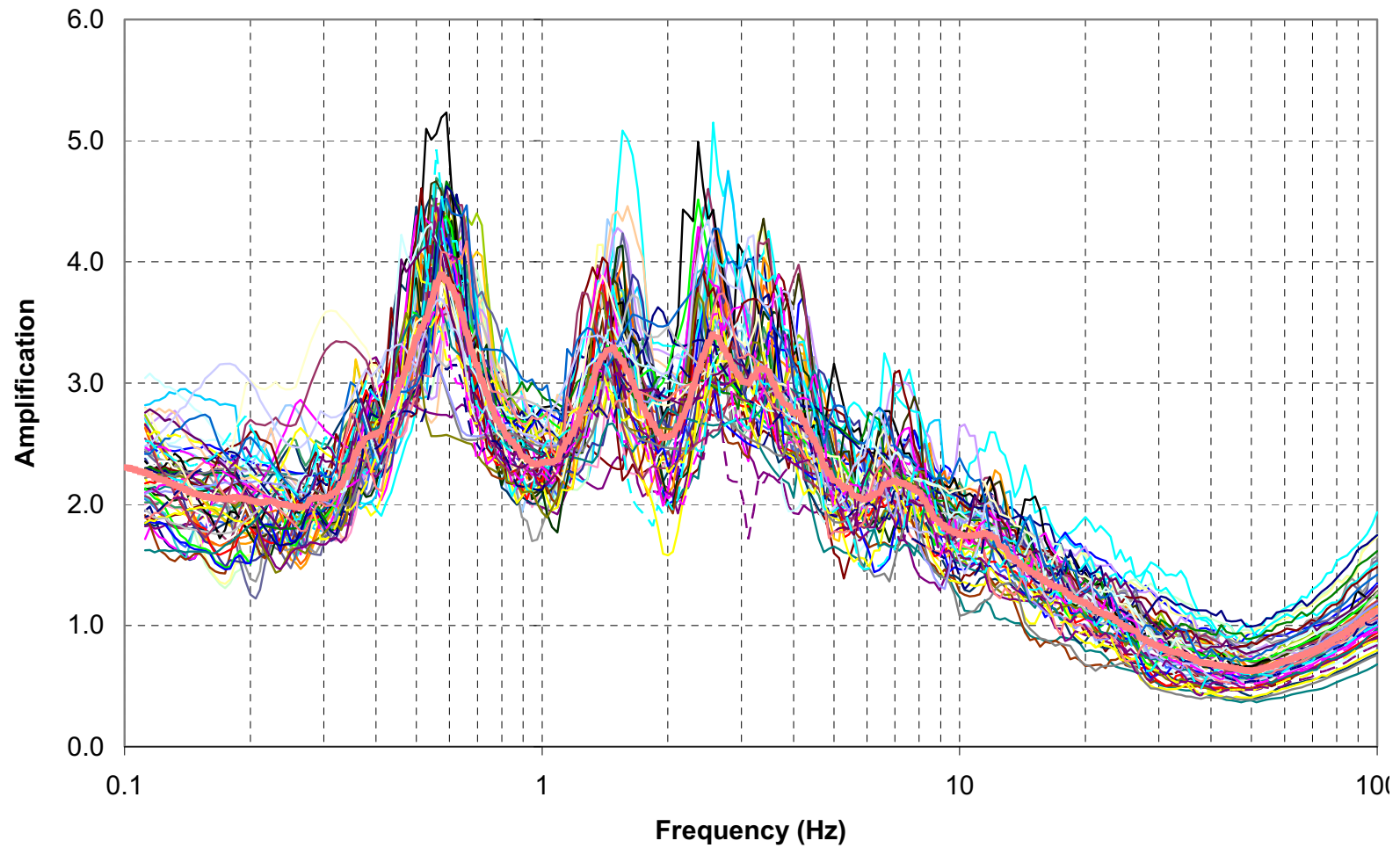


Figure 2.5-306
Typical Results of Spectral Amplification at 40-ft Horizon Outcrop Motion
Using EPRI Degradation Curves for High-Frequency Time Histories
of 10^{-4} MAFE Input Motion Level

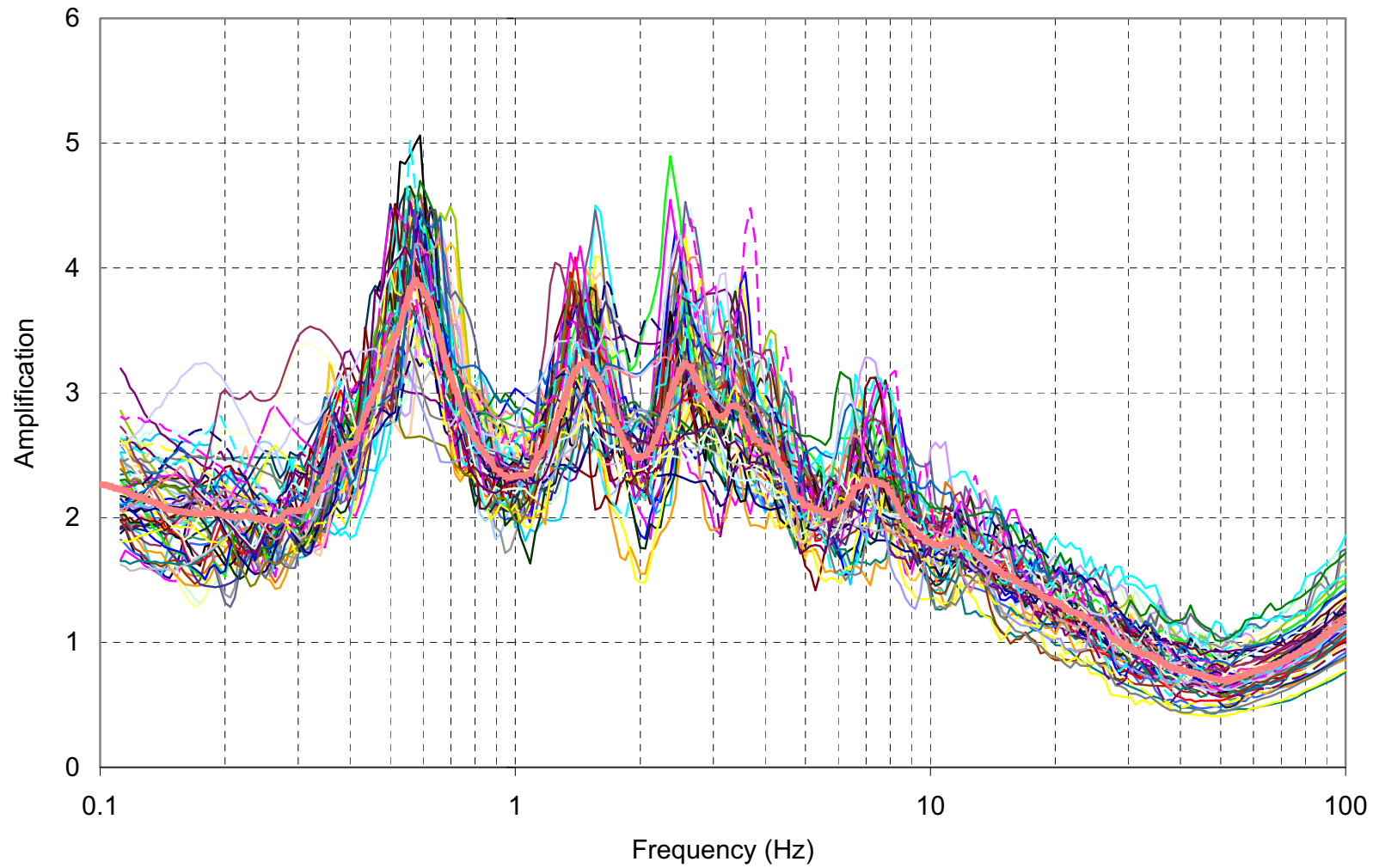


Figure 2.5-307
Typical Results of Spectral Amplification Ground Surface
using EPRI Degradation Curves for High Frequency Time Histories
of 10^{-4} MAFE Input Motion Level

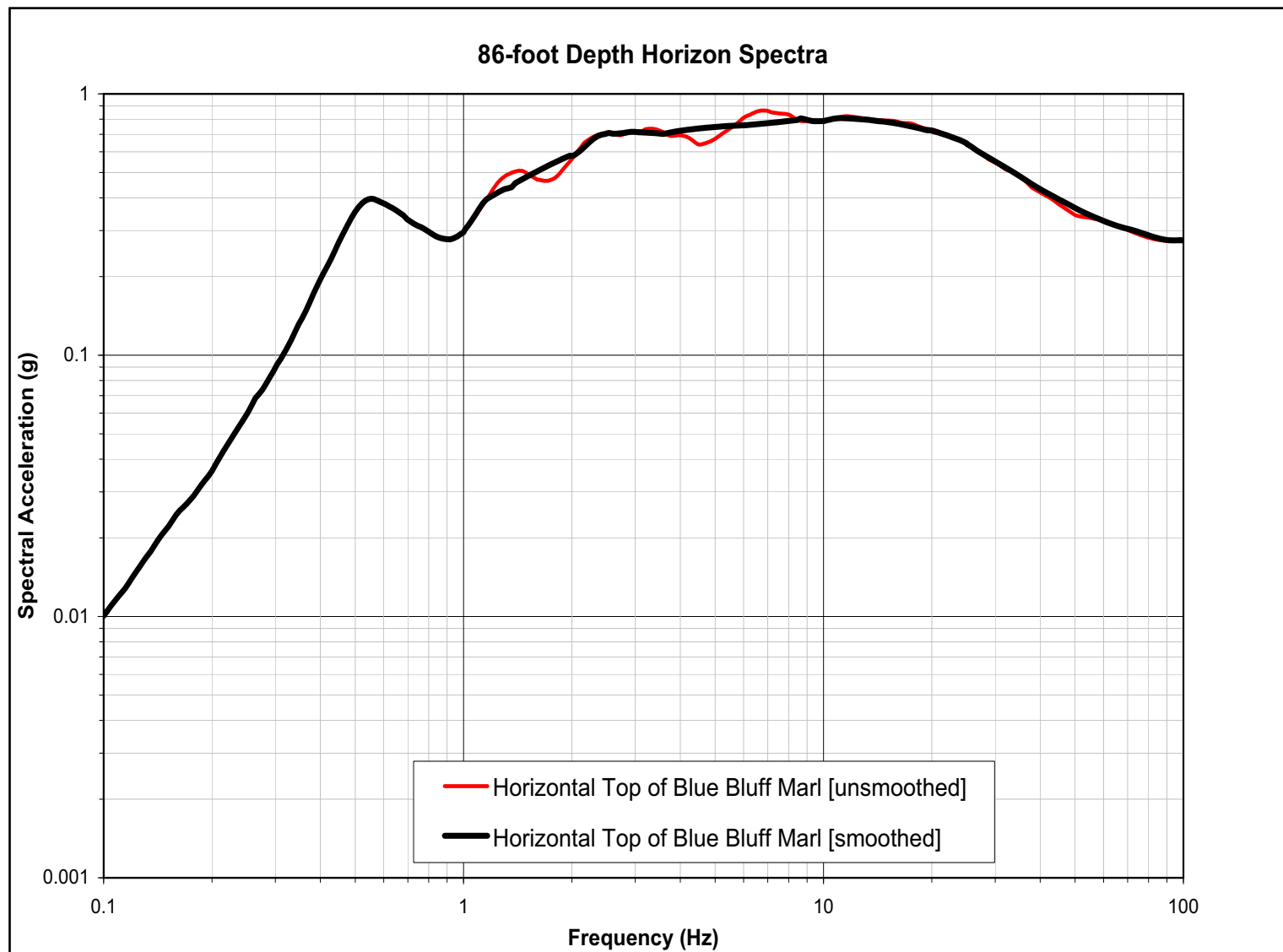


Figure 2.5-308
Horizontal Raw and Smoothed, Top of Blue Bluff Marl

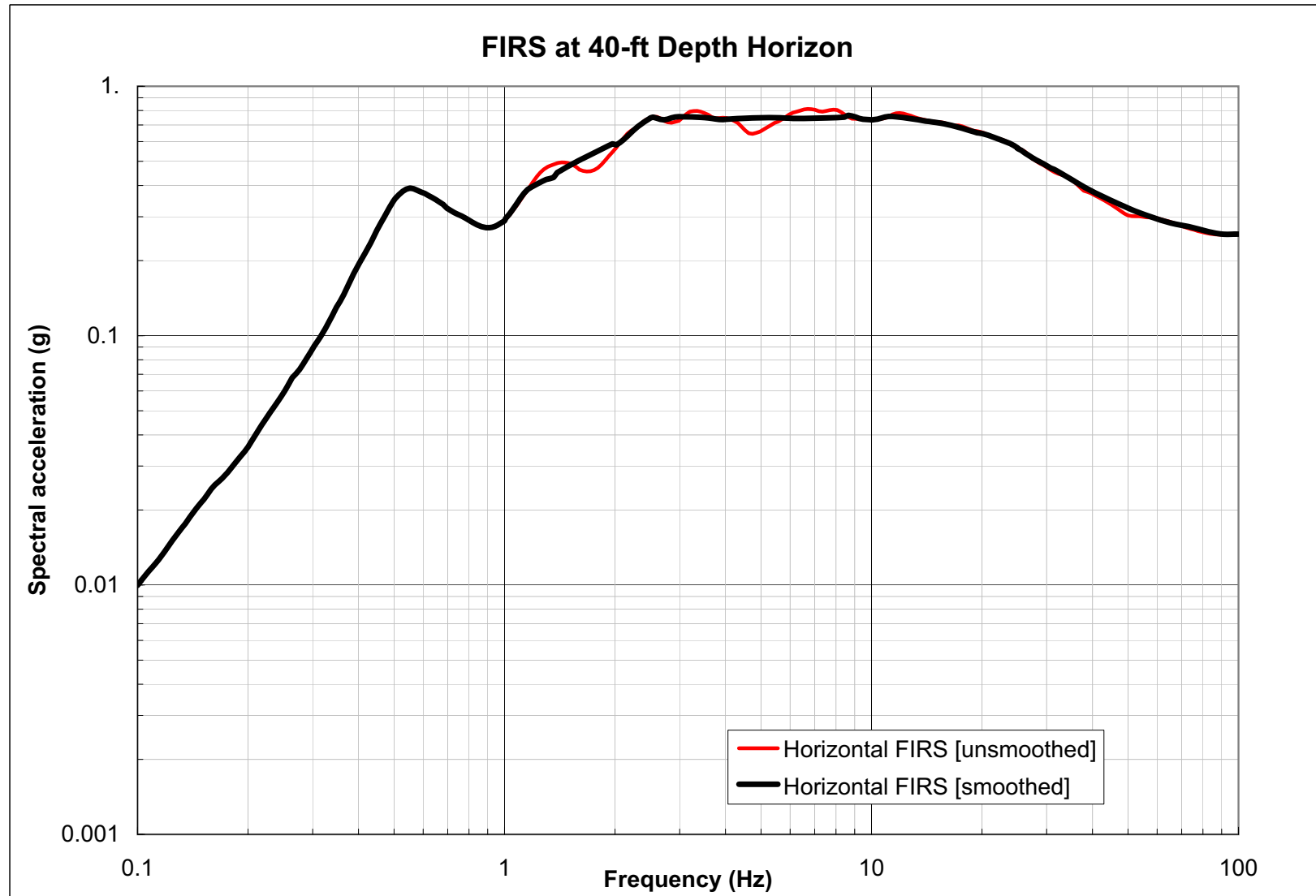


Figure 2.5-309
Horizontal Raw and Smoothed FIRS, 40-ft Depth Horizon

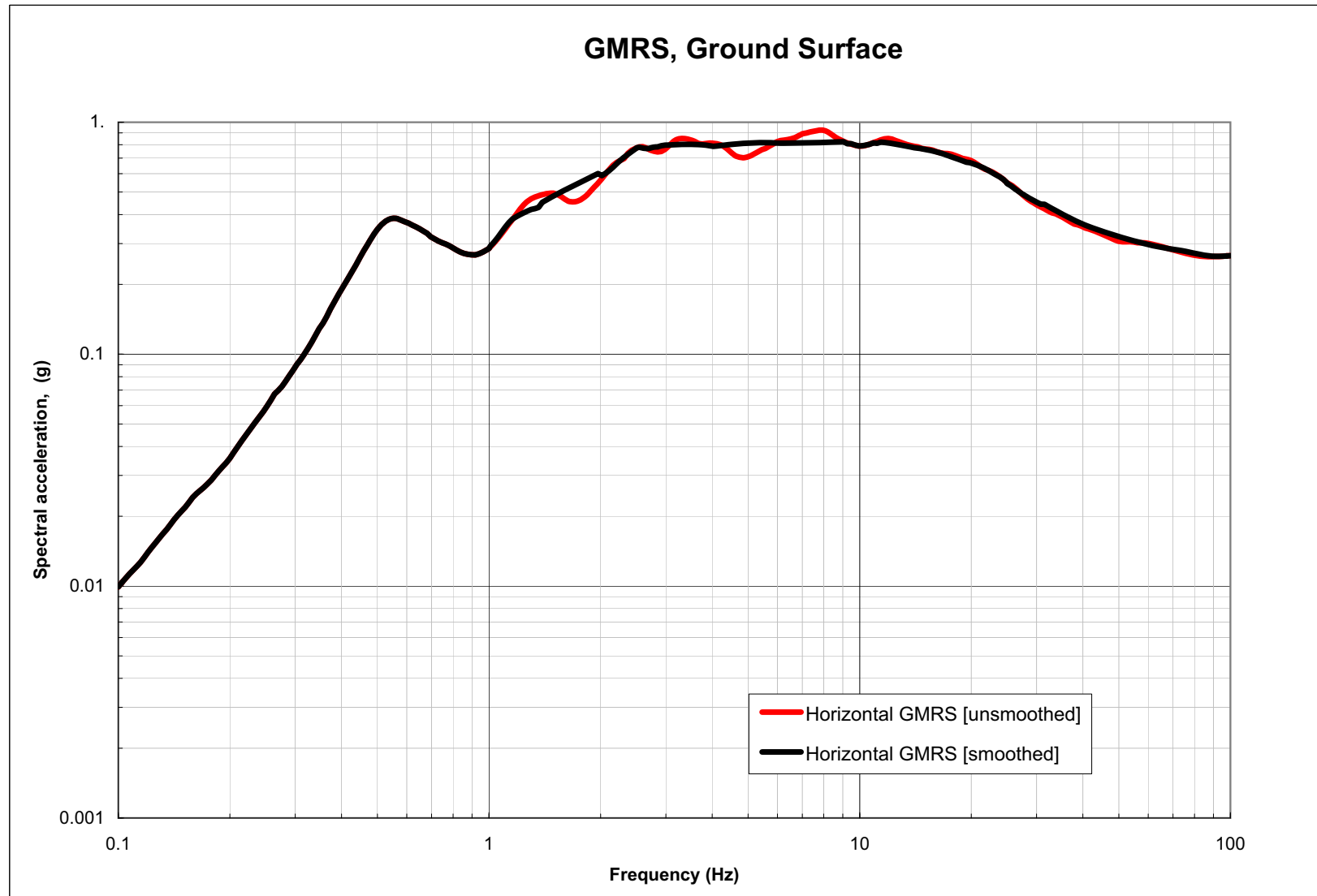


Figure 2.5-310
Horizontal Raw and Smoothed GMRS, Ground Surface

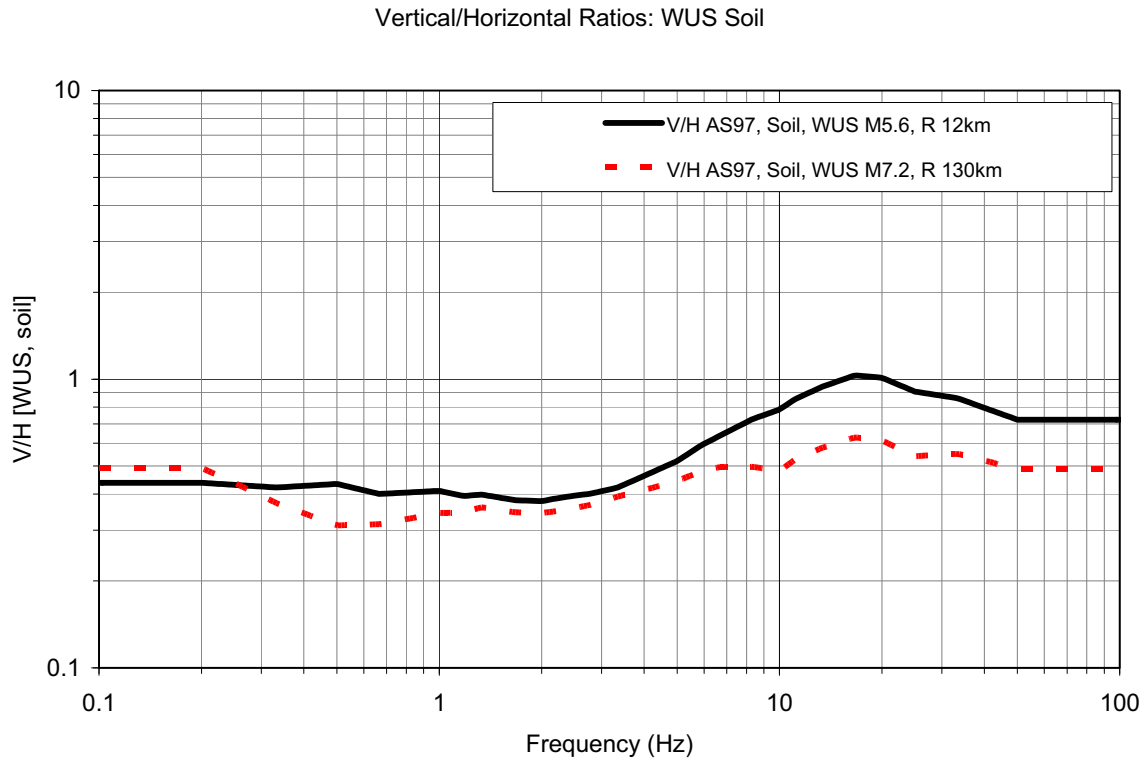
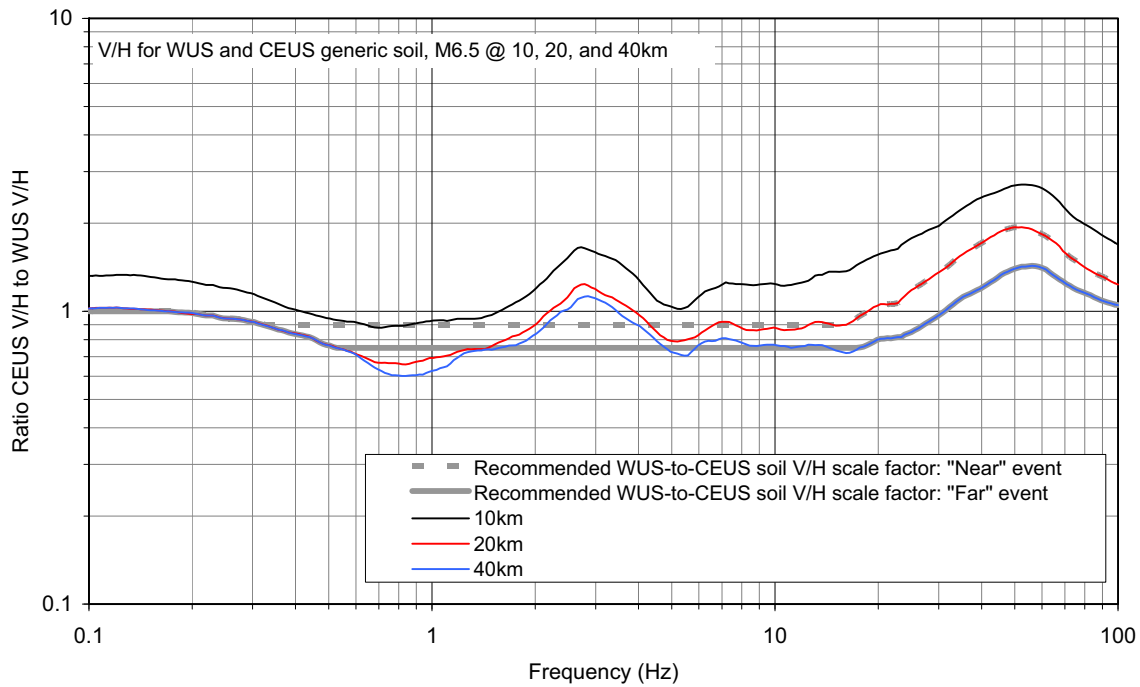


Figure 2.5-311

**Plots of V/H_{WUS,Soil}, Empirical Term of Equation 2.5.2-6
for “Near” [M5.6 at a Distance of 12 km] and “Far” [M7.2 at a Distance
of 130 km] Events Using the Attenuation Relation of Abrahamson and Silva (1997)**

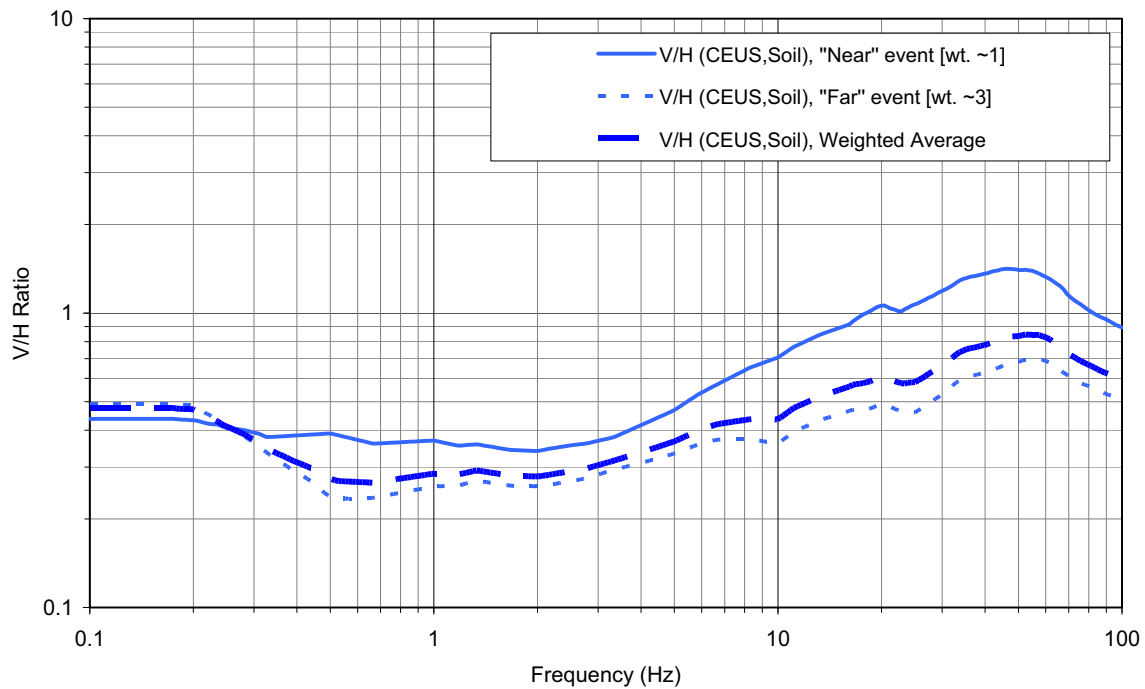
NUREG/CR-6728, Figure J-31 and J-32



Note: The "near" and "far" ratios of V/H ratios recommended for this study are also shown.

Figure 2.5-312
Plots of $[V/H_{CEUS, Soil, Model} / V/H_{WUS, Soil, Model}]$ Term
of Equation 2.5.2-6 for M6.5 and Distances of 10, 20, and 40 km,
as Available in NUREG/CR-6728 (McGuire et al 2001)

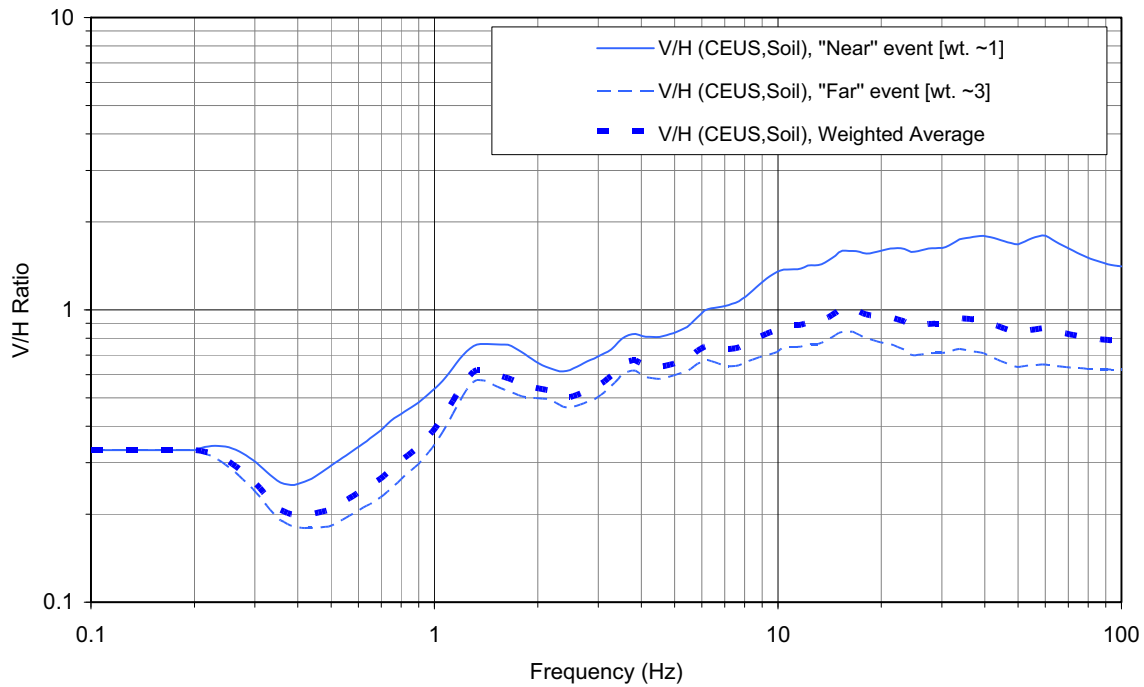
Application of NUREG/CR-6728 Method and Available Results



Note: Considering the relative contribution of the “near” and “far” events to the horizontal SSE design response spectrum, the approximately 1:3 weighted average is the recommended $V/H_{\text{CEUS,Soil}}$.

Figure 2.5-313
Plots of Recommended $V/H_{\text{CEUS,Soil}}$ from Equation 2.5.2-6
for “Near” and “Far” Events Using Results
from NUREG/CR-6728 (McGuire et al 2001)

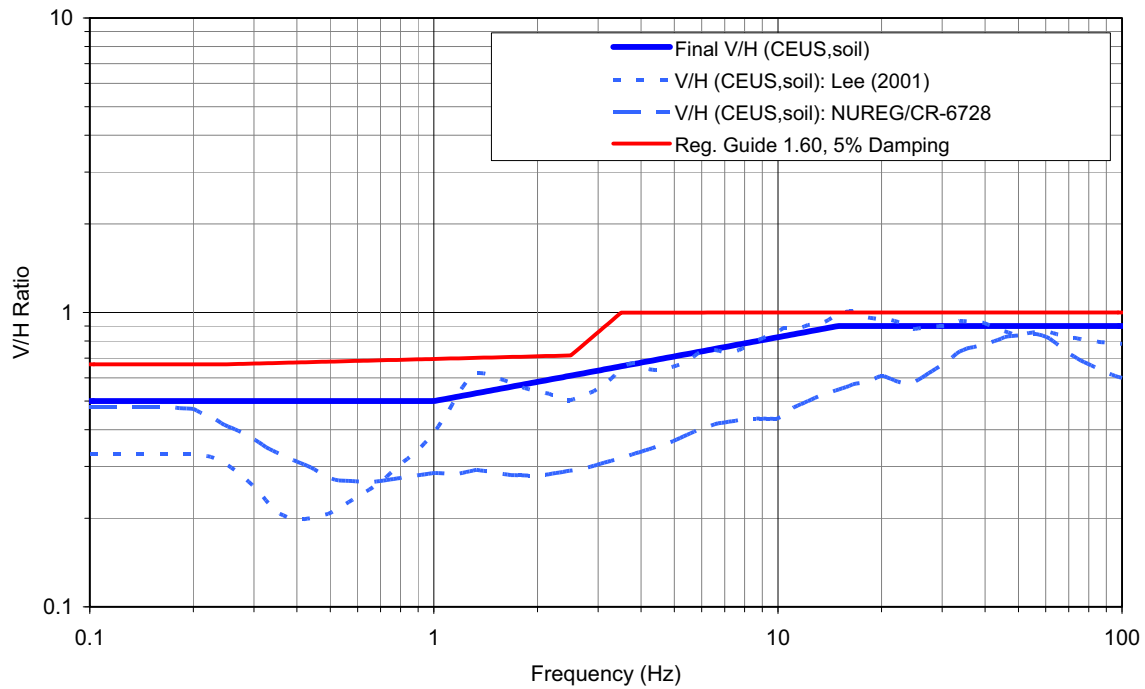
Application of Lee (2001) Results



Note: Considering the relative contribution of the “near” and “far” events to the horizontal SSE design response spectrum, the approximately 1:3 weighted average is shown.

Figure 2.5-314
Plots of Recommended V/HCEUS,Soil from Equation 2.5.2-6
for “Near” and “Far” Events Using Results from Lee (2001)

Application of NUREG/CR-6728 & Lee (2001)



Note: Considering the site-specific aspects of the Lee (2001), it is preferred, guiding the recommended final $V/H_{CEUS,Soil}$ (blue solid). The V/H from RG 1.60 is shown (red) for comparison.

Figure 2.5-315
Plots of $V/H_{CEUS,Soil}$ (Blue Patterned) Derived from Results
from NUREG/CR-6728 (McGuire et al 2001) and Lee (2001)

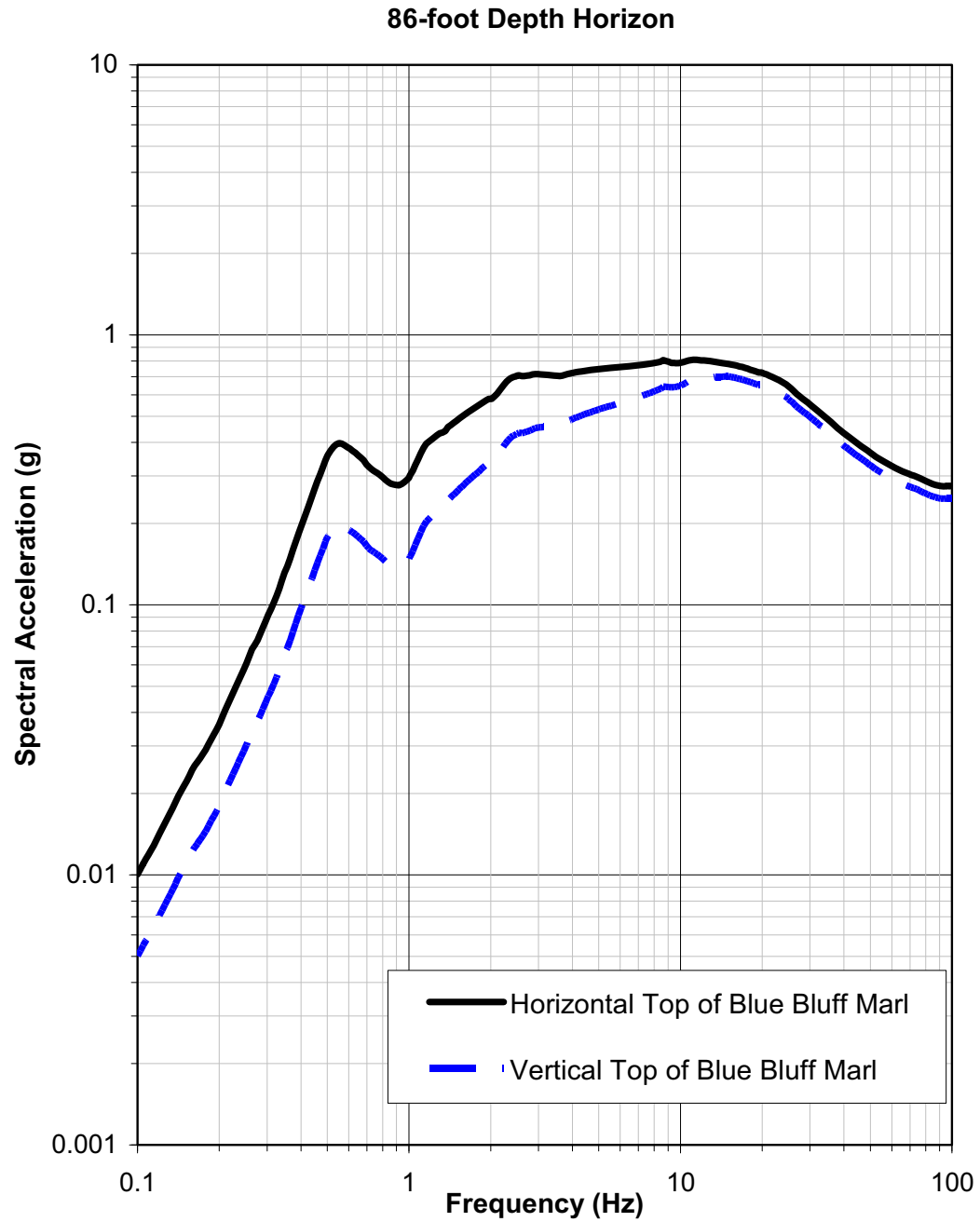


Figure 2.5-316

VEGP ESP Horizontal and Vertical Top of Blue Bluff Marl (5% Damping)

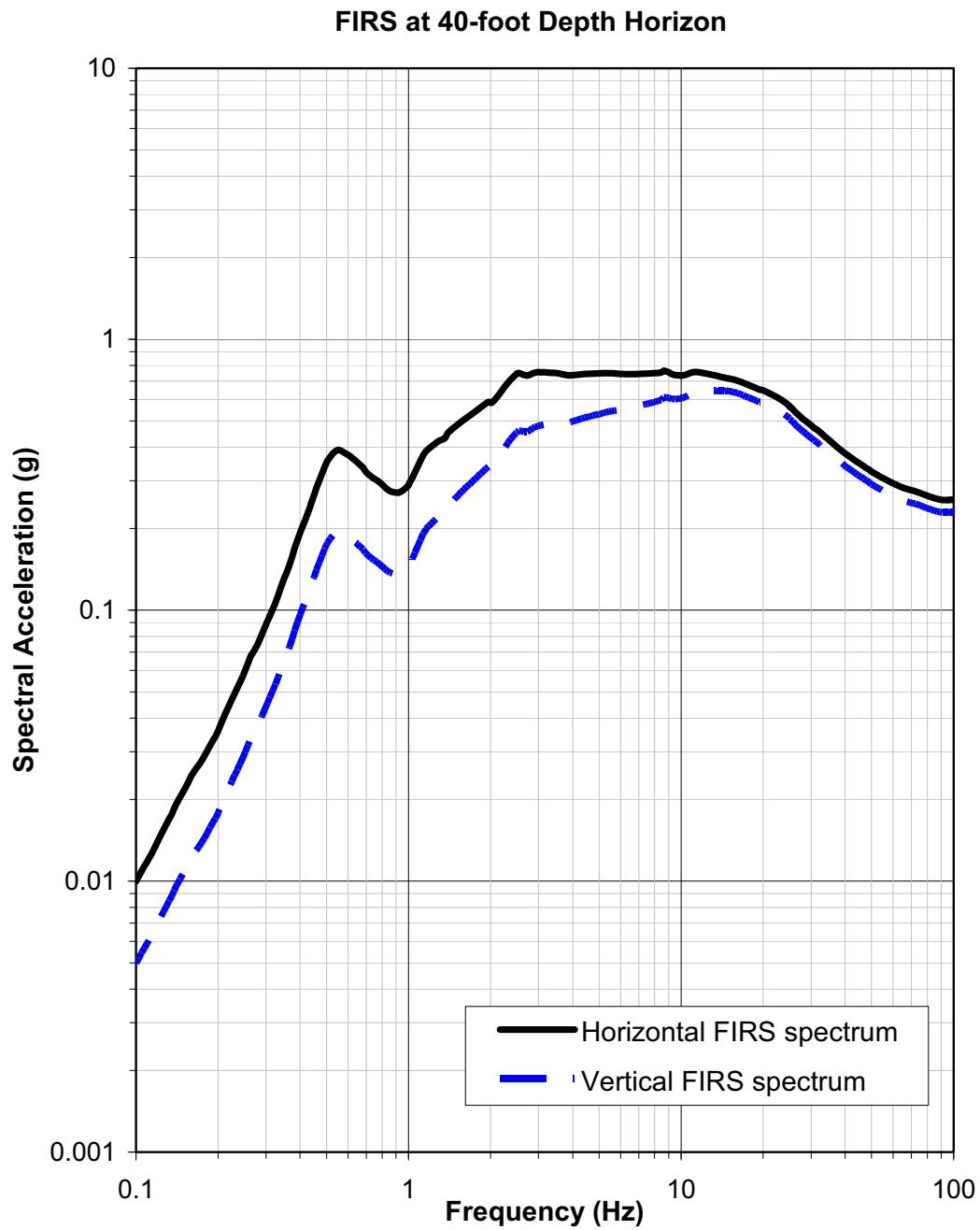


Figure 2.5-317

VEGP ESP Horizontal and Vertical FIRS Spectra, at the 40-ft Depth Horizon

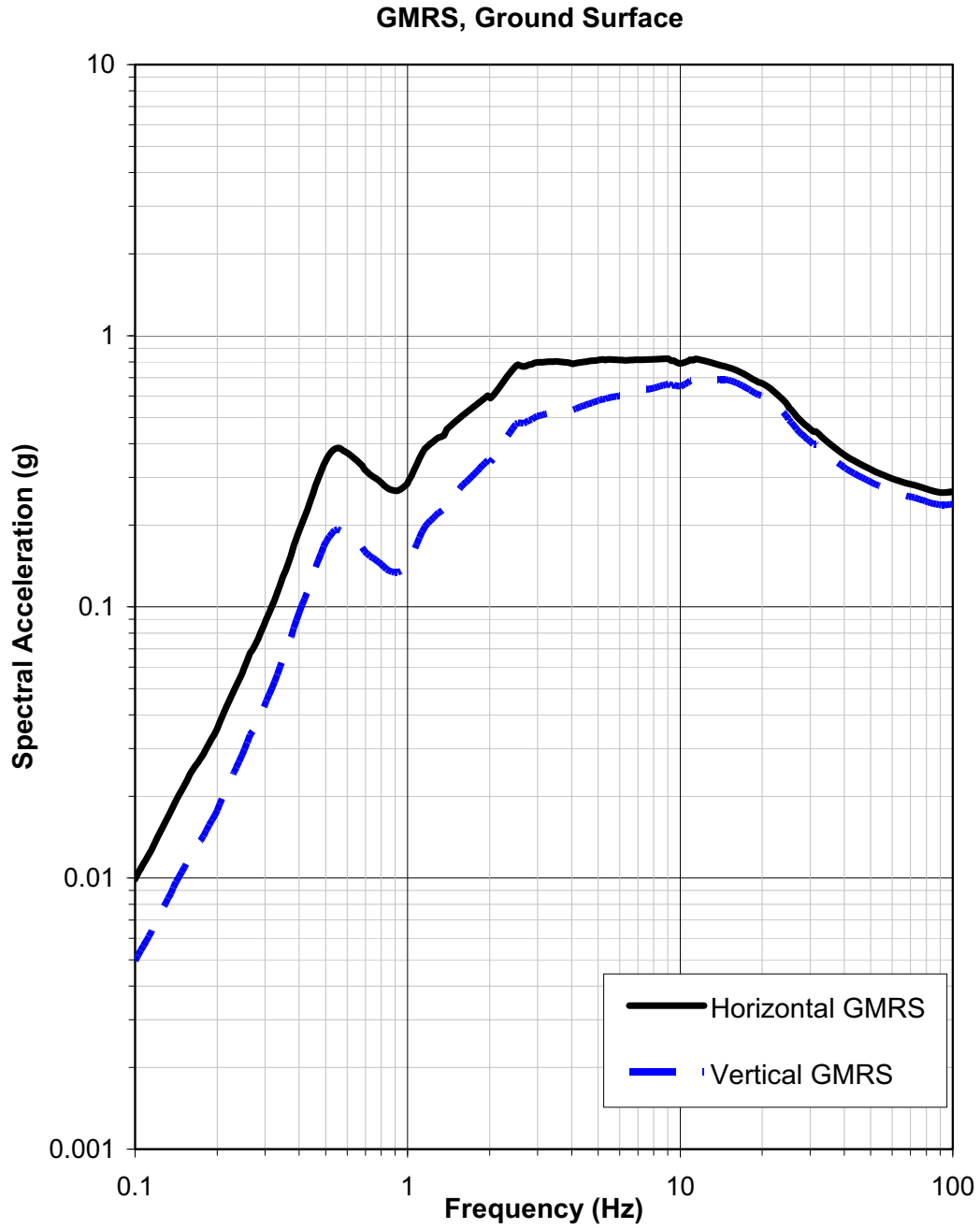


Figure 2.5-318

VEGP ESP Horizontal and Vertical GMRS Spectra (5% Damping)

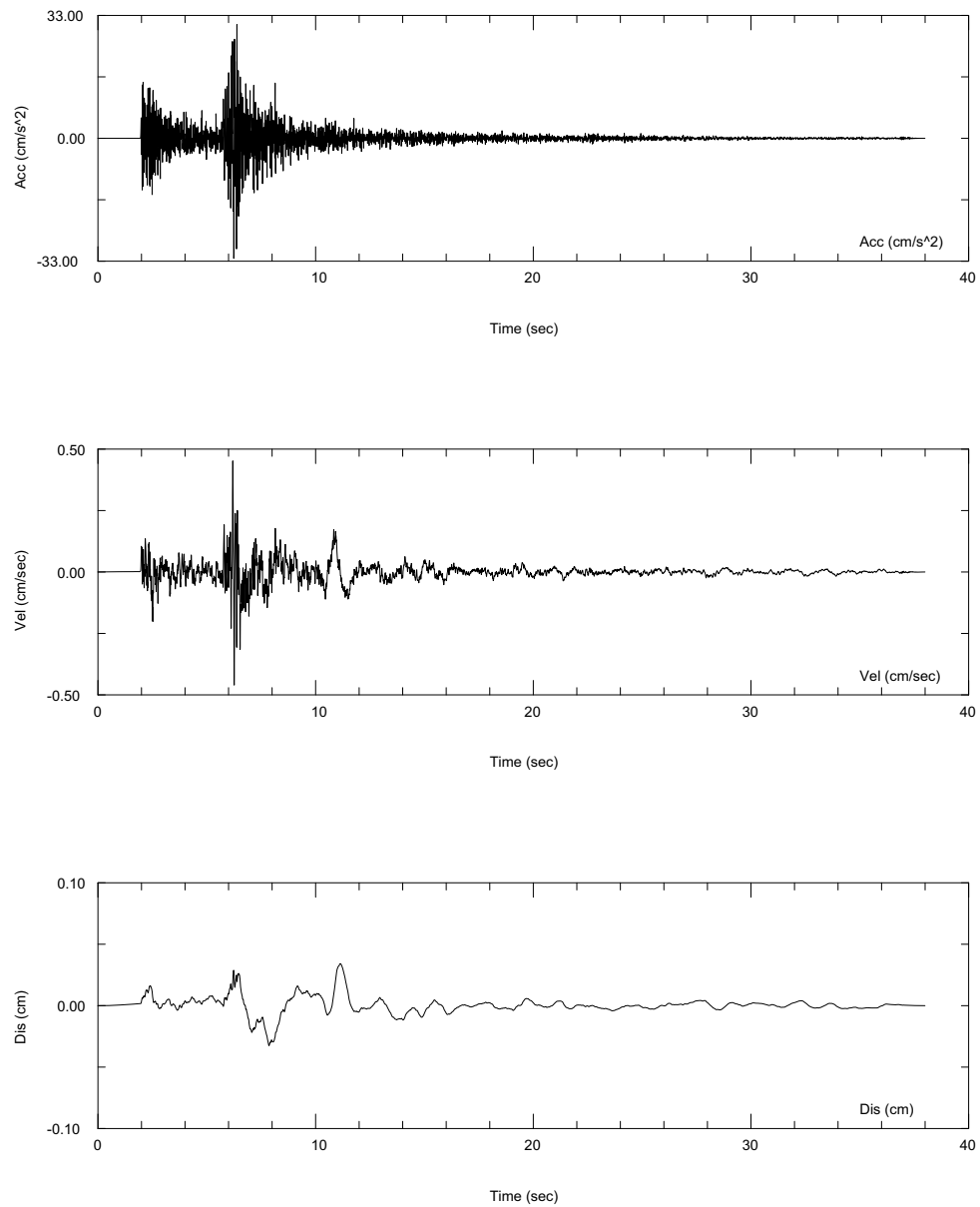


Figure 2.5-319
Example of Initial Seed Input Time Acceleration, Velocity,
and Displacement Time Histories (One of Thirty)
for High Frequency Target Spectrum

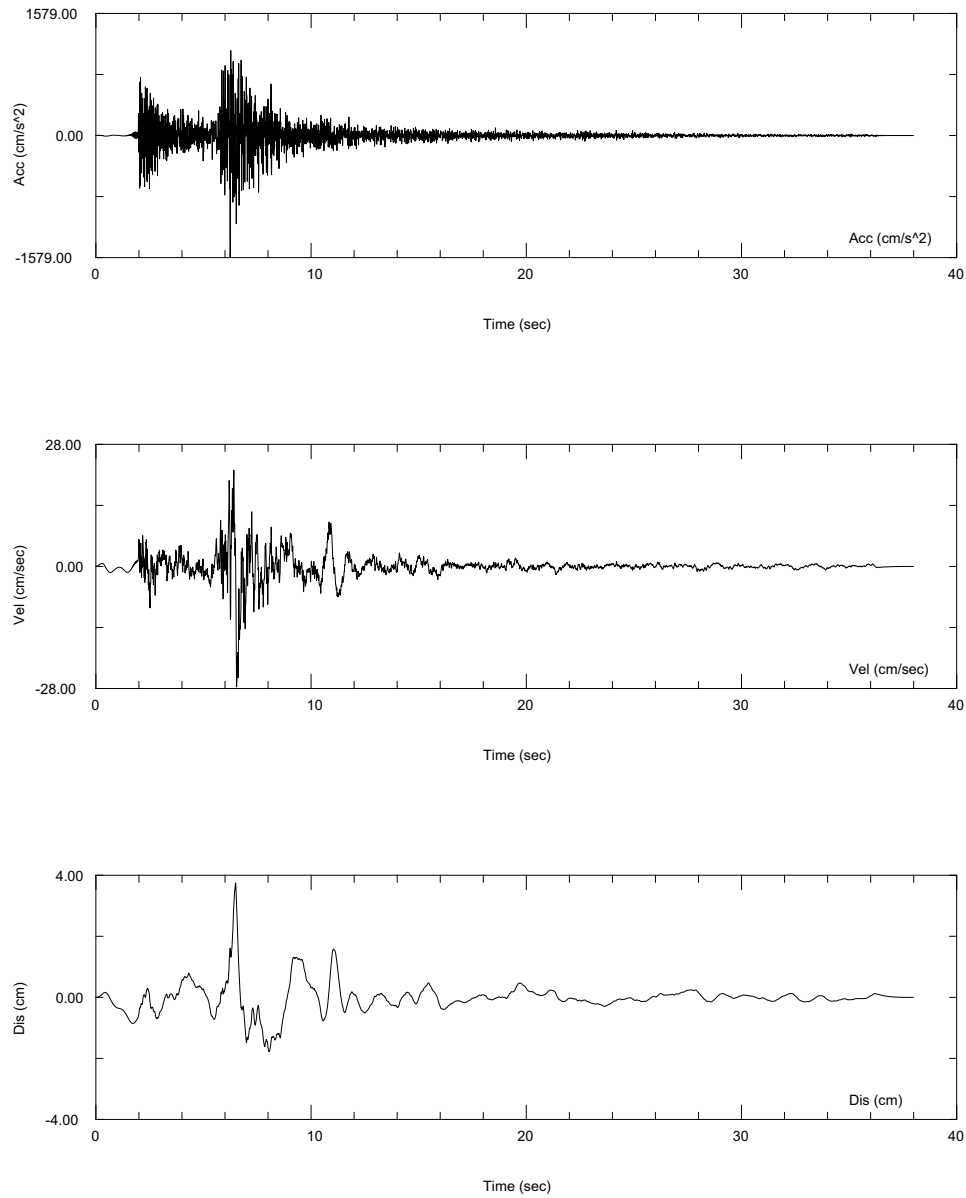


Figure 2.5-320
Final Modified Spectrum-Compatible Acceleration, Velocity,
and Displacement Time Histories (One of Thirty)
for 10^{-6} High Frequency Target Spectrum

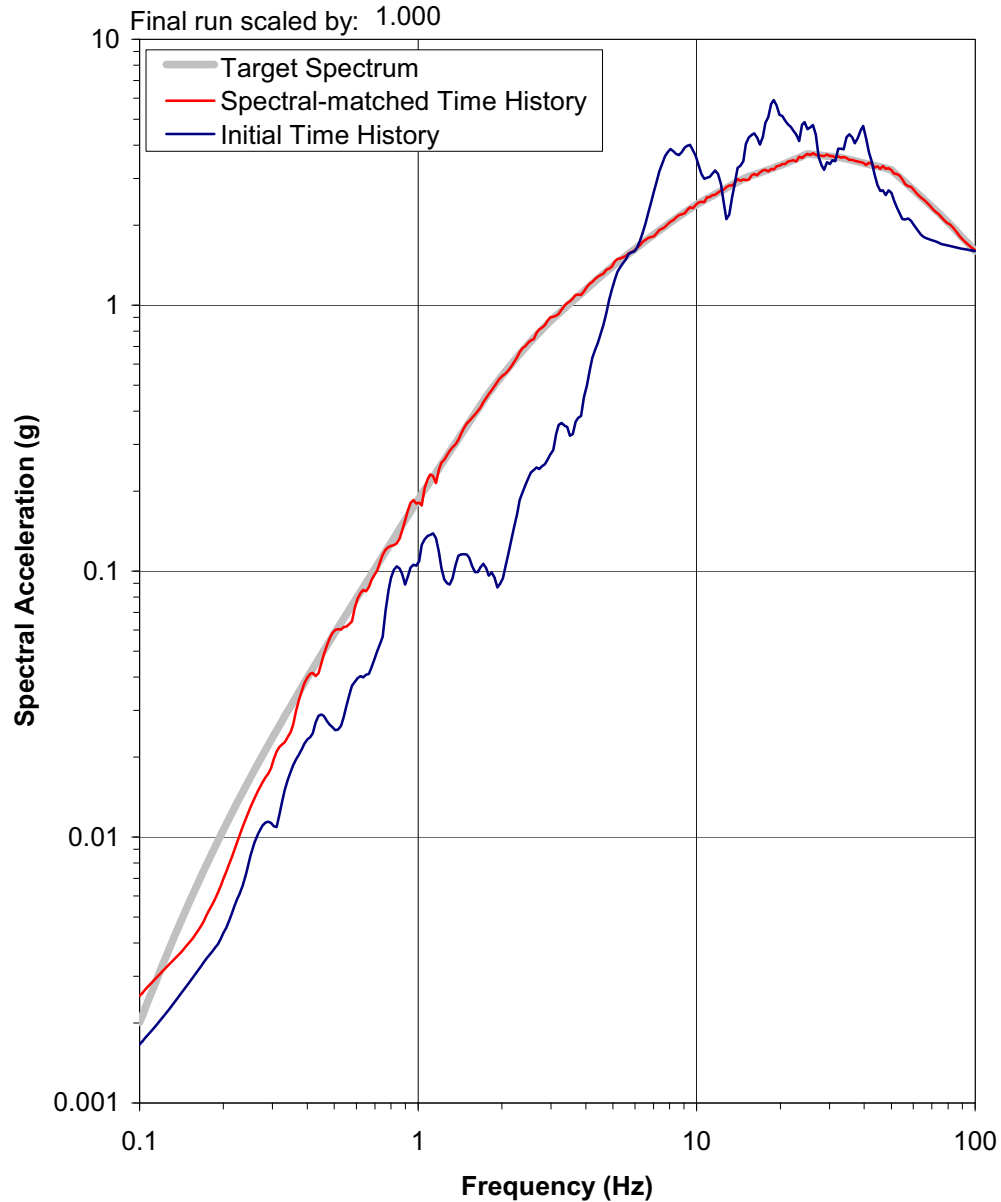


Figure 2.5-321
Comparison of 10^{-6} High Frequency Target Spectrum (Thick Grey Line), Response Spectrum from Initial Seed Input Acceleration Time History Scaled to Target PGA (Thin Blue Line), and Acceleration Response Spectrum for Final Modified Spectrum Compatible Time History (Thin Red Line)

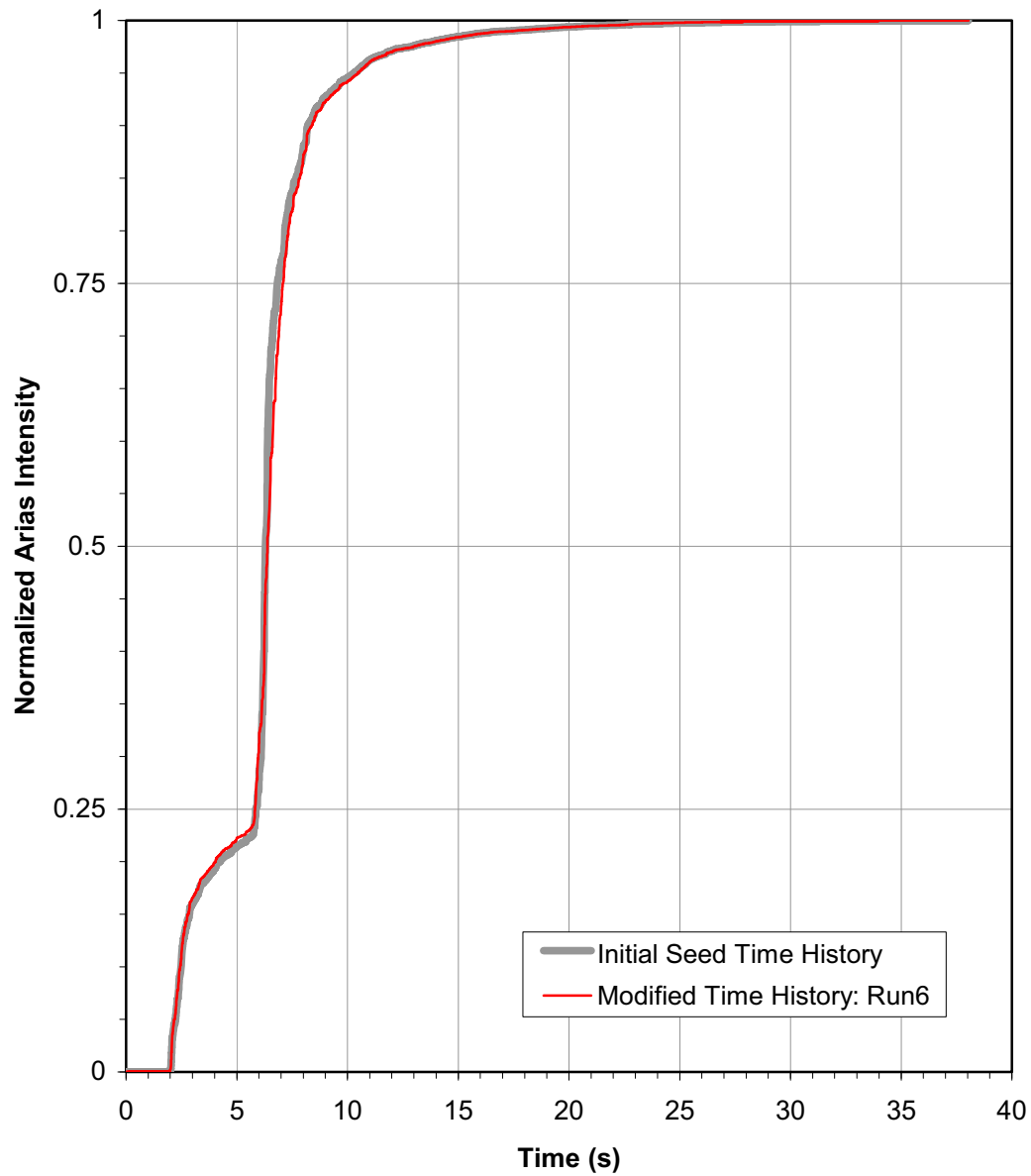


Figure 2.5-322
Comparison of Normalized Arias Intensity from Initial Seed Input Time History (Thick Grey Line) and Final Modified Spectrum Compatible (10^{-6} High Frequency Target Spectrum) Time History (Thin Red Line) for an Example Case

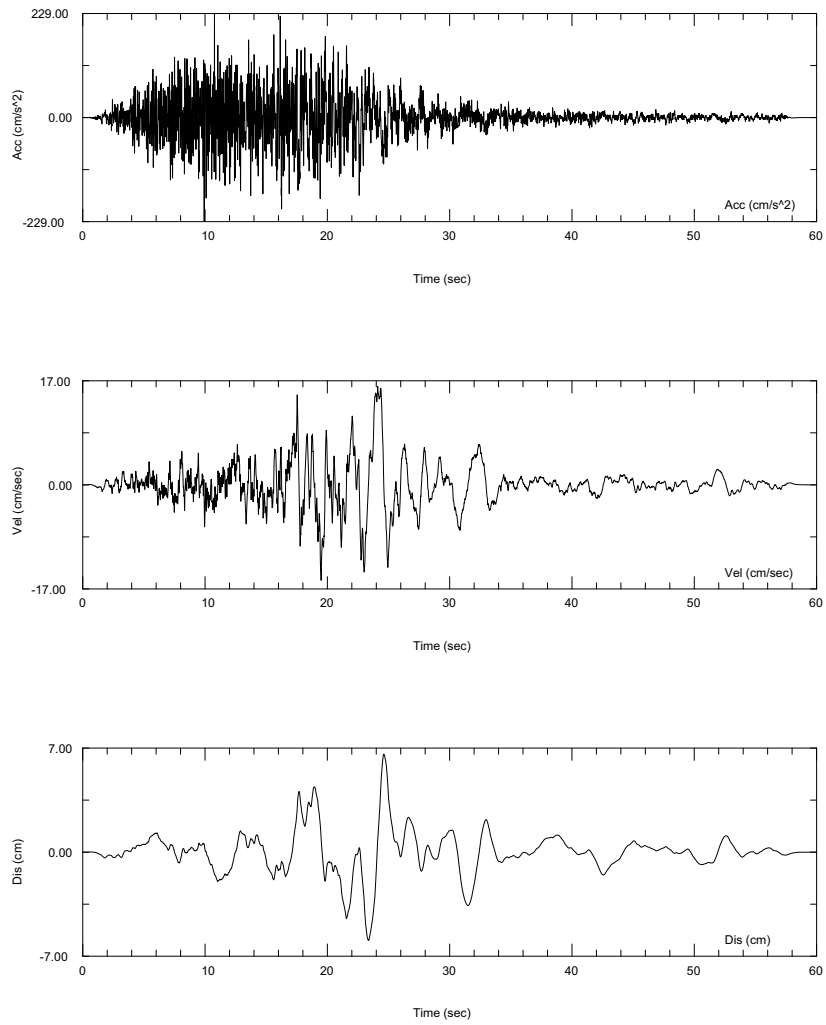


Figure 2.5-323
Horizontal Component 1 Modified Spectrum Compatible Time Acceleration,
Velocity, and Displacement Time Histories for FIRS Horizontal Target Spectrum
Prior to Application of 1.01 Scale Factor

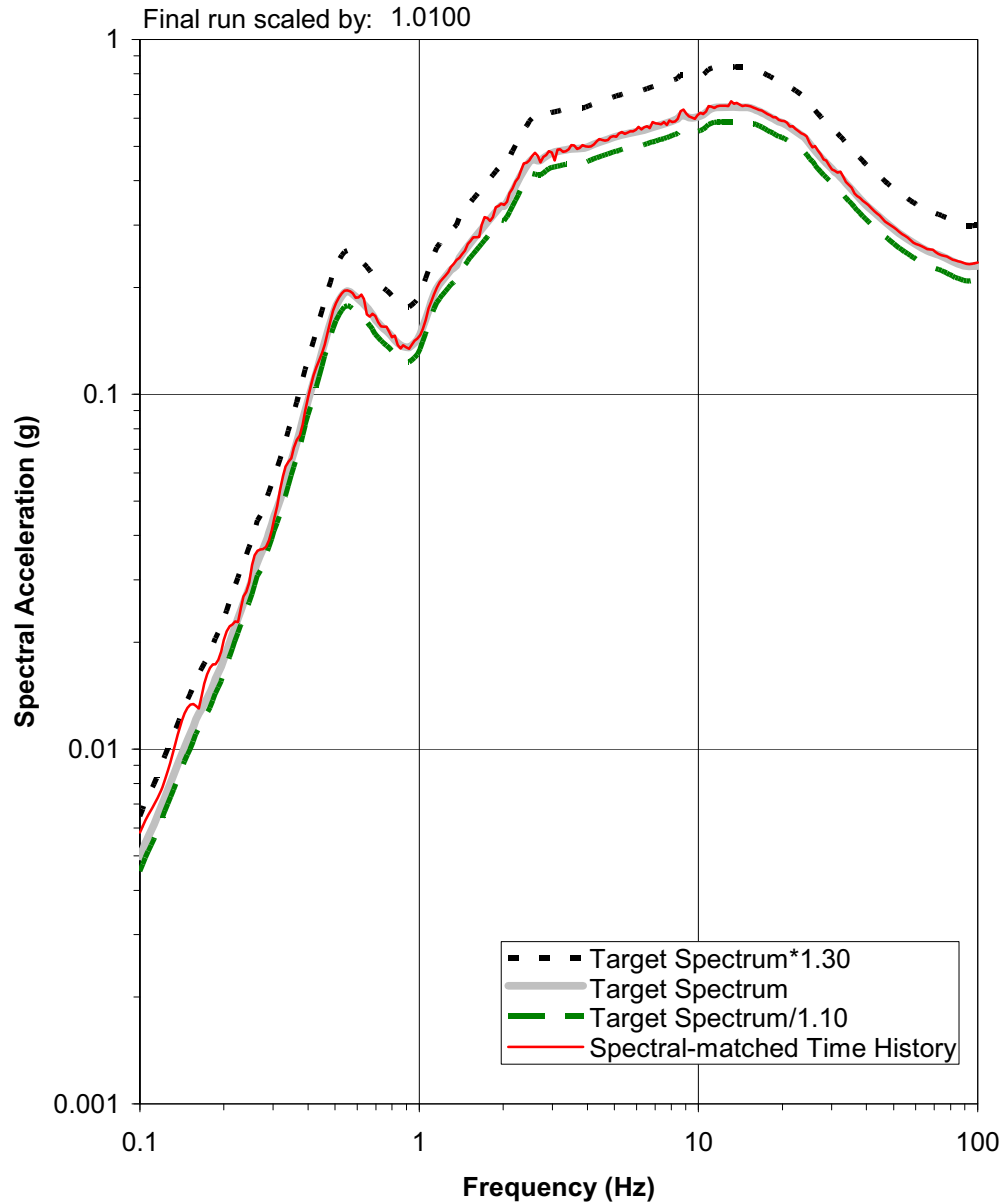


Figure 2.5-324
Comparison of Horizontal FIRS Target Spectrum (Thick Grey Line),
1.3*FIRS Target Spectrum (Dashed Black Line), 0.9*FIRS Target Spectrum
(Dashed Green Line), and Acceleration Response Spectrum
for Final Modified Spectrum Compatible Time History (Thin Red Line)
Including Application of 1.01 Scale Factor for Horizontal Component 1

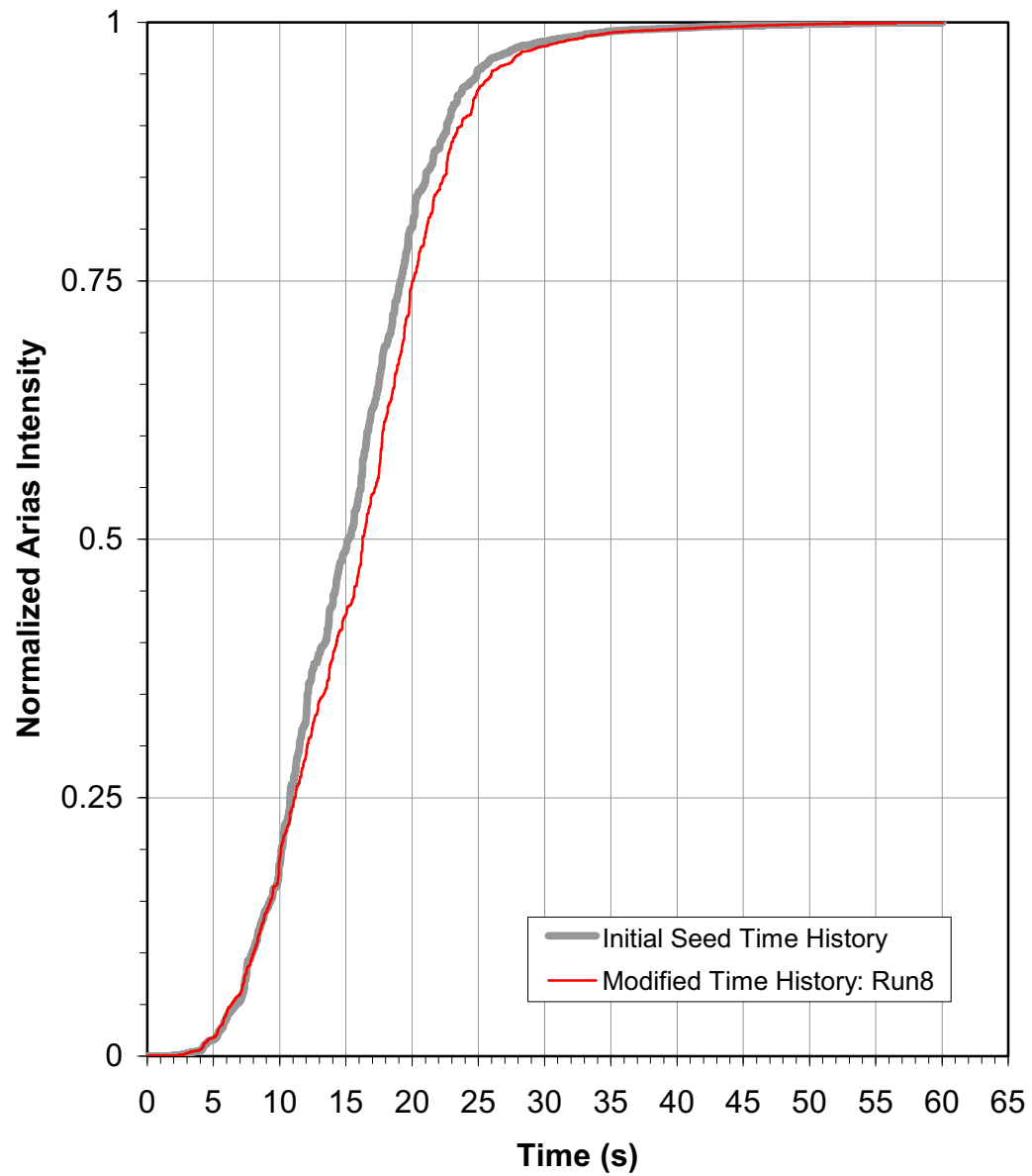


Figure 2.5-325
Comparison of Normalized Arias Intensity from Initial Seed Input Time History
(Thick Grey Line) and Final Modified Spectrum Compatible Time History
(Thin Red Line) Including Application of 1.01 Scale Factor
for Horizontal Component 1

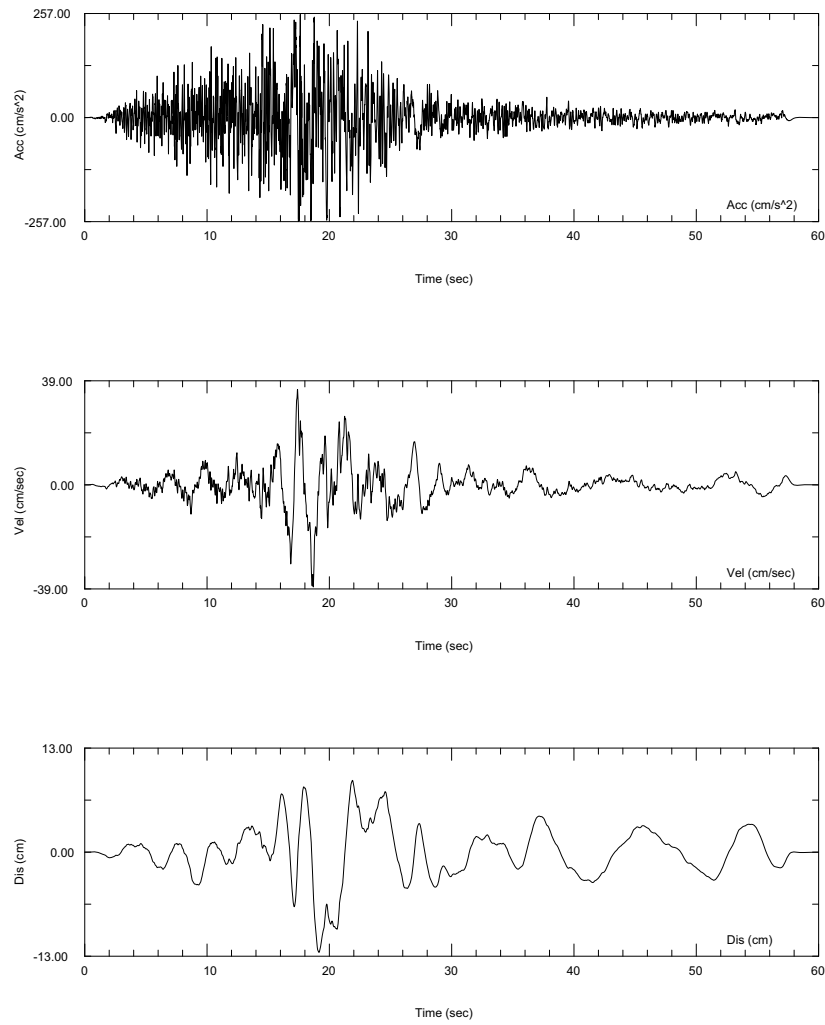


Figure 2.5-326
Horizontal Component 2 Modified Spectrum Compatible Time Acceleration,
Velocity, and Displacement Time Histories for FIRS Horizontal Target Spectrum
Prior to Application of 1.01 Scale Factor

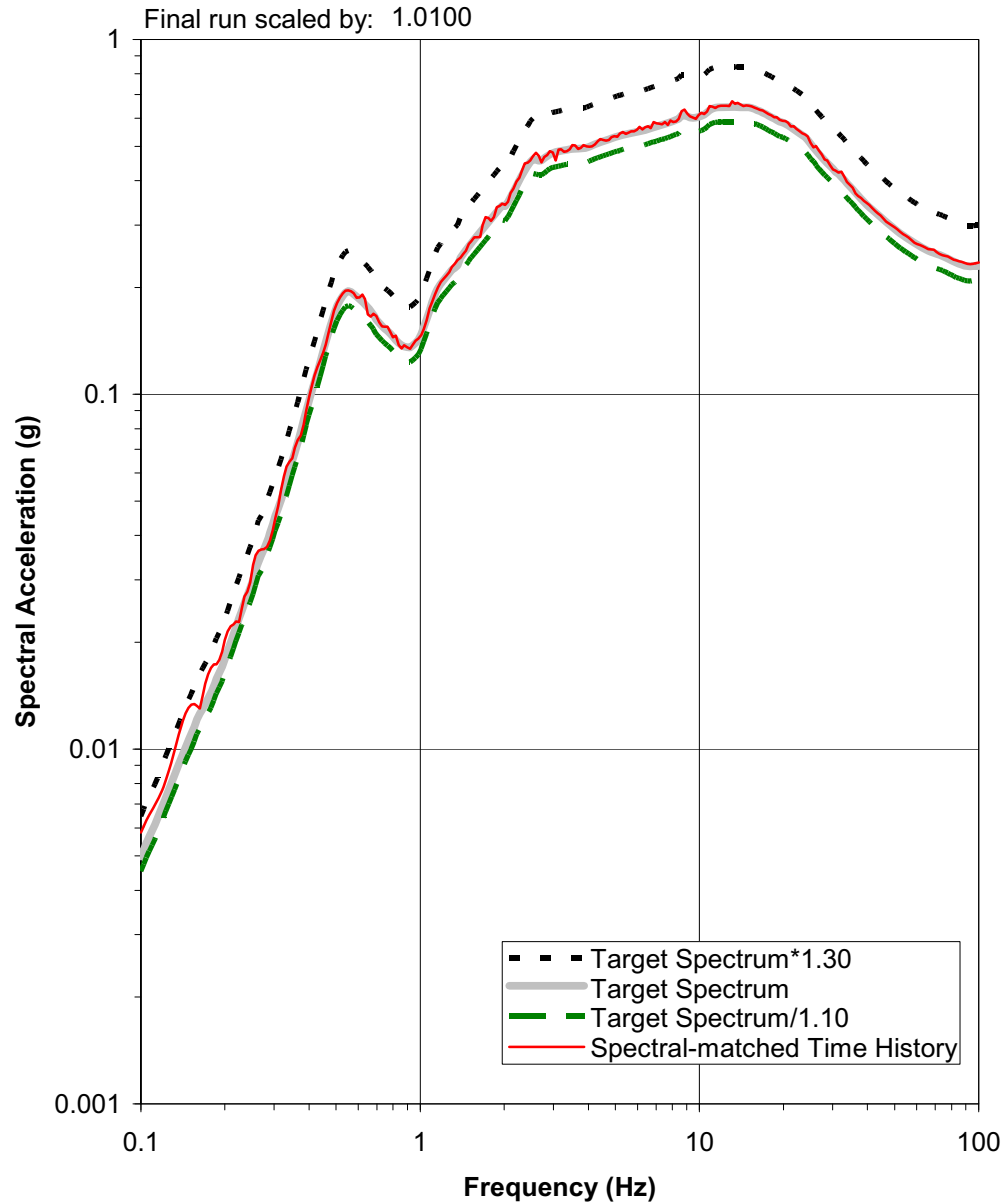


Figure 2.5-327
Comparison of Horizontal FIRS Target Spectrum
(Thick Grey Line), 1.3*FIRS Target Spectrum (Dashed Black Line),
0.9*FIRS Target Spectrum (Dashed Green Line), and Acceleration Response
Spectrum for Final Modified Spectrum Compatible Time History (Thin Red Line)
Including Application of 1.01 Scale Factor for Horizontal Component 2

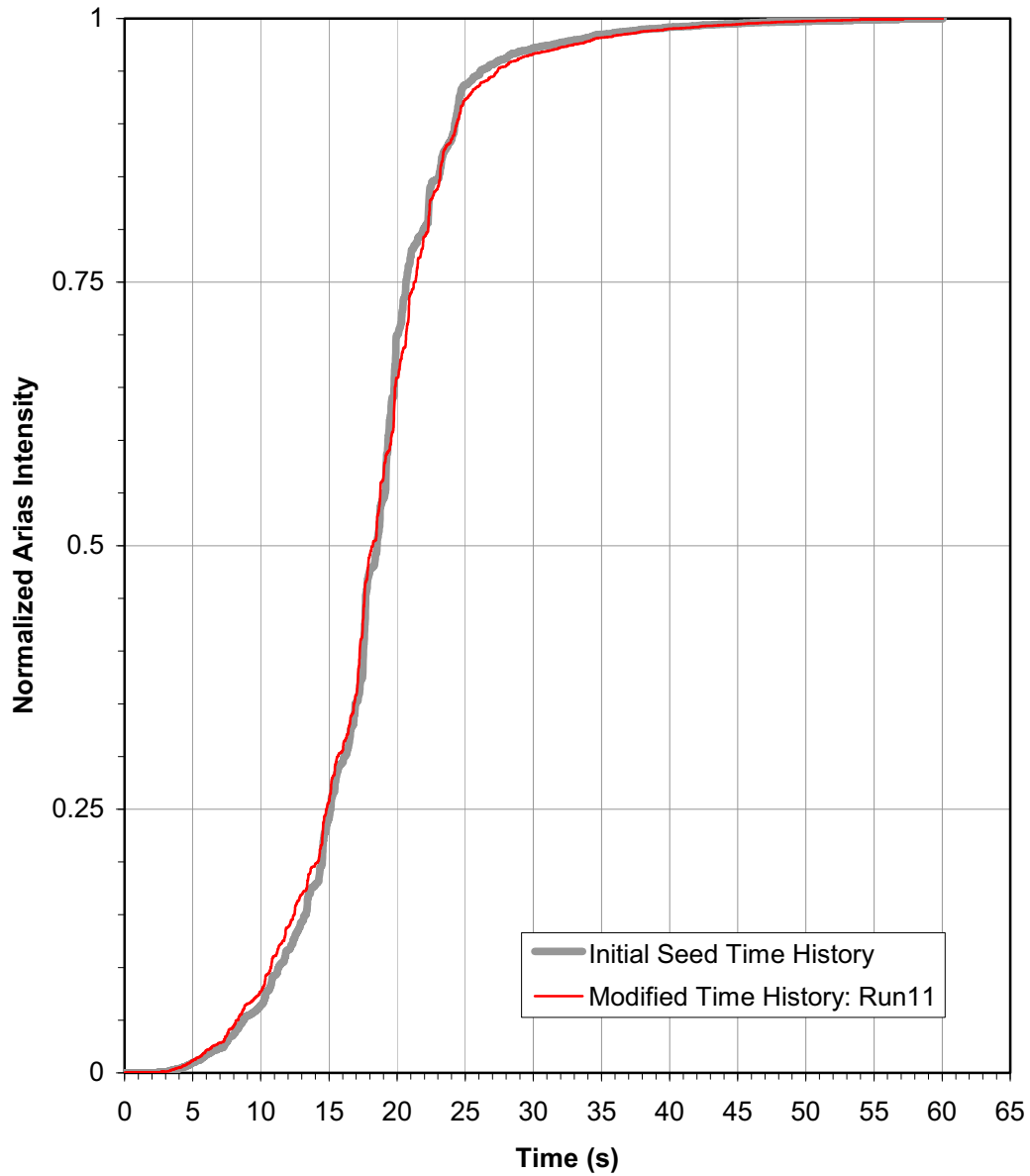


Figure 2.5-328
Comparison of Normalized Arias Intensity from Initial Seed Input Time History
(Thick Grey Line) and Final Modified Spectrum Compatible Time History
(Thin Red Line) Including Application of 1.01 Scale Factor
for Horizontal Component 2

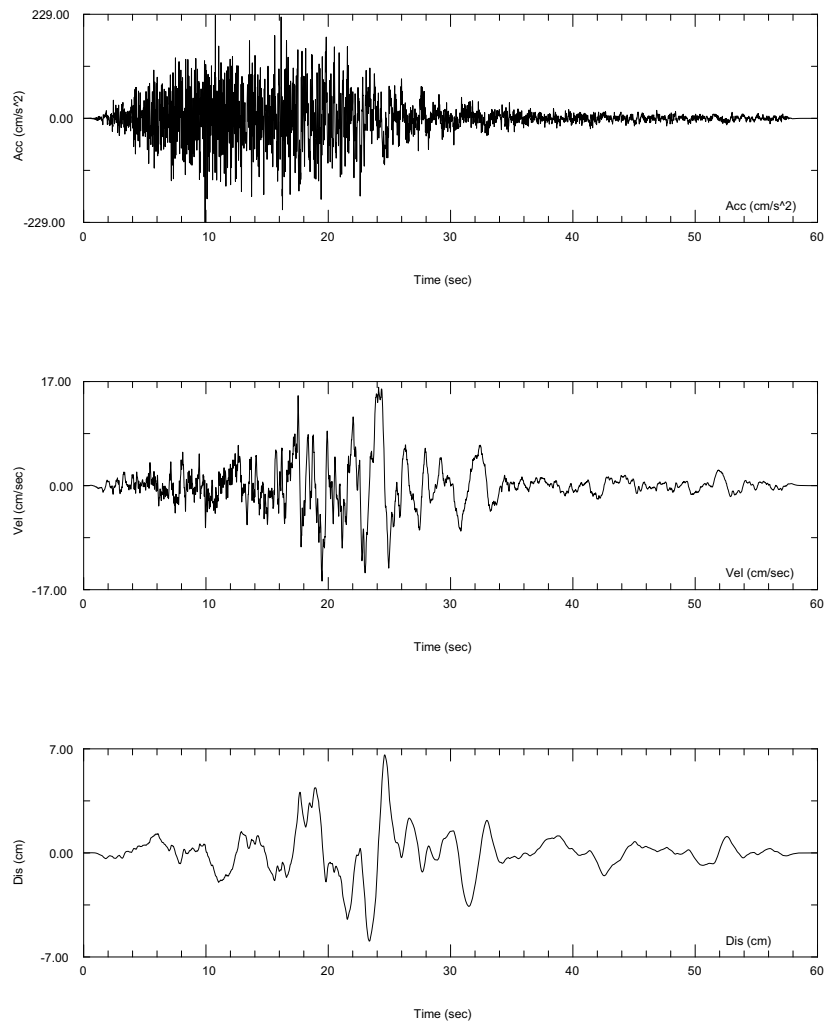


Figure 2.5-329
Vertical Component Modified Spectrum Compatible Time Acceleration,
Velocity, and Displacement Time Histories for FIRS Vertical Target
Spectrum Prior to Application of 1.01 Scale Factor

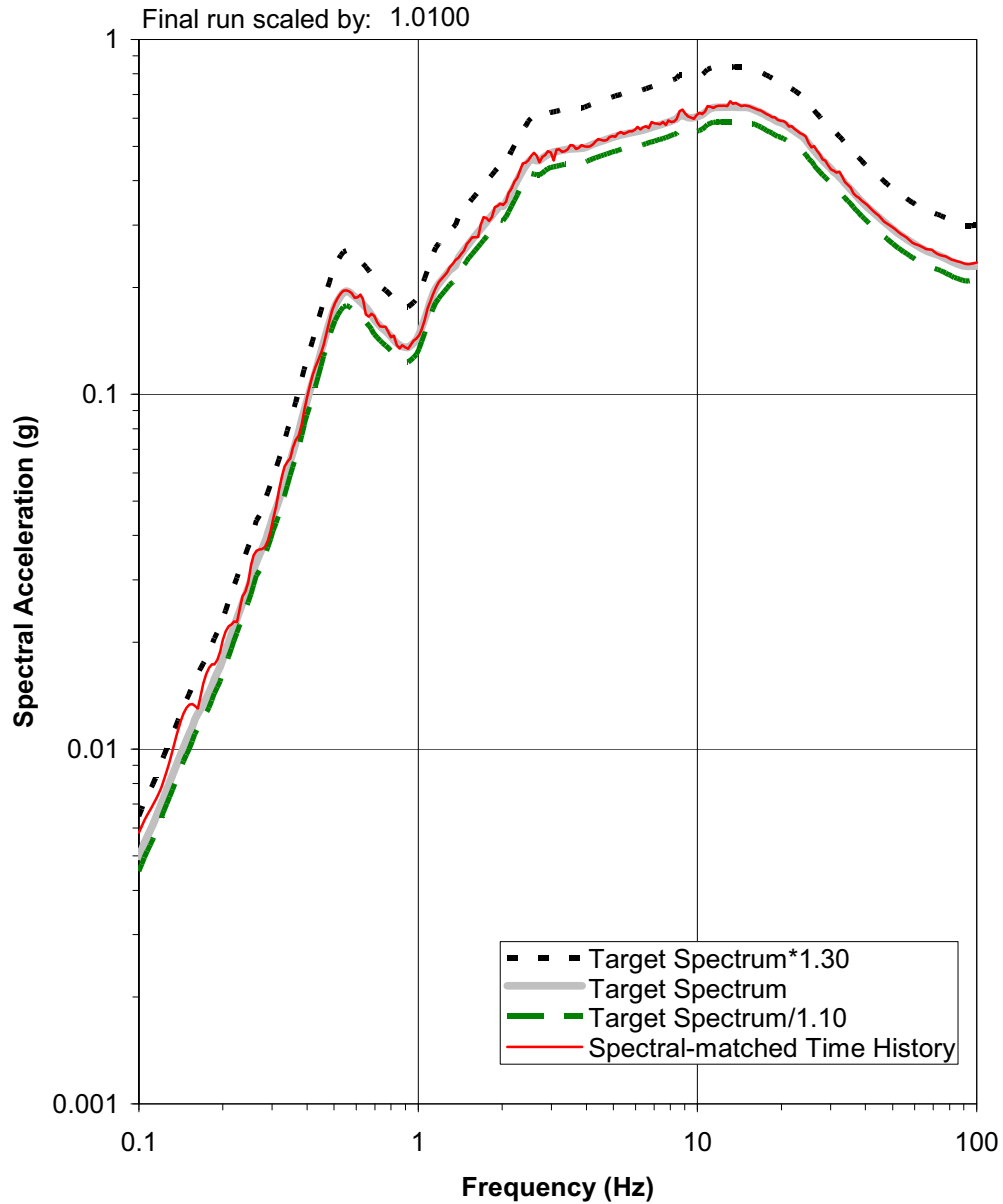


Figure 2.5-330
Comparison of Vertical FIRS Target Spectrum (Thick Grey Line),
1.3*FIRS Target Spectrum (Dashed Black Line), 0.9*FIRS Target Spectrum
(Dashed Green Line), and Acceleration Response Spectrum
for Final Modified Spectrum Compatible Time History (Thin Red Line)
Including Application of 1.01 Scale Factor for Vertical Component

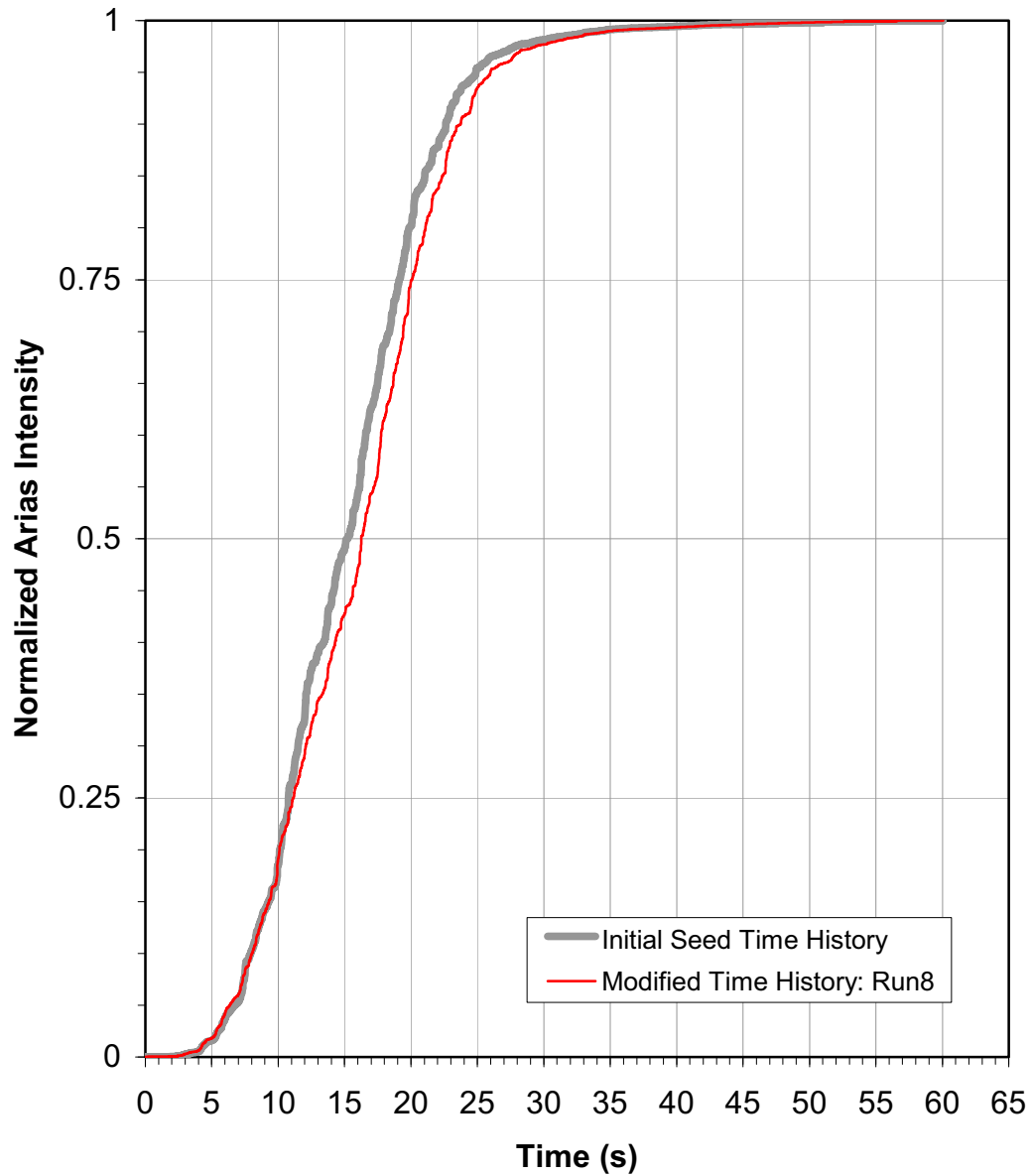


Figure 2.5-331
Comparison of Normalized Arias Intensity from Initial Seed Input Time History (Thick Grey Line) and Final Modified Spectrum Compatible Time History (Thin Red Line) Including Application of 1.01 Scale Factor for Vertical Component

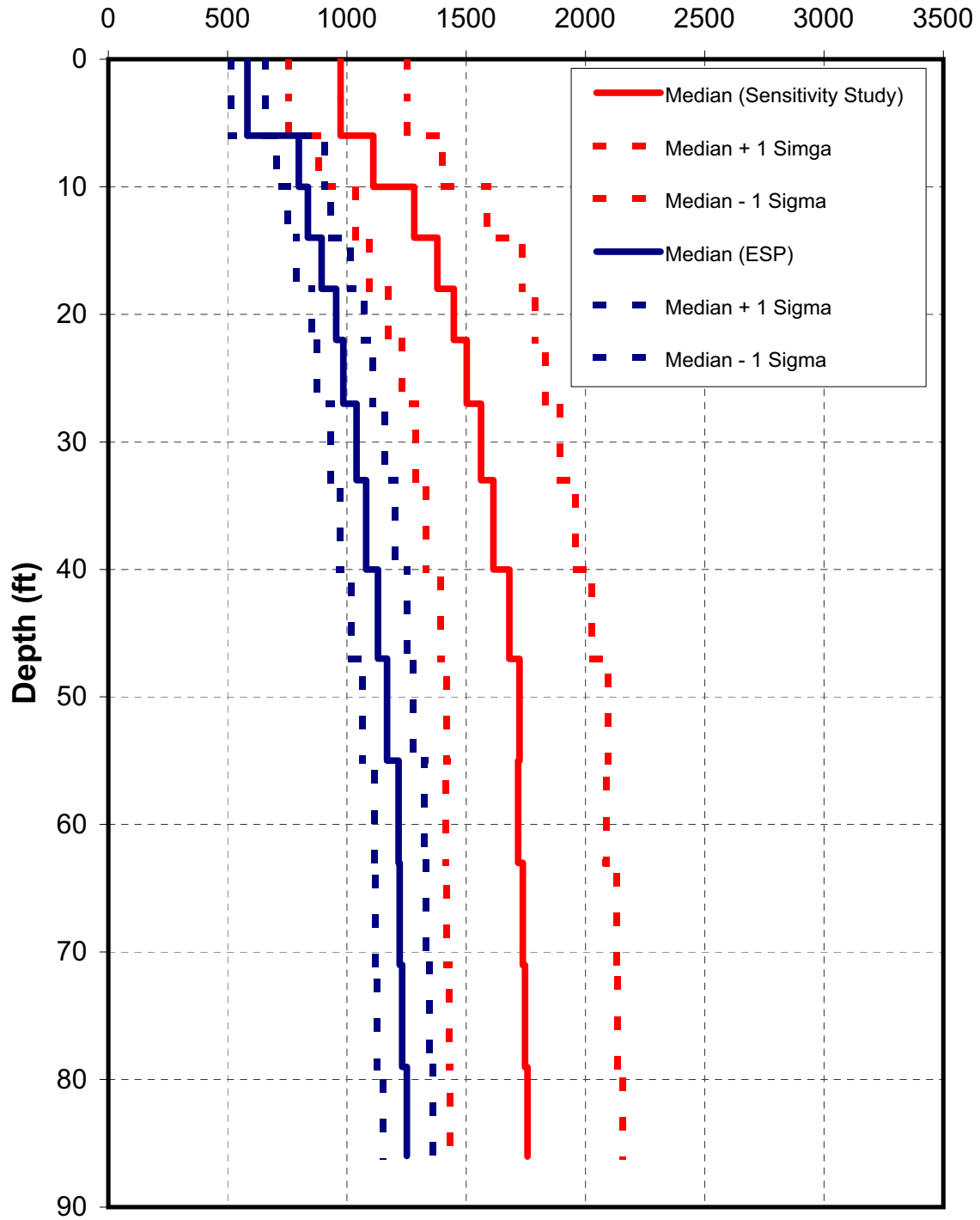


Figure 2.5-332
Low Strain Backfill Shear Wave Velocity (ft/sec)

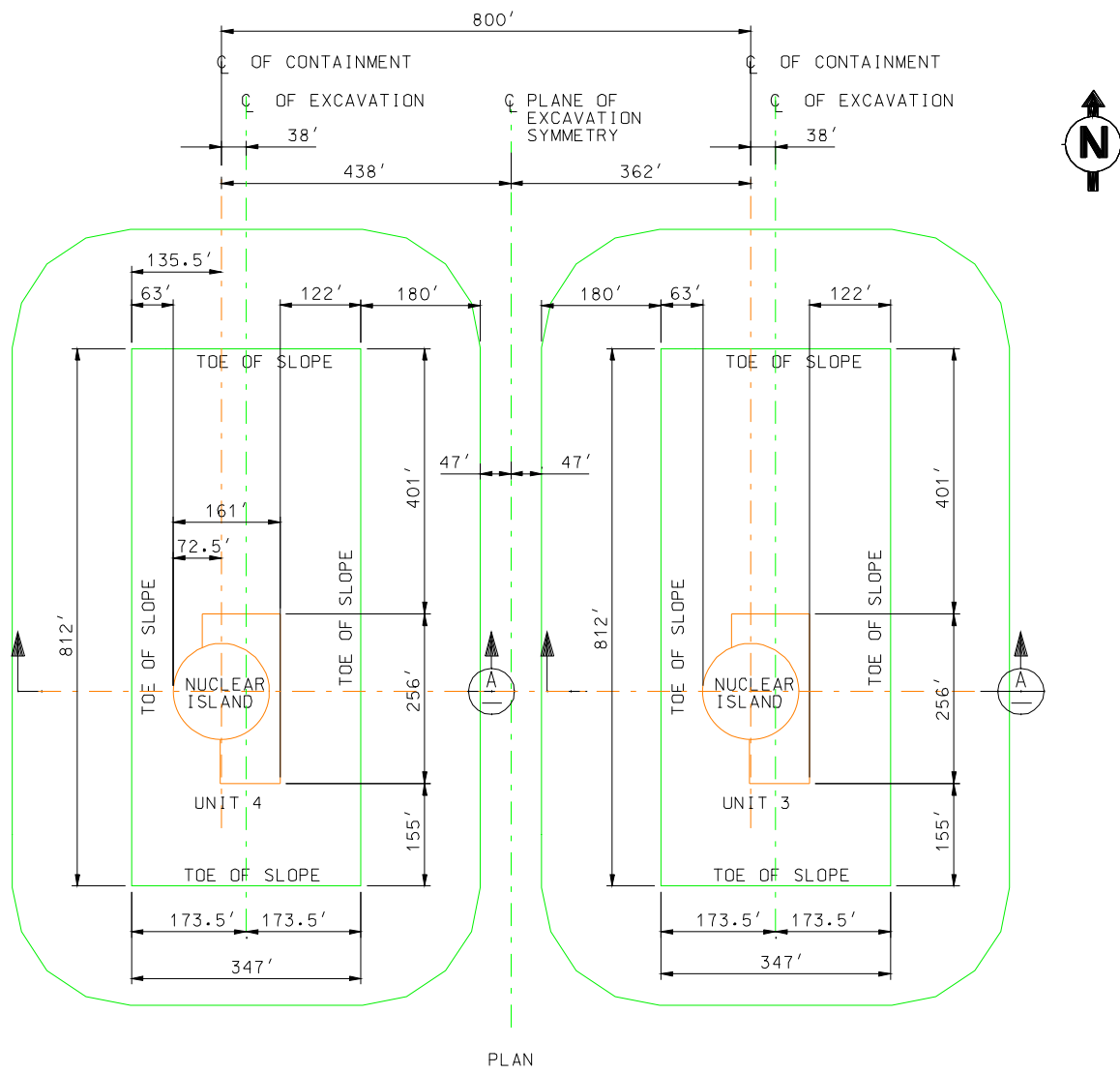


Figure 2.5-333
Plant Layout

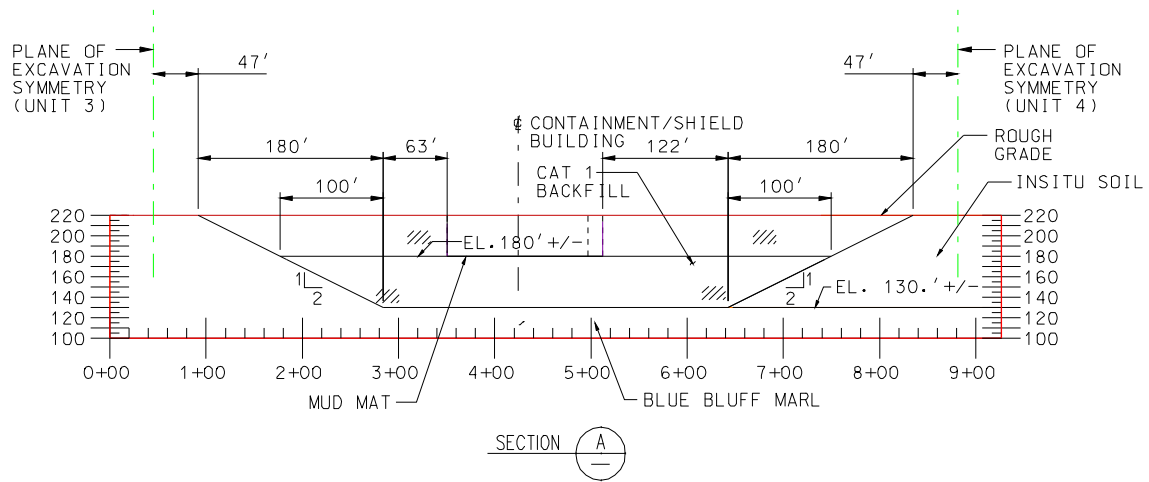


Figure 2.5-334
Cross Section A

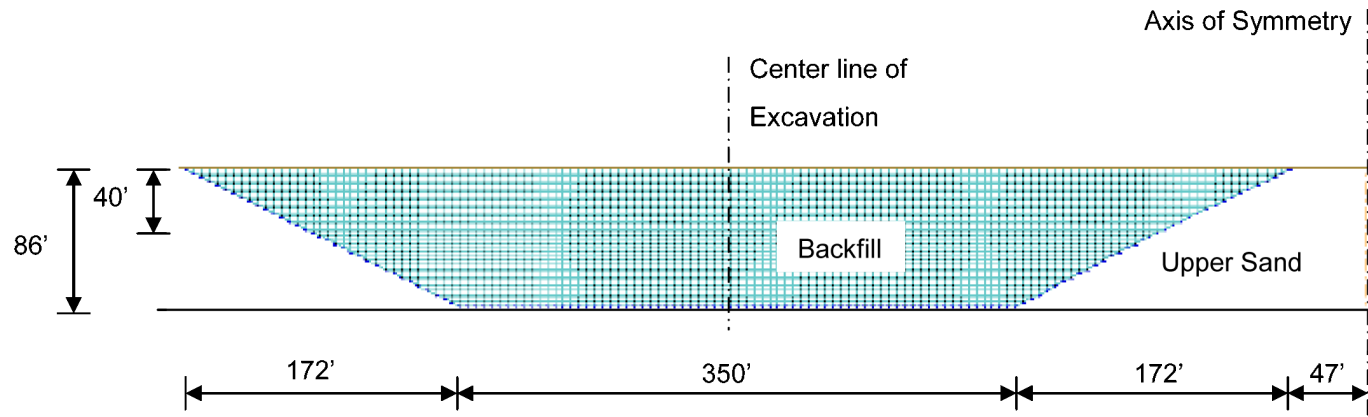


Figure 2.5-335
SASSI 2D-Model

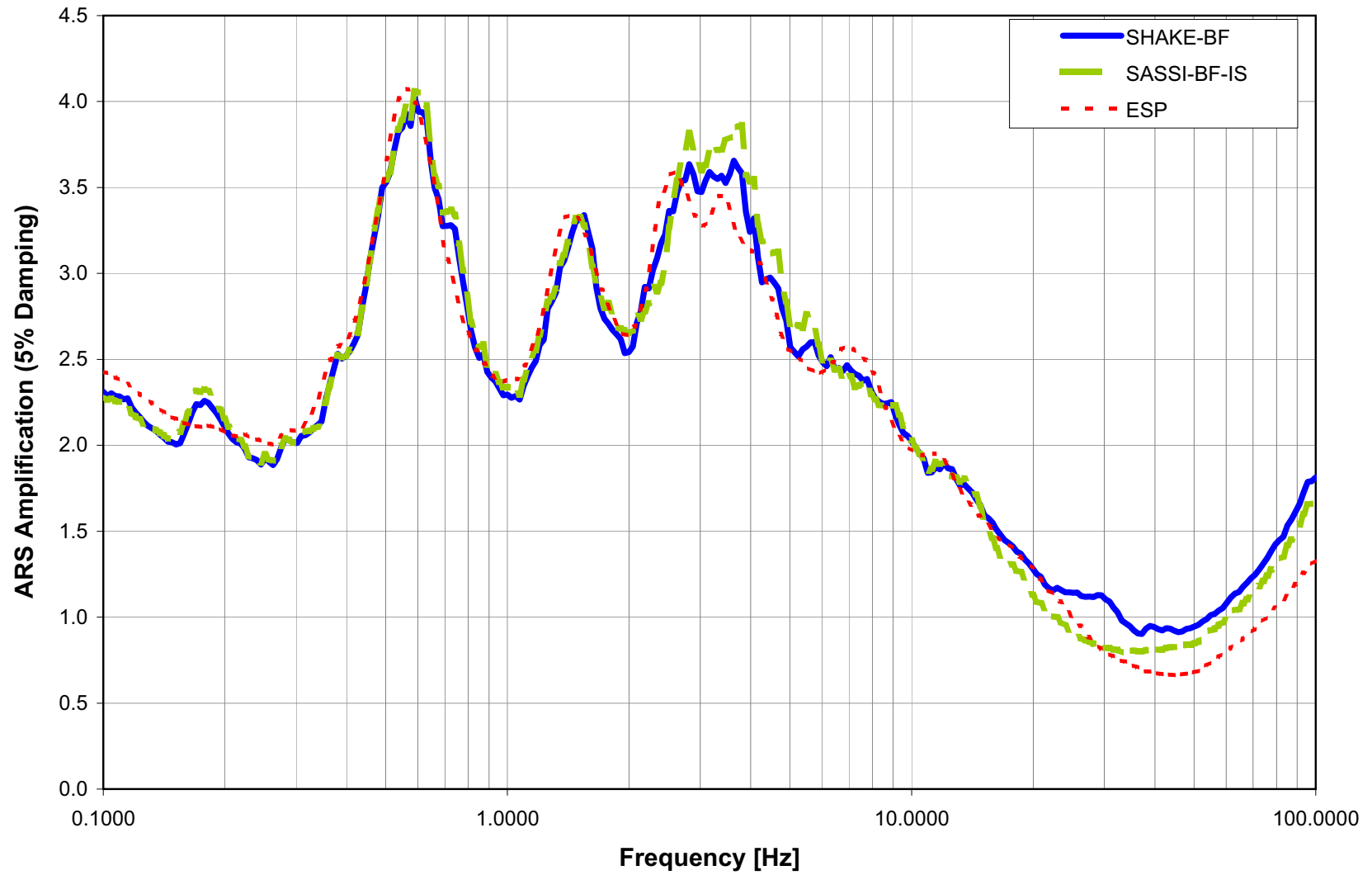


Figure 2.5-336
Amplification at 0 ft (GMRS Horizon)

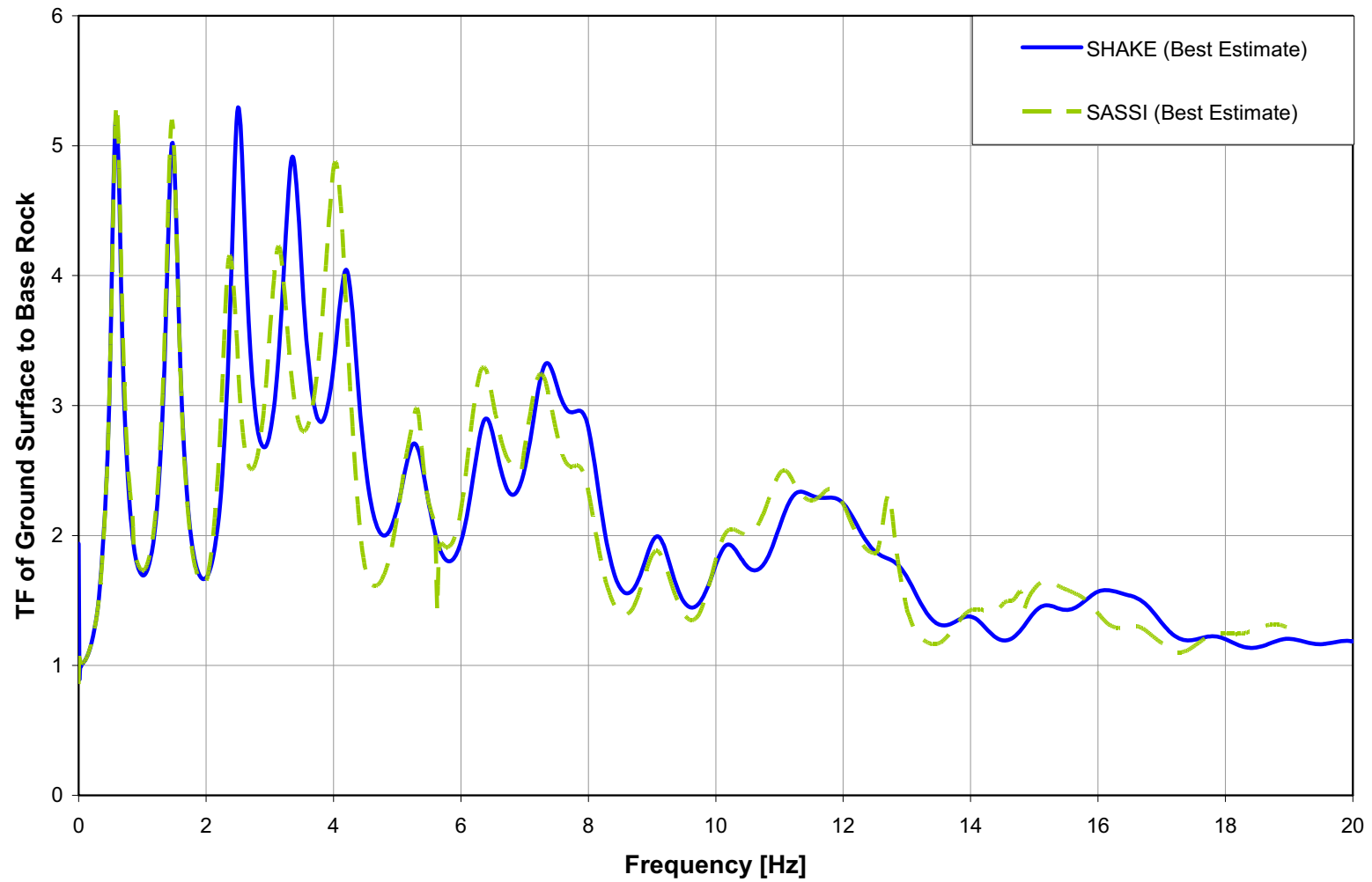


Figure 2.5-337
Transfer Functions at 0 ft (GMRS Horizon)

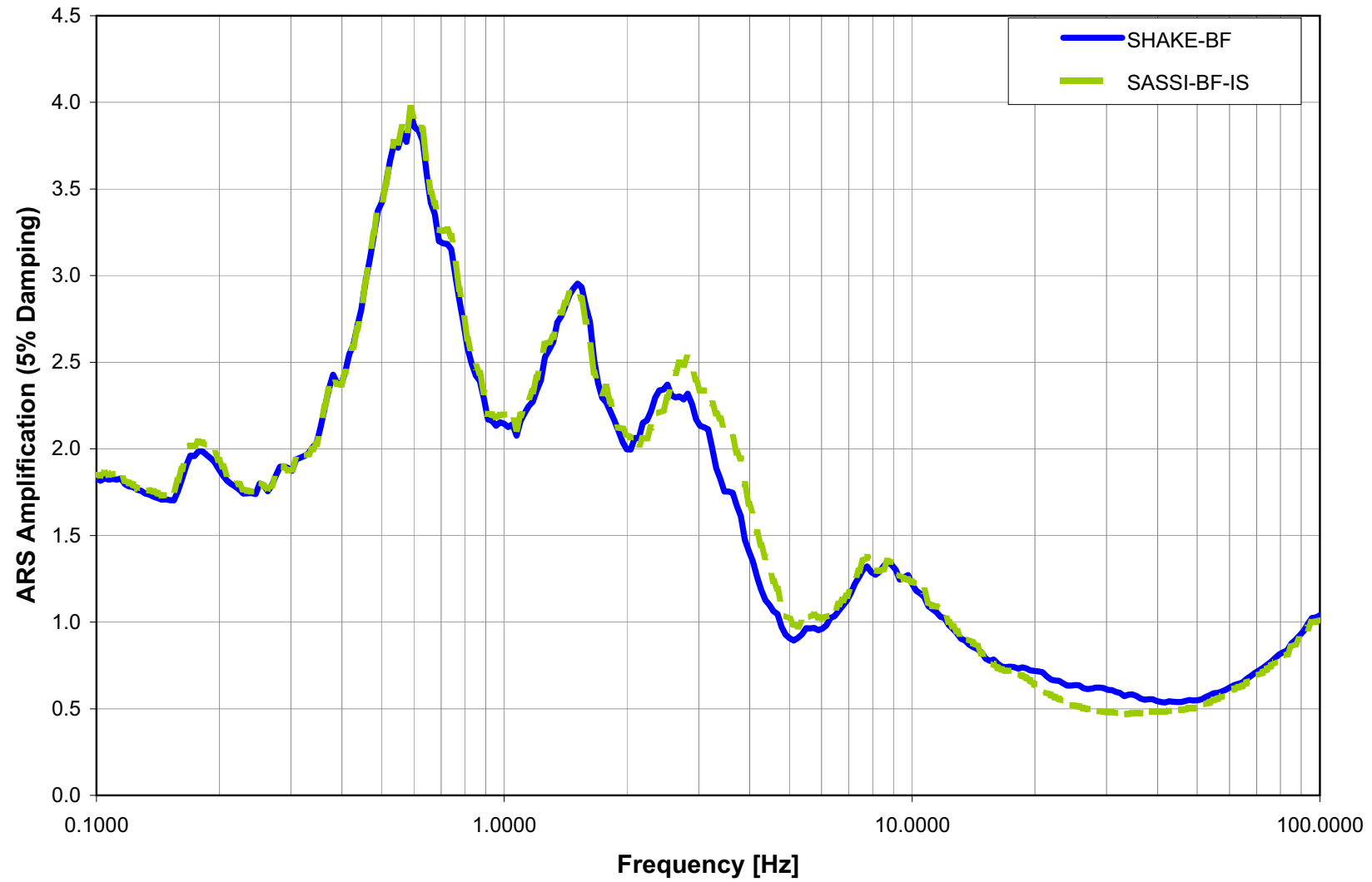


Figure 2.5-338
Amplification at 40 ft depth (FIRS horizon)

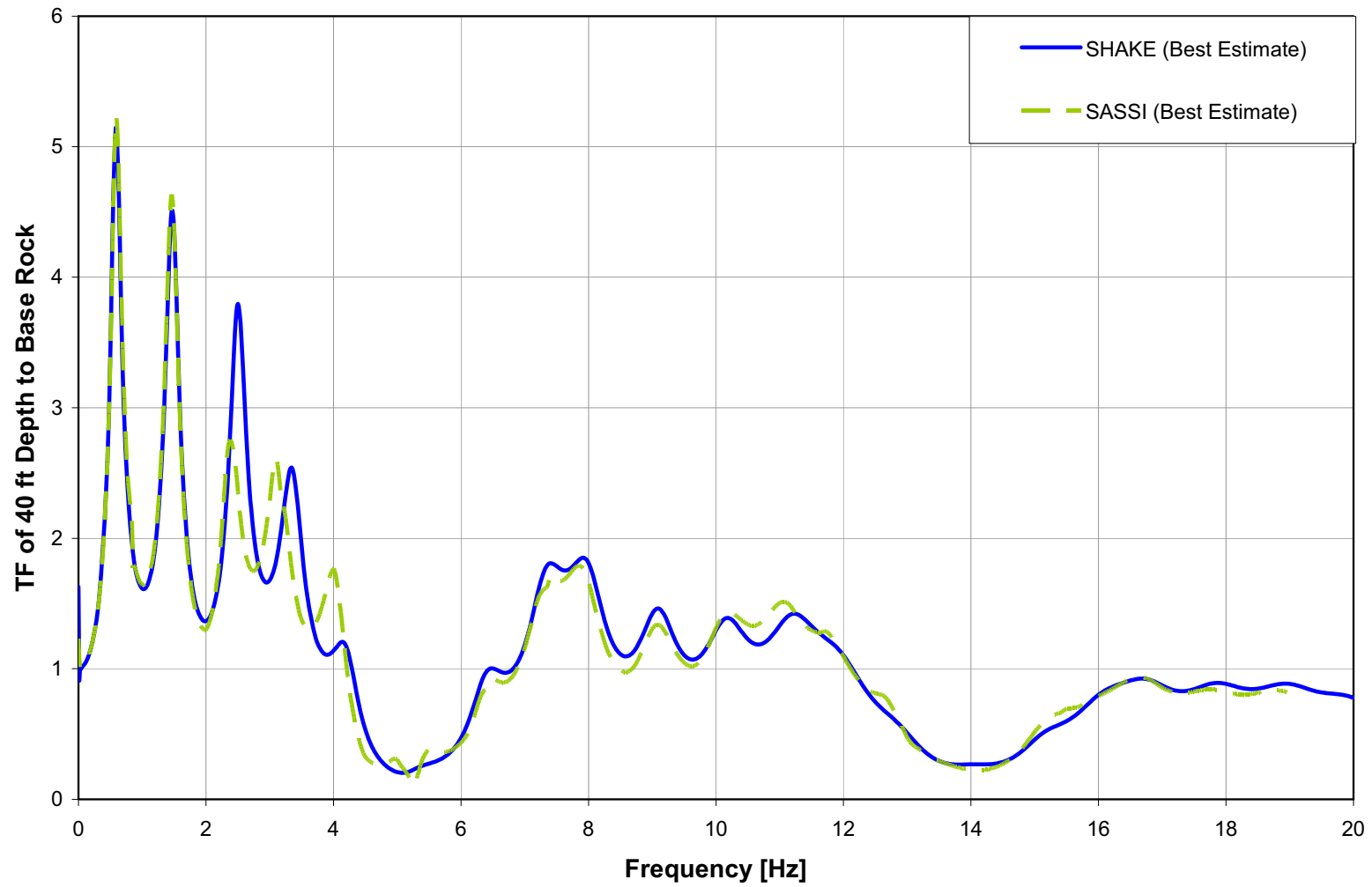


Figure 2.5-339
Transfer Functions at 40 ft (FIRS Horizon)

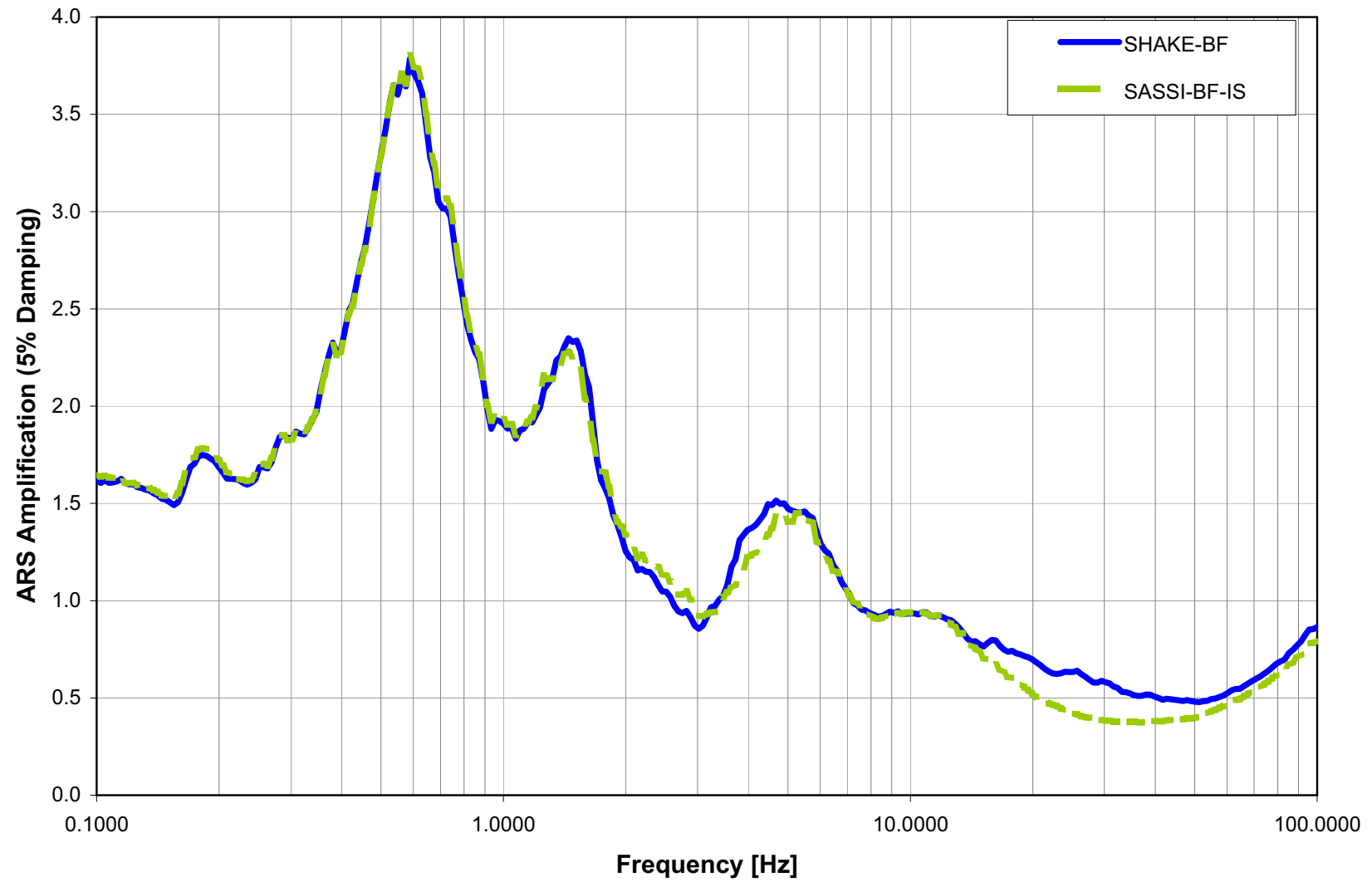


Figure 2.5-340
Amplification at 86 ft depth (Top of Blue Bluff Marl)

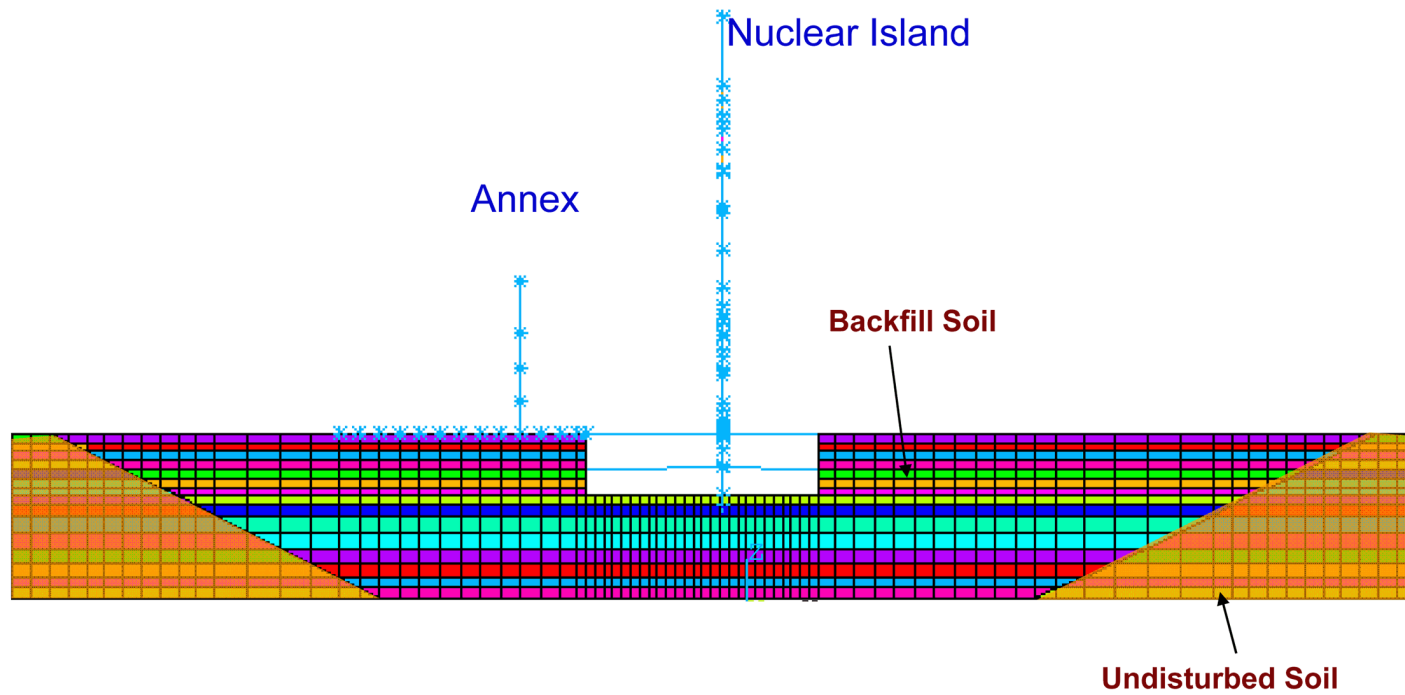


Figure 2.5-341
2D SASSI Backfill Model

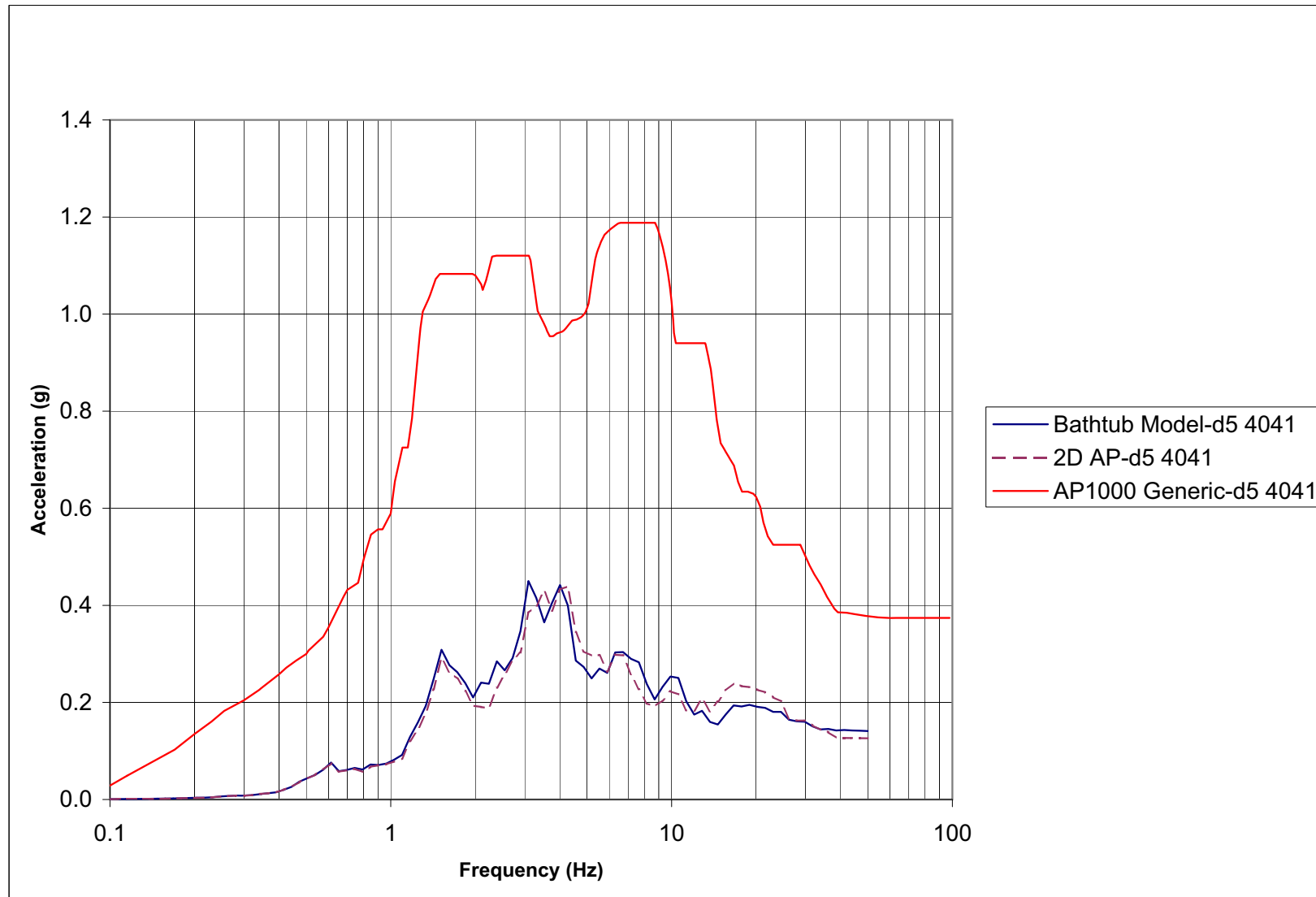


Figure 2.5-342
Node 4041 — EL 99.00 NI at Reactor Vessel Support Elevation

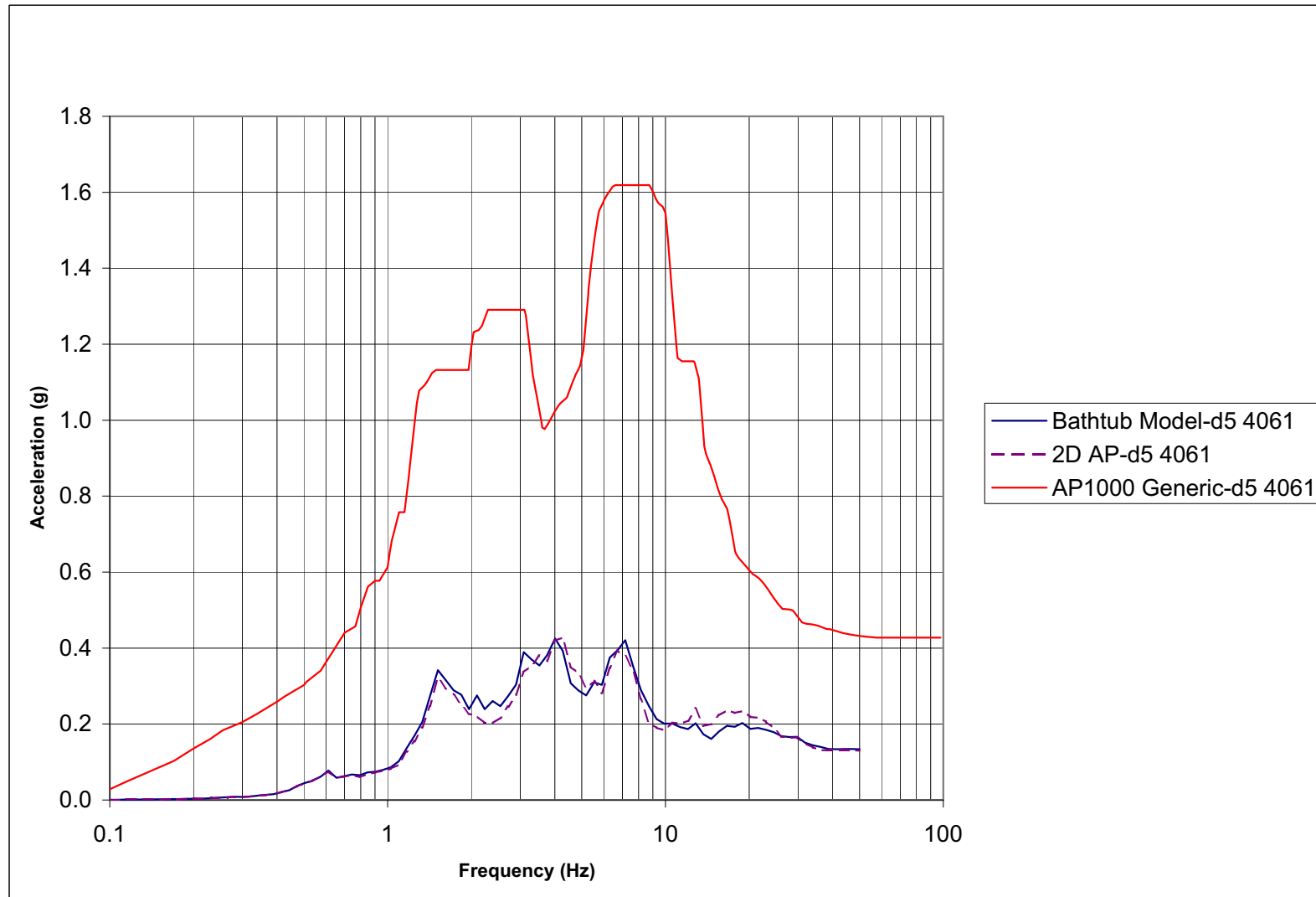


Figure 2.5-343
Node 4061 — EL 116.5 Auxiliary Shield Building at Control Room Floor

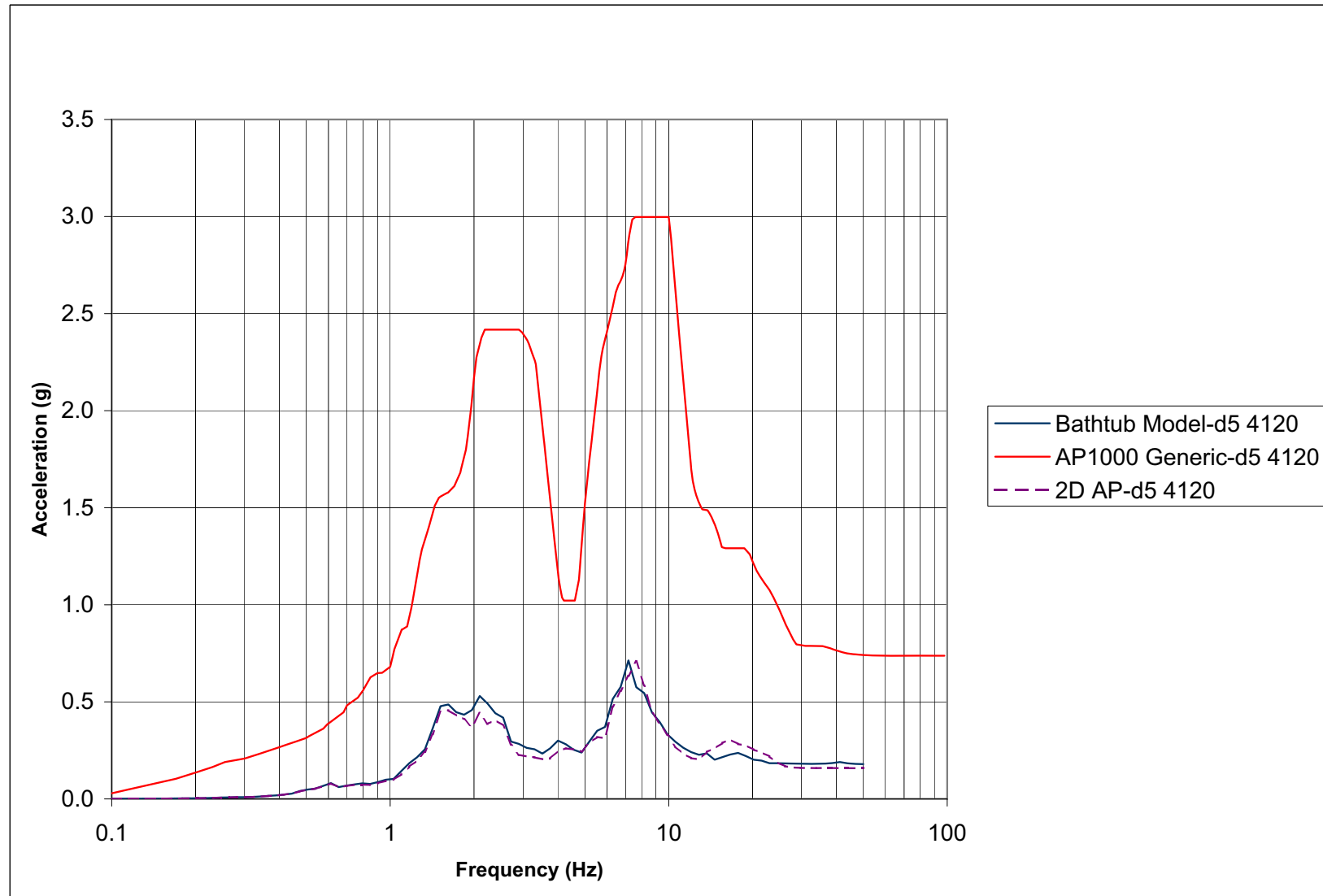


Figure 2.5-344
Node 4120 — EL 179.56 ASB Auxiliary Building Roof Area

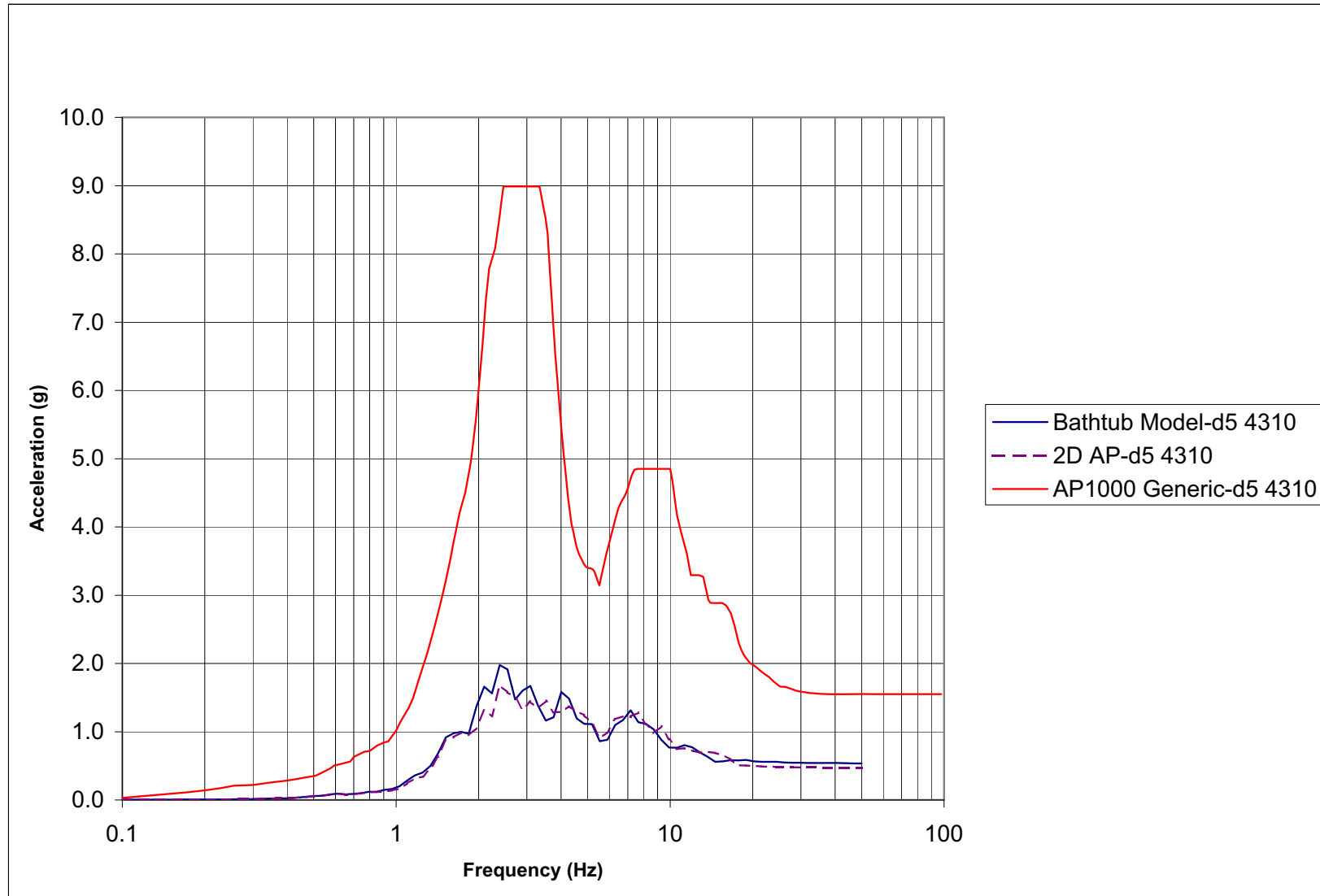


Figure 2.5-345
Node 4310 — EL 327.41 ASB Shield Building Roof Area

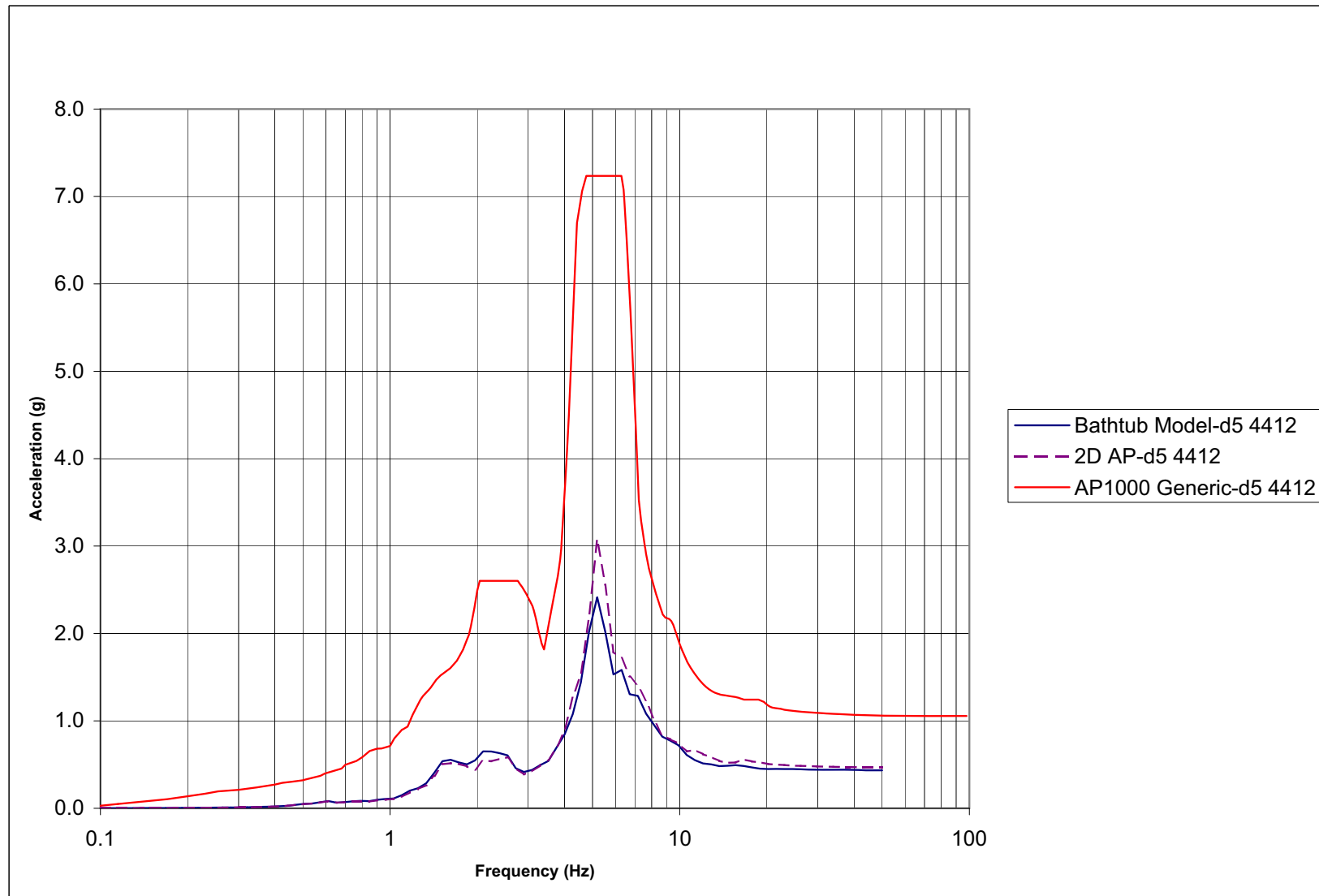


Figure 2.5-346
Node 4412 — EL 224 Steel Containment Vessel Near Polar Crane

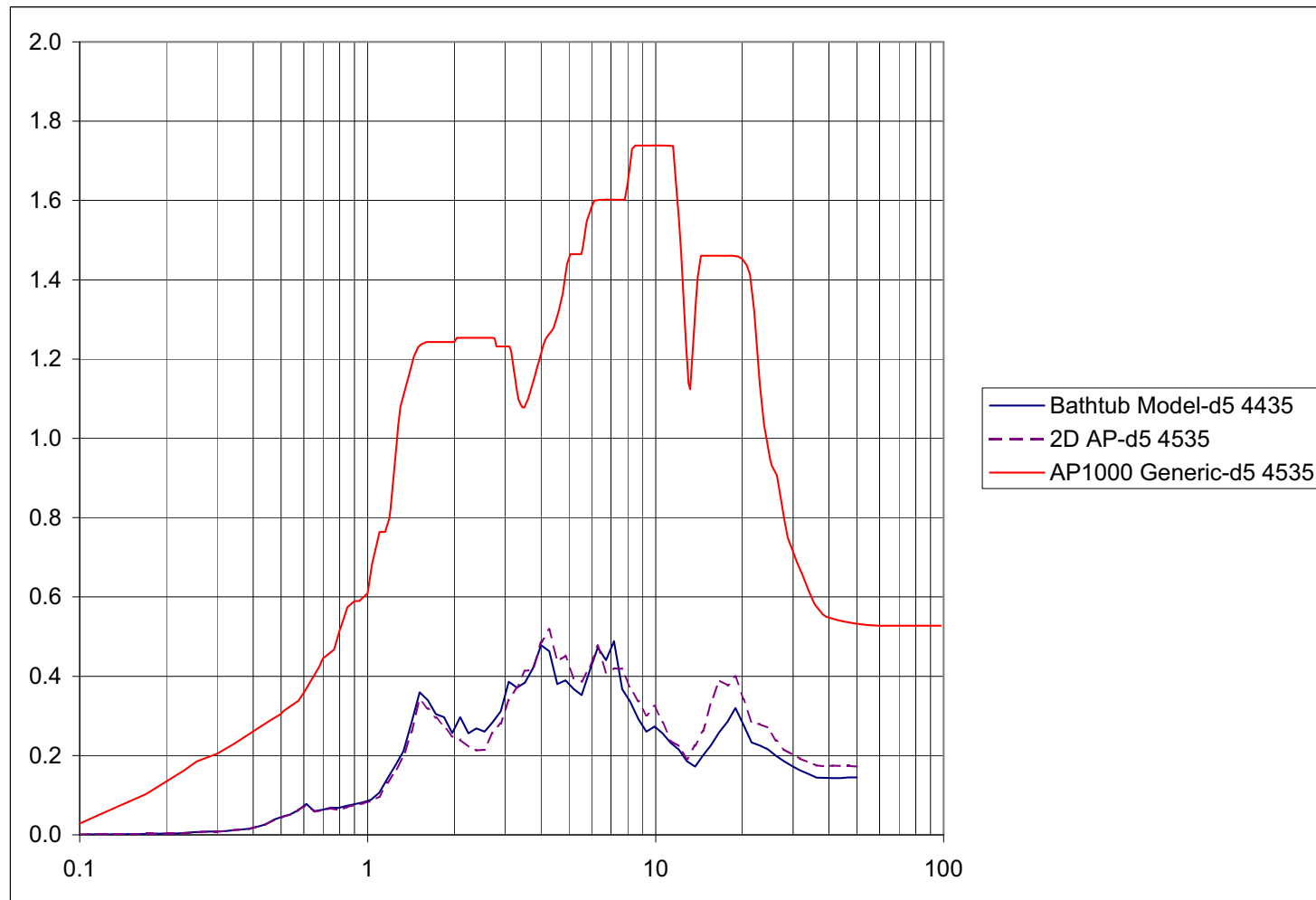


Figure 2.5-347
Node 4335 — EL 135.25 Containment Internal Structure at Operating Deck

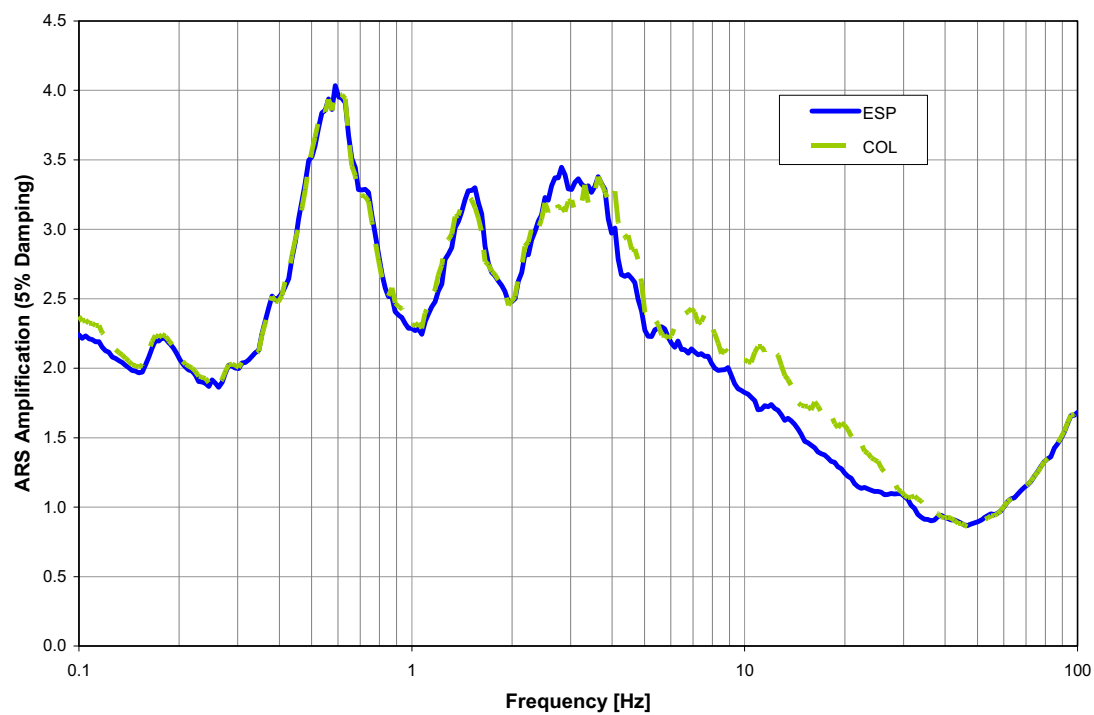


Figure 2.5-348
Amplification at 40-ft Outcrop Depth (FIRS Horizon)

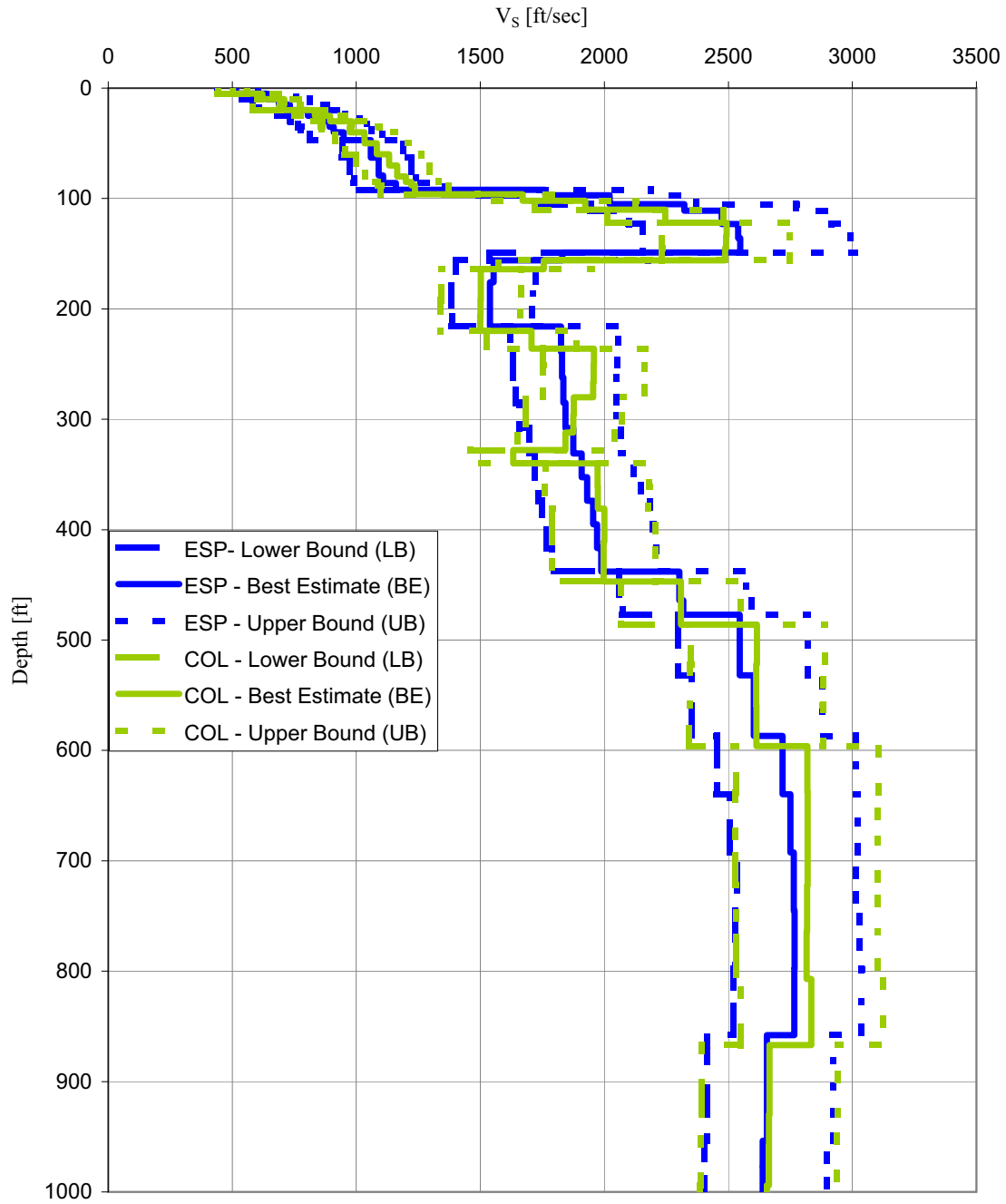


Figure 2.5-349
Vogtle Strain Compatible Profiles (S-Wave Velocity)

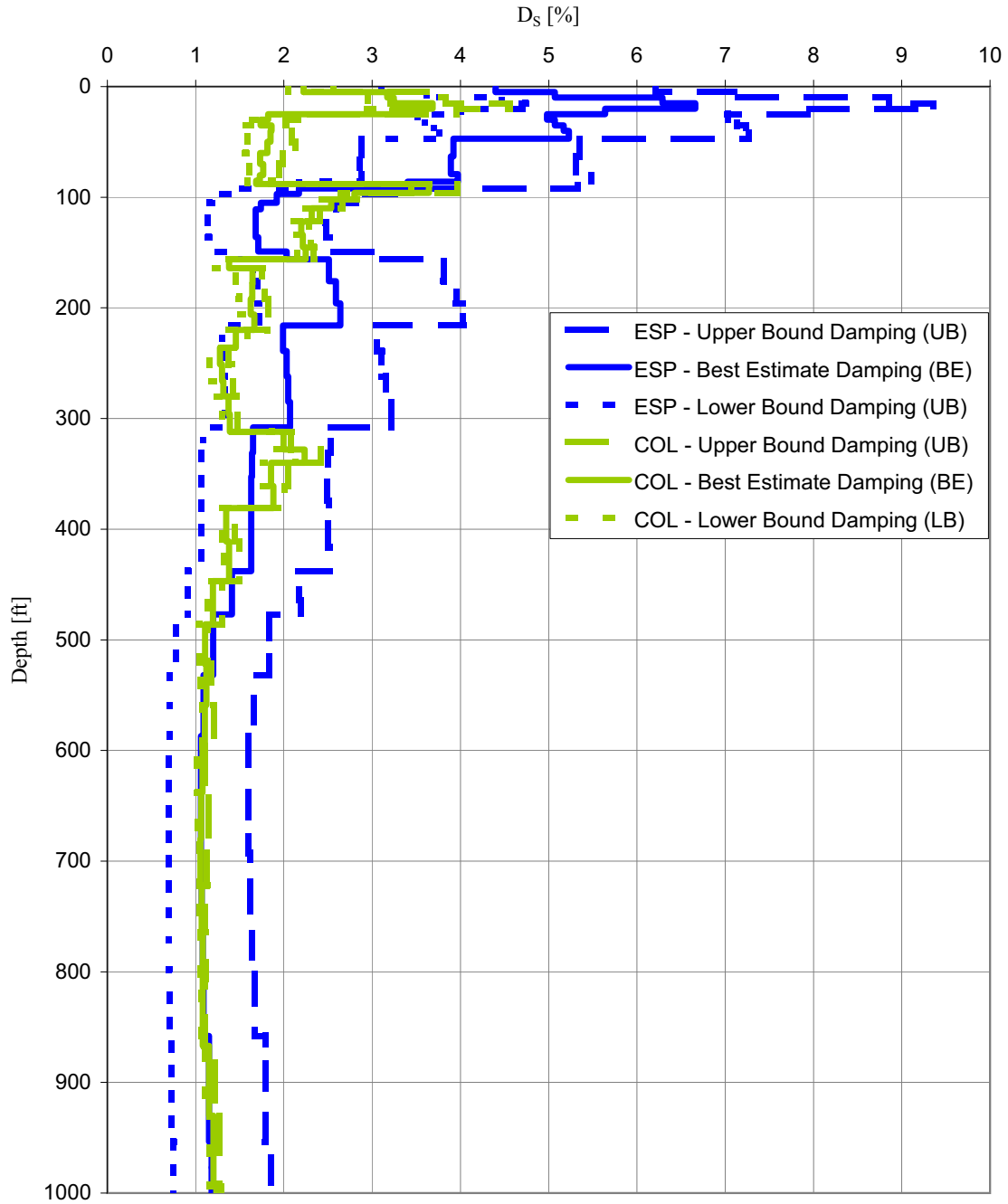


Figure 2.5-350
Vogtle Strain Compatible Profiles (S-Wave Damping)

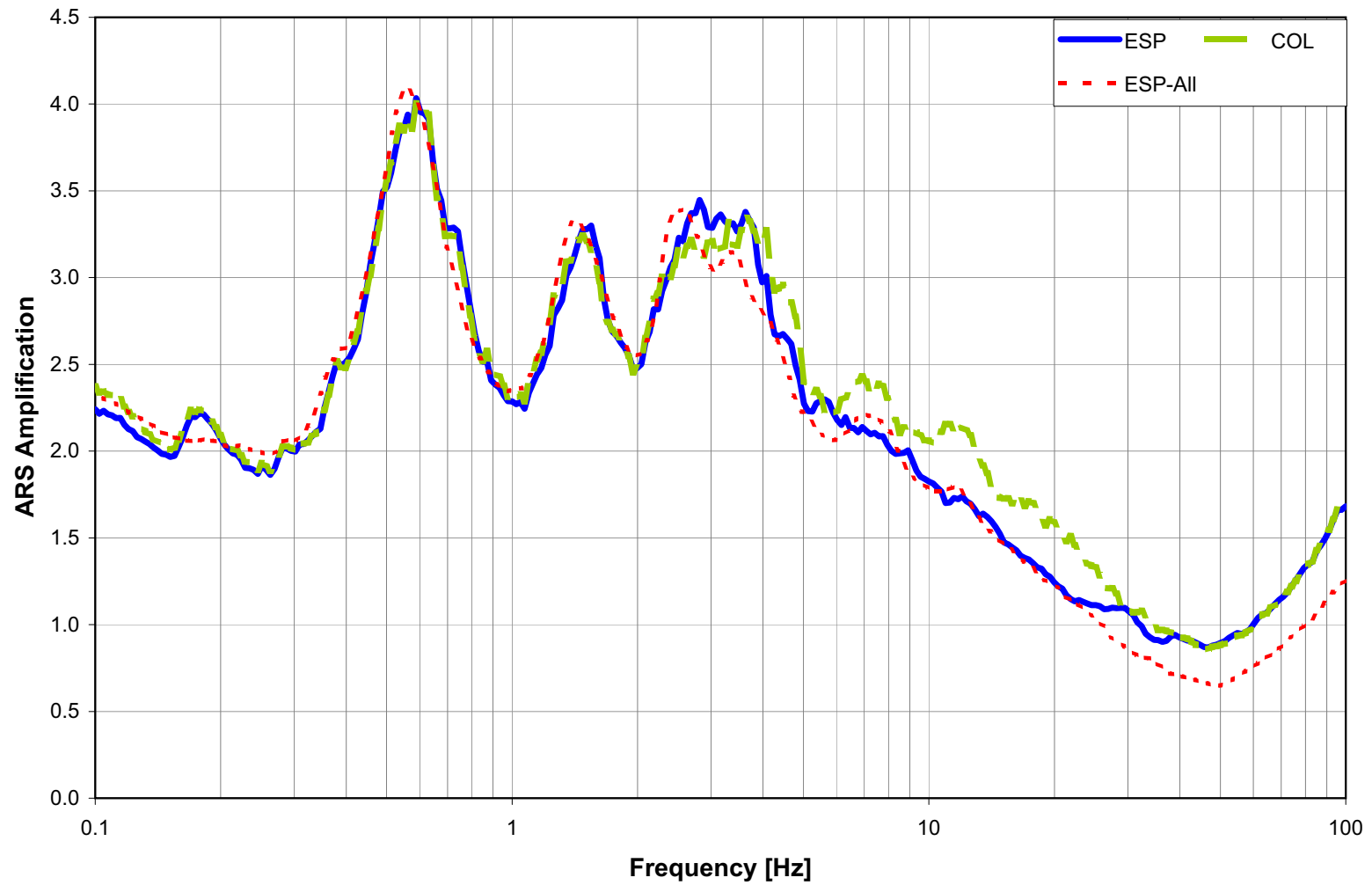


Figure 2.5-351
Envelope at 40 ft Depth (FIRS Horizon)

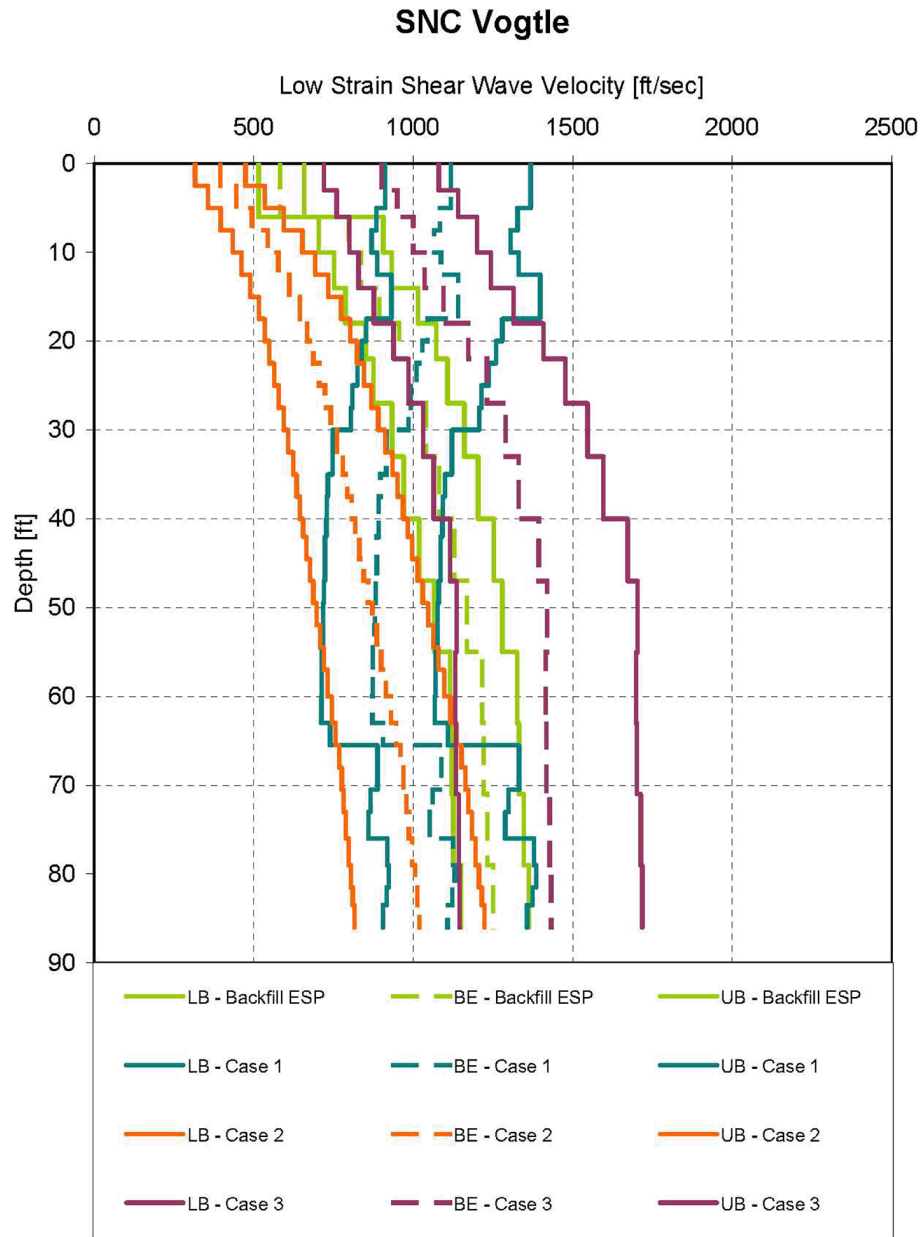


Figure 2.5-352

**Low Strain Shear Wave Velocity Profile Cases
(LB, BE, UB) - Study for Material Over Excavation Slopes**

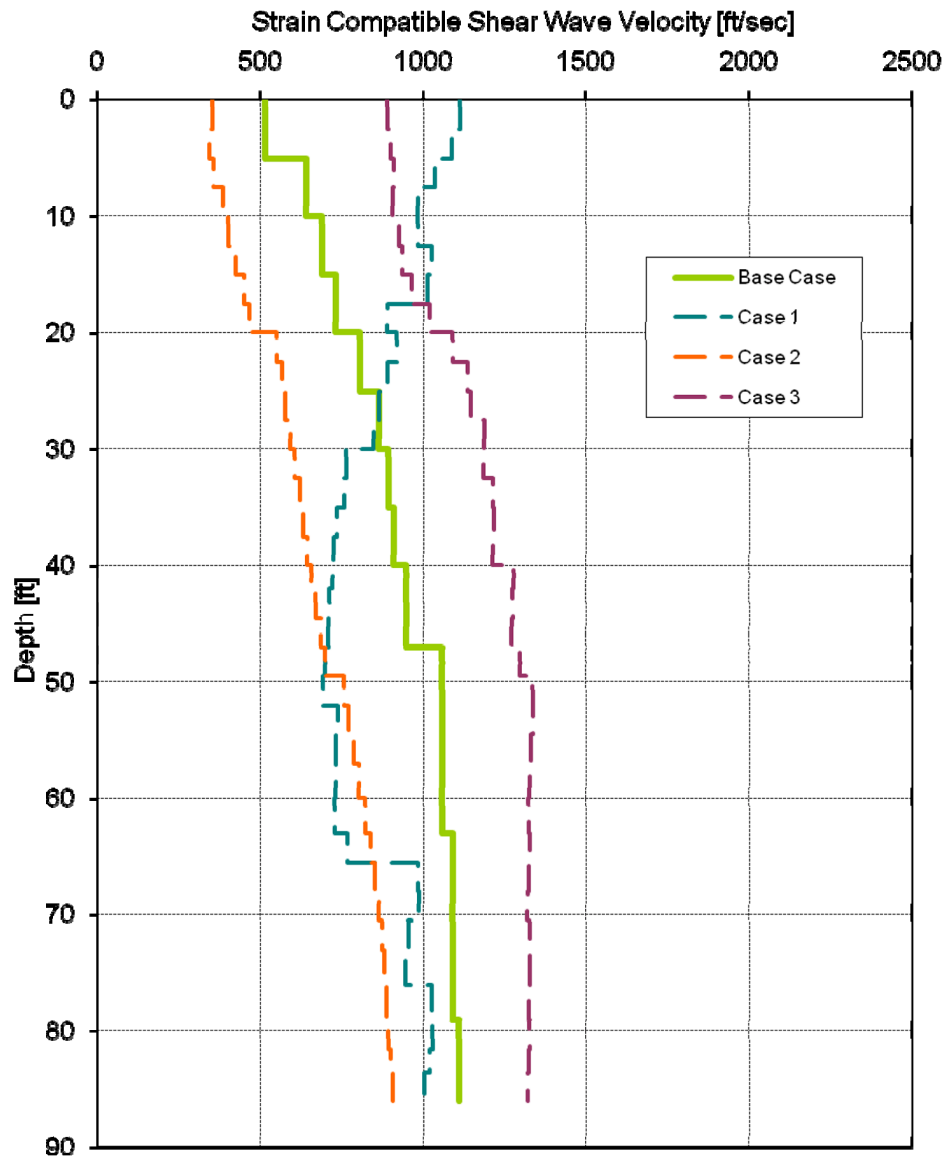
SNC Vogtle

Figure 2.5-353
Strain Compatible BE Shear Wave Velocity Profiles
Cases-for Material Over Excavation Slopes
(2D SASSI SSI Bathtub Analyses)

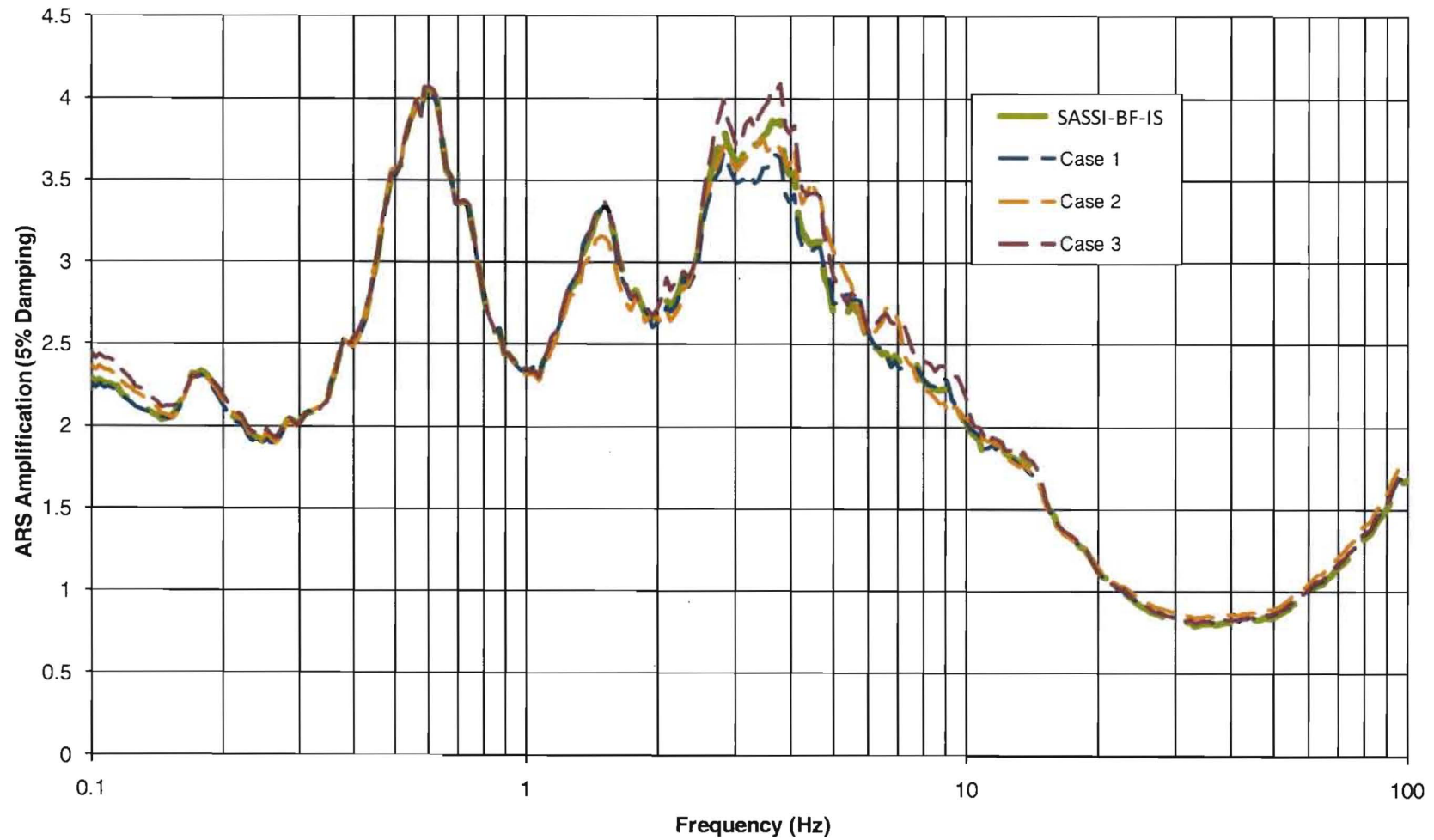


Figure 2.5-354
Comparison of SASSI 2D Bathtub Model Site Response:
Amplification at 0 ft (GMRS horizon)

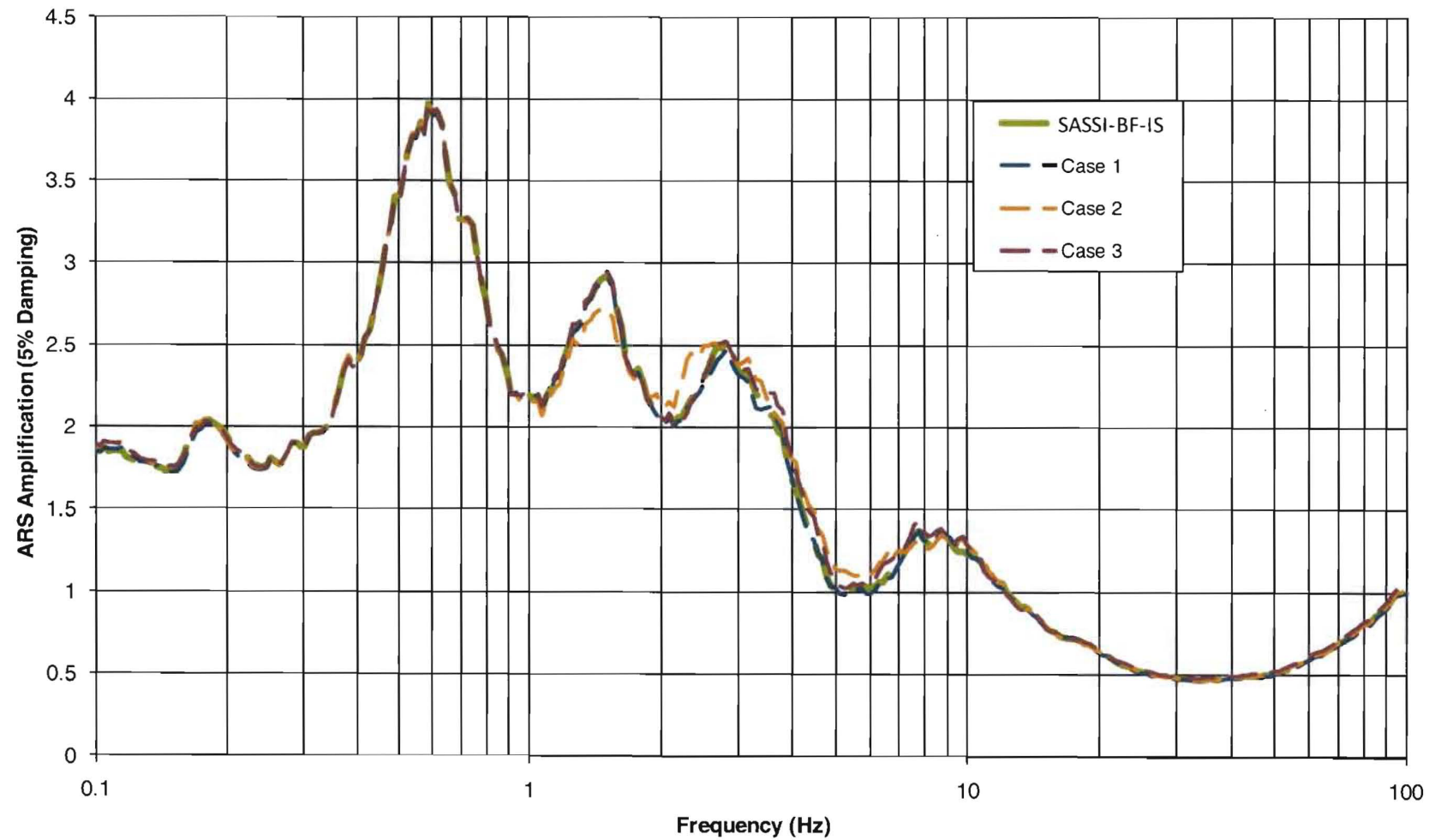


Figure 2.5-355
Comparison of SASSI 2D Bathtub Model Site Response:
Amplification at 40 ft depth (FIRS horizon)

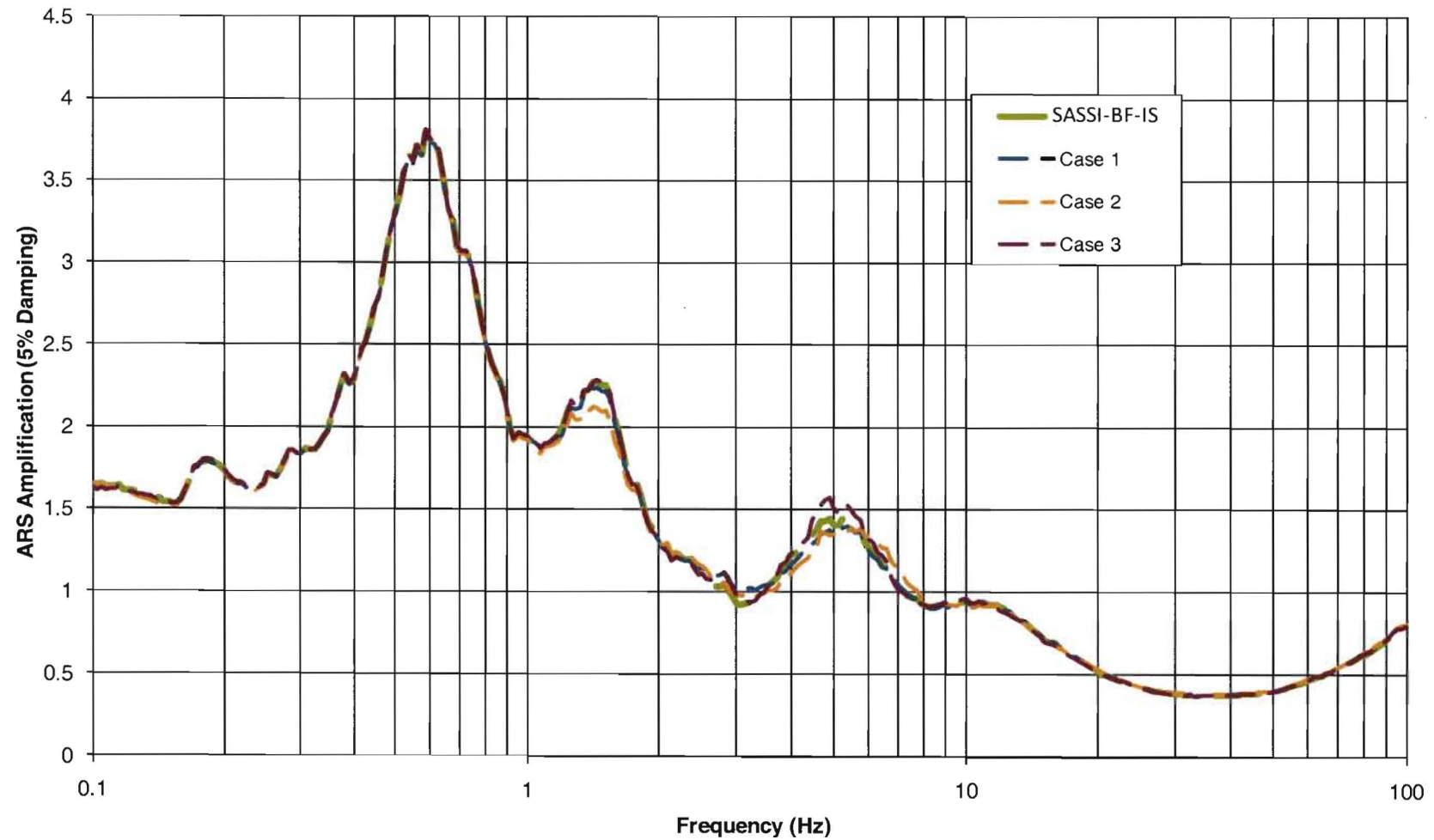


Figure 2.5-356
Comparison of SASSI 2D Bathtub Model Site Response:
Amplification at 86 ft depth (Top of Blue Bluff Marl)

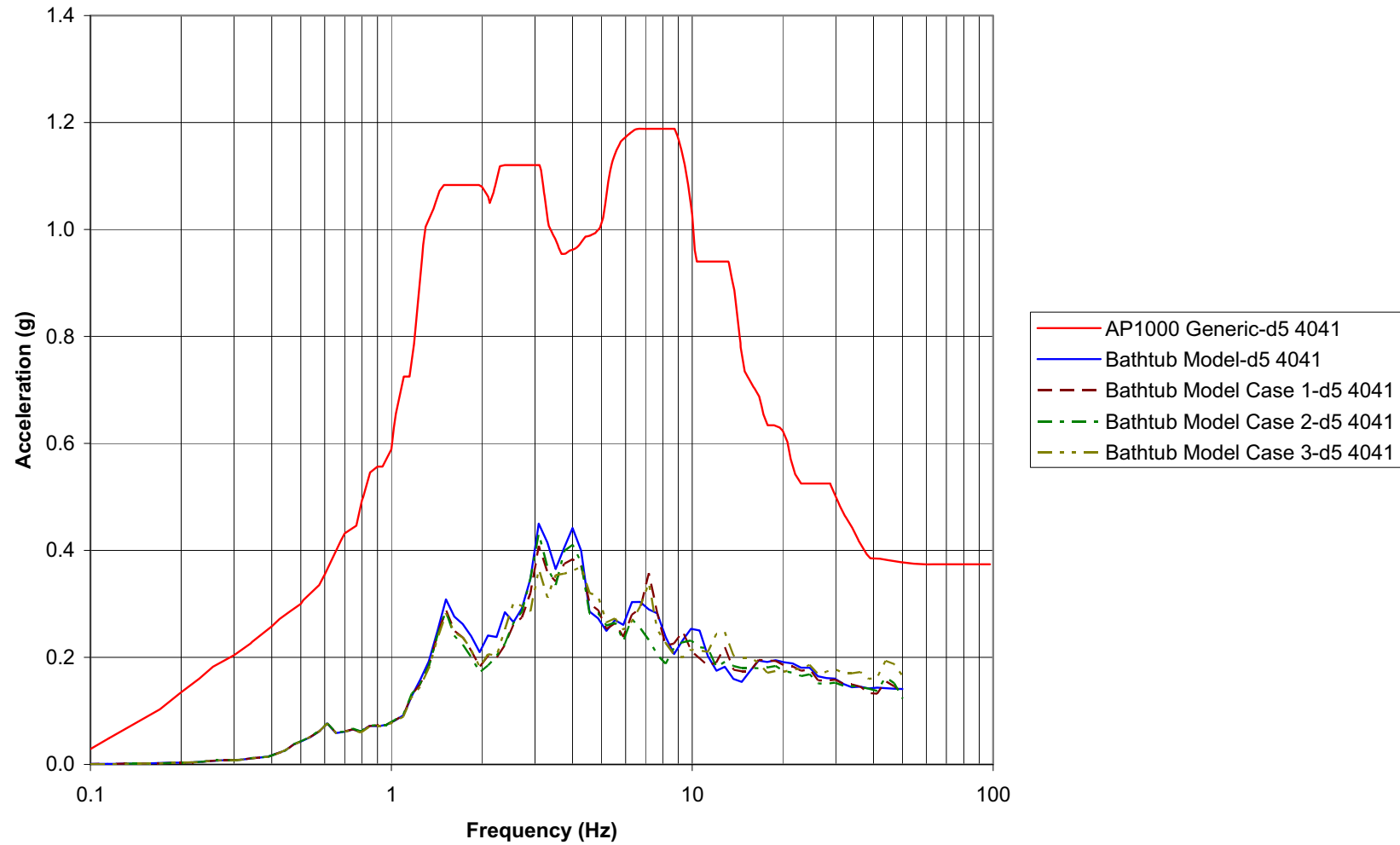


Figure 2.5-357
Comparison of SASSI 2D Bathtub NI Model SSI Responses:
Node 4041-EL 99 NI at Reactor Vessel Support Elevation

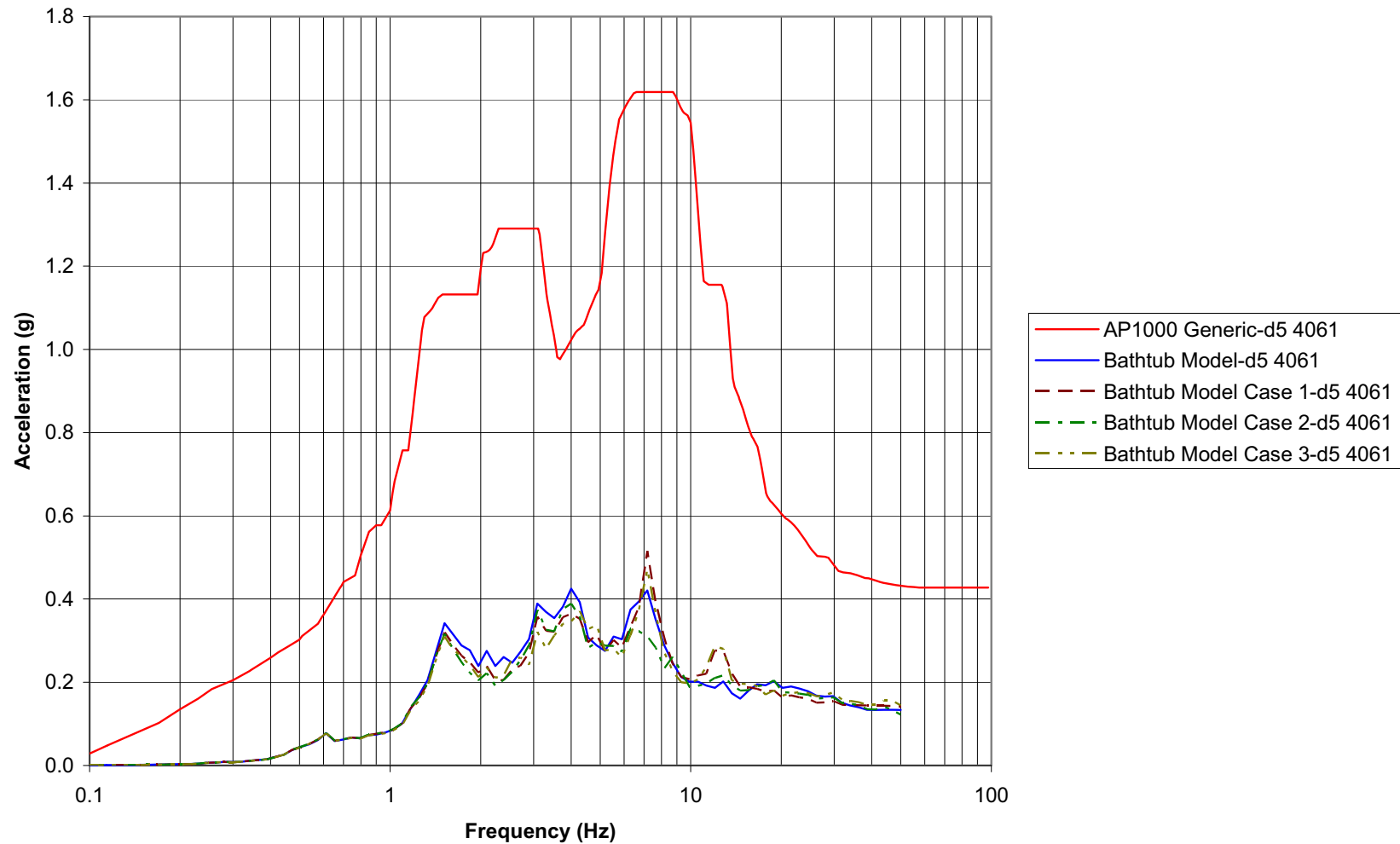


Figure 2.5-358
Comparison of SASSI 2D Bathtub NI Model SSI Responses:
Node 4061-EL 116.5 Auxiliary Shield Building at Control Room Floor

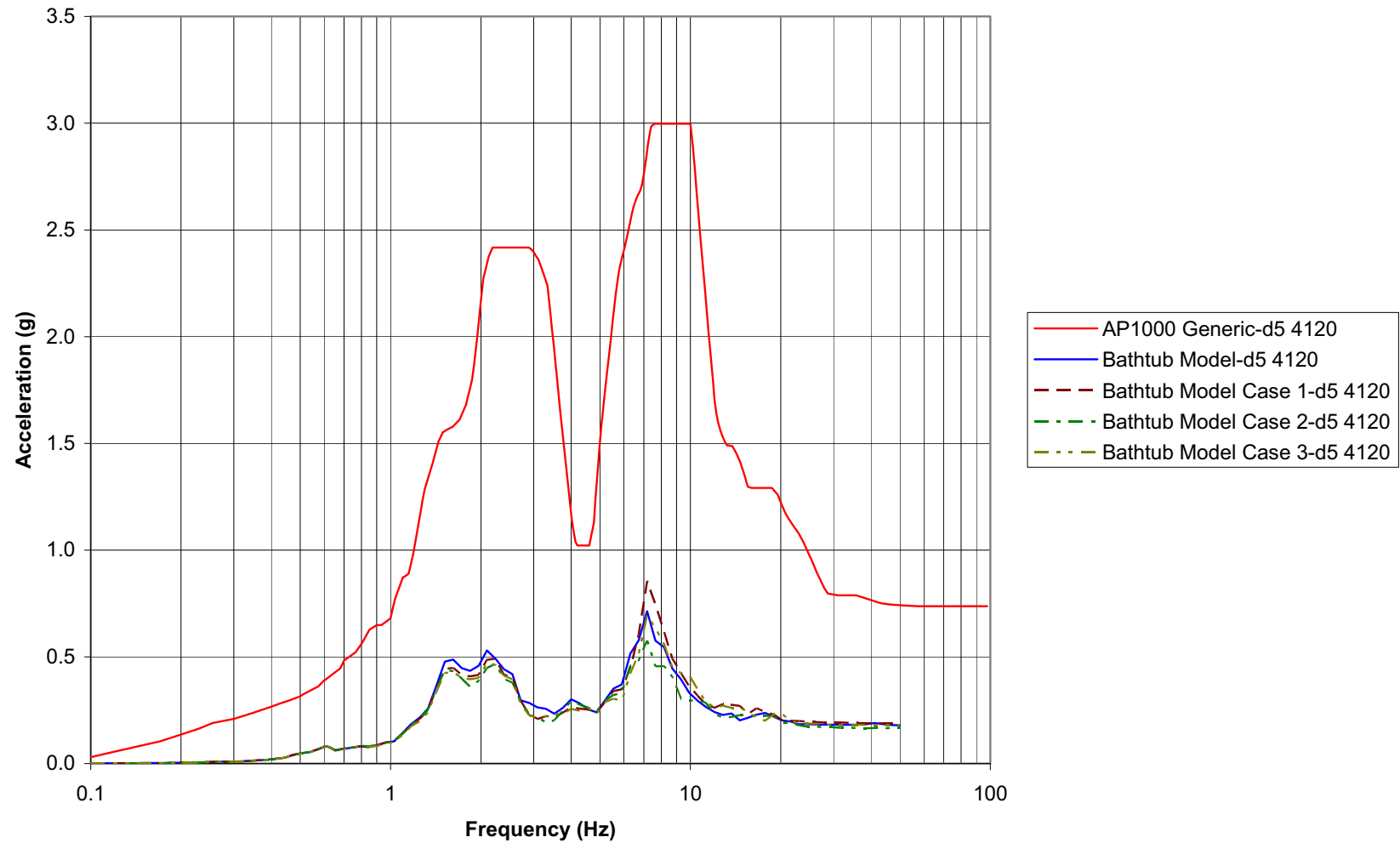


Figure 2.5-359
Comparison of SASSI 2D Bathtub NI Model SSI Responses:
Node 4120-EL 179.56 ASB Auxiliary Building Roof Area

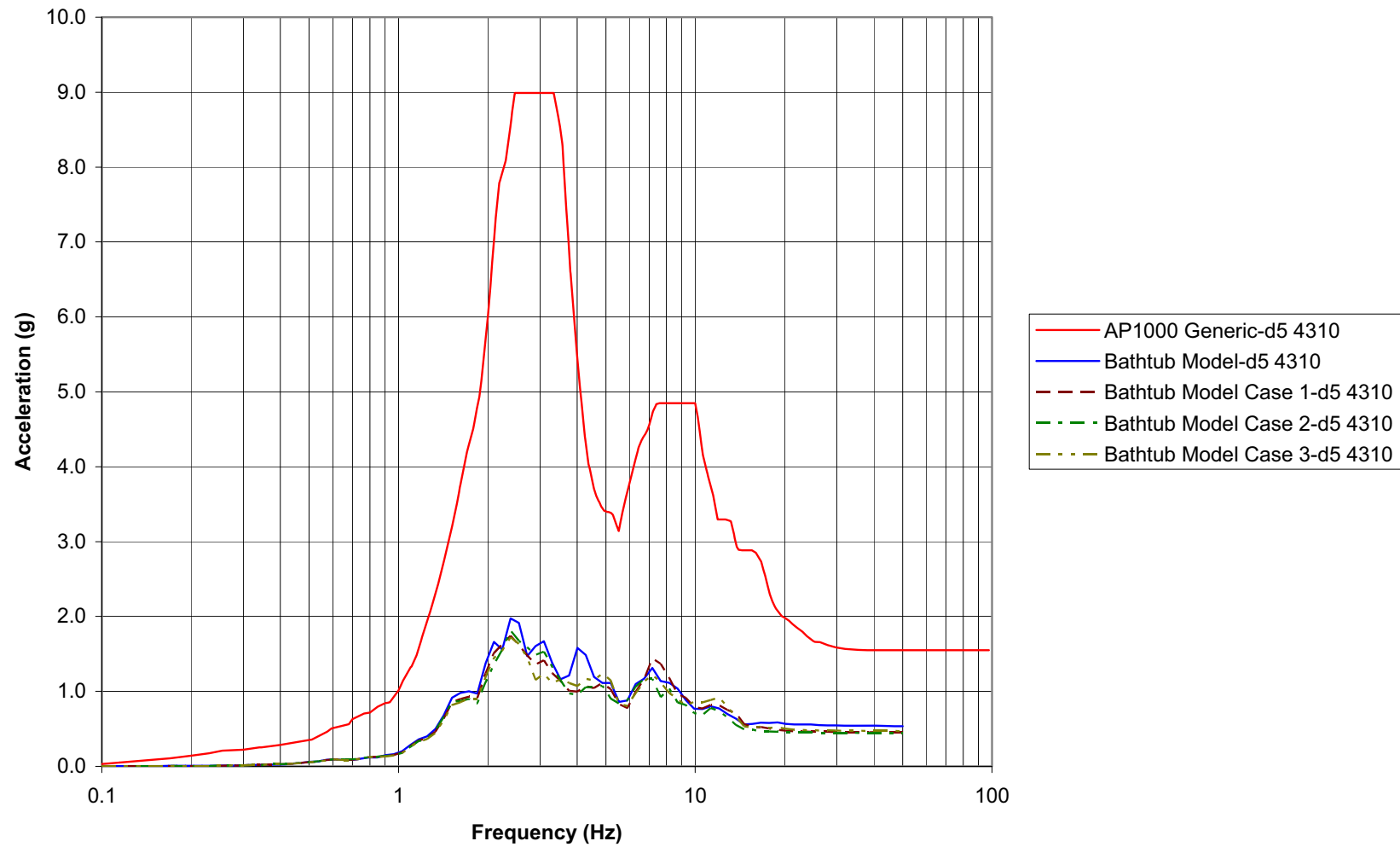


Figure 2.5-360
Comparison of SASSI 2D Bathtub NI Model SSI Responses:
Node 4310-EL 327.41 ASB Shield Building Roof Area

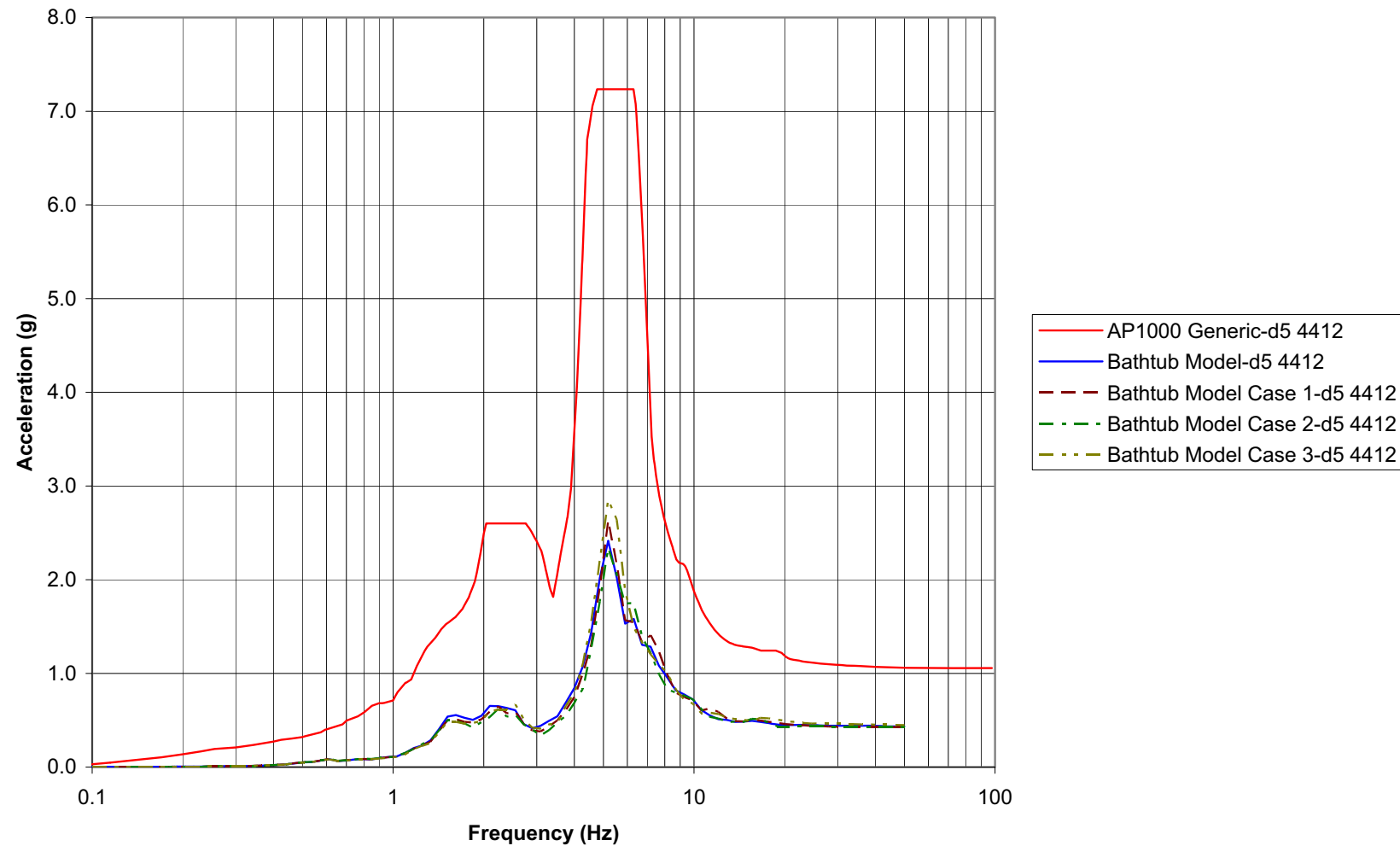


Figure 2.5-361
Comparison of SASSI 2D Bathtub NI Model SSI Responses:
Node 4412-EL 224 Steel Containment Vessel Near Polar Crane

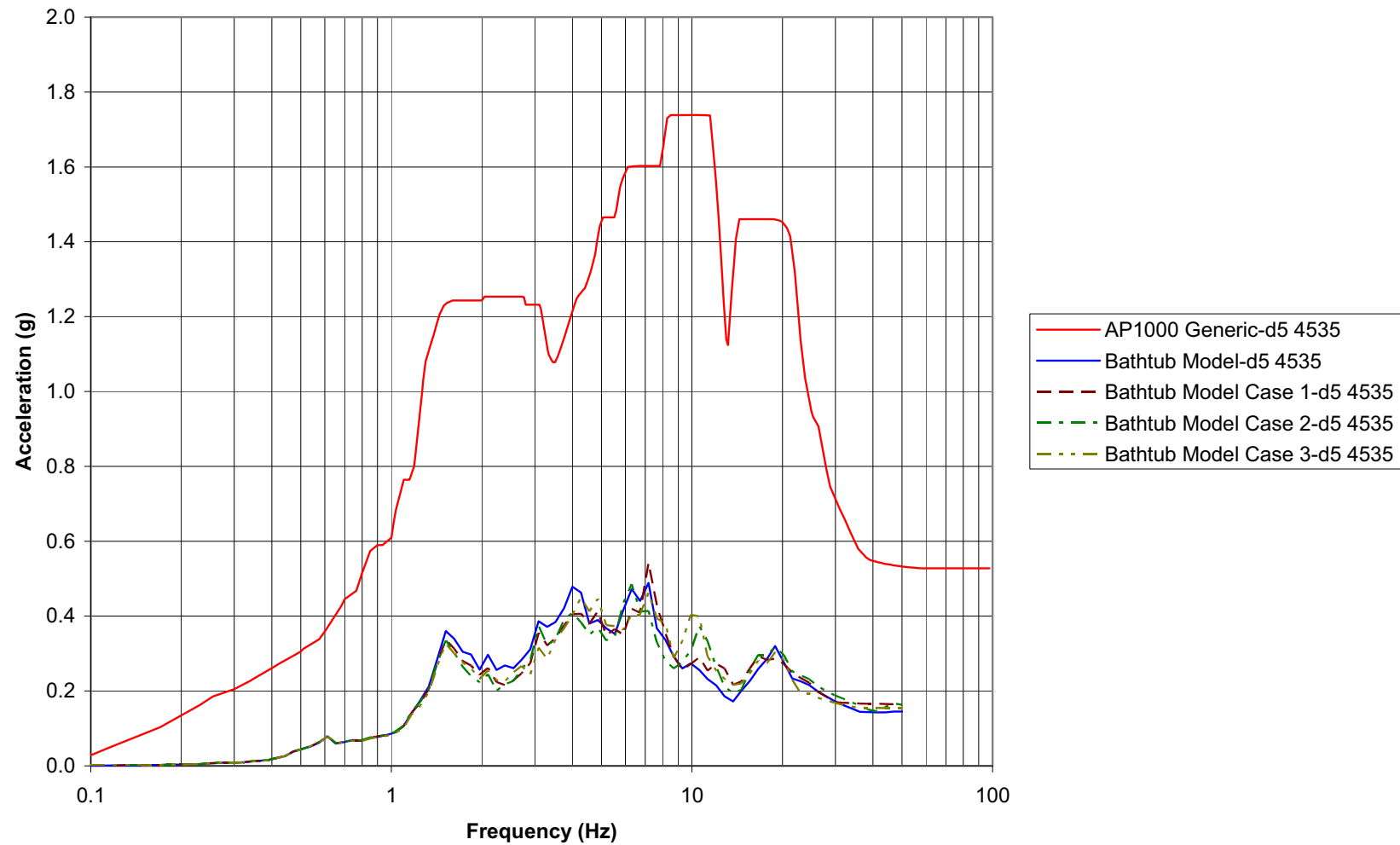
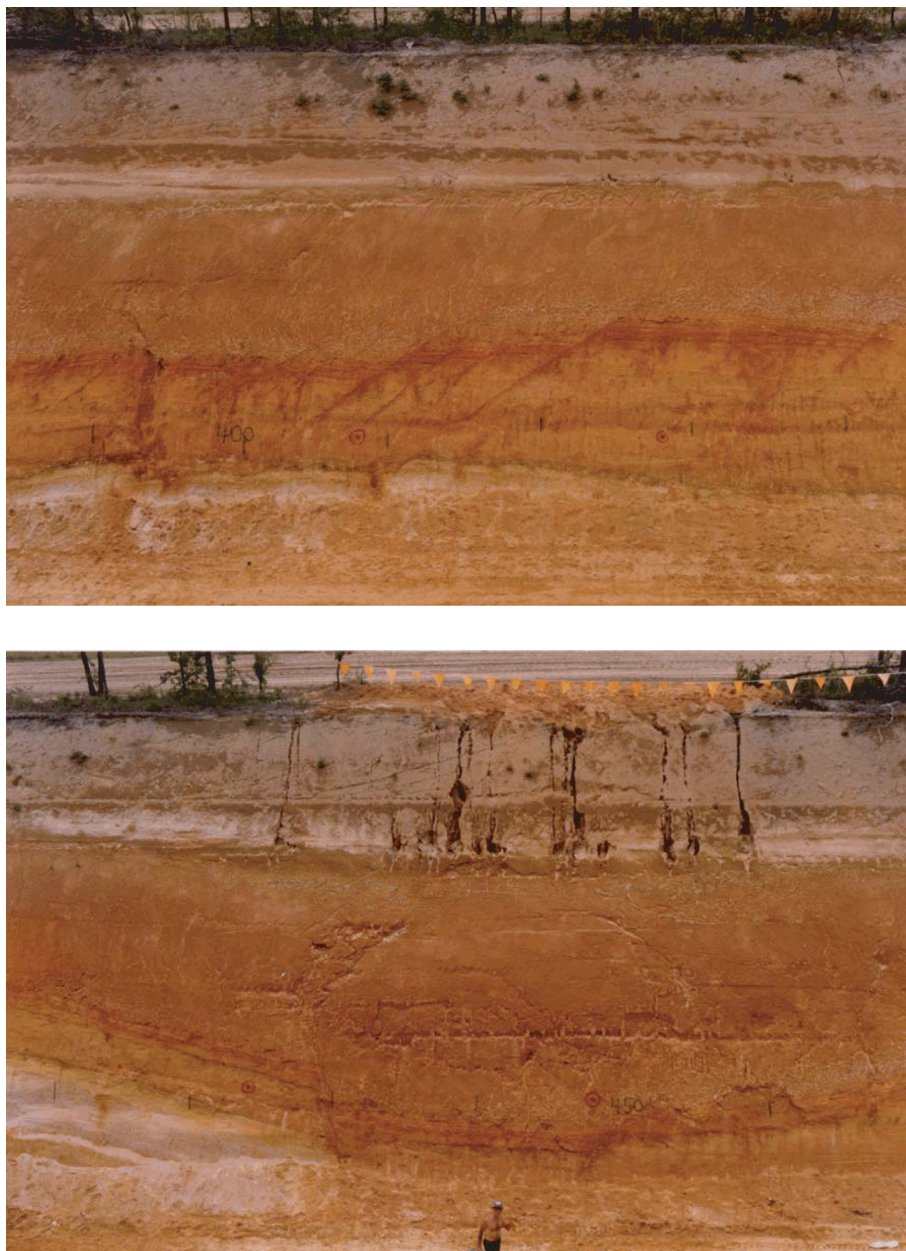


Figure 2.5-362
Comparison of SASSI 2D Bathtub NI Model SSI Responses:
Node 4535-EL 135.25 Containment Internal Structure at Operating Deck



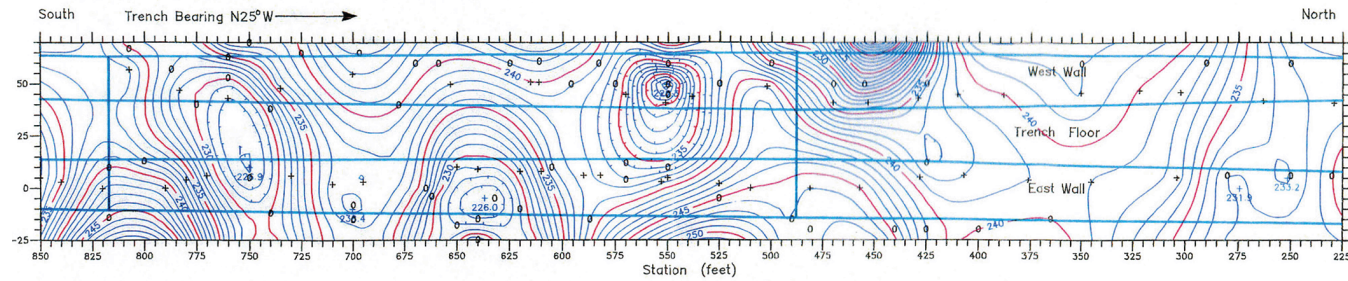
Source: Bechtel 1984b

Figure 2.5-363
Contorted Bedding in Garbage Trench at VEGP Site



Source: Bechtel 1984b

Figure 2.5-364
West Wall of Garbage Trench Showing Small Offsets (1–24 inches) (Upper)
and Arcuate Fractures and Clastic Dikes Over Center of Depression (Lower)



Structure Contour Map, Surface of Unit F – Trench Plan View

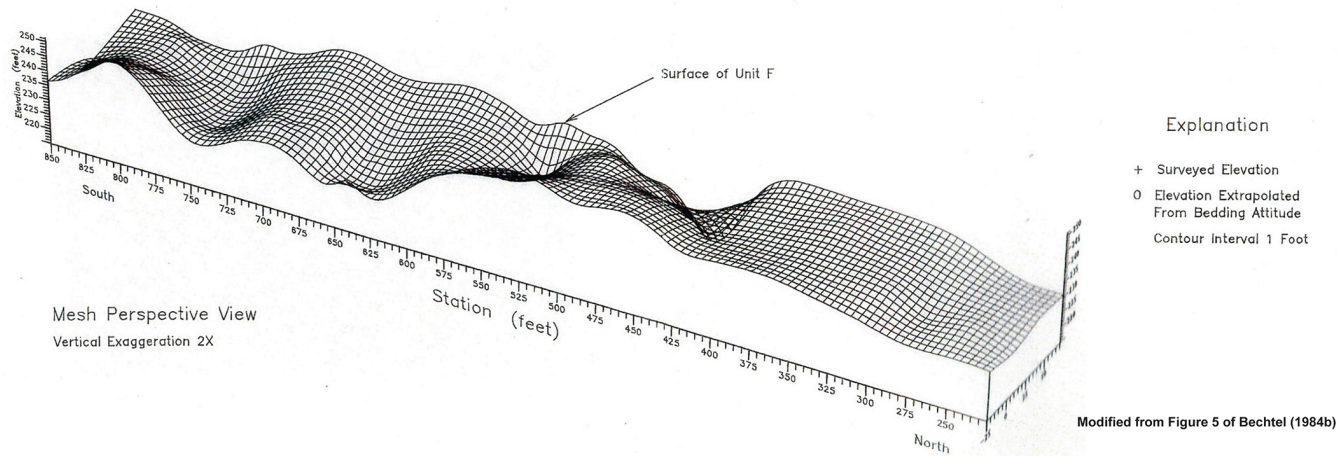


Figure 2.5-365
Surface Geometry of Unit F Illustrating Localized Nature of Deformation

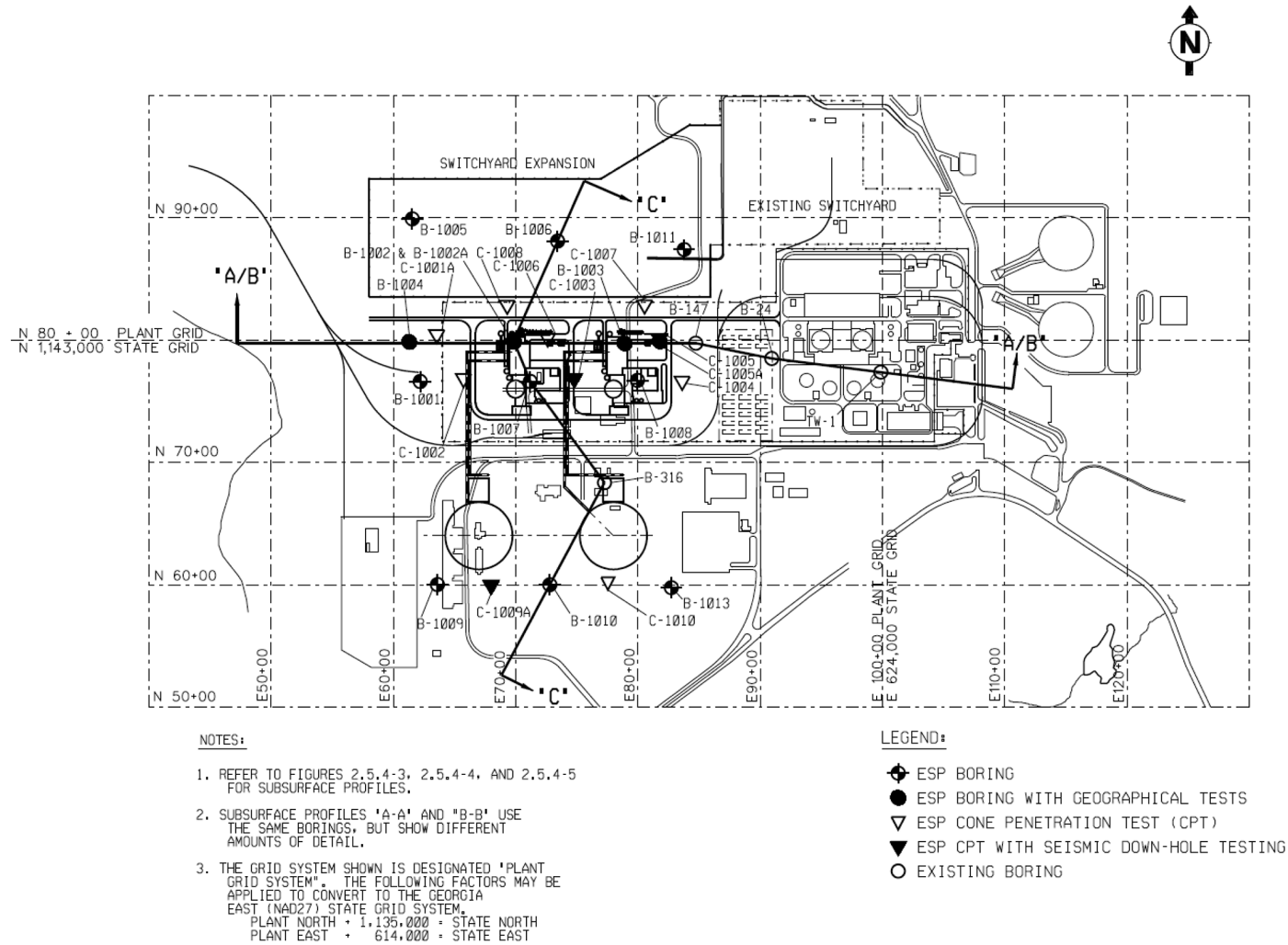


Figure 2.5-366
ESP Study Boring Location Plan



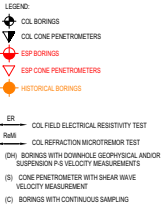


Figure 2.5-368
COL Power Block — Cooling Tower Boring Location

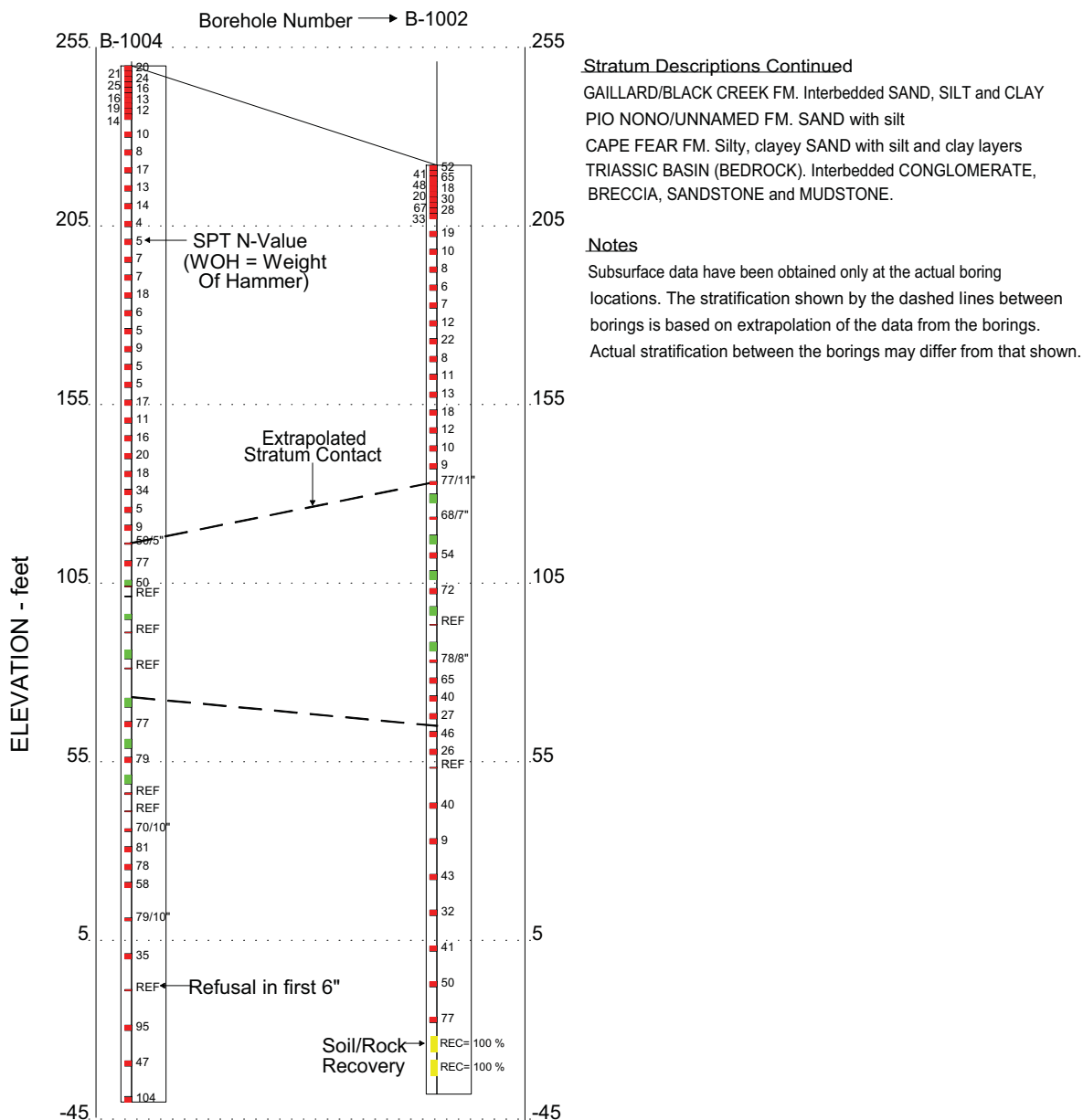


Figure 2.5-369
Subsurface Profile Legend



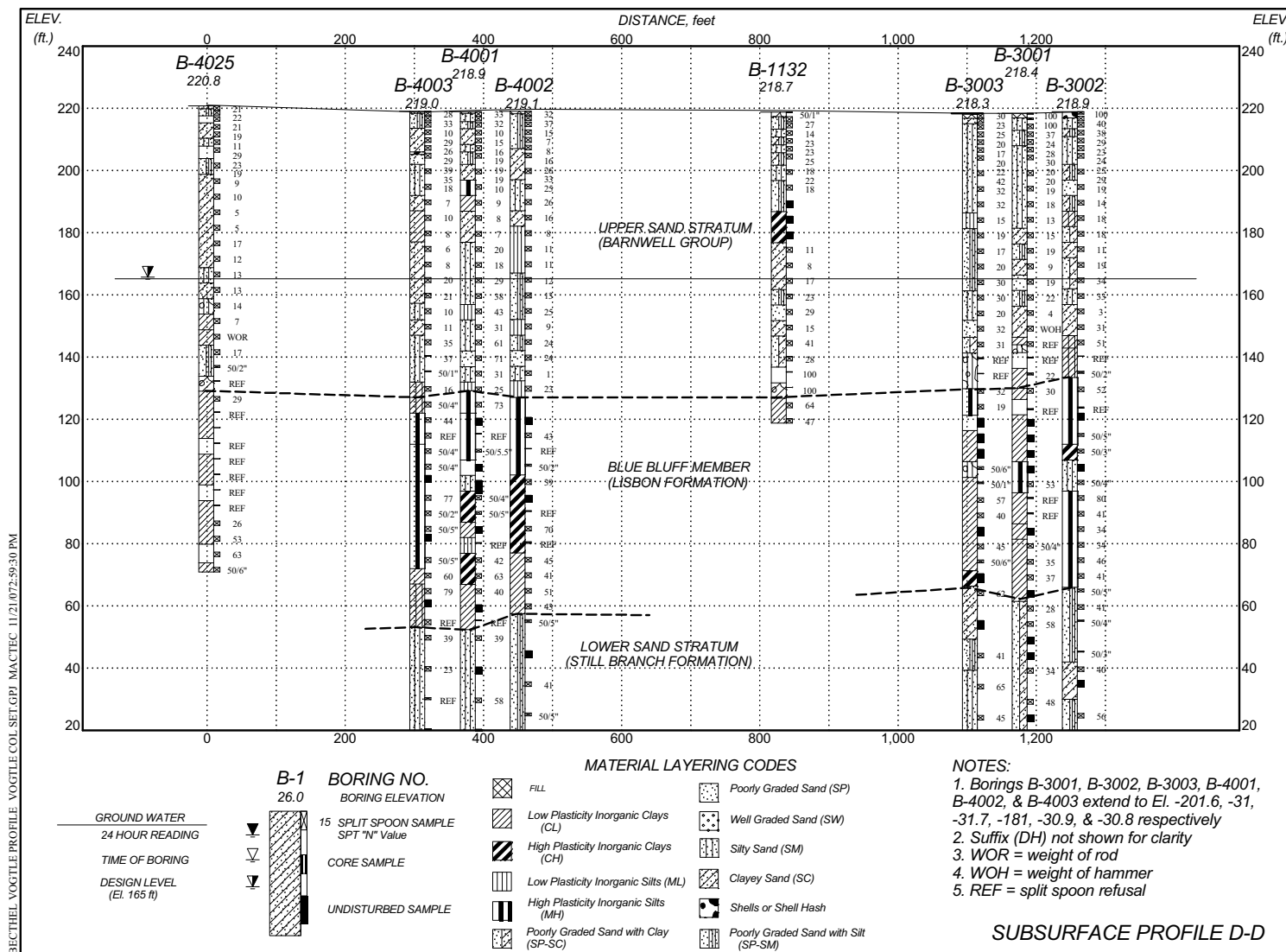
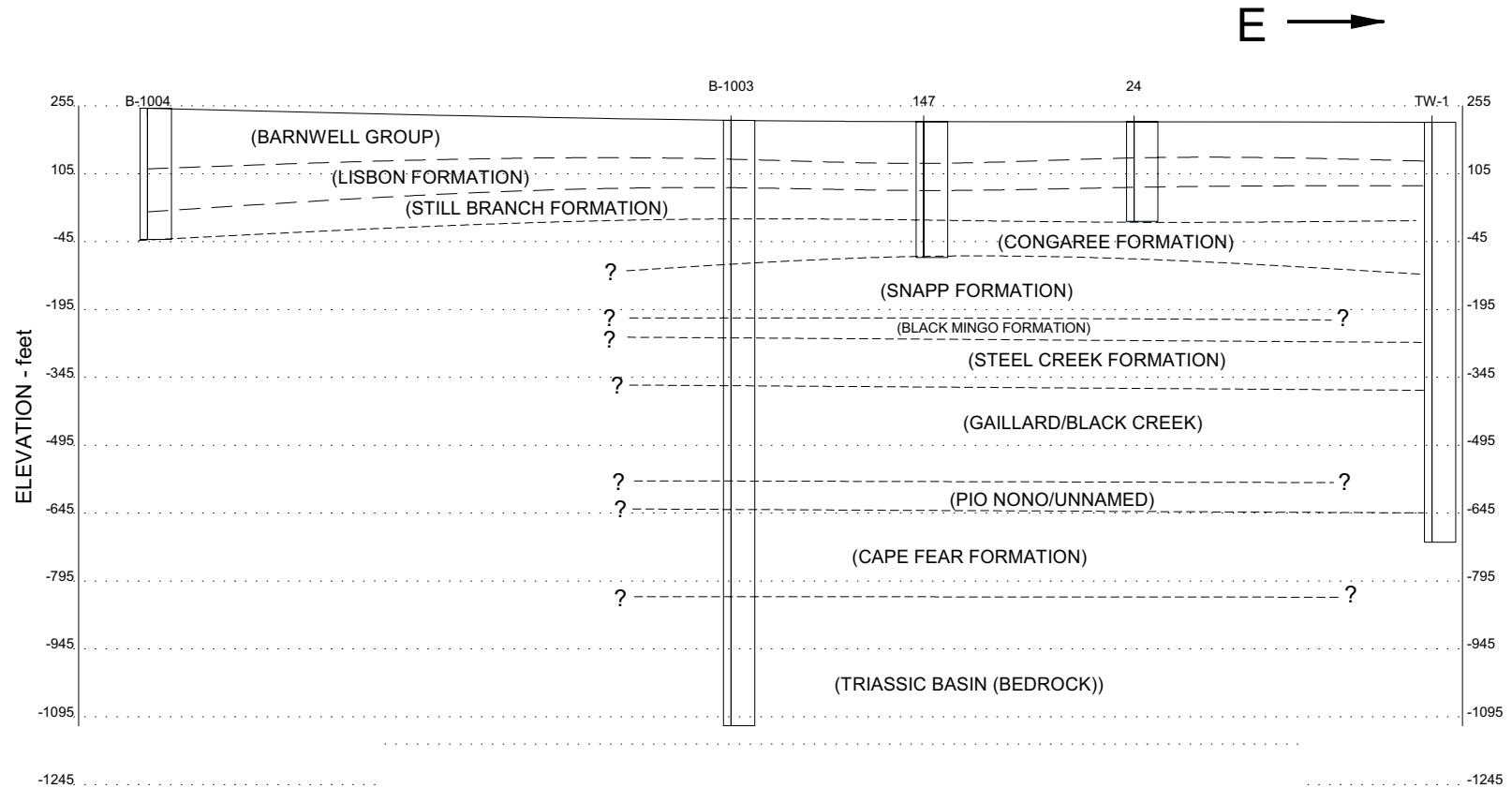


Figure 2.5-371
Subsurface Profile D-D'



Vertical Exaggeration = 1.36x

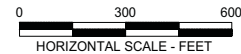


Figure 2.5-372
Subsurface Profile B-B'

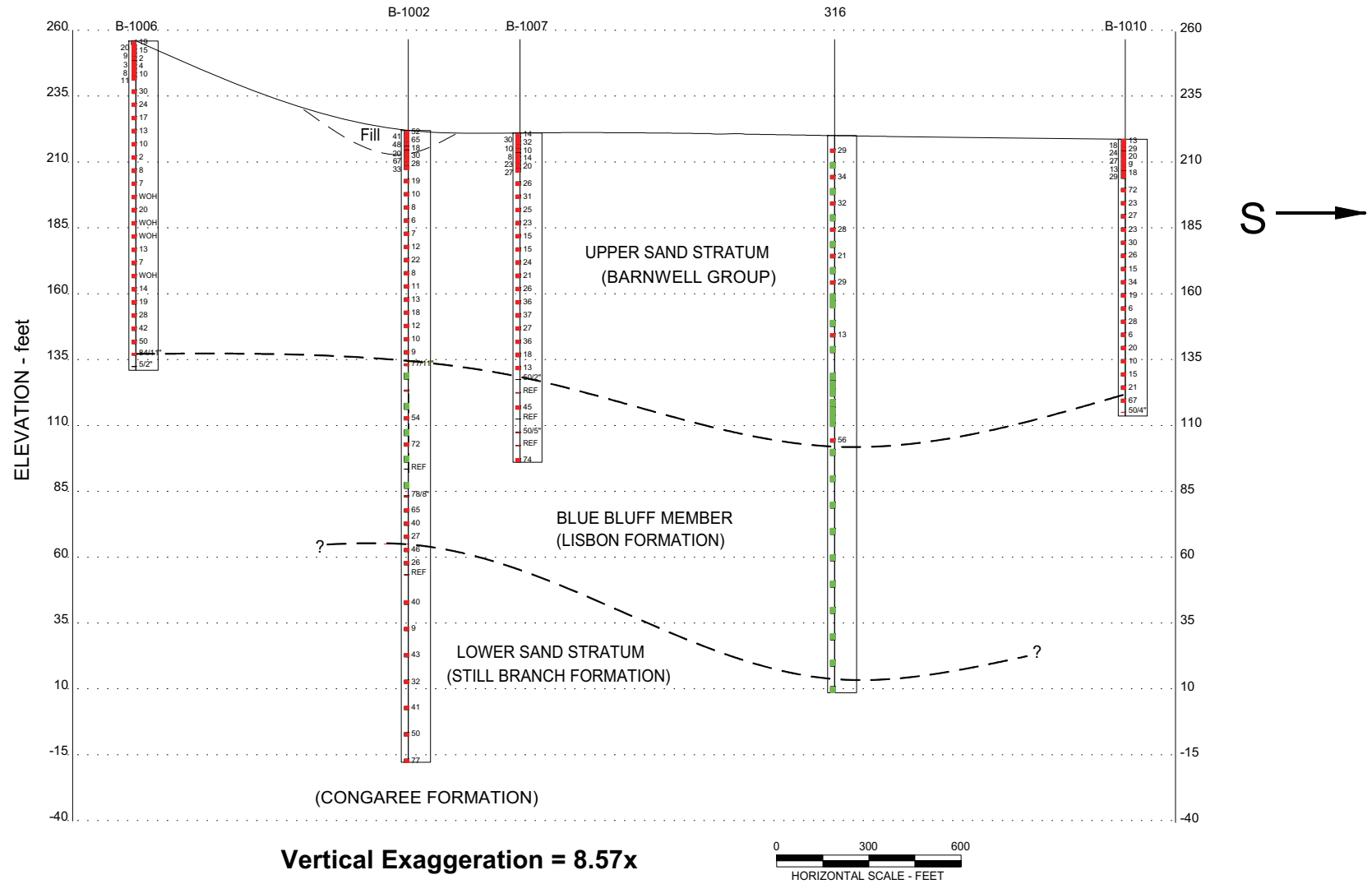


Figure 2.5-373
Subsurface Profile C-C'

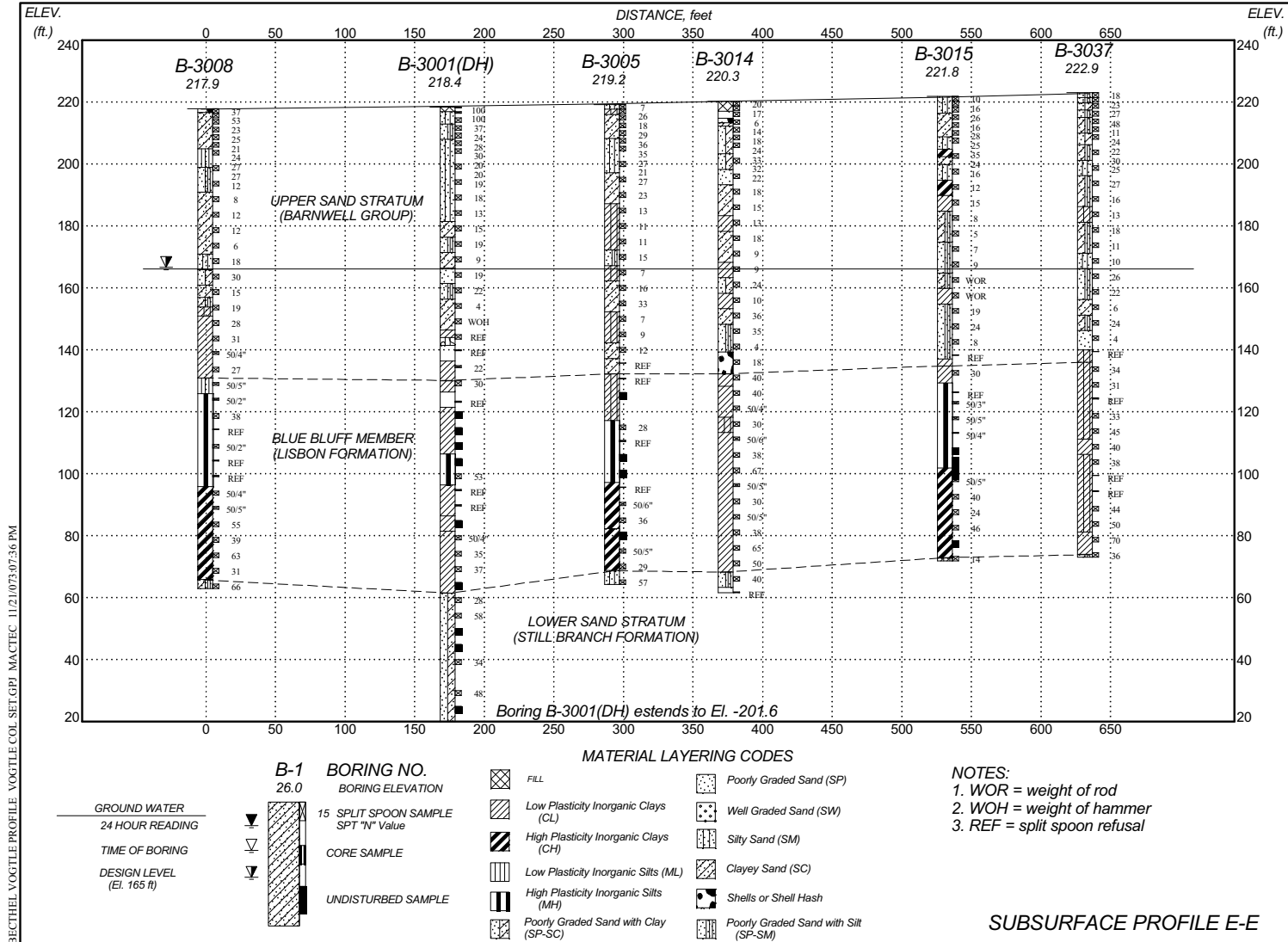


Figure 2.5-374
Subsurface Profile E-E'

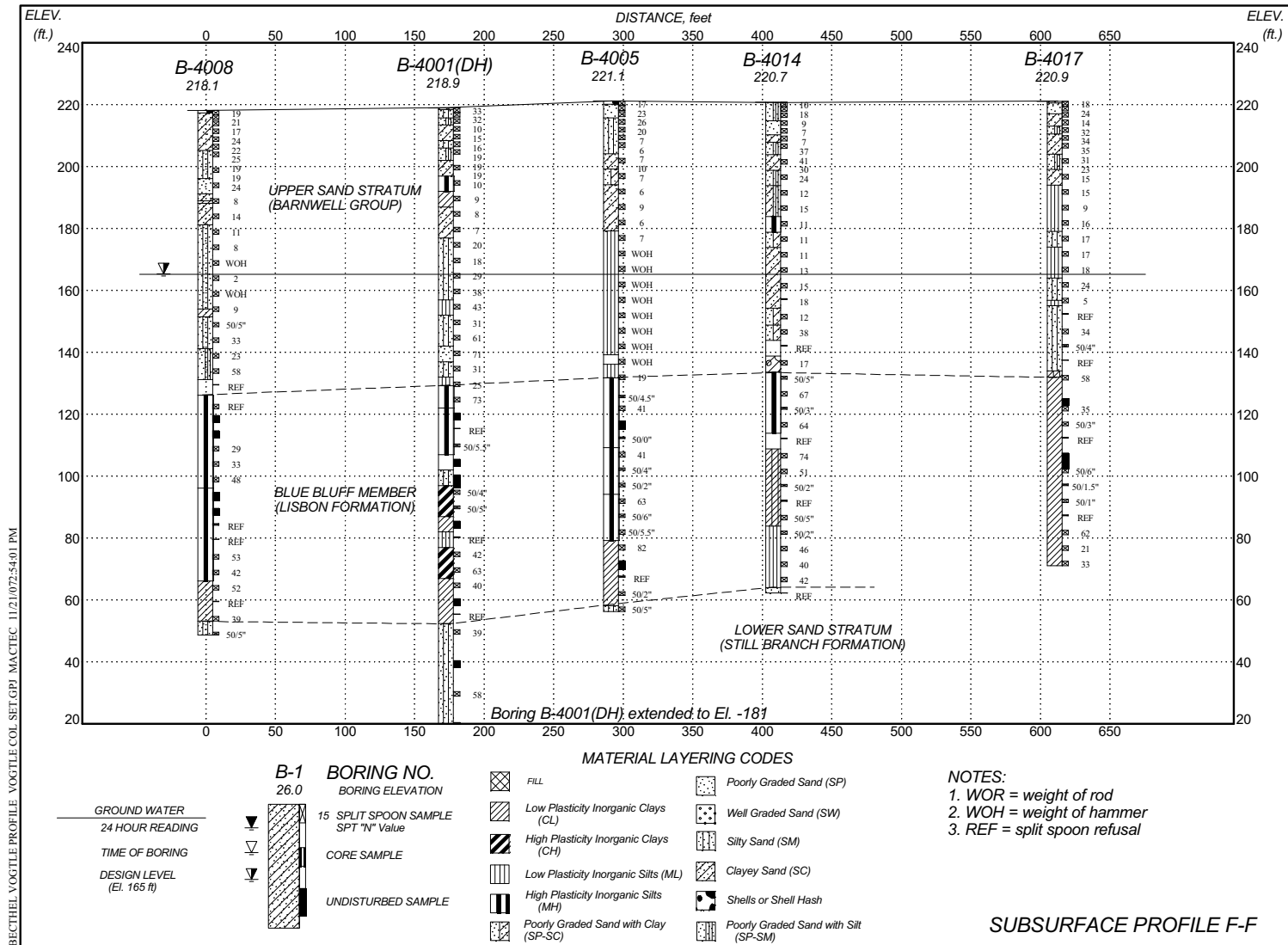


Figure 2.5-375
Subsurface Profile F-F'

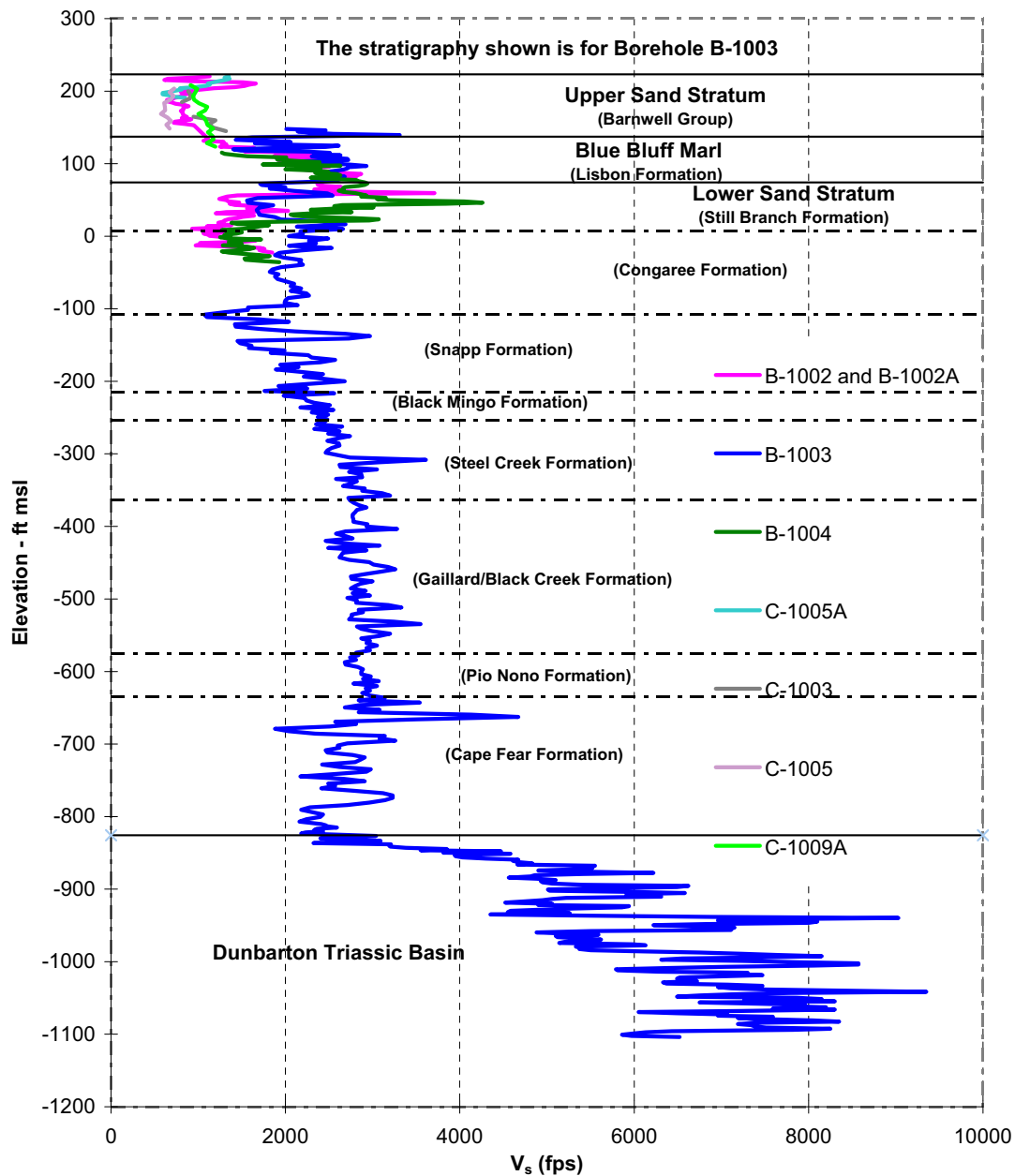


Figure 2.5-376
Shear Wave Velocity Measurements

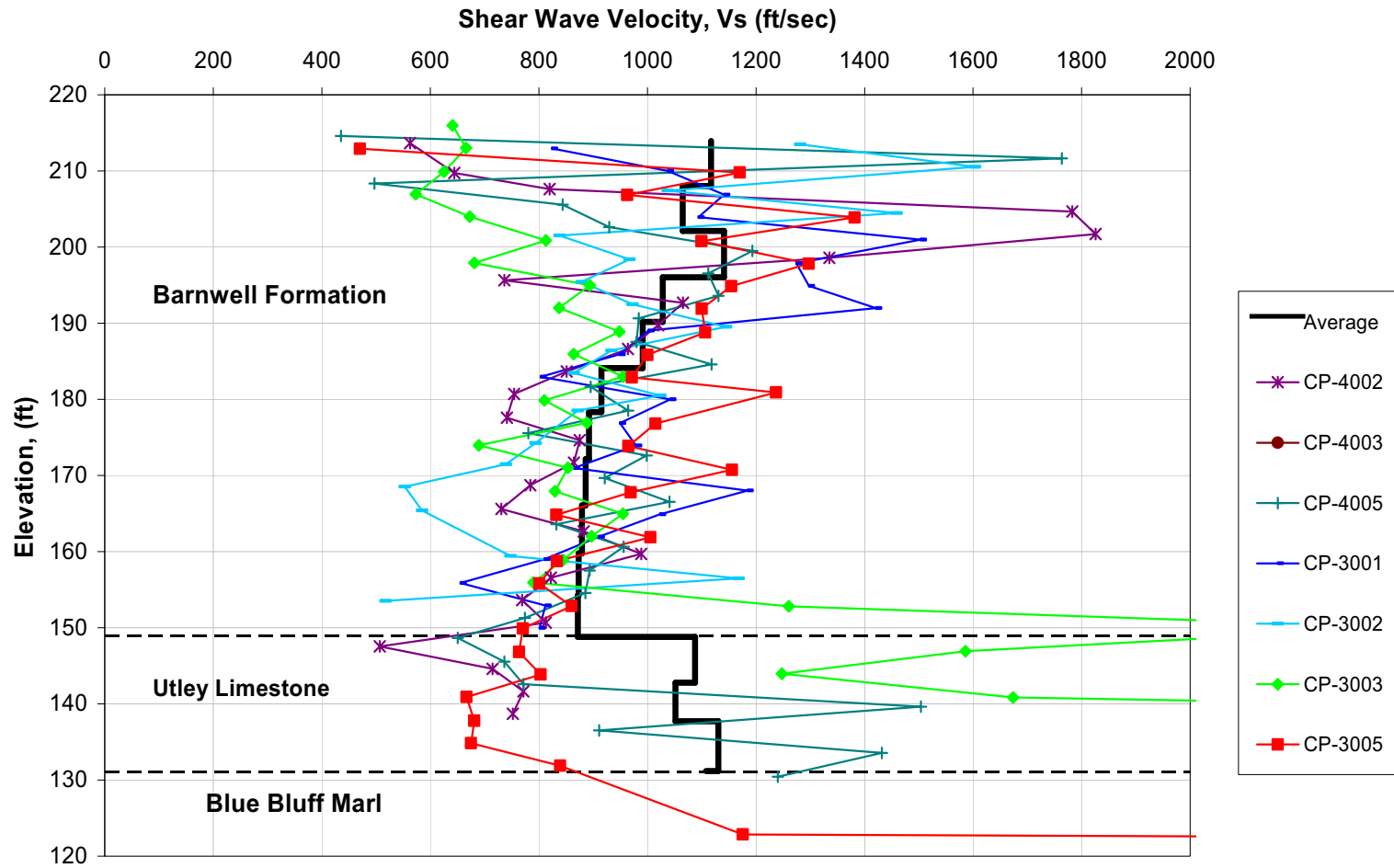


Figure 2.5-377
Shear Wave Velocity Measurements in the Upper Sand Stratum as Measured by COL SCPT

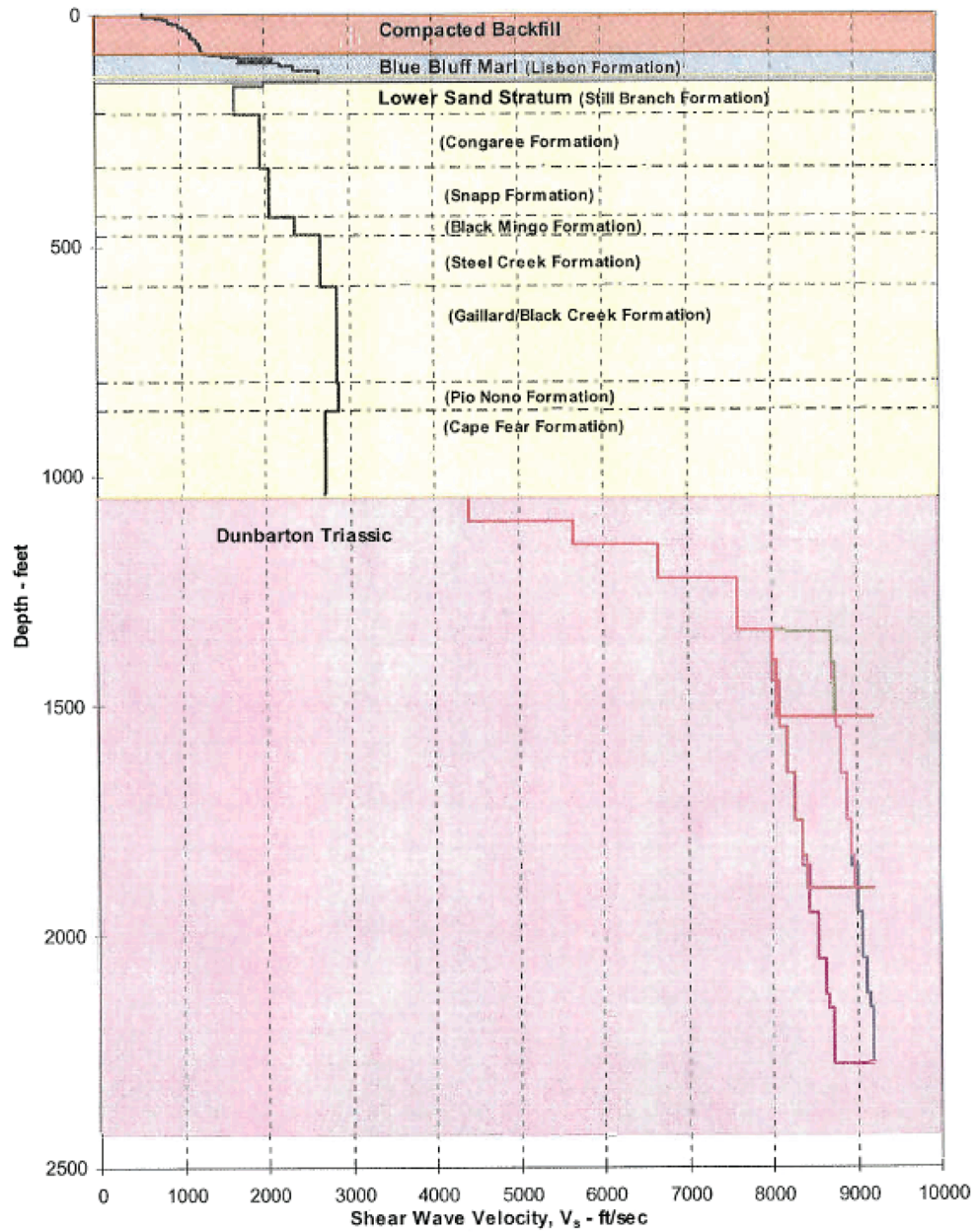


Figure 2.5-378
Shear Wave Velocity Profile for SHAKE Analysis

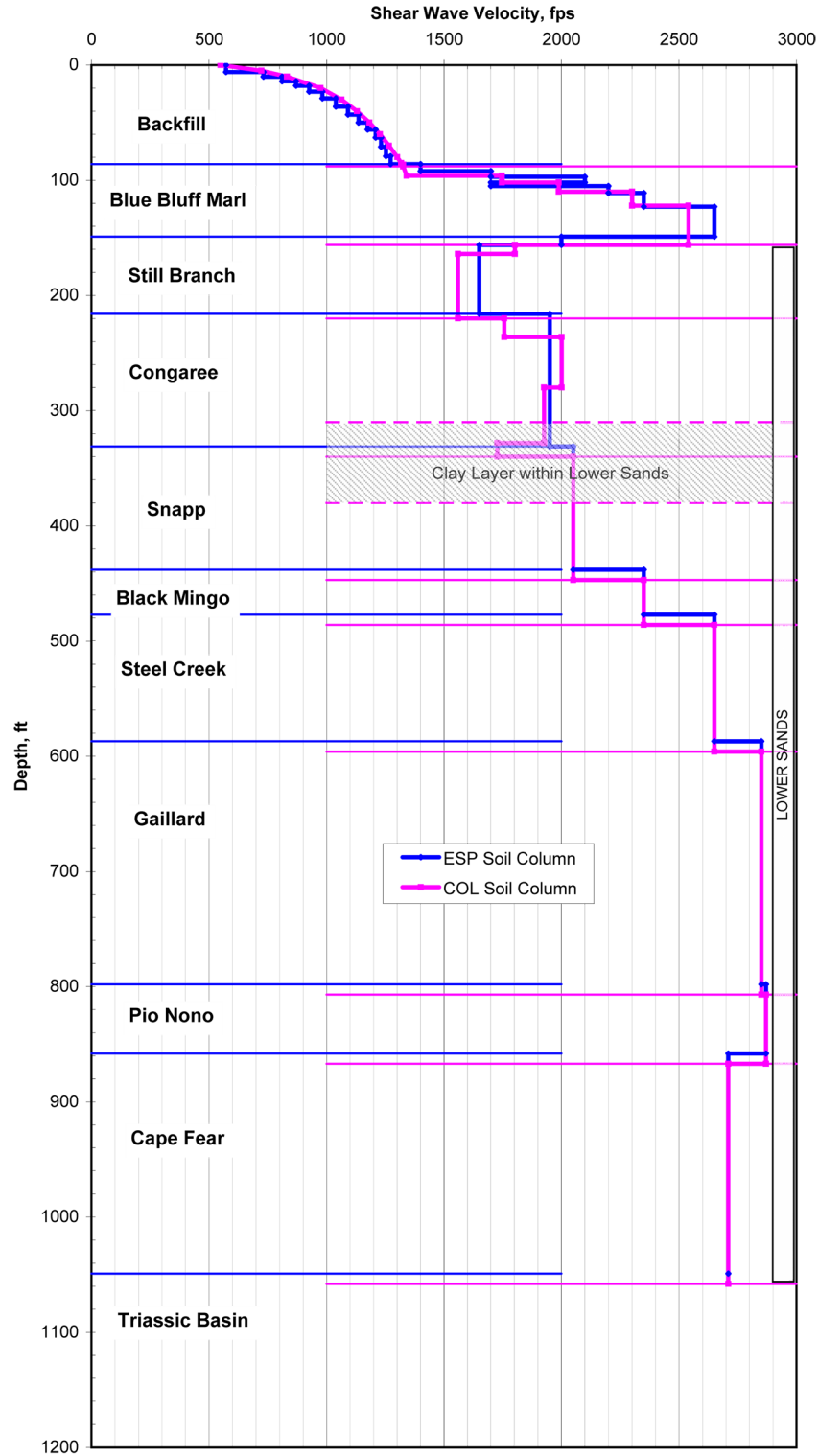


Figure 2.5-379
Shear Wave Velocity Profile — ESP and COL Soil Columns

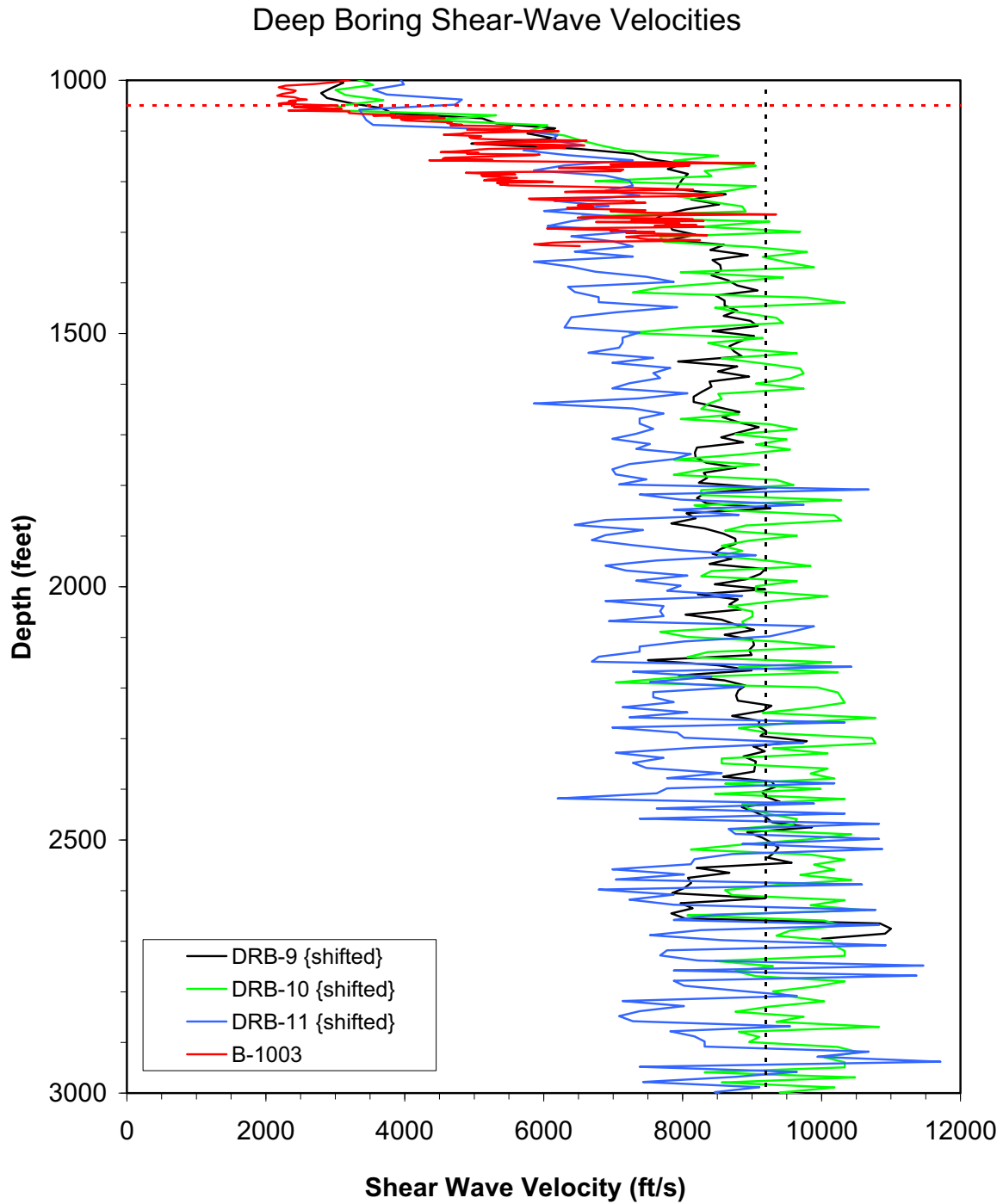


Figure 2.5-380

Rock shear-wave velocities for three SRS sites [DRB] (SRS 2005) and B-1003 [Figure 2.5.4-6]. The DRB data has been shifted in depth so that the depth to top of rock is consistent with B-1003.

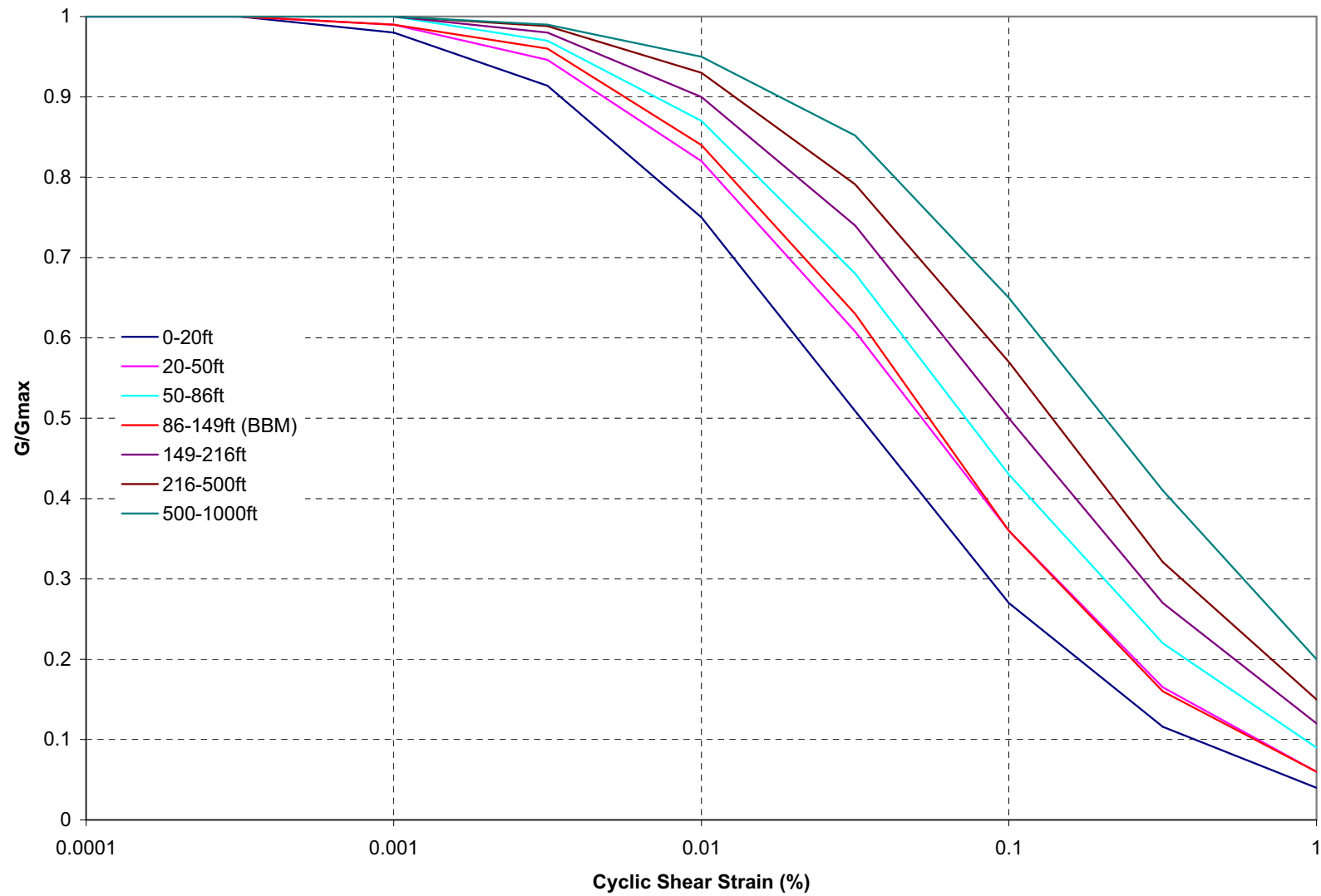


Figure 2.5-381
Shear Modulus Reduction Curves for SHAKE Analysis – EPRI Curves

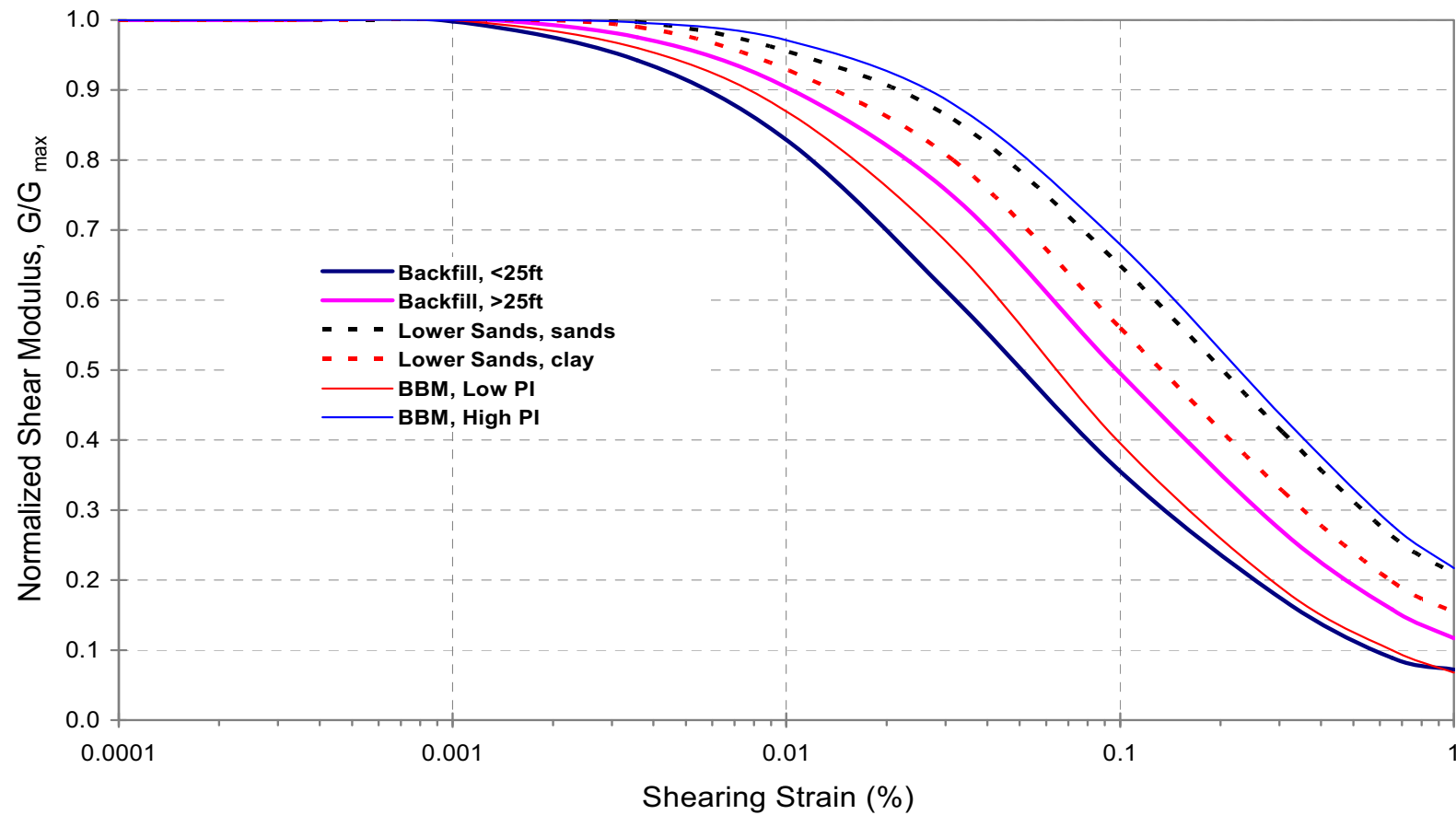


Figure 2.5-382
Site-Specific Shear Modulus Reduction Curves

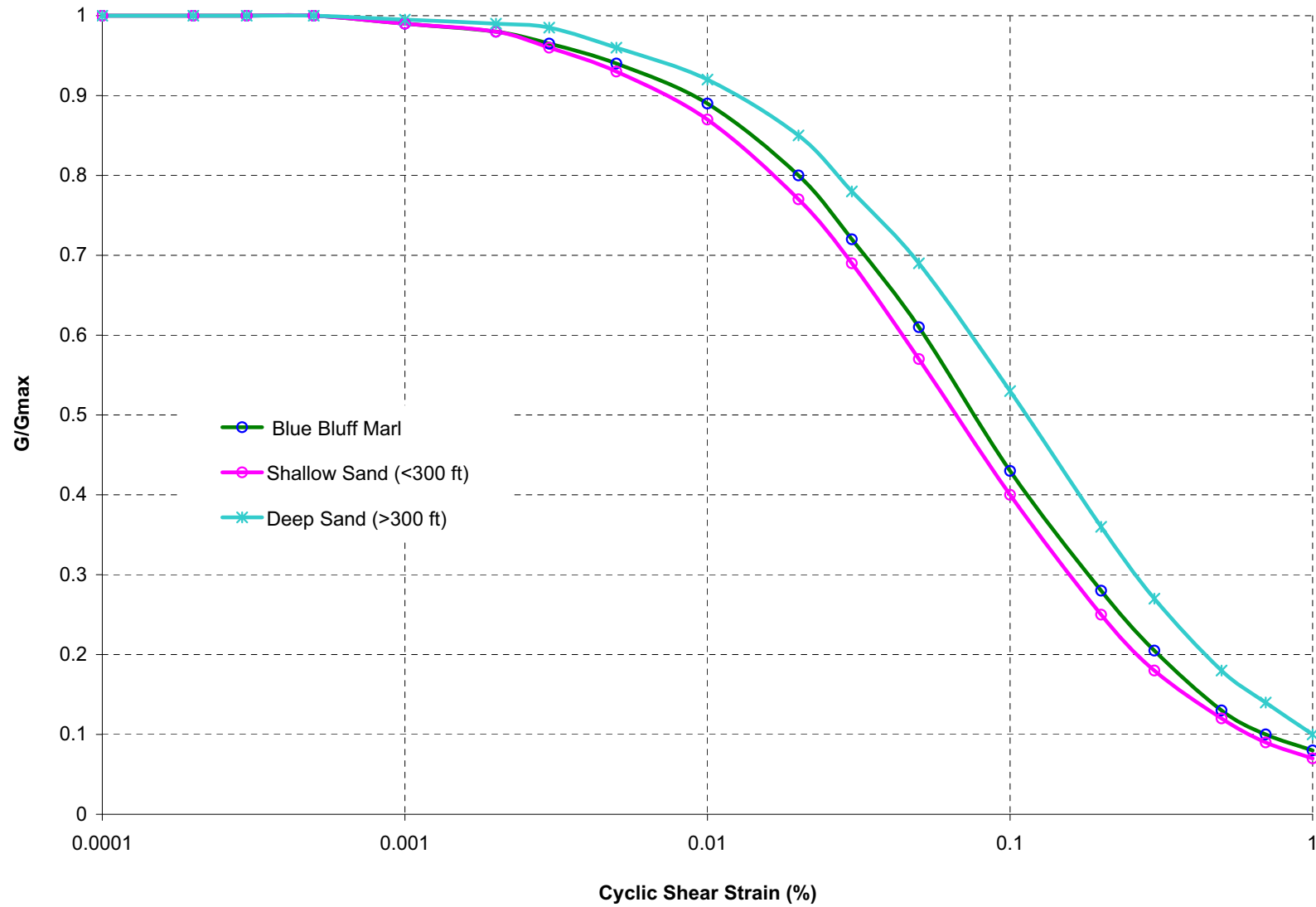


Figure 2.5-383
Shear Modulus Reduction Curves for SHAKE Analysis – SRS Curves

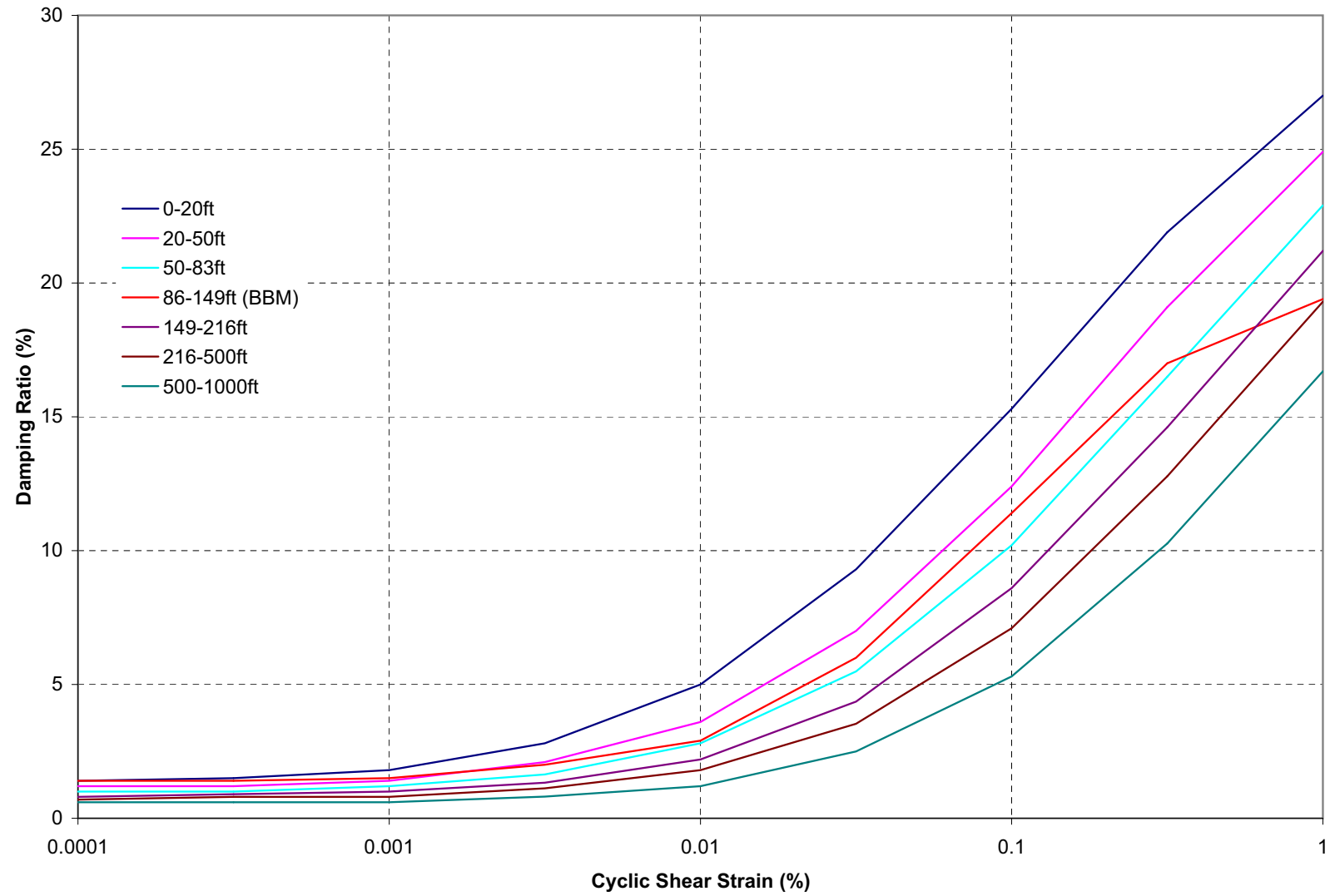


Figure 2.5-384
Damping Ratio Curves for SHAKE Analysis – EPRI Curves

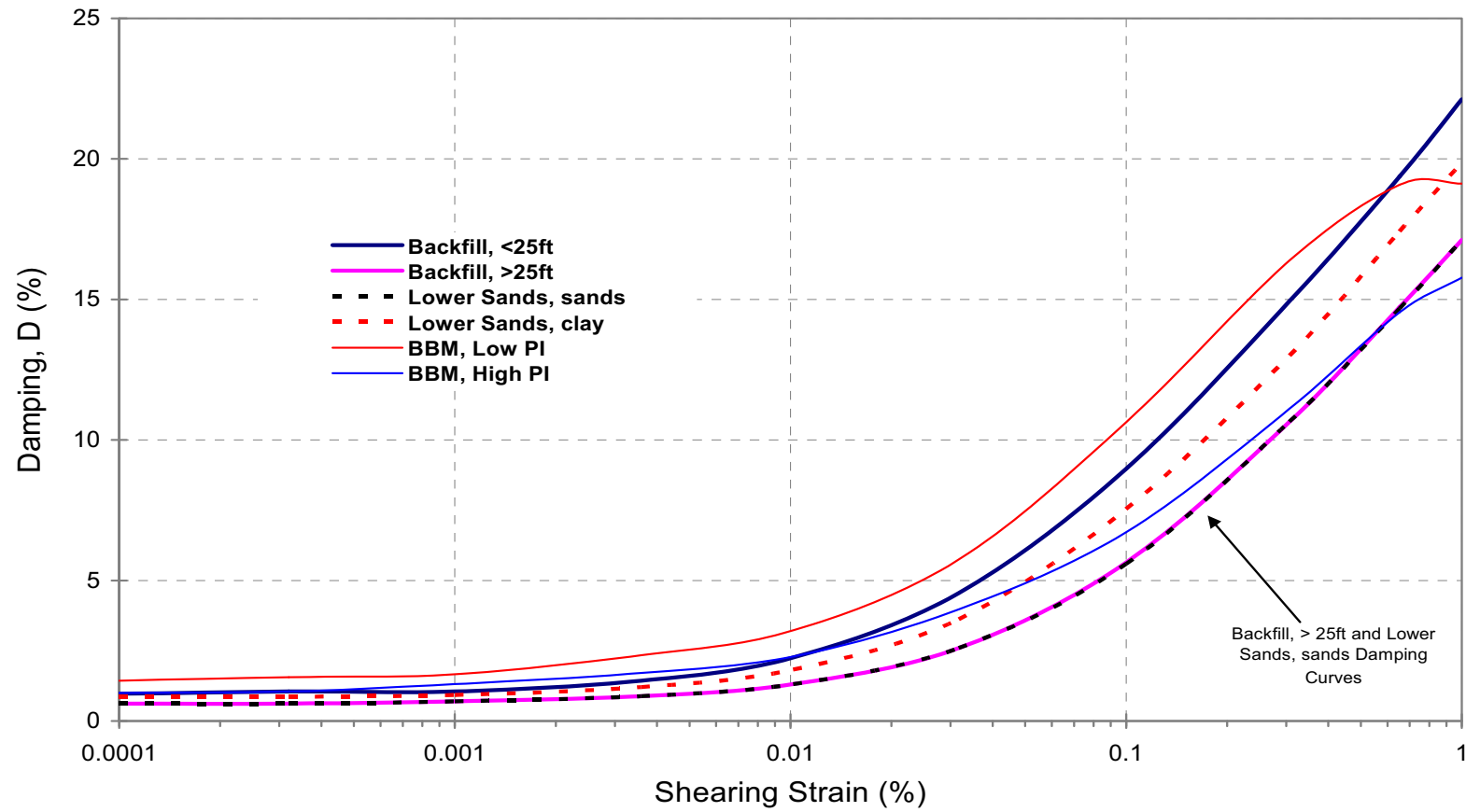


Figure 2.5-385
Site-Specific Damping Ratio Curves

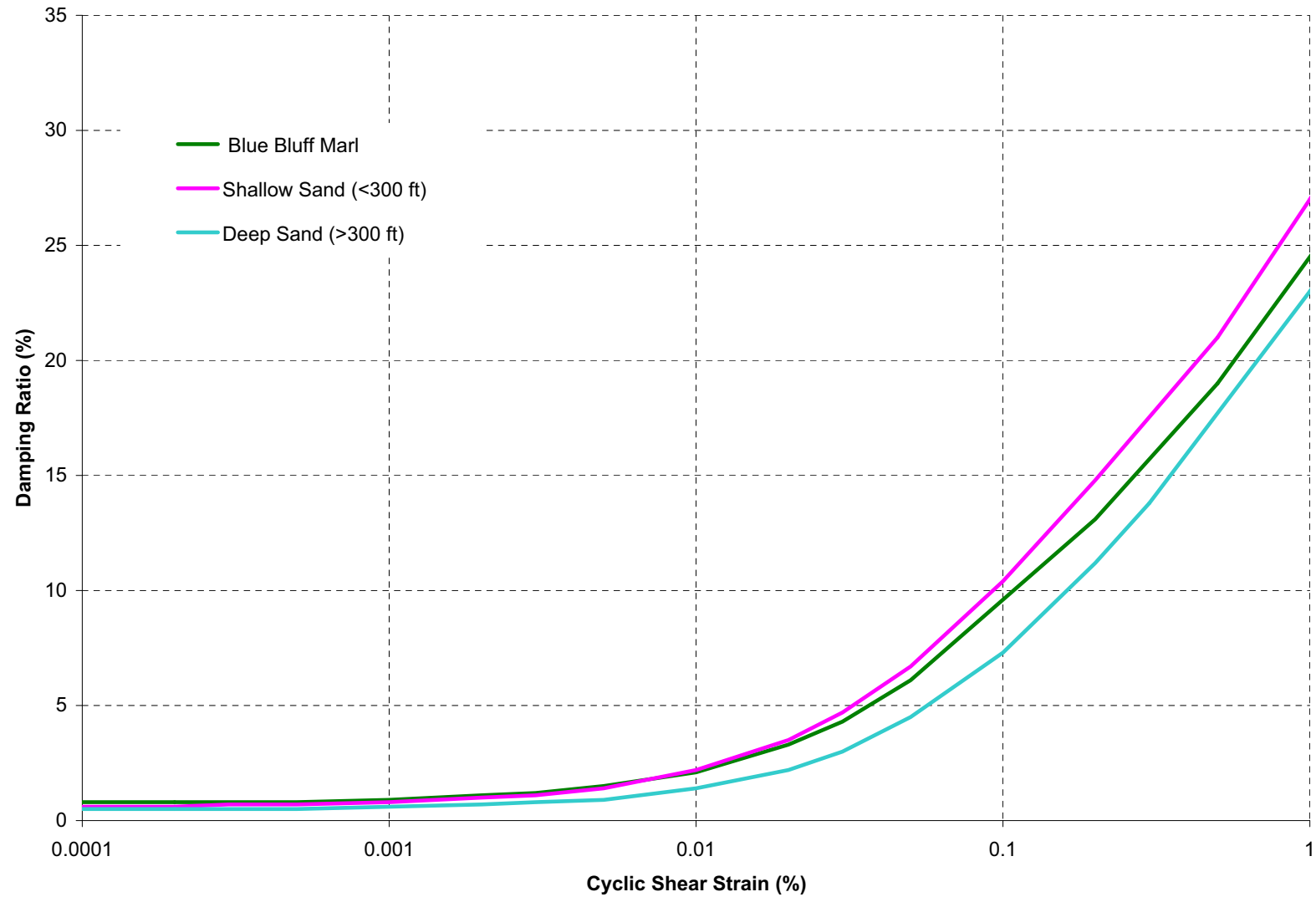


Figure 2.5-386
Damping Ratio Curves for SHAKE Analysis – SRS Curves

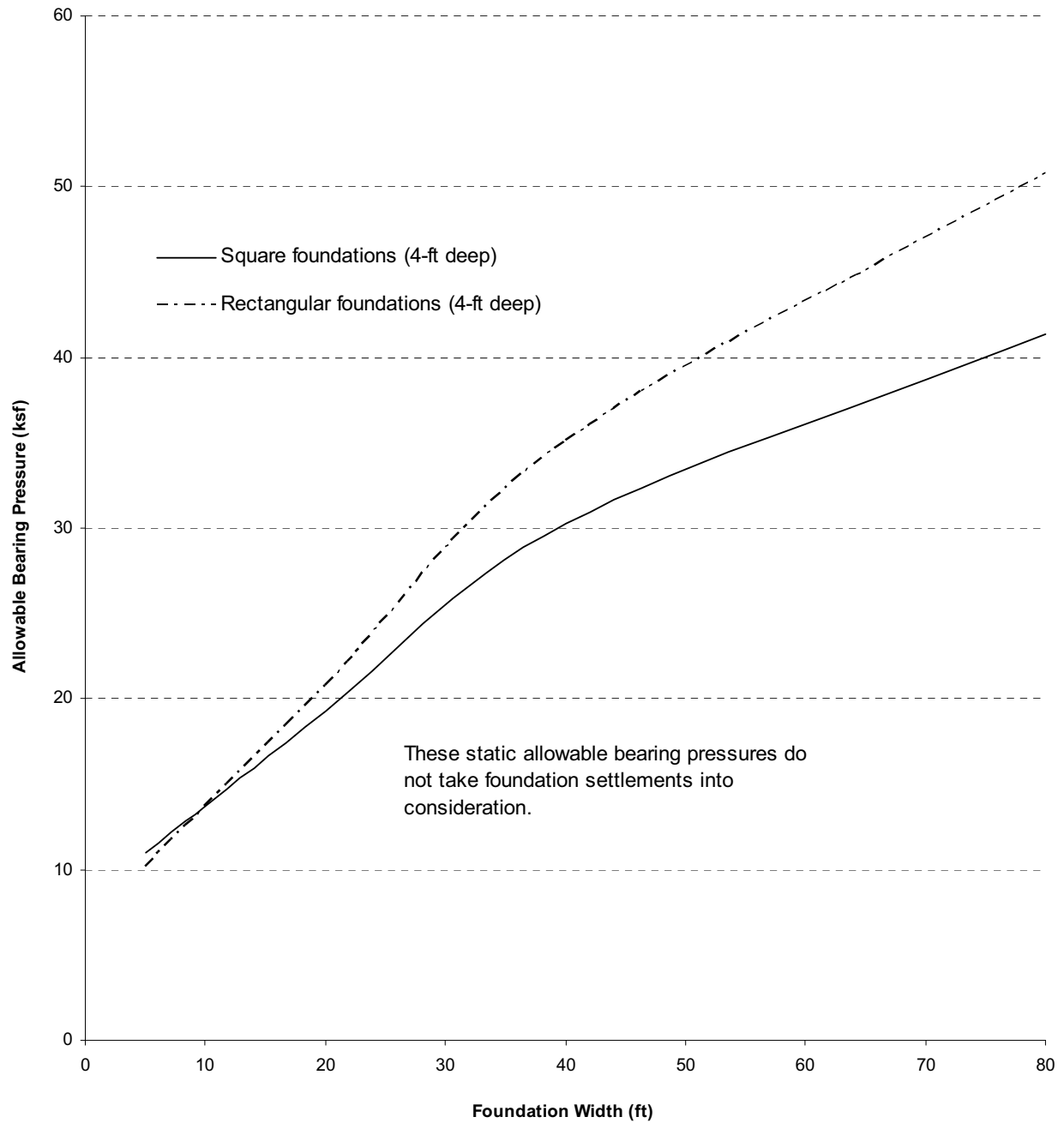


Figure 2.5-387
Allowable Bearing Capacity of Typical Foundation

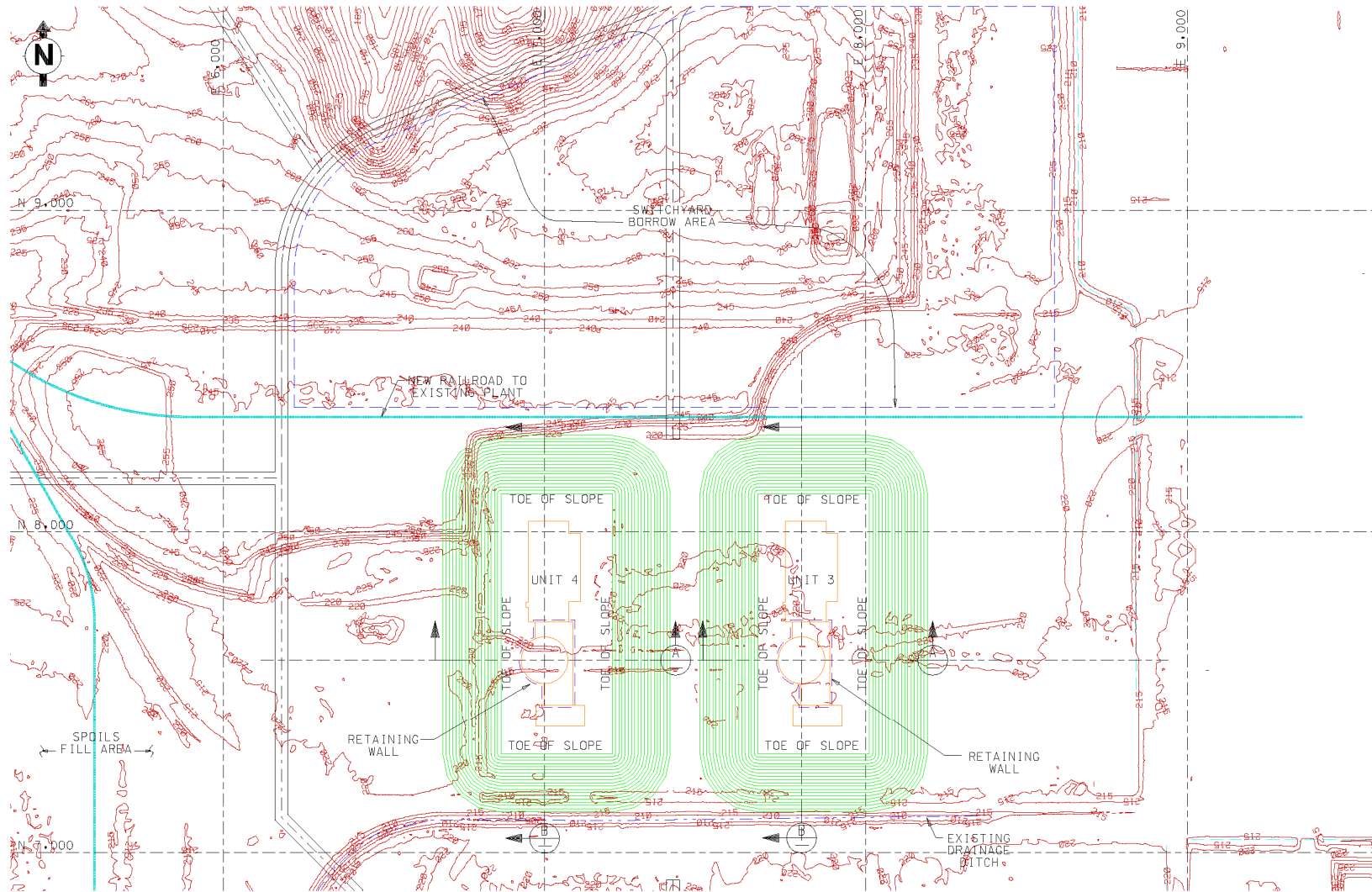


Figure 2.5-388
Power Block Excavation and Switchyard Borrow Area

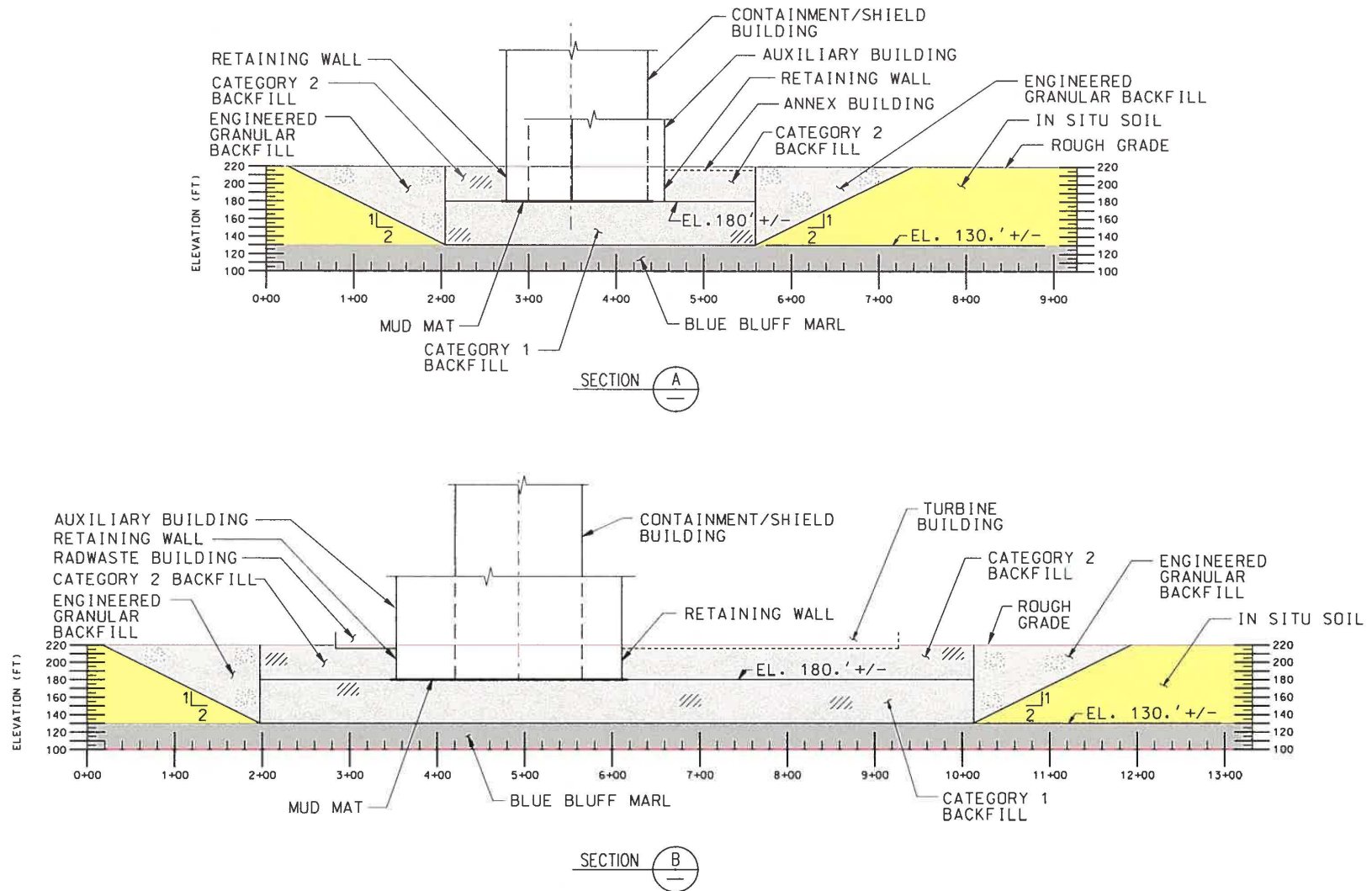


Figure 2.5-389
Power Block Excavation Sections

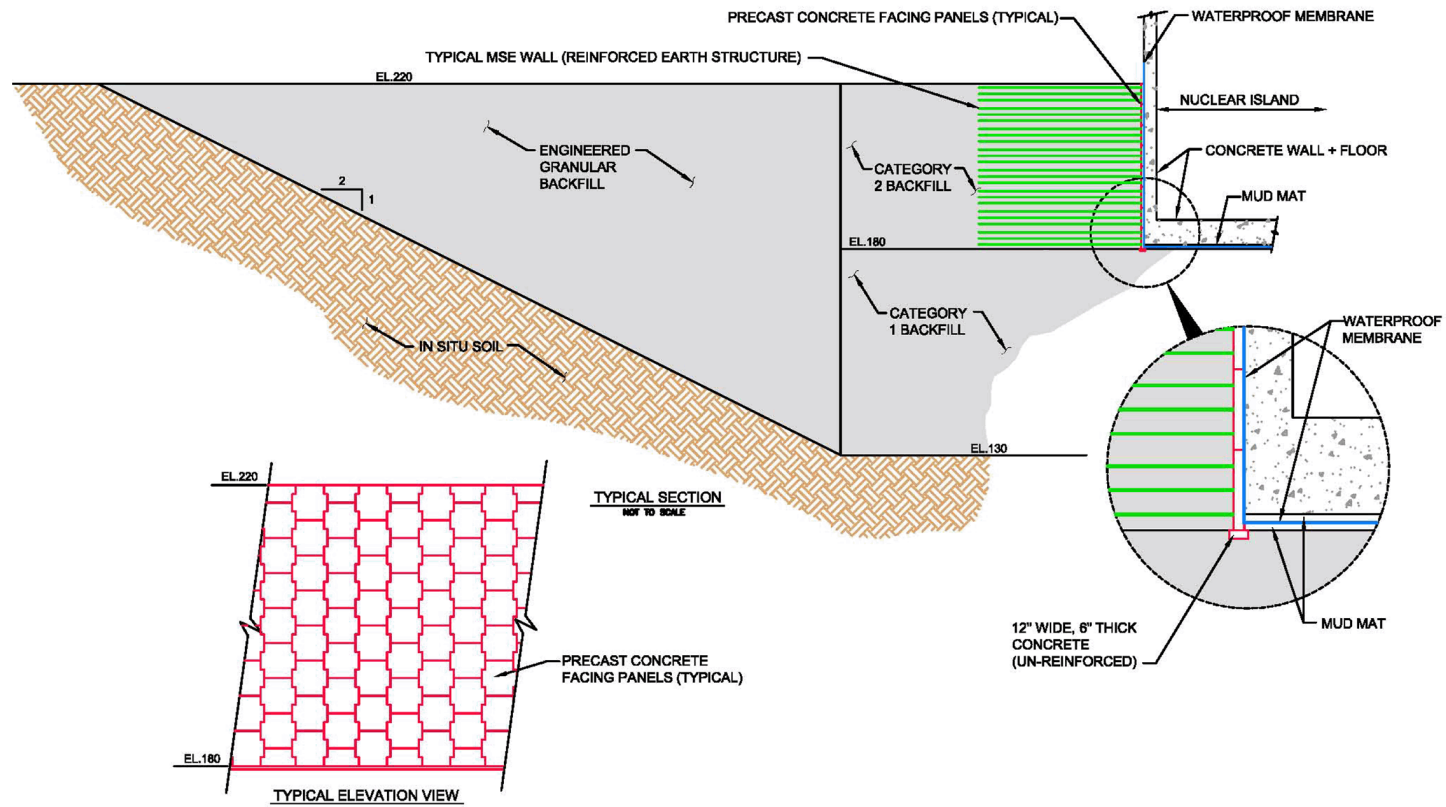


Figure 2.5-390
Nuclear Island Temporary Retaining Wall

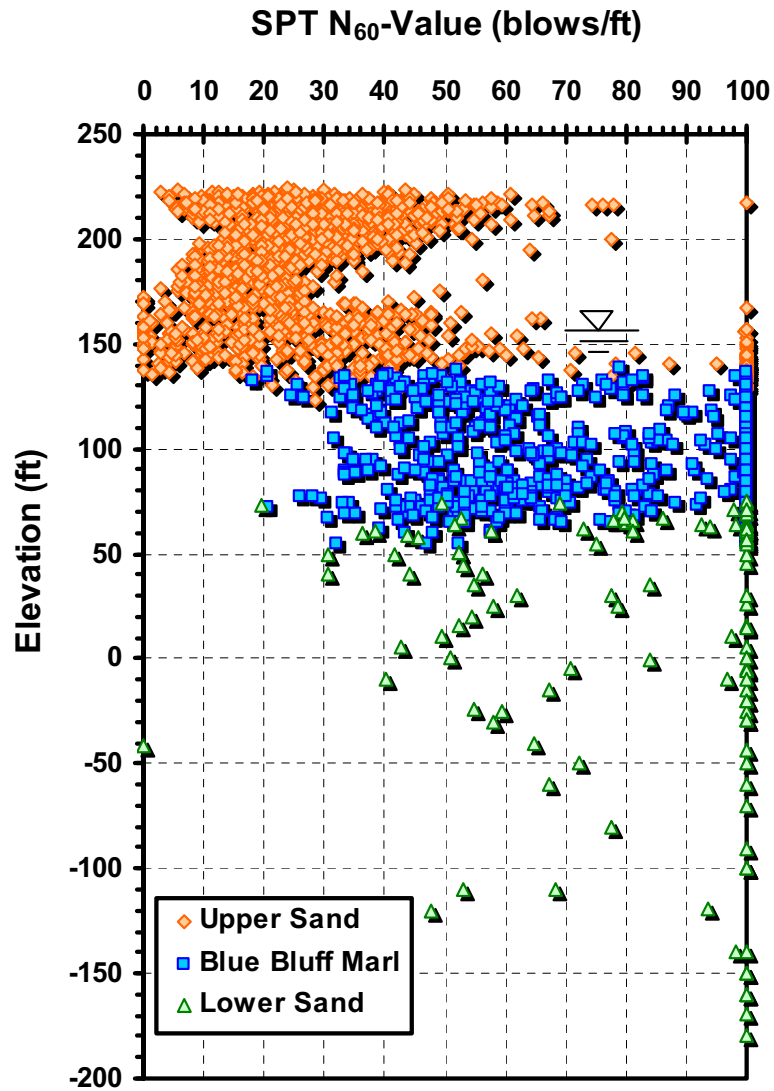


Figure 2.5-391
Distribution of SPT N_{60} -Value with Elevation (COL)

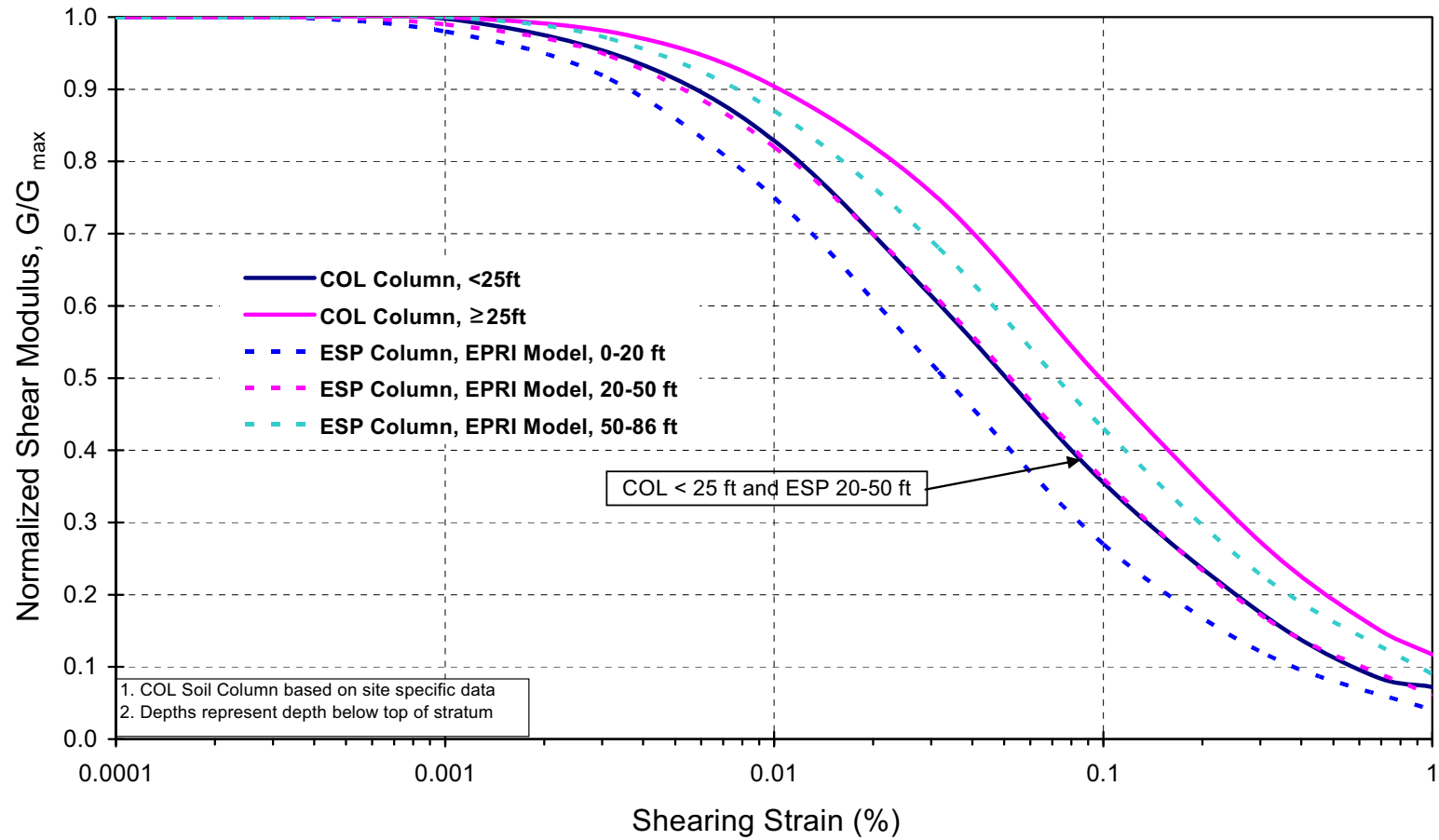


Figure 2.5-392
Comparison of Shear Modulus Reduction Curves - Backfill Soils

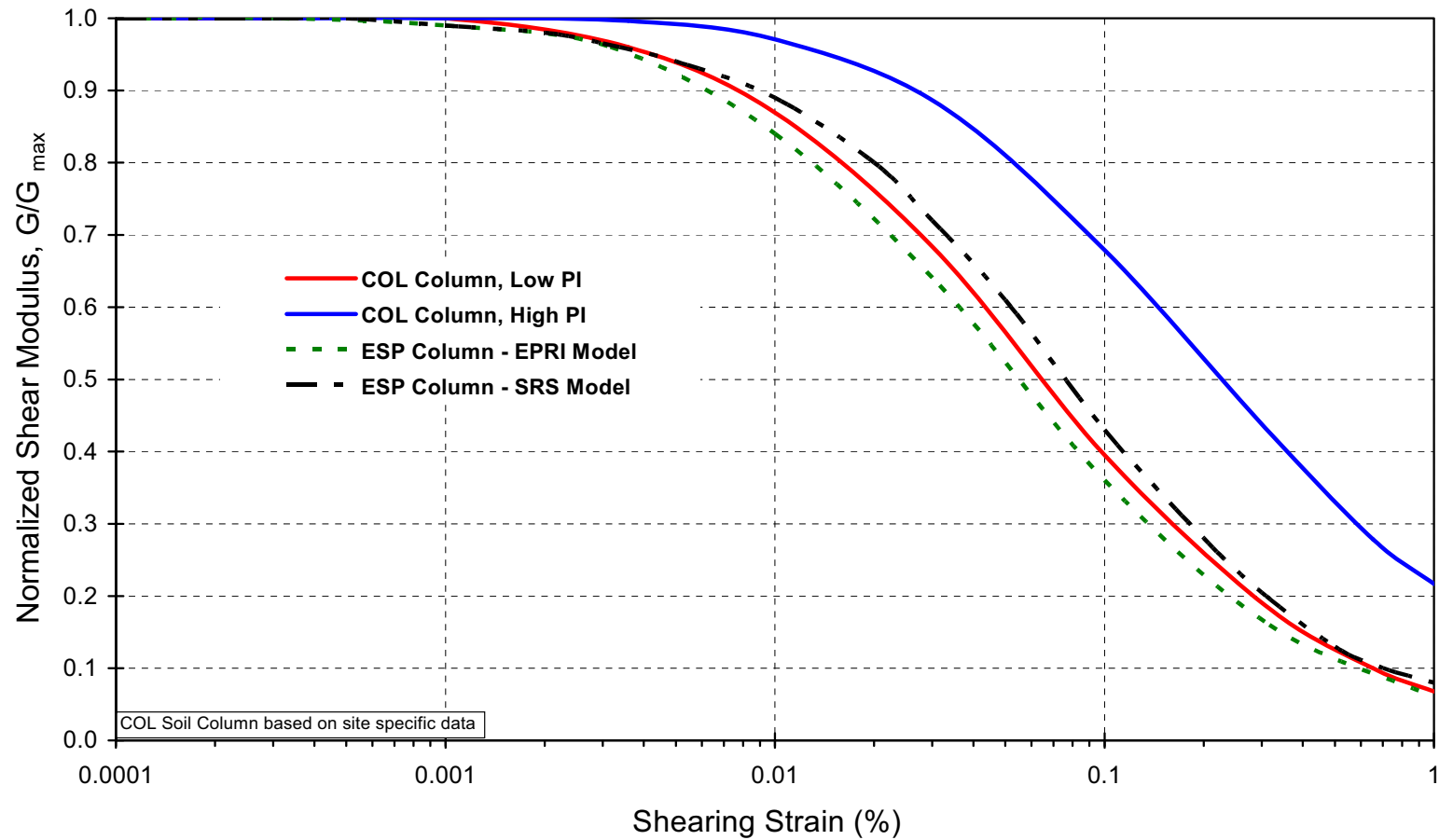


Figure 2.5-393
Comparison of Shear Modulus Reduction Curves - Blue Bluff Marl

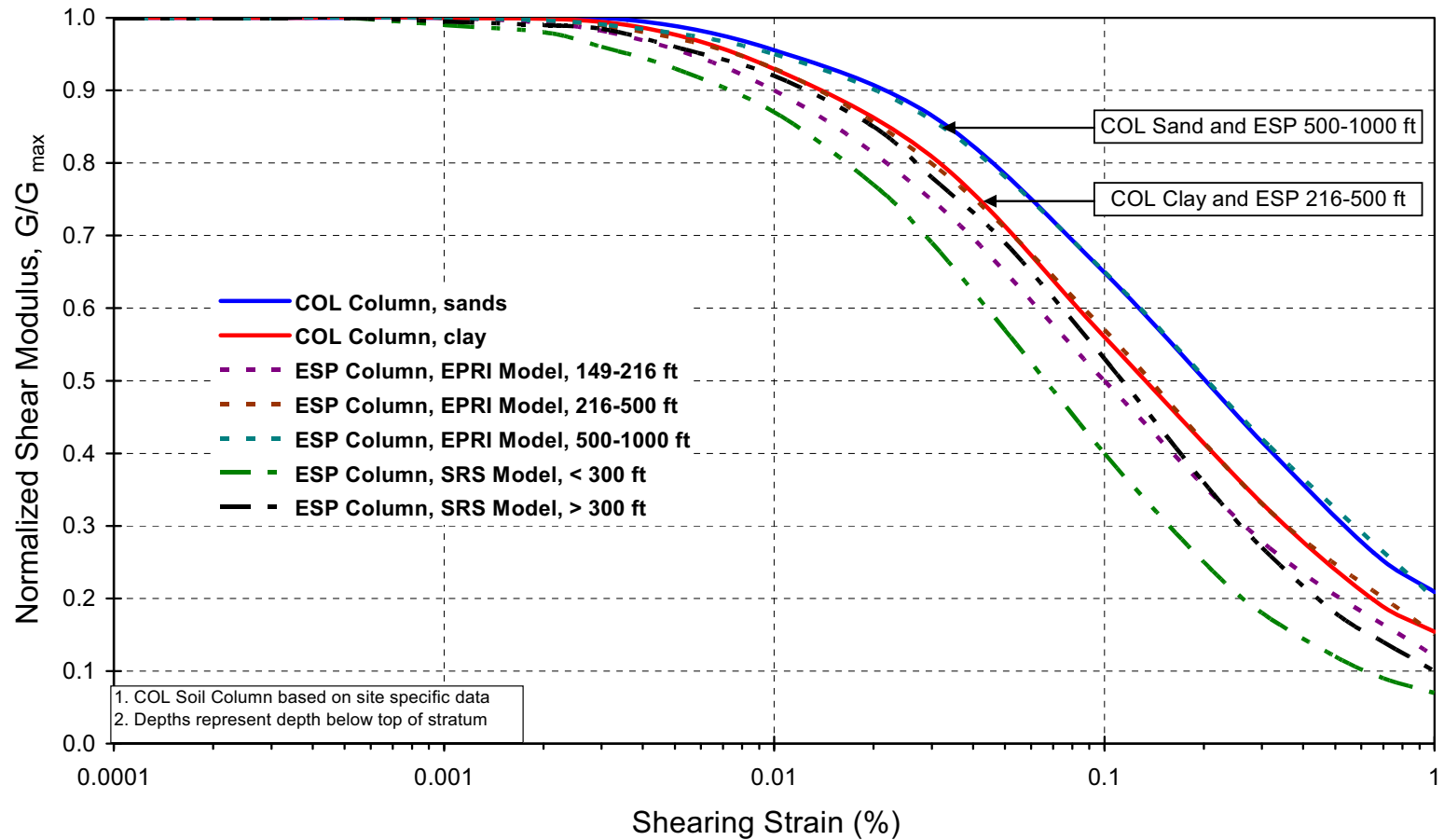


Figure 2.5-394
Comparison of Shear Modulus Reduction Curves - Lower Sands

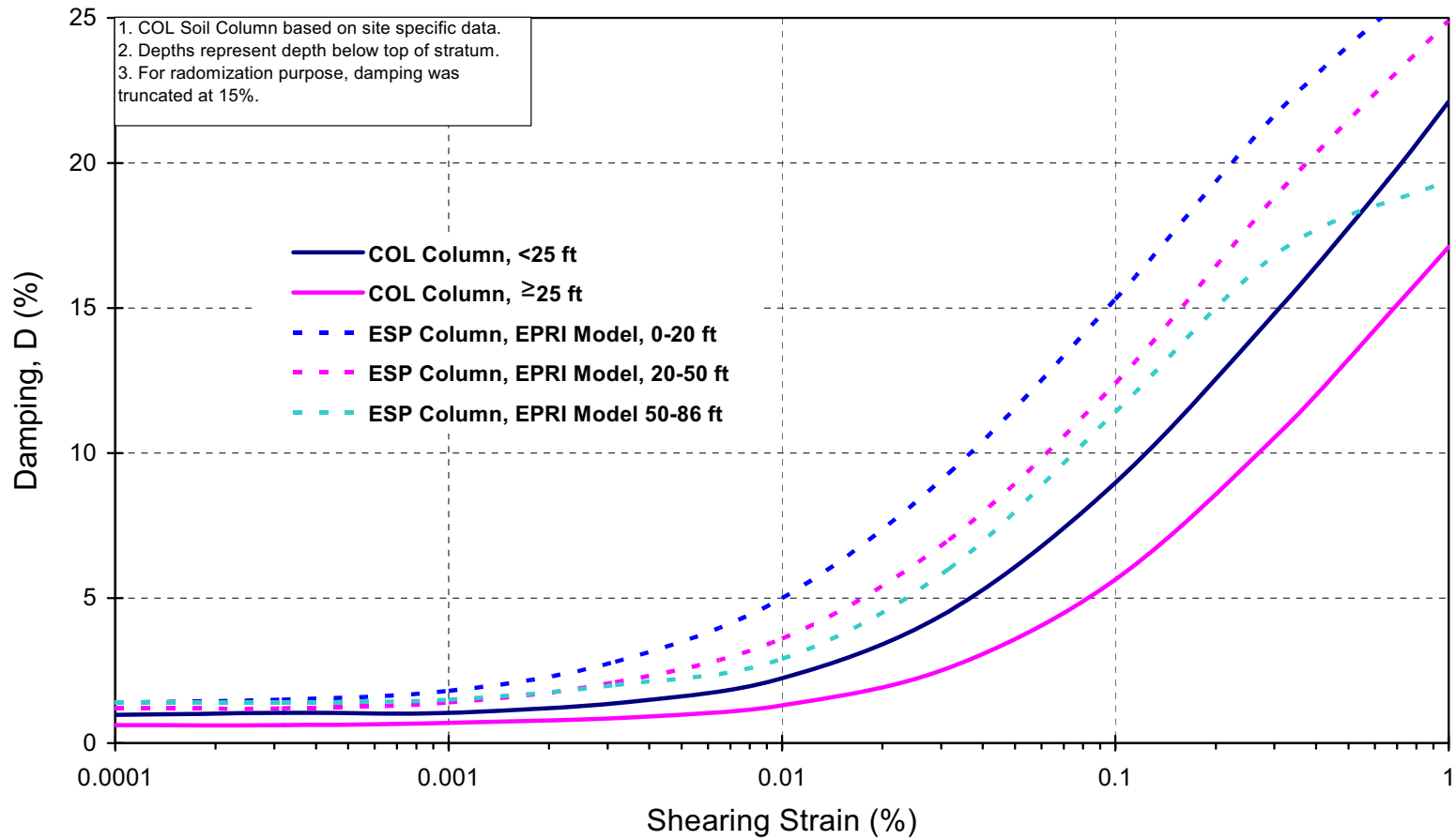


Figure 2.5-395
Comparison of Damping Ratio Curves - Backfill Soils

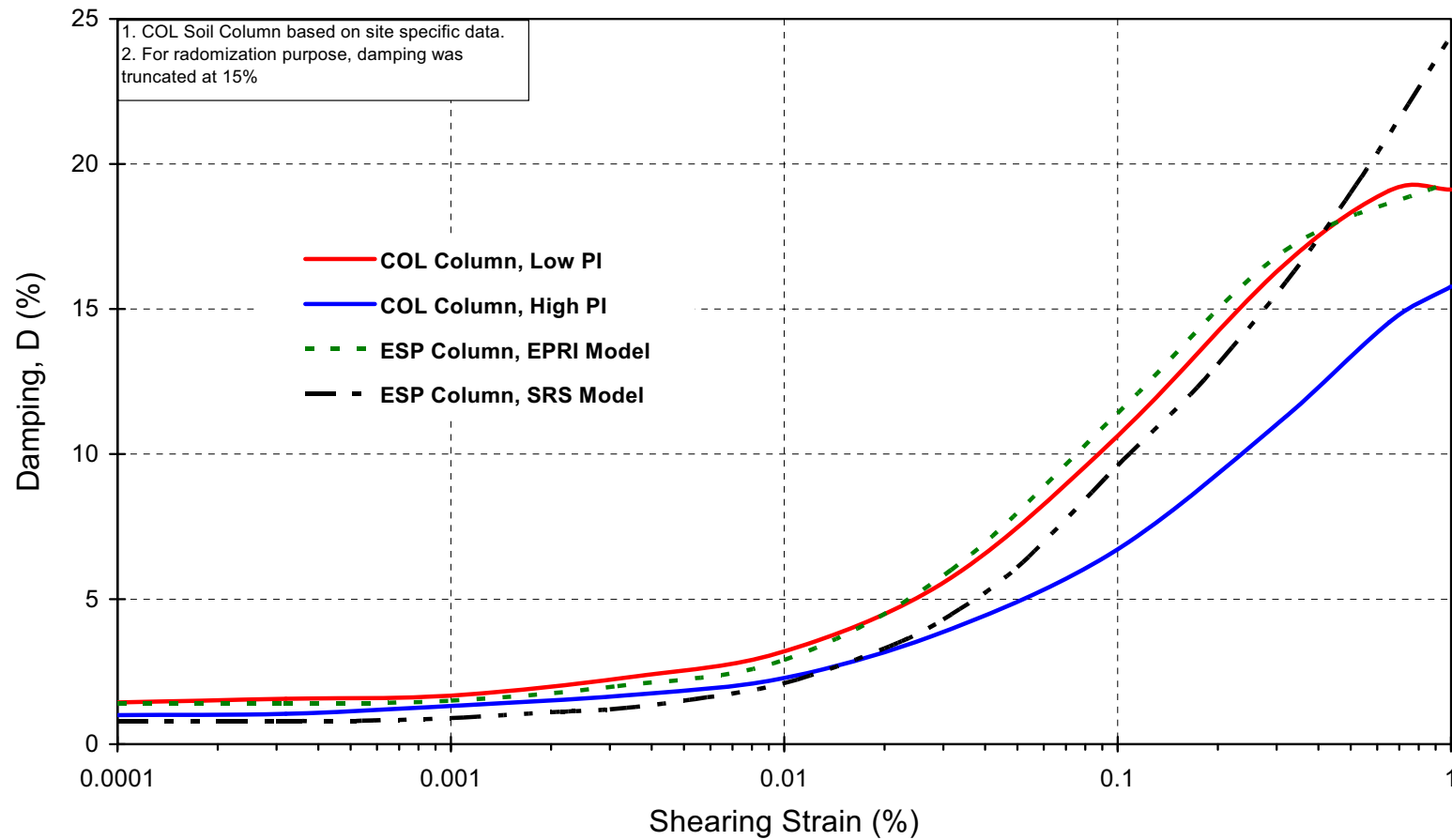


Figure 2.5-396
Comparison of Damping Ratio Curves - Blue Bluff Marl

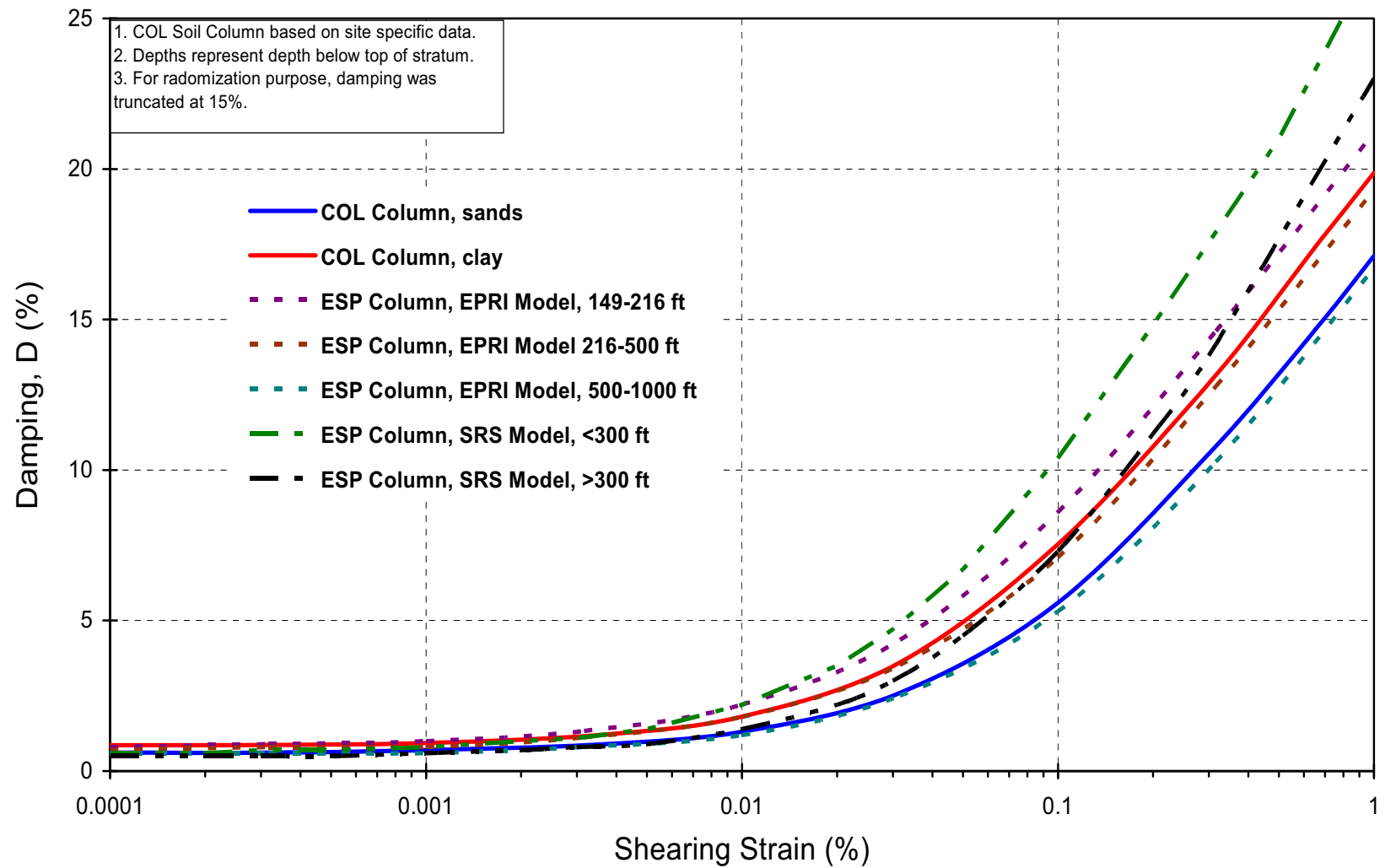


Figure 2.5-397
Comparison of Damping Ratio Curves - Lower Sands